

UNIVERSIDADE DE LISBOA

FACULDADE DE FARMÁCIA



**IRREVERSIBLE INHIBITORS OF SERINE PROTEASES
BASED ON THE β -LACTAM SCAFFOLD AS
POTENTIAL DRUG CANDIDATES**

Jalmira Hasmuklal Mulchande

DOUTORAMENTO EM FARMÁCIA

(Química Farmacêutica)

2009

UNIVERSIDADE DE LISBOA

FACULDADE DE FARMÁCIA



**IRREVERSIBLE INHIBITORS OF SERINE PROTEASES
BASED ON THE β -LACTAM SCAFFOLD AS
POTENTIAL DRUG CANDIDATES**

Jalmira Hasmuklal Mulchande

Tese orientada pelo Professor Doutor Rui Moreira

**Dissertação apresentada à Faculdade de Farmácia da Universidade de Lisboa,
com vista à obtenção do grau de Doutor em Farmácia (Química Farmacêutica)**

Lisboa 2009

Este trabalho foi desenvolvido sob orientação científica do Professor Doutor Rui Moreira, no Centro de Estudos de Ciências Farmacêuticas (CECF)/iMed.UL (Institute for Medicines and Pharmaceutical Sciences), Faculdade de Farmácia da Universidade de Lisboa.

O trabalho foi apoiado financeiramente pela Fundação para a Ciência e a Tecnologia, através da bolsa de doutoramento SFRH/BD/17534/2004 e através do projecto PTDC/QUI/64056/2006.

This work was developed under scientific guidance of Professor Dr. Rui Moreira, at CECF/iMed.UL (Institute for Medicines and Pharmaceutical Sciences), Faculty of Pharmacy, University of Lisbon.

The work was financially supported by Fundação para a Ciência e a Tecnologia, through the doctoral grant SFRH/BD/17534/2004 and through the project PTDC/QUI/64056/2006.

*The most beautiful experience we can have is the mysterious.
It is the fundamental emotion that stands at the cradle of true art and true science.
(...) I am satisfied with the mystery of life's eternity and with a knowledge,
a sense, of the marvelous structure of existence — as well as
the humble attempt to understand even a tiny portion of the
Reason that manifests itself in nature.*

Albert Einstein

(1879 - 1955)

To my parents.

To Febin and Jhit.

ACNOWLEDGMENTS

I sincerely thank Professor Rui Moreira (PhD), head of the Medicinal Chemistry Unit and supervisor of this thesis, for scientific support, continuous guidance and encouragement, and for this opportunity given to me to do research in medicinal chemistry.

I gratefully acknowledge Professor Jim Iley (PhD), from The Open University, not only for valuable suggestions and work discussions, but also for kindly receiving me at The Open University, UK, providing outstanding facilities. I also want to thank to the members of his lab for the assistance during my stay, in particular to Dr. Praveen Patel.

I warmly thank Dr. Luísa Martins (PhD), not only for introducing me to elastase and sharing expertise in enzyme inhibition kinetics, but also for friendship, interesting discussions and encouragement. Particularly, her Master thesis was very important in the context of the doctoral programme and it will be referred many times in the present work, enabling this study a comprehensive discussion of results.

To Professor Margarida Archer (PhD) and Dr. Tânia Oliveira, from the ITQB, UNL, at Oeiras, I thank for all the availability in performing X-ray crystallography studies of this project.

To Dr. Rita C. Guedes (PhD), from iMed.UL, for all the molecular modeling studies.

To Professor Luís Gouveia, (PhD), from iMed.UL, for the development of ENZFIT software, invaluable for slow-binding enzyme inhibition kinetic analysis by non-linear regression.

To Dr. Sandra I. Simões (PhD), from INETI/iMed.UL for the availability and kindness in performing a biodistribution study of a 4-oxo- β -lactam in mice and to Professor M. Eugénia M. Cruz (PhD), head of the Department, for making possible this fruitful collaboration. To Dr. Maria M. Gaspar (PhD) and Dr. Carla V. Eleutério for generous assistance in performing HPLC studies in mice blood and tissues.

To Dr. Rudi Oliveira, for kindly performing the hydrolysis studies in phosphate buffer and human plasma of this project.

To Dr. João Neres (PhD) for the synthesis of some β -lactams.

To Professor Michael I. Page (PhD), and Dr. W. Tsang (PhD), for a nice collaboration with Paper III.

To Professor Francisca Lopes (PhD) for a nice collaboration with Publication VI.

To Fundação para a Ciência e a Tecnologia (FCT), for financial support.

I wish to express my sincere gratitude to all research assistants and technical staff of my department as well as to past and present labmates. Thank you for everything: from the help in practical issues, support and assistance, to the trips to the Faculty of Sciences to run NMR spectra, and for sharing my joys, anxieties and frustrations, and surrounding me with a pleasant working environment!

Rita and João, I greatly appreciate for reading the thesis manuscript!

To Dixita, for taking such good care of my son since the ending of maternity leave till the nursery.

To my dear friends, both near and far, for care, support and enjoyable moments spent together! I feel very privileged in having your friendship!

My dearest thanks to my parents for their love, support and encouragement and for being there whenever needed! I dedicate this thesis to you!

I warmly thank my parents-in-law for their love, understanding and encouragement, and my siblings and brothers-in-law for their generous help and support.

My heartfelt thanks are due to my husband Febin, for his love, care, understanding and support. To my lovely son Jhit, for daily pleasant moments, giving me more than that I ever dreamed of. Febin and Jhit, this thesis is dedicated to you both too! I am so lucky to have you in my life!

Thank you all! Without you I would not made it this far.

GENERAL INDEX

ABBREVIATIONS AND SYMBOLOGY.....	i
INDEX OF FIGURES.....	iii
INDEX OF TABLES.....	xii
INDEX OF SCHEMES.....	xiv
INDEX OF EQUATIONS.....	xvi
ABSTRACT.....	xvii
RESUMO.....	xix

1. INTRODUCTION.....	1
1.1. Overview of Proteases.....	1
1.2. Serine Proteases.....	1
1.2.1 Serine Proteases as Therapeutic Targets.....	1
1.2.2 Active Site Topology and Catalytic Mechanism.....	5
1.3. Chymotrypsin Superfamily.....	7
1.4. Neutrophil Serine Proteases.....	7
1.4.1 Human Leukocyte Elastase (HLE).....	8
1.4.2 Proteinase 3 (PR3).....	8
1.4.3 Cathepsin G (Cat G).....	8
1.4.4 Physiological Functions.....	9
1.4.5 Roles in Human Disease.....	10
1.4.5.1 Chronic Obstructive Pulmonary Disease.....	11
1.4.5.2 The Protease-Antiprotease Hypothesis and the Relevance of HLE.....	11
1.5. Synthetic Inhibitors of Human Leukocyte Elastase.....	12

1.5.1 Transition State Analogue Inhibitors.....	13
1.5.2 Affinity Labels	16
1.5.3 Acylating Agents (Alternate Substrate Inhibitors).....	17
1.5.4 Mechanism-Based Irreversible Inhibitors	20
1.6. β-Lactams Inhibitors of HLE.....	21
1.6.1 Cephalosporins Derivatives.....	23
1.6.2 Monocyclic β -Lactams Derivatives	25
1.6.2.1 Monocyclic β -Lactams with the Leaving Group on a Different Position than C-4	30
1.6.2.2 Monocyclic β -Lactam Analogues Acylating Agents of HLE	33
1.7. Porcine Pancreatic Elastase.....	35
1.8. Design of Potential Irreversible Inhibitors of HLE.....	36
1.8.1 The Second-Order Rate Constant for Alkaline Hydrolysis, k_{OH^-} , as an Important Tool in Drug Design	38
1.9. Aim of the Thesis	38
1.9.1 C-4 Substituted Azetidin-2-ones (Simple β -Lactams) as Inhibitors of Serine Proteases.....	39
1.9.2 Azetidine-2,4-diones (4-Oxo- β -lactams) as Inhibitors of Serine Proteases	40
2. C-4 SUBSTITUTED N-CARBAMOYL AZETIDIN-2-ONES: CHEMICAL REACTIVITY AND ENZYME INHIBITION	45
2.1. Synthesis	45
2.1.1 NMR Spectral Characterisation.....	49
2.1.2 IR Spectroscopy	52
2.2. Alkaline hydrolysis studies	52
2.2.1 Introductory Remarks	52
2.2.2 Results and Discussion	53
2.2.2.1 Free Energy Relationships for the Alkaline Hydrolysis of 47	55
2.2.2.2 Mechanism of the Alkaline Hydrolysis Reaction of 47	60
2.3. Enzyme Inhibition Studies.....	64
2.3.1 PPE Inhibition Studies.....	64
2.3.1.1 Introductory remarks	64
2.3.1.2 Determination of the K_m	65

2.3.1.3	Inhibition Assays	66
2.3.1.4	Results and Discussion	67
2.3.2	HLE Inhibition Studies	78
2.3.2.1	Introductory Remarks	78
2.3.2.2	Results and Discussion	79
3.	AZETIDINE-2,4-DIONES (4-OXO-β-LACTAMS): SYNTHESIS, AND PRELIMINARY STUDIES AS ENZYME INHIBITORS	95
3.1.	Introductory Remarks	95
3.1.1	Molecular Modelling	95
3.2.	Synthesis	96
3.2.1	Attempted Synthesis of <i>N</i> -Unsubstituted 4-Oxo- β -lactams, Using Published Routes	97
3.2.1.1	Ring closure of 2,2-Diethyl Malonic Acid Monoamide (Malonic Acid) and Derivatives	98
3.2.2	Condensation of Malonyl Dichlorides with Primary Amines to give C-3 and N- 1 Substituted 4-Oxo- β -lactams	101
3.2.3	Attempted Synthesis of <i>N</i> -Unsubstituted 4-Oxo- β -lactam from <i>N</i> -Protected Azetidine-2,4-diones	102
3.2.3.1	Attempted Oxidative <i>N</i> -Dearylation of <i>N</i> -(<i>p</i> -Methoxy)- phenylazetidine-2,4-dione, 77c	103
3.2.3.2	Attempted <i>N</i> -Debenzylation of 77b by Catalytic Hydrogenation	104
3.2.3.3	Attempted Deprotection of <i>N</i> -benzhydryl azetidine-2,4-dione 79	105
3.2.4	Attempted Bromination at C-1' of Azetidine-2,4-diones	105
3.2.5	NMR Spectral Characterisation	106
3.2.6	IR Spectroscopy	108
3.2.7	Mass Spectroscopy	109
3.3.	Alkaline Hydrolysis Studies of 4-Oxo-β-lactams	110
3.3.1	Results and Discussion	110
3.3.1.1	Structure Activity Relationships for the Alkaline Hydrolysis	113
3.4.	PPE Inhibition Studies	117
3.4.1	Results and Discussion	117
3.4.1.1	Structure Activity Relationships and Molecular Modeling	125

4. AZETIDINE-2,4-DIONES (4-OXO-β-LACTAMS) AS POTENT AND SELECTIVE INHIBITORS OF HLE	137
4.1. 4-Oxo-β-lactam-Based Inhibitor Design Rationale	137
4.2. Synthesis	139
4.2.1 Cicloaddition of ketenes generated in situ with isocyanates	141
4.2.2 Thioether Functionalized <i>N</i> -aryl-azetidine-2,4-diones	146
4.2.3 NMR Spectral Characterisation.....	148
4.2.4 IR Spectroscopy	149
4.2.5 Mass Spectroscopy	149
4.3. Enzyme Inhibition Studies	151
4.3.1 HLE Inhibition Studies: Results and Discussion.....	151
4.3.1.1 Structure Activity Relationships.....	160
4.3.1.2 Molecular Modeling Studies	165
4.3.2 Selectivity Studies	167
4.3.2.1 Proteinase 3 Inhibition Studies	167
4.3.2.2 Cathepsin G Inhibition Studies.....	168
4.3.2.3 Papain Inhibition Studies.....	170
4.3.2.4 PPE Inhibition <i>versus</i> HLE inhibition	170
4.4. Hydrolytic Stability Studies	171
4.4.1. The Product of Hydrolysis of 103	172
4.4.2 Stability in pH 7.4 Buffer and in 80% Human Plasma.....	174
4.5. Biodistribution Studies of a Selected 4-Oxo-β-lactam.....	176
5. CONCLUSIONS.....	183
6. EXPERIMENTAL SECTION	189
6.1. Synthesis	189
6.1.1 Reagents, solvents and chromatography	189
6.1.2 Equipment	189
6.1.3 Experimental Procedures and Product Characterization	190
6.2. Alkaline Hdrolisis Studies (Chemical Kinetics).....	225

6.3. Enzyme Inhibition Studies.....	225
6.3.1 PPE Inhibition Studies.....	225
6.3.1.1 PPE Inactivation by the Incubation Method.....	225
6.3.1.2 PPE Inactivation by the Progress Curve Method	226
6.3.1.3 Titration of PPE (Partition Ratio).....	226
6.3.2 HLE Inhibition Studies.....	227
6.3.3 HLE Inactivation by the Progress Curve Method	227
6.3.4 HLE Inactivation by the Incubation Method.....	227
6.3.4.1 Titration of HLE (Partition Ratio)	228
6.3.5 Inhibition Assay for Cathepsin G	228
6.3.6 Inhibition Assay for Proteinase 3	228
6.3.7 Inhibition Assay for Papain.....	229
6.4. X-Ray Crystallography Studies.....	229
6.5. Hydrolysis of Selected 4-Oxo-β-lactams in Phosphate Buffer Solution and Human Plasma.....	230
6.5.1 Hydrolysis of Selected β -Lactams in pH 7.4 Phosphate Buffer Solution	230
6.5.2 Hydrolysis in Human Plasma	230
6.5.3 HPLC Analysis.....	231
6.6. Biodistribution Study in Mice	231
6.6.1 Determination of 103k by HPLC in Mice Blood and Tissues	231
6.6.1.1 Chromatographic System	231
6.6.1.2 Preparation of Standard Solutions	232
6.6.1.3 Extraction of 103k from Blood and Tissues.....	232
6.7. Molecular Modeling	233
6.7.1 Virtual Screening.....	234
6.7.2 Molecular Docking.....	234

APPENDIX 1.....	237
A1.1 Alkaline Hydrolysis of Compounds 47b , 47e and 47f	237
A1.2 Determination of the Molar Extinction Coefficient for <i>p</i> -Nitroaniline.....	239
A1.3 Determination of the K_m	239
A1.4 PPE Inhibition Studies.....	241
A1.5 HLE Inhibition Studies.....	244
APPENDIX 2.....	246
APPENDIX 3.....	258
A3.1 Alkaline Hydrolysis Studies of 4-Oxo- β -lactams 77	258
A3.2 PPE Inhibition by 4-Oxo- β -lactams 77	260
A3.2.1 Analysis of the Inhibition Kinetics and Determination of K_i for 77e	261
A3.2.2 Inhibition of PPE by Compounds 77h-i	264
A3.2.3 Molecular Modeling of 77h at the Active Site of PPE.....	266
APPENDIX 4.....	267
A4.1 HLE Inactivation Studies by 4-Oxo- β -lactams (77 and 103).....	267
A4.1.1 Obtained Pseudo-first-order Rate Constants of HLE Inhibition.....	267
A4.1.2 Plots of the Linear Dependence of k_{obs} with Inhibitor Concentration for the HLE Inhibition by 77 and 103 (Mechanism A).....	271
A4.1.3 Determination of K_i for 4-Oxo- β -lactams HLE Inhibitors (Mechanism A)..	277
A4.1.4 Determination of Kinetic Parameters for HLE inhibition (Mechanism B)....	289
A4.1.5 Titration of HLE Activity by 77g	293
A4.2 Proteinase 3 Inhibition Studies.....	293
A4.3 Cathepsin G Inhibition Studies.....	295
A4.4 Hydrolytic Stability Studies.....	296
A4.4.1 Calibration Curves.....	296
A4.4.2 Stability in pH 7.4 Phosphate Buffer Saline.....	298
A4.4.3 Stability in 80% Human Plasma.....	299
A4.5 Biodistribution Studies.....	301
REFERENCES.....	305
PUBLICATIONS RESULTING FROM THIS THESIS.....	325

ABBREVIATIONS AND SYMBOLOGY

Amino acids are written in three-letter code. Other abbreviations are:

abs	absolute
Anal. Calcd.	analysis calculated
asymm.	asymmetric
br	broad
brs	broad singlet
Bu	butyl
Bz	benzyl
Cat G	cathepsin G
COPD	chronic obstructive pulmonary disease
¹³ C NMR	carbon isotope C-13 nuclear magnetic resonance
d	doublet
DCM	dichloromethane
dd	doublet of doublets
ddd	doublet of doublet of doublets
DEPT	distortionless enhancement by polarization transfers
DMSO	dimethylsulfoxide
dt	doublet of triplets
dq	doublet quartet
EREF	enzyme rate enhancement factor
MS	mass spectrometry
Et	ethyl
EtOAc	ethyl acetate
EtOH	ethanol
eq.	equivalent
EWG	electron-withdrawing group
exc.	excess
h	hour
HCMV	human cytomegalovirus
HCV	hepatitis C virus
HEPES	<i>N</i> -(2-Hydroxyethyl)piperazine- <i>N'</i> -(2-ethanesulfonic acid)
HLE	human leukocyte elastase
¹ H NMR	proton nuclear magnetic resonance

HOMO	highest occupied molecular orbital
HPLC	high performance liquid chromatography
<i>i</i> Pr	isopropyl
IR	infrared
<i>J</i>	proton-proton coupling constant
LG	leaving group
lit.	literature
LUMO	lowest unoccupied molecular orbital
m	multiplet
(M) ⁺	molecular ion peak (in mass spectrometry)
Me	methyl
MMP	matrix metalloproteases
m.p.	melting point
MW	molecular weight
m/z	mass to charge ratio
Naph	naphthyl
NMR	nuclear magnetic resonance
PBS	phosphate buffer solution
Ph	phenyl
PR3	proteinase 3
PPE	porcine pancreatic elastase
Pyr	pyridine
q	quartet
rt	room temperature
s	singlet (in the context of NMR data) or seconds
symm.	symmetric
t	triplet
TEA	triethylamine
TLC	thin layer chromatography
UV	ultraviolet
ν_{\max}	maximum wave number
v/v	volume/volume fraction solution

INDEX OF FIGURES

Figure 1.1 - Interactions between the specific subsites of a protease and the respective residues of the substrate. ²²	5
Figure 1.2 - General catalytic mechanism of serine proteases. ^{23, 24}	6
Figure 1.3 - Design of a peptidic transition state analogue inhibitor of HLE from a peptidic substrate. ⁶⁴	14
Figure 1.4 - Scheme of binding mode of pyridone-containing trifluoromethyl ketones to HLE. ⁶⁸	15
Figure 1.5 - Proposed mechanism of inhibition of serine proteases by peptidyl chloromethyl ketones. ²⁵	17
Figure 1.6 - Formation of an acyl-enzyme complex between 2-amino-4H-3,1-benzoxazin-4-ones and HLE and deacylation pathways to regenerate free enzyme. ⁷⁷	19
Figure 1.7 - Proposed “double-hit” mechanism of HLE inactivation by cephalosporin derivatives. ⁹⁰	24
Figure 1.8 - Proposed mechanism of inhibition of HLE by monocyclic β -lactams with a leaving group LG at C-4. ⁹⁵	26
Figure 1.9 - Potential suicide-type mechanism of HLE inhibition by <i>N</i> -acyloxymethylazetidin-2-ones. ¹⁰⁶	31
Figure 1.10 - Postulated suicide-type mechanism of HLE inhibition by functionalized <i>N</i> -aryl azetidin-2-ones. ¹¹⁰	32
Figure 1.11 - Inhibition of HLE by 1,3-diazetidone-2,4-diones. ¹¹²	33
Figure 1.12 - Nucleophilic attack at 3-oxo- β -sultam. PPE inhibition involves C-N fission while alkaline hydrolysis involves S-N fission. ¹¹⁵	35
Figure 1.13 - General acyl transfer process (Nu = nucleophile; LG = leaving group).	36
Figure 1.14 - Rational design of C-4 substituted <i>N</i> -carbamoylazetidin-2-ones.....	40
Figure 2.1 - Expansion of the observed signals of the spectrum of ¹ H NMR for the protons at C-3 of compound 43a	49
Figure 2.2 -Splitting pattern diagram of the signal corresponding to a <i>ddd</i> for the proton at C-3 of compound 43a	50
Figure 2.3 - Expansion of the observed signals of the spectrum of ¹ H NMR for the -CH ₂ protons of the diethyl group at C-3 of compound 47f	50
Figure 2.4 - Splitting pattern diagram of the signal corresponding to a doublet of quadruplets (Figure 2.3, left) for a methylene proton of the diethyl group at C-3 of compound 47f	51

Figure 2.5 - Expansion of the observed signals of the spectrum of ^1H NMR for the methylene NHCH_2Ph protons of compound 47f .	51
Figure 2.6 -Time course for the alkaline hydrolysis of 47f .	53
Figure 2.7 - Plot of the pseudo-first-order rate constants, k_{obs} for the alkaline hydrolysis of compound 47b , against hydroxide concentration, at 25 °C and ionic strength 0.5 M.	54
Figure 2.8 - Plot of the pseudo-first-order rate constants, k_{obs} for the alkaline hydrolysis of compound 47e , against hydroxide concentration, at 25 °C and ionic strength 0.5 M.	54
Figure 2.9 - Plot of the pseudo-first-order rate constants, k_{obs} for the alkaline hydrolysis of compound 47f , against hydroxide concentration, at 25 °C and ionic strength 0.5 M.	55
Figure 2.10 - Linear correlation between the second-order rate constants for the alkaline hydrolysis, k_{OH^-} of C-3 unsubstituted β -lactams 47a-d and C-3 gem-diethyl β -lactams 47e-j and the Taft σ_1 value for the X substituents in C-4.	58
Figure 2.11 - Tetrahedral intermediate 52 resulting from hydroxide ion attack at a 3,3-diethyl derivative, 47e , $\text{R}=\text{CONHCH}_2\text{Ph}$, and the respective Newman projection obtained from looking along the C2-C3 bond of the β -lactam.	58
Figure 2.12 - Mechanism of ring-opening of a cephalosporin with a leaving group X at C-3' by nucleophilic attack at the β -lactam carbonyl carbon. ¹²⁸	59
Figure 2.13 - Proposed mechanism of alkaline hydrolysis of C-3 substituted derivatives 47 .	60
Figure 2.14 - The enolate of 3-oxopropanamide, 54 , formed by the alkaline hydrolysis of C-3 unsubstituted 4-aryloxy and 4-arylthioazetidin-2-ones, and <i>N</i> -acyloxymethylazetidin-2-ones.	61
Figure 2.15 - Proposed mechanism of alkaline hydrolysis of C-3 unsubstituted derivatives 47 .	62
Figure 2.16 - Hydrolysis of the chromogenic substrate <i>N</i> -suc-(L-Ala) ₃ - <i>p</i> -nitroanilide, 58 . ¹³⁴	64
Figure 2.17 - Lineweaver-Burke plot for the PPE-catalyzed hydrolysis of <i>N</i> -suc-(L-Ala) ₃ - <i>p</i> -nitroanilide, 58 , in 0.1 M HEPES buffer, pH 7.2, at 25 °C.	65
Figure 2.18 - Plot of the PPE remaining activity against incubation time for compound 47d , at 10 μM , 20 μM , 40 μM , and 50 μM , in the incubation mixture, at 25 °C, in 0.1 M HEPES buffer, pH 7.2.	68
Figure 2.19 - Plot of the pseudo-first-order rate constants, k_{obs} for the inactivation of PPE by compounds 47b , and 47c , against inhibitor concentration, at 25 °C and pH 7.2 buffer.	68

Figure 2.20 - Plot of the pseudo-first-order rate constants, k_{obs} for the inactivation of PPE by compound 47d , against inhibitor concentration, at 25 °C and pH 7.2 buffer.	69
Figure 2.21 - Inactivation of porcine pancreatic elastase as a function of the molar ratio of inhibitor 47d to enzyme. PPE (10 μM) and various amounts of inhibitor 47d (20-0.4 μM) in 0.1 M HEPES buffer, pH 7.2, were incubated at 25 °C for 30 min, and aliquots were withdrawn for assay.	72
Figure 2.22 - A) A stereoview of the $ F_0 - F_c $ electron density map calculated, with Ser-195 and inhibitor 47d (code JM54) omitted from the model. B) Detail of the crystal structure of the acyl-enzyme complex, with the α -carbon trace of the protein displayed as a ribbon.	74
Figure 2.23 - The structure of the crystallized acyl-enzyme 59 resulting from PPE-catalyzed hydrolysis of 47d	75
Figure 2.24 - By reaction of 47d with excess of MeO^- in MeOH, compound 60 is formed.	75
Figure 2.25 - The β -lactam ring-opening of 47d catalyzed by PPE involves the departure of phenylsulfinate from C-4, generating an imine 61 and tautomers enamines 62 or 63 . .76	76
Figure 2.26 - Proposed reaction mechanism of tazobactam with SHV-1 β -lactamase. ¹³⁸	77
Figure 2.27 - Progress curves for HLE inhibition by compound 47g	80
Figure 2.28 - General mechanisms of slow binding inhibition of enzyme-catalyzed reactions. ¹⁴¹	80
Figure 2.29 - Plot of the pseudo-first-order rate constants, k_{obs} for the HLE inhibition by compound 47f , against inhibitor concentration, at 25 °C and pH 7.2 buffer.	84
Figure 2.30 - Plot of the steady-state rates versus [I] for the inhibition of HLE by compound 47f	84
Figure 2.31 - Plot of the pseudo-first-order rate constants, k_{obs} for the HLE inhibition by compound 47g , against inhibitor concentration, at 25 °C and pH 7.2 buffer.	85
Figure 2.32 - Plot of the pseudo-first-order rate constants, k_{obs} for the HLE inhibition by compound 47h , against inhibitor concentration, at 25 °C and pH 7.2 buffer.	85
Figure 2.33 - Plot of the pseudo-first-order rate constants, k_{obs} for the HLE inhibition by compound 47k , against inhibitor concentration, at 25 °C and pH 7.2 buffer.	86
Figure 2.34 - Linear correlation between the second-order rate constants for HLE inactivation by 3,3-diethyl β -lactams 47e-f , and the σ_1 value for the X substituents in C-4, giving a ρ_1 value of 2.5. For comparison, the linear correlation for the alkaline hydrolysis, k_{OH^-} for the same compounds was included, giving a ρ_1 value of 3.4.	88

Figure 2.35 - Plot of the second-order rate constants for HLE inactivation by 3,3-diethyl β -lactams 47e-f against the second-order rate constants for alkaline hydrolysis, k_{OH^-} by the same compounds.....	90
Figure 3.1 - Expansion of the observed signals of the spectrum of 1H NMR for the methylene protons $-CH_2CH_3$ of the diethyl substituent of compound 73	106
Figure 3.2 - Splitting pattern diagram for each methylene proton of the diethyl group of compound 73	107
Figure 3.3 - Expansion of the observed signals of the spectrum of 1H NMR for <i>a</i>) the singlet corresponding to two methylene protons $-CH_2Ph$, <i>b</i>) the quartet corresponding to four CH_2CH_3 protons of the diethyl substituent and <i>c</i>) the triplet corresponding to six CH_2CH_3 protons of the diethyl substituent of 77b	107
Figure 3.4 - AA'BB' protons in a 1,4-disubstituted aromatic ring.....	108
Figure 3.5 - Plot of the pseudo-first-order rate constants, k_{obs} for the alkaline hydrolysis of the <i>N</i> -benzyl derivatives 77b and 77h , against hydroxide concentration, at 25 °C, ionic strength 0.5 M.....	111
Figure 3.6 - Plot of the pseudo-first-order rate constants, k_{obs} for the alkaline hydrolysis of the 3,3-diethyl- <i>N</i> -(<i>p</i> -methoxyphenyl)-azetidine-2,4-dione 77c , and <i>N</i> -(<i>p</i> -methylphenyl) counterpart 77d , against hydroxide concentration, at 25 °C, ionic strength 0.5 M.....	111
Figure 3.7 - Plot of the pseudo-first-order rate constants, k_{obs} for the alkaline hydrolysis of the <i>p</i> -unsubstituted, 77e , the <i>p</i> -chloro 77f and the <i>p</i> -cyanophenyl 77g 4-oxo- β -lactams, against hydroxide concentration, at 25 °C, ionic strength 0.5 M.....	112
Figure 3.8 - Plot of the pseudo-first-order rate constants, k_{obs} for the alkaline hydrolysis of 77i against hydroxide concentration, at 25 °C, ionic strength 0.5 M.....	112
Figure 3.9 - Comparison of the chemical reactivity towards hydroxide between the less reactive 3,3-diethyl- <i>N</i> -aryl derivative 77c , and the most reactive one, 77g , at 25 °C.	114
Figure 3.10 - Hammett plot for the second-order rate constants for the alkaline hydrolysis, k_{OH^-} , of 77c-g at 25°C, yielding a ρ_p value of 0.96.....	115
Figure 3.11 - The mechanism of alkaline hydrolysis of 4-oxo- β -lactams 77	116
Figure 3.12 - Progress curves for slow-binding inhibition of PPE by 77f	118
Figure 3.13 - Effect of inhibitor concentration on the onset of inhibition of PPE by 77c and 77d , at 25 °C.....	119
Figure 3.14 - Effect of inhibitor concentration on the onset of inhibition of PPE by 77e at 25 °C.....	119
Figure 3.15 - Effect of inhibitor concentration on the onset of inhibition of PPE by 77f and 77g	120

Figure 3.16 - Plot of the remaining PPE activity after incubation with 77i ([I] = 15 mM) at 25 °C, pH 7.2, [I]/[E] = 15, leading to a rapid increase of enzymatic activity.....	121
Figure 3.17 - Time-dependent loss of enzymatic activity. Excess of inhibitor 77f ([I] = 150 μM) was incubated with PPE ([E] = 10 μM) in 0.1 M HEPES buffer, pH 7.2, 25 °C.	122
Figure 3.18 - Lineweaver-Burke plot for the PPE catalyzed hydrolysis of the substrate: in the absence of inhibitor; and in the presence of 77i at 100 μM, [I]/[E] = 100 (Δ) and at 60 μM, [I]/[E] = 60.	122
Figure 3.19 - Lineweaver-Burke plot for the PPE catalyzed hydrolysis of the substrate, in the absence of inhibitor and in the presence of inhibitor 77h at 30 μM, [I]/[E] = 30 and at 100 μM, [I]/[E] = 100.	123
Figure 3.20 - Hammett plots for the second-order rate constants, k_{on} , for the inhibition of PPE by 4-oxo-β-lactams 77c-g and for the hydroxide-ion-catalyzed hydrolysis, k_{OH^-} , of the same compounds at 25°C.	125
Figure 3.21 - The hydrolysis of 4-oxo-β-lactams mediated by PPE.....	126
Figure 3.22 - Comparison between the effect of 4-oxo-β-lactam concentration on the onset of inhibition of PPE by 77c , the most potent inhibitor of the series and 77g , the less potent one, at 25 °C.....	127
Figure 3.23 - Linear correlation between the second-order rate constant for PPE inhibition, k_{on} and the second-order rate constant for alkaline hydrolysis, k_{OH^-}	128
Figure 3.24 - Docking of 77g (A), 77c (B) and 77d (C) in the active site of PPE (see text for details).....	129
Figure 4.1 – Schematic drawing of the spatial arrangement of C-3 and N-1 substituents of azetidine-2,4-diones in the active site of HLE.....	137
Figure 4.2 - Typical progress curves for the inhibition of HLE by 77a	152
Figure 4.3 - Typical progress curves for the inhibition of HLE by 77l	152
Figure 4.4 - Typical progress curves for HLE inhibition by compound 103f	153
Figure 4.5 - Effect of inhibitor concentration on the onset of inhibition of HLE by 77l	155
Figure 4.6 - Plot of the steady-state rates versus [I] for the inhibition of HLE by compound 77l	155

Figure 4.7 - Effect of inhibitor concentration on the onset of inhibition of HLE by 103f . The values for the pseudo-first order rate constants were obtained from fits to the data shown in Figure 4.4, using Equation 4.1.	156
Figure 4.8 - Inactivation of HLE as a function of the ratio [77g]/[enzyme] at a fixed [HLE] of 10 μ M. Various amounts of inhibitor 77g (25-800 nM) in 0.1M pH 7.2 HEPES buffer were incubated at 25 $^{\circ}$ C for 30 min, then aliquots were withdrawn and measured for the remaining enzyme activity.	160
Figure 4.9 - 1 μ M of inhibitor 103a was incubated with 0.2 μ M of HLE in 0.1 M pH 7.2 HEPES buffer, at 25 $^{\circ}$ C.....	164
Figure 4.10 - 1 μ M of inhibitor 103e was incubated with 0.2 μ M of HLE in 0.1 M pH 7.2 HEPES buffer, at 25 $^{\circ}$ C.....	164
Figure 4.11 - Docking poses of 103e (A), 103f (B), and 103i (C) in the active site of HLE, obtained from PDB 1HNE. Pictures were prepared using Pymol. ¹⁶⁷	166
Figure 4.12 - Docking pose of 77p in the active site of HLE, obtained from PDB 1HNE. (Picture prepared using Pymol). ¹⁶⁷	167
Figure 4.13 - UV spectra depicting the reactions, at 25 $^{\circ}$ C of (a) 103f (150 μ M) and (b) 2-mercaptobenzoxazole (150 μ M) in 10 mM NaOH, containing NaClO ₄ to maintain the ionic strength at 0.5 M.....	172
Figure 4.14 - Profile of concentration of 103a versus time after incubation in phosphate buffer saline, at 37 $^{\circ}$ C..	174
Figure 4.15 - Profile of concentration of 103a versus time after incubation in 80% human plasma, at 37 $^{\circ}$ C.	175
Figure 4.16 - Mean pharmacokinetic profile in total mice blood after administration of a ip 30 mg/kg dosage of 103k . Data are mean \pm sd.....	177
Figure 4.17 - Mean pharmacokinetic profile in mice spleen after administration of ip 30 mg/kg dosage of 103k . Data are mean \pm sd.....	178
Figure 4.18 - Mean pharmacokinetic profile in mice lung after administration of a ip 30 mg/kg dosage of 103k . Data are mean \pm sd.....	178

Figure A1.1 - Brönsted plot for the second-order rate constant for alkaline hydrolysis of 47a-d against the pK_a of the corresponding leaving groups at C-4, at 25°C, in 20% acetonitrile (v/v).....	238
Figure A1.2 - Brönsted plot for the second-order rate constant for alkaline hydrolysis of 47e-j against the pK_a of the corresponding leaving groups at C-4, at 25°C, in 20% acetonitrile (v/v).....	238
Figure A1.3 - Beer-Lambert plot for determination of the molar extinction coefficient for <i>p</i> -nitroaniline, at 390 nm, ϵ_{390} , 25 °C, in 0.1 M HEPES buffer, pH 7.2, 6% DMSO (v/v).....	239
Figure A1.4 – Michaelis-Menten plot for the hydrolysis of the chromogenic substrate of PPE, at 390 nm, 25 °C, in 0.1 M pH 7.2 HEPES buffer, 6% DMSO (v/v).	240
Figure A1.5 – Brönsted plot of the second-order rate constant for PPE inactivation $k_{obs}/[I]$ by 47b-d against the pK_a of the leaving group at C-4.....	242
Figure A1.6 - Plot of the second-order rate constants for PPE inactivation, $k_{obs}/[I]$, by 47b-d against the σ_I value of the substituent at C-4.	242
Figure A1.7 - Beer-Lambert plot for determination of the molar extinction coefficient for <i>p</i> -nitroaniline, at 410 nm, ϵ_{410} , 25 °C, in 0.1 M HEPES buffer, pH 7.2.	244
Figure A1.8 – Brönsted plot of the second-order rate constant for HLE inactivation k_{inact}/K_i against the pK_a of the leaving group at C-4, giving a β_{lg} value of -0.047.	245
Figure A3.1 - UV spectra depicting the reaction, at 25 °C, of 77d (10^{-4} M) with OH^- 0.1 M (ionic strength 0.5 M).....	258
Figure A3.2 - Progress curves for the slow-binding inhibition of PPE by compound 77e ..	261
Figure A3.3 - Plot of the steady-state rates versus $[I]$ for the inhibition of PPE by compound 77e	263
Figure A3.4 - Michaelis-Menten plot for the hydrolysis of the chromogenic substrate of PPE, in the absence of inhibitor 77i , and in the presence of 60 μ M and 100 μ M of 77i , at 390 nm, 25 °C, in 0.1 M HEPES buffer, pH 7.2, 6% DMSO (v/v).....	264
Figure A3.5 - Michaelis-Menten plot for the hydrolysis of the chromogenic substrate of PPE, in the absence of inhibitor 77h , and in the presence of 30 μ M and 100 μ M of 77h , at 390 nm, 25 °C, in 0.1 M HEPES buffer, pH 7.2, 6% DMSO (v/v).....	265
Figure A3.6 - Docking of 77h at the active site of PPE. The aromatic ring of the <i>N</i> -benzyl moiety lies in the S_1 pocket of PPE.....	266

Figure A4.1 - Effect of inhibitor concentration on the onset of inhibition of HLE by 77a and 77b	271
Figure A4.2 - Effect of inhibitor concentration on the onset of inhibition of HLE by 77c and 77e	271
Figure A4.3 - Effect of inhibitor concentration on the onset of inhibition of HLE by 77h	272
Figure A4.4 - Effect of inhibitor concentration on the onset of inhibition of HLE by 77i	272
Figure A4.5 - Effect of inhibitor concentration on the onset of inhibition of HLE by 77j	273
Figure A4.6 - Effect of inhibitor concentration on the onset of inhibition of HLE by 77k	273
Figure A4.7 - Effect of inhibitor concentration on the onset of inhibition of HLE by 77m	274
Figure A4.8 - Effect of inhibitor concentration on the onset of inhibition of HLE by 77n and 77r	274
Figure A4.9 - Effect of inhibitor concentration on the onset of inhibition of HLE by 77o and 77p	275
Figure A4.10 - Effect of inhibitor concentration on the onset of inhibition of HLE by 103d	275
Figure A4.11 - Effect of inhibitor concentration on the onset of inhibition of HLE by 103e , 103h and 103i	276
Figure A4.12 - Effect of inhibitor concentration on the onset of inhibition of HLE by 103j and 103k	276
Figure A4.13 - Plot of the steady-state rate <i>versus</i> [I] for the inhibition of HLE by 77a	280
Figure A4.14 - Plot of the steady-state rate <i>versus</i> [I] for the inhibition of HLE by 77b	280
Figure A4.15 - Plot of the steady-state rate <i>versus</i> [I] for the inhibition of HLE by 77c	281
Figure A4.16 - Plot of the steady-state rate <i>versus</i> [I] for the inhibition of HLE by 77e	281
Figure A4.17 - Plot of the steady-state rate <i>versus</i> [I] for the inhibition of HLE by 77h	282
Figure A4.18 - Plot of the steady-state rate <i>versus</i> [I] for the inhibition of HLE by 77i	282
Figure A4.19 - Plot of the steady-state rate <i>versus</i> [I] for the inhibition of HLE by 77j	283
Figure A4.20 - Plot of the steady-state rate <i>versus</i> [I] for the inhibition of HLE by 77k	283
Figure A4.21 - Plot of the steady-state rate <i>versus</i> [I] for the inhibition of HLE by 77m	284
Figure A4.22 - Plot of the steady-state rate <i>versus</i> [I] for the inhibition of HLE by 77n	284
Figure A4.23 - Plot of the steady-state rate <i>versus</i> [I] for the inhibition of HLE by 77o	285
Figure A4.24 - Plot of the steady-state rate <i>versus</i> [I] for the inhibition of HLE by 77p	285
Figure A4.25 - Plot of the steady-state rate <i>versus</i> [I] for the inhibition of HLE by 77r	286
Figure A4.26 - Plot of the steady-state rate <i>versus</i> [I] for the inhibition of HLE by 103d	286

Figure A4.27 - Plot of the steady-state rate <i>versus</i> [I] for the inhibition of HLE by 103e .	287
Figure A4.28 - Plot of the steady-state rate <i>versus</i> [I] for the inhibition of HLE by 103h .	287
Figure A4.29 - Plot of the steady-state rate <i>versus</i> [I] for the inhibition of HLE by 103i .	288
Figure A4.30 - Plot of the steady-state rate <i>versus</i> [I] for the inhibition of HLE by 103j .	288
Figure A4.31 - Plot of the steady-state rate <i>versus</i> [I] for the inhibition of HLE by 103k .	289
Figure A4.32 - Plot of the pseudo-first order rate constants for HLE inhibition by 77d .	289
Figure A4.33 - Plot of the pseudo-first order rate constants for HLE inhibition by 77f .	290
Figure A4.34 - Plot of the pseudo-first order rate constants for HLE inhibition by 77g .	290
Figure A4.35 - Plot of the pseudo-first order rate constants for HLE inhibition by 103a .	291
Figure A4.36 - Plot of the pseudo-first order rate constants for HLE inhibition by 103b .	291
Figure A4.37 - Plot of the pseudo-first order rate constants for HLE inhibition by 103c .	292
Figure A4.38 - Plot of the pseudo-first order rate constants for HLE inhibition by 103g .	292
Figure A4.39 - Progress curve for PR3 inhibition by 103i .	293
Figure A4.40 - Progress curve for Cat G inhibition by 77m .	295
Figure A4.41 - Calibration curve for 103a .	296
Figure A4.42 - Calibration curve for 103e .	296
Figure A4.43 - Calibration curve for 103i .	297
Figure A4.44 - Calibration curve for 103k .	297
Figure A4.45 - Profile of concentration of 103e <i>versus</i> time after incubation in pH 7.4 PBS, at 37 °C.	298
Figure A4.46 - Profile of concentration of 103i <i>versus</i> time after incubation in PBS, at 37 °C.	298
Figure A4.47 - Profile of concentration of 103k <i>versus</i> time after incubation in PBS, at 37 °C.	299
Figure A4.48 - Profile of concentration of 103e <i>versus</i> time after incubation in 80% human plasma, at 37 °C.	299
Figure A4.49 - Profile of concentration of 103i <i>versus</i> time after incubation in 80% human plasma, at 37 °C.	300
Figure A4.50 - Profile of concentration of 103k <i>versus</i> time after incubation in 80% human plasma, at 37 °C.	300

INDEX OF TABLES

Table 1.1 Example of some serine proteases with relevance as drug targets and therapeutic indication of their inhibitors.....	2
Table 1.2 - Serine protease inhibitors approved for clinical use.....	4
Table 1.3 - Main characteristics of human leukocyte elastase (HLE), proteinase 3 (PR3) and cathepsin G (Cat G)	9
Table 1.4 - HLE inhibition by 8 . Impact of R and R ⁵ substituents on K_i , k_1 e k_{off}	19
Table 2.1 - <i>N</i> -unsubstituted key intermediates synthesized 43-46	47
Table 2.2 - Final <i>N</i> -carbamoylazetid-2-ones 47 studied in this work.	48
Table 2.3 - The second-order rate constants for the alkaline hydrolysis of 4-substituted <i>N</i> -carbamoylazetid-2-ones, k_{OH^-} , at 25 °C, and the p <i>K</i> _a and σ_1 for the C-4 substituents. ...	56
Table 2.4 - Second-order rate constants for the time-dependent inactivation of PPE in pH 7.2 buffer at 25 °C and for the hydroxide-catalyzed hydrolysis of compounds 47a-f	70
Table 2.5 - Percentage of remaining PPE activity, v_t/v_i , after a 30 min incubation period with 47d at 25 °C, versus the initial ratio of inhibitor to enzyme, $[I]/[E]_0$	72
Table 2.6 - Second-order rate constants for the time-dependent inactivation of HLE, k_{on} , at 25 C, pH 7.2 buffer and for the hydroxide-catalyzed hydrolysis of compounds 47e-k at 25 °C.	87
Table 3.1 - Synthesized 4-oxo- β -lactams 77a-i	102
Table 3.2 - Azetidine-2,4-diones (4-oxo- β -lactams) studied in the present work on the intrinsic chemical reactivity and indication of the selected wavelength for kinetic measurements by UV spectroscopy.....	110
Table 3.3 - The second-order rate constants, k_{OH^-} , for the alkaline hydrolysis of 4-oxo- β -lactams 77 , at 25 °C and ionic strength adjusted to 0.5 M with NaClO ₄ . The σ_p values are given as an indicator of the polar effect of the substituent in the <i>para</i> position of the aromatic ring.....	113
Table 3.4 - Kinetic parameters for PPE inhibition at pH 7.2 and 25 °C by 4-oxo- β -lactams 77 . For comparison, k_{OH^-} for the alkaline hydrolysis of the same compounds at 25 °C are included and also the respective EREFs.	124
Table 4.1 - Azetidine-2,4-diones 77 synthesized using the method illustrated in Scheme 4.2.	141
Table 4.2 - Synthesized <i>N</i> -heteroarylthiomethyl azetidine-2,4-diones 103a-k	147
Table 4.3 - Key intermediates <i>N</i> -bromomethylaryl azetidine-2,4-diones 102a-c	148

Table 4.4 - k_{obs} and v_s obtained from non-linear regression analysis using Equation 2.6 for HLE inhibition by compound 77l	154
Table 4.5 - Kinetic data for HLE inhibition by 4-oxo- β -lactams. See text for definition of each kinetic parameter.	158
Table 4.6 - Inhibitory activity of selected 4-oxo- β -lactams against neutrophil serine proteases HLE, PR3 and Cat G.....	169
Table 4.7 - Aqueous and plasma stability at 37 °C for compounds 103a , 103e , 103i and 103k	175
Table A1.1 - Effect of concentration of OH ⁻ on the pseudo-first-order rate constant for the alkaline hydrolysis of compounds 47b , 47e and 47f , at 25 °C and ionic strength adjusted to 0.5 M with NaClO ₄	237
Table A1.2 - Concentrations of the chromogenic substrate used for determination of the K_m and the respective initial rates of PPE-mediated hydrolysis, in $\Delta A \text{ s}^{-1}$ and Ms^{-1} , at 390 nm, 25 °C, in 0.1 M pH 7.2 HEPES buffer, 6% DMSO (v/v).	240
Table A1.3 - Pseudo-first-order rate constant, k_{obs} , for the inactivation of PPE by β -lactams 47b-d , at 25 °C, in 0.1 M HEPES buffer, pH 7.2.	241
Table A1.4 . Data collection and crystallographic refinement statistics for the porcine pancreatic structure bound to 47d	243
Table A1.5 Pseudo-first-order rate constant, k_{obs} , for the inactivation of HLE by β -lactams 47f-h and 47k at 25 °C, in 0.1 M HEPES buffer, pH 7.2.	244
Table A1.6 The dependence of the steady-state rate, v_s , with the inhibitor concentration for compound 47f , allowing the determination of K_i	245
Table A2.1 - Database of 4-oxo- β -lactams created for virtual screening studies with HLE:	246
Table A3.1 - Effect of concentration of OH ⁻ on the pseudo-first-order rate constant for the alkaline hydrolysis of compounds 77b-i , at 25 °C and ionic strength adjusted to 0.5 M with NaClO ₄	259
Table A3.2 - Pseudo-first-order rate constant, k_{obs} , for the inactivation of PPE by 4-oxo- β -lactams 77c-g , at 25 °C, in 0.1 M HEPES buffer, pH 7.2.	260
Table A3.3 - The dependence of the kinetic parameters of PPE inhibition, k_{obs} , v_i and v_s with the inhibitor concentration for the 4-oxo- β -lactam 77e	262
Table A3.4 - Kinetic data for the hydrolysis of the chromogenic substrate of PPE in the presence and absence of 77i	264

Table A3.5 - Kinetic data for the hydrolysis of the chromogenic substrate of PPE in the presence and absence of 77h	265
Table A4.1 - Pseudo-first-order rate constant, k_{obs} , for the inactivation of HLE by 4-oxo- β -lactams 77 and 103 , at 25 °C, in 0.1 M HEPES buffer, pH 7.2.....	267
Table A.4.2 - The dependence of the steady-state rates, v_s , with the inhibitor concentration for HLE inhibition.....	277
Table A4.3 - Percentage of remaining HLE activity, v_t/v_i versus the initial ratio of inhibitor to enzyme, $[I]/[E]_0$, after a 30 min. incubation period with 77g at 25 °C.	293
Table A4.4 - Pseudo-first-order rate constant, k_{obs} , for the time-dependent inactivation of PR3 by 4-oxo- β -lactams, at 25 °C, in 0.1 M, pH 7.2 HEPES buffer.	294
Table A4.5 - PR3 inhibition by 77g and 77p	294
Table A4.6 - Pseudo-first-order rate constant, k_{obs} , for the time-dependent inactivation of CatG by 4-oxo- β -lactams, at 25 °C, in 0.1 M, pH 7.5 HEPES buffer.	295
Table A4.7 - Data for calibration curves of 103k in mice blood, spleen, lung and liver	301

INDEX OF SCHEMES

Scheme 1.1 - General kinetic scheme for an alternate substrate inhibitor.	18
Scheme 1.2 - General kinetic scheme for a mechanism-based irreversible inhibitor.....	20
Scheme 2.1 - Synthesis of <i>N</i> -carbamoylazetid-2-ones.....	46
Scheme 2.2 - Synthesis of 3,3-diethyl-4-acetoxy-azetid-2-one, 42b	47
Scheme 2.3 - Synthesis of 2-mercaptobenzoxazole-5-carboxylic acid 51	48
Scheme 2.4 - The general reaction of hydroxide-ion catalyzed hydrolysis.	52
Scheme 2.5 - Kitz and Wilson's model for irreversible enzyme inhibition.	67
Scheme 2.6 –Mechanism A of slow binding inhibition.	81
Scheme 2.7 - Mechanism B of slow binding inhibition.	82
Scheme 3.1 - Retrosynthetic analysis of <i>N</i> -carbamoylazetid-2,4-diones.	97
Scheme 3.2 - Strategic routes for the synthesis of <i>N</i> -unsubstituted 4-oxo- β -lactams based on published procedures.	97

Scheme 3.3 - Alkylation of the cyano-ester 72 to give a gem-diethyl derivative 73 , which was hydrolysed to give 74 ..	98
Scheme 3.4 - Attempted ring closure of malonic acid monoamide to give <i>N</i> -unsubstituted azetidine-2,4-dione 71 . ^{145, 146}	98
Scheme 3.5 - The nitrile bond of compound 75 results from reaction of thionyl chloride with the amide carbonyl carbon atom.	99
Scheme 3.6 - Synthesis of 76 from acid hydrolysis of 73 .	99
Scheme 3.7 - Attempted synthesis of 3,3-diethylazetidine-2,4-dione 71 by cyclisation of 76 catalyzed by base.	100
Scheme 3.8 - Synthesis of azetidine-2,4-diones 77 , using the method described by Golik.	101
Scheme 3.9 - Attempted synthesis of <i>N</i> -unsubstituted 4-oxo- β -lactams based on <i>N</i> -protected azetidine-2,4-diones.	103
Scheme 3.10 - Attempted synthesis of <i>N</i> -unsubstituted 4-oxo- β -lactam from 77c ..	104
Scheme 3.11 - Attempted synthesis of <i>N</i> -unsubstituted 4-oxo- β -lactam from 77b ..	104
Scheme 3.12 - Attempted bromination of 77a .	105
Scheme 3.13 - Fragmentation of 3,3-diethylazetidin-2,4-diones with formation of diethylketene and the respective isocyanate.	109
Scheme 3.14 - Further fragmentation of the diethylketene ion.	109
Scheme 3.15 – Competitive reversible enzyme inhibition mechanism.	123
Scheme 4.1 Expected “double-hit” mechanism for HLE inactivation by 4-oxo- β -lactams containing a potential thiol leaving group.	138
Scheme 4.2 - Synthesis of 4-oxo- β -lactams 77 . Reagents and conditions: (i) R^3NH_2 , TEA, dioxane, reflux.	139
Scheme 4.3 - Synthesis of disubstituted malonyl dichlorides 89 from the appropriate malonates 90 ..	140
Scheme 4.4 - Proposed mechanism for the cycloaddition of ketenes and isocyanates. ...	142
Scheme 4.5 - Ketene generated by reaction of the respective acid chloride with triethylamine.	142
Scheme 4.6 - Attempted synthesis of 3-butyl-3-ethyl- <i>N</i> -tosylazetidine-2,4-dione 96 ...	143
Scheme 4.7 - Attempted synthesis of 3-butyl-3-ethyl- <i>N</i> -phenylcarbamoylazetidine-2,4-dione 98 ..	145
Scheme 4.8 – Synthesis of <i>N</i> -heteroarylthiomethyl azetidine-2,4-diones 103a-k ..	146
Scheme 4.9 - Fragmentation of 3,3-diethyl- <i>N</i> -(4-(bromomethyl)phenyl)-azetidine-2,4-dione, 102a .	150

Scheme 4.10 - The product of the alkaline hydrolysis of 4-oxo- β -lactam **103** is the corresponding α -amidoacid, **104**, without departure of the thiol leaving group. 173

INDEX OF EQUATIONS

Equation 2.1	52
Equation 2.2	52
Equation 2.3	66
Equation 2.4	67
Equation 2.5	67
Equation 2.6	79
Equation 2.7	81
Equation 2.8	81
Equation 2.9	82
Equation 2.10	82
Equation 2.11	82
Equation 2.12	83
Equation 2.13	83
Equation 3.1	123
Equation 4.1	151
Equation 4.2	151
Equation 4.3	156

ABSTRACT

Human leukocyte elastase (HLE, EC 3.4.21.37) is a neutrophil serine protease capable of degrading a great variety of proteins, such as elastin and collagens. HLE is an attractive therapeutic target since unregulated activity of this enzyme has been implicated in many inflammatory disorders, such as chronic obstructive pulmonary disease. The present work focused on the design of synthetic irreversible inhibitors of HLE based on the β -lactam scaffold (azetidin-2-ones and azetidine-2,4-diones), as potential drug candidates. Kinetic studies of enzyme inhibition *in vitro* were performed to determine the inhibitory potency. Intrinsic chemical reactivity studies, using hydroxide as a model of serine residue, were performed to evaluate the stability towards non-specific nucleophiles.

The effect of different leaving groups at C-4 on the intrinsic chemical reactivity and elastases (PPE and HLE) inactivation by *N*-carbamoylazetidin-2-ones is described. In both cases, the rate limiting step is the formation of the tetrahedral intermediate, and the β -lactam ring opening is not concerted with the departure of the substituent from C-4. 3,3-Unsubstituted derivatives inhibited PPE (k_{on} ranging from 11.3 to 290 $M^{-1}s^{-1}$), while 3,3-diethyl counterparts inhibited HLE (k_{on} ranging from 310 to 14600 $M^{-1}s^{-1}$). Taft ρ_I values suggests that the HLE catalyzed hydrolysis occurs in an earlier position along the reaction coordinate than the alkaline hydrolysis, due to favorable binding interactions of the inhibitor to the enzyme. Sulfones at C-4 improve the inhibitory potency, activating the β -lactam and leading to an irreversible covalent enzyme-inhibitor adduct with sulfinate departure, as shown by X-ray crystallography.

Azetidine-2,4-diones were designed as isosteric analogues of highly reactive 3-oxo- β -sultams inhibitors of PPE. The synthesis and preliminary studies as PPE inhibitors are described. The inhibitory activity is a result of nucleophilic attack by catalytic serine residue to a carbonyl carbon and four-membered ring opening to form the acyl-enzyme complex. Good Hammett correlations were found for the *para*-substituted derivatives, giving a ρ_p value lower for PPE inhibition than the obtained for the chemical process. This result agrees with favorable binding interactions of the inhibitor within the active site, as revealed by docking studies. 4-Oxo- β -lactams were found to be novel, potent time-dependent irreversible inhibitors of PPE, while decreasing dramatically the reactivity towards hydroxide ion when compared to the 3-oxo- β -sultams analogues.

A comprehensive SAR study of 4-oxo- β -lactams is described, including differently substituted derivatives at C-3 and N-1 for exploiting S and S' subsites of HLE, which gave potent irreversible inhibitors of HLE (k_{on} ranging from 2×10^2 to 3×10^6 $M^{-1}s^{-1}$). Inhibitory activity is strongly dependent on the nature of substituents at C-3. 3,3-Diethyl derivatives with a *para*-heteroarylthiomethyl group on the N^1 -aryl moiety were found to be potent acylating agents of HLE, with higher than 10^6 $M^{-1}s^{-1}$ k_{on} values and K_i values ranging from 0.50 to 9.5 nM. Inhibition is a result of ring-opening to form a tight enzyme-inhibitor adduct, but with no expulsion of the thiol leaving group. 4-Oxo- β -lactams were selective towards HLE rather than PPE, proteinase 3 or cathepsin G and were inactive against cysteine protease papain. The stability of some compounds at 37 °C in pH 7.4 phosphate buffer and human plasma as well as a biodistribution study in mice for a selected derivative were also performed. The results from this thesis demonstrate convincingly the superiority of the azetidine-2,4-dione scaffold over 3-oxo- β -sultams and simple β -lactams in the design of inhibitors of serine proteases.

KEYWORDS: β -lactam, azetidine-2,4-dione, serine proteases, irreversible inhibitors, elastase, reactivity.

RESUMO

A elastase leucocitária humana (HLE, EC 3.4.21.37) é uma protease de serina dos neutrófilos capaz de degradar uma grande variedade de proteínas, como o colagénio e a elastina. A HLE é um interessante alvo terapêutico, uma vez que a actividade descontrolada desta enzima está associada a várias patologias inflamatórias, como a doença pulmonar obstrutiva crónica. O presente trabalho teve como objectivo o desenho de inibidores irreversíveis da HLE com base no núcleo β -lactâmico (azetidina-2-onas e azetidina-2,4-dionas), numa perspectiva terapêutica. Neste âmbito, foram realizados estudos cinéticos de inibição enzimática *in vitro*, de forma a determinar a potência inibitória e, também, estudos de reactividade química intrínseca, usando o ião hidróxido como modelo do resíduo serina, de forma a avaliar a estabilidade dos compostos perante nucleófilos não específicos.

É descrito o efeito relativo de diferentes grupos abandonantes em C-4 quer na reactividade química quer na inibição enzimática por *N*-carbamoilazetidina-2-onas. Em ambos os casos, a etapa determinante da velocidade da reacção é a formação do intermediário tetraédrico e a abertura do anel β -lactâmico não é concertada com a saída do substituinte em C-4. Os derivados não substituídos em C-3 inibiram a PPE (k_{on} variou entre 11.3 a 290 $M^{-1}s^{-1}$), enquanto que os 3,3-dietilsubstituídos inibiram a HLE (k_{on} variou de 310 a 14600 $M^{-1}s^{-1}$). Valores de Taft ρ_I sugerem que a reacção catalisada pela HLE envolve um estado de transição precoce na coordenada da reacção em relação ao processo químico, devido a interacções favoráveis entre a enzima e o inibidor. Sulfonas em C-4 aumentaram a potência inibitória por activação do anel β -lactâmico (efeito indutivo), resultando numa inibição irreversível por formação da acil-enzima e expulsão do sulfinato, como demonstrado por estudos de cristalografia de raios-X.

É descrita a síntese bem como estudos preliminares de inibição enzimática de azetidina-2,4-dionas. Estas foram desenvolvidas como isósteros de 3-oxo- β -sultamas, as quais são inibidores da PPE com uma elevada reactividade química intrínseca. A actividade inibitória de azetidina-2,4-dionas resulta do ataque nucleofílico do resíduo serina do centro activo a um dos carbonos carbonílicos, com abertura do anel de quatro membros para formar o aducto inibidor-enzima. Boas correlações de Hammett foram obtidas para os derivados *para*-substituídos, tendo-se verificado um valor de Hammett ρ_p para a

inibição da PPE inferior do que para o processo químico. Este resultado sugere a existência de interações favoráveis entre o inibidor e a enzima, tal como indicado por estudos de docking. As azetidine-2,4-dionas representam uma nova classe de potentes inibidores irreversíveis da protease de serina PPE, apresentando uma reactividade química intrínseca drasticamente inferior aos isómeros 3-oxo- β -sultamas.

É descrito um abrangente estudo de relação-estrutura-actividade de 4-oxo- β -lactamas, incluindo derivados com diferentes substituintes em C-3 e N-1 para explorar bolsas de ligação S e S' da HLE. Obtiveram-se potentes inibidores irreversíveis da HLE (k_{on} entre 2×10^2 to 3×10^6 $M^{-1}s^{-1}$). A potência inibitória depende fortemente da natureza do substituinte em C-3. Derivados 3,3-dietil *para*-substituídos em N¹-aril com um grupo heteroarilmetil revelaram-se potentes agentes acilantes da HLE, com valores de k_{on} notáveis, acima de 10^6 $M^{-1}s^{-1}$ e valores de K_i entre 0.50 e 9.5 nM. A inibição resulta da abertura do anel de quatro membros para formar um aducto enzima-inibidor estável, todavia sem ocorrer expulsão do grupo abandonante tiol. As 4-oxo- β -lactamas mostraram-se selectivas para a HLE quando comparadas com a PPE, a proteinase 3, ou a catepsina G e foram inactivas contra a protease de cisteína papaína. Foram ainda efectuados estudos de estabilidade de alguns compostos a 37 °C em tampão fosfato pH 7.4 e plasma humano bem como um estudo de biodistribuição em ratinhos. Os resultados obtidos demonstram a clara superioridade das azetidine-2,4-dionas sobre 3-oxo- β -sultamas e azetidina-2-onas no desenho de inibidores de proteases de serina.

PALAVRAS-CHAVE: β -lactama, azetidine-2,4-diona, proteases de serina, inibidores irreversíveis, elastase, reactividade.

CHAPTER 1

INTRODUCTION

1. INTRODUCTION

1.1. OVERVIEW OF PROTEASES

Proteases, also known as peptidases, are enzymes that selectively catalyse the hydrolysis of peptide bonds. Proteases are classified as hydrolases (Class E.C. 3), by the Enzyme Commission of the International Union of Biochemistry and Molecular Biology, and, under hydrolases, they belong to Subclass E.C. 3.4, the Peptidases.¹ Based on their catalytic mechanism, there are six types of proteases known: Serine-, Cysteine-, Aspartic-, Threonine-, Glutamic- and Metallo-proteases.² These are further classified into clans that share structural homology and then into families with similar sequence.

1.2. SERINE PROTEASES

Serine proteases are so named due to the common nucleophilic serine residue present at the active site. Serine proteases are endopeptidases (E.C. 3.4.21), cleaving peptide bonds internally in peptides and proteins.³ Almost one-third of all proteases can be classified as serine proteases. These enzymes are widely distributed in nature and found in all kingdoms of cellular life. Over 26000 serine proteases are grouped into 13 clans and 40 families in the MEROPS database (<http://merops.sanger.ac.uk>). Clan PA of serine proteases is the largest and well-studied, from which chymotrypsin is the prototype member.

1.2.1 Serine Proteases as Therapeutic Targets

By cleaving proteins, serine proteases play multifarious roles in physiological events, including digestion, blood coagulation, signal transduction, reproduction, cell differentiation, tissue homeostasis, the immune response and apoptosis.⁴⁻⁷ It is known that serine proteases are involved in vital processes not only in humans but also in pathogens.

At present, proteases are recognized not only as protein degrading enzymes, but also as important signalling molecules of a complex biochemical network, requiring tight regulation.⁸ Disorders in protease regulation are known to be related with aetiology and progression of several pathologies. In particular, excessive proteolysis, which is most often a result of unwanted activation of protease signalling pathways, is related to tissue damage and/or aberrant processing of other proteins, playing a crucial role in cancer, cardiovascular, inflammatory, immunological, respiratory, neurodegenerative diseases, diabetes and infections.^{9, 10} Thus, serine proteases, have emerged as important drug targets and one of the great challenges in medicinal chemistry is the design and development of serine protease inhibitors.^{6, 8, 11} In Table 1.1 some known serine proteases targeted for pharmacological intervention are listed. Most of them have inhibitors currently under clinical trials.⁹

Table 1.1 Example of some serine proteases with relevance as drug targets and therapeutic indication of their inhibitors.

Targeted-Serine Proteases	Therapeutic Indication
HCMV protease ⁶	Cytomegalic inclusion disease (viral infection)
HCV NS3 protease ^{6, 9, 12}	Hepatitis C (viral infection)
Urokinase type plasminogen activators ^{6, 13}	Cancer
Prostate Specific Antigen ¹⁴	Cancer
Tryptase ^{6, 9, 15}	Allergic asthma, rhinitis, urticaria
Human leukocyte elastase ^{6, 9, 16}	Respiratory diseases (including COPD), inflammation
Proteinase 3 ^{16, 17}	Respiratory diseases (including COPD), inflammation, Wegener's granulomatosis
Cathepsin G ¹⁶	Inflammation
Dipeptidyl peptidase IV ^{8, 9}	Diabetes type 2
Thrombin ^{6, 9, 18}	Thrombosis
Factor VIIa ^{6, 9, 18}	Thrombosis
Factor IXa ^{6, 9, 18}	Thrombosis
Factor Xa ^{6, 9, 18}	Thrombosis

However, from the many thousands of serine proteases inhibitors already developed, only a few have successfully progressed through clinical trials and been approved for commercial use (Table 1.2).^{8, 9} For example, although proteases related with coagulopathies have been validated targets for more than a half century, only a few direct thrombin inhibitors have been launched in the market, but almost all of them have the inconvenience of being restricted to parenteral administration.⁸ Only one thrombin inhibitor for oral administration is currently available, **1** (Table 1.2), commercialized in European Union very recently, in April 2008, as a prodrug.¹⁹

Despite great efforts over more than 30 years in the design of human leukocyte elastase inhibitors (discussed later in this chapter), only one drug for inhibition of this enzyme was approved for clinical use, in Japan, sivelestat (ONO-5046) (**3**, Table 1.2), as an injectable formulation.⁹

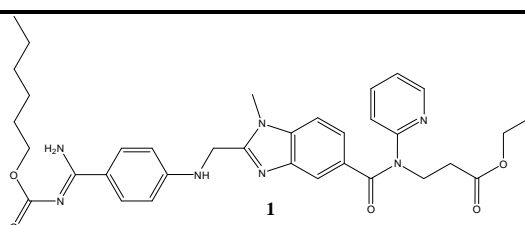
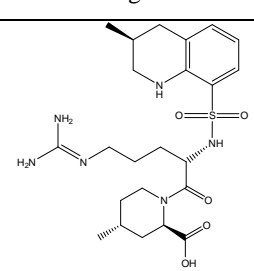
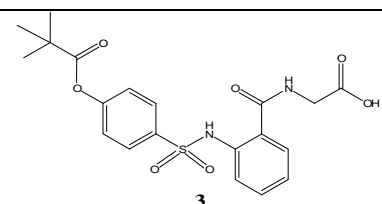
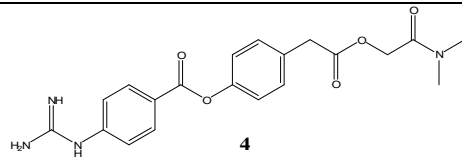
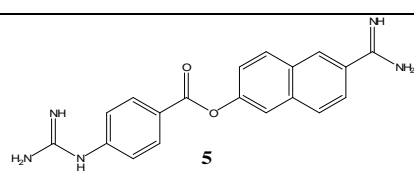
As far as the author knows, besides thrombin inhibitors and **3**, there are only two more direct inhibitors of serine proteases available in the marketplace to date (in Japan): **4** and **5** (Table 1.2), both indicated for treatment of pancreatitis. Their mechanism has not been fully understood, but involves broad-spectrum/trypsin-like serine protease inhibition.^{8,9}

With this background, it is of interest to improve serine protease inhibitors. However, a case of success of protease inhibition in clinic is the well-known and widely use of β -lactam antibiotics, such as penicillins and cephalosporins, inhibitors of bacterial serine enzymes transpeptidases.²⁰ These bacterial enzymes are related with serine proteases, but differ by these because of being carboxypeptidases.¹

At present, protease-targeted therapy is a promising area, taking advantage of recent developments in genomics, proteomics and combinatorial chemistry, and using a variety of tools, such as X-ray crystallography and high-field NMR.

The attractiveness of serine proteases as therapeutic targets results not only from their pathophysiological role in disease, but also from structural determinants of their catalysis. In particular, either the structure of the active site, suitable for high-affinity interactions with inhibitors, or features of the catalytic mechanism, make protease inhibition a fascinating area for therapeutic intervention.²¹

Table 1.2 - Serine protease inhibitors approved for clinical use.⁸

Target	Compound	Company
Thrombin	 <p style="text-align: center;">1</p> <p style="text-align: center;">Dabigatran</p>	Boehringer-Ingelheim
Thrombin	 <p style="text-align: center;">2</p> <p style="text-align: center;">Argatroban</p>	Mitsubishi Pharma
Thrombin	Naturally occurring in the salivary glands of medicinal leeches hirudin-based peptide drug.	Aventis
	Lepirudin	
Thrombin	Naturally occurring in the salivary glands of medicinal leeches hirudin-based peptide drug.	Novartis
	Desirudin	
Human leukocyte elastase	 <p style="text-align: center;">3</p> <p style="text-align: center;">Sivelestat (ONO-5046)</p>	Ono
Trypsin-like serine proteases	 <p style="text-align: center;">4</p> <p style="text-align: center;">Camostat mesilate</p>	Ono
Broad-spectrum	 <p style="text-align: center;">5</p> <p style="text-align: center;">Nafomostat mesilate</p>	Japan Tobacco

1.2.2 Active Site Topology and Catalytic Mechanism

Serine proteases active site involves not only the catalytic triad, formed by Ser-195, His-57 and Asp-102 (chymotrypsin numbering), but also extended molecular recognition binding sites for interaction with the peptidic substrate.

The Schechter and Berger nomenclature²² is used to define the interaction of a protease with a substrate. The amino acid residues of the substrate are named $P_1, P_2, P_3, \dots, P_n$ from the scissile peptide bond to the amino-terminus, while those towards carboxyl-terminus direction are designated $P_{1'}, P_{2'}, P_{3'}, \dots, P_{n'}$. These residues are accommodated in the corresponding binding sites of the enzyme, referred to $S_1, S_2, S_3, \dots, S_n$ and $S_{1'}, S_{2'}, S_{3'}, \dots, S_{n'}$, respectively (Figure 1.1). These sites are located in clefts and crevices in the protein and are determinant for substrate specificity. S_1 is the primary specificity binding pocket in serine proteases, being critical to the molecular recognition (complementary).

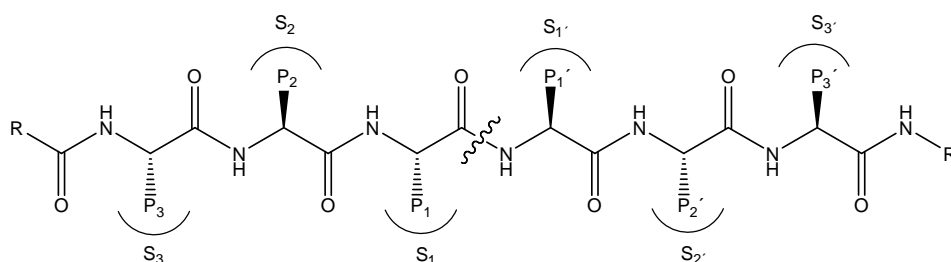


Figure 1.1 - Interactions between the specific subsites of a protease and the respective residues of the substrate.²²

The initial interactions between the inhibitor and the enzyme are noncovalent and reversible, and provide a specific orientation of the substrate at the active site, aligning the catalytic triad.

The general catalytic mechanism of serine proteases is presented in Figure 1.2. Once the substrate is non-covalently bound, the carbonyl carbon of the scissile peptide bond is attacked by the hydroxyl group of the catalytic Ser-195 residue. His-57 acts as a general base catalyst and enhances the nucleophilicity of Ser-195, by removing the hydroxyl proton. This process is facilitated by the polarising effect of Asp-102 (Figure 1.2a).

1. Introduction

The tetrahedral intermediate (TI) is formed and its oxyanion is stabilized by hydrogen bonds formed to the backbone NH groups of Ser-195 and Gly-193 residues. This region is named the oxyanion hole. The imidazolium ion of His-57 assists the collapse of the TI via general acid catalysis, by protonation of the amine leaving group, releasing the amino-terminus peptide (Figure 1.2b). Simultaneously, the peptide bond is broken and the acyl-enzyme complex is formed.

Subsequently, (Figure 1.2c), a water molecule attacks the acyl-enzyme, assisted by general base catalysis by His-57, forming a new TI (omitted in Figure 1.2). By breakdown of this intermediate, Ser-195 recovers its hydrogen from His-57, while the acid product (carboxy-terminus peptide) diffuses out (Figure 1.2d).^{23,24}

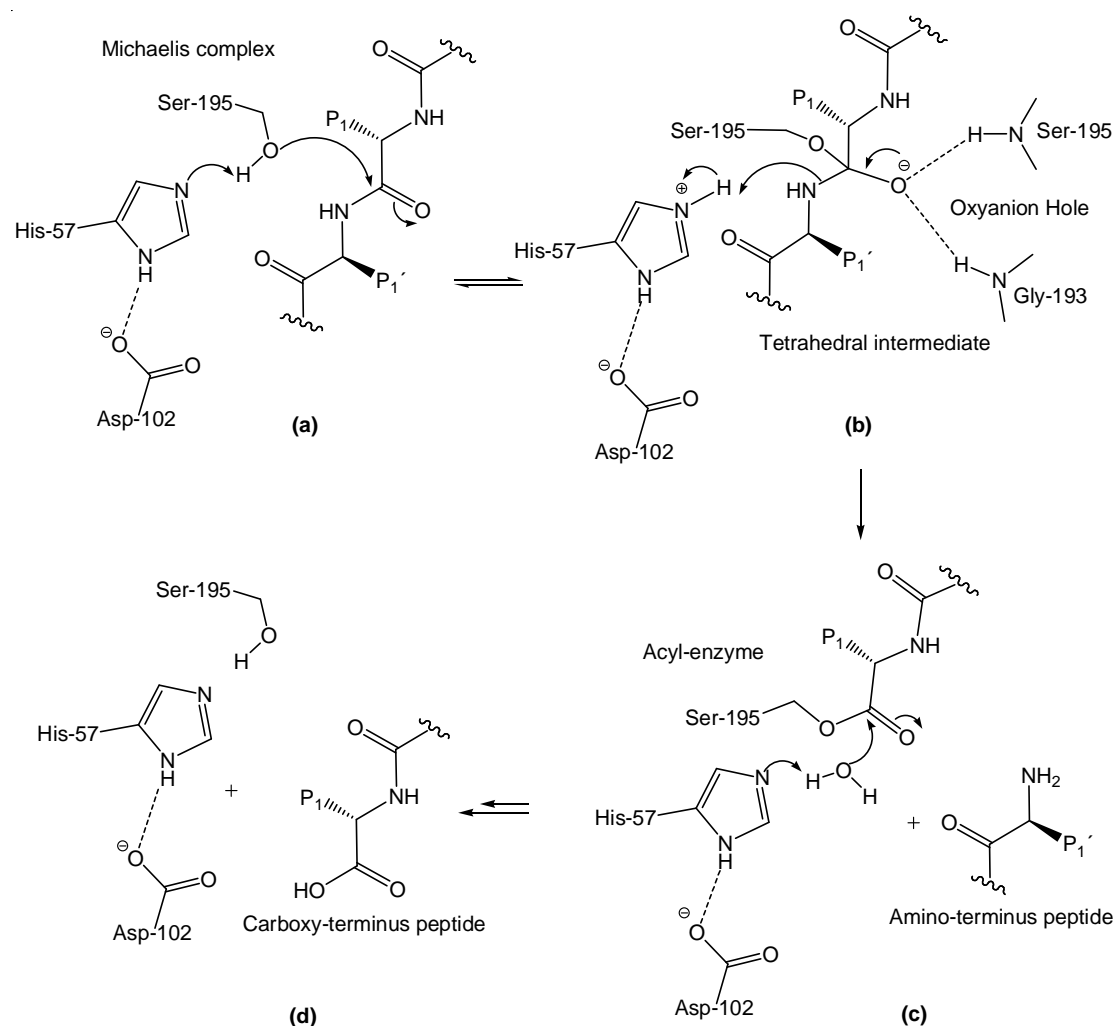


Figure 1.2 - General catalytic mechanism of serine proteases.^{23,24}

1.3. CHYMOTRYPSIN SUPERFAMILY

The chymotrypsin superfamily, which belongs to clan PA, is the largest group of serine proteases. Serine proteases of the chymotrypsin superfamily consist of two similar domains, each of which is an antiparallel β -barrel structure and these enzymes are classified based on the nature of the P₁ residue in the peptidic substrate.²⁵ Subtle differences in primary sequence of these enzymes account for differences in substrate specificity. There are three major classes of chymotrypsin superfamily serine proteases: trypsin-like accepts positively charged side chains at P₁, chymotrypsin-like accepts aromatic hydrophobic residues and elastase-like prefers small hydrophobic ones.⁴ Based on the combined knowledge of the active site topology, the catalytic mechanism, and regulation pathways, research groups worldwide undertook studies to design more selective inhibitors of these enzymes. In particular, human leukocyte elastase, a validated target for therapeutic intervention, as mentioned earlier, is the major target of this work. Human leukocyte elastase is a neutrophil serine protease of the chymotrypsin superfamily implicated in several inflammatory disorders. Therefore, a short description of neutrophil serine proteases and their role in health and disease will follow.

1.4. NEUTROPHIL SERINE PROTEASES

Neutrophils are leukocytes of the first line of defence against infection, presenting a potent antimicrobial arsenal for degradation of foreign materials. In particular, in their azurophil granules, neutrophils have many degradative enzymes, including three serine proteases: human leukocyte elastase, proteinase 3 and cathepsin G. These serine enzymes are synthesized as zymogens, but stored in the azurophil granules in the active form. Other serine proteases are also present in neutrophils²⁶, but in granules different than the azurophil ones and will not be discussed here. In Table 1.3 the main characteristics of these enzymes are listed.

1.4.1 Human Leukocyte Elastase (HLE)

HLE is a glycoprotein containing 218 amino acid residues and four intramolecular disulfide bonds. There are at least four isoforms of HLE, differing in carbohydrate content.²⁷ In the promyelocytic stage of granulocyte development, HLE is produced, post-translationally processed and stored.²⁸ The S₁ binding pocket of HLE is hydrophobic in nature, containing Val-190, Phe-192, Ala-213, Val-216, Phe-228 and a disulfide bond Cys-191-Cys-220. HLE prefers small hydrophobic residues at S₁, such as valine, leucine, norvaline and isoleucine (Table 1.3).²⁹ The preferred residue in S₂ is proline. Nearly 67000 molecules of HLE are stored in each azurophil granule, at a mean concentration of 5.33 mM. The term elastase is partly a misnomer, as not only HLE degrades elastin, but also degrades almost all extracellular matrix and plasma proteins.³⁰

1.4.2 Proteinase 3 (PR3)

PR3 is a glycoprotein containing 222 amino acid residues which has three isoforms, differing in their carbohydrate. PR3 is not restricted to the azurophil granules (major source), since it is also present in secondary granules and at membrane of secretory vesicles of neutrophils. PR3 is an elastase-like serine protease, being highly homologous with HLE (57%)²⁹. The S₁ binding pocket of PR3 is hemispheric, hydrophobic, but smaller than that of HLE (Table 1.3), due to the replacement of both Val/Ile at position 190 and Ala/Asp at position 213.²⁹ The S_n' subsites are more polar than that of HLE. PR3 is involved in Wegener's granulomatosis disease, a systemic autoimmune vasculitis characterized by circulating antineutrophil cytoplasmic antibodies (ANCA) that recognize PR3.³¹

1.4.3 Cathepsin G (Cat G)

Cathepsin G is a glycoprotein containing 235 amino acid residues and three disulfide bridges, presenting moderate homology with HLE (37%).^{29, 32} The S₁ binding pocket is larger than that of HLE and PR3 (Table 1.3). Unlike HLE and PR3, Cat G

accommodates both basic and aromatic P₁ residues (trypsin and chymotrypsin-like preference), due to the presence of a glutamate residue (Glu-226) at the bottom of the S₁ subsite, and the absence of the Cys-191–Cys-220 disulfide bond. Thus, Cat G may accept at S₁ Phe, Tyr, Lys, Arg.²⁹

Table 1.3- Main characteristics of human leukocyte elastase (HLE), proteinase 3 (PR3) and cathepsin G (Cat G)²⁹

	HLE	PR3	Cat G
EC number	EC.3.4.21.37	EC.3.4.21.76	EC.3.4.21.20
Gene, locus	<i>ELA2</i> , 19p13.3	<i>PRTN3</i> , 19p13.3	<i>CTSG</i> , 14q11.2
MW (kDa)	29-33	29-32	28.5
Residues	218	222	235
Substrate P₁	Small hydrophobic Val, Leu, Met, Ile, Ala, norVal	Small hydrophobic Val, Leu, Ala	Aromatic or positively charged: Phe, Tyr, Lys, Arg
Source	Neutrophil (major) Monocyte Mastocyte Eosinophil	Neutrophil (major) Monocyte Basophil Mastocyte	Neutrophil (major) Monocyte

1.4.4 Physiological Functions

In response to infection, neutrophils migrate from blood to the tissue and engulf pathogens. Upon such inflammatory stimuli, neutrophil serine proteases are released from their granules and act intracellularly within phagolysosomes to destroy pathogens, via combination of reactive oxygen species and antimicrobial peptides.³³ These enzymes are also released to the extracellular medium, where they can inactivate microorganisms³⁴, facilitate neutrophil migration through tissue, degrade extracellular matrix proteins (elastin, collagen, fibronectin and proteoglycans) or remodel damage tissue.³⁵ It appears that elastase is the most efficient neutrophil serine protease in the turnover of these proteins, presenting a broad range of substrates and a powerful

proteolytic activity.³⁶ Elastase can also activate several matrix metalloproteases (MMP-2, -3, -9), playing an important role in tissue repair.³⁷

Recently, it has become clear that neutrophil serine proteases also play an important role in modulation of the inflammatory response.³⁸ These enzymes are mediators and secretagogues in inflammation, due to proteolysis of chemokines (chemoattractant proteins that play an important role in recruiting leukocytes to the sites of inflammation), and growth factors; activation/inactivation of cytokines, such as interleukin 1 (IL-1) and tumor necrosis factor- α (TNF- α), and activation of specific cell surface receptors.^{29, 33, 38, 39} Furthermore, it was suggested that these enzymes can induce cellular apoptosis at the sites of inflammation, due to a caspase-like activity.³³

Under physiological conditions, tissues are protected from excessive proteolysis due to strict regulation through compartmentalization or natural inhibitors.²⁷ The most relevant natural inhibitor is α_1 -antitrypsin (also called α_1 -antiproteinase inhibitor), and belongs to serpins, a family of serine protease inhibitors.⁴⁰ Other inhibitors of neutrophil serine proteases are α_2 -macroglobuline, secretory leukocyte proteinase inhibitor (SLPI) and elafin.³¹

1.4.5 Roles in Human Disease

Unregulated extracellular activities of these enzymes are implicated in the aetiology and development of a variety of diseases associated with a massive influx of neutrophils. In particular, excessive proteolysis of elastin (an essential component of lung connective tissue, arteries, skin and ligaments), and other structural proteins cause tissue damage implicated in inflammatory diseases, such as glomerulonephritis^{41, 42}, atherosclerosis⁴³, arthritis⁴⁴ and mostly respiratory diseases, including chronic obstructive pulmonary disease (COPD),^{45, 46} acute respiratory distress syndrome^{28, 47} and cystic fibrosis.^{30, 48} A brief description of COPD and the pathophysiologic role of neutrophil serine proteases will follow.

1.4.5.1 Chronic Obstructive Pulmonary Disease

COPD is the fourth leading cause of death in the world^{49, 50} and is predicted to become the third by 2020.⁵¹ COPD is an inflammatory disorder characterized by a slowly, progressive development of airflow limitation that is not fully reversible.⁵⁰ One type of COPD is pulmonary emphysema, which involves an enlargement of airspaces and destruction of the lung parenchyma, with loss of lung elasticity.⁴⁶

Cigarette smoking is the most common cause of COPD (more than 95%). The mechanism of development and progression of the disease involves the interplay of multiple processes, including a protease-antiprotease imbalance, which leads to excessive proteolytic activity, inflammation, oxidative stress, matrix remodelling and straining mechanical forces.^{52, 53} As no currently available treatment halt the progression of the disease,⁵⁴ the research for new drugs has considerable interest.

1.4.5.2 The Protease-Antiprotease Hypothesis and the Relevance of HLE

This hypothesis considers the imbalance of protease-antiprotease as a major pathogenic contributor of tissue destruction in inflammatory diseases⁵⁵ as COPD, and it results from some experimental findings.

- It is known that the genetic deficiency in α_1 -antitrypsin, the major natural inhibitor of HLE, is responsible for the early onset of pulmonary emphysema.⁵⁶ This situation is especially notable for individuals with exposure to cigarette smoking.⁴⁰ α_1 -Antitrypsin is produced in the liver and circulates from there to the lung where it provides the major anti-HLE protection in the lower respiratory tract.

- On the other hand, in normal individuals, α_1 -antitrypsin can be inactivated by oxygen radicals, released by neutrophils under circumstances of overwhelming stimuli.

- Furthermore, cigarette smoking may cause a protease-antiprotease imbalance in the lung of normal individuals, not only by oxidative inactivation of α_1 -antitrypsin, but also because it promotes the increase of the number of neutrophils in the pulmonary parenchyma, with release of proteolytic enzymes.^{40, 57} Thus, it leaves the activity of proteases unchecked for excessive proteolysis, especially elastolysis, leading to

emphysema. The acquired functional deficiency of α_1 -antitrypsin is transient. In fact, cessation of cigarette smoking is the only therapeutic intervention capable to reduce progression of diseases as COPD.^{58, 59}

- It was demonstrated that intra-tracheal injection of HLE in animals induces emphysema, supporting the protease-antiprotease hypothesis.⁶⁰ In addition, a correlation between the severity of emphysema and proteolytic burden was found.⁴⁵ Within neutrophil serine proteases, HLE is likely to play the major role in devastating the extracellular matrix, not only because it has a powerful proteolytic activity,⁶¹ but also because activates other proteases and upregulates inflammation.³⁷ In addition, HLE has the ability to cleave lung surfactant,⁶² to inhibit ciliary motility and to induce airway submucosal gland mucus secretion,⁴⁸ with consequent implications in aggravating disorders, such as emphysema, cystic fibrosis and bronchitis. Indeed, millimolar concentrations of HLE released from azurophil granules of activated neutrophils lead to evanescent quantum bursts of proteolysis. When the fine balance between HLE and its endogenous inhibitors is disturbed, the deleterious effect of HLE is responsible of tissue injury.

Thus, an attractive therapeutic strategy for treatment of COPD and other inflammatory disorders is restoring the balance protease-antiprotease.^{59, 63} Therefore, intensive efforts have been made in the discovery of inhibitors of neutrophil serine proteases, in particular, HLE inhibitors.^{6, 9, 25, 64}

1.5. SYNTHETIC INHIBITORS OF HUMAN LEUKOCYTE ELASTASE

Strategies to re-establish the balance protease-antiprotease include:

- the use of external supplement of naturally-occurring/recombinant proteic inhibitors (α_1 -antitrypsin, secretory leukocyte proteinase inhibitor, elafin)
- the use of low molecular weight synthetic inhibitors of HLE.

The first strategy has some disadvantages, in particular: risk of immunological response, low serum half-life, high cost-effectiveness ratio (involving maintenance of plasmatic levels of purified protein, typically by i.v. administration) and the need of

an alternative drug delivery system as aerosolization. The inhaled mode of delivery may complicate the determination of dose responsiveness and clinical efficacy.^{63, 65}

In contrast, low molecular weight synthetic inhibitors are promising therapeutic agents for inflammatory diseases, as a result of a potential greater oral absorption with potential oral activity, decreased risk of immunological reactions and a less expensive therapy, in particular for long-term use as required for chronic diseases, such as COPD.

A general approach to design synthetic inhibitors of serine proteases involves somehow trapping the nucleophilic serine residue. Therefore, a relatively stable enzyme-inhibitor adduct is formed, taking advantages of binding interactions with the catalytic machinery. X-ray crystal structural data for neutrophil serine proteases are available in the PDB databank and in particular for HLE.⁶⁶ A number of therapeutic strategies involve peptide and non-peptide inhibitors, with reversible and irreversible mechanism of action. The most important classes of enzyme inhibitors in drug design are the transition state analogues, the affinity labels, the acylating agents (alternate substrate inhibitors) and the mechanism-based inhibitors.

1.5.1 Transition State Analogue Inhibitors

This class of inhibitors were designed keeping in mind the ability of the enzyme to stabilize the transition state. They react with the enzyme to form stable tight-binding tetrahedral transition state-like complexes, through non-covalent binding interactions with the subsites of the enzyme and a covalent bond to Ser-195. No acyl-enzyme complex is released, due to the absence of a leaving group.²¹ Kinetically, transition state analogues behave as slow tight-binding inhibitors. In principle, slow tight-binding inhibitors have clinical advantages over rapidly reversible inhibitors. In fact, the high affinity for their target, and an extended residence time on the enzyme, due to a long dissociation half-life, allow minimizing the drug dose and its intervals, with a much longer duration of action, less side effects, improving clinical efficacy.²¹

Peptidic aldehydes were the first transition state analogue inhibitors of HLE. They were designed retaining a recognition sequence of the peptidic substrate, and terminating it in an aldehyde function (Figure 1.3, X = H), which acts as a serine trap.

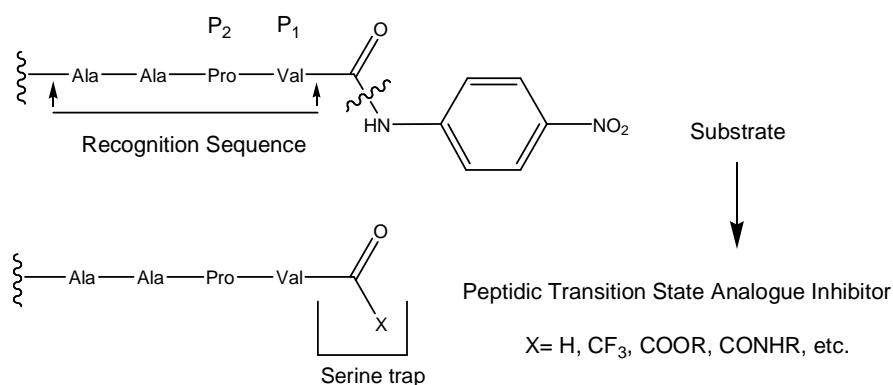


Figure 1.3 - Design of a peptidic transition state analogue inhibitor of HLE from a peptidic substrate.⁶⁴

By reaction with the enzyme, these inhibitors lead to a hemiacetal enzyme-inhibitor complex. However, aldehydes are easily oxidized to the corresponding carboxylic acids, prone to racemization or may also inhibit cysteine proteases,²³ leading to toxicity and poor bioavailability. To avoid these problems, other types of serine trap were developed such as peptidyl ketones.

Electron-withdrawing substituents were used to increase the electrophilicity of the carbonyl carbon of the ketone, for activation towards nucleophilic attack by Ser-195. The ketone-activating group also stabilizes the charged hemiketal of the enzyme-inhibitor adduct. Some examples of highly electrophilic ketones are peptidyl α -trifluoromethyl ketones (Figure 1.3, X = CF₃), α -ketoesters (X = COOR), α -ketoamides (X = CONHR)⁶⁴ and α -ketoheterocycles, as α -ketobenzoxazoles.⁶⁷

To overcome unsuitable pharmacokinetic properties of most peptidic compounds, a more challenging goal consists on designing non-peptidic inhibitors. A rational approach involves retaining the serine trap, and exploiting multiple non-covalent binding interactions at the active site of the enzyme, in order to increase the adduct stability and improve the inhibitory potency.

For example, pyridone trifluoromethyl ketones are potent non-peptidic inhibitors of HLE. They were designed from peptidic substrate structures, by use of computer modelling, X-ray crystallography and structure activity relationship (SAR) studies.

Besides the covalent bond formed between the electrophilic carbonyl carbon and Ser-195, many non-covalent binding interactions are established (Figure 1.4):

- the oxyanion is stabilized in the oxyanion hole (hydrogen bonds)
- the *iso*-propyl group of the inhibitor lies in the S₁ binding pocket (hydrophobic interactions);
- the phenyl substituent on the 6-position lies in the S₂ subsite (hydrophobic interactions);
- the 3-amino and the carbonyl groups of the pyridone ring form antiparallel hydrogen bonding with Val-216 of the enzyme.

These favorable binding interactions stabilized the final enzyme-inhibitor complex. This model of binding was supported by X-ray crystallography studies of a hemiketal adduct, obtained from a pyridone trifluoromethyl ketone and a closely related enzyme, porcine pancreatic elastase, (PPE).⁶⁸

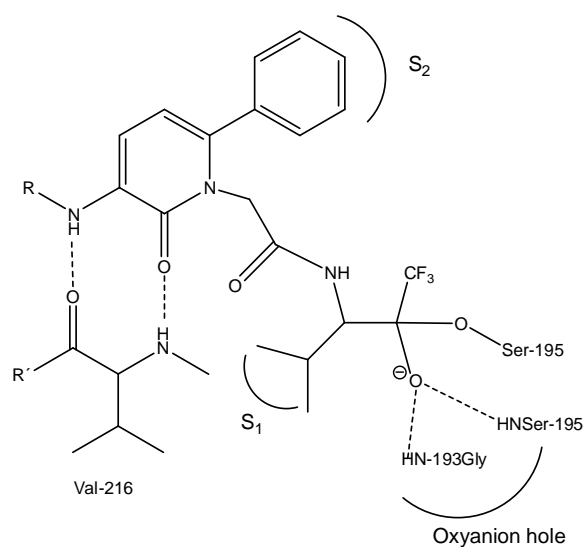
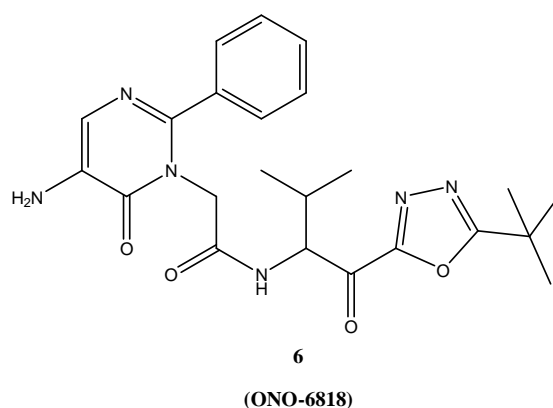


Figure 1.4 - Scheme of binding mode of pyridone-containing trifluoromethyl ketones to HLE.⁶⁸

Some potent orally active pyridone trifluoromethyl ketone derivatives were developed, by an appropriate substitution on the amino group of the pyridone ring (ex.: R = SO₂CH₂Ph, Figure 1.4).

Another approach was the development of non-peptidic orally active inhibitors containing an α -keto-1,3,4-oxadiazole moiety as serine trap, such as ONO-6818, **6**. ONO-6818 binds to HLE in a similar mode to that of pyridone-containing trifluoromethyl ketones. In addition, the oxadiazole ring allows hydrogen bonding with the imidazol group of His-57, contributing to the stabilization of the hemiketal adduct.⁶⁹ ONO-6818 was in Phase II Clinical Trials for treatment of COPD, but it was discontinued (2002) due to hepatic toxicity.⁷⁰



In fact, because of the reactive electrophilic function present in these inhibitors, they may lead to toxic side effects. On the other hand, due to the reversible nature of the established bonds, the enzyme may recover its activity. Thus, irreversible inactivators of HLE, presenting a leaving group which departure may release an acyl-enzyme complex, have emerged as an alternative strategy in drug design.

1.5.2 Affinity Labels

An affinity label is an active site-directed irreversible inhibitor containing a chemically reactive functionality (electrophilic) that modifies covalently a nucleophile at the active site. Once the inhibitor is reversibly bound to the enzyme, it reacts with the enzyme by acylation or alkylation (S_N2) mechanisms.

The first affinity labels irreversible inhibitors of HLE were derivatives of peptidyl chloromethyl ketones, **7** (Figure 1.5)²⁵. They were designed from the structure of the peptidic substrate, retaining the recognition sequence attached to a serine trap. By

contrast to transition state analogues, in this case, the serine trap is a α -chloromethyl ketone moiety (Figure 1.3, X = CH₂Cl), presenting a chloride leaving group. These compounds function as alkylating agents of the active site histidine residue, accordingly to the mechanism depicted in Figure 1.5.

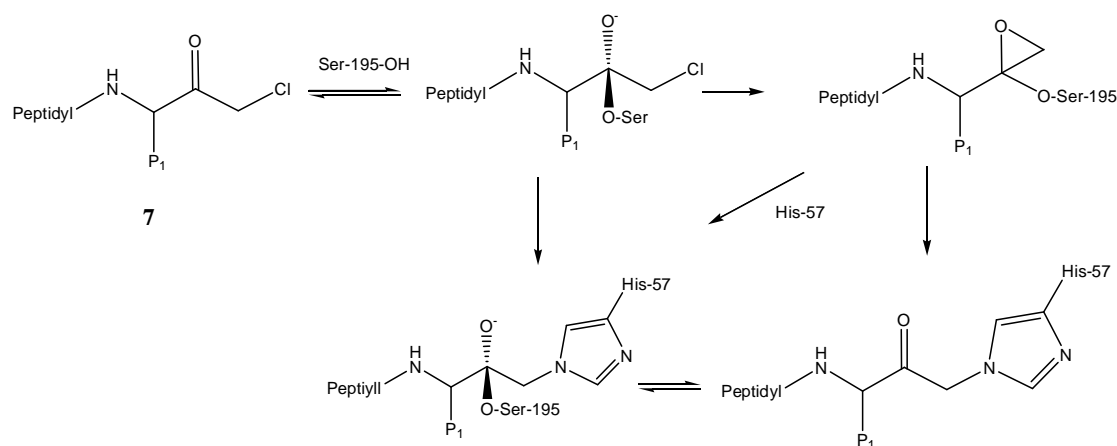


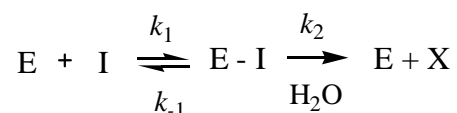
Figure 1.5 - Proposed mechanism of inhibition of serine proteases by peptidyl chloromethyl ketones.²⁵

However, they are chemically reactive towards other serine or cysteine proteases, or also bionucleophiles such as glutathione, leading to loss of selectivity and toxic effects.²³ Thus, the lack of target enzyme specificity is a critical liability for these agents as drug candidates. Furthermore, because highly reactive compounds exacerbate the formation of irreversible protein-drug conjugates, the risk of idiosyncratic immunological reactions in the turnover of those conjugates is another problem for clinical safety of affinity labels. All these aspects make this class of inhibitors less attractive for therapeutics.²¹

1.5.3 Acylating Agents (Alternate Substrate Inhibitors)

An acylating agent, also known as alternate substrate inhibitor, reacts with the enzyme to form a stable acyl-enzyme covalent complex that suspended the enzyme activity at a point within the catalytic process (Scheme 1.1). The acyl-enzyme complex [E-I] undergoes very slow deacylation (hydrolysis k_2), leading in practical terms, to an irreversible inhibition.⁷¹ The acylation rate, k_{on} is equivalent to k_1 , and the off rate,

k_{off} , is given by the sum of all pathways of breakdown of the acyl-enzyme complex [E-I], $k_{\text{off}} = k_{-1} + k_2$. The steady-state dissociation constant of the enzyme-inhibitor complex is given by $K_i = k_{\text{off}}/k_{\text{on}}$.



Scheme 1.1 - General kinetic scheme for an alternate substrate inhibitor.⁷¹

The stability of [E-I] is dependent on electronic and steric effects, in order to increase the acylation rate and decrease the deacylation rate.⁷² The mechanism of "acylation-deacylation" of alternate substrate inhibitors is important for their safety profile relative to completely irreversible inhibitors.

Many acylating agent of HLE were already developed, using different templates, such as the pivaloyloxybenzene derivatives⁷³, which include the unique commercially marketed inhibitor of HLE, sivelestat, **3** (mentioned earlier),⁷⁴ launched in Japan as an injectable formulation. Sivelestat is a potent inhibitor of HLE (IC₅₀ 0.044 μM), and suppresses lung damage induced in hamsters by elastase administered intratracheally (ID₅₀ 82 $\mu\text{g}/\text{Kg}$).⁷⁵ This inhibitor works via acylation of the catalytic serine residue by its pivaloyl group.

Other acylating agents scaffolds include 2-amino-4H-3,1-benzoxazin-4-ones **8** (Figure 1.6).⁷⁶ The reaction of HLE with **8** leads to the formation of an acyl-enzyme complex **9**, due to Ser-195 nucleophilic attack at the C-4 carbonyl carbon and ring opening. The deacylation of **9** occurs by two ways, being the intramolecular cyclization (k_2) a rapid process. It is of interest to obstruct deacylation pathways k_{off} , $k_{\text{off}} = k_{-1} + k_2 + k_3$ (Figure 1.6), in order to increase the lifetime of **9** and improve the inhibitory potency.

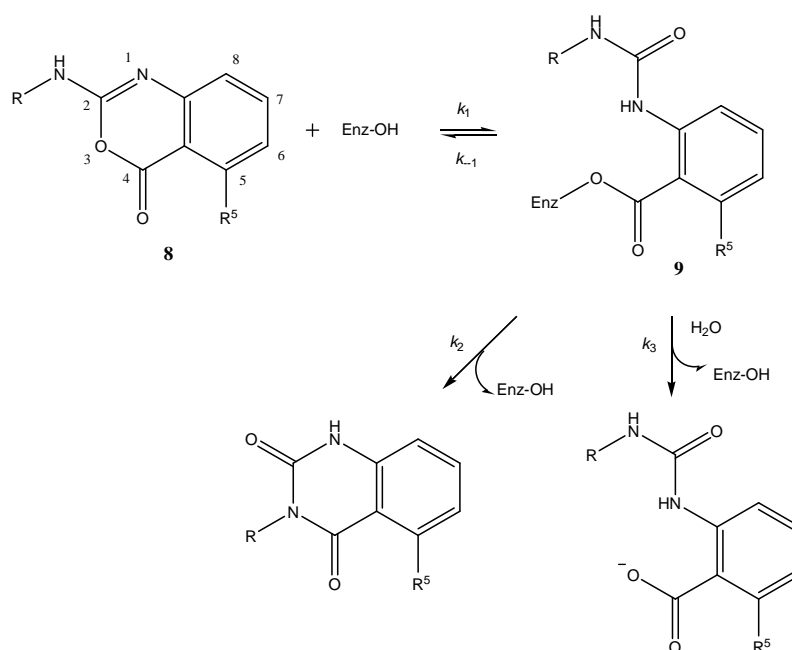


Figure 1.6 - Formation of an acyl-enzyme complex between 2-amino-4H-3,1-benzoxazin-4-ones and HLE and deacylation pathways to regenerate free enzyme.⁷⁷

The impact of R and R⁵ substituents on the HLE inhibition by benzoxazinones is presented in Table 1.4.⁷⁷

Table 1.4 - HLE inhibition by 8. Impact of R and R⁵ substituents on K_i , k_1 e k_{off} .⁷⁷

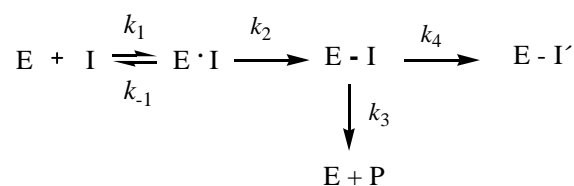
R	R ⁵	K_i , μM	k_1 , $\text{M}^{-1}\text{s}^{-1}$	k_{off} , s^{-1}
H	H	63	810	0.051
<i>i</i> -Pr	H	0.052	59000	0.0030
<i>i</i> -Pr	Et	0.00094	70000	0.000066

The incorporation of a bulky R substituent, such as R = *i*-Pr, depresses the cyclization rate of deacylation k_2 (steric effect). On the other hand, substitution at *ortho* position to the carbonyl carbon, C-5, such as R⁵ = Et, shield the carbonyl carbon of 9 from nucleophilic attack. Furthermore, the combined substitution on R and R⁵ has a

synergistic effect in HLE inhibition, as 2-(isopropylamino)-5-ethylbenzoxazinone results in 86-fold increase in k_1 and a 770-fold decrease in k_{off} versus **8** (Figure 1.6, R = H, R⁵ = H).^{76,77}

1.5.4 Mechanism-Based Irreversible Inhibitors

Mechanism-based irreversible inhibitors are not inherently reactive, but they are transformed by reaction with the target enzyme to reactive inhibitory compounds, which inactivates the enzyme through the formation of stable enzyme-inhibitor complexes (suicide type inhibition). Because unmasking of the reactive functionality requires catalysis by the enzyme, these inhibitors are quite selective for their target. Enzyme inactivation involves a “double hit” mechanism, *i.e.*, after the nucleophilic attack by serine residue, a reactive specie, capable of forming a second covalent bond to the active site, is formed only after the normal catalytic mechanism has taken place.⁷⁸

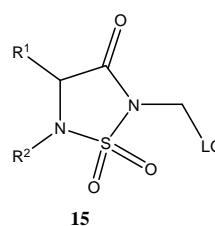
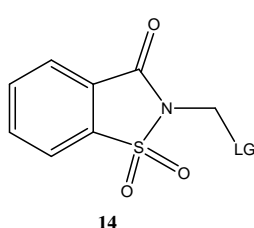
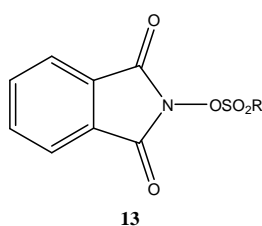
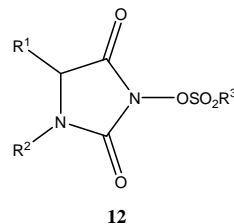
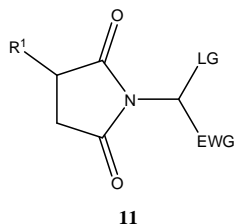
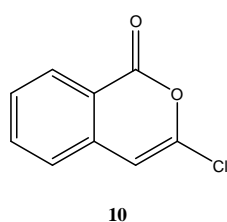


Scheme 1.2 - General kinetic scheme for a mechanism-based irreversible inhibitor.⁷⁸

Thus, the reactive acyl-enzyme [E-I] undergoes either further reaction with a second nucleophile of the active site (presumably with His-57), leading to permanent inactivation of the enzyme [E-I'], or undergoes deacylation, escaping from the active site to regenerate the free enzyme (k_3) (Scheme 1.2). Therefore, for a persistent irreversible inhibition, the stoichiometry of inactivation must be less than 1:1 and must occur prior to release of the reactive specie from the active site.²¹ The ratio k_3/k_4 is called partition ratio r , which means the number of turnovers that gives a released product per inactivation event, being indicative of the number of molecules of inhibitor necessary to inactivate a single molecule of enzyme. An ideal inhibitor has a partition rate $r=0$, thus the reactive intermediate does not escape to react with off-target enzymes, being exclusively sequestered to form [E-I'].

As the equilibrium k_1/k_{-1} is set up rapidly and k_4 is a fast step, the rate limiting step is given by k_2 , being the inactivation rate constant, k_{inact} . The inactivation kinetics is saturable (the pseudo-first-order rate constant for enzyme inhibition, k_{obs} is a rectangular hyperbolic function of [I]) and increasing substrate concentration protects against enzyme inhibition. These inhibitors display a slow tight-binding behaviour, with a time-dependent inhibition. Thus, besides target selectivity, mechanism-based inhibitors explore the same potential advantages described above for tight binding inhibitors, but requiring fewer doses. Therefore, they are very attractive in drug design.^{21, 78}

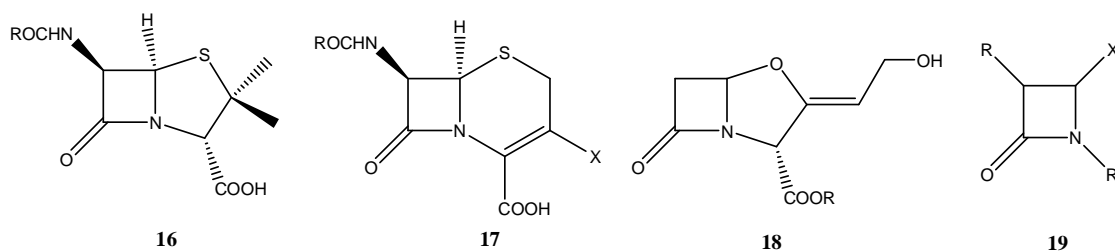
The design of HLE mechanism-based inhibitors requires a suitable template presenting not only elements for molecular recognition but also intrinsic reactivity on the carbonyl carbon. Several heterocyclic templates are used in this purpose, such as isocoumarins **10**,^{79, 80} succinimides **11**,⁸¹ hydantoins **12**,⁸² phthalimides **13**,⁸³ saccharins **14**,⁸⁴ 1,2,5-thiadiazolidin-3-one 1,1 dioxides **15**,⁸⁵⁻⁸⁷ and β -lactams.^{88, 89}



1.6. β -LACTAMS INHIBITORS OF HLE

β -Lactams are widely used in clinic due to antibiotic properties, including well-known penicillins **16** and cephalosporins **17**. These agents inhibit bacteria cell wall synthesis

via inactivation of transpeptidases, such as penicillin binding proteins (PBPs). These bacterial enzymes are related with serine proteases because they have a catalytic serine residue at the active site. Inhibition of transpeptidases by β -lactam antibiotics involves the formation of a stable covalent enzyme-inhibitor complex with acylation of the catalytic serine residue. Other β -lactams largely used in clinic, such as **18** (R = H, clavulanic acid), are well-known inhibitors of bacterial Class A and Class C β -lactamases.²⁰



The first study that demonstrated that β -lactams derivatives are inhibitors of HLE was developed by Merck Research Laboratories, in 1986: benzyl clavulanate, **18** (R=CH₂Ph) was found to be an inhibitor of HLE. It was the first time that β -lactams compounds were used in a different purpose than the antibiotic therapy. Since then, there has been a growing interest in studying these compounds as inhibitors of serine proteases, and in particular, HLE inhibitors. Other serine enzymes inhibited by β -lactam derivatives include Cytomegalovirus protease, prostate specific antigen, thrombin, co-enzyme A independent transacylase, γ -amino-butyric acid (GABA) aminotransferase and phospholipase A₂.²⁰

Within the β -lactam derivatives developed as inhibitors of HLE, cephalosporins (bicyclic structures) and azetidin-2-ones (monocyclic- β -lactam) **19** are the most important inhibitors.

1.6.1 Cephalosporins Derivatives

The Merck pioneered study discovered that the cephalosporin nucleus, **17**, after appropriate structural adjustments, can selectively inhibit HLE.⁸⁸ One requirement to develop irreversible inhibitors of HLE is C-4 carboxyl acid esterification or amidation. Free acids are inactive towards HLE (this enzyme is an endopeptidase while transpeptidases are carboxypeptidases).

In addition, other structural elements improve inhibitory potency, such as:

- the incorporation of a α -substituent at C-7, such as 7 α -methoxy, allowing interaction with the enzyme's small S₁ binding pocket. A 7 α -chloro moiety also increases the intrinsic chemical reactivity of the β -lactam.
- the oxidation of the sulfur atom into a sulfone (cephalosporin 1,1-dioxide), enhancing chemical reactivity and hydrogen bonding opportunities.
- electron-withdrawings substituents on the leaving group in C-3 '.

An example of a cephalosporin inhibitor of HLE is compound **20** (Figure 1.7), which is a mechanism-based irreversible inhibitor of elastase, as revealed by X-ray crystallography studies.⁹⁰ Inhibition occurs as a result of the nucleophilic attack of Ser-195 on the β -lactam carbonyl carbon, with formation of a tetrahedral intermediate (TI), which collapses with β -lactam ring opening by N5-C8 bond fission.

The resulting acyl-enzyme intermediate may hydrolyze or react further, with expulsion of the acetate from C3', loss of HCl, generating a α,β -unsaturated reactive imine, trapped by His-57 in a Michael addition. Thus, a stable adduct is formed, with two covalent bonds at the active site of the enzyme: acylation of Ser-195 and alkylation of His-57, in "double-hit" mechanism (Figure 1.7).⁹⁰

For 7 α -methoxy derivatives, the reaction with HLE also involves a "double-hit" mechanism, but this group is not lost throughout catalysis.⁹¹

Although being potent inhibitors of HLE, cephalosporin derivatives suffer some drawbacks for therapeutic use, such as poor oral bioavailability and low chemical stability in plasma.⁹² Thus, these derivatives were not useful for systemic administration.

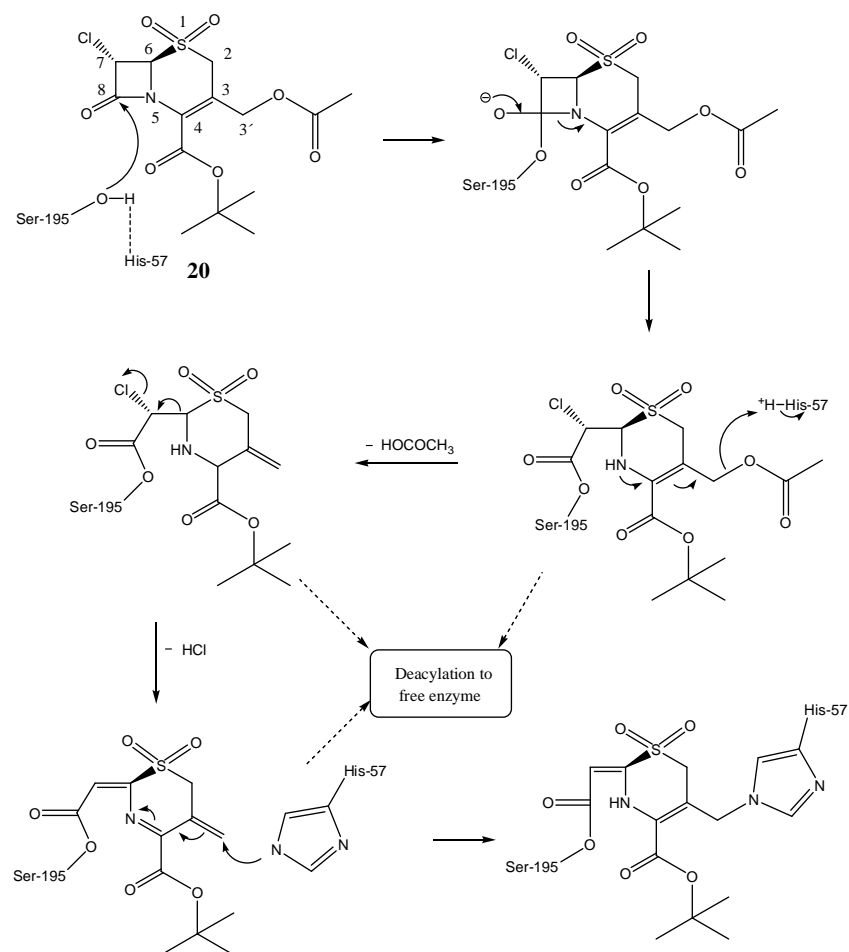
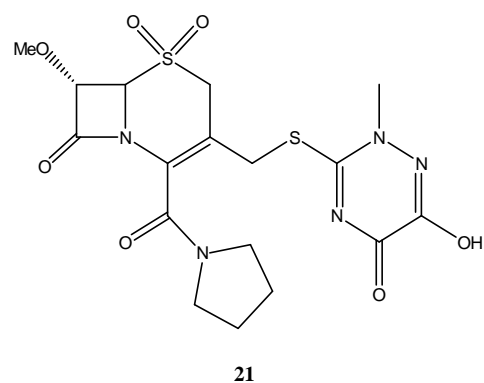


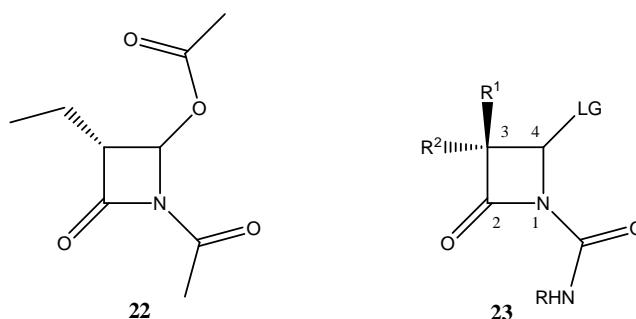
Figure 1.7 - Proposed “double-hit” mechanism of HLE inactivation by cephalosporin derivatives.⁹⁰

The best compromise between stability and activity of cephalosporin mechanism-based inhibitors was found with compound **21** (L-658,758), $k_{\text{inact}} = 0.007 \text{ s}^{-1}$, $K_i = 1.7 \text{ }\mu\text{M}$, giving a second-order rate constant for HLE inhibition, $k_{\text{inact}}/K_i = 4.1 \times 10^3 \text{ M}^{-1}\text{s}^{-1}$. This inhibitor was developed by Merck Research Laboratories and selected for clinical studies in a aerosol delivery system.⁹³



1.6.2 Monocyclic β -Lactams Derivatives

These compounds emerged in order to optimize pharmacokinetic properties limited in bicyclic derivatives (especially the need of oral bioavailability) to achieve systemically useful inhibitors of HLE. Such optimization results of an advantageous balance between stability, inhibitory potency and selectivity. Merck researchers anticipated that monocyclic β -lactams (azetidine-2-ones), containing structural requirements for both molecular recognition and chemical reactivity, were able to ensure the “double-hit” mechanism for HLE inactivation, seen in bicyclic structures.⁹⁴ The initial lead structure for design of monocyclic β -lactam inhibitors of HLE was **22**.



By SAR studies, the lead structure **23** was found, in which R¹ and R² are small alkyl substituents and LG is a leaving group, such as an acetoxy moiety. The mechanism of HLE inhibition by **23** is shown in Figure 1.8. The nucleophilic serine residue attacks on β -lactam carbonyl carbon, C-2, which leads to the ring opening (C-2 and N-1 bond fission), and can result in expulsion of the leaving group at C-4. Consequently, a reactive imine is formed (N-1 and C-4), which can be trapped by the active site histidine in a Michael addition (“double-hit” mechanism).

However, an alternative mechanism may occur, with nucleophilic attack of a water molecule instead of His-57 to the reactive imine, to form a carbinolamine. In fact, the formation of the carbinolamine was demonstrated using ESI-MS and two-dimensional NMR techniques. Mass spectrum data indicates an increase of 18 mass units in the acyl-enzyme complex generated after expulsion of the leaving group. That increment can be explained by addition of water.⁹⁵

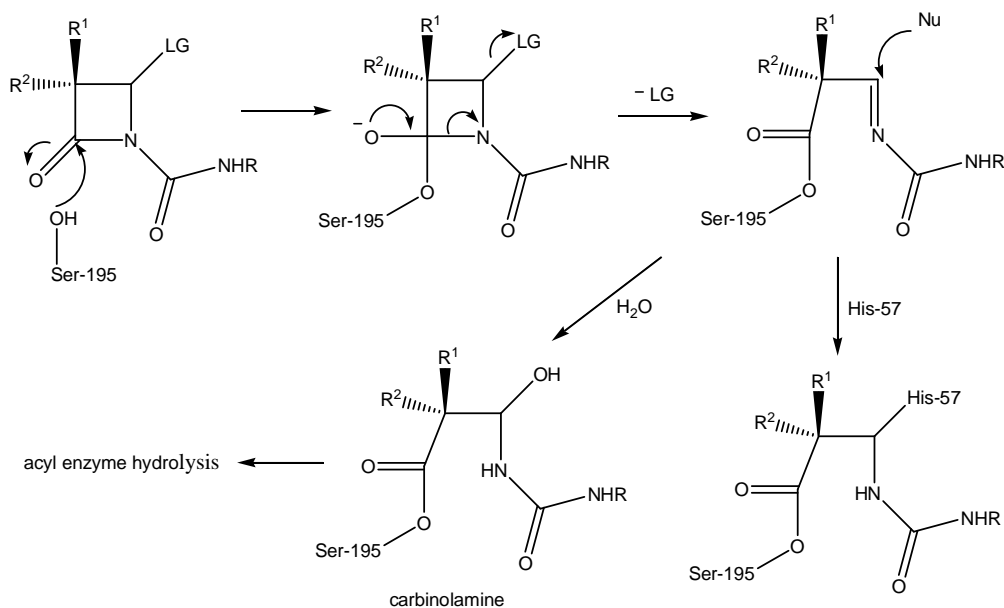
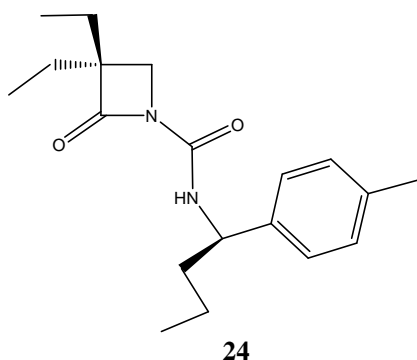


Figure 1.8 - Proposed mechanism of inhibition of HLE by monocyclic β -lactams with a leaving group LG at C-4.⁹⁵

Indeed, the carbinolamine is a stable acyl-enzyme complex, in which the hydroxyl group can be stabilized by hydrogen bonding with the active site histidine residue. Thus, the “double-hit” mechanism of inhibition suffers the competition of addition of water (Figure 1.8).⁹⁵



Nevertheless, it was suggested that the substituent at C-4 is not essential to achieve an irreversible inhibition. In fact, compound **24**, which lacks a leaving group at C-4, shows a fast inactivation and low reactivation rates of HLE, yielding a stable acyl-enzyme complex (at least as stable as that derived from inhibitors presenting a good leaving group).⁹⁶ However, opening of the β -lactam ring of **24** cannot generate an electrophilic imine. It was demonstrated by mass spectroscopy that the enzyme-inhibitor complex derived from **24** was consistent with the mass of the entire inhibitor.⁹⁵ These observations suggest

that a simple β -lactam, without leaving group at C-4, may react in complex hydrolytic pathways to protect the acyl-enzyme from hydrolysis. Thus, the stability of the acyl-enzyme is independent of the nature of the C-4 leaving group.⁹⁶ Furthermore, these data suggest that the formation of stable complexes between the HLE and β -lactam inhibitors does not necessarily require the “double-hit” mechanism.⁹⁵

Several SAR studies were conducted in order to optimize the inhibitory potency and stability of monocyclic β -lactam inhibitors of HLE.

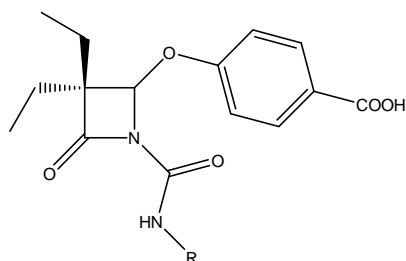
Effect of the Substituents at C-3. It was found that small hydrophobic substituents at C-3 α , as **23**, R² = ethyl group, can interact with the hydrophobic S₁ pocket of HLE. Thus, this group was selected for C-3 α position. In addition, the incorporation of a C-3 β group larger than methyl not only increases hydrolytic stability, by preventing the attack on the carbonyl carbon by nonspecific nucleophiles, but also improves inhibitory potency. This C-3 β group does not impair inhibition, since the hydroxyl group of Ser-195 attacks the α -face of the β -lactam ring.^{97, 98} Retaining the 3 α -ethyl group, the 3 β -ethyl and 3 β -*n*-propyl derivatives showed improved both stability and in vivo activity. Although 3 β -*n*-butyl analogue showed to be more potent than 3 β -ethyl in vitro, there was a loss of activity in vivo, probably related with an increased protein-binding of the more lipophilic derivative. Thus, the diethyl substituent was chosen at C-3.⁹⁷

Effect of the Substituents at C-4. The C-4 acetoxy group is unstable to nucleophiles. Studies performed in order to evaluate the effect of C-4 substituents in **23** revealed that these substituents are important to achieve oral activity. Incorporating an appropriate substituted phenol in this position retains inhibitory activity and improves aqueous solubility. These effects are remarkable for carboxylic acid derivatives, such as 4-hydroxybenzoic acid and 4-hydroxyphenylacetic acid ethers.⁹⁹

A substituent with *S* configuration at C-4 increases the inhibitory potency compared to the configuration *R*, which may be explained by interaction of the *S*-aryl carboxylic acid ether with the enzyme subsites S₂ - S₃. In contrast, the *R* configuration does not allow this interaction.⁹⁷ Conversely to what one might expect the nature of the leaving

group is not a crucial factor to influence the rate of acylation. In fact, there is a weak correlation between enzyme inhibition and the ability of the leaving group, expressed by the pK_a of the substituted phenol.⁹⁹

Effect of the Substituents at N-1. Many SAR studies were performed in order to optimize the substituent at *N*-1.^{98, 100, 101} The *N*-acetyl group of the lead structure **22** is labile and prompted the search for more stable substituents. It was found that the *N*-carbamoyl substituent (giving a urea moiety, as in **23**) improves the hydrolytic stability of monocyclic β -lactams, as this group is less electron-withdrawing than an acyl substituent. Derivatives incorporating a benzylurea substituent, **25**, were the first orally active β -lactams inhibitors of HLE.⁹⁸ Using **25** as lead structure, several SAR studies were performed in order to select the substituent on the urea moiety, to achieve potent inhibitors both in vitro and in vivo. In vivo studies involve measurement of the percentage of inhibition of HLE-induced lung hemorrhage in animals, with β -lactams inhibitors administrated orally prior of lung hemorrhage induction.¹⁰²



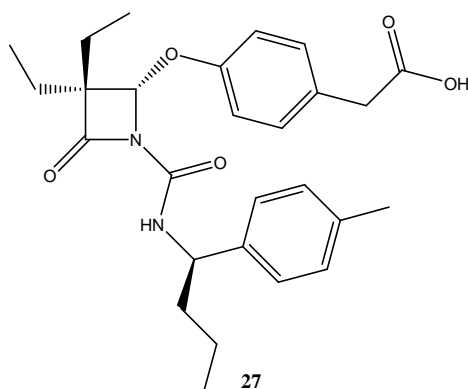
		$k_{\text{obs}}/[\text{I}] / \text{M}^{-1}\text{s}^{-1}$	Lung Hemorrhage % inhibition
25	R = CH ₂ Ph	1500	56
26	R = (CH ₂) ₄ Ph	9200	35

Compound **26**, which contains a four-carbon link between the nitrogen atom and the aromatic ring, is a better in vitro inhibitor of HLE than **25**. However, in vivo activity diminishes due to an increase in hydrophobicity.⁹⁸

In contrast, it was found that the incorporation of an alkyl substituent on the benzylurea methylene group, with an *R* configuration in this position, allows interaction with a hydrophobic pocket of the enzyme, improving inhibitory potency. Thus, Merck Research Laboratories developed potent, selective orally active

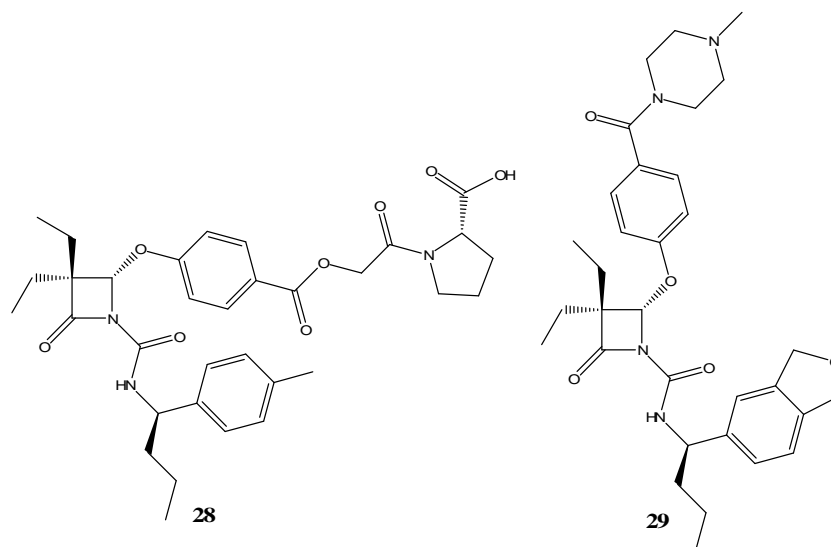
inhibitors of HLE, such as compound **27**, L-680,833, which second-order rate constant for enzyme inhibition is $k_{\text{inact}}/K_i = 6.22 \times 10^5 \text{ M}^{-1}\text{s}^{-1}$.¹⁰³

By ESI-MS and NMR spectroscopic studies, it was demonstrated that the mechanism of HLE inhibition by **27** involves a carbinolamine as a stable acyl-enzyme complex.⁹⁵



Oral bioavailability studies of **27** were performed in rodents and Rhesus monkeys, with effective inhibition of HLE-mediated lung injury. In addition, an excellent specificity against HLE was demonstrated, not only in studies performed with monkey, rat, dog and human elastases, but also in experiments with other serine proteases.¹⁰⁴ These results suggest that low-molecular-weight synthetic inhibitors of HLE such as monocyclic β -lactam **27** have promising therapeutic value.

Indeed, the analogue β -lactam **28**, also developed by Merck, is one of the most potent derivatives ever reported, with a second-order rate constant of enzyme inhibition of $1.25 \times 10^7 \text{ M}^{-1}\text{s}^{-1}$.¹⁰⁵ In addition, it was reported that compound **29**, DMP-777, presenting a k_{on} value of $3.78 \times 10^6 \text{ M}^{-1}\text{s}^{-1}$,¹⁰⁶ was in Phase II clinical trials for cystic fibrosis, juvenile rheumatoid arthritis and emphysema.⁶



1.6.2.1 Monocyclic β -Lactams with the Leaving Group on a Different Position than C-4

A different strategy to design monocyclic β -lactam as potential mechanism-based irreversible inhibitors of HLE is to incorporate the leaving group on C-1' instead of C-4. Thus, after acylation of the catalytic serine residue, and departure of the leaving group, a reactive imine is formed, serving as electrophile for a second nucleophile of the active site.⁹⁴ Examples of time-dependent irreversible inhibitors of HLE with the leaving group on C-1' are the *N*-acyloxymethyl- and *N*-aminocarbonyloxymethyl azetidin-2-ones, **30** (Figure 1.9), previously developed at the host laboratory.¹⁰⁷ The leaving group on C-1' is a carboxylic or a carbamic acid. X is an electron-withdrawing group, such as a phenylsulfone moiety, that increases the acylating power of the β -lactam by reducing the pK_a of the amine leaving group by ring opening (C-N fission). The diethyl substituent at C-3 interacts with the S_1 pocket of HLE. The proposed mechanism of HLE inhibition is shown in Figure 1.9.

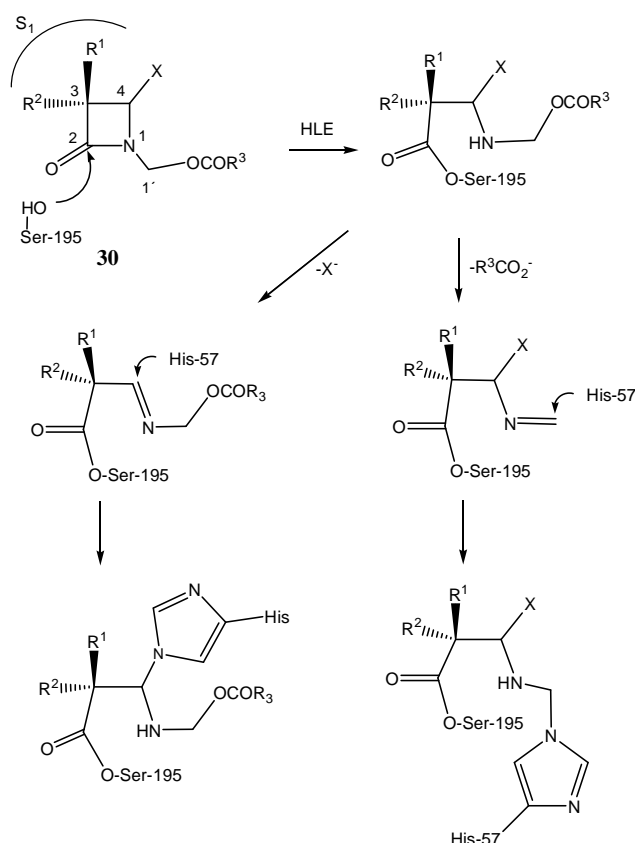
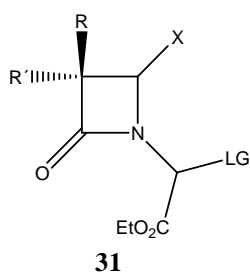


Figure 1.9 - Potential suicide-type mechanism of HLE inhibition by *N*-acyloxymethylazetidin-2-ones.¹⁰⁷

Docking studies suggests that enzyme inhibition involves departure of the leaving group on C-1' rather than at C-4. The oxidation state of the sulfur atom in the C-4 substituent plays an important role in inhibitory potency, as phenylsulfones were found to be more potent inhibitors than the correspondent sulfides.¹⁰⁷ This result is in conformity with the higher HLE inhibitory activity presented by cephalosporins sulfones compared to the correspondent sulfides.⁸⁸



Similarly, *N*- α -heterofunctionalized compounds, as **31**, were reported as irreversible inhibitors of HLE, in which LG is a leaving group. X can be an electron-withdrawing substituent, such as a phenylsulfone moiety.^{108, 109} The electron-withdrawing ethoxycarbonyl group activates the intermediate imine generated after ring opening, allowing a potential

suicide type inhibition pathway. A diethyl substituent at C-3 ($R = R' = \text{Et}$) interacts with the S_1 binding pocket of HLE.¹⁰⁹

Monocyclic β -lactam inhibitors of HLE with a leaving group in a different position are the functionalized *N*-aryl azetidion-2-ones, such as **32**,¹¹⁰ reported as being potential mechanism-based inhibitors of HLE.^{111, 112} The susceptibility to release a latent quinoniminium methide function with the formation of the acyl-enzyme allows the suicide type inhibition (Figure 1.10).

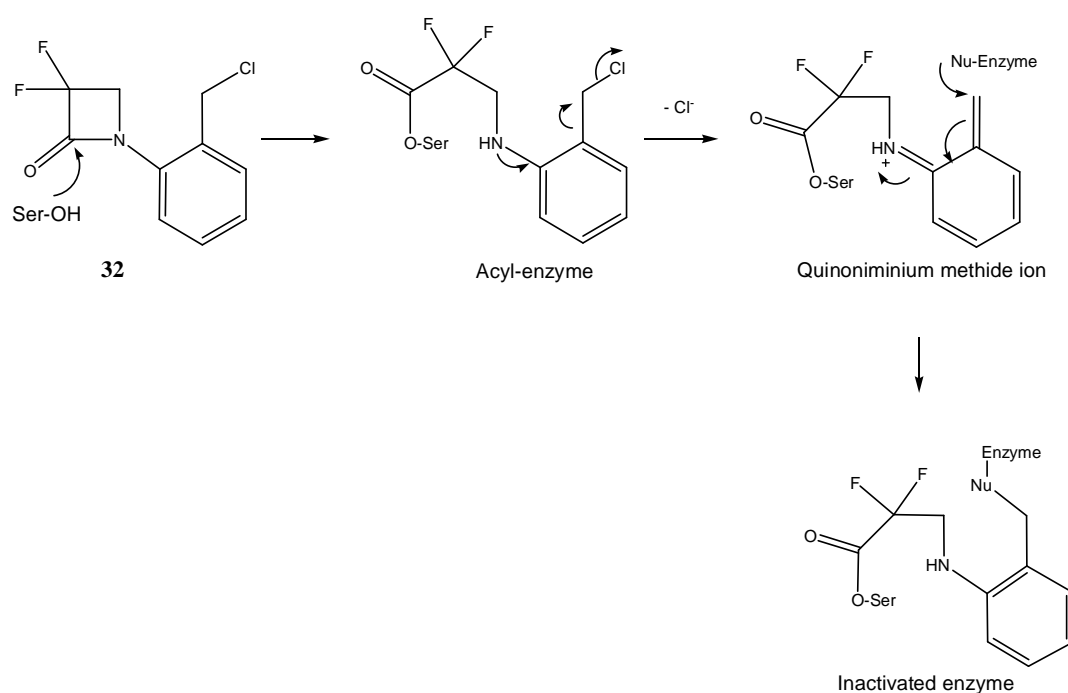


Figure 1.10 - Postulated suicide-type mechanism of HLE inhibition by functionalized *N*-aryl azetidion-2-ones.¹¹¹

The presence of a gem-dihalogeno group at C-3 reduces the pK_a of the aniline leaving group (inductive effect) and activates the carbonyl carbon towards nucleophilic attack. It was found that compounds displaying the functionalized methylene group in the *ortho* position, as in **32**, were more potent inhibitors than the *para*-analogues.

1.6.2.2 Monocyclic β -Lactam Analogues Acylating Agents of HLE

As the “double-hit” mechanism is not necessary to achieve a persistent inhibition (as mentioned earlier), it has highlighted different strategies to design monocyclic β -lactam derivatives as acylating agents of HLE.

An example is the symmetric 1,3-diazetidone-2,4-dione, **33** (Figure 1.11), which is a functionalized β -lactam used as a peptidomimetic template.¹¹³ On both nitrogen atoms of the heterocycle are incorporated small alkyl substituents. One of the P₁ substituent interacts with the S₁ pocket of HLE (ex.: P₁ = Et), being involved in molecular recognition. After nucleophilic attack of Ser-195 at one of the carbonyl carbons, an acyl-enzyme complex is generated by ring opening (C-N fission), as illustrated in Figure 1.11. By changing the nature of the P₁ substituent, one can modulate the selectivity towards other serine proteases. Interestingly, the correspondent azetidin-2-one analogue of **33** (lacking one nitrogen and one carbonyl group), *i.e.*, a typical β -lactam, showed no inhibitory activity. These results suggest that 1,3-diazetidone-2,4-dione nucleus is much more reactive than the correspondent azetidin-2-one, and activates the carbonyl carbon through electronic effects and bond angle strain.¹¹³

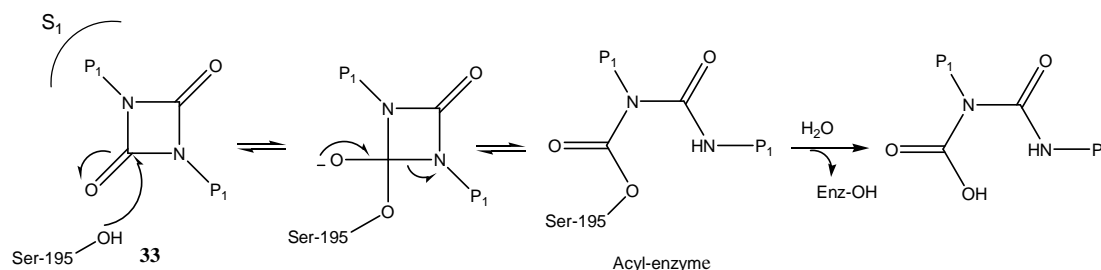
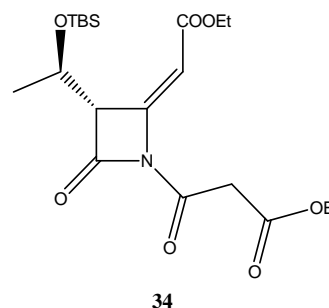


Figure 1.11 - Inhibition of HLE by 1,3-diazetidone-2,4-diones.¹¹³

A different strategy involved the design of 4-alkyliden- β -lactams, such as **34**, containing a double carbon-carbon bond on the C-4 position, in order to activate the carbonyl carbon towards nucleophilic attack. These compounds, in which OTBS is a *tert*-butyldimethylsilyloxy group, were reported as being potent inhibitors of HLE. It was reported that the IC₅₀ for **34** (IC₅₀ = 4 μ M) was better than that for the reference azetidin-2-one L-680,833 (**27**, IC₅₀ = 9 μ M).¹¹⁴

By contrast, the correspondent C-4 saturated analogue of **34** was found to be a weak inhibitor of HLE (20% inhibition at 100 μM versus 82% inhibition at 100 μM for **34**). These results reflect the activator effect of the presence of a C=C double bond on the acylating power of 4-alkyliden- β -lactams.^{114, 115}



Another approach to design β -lactam analogues as acylating agents of elastase is to incorporate a sulfonyl group next to the nitrogen within the four-membered ring, giving a 3-oxo- β -sultam, **35**. This compound is simultaneously a β -sultam and a β -lactam, thus it has two electrophilic centers available for nucleophilic attack. Therefore, nucleophilic attack at **35** could involve either attack at the carbonyl group, ring opening by C-N bond fission and expulsion of the sulfonamide leaving group (acylating agent) or attack at the sulfonyl group, S-N bond fission and expulsion of an amide leaving group (sulfonylating agent).¹¹⁶

3-Oxo- β -sultam **35** was reported as being a time-dependent inhibitor of porcine pancreatic elastase, PPE (which is a model of HLE as discussed in section 1.7). PPE inhibition is a result of acylation of the catalytic serine residue, C-N bond fission and expulsion of a sulfonamide (Figure 1.12). The second-order rate constant for enzyme inhibition by **35** is $768 \text{ M}^{-1}\text{s}^{-1}$ at pH 6.¹¹⁶ However, alkaline hydrolysis of the 3-oxo- β -sultam takes place at the sulfonyl group with S-N fission (Figure 1.12), as demonstrated by NMR and ESI-MS techniques.¹¹⁷ This is a very rapid process, occurring with a second-order rate constant for alkaline hydrolysis, k_{OH^-} , of *ca.* $2 \times 10^5 \text{ M}^{-1}\text{s}^{-1}$.¹¹⁶ In fact, the 3-oxo- β -sultam is chemically extraordinarily reactive, and its k_{OH^-} value is nearly 10^6 times higher than those of most clinically useful β -lactams ($k_{\text{OH}^-} 10^{-1} - 1.0 \text{ M}^{-1}\text{s}^{-1}$).⁹² Highly reactive inhibitors may lead to off-target reactions, toxic effects, loss of selectivity and reduced bioavailability.⁷² Thus, one may conclude that the 3-oxo- β -sultam is not a suitable scaffold for studies towards therapeutic application.

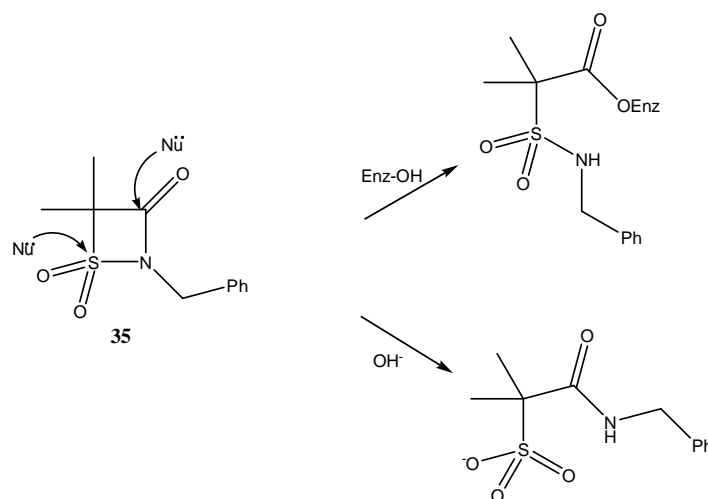


Figure 1.12 - Nucleophilic attack at 3-oxo-β-sultam. PPE inhibition involves C-N fission while alkaline hydrolysis involves S-N fission.¹¹⁶

1.7. PORCINE PANCREATIC ELASTASE

Several elastase inhibition studies are performed using porcine pancreatic elastase, PPE, which is a serine protease readily available and economically more accessible than HLE.

PPE (EC 3.4.21.36) is presented as a single chain peptide of 240 amino acid residues depending on the cation Ca²⁺ for its stabilization, and it has no carbohydrates as prosthetic group. PPE is topologically close to HLE, with 40% homology, being the two enzymes particularly similar in their active site regions (catalytic triad and residues forming the central core of the binding site).²⁷ X-Ray crystallography studies have contributed to the elucidation of their structures. PPE has the advantage that it crystallizes easily and numerous crystallographic studies of PPE in complexes with inhibitors are documented. In particular, this technique demonstrated that a cephalosporin inhibited PPE by a “double-hit mechanism”.⁹⁰ On the other hand, X-ray crystallography studies are less documented for HLE, since the crystals of native or inhibitor-complexed enzyme are obtained with difficulty.²⁷

Both enzymes have similar substrate specificities, as a result of a similar geometry and hydrophobic nature of the S₁ binding pocket. However, due to steric constraints,

this pocket is smaller in PPE, consistent with the preference for alanine by this enzyme. By contrast, HLE also accepts Val and Leu. In this context, it is important to stress that the chromogenic substrate used in vitro for HLE is *N*-methoxy-succinyl-L-Ala-L-Ala-L-Pro-L-Val-*p*-nitroanilide, while for PPE is *N*-succinyl-L-Ala-L-Ala-L-Ala-*p*-nitroanilide. These features emphasize that the design of irreversible inhibitors of HLE requires human sources of elastase. SAR studies of potent inhibitors for PPE do not necessarily lead to potent inhibitors against HLE.²⁷

1.8. DESIGN OF POTENTIAL IRREVERSIBLE INHIBITORS OF HLE

As a summary of what has been discussed before, an irreversible enzyme inhibition involving a covalent modification may be achieved using monocyclic β -lactams as an enzyme acylating agent. The acyl-enzyme must be stable in order to achieve an effective inhibition, thus the regeneration of the enzyme, by reaction with nucleophiles such as water, must be a very slow process.⁷²

The reaction of HLE with an acylating agent involves an acyl transfer process, which occurs in a stepwise process. First, it involves the nucleophilic attack of the catalytic serine residue at the carbonyl carbon to generate a four-coordinate tetrahedral intermediate. The tetrahedral intermediate breaks down back to the reactants or gives the product, with displacement of a leaving group (Figure 1.13). Therefore, the rate limiting step can be the formation ($k_{-1}, k_2 > k_1$) or the breakdown ($k_{-1}, k_1 > k_2$) of the tetrahedral intermediate.

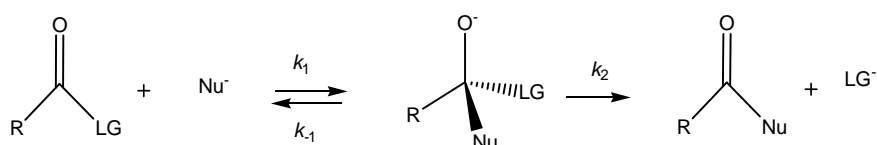


Figure 1.13 - General acyl transfer process (Nu = nucleophile; LG = leaving group).

The main requirements for an effective enzyme inhibition by an acylating agent are:

1. the rate of acylation must be faster than the rate of the turnover of the natural substrate;
2. the inhibitor must be relatively stable under in vivo conditions.

With regard to the rate of acylation, it depends on two important factors:

- i) the “chemical” reactivity of the inhibitor
- ii) the molecular recognition by the target enzyme.⁷²

The chemical reactivity is related with electronic effects, such as the electrophilic nature of the carbonyl group and the nucleofugacity (leaving group ability) of the group displaced. In addition, it involves steric and strain effects that influence the intrinsic chemical reactivity of the inhibitor.^{72, 118} Increasing the intrinsic chemical reactivity of an inhibitor may lead to a faster rate of reaction with the target enzyme.⁷² On the other hand, extremely reactive scaffolds (ex. **35**) may cause a decrease in selectivity, increasing hydrolytic instability and reactions with non-specific nucleophiles, with potential toxic effects.

Molecular recognition allows a gain in the enzyme catalyzed reaction rate, since it involves using the enzymatic apparatus for favorable non-covalent interactions at the various subsites of the enzyme and inhibitor. Thus, the ideal inhibitor should have an optimal molecular recognition by hydrophobic and other non-covalent interactions with the enzyme, minimizing the enzyme inactivation by a covalent modification.

Improving the inhibition properties of a compound may be achieved by:

- modifying the chemical reactivity
- the molecular recognition
- or a combination of both.

Structural modifications of the inhibitor in order to increase chemical reactivity can affect the ease of bond-making and breaking by electronic factors (such as inductive and resonance) and steric effects. However, the variation in rate constants for the various inhibitors reacting with the enzyme, which reflects the difference in energies between the initial reactant and the transition state, is affected not only by the chemical reactivity but also by favorable binding energies due to molecular recognition.⁷²

1.8.1 The Second-Order Rate Constant for Alkaline Hydrolysis, k_{OH^-} , as an Important Tool in Drug Design

It was suggested that the magnitude of the second-order rate constant for alkaline hydrolysis, k_{OH^-} , is a crude guide to determine the usefulness of a potential inhibitor as an enzyme acylating agent.⁷² It was suggested the use of the alkaline hydrolysis model as hydroxide mimics the reaction of the catalytic serine residue with the potential irreversible inhibitor. On the other hand, k_{OH^-} value is also useful since is indicative of the metabolic stability towards non-specific nucleophiles. In order to deduce the importance of the molecular interactions between the enzyme and the inhibitor on the enzyme-catalyzed hydrolysis, it is necessary to separate intrinsic chemical effects from specific binding interactions. Thus, the “enzyme rate enhancement factor”, EREF, which is given by the ratio of the second-order rate constant of the enzyme catalyzed reaction, k_{on} , by k_{OH^-} ,^{72, 119} is indicative of the ability of the enzyme to use its catalytic machinery to increase the rate of the reaction.

Modifications in the structure of an enzyme acylating agent attempt to increase molecular recognition, as well as the rate of acylation of the target enzyme, without prejudice of aspects of hydrolytic stability. Similarly, substitutions in the structure can reduce the susceptibility towards non-specific hydrolysis, maintaining the acylating power.⁷² Thus, alkaline hydrolysis studies (and in particular k_{OH^-} value) are an important tool in drug design.

1.9. AIM OF THE THESIS

The main purpose of this thesis was to contribute to the research of β -lactam-based irreversible inhibitors of serine proteases, in particular HLE inhibitors, as potential candidates for the treatment of several inflammatory disorders, such as COPD, adding a small piece in the puzzle of rational drug design, in the context of drug discovery.

The rationale underlying the inhibitor design is based on the following considerations:

- The monocyclic β -lactam scaffold has been successfully used to develop potent time-dependent acylating agents and mechanism-based inhibitors of HLE, some of

them presenting oral activity. Moving away from the well-known, simple and versatile β -lactam core scaffold would be difficult and time-consuming.

- It is known the preference for small alkyl substituents at C-3 on the β -lactam template to allow hydrophobic interaction for molecular recognition at the S_1 binding pocket of HLE.

- Taking into account that increasing the intrinsic chemical reactivity of a compound may lead to a faster rate of reaction with the target enzyme,⁷² it was reasoned that monocyclic β -lactams, retaining elements for molecular recognition, and presenting electron-withdrawing groups that increase the intrinsic chemical reactivity, provide an interesting motif for development of irreversible inhibitors of HLE with an improved inhibitory potency. To achieve this goal, the present project was subdivided in two main tasks: i) the development of irreversible inhibitors of HLE based on azetidin-2-ones presenting different substituents at C-4 and ii) the development of azetidine-2,4-diones (4-oxo- β -lactams) as a new template for drug design.

1.9.1 C-4 Substituted Azetidin-2-ones (Simple β -Lactams) as Inhibitors of Serine Proteases

This part of the present study was integrated in the stepwise methodological training of the doctoral program and involved synthesis, alkaline hydrolysis studies and serine proteases PPE and HLE inhibition studies (enzyme kinetics and in vitro inhibitory potency), following studies on *N*-carbamoylazetidin-2-ones started by Dr. Luísa Martins at the host laboratory.¹²⁰

The inhibitor design rational was based on previous work on β -lactams as irreversible inhibitors of elastase. Merck Research Laboratories, as mentioned in Section 1.6., developed cephalosporins sulfones and *N*-carbamoylazetidin-2-ones, such as **27** (which the structure is appropriately repeated in Figure 1.14), as potent HLE inhibitors. Since it is known that *N*-carbamoylazetidin-2-ones are much more stable in blood than bicyclic structures, they were chosen as a template for elastase inhibition studies. In order to modify the intrinsic chemical reactivity of the β -lactam motif, different substituents at C-4 were chosen, including compounds presenting a sulfone

function, in analogy to the cephalosporin sulfone **36** (Figure 1.14); and also a phenoxy substituent, in analogy to **27**. Since it is known that the gem-diethyl substituent at C-3 of **27** interacts with the S₁ binding pocket of the enzyme, this substituent was retained in the design of HLE inhibitors (Figure 1.14).

Therefore, the aims of this study were to:

- synthesize azetidin-2-ones with different substituents at C-4.
- elucidate how the C-4 substituents contribute to the chemical reactivity towards hydroxide and to the enzymatic reactivity towards the catalytic serine residues of PPE and HLE, in a mechanistic study of hydrolysis.
- to find out if there was any correlation between intrinsic chemical reactivity and serine proteases inhibition in C-4 substituted β -lactams. (Chapter 2) (Papers I and II).

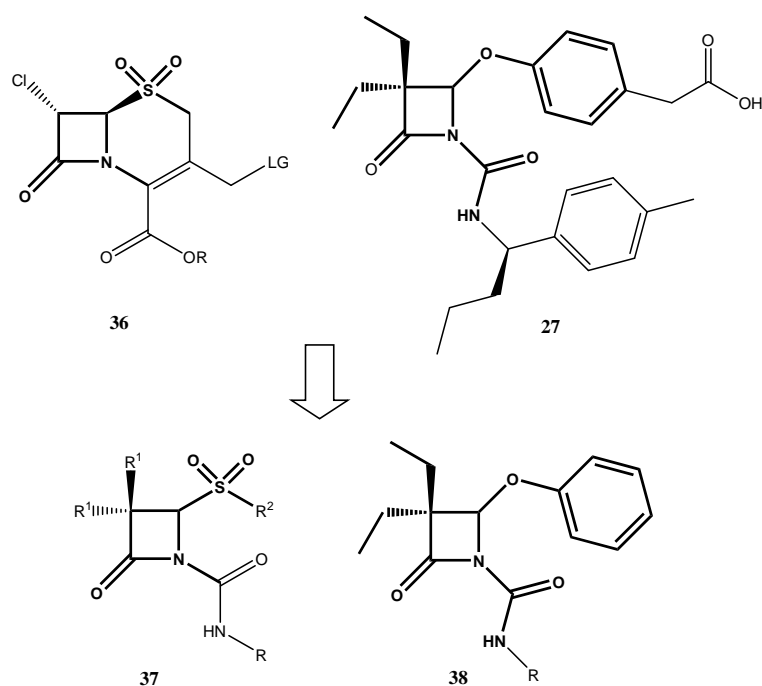


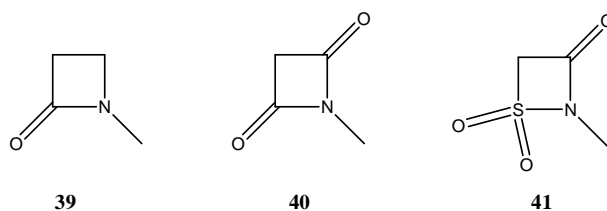
Figure 1.14 - Rational design of C-4 substituted *N*-carbamoylazetidin-2-ones.

1.9.2 Azetidine-2,4-diones (4-Oxo- β -lactams) as Inhibitors of Serine Proteases

In a second phase, the aim of this project was to develop azetidine-2,4-diones (4-oxo- β -lactams), as a novel class of irreversible inhibitors of serine proteases, with

improved activity when compared to known simple β -lactam (azetidin-2-one) inhibitors.

On the basis of the design rationale, it was reasoned that incorporating a second sp^2 carbonyl carbon at C-4 within the four-membered ring, i.e., converting the azetidin-2-one **39** into an azetidine-2,4-dione **40**, increases the intrinsic chemical reactivity of the inhibitor, which may improve the inhibitory potency against elastase. Thus, as a result of i) an increased susceptibility of the carbonyl carbon towards nucleophilic attack, as well as ii) an enhanced nucleofugacity of the leaving group amide, facilitating the C-N bond fission and ring opening, and also iii) a distortion on the β -lactam ring with increased ring strain, the azetidine-2,4-dione may lead to a greater acylating power. On the other hand, the azetidine-2,4-diones **40** were designed as a result of an isosteric substitution on 3-oxo- β -sultam **41**, replacing the sulfonyl group responsible for hydrolytic lability, by a carbonyl group, in order to improve hydrolytic stability and reduce off-target reactions by non-specific nucleophiles.



Firstly, the research interest was focused on a computer assisted drug-design, including *N*-carbamoylazetidine-2,4-diones, for comparison with the *N*-carbamoylazetidin-2-ones with a leaving group at C-4. Due to problems related with synthesis, only *N*-aryl and *N*-alkyl azetidine-2,4-diones were prepared. Preliminary enzymatic studies were performed with PPE and the main goals were to compare the results for inhibitory activity with those obtained for alkaline hydrolysis of the same compounds, in order to provide information on the effectiveness of the 4-oxo- β -lactam scaffold as a therapeutically useful acylating agent, on the sensitivity of the enzyme to the intrinsic chemical reactivity versus molecular recognition, and on the mechanism of hydrolysis (Chapter 3) (Paper III).

In order to explore S and S' subsites of HLE for molecular recognition, azetidine-2,4-dione derivatives with different substituents on C-3 and N-1 were prepared, as both acylating agents and potential mechanism-based inhibitors of HLE. In particular, a mechanism-based inhibition may be achieved with functionalized *N*-aryl azetidine-2,4-diones containing a potential thiol leaving group. Enzyme kinetic studies with HLE and biochemical assays on serine proteases human cathepsin G and proteinase 3 and against a cysteine protease, papain, were performed. The stability in human plasma for selected compounds and finally a biodistribution study in mice were described, in anticipation of using these inhibitors in rodent efficacy models (Chapter 4) (Papers IV and V).

CHAPTER 2

C-4 SUBSTITUTED N-CARBAMOYL

AZETIDIN-2-ONES: CHEMICAL REACTIVITY AND

ENZYME INHIBITION

2. C-4 SUBSTITUTED N-CARBAMOYLAZETIDIN-2-ONES: CHEMICAL REACTIVITY AND ENZYME INHIBITION

Integrated in the research-oriented doctoral program, this part of the project was developed following the study of hydrolysis of *N*-carbamoylazetidin-2-ones started by Dr. Luísa Martins at the host laboratory.¹²⁰

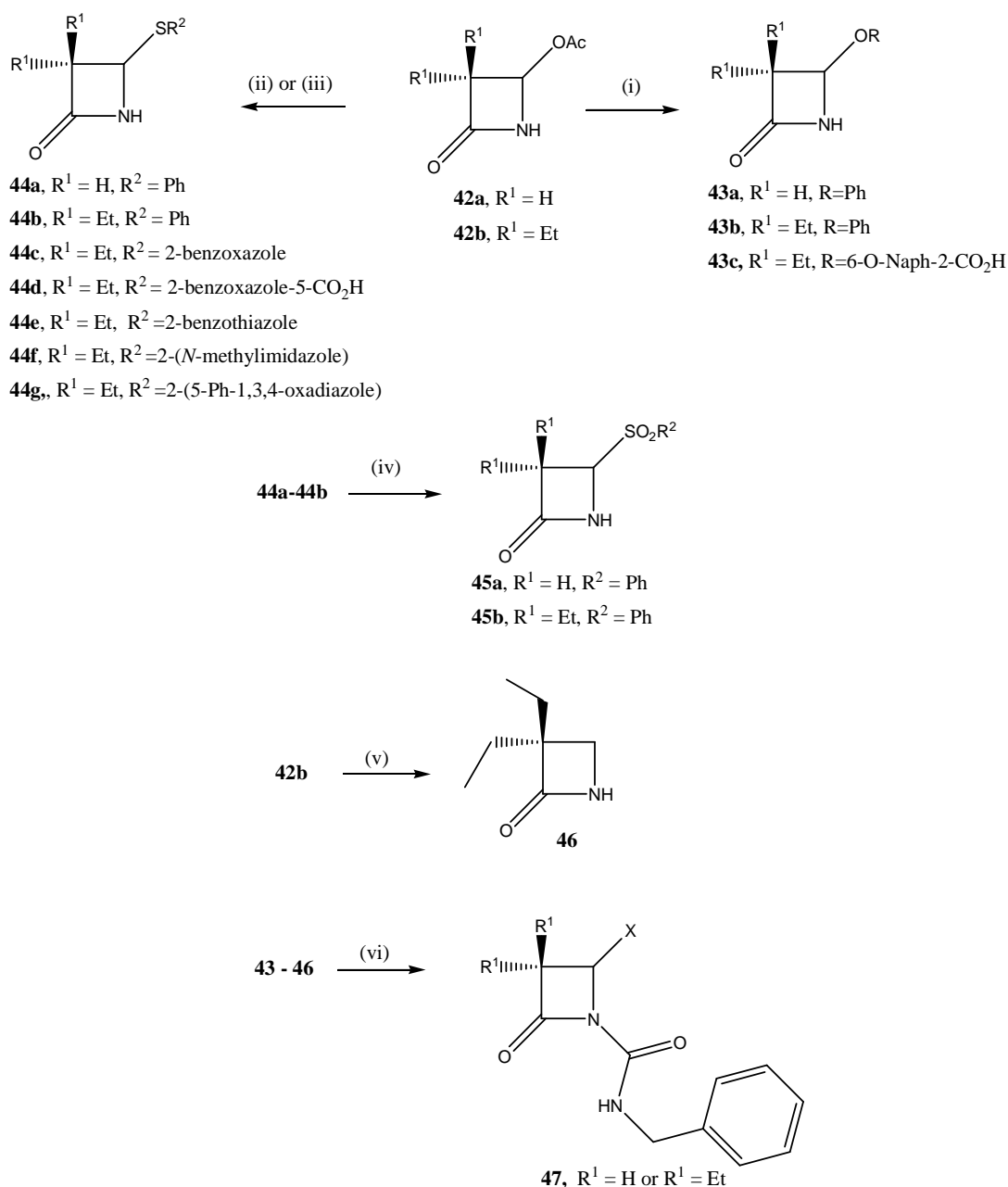
2.1. SYNTHESIS

β -Lactams (azetidin-2-ones) presenting different substituents on C-4 were synthesized using methodologies described in the literature.⁹⁸ The choice of the substituents was based on previous studies performed on β -lactams as irreversible inhibitors of HLE,^{97-99, 120} as mentioned earlier. Two series of *N*-carbamoylazetidin-2-ones (**2.6**, Scheme 2.1) were synthesized: the C-3 gem-diethyl derivatives were prepared for S_1 molecular recognition by HLE; the C-3 unsubstituted compounds were prepared to assess the impact of the C-4 substituents on PPE inhibition when interaction with the S_1 pocket is reduced.

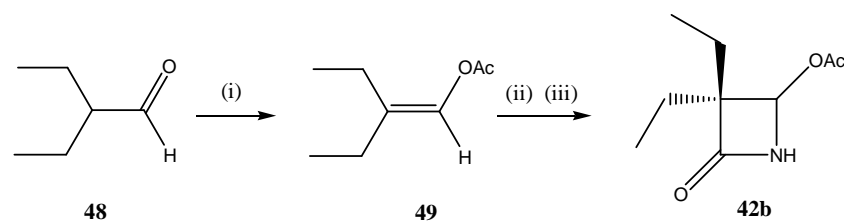
The synthetic pathway to give direct access to differently C-4 substituted azetidin-2-ones key intermediates **43** and **44** or **46** used the appropriate 4-acetoxy-azetidin-2-one **42** as the starting material (Scheme 2.1). The C-3 unsubstituted **42a** is commercially available, while the **42b** counterpart was prepared as described in the literature, involving a [2+2] cycloaddition of *N*-chlorosulfonyl isocyanate with a previously synthesized enol ester **49** (Scheme 2.2).⁹⁸

Reaction of **42** with nucleophiles, such as phenol or thiols, involving elimination-nucleophilic addition, gave compound **43-44** as racemic mixtures. Two different routes were used to synthesize compounds **44**: i) reaction of **42** with the respective thiol and sodium hydroxide in acetone at room temperature¹²¹ or ii) reflux in benzene in the presence of a catalytic amount of triethylamine.¹²² Interestingly, the second procedure, carried out in absence of water, provided superior yields. Treatment of thioethers **44** with 3-chloroperbenzoic acid (MCPBA) yielded the corresponding

sulfones **45**. The C-4 unsubstituted 3,3-diethylazetid-2-one **46** intermediate was prepared by reduction of **42b** with NaBH₄ in ethanol at 0 °C.¹⁰⁹ The correspondent C-3 unsubstituted analogue is commercially available. The synthesized *N*-unsubstituted intermediates **43-46** are listed in Table 2.1. Finally, reaction of intermediates with benzyl isocyanate gave the *N*-carbamoyl β-lactams **47** in good yield (Scheme 2.1).



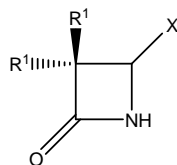
Scheme 2.1 - Synthesis of *N*-carbamoylazetid-2-ones. Reagents and conditions: (i) ArOH, NaOH, acetone; (ii) R²SH, NaOH, acetone; (iii) R²SH, TEA, C₆H₆, reflux; (iv) MCPBA, DCM; (v) NaBH₄, EtOH, 0 °C; (vi) PhCH₂NCO, TEA, DCM.



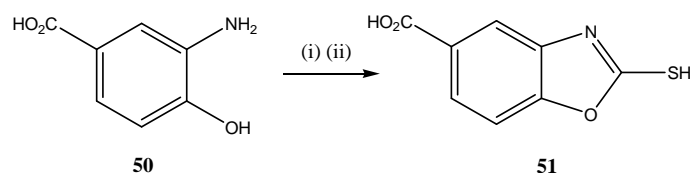
Scheme 2.2 - Synthesis of 3,3-diethyl-4-acetoxy-azetid-2-one, 42b. Reagents and conditions: (i) acetic anhydride, sodium acetate; (ii) *N*-chlorosulfonyl isocyanate, DCM; (iii) H₂O.

Table 2.1 - *N*-unsubstituted key intermediates synthesized 43-46.

Compound	R ₁ = R ₂	X
43a	H	OPh
43b	Et	OPh
43c	Et	
44a	H	SPh
44b	Et	SPh
44c	Et	
44d	Et	
44e	Et	
44f	Et	
44g	Et	
45a	H	SO ₂ Ph
45b	Et	SO ₂ Ph
46	Et	H



To prepare compound **44d**, the respective thiol 2-mercaptobenzo[d]oxazole-5-carboxylic acid **51** (Scheme 2.3) was synthesized, by refluxing 3-amino-4-hydroxybenzoic acid **50** and potassium ethyl xanthate (EtOCS₂K) in aqueous ethanol, adapting described techniques.¹²³



Scheme 2.3 - Synthesis of 2-mercaptobenzoxazole-5-carboxylic acid 51. Reagents and conditions: (i) EtOCS₂K, EtOH 95%, H₂O, reflux; (ii) HCl, H₂O.

The final *N*-carbamoylazetid-2-ones synthesized in this work were **47a-g** (Table 2.2). Compounds **47j-k** were synthesized by Dr. João Neres and are also listed in this table because they were studied in this work as inhibitors of HLE. Compounds **47h-i** were synthesized and studied at the host laboratory by Dr. Luísa Martins,¹²⁰ but were also included in Table 2.2, since the obtained results are relevant to be discussed here. Compound **47k**, developed by Merck Research Laboratories¹⁰³ as an inhibitor of HLE, was used in the present work as standard for HLE inhibition assays.

Table 2.2 - Final *N*-carbamoylazetid-2-ones 47 studied in this work.

Compound	R ₁ = R ₂	X
47a	H	H
47b	H	OPh
47c	H	SPh
47d	H	SO ₂ Ph
47e	Et	H
47f	Et	OPh
47g	Et	SPh
47h^a	Et	SO ₂ Ph
47i^a	Et	SCH ₂ Ph
47j^b	Et	SO ₂ CH ₂ Ph
47k^{b,c}	Et	OC ₆ H ₄ -4-CO ₂ H

^a Synthesized and studied by Dr. Luísa Martins.¹²⁰; ^b Synthesized by Dr. João Neres; ^c Merck's Research Laboratories compound¹⁰³.

2.1.1 NMR Spectral Characterisation

All C-4 substituted azetid-2-ones synthesized were racemic mixtures, presenting a chiral stereocenter at C-4. Thus, the adjacent protons are chemically and magnetically non-equivalent, being diastereotopic to one another.

Inspection of the ^1H NMR spectra of the C-3 unsubstituted derivatives reveals *dd* signals for the C-3 methylene protons, as a result of geminal coupling with each other and with the neighbour C-4 proton. For some synthesized *N*-unsubstituted azetid-2-ones, such as **43a**, the C-3 methylene protons give peculiar signals (Figure 2.1). One C-3 proton consists of a *d* signal (Figure 2.1, at right), while the other is a *ddd* (Figure 2.1, at left). This can be explained as follows: the coupling constant of one proton at C-3 with the proton at C-4 is small and the signal seems like a doublet. For the other proton at C-3, which presents a *ddd* signal, an additional coupling with the N-H proton over long distance occurs, as revealed by COSY. Thus, the splitting pattern illustrated in Figure 2.2 is proposed for the proton whose signal appears as a *ddd*: geminal coupling ($^2J = 15.8$ Hz), vicinal coupling with the proton at C-4 ($^3J = 3.6$ Hz) and long distance coupling with the proton at N-1 ($^4J = 2.4$ Hz).

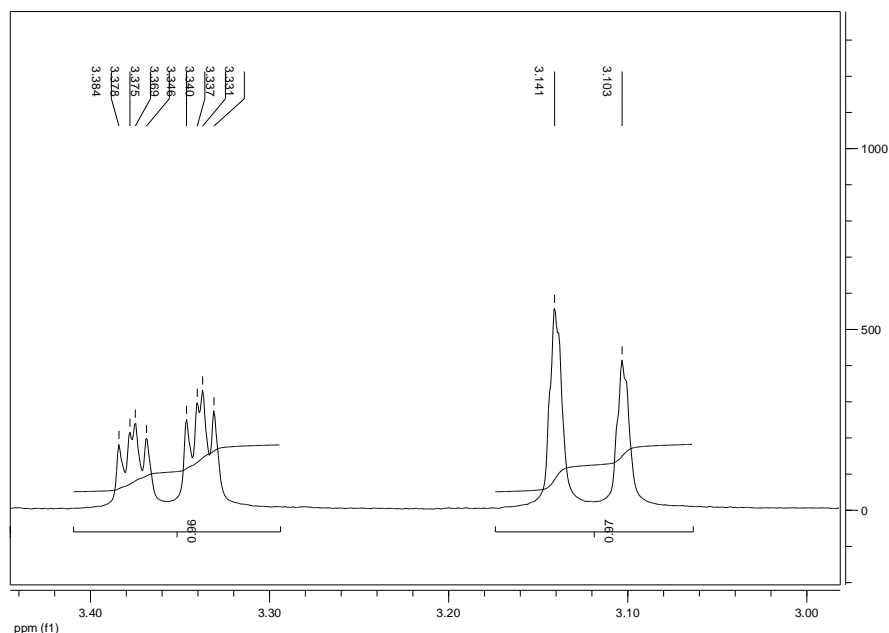


Figure 2.1 - Expansion of the observed signals of the spectrum of ^1H NMR for the protons at C-3 of compound **43a**.

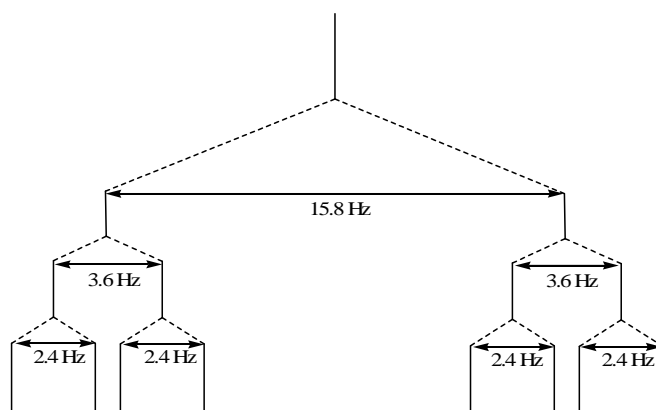


Figure 2.2 -Splitting pattern diagram of the signal corresponding to a *ddd* for the proton at C-3 of compound 43a.

Similarly, for the C-3 substituted derivatives, the methylene protons of the diethyl group at this position are diastereotopic and present distinct signals in the ^1H NMR spectra. Each of these protons present a doublet of quadruplets, due to geminal coupling with each other and with the neighbours $-\text{CH}_2\text{CH}_3$ (Figure 2.3).

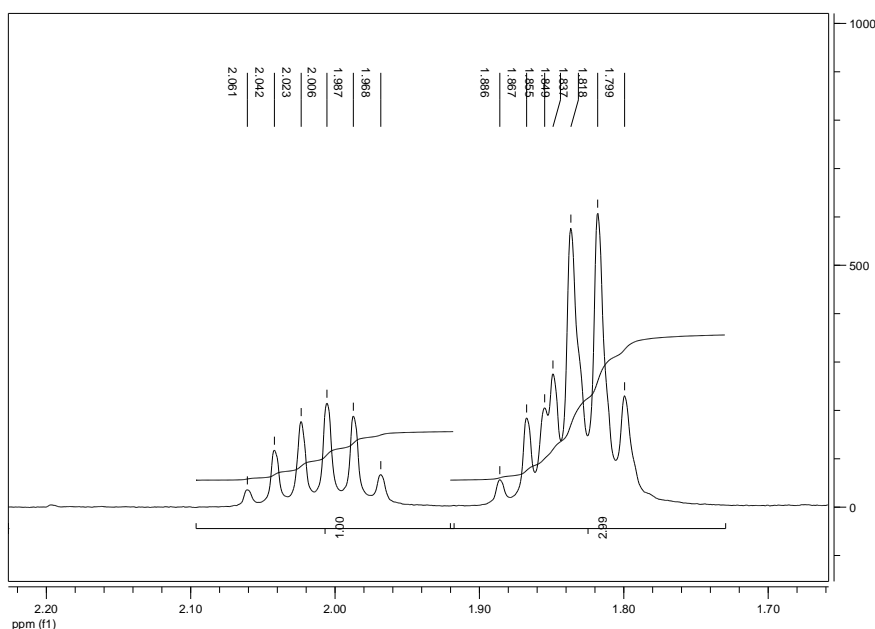


Figure 2.3 - Expansion of the observed signals of the spectrum of ^1H NMR for the $-\text{CH}_2$ protons of the diethyl group at C-3 of compound 47f.

The multiplet at right in Figure 2.3 consists of coincided resonance frequencies which integrate for 3 protons. The signal in the left is a doublet of quadruplets (${}^2J = 14.4$ Hz; ${}^3J = 7.2$ Hz) and integrates for 1 proton. The proposed splitting pattern for this proton is illustrated in Figure 2.4.

For the C-4 substituted N-carbamoylazetid-2-ones **47**, the methylene protons of the benzylurea moiety are also diastereotopic, exhibiting doublet of doublets for each methylene proton in the ${}^1\text{H}$ NMR spectra (Figure 2.5), in an AB splitting pattern.

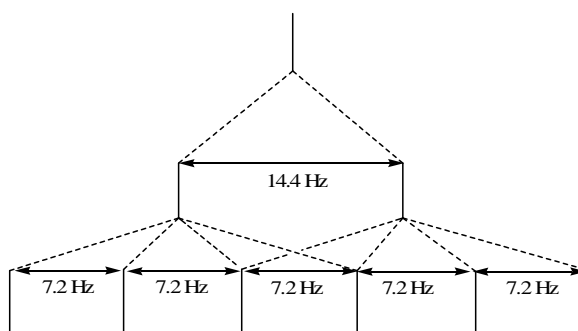


Figure 2.4 - Splitting pattern diagram of the signal corresponding to a doublet of quadruplets (Figure 2.3, left) for a methylene proton of the diethyl group at C-3 of compound **47f**.

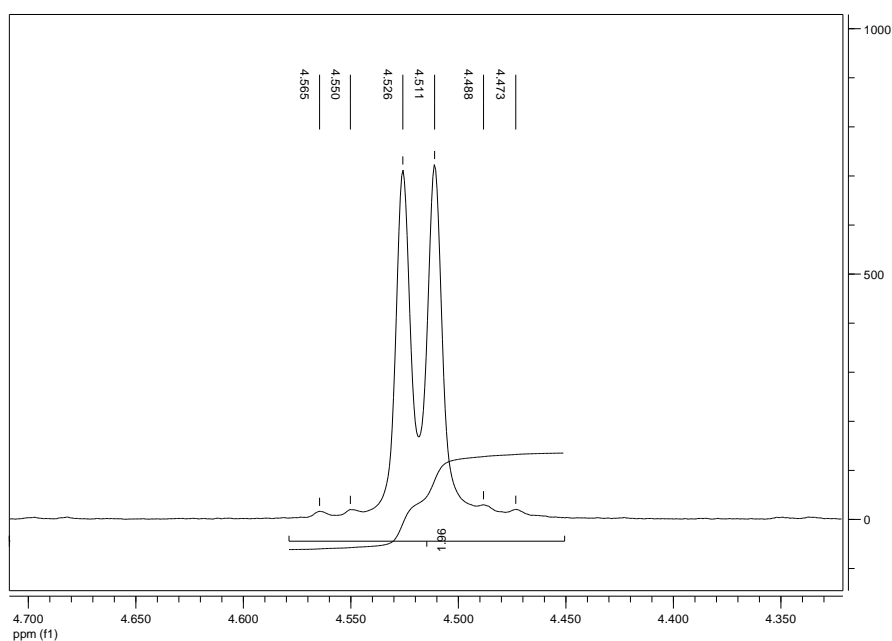


Figure 2.5 - Expansion of the observed signals of the spectrum of ${}^1\text{H}$ NMR for the methylene NHCH_2Ph protons of compound **47f**.

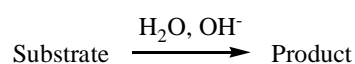
2.1.2 IR Spectroscopy

All synthesized compounds presented the characteristic β -lactam C=O IR stretching frequency, nearly 1745 cm^{-1} . The *N*-unsubstituted synthesized derivatives, **42**, **43** to **46** presented the N-H stretching frequencies ($3200\text{-}3280\text{ cm}^{-1}$). Compounds **47** exhibited an additional C=O IR stretching frequency, corresponding to the carbonyl group of the urea moiety (1700 cm^{-1}).

2.2. ALKALINE HYDROLYSIS STUDIES

2.2.1 Introductory Remarks

As already mentioned, alkaline hydrolysis studies are an important tool in the design of serine protease inhibitors. The general reaction of hydroxide-ion catalyzed hydrolysis is presented in Scheme 2.4, and the rate law can be described by Equation 2.1,



Scheme 2.4 - The general reaction of hydroxide-ion catalyzed hydrolysis.

$$-d[S]/dt = k_0[S] + k_{\text{OH}^-}[\text{OH}^-][S] \quad (2.1)$$

where $[S]$ is the concentration of the substrate, k_0 is the kinetic constant of the uncatalyzed reaction (spontaneous) and k_{OH^-} is the kinetic constant of the reaction catalyzed by hydroxide ion. Since the concentration of hydroxide ion, $[\text{OH}^-]$, is much higher than $[S]$, it is assumed that it remains constant (pseudo-first order conditions), giving:

$$k_{\text{obs}} = k_0 + k_{\text{OH}^-}[\text{OH}^-] \quad (2.2)$$

being k_{obs} the pseudo-first-order rate constant and k_{OH^-} the second-order rate constant for alkaline hydrolysis. Kinetic studies were performed by UV-spectroscopy at 25 °C, in aqueous buffers of sodium hydroxide, with 0.5 M ionic strength (NaClO_4) and 20% (v/v) acetonitrile, under pseudo-first-order conditions.

2.2.2 Results and Discussion

First, the wavelengths to be used in the kinetic studies were selected, by following the reaction of hydroxide with each compound, in a repeated spectral scanning over the wavelength range of 400-200 nm. Then, the kinetic measurements were performed at the selected wavelength in a time course mode. The hydrolysis showed first-order kinetics and the k_{obs} values were determined following the absorbance decrease or increase until at least 4 half-lives. In Figure 2.6 are represented the progress curves of the alkaline hydrolysis of **47f** in three different concentrations of hydroxide.

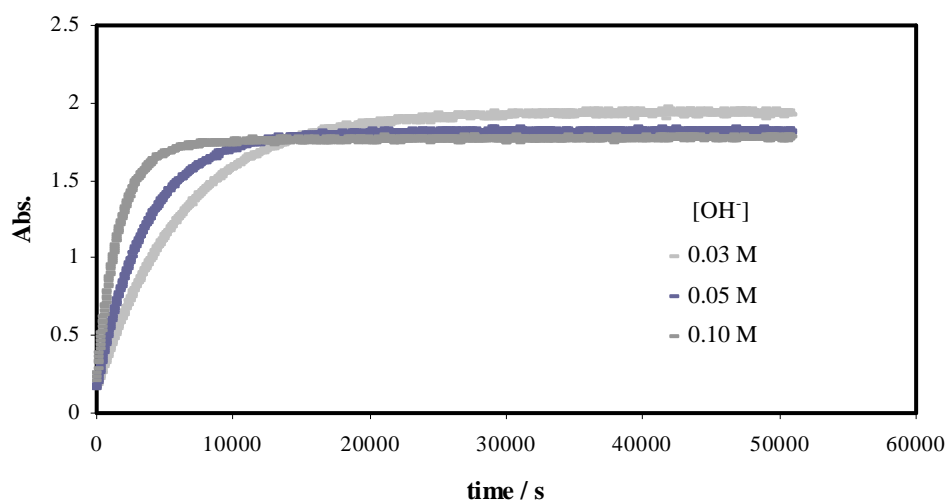


Figure 2.6 -Time course for the alkaline hydrolysis of **47f**. Concentrations of sodium hydroxide: 0.03 M, 0.05 M and 0.10 M (25 °C, ionic strength = 0.5 M, $\lambda = 238$ nm).

A linear dependence between k_{obs} and the concentration of hydroxide ion $[\text{OH}^-]$ was observed for all compounds (k_{obs} values presented in *Appendix 1, Section A1.1*), and the gradients of the plots of k_{obs} versus $[\text{OH}^-]$ gave the second-order rate constant for

alkaline hydrolysis, k_{OH^-} . The intercepts of those plots were indistinguishable from zero, thus accordingly to Equation 2.2, k_0 is zero. Next, the results for the determination of k_{OH^-} are presented and the final k_{OH^-} values are listed in Table 2.3.

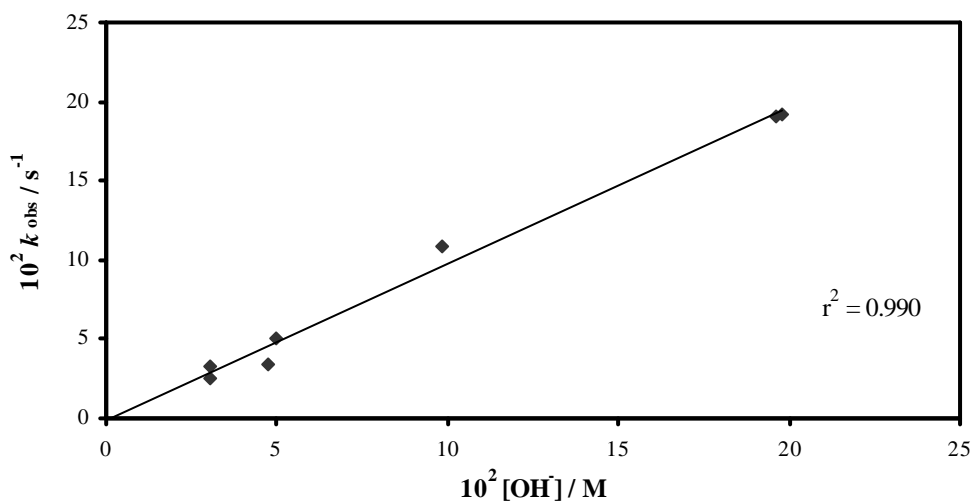


Figure 2.7 - Plot of the pseudo-first-order rate constants, k_{obs} for the alkaline hydrolysis of compound 47b, against hydroxide concentration, at 25 °C and ionic strength 0.5 M. Points are experimental and the line is from linear regression analysis of the data.

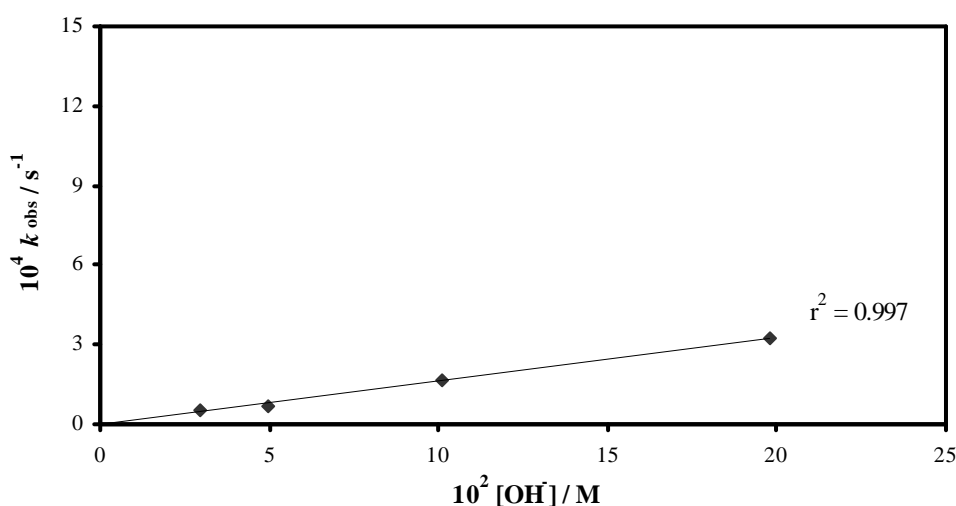


Figure 2.8 - Plot of the pseudo-first-order rate constants, k_{obs} for the alkaline hydrolysis of compound 47e, against hydroxide concentration, at 25 °C and ionic strength 0.5 M. Points are experimental and the line is from linear regression analysis of the data.

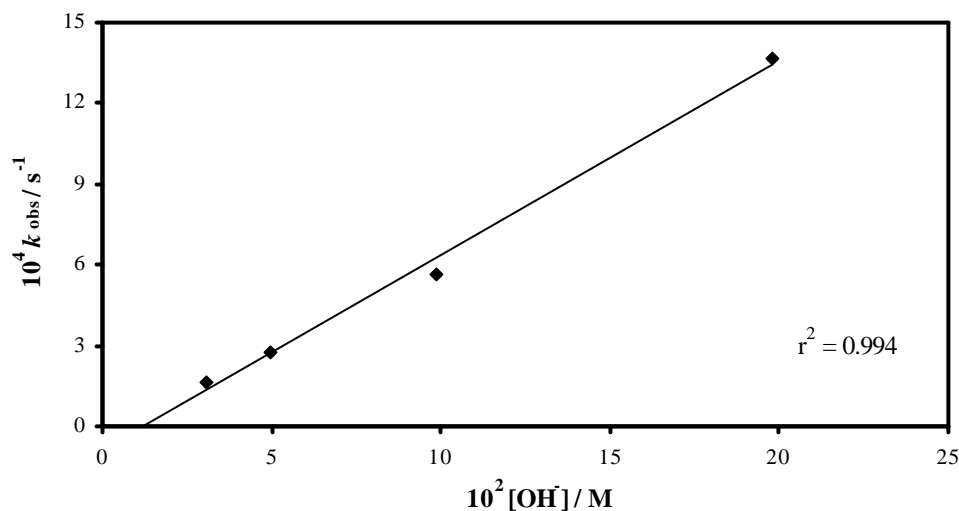


Figure 2.9 - Plot of the pseudo-first-order rate constants, k_{obs} for the alkaline hydrolysis of compound **47f**, against hydroxide concentration, at 25 °C and ionic strength 0.5 M. Points are experimental and the line is from linear regression analysis of the data.

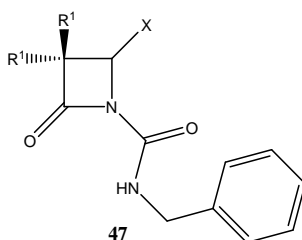
2.2.2.1 Free Energy Relationships for the Alkaline Hydrolysis of **47**

The alkaline hydrolysis of C-4 substituted *N*-carbamoylazetid-2-ones **47** involves nucleophilic attack of hydroxide at the carbonyl carbon of the β -lactam, in a ring-opening reaction, with expulsion of the leaving group at C-4, as previously demonstrated by Merck Research Laboratories¹⁰⁴ and also by Dr. Luísa Martins at the host laboratory.¹²⁰ In this work we investigated the effect of the C-4 substituents on the intrinsic chemical reactivity and on the mechanism of hydrolysis, and the results are presented in this section. It was of interest to investigate if the departure of the leaving group at this position was concerted with the β -lactam ring opening, as previously suggested by Merck.¹⁰⁴ Thus, combining the kinetic data of alkaline hydrolysis obtained by Dr. Luísa Martins¹²⁰ with the results of the present study, two series of Taft of *N*-carbamoylazetid-2-ones with different substituents at C-4 of general structure **47** are obtained (Table 2.3).

One of the series is not substituted at C-3, and it includes compound **47b**. The other series is substituted at this position, and it includes compounds **47e** and **47f**. Thus, from the data set of Table 2.3, it is possible to establish empirical correlations of

kinetics of each series with the substituent at C-4, using the respective linear free energy relationships for alkaline hydrolysis.

Table 2.3 - The second-order rate constants for the alkaline hydrolysis of 4-substituted N-carbamoylazetid-2-ones, k_{OH^-} , at 25 °C, and the $\text{p}K_{\text{a}}$ and σ_{I} for the C-4 substituents.



C-3 unsubstituted series				
$R_1 = \text{H}$				
Compound	X	$\text{p}K_{\text{a}}$ (XH)	σ_{I} ^c	$k_{\text{OH}^-} / \text{M}^{-1}\text{s}^{-1}$
47a	H	35 ^a	0	0.130 ^d
47b	PhO	9.92 ^b	0.39	0.990
47c	PhS	6.52 ^b	0.3	0.441 ^d
47d	PhSO ₂	1.29 ^b	0.57	4.16 ^d
C-3 gem-diethyl substituted series				
$R_1 = \text{Et}$				
Compound	X	$\text{p}K_{\text{a}}$ (XH)	σ_{I} ^c	$k_{\text{OH}^-} / \text{M}^{-1}\text{s}^{-1}$
47e	H	35 ^a	0	1.64×10^{-3}
47f	PhO	9.92 ^b	0.39	7.22×10^{-3}
47g	PhS	6.52 ^b	0.3	7.13×10^{-3} ^d
47h	PhSO ₂	1.29 ^b	0.57	1.42×10^{-1} ^d
47i	PhCH ₂ S	9.27 ^b	0.25	3.62×10^{-3} ^d
47j	PhCH ₂ SO ₂	1.45 ^b	0.6	1.27×10^{-1} ^d

^a From ref. ¹²⁴, ^b From ref. ¹²⁵, ^c From ref. ¹²⁶; ^d Data from ref. ¹²⁰.

Effect of the pK_a of the leaving group at C-4. A consequence of the dependency of the hydroxide-ion catalyzed hydrolysis upon the C-4 leaving group ability would be rate dependency on the pK_a of the leaving group. However, comparison of the k_{OH^-} values presented in Table 2.3 reveals that the reactivity of β -lactams **47**, for both C-3 substituted and unsubstituted series, correlates poorly to the pK_a of the leaving group at C-4 of the β -lactam moiety. For example, compound **47c** is only two-fold more reactive than **47a**, despite the 5-fold difference on the pK_a of the substituent at C-4. A poor correlation ($r^2 = 0.734$) was found between $\log k_{OH^-}$ values and the pK_a of the leaving group at C-4 for compounds **47a-d**, corresponding to a β_{lg} value of -0.04. Furthermore, for the 3,3-diethyl series **47e-j**, a poorer correlation was observed ($r^2 = 0.588$), corresponding to a β_{lg} value of -0.05 (for Brønsted plots, see *Appendix 1, Figures A1.1 and A1.2*). These small β_{lg} values are indicative that there is effectively no change in the effective charge on the leaving group on going from the ground state to the transition state for both series.

Effect of the Electronic Properties (σ_I) of the C-4 Substituent. The rate of alkaline hydrolysis ($\log k_{OH^-}$) is linearly correlated with σ_I values for the substituents at C-4, yielding ρ_I values of 2.8 and 3.4 for the series **47a-d** and **47e-j**, respectively (Figure 2.10). It is important to stress that the C-4 substituent in compounds **47a** and **47e** is X = H, and departure of the C-4 substituent would involve the expulsion of hydride ion, which does not occur. However, for each series, the substituents at C-4 which might be and those which cannot be expelled are correlated in the same correlations of free energies. These results suggest that the nucleophilic attack by hydroxide to the β -lactam carbonyl carbon atom is not concerted with the departure of the leaving group at C-4 and there is no expulsion of the leaving group at C-4 in the rate-limiting step of hydrolysis.

These ρ_I values are large end positive (Figure 2.10), and are consistent with the development of substantial negative charge in the transition-state, suggesting that the rate-limiting step is the attack of hydroxide-ion on the β -lactam carbonyl atom and that the effect exerted by C-4 substituents on the alkaline hydrolysis of **47** is purely inductive.

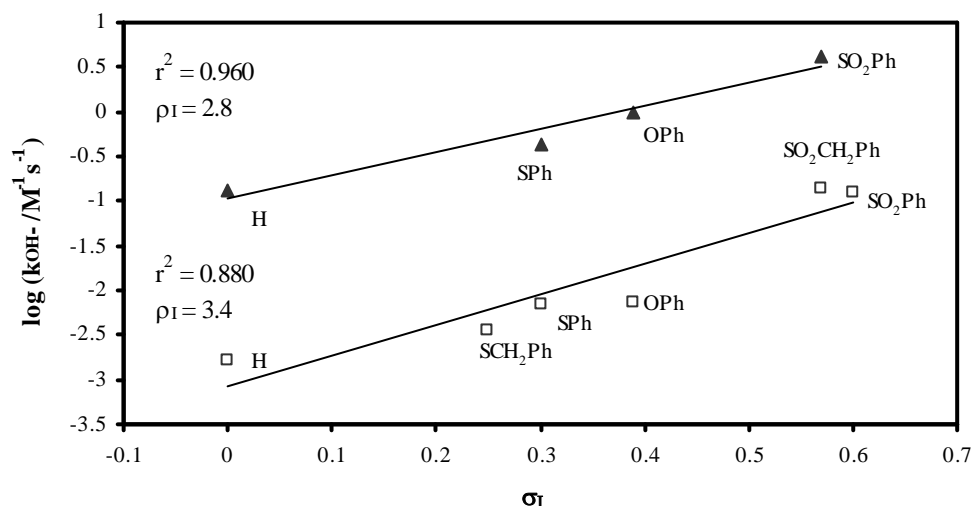


Figure 2.10 - Linear correlation between the second-order rate constants for the alkaline hydrolysis, k_{OH^-} of C-3 unsubstituted β -lactams 47a-d (▲) and C-3 gem-diethyl β -lactams 47e-j (□) and the Taft σ_{I} value for the X substituents in C-4, yielding ρ_{I} values of 2.8 and 3.4 for the series 47a-d and 47e-j, respectively. Lines are from linear regression analysis of data.

The higher ρ_{I} value determined for the 3,3-diethyl series compared to the C-3 unsubstituted series is consistent with a less favourable high energy tetrahedral intermediate, **52** (Figure 2.11) in which the two C-O bonds are eclipsed with the ethyl groups at C-3. According to the Hammond postulate,¹²⁷ this higher ρ_{I} value corresponds to a later transition state for the C-3 diethyl series, with significant negative charge buildup, and thus more susceptible to the stabilizing effect of electron-withdrawing groups at C-4.

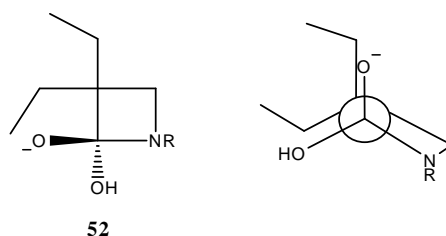


Figure 2.11 - Tetrahedral intermediate **52** ($\text{R}=\text{CONHCH}_2\text{Ph}$) for hydroxide ion attack at a 3,3-diethyl derivative, 47e, and the respective Newman projection obtained from looking along the C2-C3 bond of the β -lactam, showing the two C-O bonds eclipsed with the ethyl groups at C-3.

The results obtained for β -lactams **47** are comparable to those previously reported for the alkaline hydrolysis of the vinylogous cephalosporins containing a potential leaving group X at C-3', **53** (Figure 2.12). It was suggested that the mechanism of base-catalyzed hydrolysis of cephalosporins **53** involves nucleophilic attack on the β -lactam carbonyl carbon concerted with expulsion of the leaving group at C-3' (Figure 2.12, path a).¹²⁸

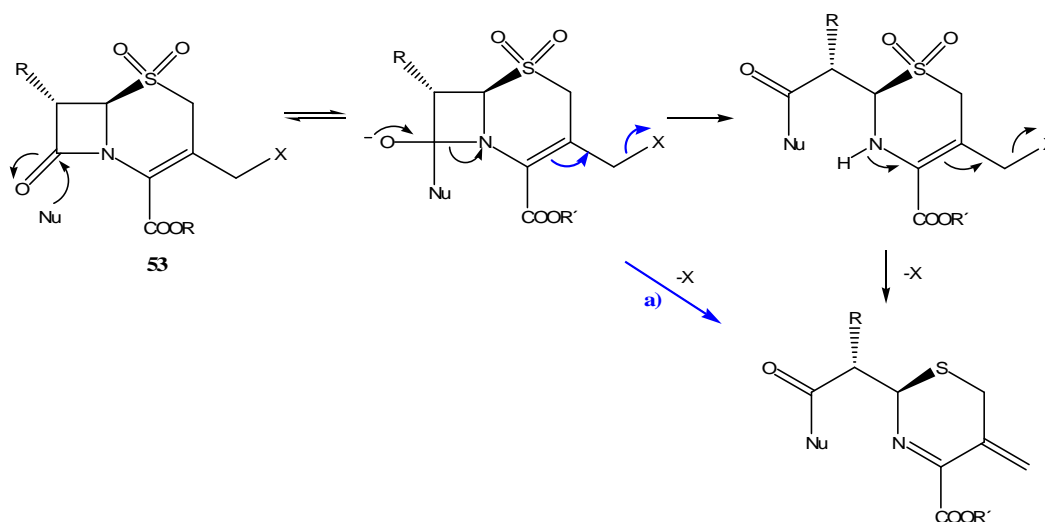


Figure 2.12 - Mechanism of ring-opening of a cephalosporin with a leaving group X at C-3' by nucleophilic attack at the β -lactam carbonyl carbon.¹²⁹

However, a Brønsted β_{lg} value close to zero was reported for the substituents at C-3' in alkaline hydrolysis of cephalosporins **53** ($\beta_{lg} = -0.06$),¹³⁰ which is comparable with the β_{lg} found in the present study for the alkaline hydrolysis of **47**. In addition, for the cephalosporin **53** in which X = H, the chemical reactivity was also similar to that of derivatives presenting a leaving group in this position. Furthermore, a thermodynamic correlation of $\log k_{OH^-}$ and σ_I values for the substituents at C-3' of **53** was found, including the compound in which X = H, giving a ρ_I value of 1.35.⁹² Thus, the effect exerted by the substituents at C-3' of cephalosporins **53** was purely inductive, and the rate-limiting step for the alkaline hydrolysis of **53** was the formation of the tetrahedral intermediate, similarly to the effect exerted by the C-4 substituents in the alkaline hydrolysis of **47**.

The difference in the magnitude of ρ_1 values of **53** and the compounds of the present study almost certainly reflects the shorter distance between the substituents and the nitrogen atom in the β -lactam scaffold of **47**.

2.2.2.2 Mechanism of the Alkaline Hydrolysis Reaction of **47**

C-3 Substituted Series. Previously reported studies on the alkaline hydrolysis of C-4 substituted 3,3-diethyl-N-benzylcarbamoylazetid-2-ones, included the identification of the reaction products.^{104, 120} It was demonstrated that the intermediate imine formed by expulsion of the leaving group from C-4 partitioned between hydrolysis giving benzylurea and a aldehyde-acid (path **a**, Figure 2.13) or decarboxylation, to produce a vinyl adduct (path **b**, Figure 2.13).¹⁰⁴ Taking into account these results with those obtained in the present study, the following mechanism is proposed for the alkaline hydrolysis of C-3 gem-diethyl **47e-j** derivatives. Contrary to the Merck's suggestion, it was now clarified that the nucleophilic attack of hydroxide at the β -lactam carbonyl carbon atom is not concerted with the expulsion of a leaving group at C-4.

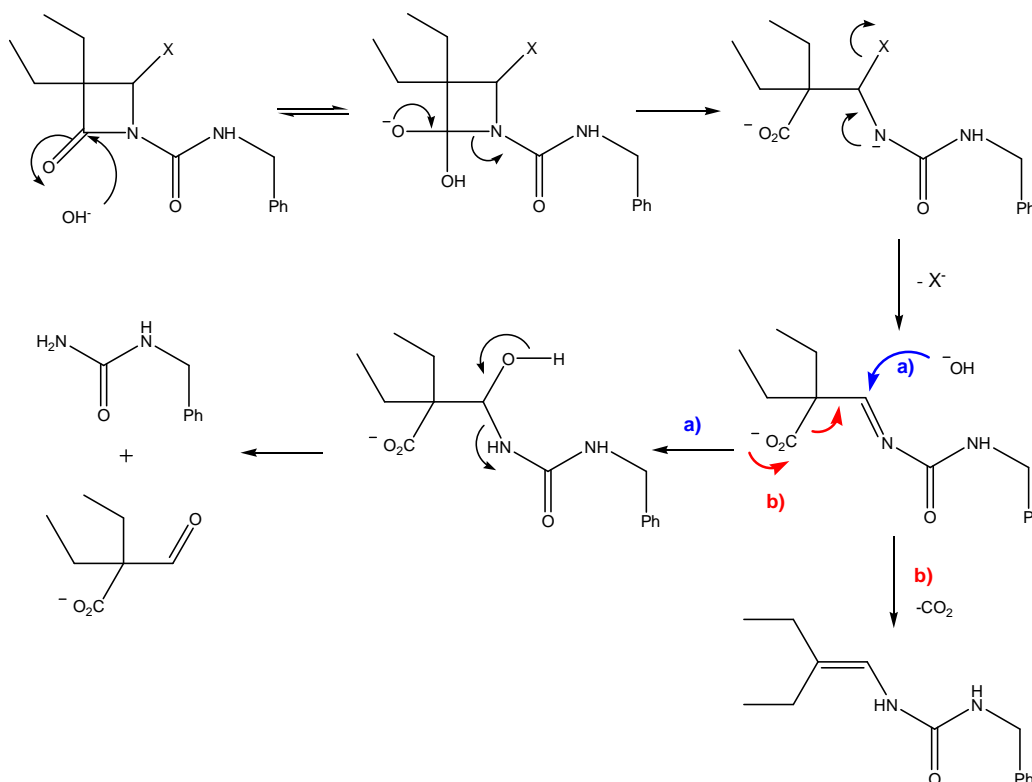


Figure 2.13 - Proposed mechanism of alkaline hydrolysis of C-3 substituted derivatives **47**.

C-3 Unsubstituted Series. The UV spectrum of the hydroxide solution containing the alkaline hydrolysis product from the C-3 unsubstituted compound **47b** had a broad maximum λ_{\max} at 255 nm. By addition of concentrated hydrochloric acid to the mixture, it was detected the emergence of a band at λ_{\max} 265 nm. After the subsequent addition of hydroxide, the band at 265 nm disappeared and the spectrum overlapped with the one acquired before the addition of acid, being indicative of an acid-base equilibrium. These data showed that a product was formed with λ_{\max} 255 nm, which did not absorb in acidic conditions. Similar observations were made by Dr. Luísa Martins for the alkaline hydrolysis of **47c-d**.¹²⁰

Analogue pH-dependent pattern of UV changes has also been reported for the alkaline hydrolysis of C-3 unsubstituted 4-aryloxy and 4-arylthioazetid-2-ones,¹²¹ and also N-acyloxymethylazetid-2-ones,¹³¹ and for such compounds it was reported to be a result of the formation of the enolate of 3-oxopropanamide, **54**, with a λ_{\max} 265 nm. Upon acidification, **54** reverted to its neutral form (Figure 2.14), with a λ_{\max} 237 nm.¹²¹

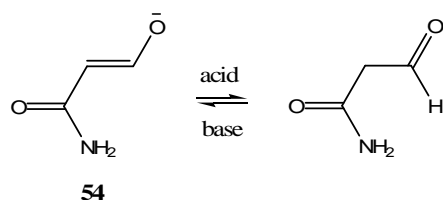


Figure 2.14 - The enolate of 3-oxopropanamide, **54**, formed by the alkaline hydrolysis of C-3 unsubstituted 4-aryloxy and 4-arylthioazetid-2-ones,¹²¹ and N-acyloxymethylazetid-2-ones.¹³¹

With this background, it seems that an enolate is also formed for the alkaline hydrolysis of C-3 unsubstituted N-carbamoyl derivatives **47** and the proposed mechanism is illustrated in Figure 2.15.

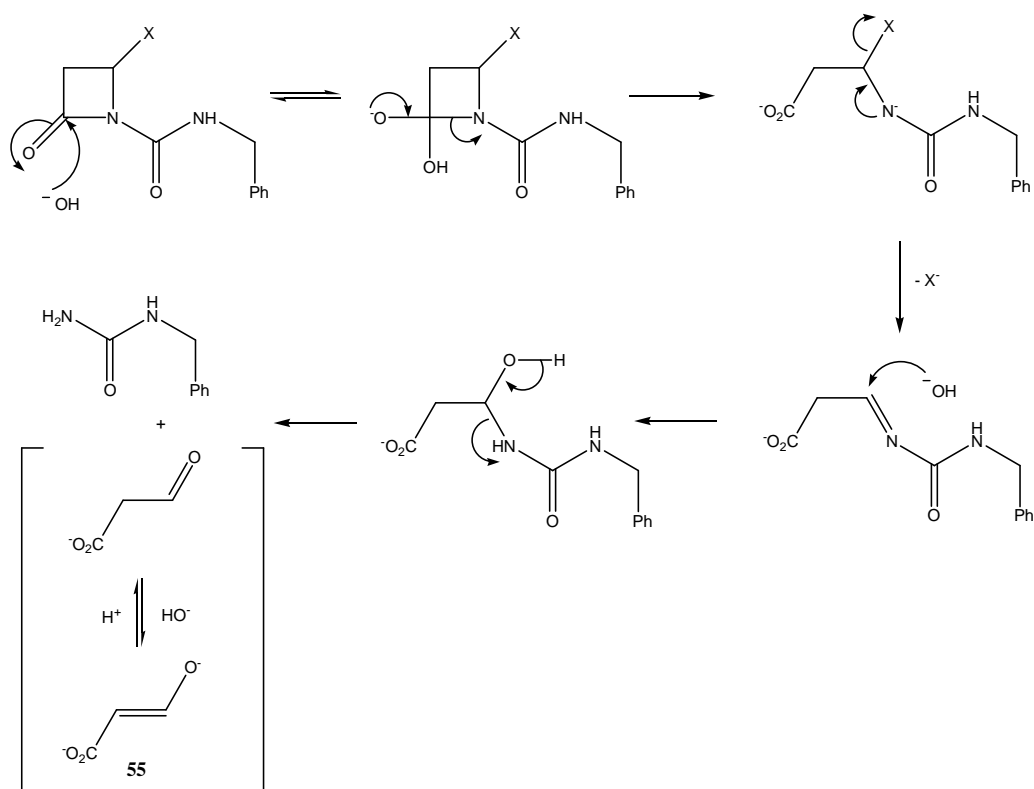


Figure 2.15 - Proposed mechanism of alkaline hydrolysis of C-3 unsubstituted derivatives 47.

Compound **55** (Figure 2.15) is likely to be the enolate responsible for the pH-dependent UV pattern, with a broad maximum λ_{max} of 255, which is near of the previously reported for the analogue enolate **54**.

Inspection of Figures 2.13 and 2.15 reveals that the alkaline hydrolysis reaction mechanism is similar for both C-3 substituted and unsubstituted series. However, the C-3 gem-diethyl analogues cannot form the enolate, thus they do not present the UV-pH dependent pattern with λ_{max} of 255.

For both series, the rate limiting step of the alkaline hydrolysis reaction is the formation of the tetrahedral intermediate. Thus, the strain energy of the four-membered ring is not released in the transition state to lower the activation energy. In fact, the reactivity of β -lactams could be a consequence of the inherent thermodynamic strain of cyclic amide within the four-membered ring, involving bond angle as well as rigid torsional strain, and the rate-limiting step could be the

breakdown of the tetrahedral intermediate. However, the reluctance of the β -lactam ring to open has been noted previously.^{132, 133} It was demonstrated that the chemical reactivity of β -lactams is not much different to that of acyclic amides, as the second-order rate constant for the alkaline hydrolysis, k_{OH^-} , of the *N*-methyl- β -lactam **56** ($6.1 \times 10^{-6} \text{ M}^{-1} \text{ s}^{-1}$) is only 3-fold superior than *N,N*-dimethyl ethanamide, **57** ($2.3 \times 10^{-6} \text{ M}^{-1} \text{ s}^{-1}$).¹³⁴ This is in contrast to the possible up to 10^{20} -fold rate enhancement estimated from releasing the strain energy of a four-membered ring ($26\text{-}29 \text{ kcal mol}^{-1}$) than an analogous acyclic system. Thus, the β -lactam ring must be intact in the rate-limiting step.¹³⁰



In the present study, the ureido anion expulsion from the tetrahedral intermediate of **47** may occur at a rate that is comparable or even faster than that for hydroxide ion. Electron-withdrawing substituents at C-4 facilitate the alkaline hydrolysis, dispersing the negative charge density at the reaction site and stabilizing the negatively charged transition state. Thus, derivatives containing the electron-withdrawing 4-phenylsulfonyl group were the most reactive for both series.

The rate of alkaline hydrolysis depends not only on the electronic properties of the substituent on C-4, but also on the substitution on C-3. Indeed, there is a large steric effect of the substituents at C-3 on the rate of the reaction, as comparison of compounds **47a** and **47f** reveals a decrease in reactivity in about 135-fold for the C-3 substituted derivative. These results are also compatible with the rate-limiting step being the formation of the tetrahedral intermediate.

2.3. ENZYME INHIBITION STUDIES

2.3.1 PPE Inhibition Studies

2.3.1.1 Introductory remarks

The inhibitory activity of PPE was determined at 25 °C, using the chromogenic substrate *N*-suc-(L-Ala)₃-*p*-nitroanilide, **58** (Figure 2.16). By PPE-catalyzed hydrolysis of this substrate, the *p*-nitroaniline is released, being the reaction monitored at 390 nm.

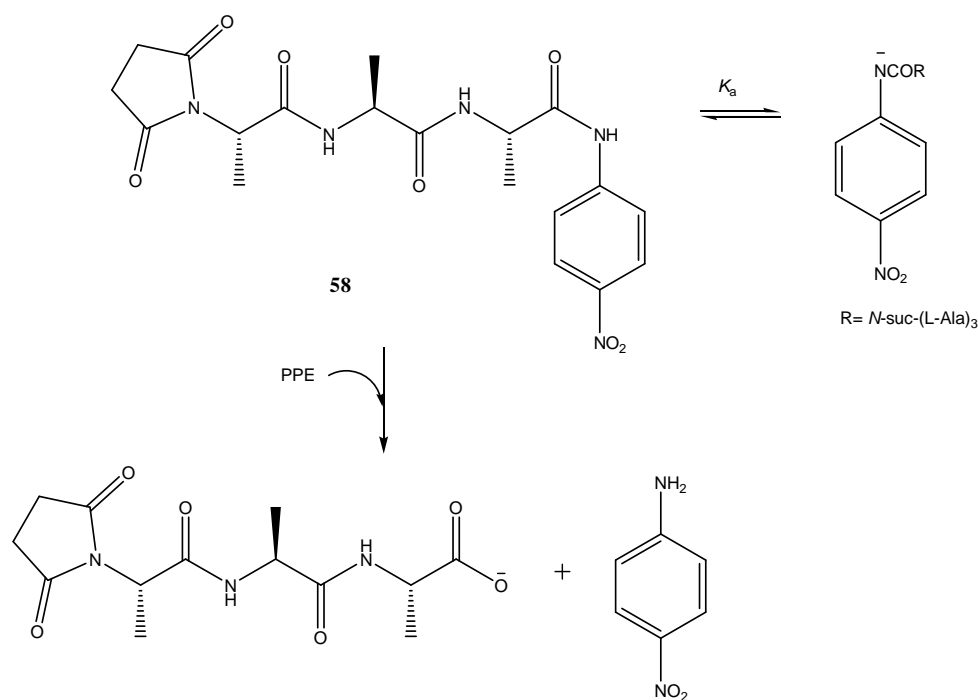


Figure 2.16 - Hydrolysis of the chromogenic substrate *N*-suc-(L-Ala)₃-*p*-nitroanilide, **58**.¹³⁵

It was demonstrated by Hinchliffe *et al* that this substrate undergoes hydrolysis in the presence of hydroxide, with a pH-independent reaction above pH 13.¹³⁵ On the other hand, accordingly to the pH-PPE-activity profile reported by the same authors, the enzyme has an active site ionisable group with a pK_a of 6.88 (presumably His-57), and it is only active when this group is deprotonated, with a pH optimum of 8.5. Thus,

inhibition assays were performed at pH 7.2, in order to avoid competition of non-enzymatic-mediated hydrolysis.

2.3.1.2 Determination of the K_m

The determination of K_m was performed at 25 °C, collecting the initial rates of the hydrolysis of the substrate **58** catalyzed by PPE, at different concentrations of substrate, with no saturation of the enzyme (*Appendix 1, Section A1.3*).

The Lineweaver-Burke plot was used to obtain the kinetic parameters of PPE catalysis (Figure 2.17). Rates in Ms^{-1} were obtained by dividing the initial absorbance increase in $\Delta A \text{ s}^{-1}$ by the molar extinction coefficient for the hydrolysis product *p*-nitroaniline at 390 nm, ϵ_{390} , which was previously determined by a Beer-Lambert plot under identical experimental conditions (data presented in *Appendix 1, Section A1.2*).

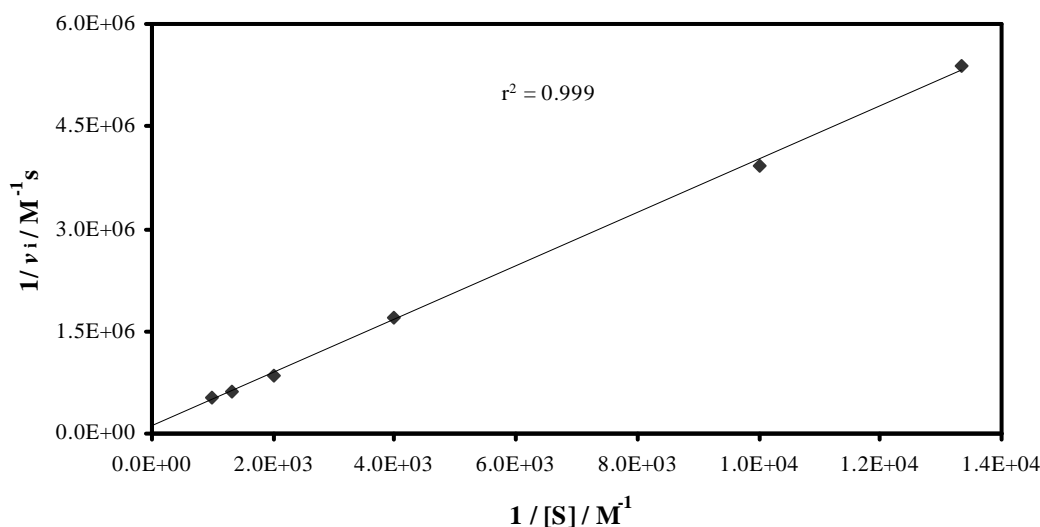


Figure 2.17 - Lineweaver-Burke plot for the PPE-catalyzed hydrolysis of *N*-suc-(L-Ala)₃-*p*-nitroanilide, **58**, in 0.1 M HEPES buffer, pH 7.2, at 25 °C, [PPE] = 1×10^{-6} M.

The obtained results are: $K_m = (3.81 \pm 0.53) \times 10^{-3}$ M, $V_{\max} = (9.75 \pm 1.02) \times 10^{-6}$ Ms^{-1} , $k_{\text{cat}} = 9.75 \text{ s}^{-1}$ and the second-order rate constant $k_{\text{cat}}/K_m = 2.56 \times 10^3 \text{ M}^{-1} \text{ s}^{-1}$. This K_m value is consistent with the one reported in the literature ($K_m = 4.92 \times 10^{-3}$ M).¹³⁵ In

fact, although being convenient for UVs assays, the substrate *N*-suc-(L-Ala)₃-*p*-nitroanilide has a relatively high K_m value, reflecting a poor degree of enzyme-substrate binding.

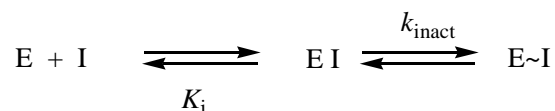
2.3.1.3 Inhibition Assays

In order to determine the effect of the substituent at C-4 of *N*-carbamoylazetid-2-ones in the PPE-mediated hydrolysis in the absence of molecular recognition elements for S₁ binding pocket, compounds **47a-d** were assayed. To determine the effect of the C-3 substituent, compound **47f** was also tested. Kinetics inhibition assays were performed using the Kitz and Wilson's pre-incubation method.¹³⁶ Thus, both PPE and inhibitor were incubated together, in 0.1 M HEPES buffer, pH 7.2, at 25 °C. Aliquots of the incubation mixture were withdrawn at different time intervals and assayed for PPE activity, monitoring spectrophotometrically the hydrolysis of *N*-suc-(L-Ala)₃-*p*-nitroanilide, **58**. The experiments were repeated at least twice for each concentration and different concentrations of inhibitor were used. For time-dependent inhibitors, the enzyme activity tends towards zero increasing incubation time and also depends on the concentration of the inhibitor.

Control assays were performed under the same conditions, but in absence of inhibitor, and the enzyme activity remained constant throughout the experiments; with the initial rate for the hydrolysis of the substrate, v_i , being equal to 100% of PPE activity. The remaining activity at incubation time t was expressed as percentage, and was given by $(v_t/v_i) \times 100$, being v_t the reaction rate at time t . The pseudo-first-order rate constants of enzyme inactivation were calculated by exponential regression-type analysis of PPE remaining activity *versus* time, using Equation 2.3 (an example is given in Figure 2.18),

$$A = A_0 e^{-kt} \quad (2.3)$$

being A the PPE activity at a time t ; A_0 the PPE activity in the control assay; k , the pseudo-first-order rate constants of PPE inactivation (k_{obs}) and t the incubation time in second. The observed rate constant k_{obs} of the reaction of an irreversible inhibitor with an enzyme may be described by Kitz and Wilson's model, (Scheme 2.5).¹³⁶



Scheme 2.5 - Kitz and Wilson's model for irreversible enzyme inhibition.¹³⁶

where K_i is the dissociation constant of the enzyme-inhibitor complex and k_{inact} is the first-order rate constant for the inactivation step. Overall, this process is described by Equation 2.4. This kinetic expression corresponds to a hyperbolic dependence of k_{obs} with the concentration of inhibitor, [I].

$$k_{\text{obs}} = k_{\text{inact}} [\text{I}] / (K_i + [\text{I}]) \quad (2.4)$$

However, when $K_i \gg [\text{I}]$, Equation 2.4 simplifies to Equation 2.5, and k_{obs} is linearly dependent on [I].

$$k_{\text{obs}}/[\text{I}] = k_{\text{inact}}/K_i \quad (2.5)$$

Thus, the second-order rate constants for PPE inhibition, $k_{\text{obs}}/[\text{I}]$, were given by the gradient of the plots of k_{obs} against the inhibitor concentration and are indicative of the inhibitory potency.

2.3.1.4 Results and Discussion

Compound **47a** was found to be non inhibitor of PPE, even when assayed at a concentration of 1 mM in the incubation mixture. Compounds **47b-d** were found to be time-dependent inhibitors of PPE, suggesting an irreversible process of inactivation. The k_{obs} values for compounds **47b-d**, calculated as shown in Figure 2.18, are listed in *Appendix 1, Table A1.3* and the final plots for determination of $k_{\text{obs}}/[\text{I}]$ for these compounds are represented in Figures 2.19 and 2.20.

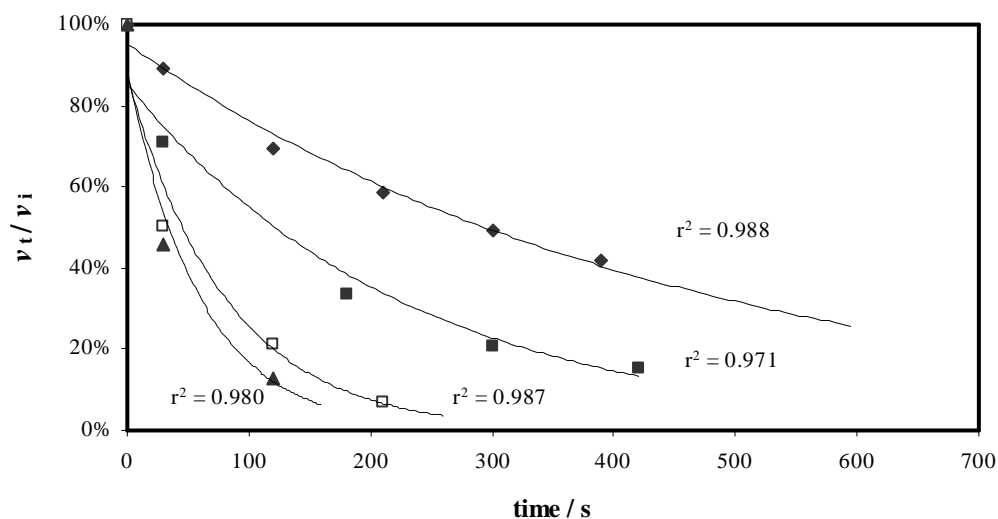


Figure 2.18 - Plot of the PPE remaining activity against incubation time for compound 47d, at 10 μM (\blacklozenge), 20 μM (\blacksquare), 40 μM (\square), and 50 μM (\blacktriangle), in the incubation mixture, at 25 $^{\circ}\text{C}$, in 0.1 M HEPES buffer, pH 7.2. Points are experimental and lines are from exponential regression analysis of the data, to yield the k_{obs} values for each concentration, accordingly to Equation 2.3.

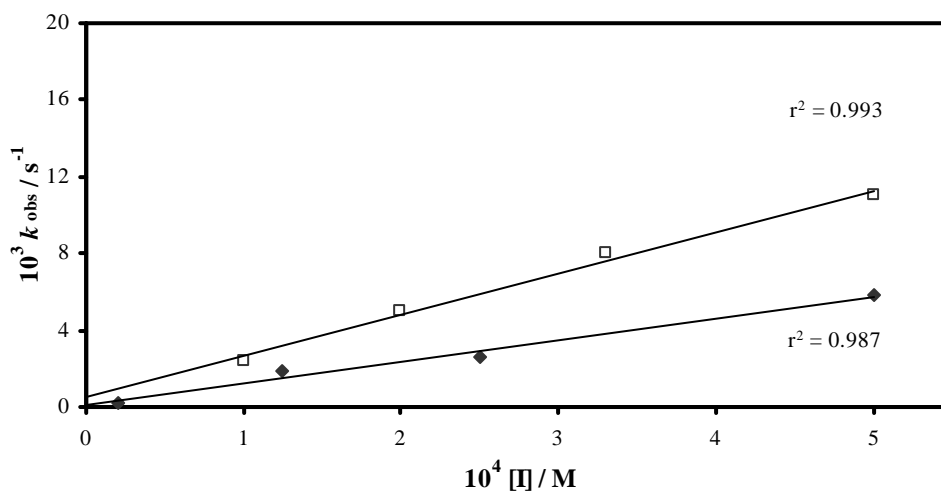


Figure 2.19 - Plot of the pseudo-first-order rate constants, k_{obs} for the inactivation of PPE by compounds 47b (\blacktriangle), and 47c (\square), against inhibitor concentration, at 25 $^{\circ}\text{C}$ and pH 7.2 buffer. Points are experimental and lines are from linear regression analysis of the data, giving the second-order rate constants, $k_{\text{obs}}/[\text{I}] = 11.33 \pm 0.92 \text{ M}^{-1}\text{s}^{-1}$ for 47b, and $k_{\text{obs}}/[\text{I}] = 21.67 \pm 1.20 \text{ M}^{-1}\text{s}^{-1}$ for 47c.

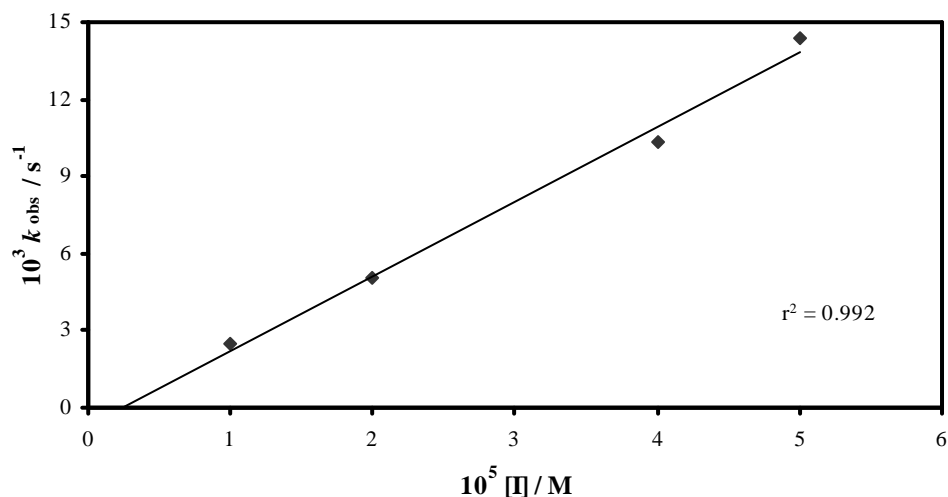


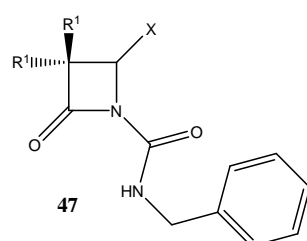
Figure 2.20 - Plot of the pseudo-first-order rate constants, k_{obs} for the inactivation of PPE by compound **47d**, against inhibitor concentration, at 25 °C and pH 7.2 buffer. Points are experimental and the line is from linear regression analysis of the data, giving the second-order rate constant for PPE inhibition $k_{obs}/[I] = 290.4 \pm 18.96 \text{ M}^{-1}\text{s}^{-1}$.

The 3,3-diethyl derivative **47f**, was completely inactive against PPE in a concentration up to 0.5 mM. The results for PPE inhibition are listed in Table 2.5. Values of k_{OH^-} were also included for comparison with the inhibitory potency as well as the respective enzyme rate enhancement factors, EREFs, given by $k_{obs}/[I]/k_{OH^-}$.

Structure Activity Relationships. The C-3 unsubstituted compounds presenting leaving groups at C-4, **47b-d**, were time-dependent inhibitors of PPE, while the compound without a leaving group **47a** was inactive. The second-order rate constants of the PPE-catalyzed hydrolysis of **47** revealed a low correlation with the pK_a of the leaving group at C-4 (values of pK_a were presented in Table 2.4). Interestingly, the Brønsted plot gave a β_{lg} value of -0.16 for the PPE-catalyzed reaction ($r^2 = 0.954$, Appendix 1, Figure A1.5), but it was determined with only three points and must be analyzed with caution. This small value may indicate a small change in charge on the leaving group on going from the ground state to the transition state. One must note that the phenylsulfonyl derivative **47d** was only 25-fold more active than its 4-phenoxy analogue, **47b**, despite the 9-fold difference between the leaving group

abilities of phenylsulfinate and phenolate. Compared with the β_{lg} value of -0.04 for the alkaline hydrolysis (data presented *Appendix 1, Figure A1.1*), this β_{lg} value of -0.16 surprisingly may indicate more change in charge, with a little more dependence of the rate of the enzyme catalyzed reaction with the inhibitor's C-4 leaving group ability.

Table 2.4 - Second-order rate constants for the time-dependent inactivation of PPE in pH 7.2 buffer at 25 °C and for the hydroxide-catalyzed hydrolysis of compounds 47a-f.



Compound	R ¹	X	$k_{obs}/[I]/ M^{-1}s^{-1}$	$k_{OH^-}/ M^{-1}s^{-1}$	EREF ^a
47a	H	H	NI ^b	0.221 ^c	–
47b	H	OPh	11.3± 0.92	0.990	11.4
47c	H	SPh	21.7± 1.20	0.441 ^c	49.0
47d	H	SO ₂ Ph	290±19.0	4.16 ^c	70.0
47f	Et	OPh	NI ^b	7.22×10 ⁻³	–

^a EREF enzyme rate enhancement factor; ^b No inhibition; ^c Data from ref. ¹²⁰.

In addition, a greater ρ_I value was found for the PPE-mediated hydrolysis of C-3 unsubstituted derivatives (data presented in *Appendix 1, Figure A1.6*), compared with the hydroxide-ion catalyzed reaction (4.7 versus 2.6). Once again, it was determined with only three points. These results may reflect a later transition state in the formation of the tetrahedral intermediate for the PPE-catalyzed reaction. This could be a result of the lack of molecular recognition elements at C-3, in such a way that it does not allow a favourable orientation of the tetrahedral intermediate for stabilization at the oxyanion hole. In this context, the magnitude of the EREF values for **47b-d** (Table 2.4) are very small compared with the EREFs values reported for an enzyme-

catalyzed reactions, which are of nearly 10^4 - 10^6 orders of magnitude.⁷² However, it is important to note that the C-3 substituted compound **47f** was found to be a non inhibitor of this enzyme. Indeed, the gem-diethyl group of **47f** may lead to a non-productive binding at the small S_1 pocket of PPE, which does not compensate the unfavourable steric hindrance introduced.

Interestingly, compound **47c**, which was chemically less reactive than **47b**, revealed a gain in molecular recognition by PPE rather than the 4-phenoxy analogue (Table 2.4, EREF). The sulfone derivative **47d** presented the higher EREF value and it was also found to be the best inhibitor of PPE of this series, with a $k_{\text{obs}}/[\text{I}]$ value of $290 \text{ M}^{-1}\text{s}^{-1}$. This result suggested that the electron-withdrawing sulfone function is a powerful activator of the β -lactam carbonyl carbon atom towards the Ser-195 hydroxyl group, even in the absence of an adequate molecular recognition moiety at C-3 in the β -lactam scaffold. Furthermore, compound **47d** was also the most reactive in the alkaline hydrolysis studies; thus increasing the intrinsic chemical reactivity led to a faster rate of enzyme inactivation (superior $k_{\text{obs}}/[\text{I}]$ value).

Inhibition of PPE by these compounds led to the β -lactam ring-opening with expulsion of the leaving group at C-4, with formation of a reactive imine which could be trapped by a second nucleophile within the active site. In fact, it could be trapped by His-57 in a possible suicide-type mechanism, or by a water molecule, in analogy with the mechanism of elastase inhibition discussed in Chapter 1, Figure 1.8. Thus, compound **47d** was further studied on the titration of enzymatic activity, to determine the partition ratio of inhibitory efficiency, and on crystallography studies of the correspondent acyl-enzyme complex.

Titration of PPE Activity by 47d. Further evidence of the efficiency of **47d** as an irreversible inhibitor of PPE comes from the determination of the partition ratio, r , which represents the number of molecules of inhibitor necessary to inactivate a single molecule of enzyme. The r value was calculated by plotting the percentage of remaining enzyme activity, v_t/v_i , after a 30 min incubation period with the inhibitor versus the initial ratio of inhibitor to enzyme, i.e. $[\text{I}]/[\text{E}]_0$ (Table 2.5). The extent of

inactivation was found to be linearly dependent on the inhibitor-to-enzyme molar ratio and extrapolation of the line to $v_t/v_i = 0$ yielded a partition ratio of ca. 1.2 equivalents for **47d** (Figure 2.21). Such high inhibitory efficiency was also reported for HLE inactivation by 3,3-diethylmonobactams.¹³⁷ For example, 1.3 equiv of the Merck's inhibitor L-680,833 are required to inactivate HLE to approximately 99%.¹³⁷

Table 2.5 - Percentage of remaining PPE activity, v_t/v_i , after a 30 min incubation period with **47d at 25 °C, versus the initial ratio of inhibitor to enzyme, $[I]/[E]_0$.**

$[I]/[E]_0$	v_t/v_i (%)
0	100.0
0.04	96.67
0.10	89.41
0.40	67.78
0.50	58.40
0.75	32.38
1.0	13.56
2.0	0

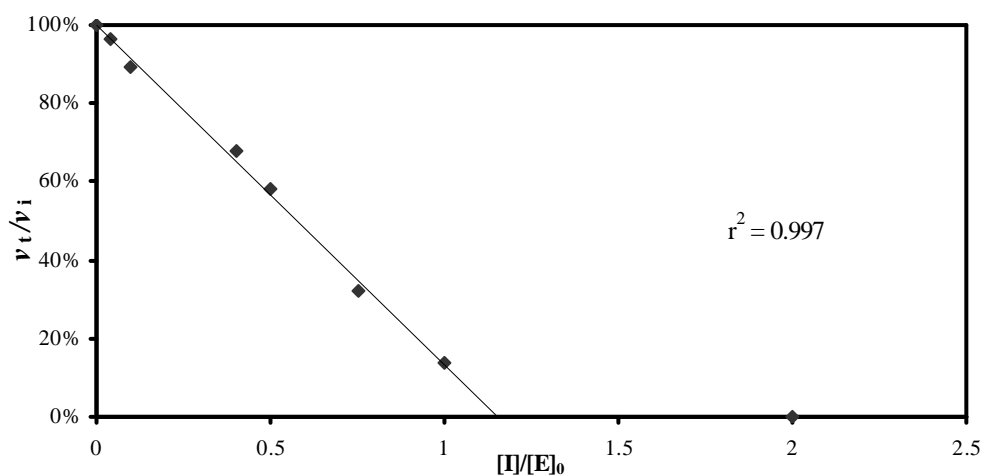


Figure 2.21 - Inactivation of PPE as a function of the molar ratio of inhibitor **47d to enzyme. PPE (10 μ M) and various amounts of inhibitor **47d** (20-0.4 μ M) in 0.1 M HEPES buffer, pH 7.2, were incubated at 25 °C for 30 min, and aliquots were withdrawn for assay. Points are experimental and the line is from linear regression analysis of the data.**

X-Ray Crystallography Studies. In order to confirm i) the formation of a covalent bond between the β -lactam carbonyl carbon of **47d** and the hydroxyl group of catalytic serine residue of PPE, and ii) the departure of the leaving group at C-4 with formation of a stable acyl-enzyme, X-ray crystallography studies were performed. These studies were kindly developed by Dr. Tania F. Oliveira and Prof. Margarida Archer, from the ITQB, Oeiras. PPE was incubated with **47d** for 30 minutes, and good quality crystals were grown and subjected to X-ray analysis. Data collection and crystallographic refinement statistics for the porcine pancreatic structure bound to **47d** are shown in Appendix 1, Table A1.4.

The electron density maps at the catalytic site and inspection of the structure determined at 1.66 Å (Figure 2.22) show that PPE inactivation by **47d** involves:

- β -lactam ring-opening, as revealed by the ester formed with Ser-195 O γ .
- departure of the leaving group phenylsulfinate from C-4.
- Interestingly, the crystal structure reveals the presence of a hydroxyl group at C-3 (β -lactam numbering), as a result of attack of a water molecule to the reactive acyl-enzyme formed. No “double-hit mechanism” adduct, due to attack of His-57 to the acyl-enzyme was found.

The structure of the crystallized acyl-enzyme is also represented in **59** (Figure 2.23). The presence of a hydroxyl group at C-3 is an unexpected result when compared with previous X-ray crystallographic studies of elastase complexed with β -lactams containing leaving groups at C-4. For example, inactivation of elastase by 4-aryloxy-3,3-diethyl- β -lactams leads to a carbinolamine acyl-enzyme, resulting from reaction of water at C-4 of the imine intermediate (discussed earlier in Section 1.6.2, Chapter 1).¹³⁸

In order to realize if this pattern of enzymatic reactivity to give **59** was inherent to the inhibitor **47d** or a function of the enzyme active site, a reaction of inhibitor **47d** was undertaken with excess of sodium methoxide in methanol, which has been reported as a good model reaction for the acylation of serine enzymes.^{72, 84} The product of the reaction was 3-benzylpyrimidine-2,4(1H,3H)-dione, **60**, in 80% yield (Figure 2.24). This result is consistent with methoxide-catalyzed β -lactam ring opening followed by

pyrimidine ring formation and phenylsulfinate elimination (or first the elimination then the ring closure).

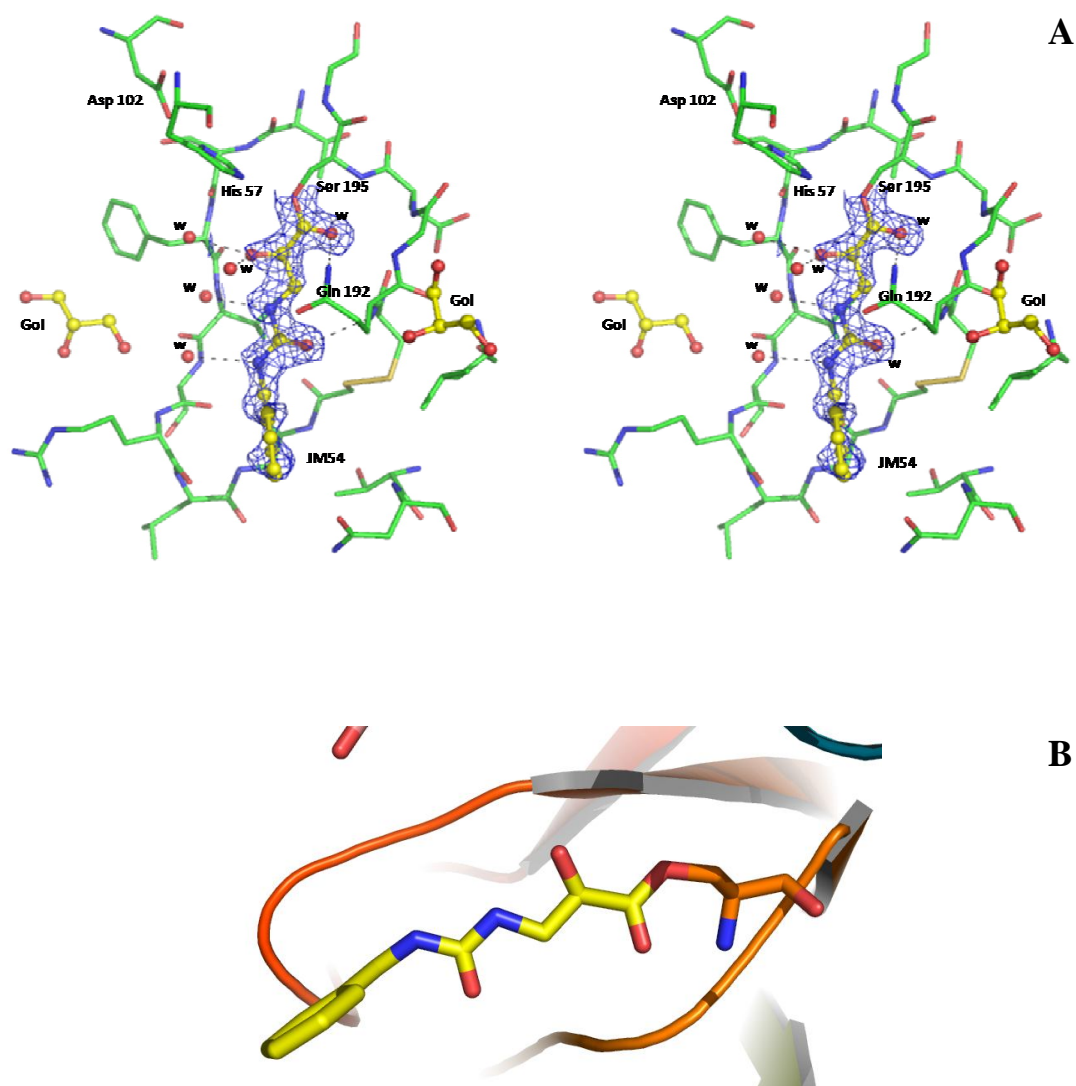


Figure 2.22 - A) A stereoview of the $|F_0| - |F_c|$ electron density map calculated, with Ser-195 and inhibitor 47d (code JM54) omitted from the model, showing the acyl-enzyme, with the β -lactam carbonyl carbon of 47d covalently linked to Ser-195, with the corresponding interactions with PPE active site. B) Detail of the crystal structure of the acyl-enzyme complex, with the α -carbon trace of the protein displayed as a ribbon.

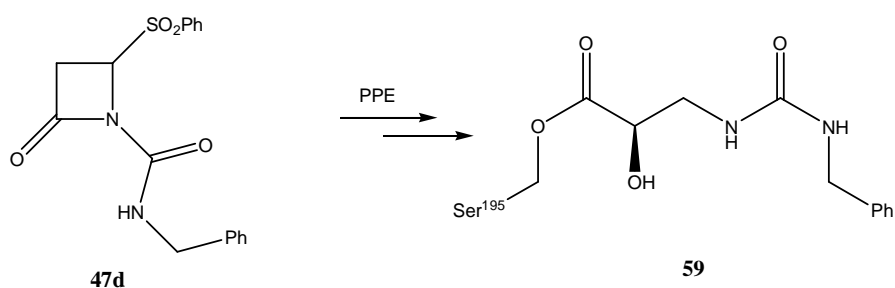


Figure 2.23 - The structure of the crystallized acyl-enzyme **59** resulting from PPE-catalyzed hydrolysis of **47d**.

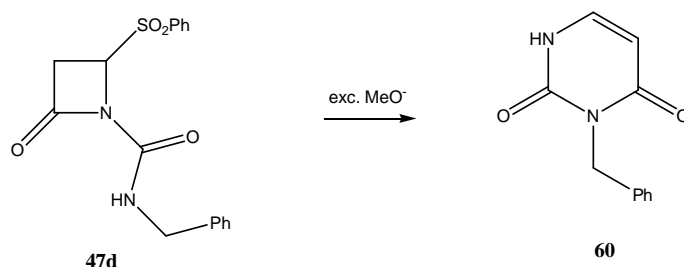


Figure 2.24 - By reaction of **47d** with excess of MeO⁻ in MeOH, compound **60** is formed.

Clearly, the enzyme active site must preclude the ring closure process. In fact, the acyl-enzyme structure equivalent to **60** would be a *cis*-enamine **62** or a *trans*-enamine **63** (Figure 2.25). It would be expected the imine **61**, or the tautomeric enamine forms **62** or **63** (Figure 2.25), to add water to C-4 (β -lactam numbering) to give **64**, rather than to the C-3 atom, in contradiction with the obtained crystal structure of **59**.

These results suggest that a different pathway may be available in the active site of PPE, subsequently to β -lactam ring-opening. In this regard, it is of interest to note that the distance between C-4 of PPE-**47d** complex and the C α of Gln-192 is only 3.4 Å. This close approach (Figure 2.22A) might suggest a reason as to why the presence of a hydroxyl group in the C-4 position is precluded.

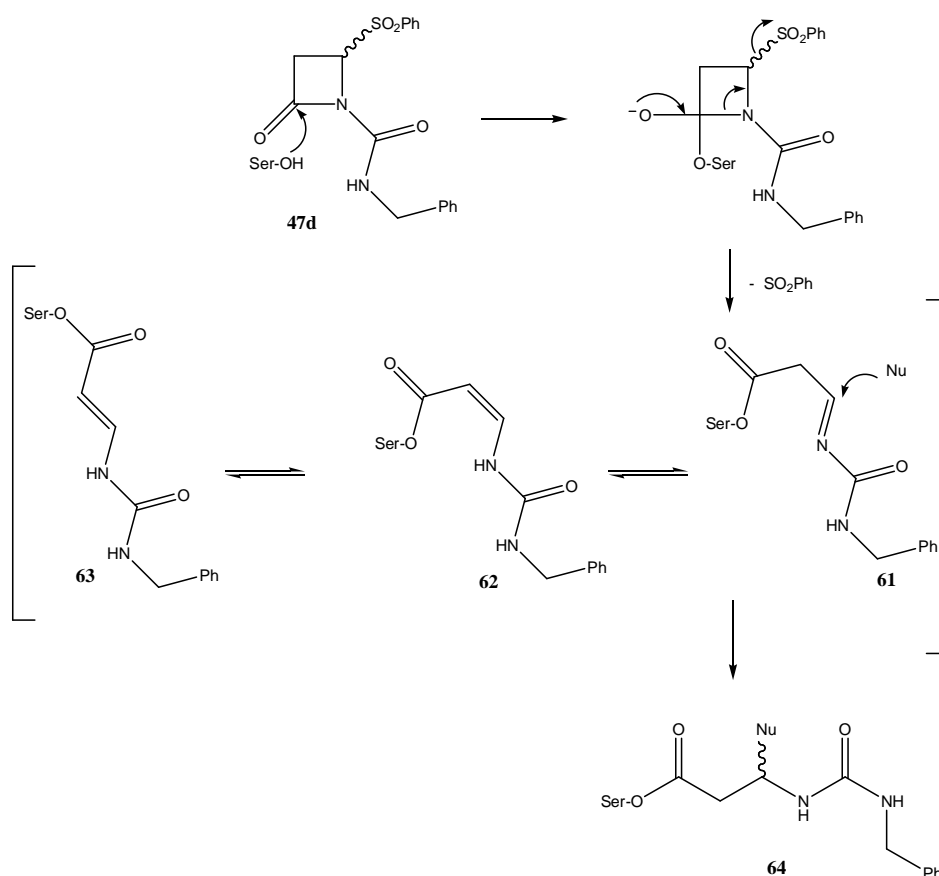


Figure 2.25 - The β -lactam ring-opening of **47d** catalyzed by PPE involves the departure of phenylsulfinate from C-4, generating an imine **61** and tautomers enamines **62** or **63**, but it would be expected to add water to C-4, to give **64**, rather than to C-3.

The obtained crystal structure **59** has an (*R*)-configuration at the C-3 chiral carbon (β -lactam numbering). This could be a result of a favourable chiral environment of the enzyme active site for this configuration. The (*S*)-diastereoisomer of the acyl-enzyme was not obtained, probably due to unfavourable geometrical differences that rely on juxtaposition of amino acid residues on the active site or, the structure, although formed, was not crystallographed.

Interestingly, X-ray crystallography studies were also reported for the reaction of C-3 unsubstituted β -lactams, in particular penem sulfones such as tazobactam (**65**), with class A β -lactamases, which contains a catalytic serine residue (Ser-70).^{139, 140} The

proposed reaction mechanism of tazobactam with a SHV-1 β -lactamase is illustrated in Figure 2.26 (suicide-type inhibition).

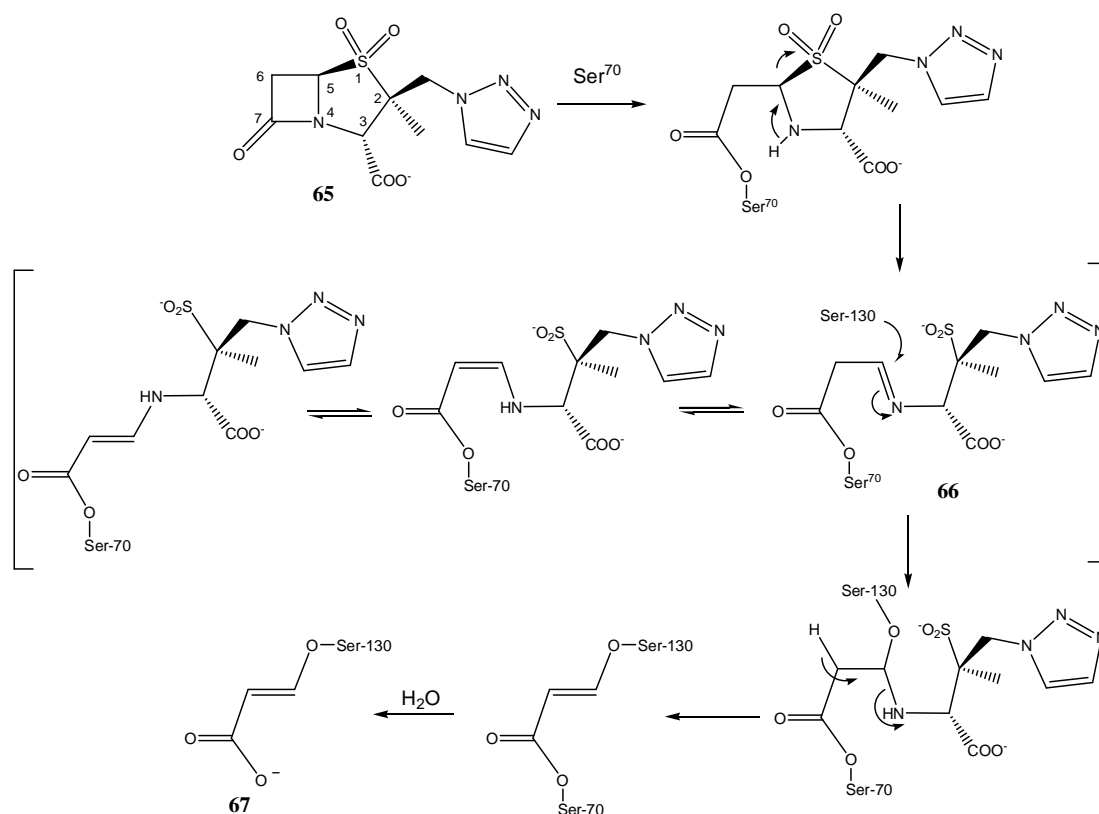


Figure 2.26 - Proposed reaction mechanism of tazobactam with SHV-1 β -lactamase.¹³⁹

The obtained crystal structure for reaction of **65** with a SHV-1 β -lactamase is a *composite* of two complexes:

- an imine acyl-enzyme intermediate, **66**, formed by β -lactam ring opening and departure of the sulfinate leaving group at the C-5 position, and
- an acrylate acid, **67**, resulting from nucleophilic attack at the acyl-enzyme intermediate by a second residue at the active site (Ser-130), followed by hydrolysis of the respective acrylate ester (Figure 2.26). It is important to note that allowing the reaction of **65** with the enzyme to go for a longer time would label all molecules in the form of **67**.¹³⁹ This mechanism allows the formation of a reactive imine, **66**, and

the tautomeric forms *cis*- and *trans*-enamine. Similar situation was discussed for PPE inactivation by **47d**. However, the isolated complex **67** results from the nucleophilic attack of Ser-130 of the β -lactamase at C-5 rather than C-6 (penem sulfone numbering), which would be equivalent to attack at C-4 of **47d**.

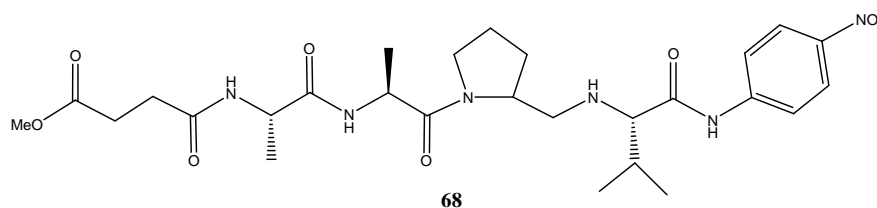
Interestingly, in the case of penem sulfones, such as **65**, the departure of the sulfinate leaving-group is not rate-limiting in the inactivation process (but is an indispensable component for the irreversible inactivation of β -lactamase).¹⁴¹ Similar situation was found in the present study for the inhibition of PPE by **47d**.

2.3.2 HLE Inhibition Studies

2.3.2.1 Introductory remarks

The compounds studied in the present work against HLE were **47e-h**. The inhibitor **47k**, developed by Merck Research Laboratories,¹⁰³ was used as standard of HLE inhibition assays. Inhibition of HLE by compounds **47i-j** was previously studied by Dr. Luísa Martins, and the obtained results will be included here for a better discussion in terms of structure activity relationships.¹²⁰

The C-3 gem-diethyl substituted compounds **47e-h** and **47k** were assayed against HLE, using MeO-Suc-(L-Ala)₂-L-Pro-L-Val-*p*-NA, **68**, as the chromogenic substrate for HLE inhibition assays. By hydrolysis of **68** mediated by the enzyme, *p*-nitroaniline is released, being the reaction monitored at 410 nm. The molar extinction coefficient for the product *p*-nitroaniline at 25 °C, 410 nm, ϵ_{410} , was previously determined by a Beer-Lambert plot, under identical experimental conditions of the enzymatic assays (data presented in *Appendix 1, Figure A1.7*).



The HLE inhibition assays were performed at 25 °C in 0.1 M HEPES buffer, pH 7.2, similarly to the PPE inhibition. However, HLE was reconstituted in 50 mM sodium acetate, pH 5.5, to avoid autolysis and to maintain stability upon reconstitution.

2.3.2.2 Results and Discussion

Inhibition assays were performed using the progress curve method, accordingly to the slow-binding inhibition described by Morrison and Walsh.¹⁴² Thus, the reaction is initiated by addition of HLE to a solution of the inhibitor and the chromogenic substrate in 0.1 M HEPES buffer, pH 7.2, at 25 °C. The characteristics non-linear progress curves of slow-binding irreversible inhibition were obtained for all inhibitors assayed against HLE, reflecting the establishment of the equilibrium between the enzyme and the inhibitor. An example is illustrated in Figure 2.27. The control assays (without inhibitor) gave a linear progression curve.

Progress curves were fitted to Equation 2.6,

$$A = v_s t + (v_i - v_s) [1 - \exp(-k_{obs} t)] / k_{obs} + A_0 \quad (2.6)$$

where A is the absorbance at 410 nm related to the concentration of 4-nitroaniline formed by enzymatic hydrolysis, A_0 is the absorbance at time $t=0$, v_i and v_s are the initial and final rates of product formation in $\Delta A/\Delta t$ units and k_{obs} is the pseudo-first-order rate constant of enzyme inhibition. The v_i , v_s and k_{obs} parameters were calculated using non-linear least-squares regression methods, using the routine ENZFIT, developed at CECF/i-Med.UL, Faculty of Pharmacy, University of Lisbon, by Prof. Luís Gouveia (fitting residuals typically less than +/-0.001 Abs units).

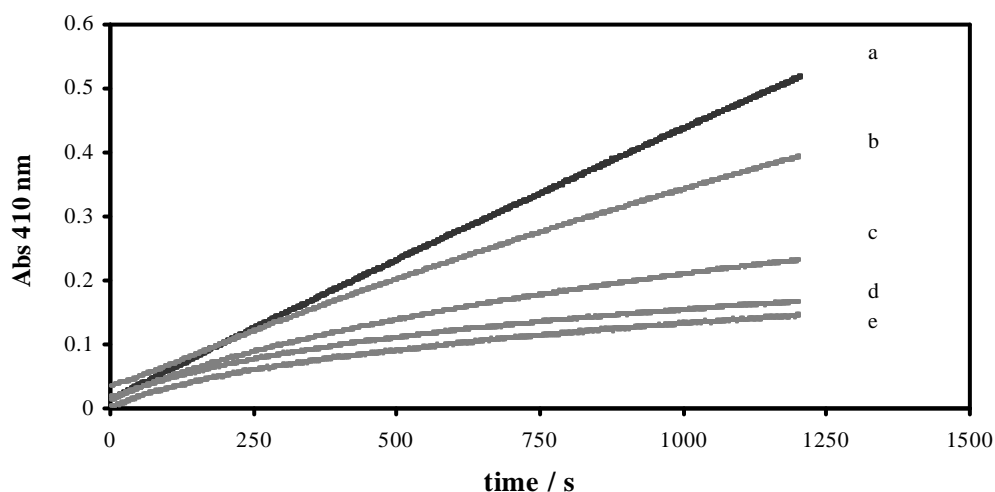


Figure 2.27 - Progress curves for HLE inhibition by compound 47g. Reaction conditions: [HLE] = 20 nM, [MeO-Suc-(L-Ala)₂-L-Pro-L-Val-p-NA] = 1mM, 0.1M HEPES buffer, pH 7.2, 3% DMSO, 25 °C. Inhibitor concentrations: (a) absence of inhibitor, (b) 2, (c) 10, (d) 50, (e) 100 μM.

Accordingly to the slow-binding inhibition kinetics described by Morrison and Walsh, two general reaction mechanisms explain the enzyme inhibition, being represented in Figure 2.28 (E is the free enzyme, I is the inhibitor and S is the substrate).¹⁴²

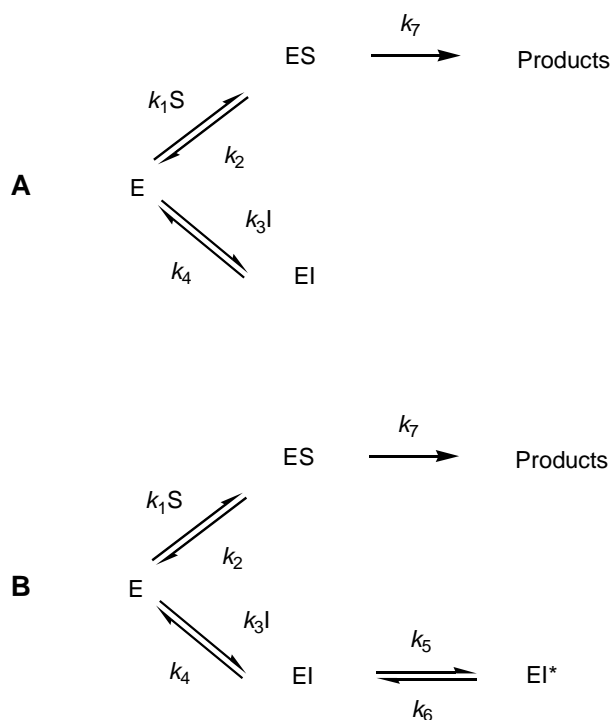
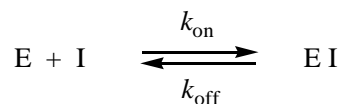


Figure 2.28 - General mechanisms of slow binding inhibition of enzyme-catalyzed reactions.¹⁴²

Mechanism A assumes that the formation of the EI complex is a single, slow step, in which the isomerization to form EI* does not occur and can be represented as follows:



Scheme 2.6 –Mechanism A of slow binding inhibition.

where k_{on} , which is equivalent to k_3 , is the second-order rate constant for HLE acylation, and expresses the inhibitory potency, and k_{off} , which equivalent to k_4 , is the first-order rate for deacylation. This is a simplified mechanism, because the product of deacylation (I) is not identical to the reactant (I). Specifically, being I a β -lactam inhibitor, the deacylation of the acyl-enzyme (hydrolysis) does not involve β -lactam ring closure to give the intact inhibitor.⁹⁵

For mechanism A, the plots of the pseudo-first order rate constant for enzyme inhibition, k_{obs} , versus concentration of [I] are linear and an apparent value, k_{on}' , is determined by the slope, accordingly to Equation 2.7.

$$k_{\text{obs}} = k_{\text{on}} [I] / + k_{\text{off}} \quad (2.7)$$

Then, it is necessary to make a correction taking into account the reaction of the enzyme with the substrate, allowing the establishment of equilibrium to form ES (Figure 2.28). Partial saturation of the enzyme by the reporter substrate slightly reduces the concentration of enzyme susceptible to inactivation. The corrected k_{on} value is given by Equation 2.8,

$$k_{\text{on}} = k_{\text{on}}' (1 + [S] / K_m) \quad (2.8)$$

being [S] the substrate concentration used (1 mM), and K_m the Michaelis constant for the substrate **68**. The K_m value had been previously determined at the host laboratory, $K_m = 1.60 \times 10^{-4}$ M.¹⁰⁹

It is important to note that for the incubation method, described previously for PPE inhibition assays, such correction is not required, because the inhibitor reacts with the enzyme in the absence of substrate (incubation mixture).

The steady-state dissociation constant of the enzyme-inhibitor complex, K_i is defined as¹⁴²

$$K_i = k_{\text{off}} / k_{\text{on}} \quad (2.9).$$

For mechanism A, K_i is calculated using the steady-state velocities, v_s together with v_0 (where v_0 is the rate for product formation in the absence of inhibitor), fitting by non-linear regression to Equation 2.10,¹⁴³ which yields an apparent K_i' . Then it is corrected using Equation 2.11 to give K_i .

$$v_s = \frac{v_0}{([I]/K_i') + 1} \quad (2.10)$$

$$K_i' = K_i(1 + [S]/K_m) \quad (2.11)$$

On the other hand, mechanism B (Figure 2.28) assumes the rapid formation of a collision complex EI that undergoes a slow and favourable isomerization to an EI* complex ($k_3 > k_5$), and can be written as in Scheme 2.7,



Scheme 2.7 - Mechanism B of slow binding inhibition.

where k_{inact} is equivalent to k_5 (Figure 2.28), being the first-order rate constant for the chemical inactivation step and k_{off} is equivalent to k_6 . When k_{off} tends to zero, the

inhibitor becomes a slow tight-binding irreversible inhibitor, leading to a stable enzyme-inhibitor complex from which the inhibitor is, in practice, not released. For mechanism B, k_{inact} and K_i , the dissociation constant for EI, are given by non-linear analysis using . It is important to note that using Equation 2.12, an apparent K_i' value is obtained, which is then corrected by Equation 2.11 to give K_i .

$$k_{obs} = \frac{k_{inact} [I]}{[K_i'] + [I]} + k_{off} \quad (2.12)$$

The second-order rate constants for the formation of EI* (HLE inactivation) are given by Equation 2.13, being an index of inhibitory potency.

$$k_{on} = k_{inact} / K_i \quad (2.13)$$

For each compound several concentrations were tested, with the exception for inhibitor **47e**. Thus, since only one concentration was carried out for **47e**, the second-order rate constant for HLE inactivation was obtained by dividing k_{obs} by the inhibitor concentration, $k_{obs}/[I]$, and then corrected due to the presence of the substrate. A linear behaviour of k_{obs} with $[I]$ was assumed, yielding a final $k_{obs}/[I]$ value of $310 \pm 73 \text{ M}^{-1}\text{s}^{-1}$ for this compound.

The k_{obs} values obtained at different concentrations of inhibitor for compounds **47f-h** and **47k** are presented in *Appendix 1, Table A1.5*, and the final plots are given in Figures 2.29, 2.31 to 2.33. From data of Figure 2.30 the K_i for **47f** was calculated, using Equations 2.10 and 2.11. The final results for HLE inhibition studies are listed in Table 2.6 (k_{OH^-} values were included for comparison and also the EREFs). For compounds **47g-h** and **47k** k_{off} was indistinguishable from zero.

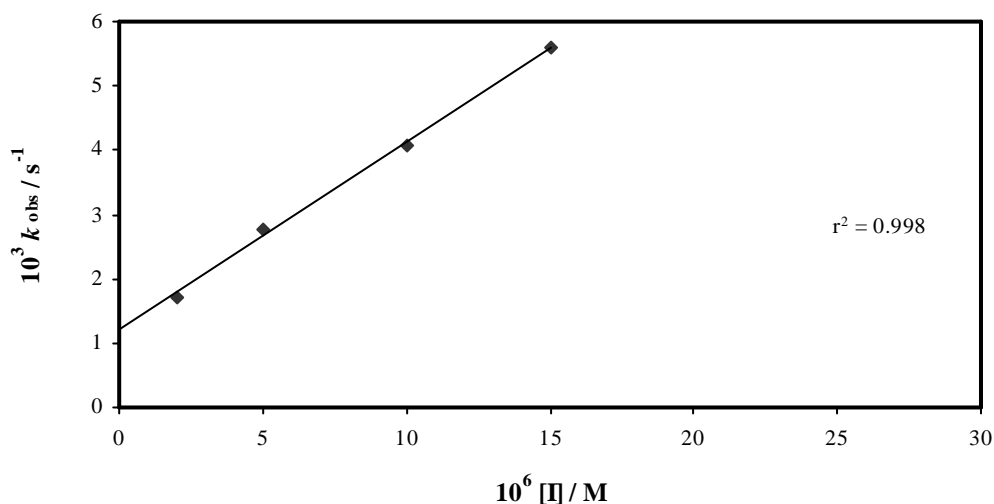


Figure 2.29 - Plot of the pseudo-first-order rate constants, k_{obs} for the HLE inhibition by compound **47f**, against inhibitor concentration, at 25 °C and pH 7.2 buffer. Points are experimental and the line is from linear regression analysis of the data (Equation 2.7). After correction using Equation 2.8, the second-order rate constant for HLE inhibition by **47f** is $k_{on} = 2120 \pm 69 \text{ M}^{-1} \text{ s}^{-1}$, accordingly to the mechanism A of Figure 2.28.

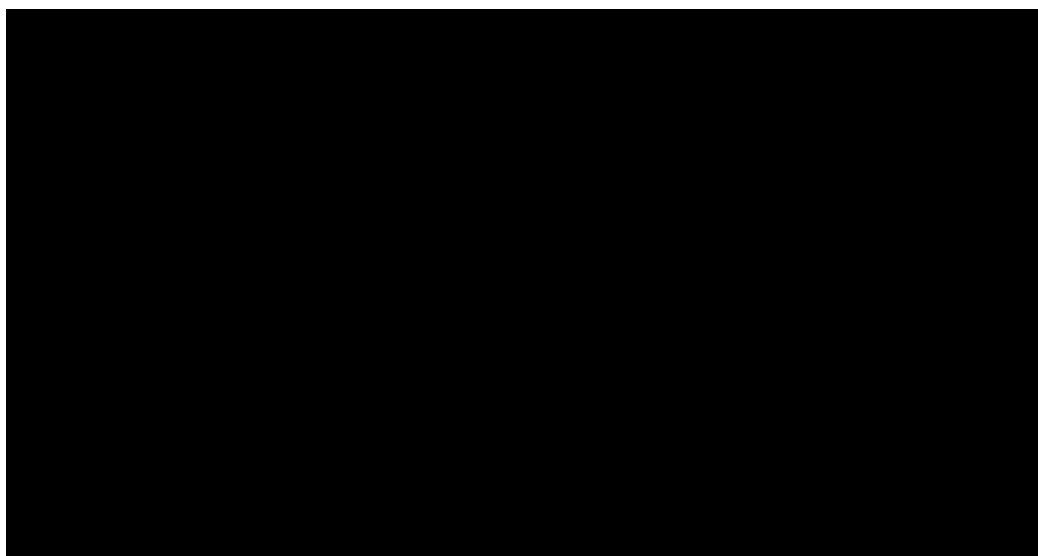


Figure 2.30 - Plot of the steady-state rates versus $[I]$ for the inhibition of HLE by compound **47f**. Points are experimental and the line is from non linear regression analysis of the data presented in Appendix 1, Table A1.6, using Equation 2.10, for $K_i' = 1.13 \mu\text{M}$, which gave after correction using Equation 2.11, $K_i = 0.16 \pm 0.02 \mu\text{M}$.

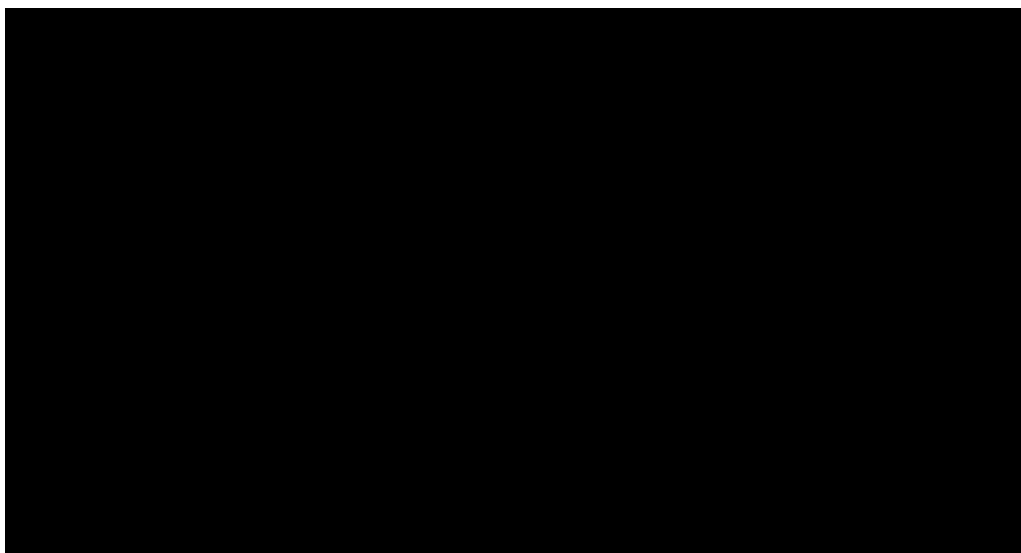


Figure 2.31 - Plot of the pseudo-first-order rate constants, k_{obs} for the HLE inhibition by compound 47g, against inhibitor concentration, at 25 °C and pH 7.2 buffer. Points are experimental and the line is from non linear regression analysis of the data to Equation 2.12, accordingly to the mechanism B of Figure 2.28, giving, $k_{\text{inact}} = (3.63 \pm 0.22) \times 10^{-3} \text{ s}^{-1}$ and $K_i' = 4.81 \pm 0.97 \text{ }\mu\text{M}$. By correction using Equation 2.11, $K_i = 0.66 \pm 0.13 \text{ }\mu\text{M}$, and k_{on} , the second-order rate constant for HLE inhibition, given by k_{inact}/K_i , is $5480 \pm 160 \text{ M}^{-1}\text{s}^{-1}$.

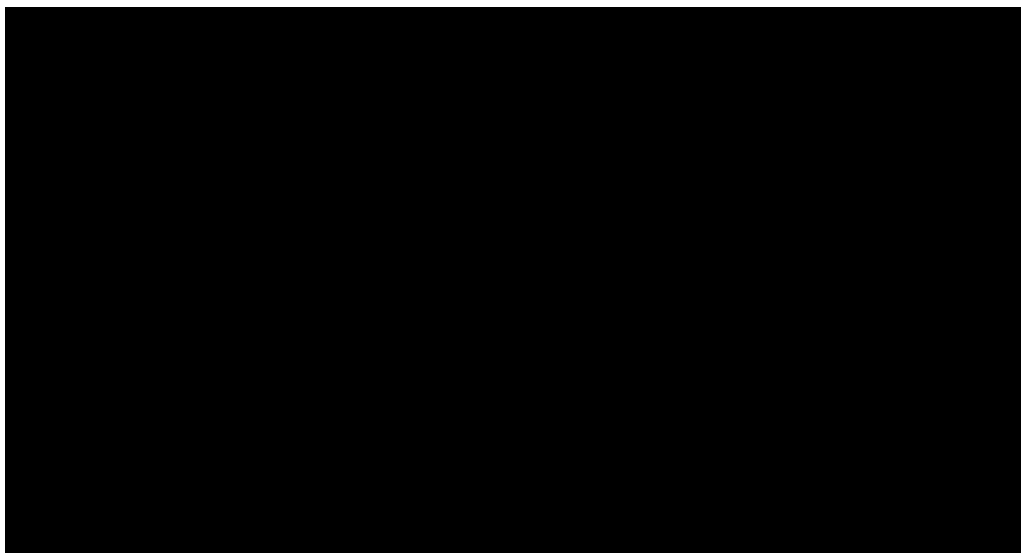


Figure 2.32 - Plot of the pseudo-first-order rate constants, k_{obs} for the HLE inhibition by compound 47h, against inhibitor concentration, at 25 °C and pH 7.2 buffer. Points are experimental and the line is from non linear regression analysis of the data to Equation 2.12, accordingly to the mechanism B of Figure 2.28, giving $k_{\text{inact}} = (4.06 \pm 0.27) \times 10^{-3} \text{ s}^{-1}$ and $K_i' = 2.01 \pm$

0.61 μM . By correction using Equation 2.11, $K_i = 0.28 \pm 0.13 \mu\text{M}$, and k_{on} , the second-order rate constant for HLE inhibition, given by k_{inact}/K_i , is $14600 \pm 443 \text{ M}^{-1}\text{s}^{-1}$.

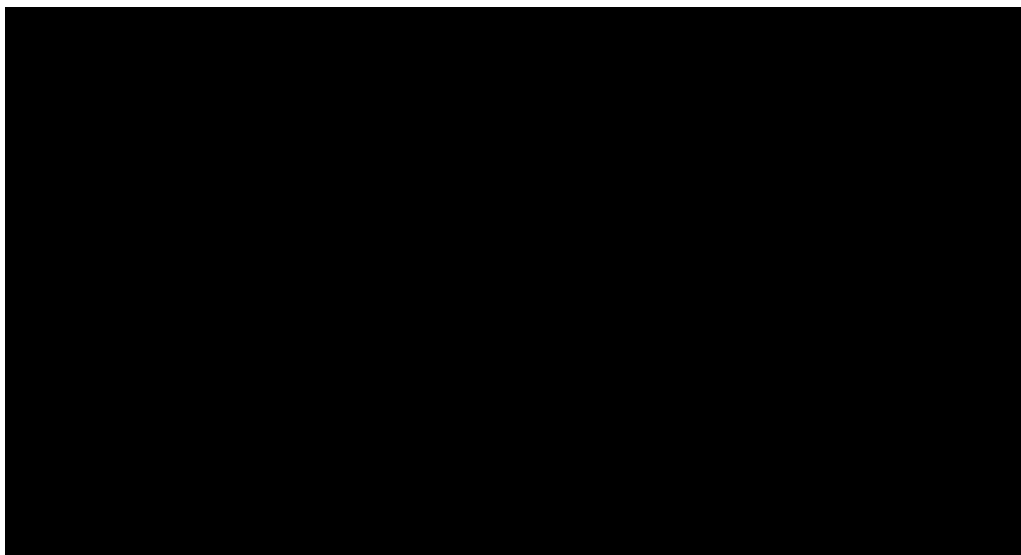
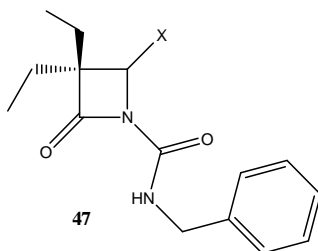


Figure 2.33 - Plot of the pseudo-first-order rate constants, k_{obs} for the HLE inhibition by compound **47k**, against inhibitor concentration, at 25 °C and pH 7.2 buffer. Points are experimental and the line is from non linear regression analysis of the data to Equation 2.12, accordingly to the mechanism B of Figure 2.28, giving $k_{\text{inact}} = (3.77 \pm 0.08) \times 10^{-3} \text{ s}^{-1}$ and $K_i' = 3.41 \pm 0.29 \mu\text{M}$. By correction using Equation 2.11, $K_i = 0.47 \pm 0.04 \mu\text{M}$, and k_{on} , the second-order rate constant for HLE inhibition, given by k_{inact}/K_i , is $8040 \pm 292 \text{ M}^{-1}\text{s}^{-1}$.

Structure Activity Relationships. Inspection of Table 2.6 reveals that 3,3-diethyl β -lactams **47** inhibited HLE very efficiently: the second-order rate constant for HLE inactivation ranges from 10^2 to 10^4 orders of magnitude. As a hyperbolic dependence of k_{obs} versus $[\text{I}]$ was found in most cases (Figures 2.31-2.33), a preassociation complex of high affinity was formed, allowing the determination of k_{inact} (Table 2.6). A comprehensive study of the C-4 substituents on the inhibitory activity will follow.

Table 2.6 - Second-order rate constants for the time-dependent inactivation of HLE, k_{on} , at 25 °C, pH 7.2 buffer and for the hydroxide-catalyzed hydrolysis of compounds 47e-k at 25 °C.

Compd	X	$k_{on}/M^{-1}s^{-1}$	$10^3 k_{inact}/s^{-1}$	$K_i/\mu M$	$k_{OH^-}/M^{-1}s^{-1}$	EREF ^a
47e	H	310 ± 73^b	-	-	1.64×10^{-3}	1.89×10^5
47f	OPh	2120 ± 69	-	0.16	7.22×10^{-3}	2.94×10^5
47g	SPh	5480 ± 160^c	3.63 ± 0.22	0.66	7.13×10^{-3d}	7.69×10^5
47h	SO ₂ Ph	14600 ± 443^c	4.06 ± 0.27	0.28	1.42×10^{-1d}	1.03×10^5
47i	SCH ₂ Ph	$4464^{c,d}$	-	-	3.62×10^{-3d}	1.23×10^6
47j	SO ₂ CH ₂ Ph	$11741^{c,d}$	-	-	1.27×10^{-1d}	9.24×10^4
47k	OC ₆ H ₄ -4-CO ₂ H	8040 ± 292^c	3.77 ± 0.08	0.47	ND ^e	ND ^e

^a EREF enzyme rate enhancement factor; ^b $k_{obs}/[I]$; ^c k_{inact}/K_i ; ^d Data from ref.¹²⁰; ^e Not determined.

Effects of the pK_a of the leaving group at C-4. A correlation was found between the logarithms of the second-order rate constants for HLE inactivation and the pK_a of the leaving group at C-4, giving a small β_{lg} value of -0.047 (see data in *Appendix 1, Figure A1.8*), suggesting that there is essentially no change in the effective charge on the leaving group from going from the ground state to the transition state. Similar results were found for alkaline hydrolysis of the same compounds, previously discussed in this chapter. The 4-phenylsulfonfyl derivative **47h** is only 7-fold more potent than its 4-phenoxy analogue, **47f**, despite the nearly 9-fold difference between the leaving group abilities of phenylsulfinate and phenolate, suggesting that the rate of enzyme inactivation is largely independent on the pK_a of the leaving group at C-4.

Effects of the Electronic Properties (σ_I) of the C-4 Substituent. A correlation was found between $\log(k_{\text{on}})$ and the σ_I values for the substituent at C-4 of compounds **47e-j**, including X=H (**47e**), yielding a corresponding ρ_I value of 2.5 (Figure 2.34). These findings suggest that the rate-limiting step in HLE inactivation is the formation of the tetrahedral intermediate and that the expulsion of the leaving group at C-4 is not concerted with the β -lactam ring opening. Thus, the C-4 substituents exerted only an inductive effect.

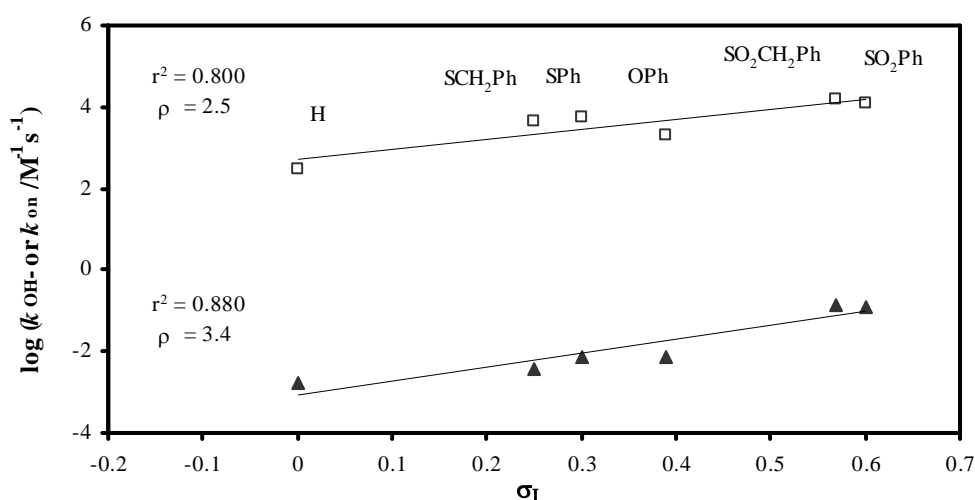


Figure 2.34 - Linear correlation between the second-order rate constants for HLE inactivation by 3,3-diethyl β -lactams **47e-f** (\square), and the σ_I value for the X substituents in C-4, giving a $\rho_I = 2.5$. For comparison, the linear correlation for the alkaline hydrolysis, k_{OH^-} (\blacktriangle) for the same compounds was included, giving a ρ_I value of 3.4. Lines are from linear regression analysis of data.

Interestingly, this ρ_I value of 2.5 is superior to that reported for the HLE inactivation by cephalosporins sulfones **53** (Figure 2.12), which gave a $\rho_I = 1.83^{144}$. This difference in magnitude of ρ_I values for HLE inhibition by **47** and cephalosporins sulfones **53** certainly reflects, once again, the shorter distance between the substituents and the nitrogen atom in the β -lactam scaffold of **47**.

It is important to note that the obtained ρ_I value of 2.5 is lower compared with the previously discussed ρ_I value of 3.4 for the alkaline hydrolysis for the same compounds (Figure 2.34). Thus, the difference in magnitude between these ρ_I values

suggest that the enzyme-mediated hydrolysis of **47e-j** involves an earlier transition state than the hydroxide-catalyzed one, consistent with the establishment of favourable binding interactions between the inhibitor and the enzyme in order to facilitate the attack by Ser-195. This can be ascribed, at least in part, to the molecular recognition at S₁ binding pocket, since it is known the hydrophobic interaction between the diethyl substituent at C-3 on the β -lactam and the S₁ pocket of HLE.⁹⁹ Thus, it allows alignment of the catalytic triad and positions the oxyanion hole of the enzyme to stabilize the negative charge in the transition state, affording a more favourable reaction pathway. This is consistent with the high magnitude of EREF values obtained for **47e-j**, ranging from 10⁵ to 10⁶ (Table 2.6). It reflects the ability of HLE to increase the rate of reaction when compared to alkaline hydrolysis, by using its catalytic apparatus.

Inspection of Table 2.6 reveals that the C-4 unsubstituted derivative **47e** is a weak inhibitor of the enzyme. Replacing the oxygen atom of the C-4 substituent of **47f** by a sulfur atom to give **47g**, increased the rate of HLE inactivation up to 2.5-fold and allowed the accumulation of a high affinity EI* complex (hyperbolic dependence of k_{obs} versus [I], Figure 2.31). This suggests a favourable orientation for **47g** rather than simple sensitivity to intrinsic chemical reactivity.

Oxidation of the sulfur atom to the respective sulfone increased the inhibitory potency. In fact, the sulfones **47h** and **47j** were the most active compounds of the series, presenting k_{inact}/K_i values superior to that of the Merck's compound **47k**, used as standard in inhibition assays

In effect, for both PPE and HLE inhibition studies, the sulfones were the most potent inhibitors and these results can be ascribed to the powerful electron-withdrawing properties of the sulfone function. Similarly, it is known that the oxidation state of the sulphur atom of cephalosporin plays an important role in the inhibitory potency against HLE, being the sulfones more potent than the correspondent sulfides or β -sulfoxides, while α -sulfoxides are inactive.^{88, 144, 145} Similar results were also found in N-acyloxymethylazetidin-2-ones inhibitors of HLE,¹⁰⁷ as mentioned in Chapter 1.

Although not being completely correct to compare the results of different enzymes, using different inhibitors and substrates, *i.e.*, to compare the results obtained for PPE and HLE inhibitions assays, it is important to note that the respective EREFs show a significant difference in magnitude (values for PPE inhibition were given in Table 2.4). Remarkably, the 3,3-gem diethyl derivatives **47e-k** exhibited EREF values *ca.* 10^4 -fold higher towards HLE than those of their C-3 unsubstituted analogues **47b-d** towards PPE. An eventual steric hindrance to the carbonyl carbon, due to the presence of the gem-diethyl substituent in derivatives **47e-k**, seems to be largely compensated by hydrophobic interactions with the S_1 pocket of HLE. This interaction probably positions the β -lactam carbonyl within the oxyanion hole of HLE, thus enhancing the rate of the reaction, with an improvement on inhibitory potency. The best EREF value was found for compound **47i**, suggesting favourable binding interactions for the 4-SCH₂Ph derivative.

A weak correlation was found between $\log(k_{\text{on}})$ for HLE inhibition and $\log(k_{\text{OH}^-})$ for compounds **47e-j**, as illustrated in Figure 2.35.

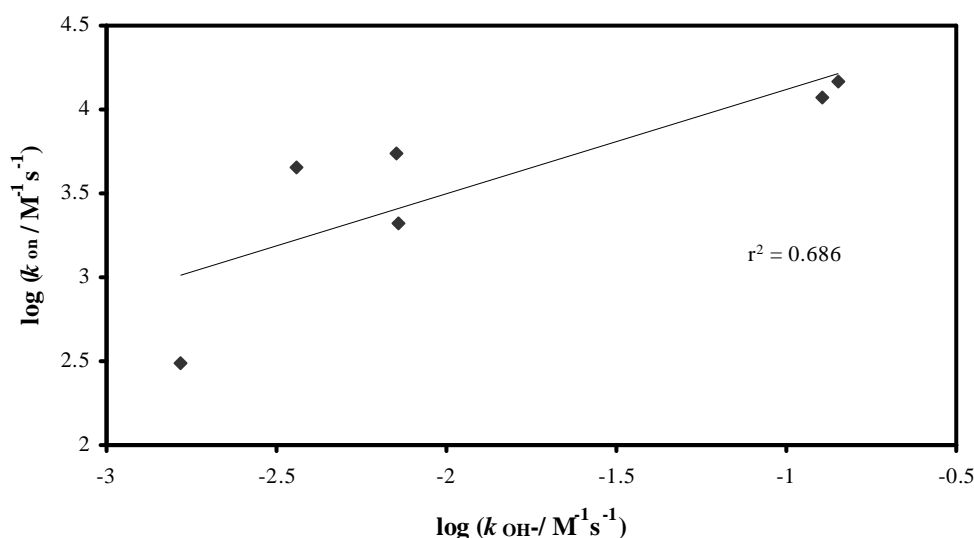


Figure 2.35 - Plot of the second-order rate constants for HLE inactivation by 3,3-diethyl β -lactams **47e-f** against the second-order rate constants for alkaline hydrolysis, k_{OH^-} by the same compounds. Line is from linear regression analysis of data.

These results suggest that increasing the intrinsic chemical reactivity of a compound may lead to a faster rate of enzyme inactivation, without detriment of favourable binding interactions. Nevertheless, the enzyme may be more sensitive to molecular recognition elements rather than intrinsic chemical reactivity (ex.: **47g** versus **47f**).

Interestingly, the sulfones were not only the best inhibitors in both series towards PPE and HLE, but also the ones that showed the greatest intrinsic chemical reactivity. These results reflect the efficiency of this substituent in activating the β -lactam scaffold towards serine proteases and hydroxide ion.

CHAPTER 3

AZETIDINE-2,4-DIONES (4-OXO- β -LACTAMS): SYNTHESIS AND PRELIMINARY STUDIES AS ENZYME INHIBITORS

3. AZETIDINE-2,4-DIONES (4-OXO- β -LACTAMS): SYNTHESIS, AND PRELIMINARY STUDIES AS ENZYME INHIBITORS

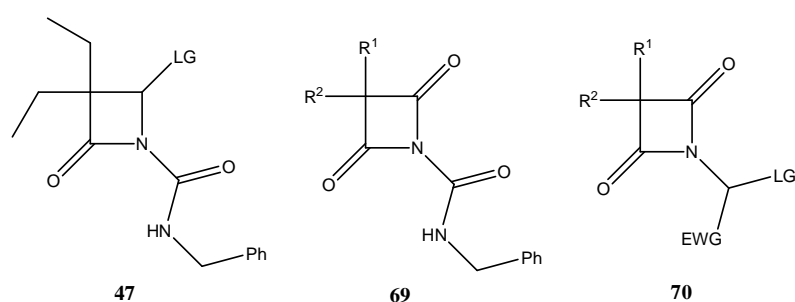
3.1. INTRODUCTORY REMARKS

As already mentioned in Section 1.9, the aim of the second phase of this project was to develop 4-oxo- β -lactams as inhibitors of elastase, and at this phase of the work, azetidine-2,4-diones had never been reported as inhibitors of elastase.

Molecular modelling techniques were used prior to synthesis, in order to select some 4-oxo- β -lactam lead structures, and speeding up the optimization to obtain highly potent inhibitors.

3.1.1 Molecular Modelling

In order to perform a computational-assisted inhibitor drug design, a database of 260 differently substituted 4-oxo- β -lactams was created (*Appendix A2*). The choice of the substituents was based on prior studies with simple β -lactams inhibitors of HLE. For example, based on the results obtained with C-4 substituted *N*-carbamoylazetidin-2-ones (Chapter 2), **47**, in which LG is a leaving group, it was of interest to synthesize compound **69** ($R^1 = R^2 = \text{Et}$) to evaluate the effect of the incorporation of a 4-oxo substituent on the inhibitory potency compared with **47**.



The presence of a second sp^2 centre at C-4 on the β -lactam ring of **69** would increase the chemical reactivity of the carbonyl carbon, and reduce the basicity of the leaving group by C-N fission, as it would change the leaving group from an amide in **47** to an imide in **69**. Interestingly, the two acyl groups would be equivalent, increasing the probability of nucleophilic attack at a “reactive” carbonyl carbon. Analogues **69** with different C-3 substituents for molecular recognition were included on the database, as $R^1 = iso\text{-Pr}$, $R^2 = H$. The *iso*-propyl substituent resembles the side chain of a valine residue, which is known that binds best in the S_1 pocket of HLE.

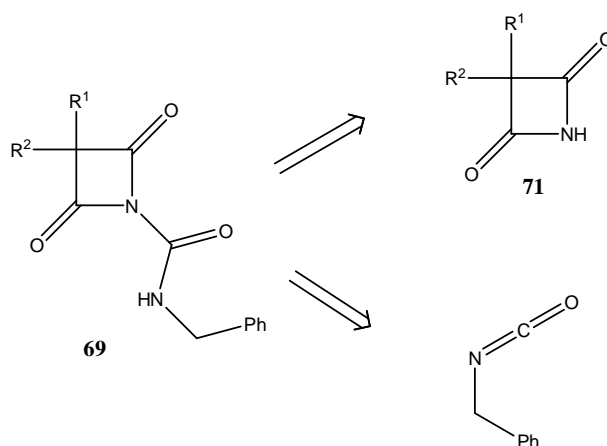
Compound **70** (LG = leaving group, EWG = electron-withdrawing group) allows a potential mechanism-based inhibition of the target, in analogy with simple *N*-hetero-functionalized β -lactams, discussed earlier in Chapter 1, Section 1.6.2.1.

A virtual screening study was carried out at the host institution, by Dr. Rita Guedes, to investigate the binding mode of potential inhibitors within the active site of HLE (see Experimental Section for details). Thus, compounds that afforded the best results were selected for synthesis. An example of an interesting candidate for synthesis was compound **70**, $R^1 = iso\text{-Pr}$, $R^2 = H$, LG = OCOPh, EWG = CO_2Et . PPE inhibition and alkaline hydrolysis assays would be performed with the selected azetidin-2,4-diones, in a preliminary study with these compounds.

3.2. SYNTHESIS

Retrosynthetic analysis indicates that *N*-carbamoylazetidine-2,4-diones should be accessible by coupling the *N*-unsubstituted azetidine-2,4-dione, **71**, with benzyl isocyanate, as illustrated in Scheme 3.1.

Since **71** is not commercially available, it was necessary to prepare it. Interestingly, *N*-unsubstituted azetidine-2,4-diones may also function as a key intermediate to prepare **70**.

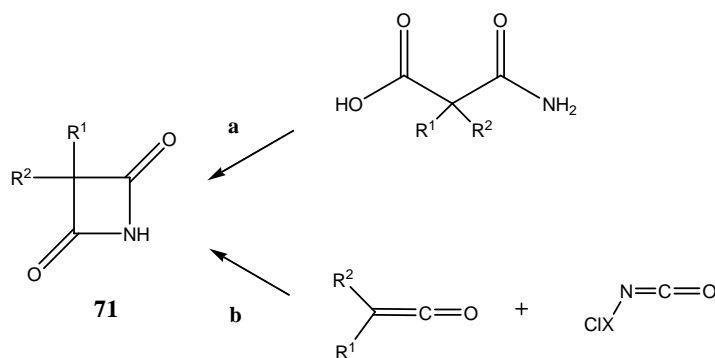


Scheme 3.1 - Retrosynthetic analysis of *N*-carbamoylazetidine-2,4-diones.

3.2.1 Attempted Synthesis of *N*-Unsubstituted 4-Oxo- β -lactams, Using Published Routes

In this phase of the project, published routes were considered for synthesis of *N*-unsubstituted azetidine-2,4-diones (4-oxo- β -lactams), **71** (Scheme 3.2):

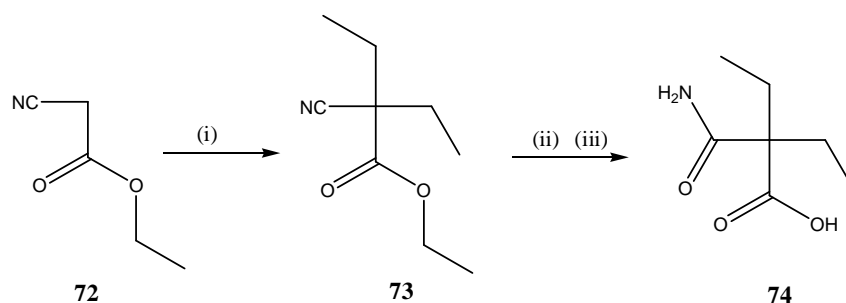
- a) ring closure of malonic acid monoamides^{146, 147}
- b) cycloaddition of ketenes with isocyanates^{148, 149}



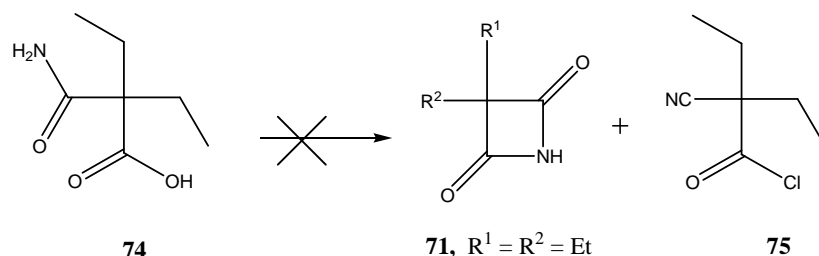
Scheme 3.2 - Strategic routes for the synthesis of *N*-unsubstituted 4-oxo- β -lactams based on published procedures (X = SO₂ or CO).

3.2.1.1 Ring closure of 2,2-Diethyl Malonic Acid Monoamide (Malonamic Acid) and Derivatives

A synthetic route involving ring closure of 2,2-diethylmalonic acid monoamide (malonamic acid) has been reported previously for the synthesis of *N*-unsubstituted 3,3-gem-diethyl derivative **71** ($R^1 = R^2 = \text{Et}$), and the described methodology was used in the present work.^{146, 147} The 2,2-diethylmalonamic acid **74** was obtained in 31% yield from hydrolysis of respective cyanoacetic ester **73** (Scheme 3.3).¹⁴⁷ Compound **73** is not commercially available and was prepared from alkylation of **72**, using sodium ethoxide and iodoethane (76% yield). It was reported that the ring closure of malonic acid monoamide **74** to give **71** was obtained by reaction with thionyl chloride and pyridine, in toluene (inert atmosphere), with formation of a by-product, as represented in Scheme 3.4. The described technique was used.¹⁴⁶

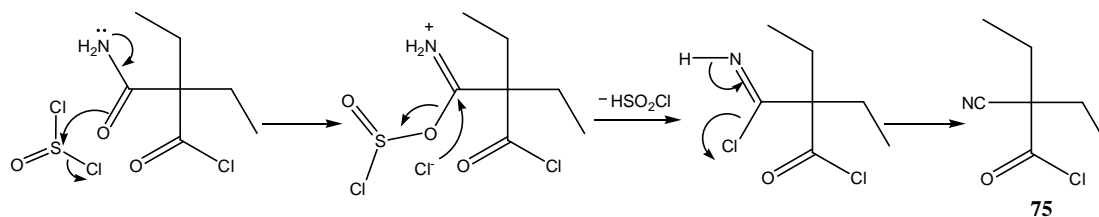


Scheme 3.3- Alkylation of the cyano-ester **72** to give a gem-diethyl derivative **73**, which was hydrolysed to give **74**. Reagents and conditions: (i) EtO⁻/EtOH at 50 °C, EtI and reflux, (ii) H₂SO₄ conc. at 110 °C for 30 min, (iii) ice.



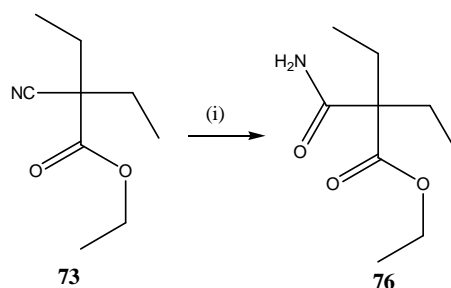
Scheme 3.4 - Attempted ring closure of malonic acid monoamide to give *N*-unsubstituted azetidine-2,4-dione **71.**^{146, 147} Reagents and conditions: SOCl₂, Pyr, toluene, reflux.

Since TLC was not useful in monitoring the reaction, it was kept in reflux during the time reported (30 min). Then, the chloridrate was filtered-off and the residue was purified by distillation under reduced pressure (0.4 mm Hg). The obtained product was characterized by NMR and ESI-MS as being the by-product **75** (Scheme 3.4), with 37 % yield. The formation of the nitrile bond of **75** is explained in Scheme 3.5.



Scheme 3.5 - The nitrile bond of compound **75** results from reaction of thionyl chloride with the amide carbonyl carbon atom.

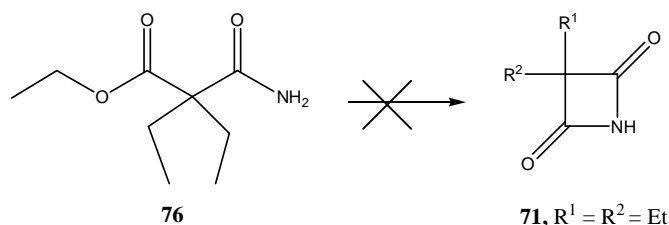
In order to prevent the formation of **75**, a different strategy was investigated to achieve ring closure, using the ethyl ester of the malonic acid monoamide as starting material, **76** (Scheme 3.6). Compound **76** was obtained by a partial hydrolysis of **73**, following a described procedure¹⁴⁷ (21% yield).



Scheme 3.6 - Synthesis of **76** from acid hydrolysis of **73**¹⁴⁷ Reagents and conditions: H₂SO₄ conc. at 90 °C for 5 min; ice.

It was reasoned that reaction of dilute **76** with ethoxide in a 1:2 molar ratio, in dry ethanol allows the cyclisation to occur (Scheme 3.7). Reaction was carried out at

room temperature and also using reflux. TLC was ineffective in monitoring the reaction. After work-up, only starting material **76** was recovered.



Scheme 3.7 - Attempted synthesis of 3,3-diethylazetidine-2,4-dione **71** by cyclisation of **76** catalyzed by base.

Thus, a stronger deprotonating agent, lithium diisopropylamide (LDA, 1.2 eq.), was chosen instead of ethoxide, but the cyclisation process also failed. Experimental attempts involving variation of the temperature and the order of addition of the reagents remained unsuccessful. It is important to note that the procedure involving malonic acid monoamides ring closure, illustrated in Scheme 3.4, was reported in an old reference (1959), and the products were only analyzed using IR and elemental analysis, with no NMR characterization.¹⁴⁶

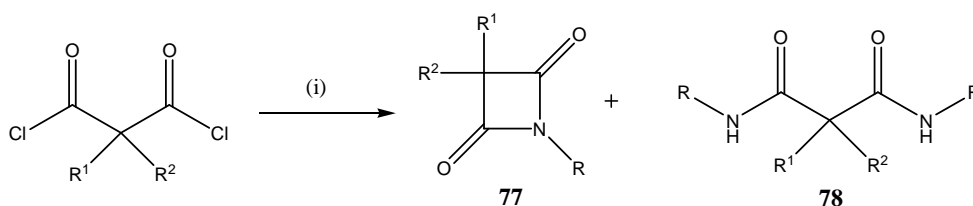
The route involving cycloaddition of ketenes with chlorosulfonyl isocyanates to prepare *N*-unsubstituted 4-oxo- β -lactam **71** was not tested, because it was reported that the resulting *N*-chlorosulfonyl 4-oxo- β -lactam was difficult to handle, due to decomposition with SO₂ evolution, prior to hydrolysis to give **71**.¹⁴⁹ However, the synthetic pathway using ketenes and isocyanates to prepare 4-oxo- β -lactams will be discussed in Chapter 4 (including a route using chlorocarbonyl isocyanate).

As a result of the unsuccessful approaches for the synthesis of *N*-unsubstituted 4-oxo- β -lactams, a different method was investigated, in order to synthesize derivatives substituted at both C-3 and N-1.

3.2.2 Condensation of Malonyl Dichlorides with Primary Amines to give C-3 and N-1 Substituted 4-Oxo- β -lactams

One reported route for the synthesis of the 4-oxo- β -lactam (azetidine-2,4-dione) nucleus involves the condensation of malonyl dichlorides with primary amines.^{150, 151} Golik reported the synthesis of a 3,3-diethyl-*N*-alkylazetidine-2,4-dione **77** (Scheme 3.8, R¹ = R² = Et, R = CH₂CO₂Et), in 12% yield, by refluxing commercially available diethyl malonyl dichloride with ethyl glycinate hydrochloride, in the presence of triethylamine as catalyst (inert atmosphere). Accordingly to the described procedure, the catalyst is added dropwise during 1.5 h to the reaction mixture. The same author reported the simultaneous formation of the disubstitution product **78** (R = CH₂CO₂Et), an acyclic malondiamide (22% yield). Both products **77** and **78** were characterized, including NMR techniques.¹⁵¹ Thus, this procedure was completely followed as described in the literature, in order to assert a synthetic pathway for 4-oxo- β -lactams. In addition, the 3,3-gem-diethyl substituent is known to be important for molecular recognition at S₁ binding pocket of elastase and, therefore, the synthesis of **77** and analogues was interesting as potential elastase inhibitors.

Based on this synthetic route, different 4-oxo- β -lactams **77** were prepared, as represented in Scheme 3.8, and they were easily purified by column chromatography, being the first fraction eluted. Since it was reported that aliphatic amines decreases the yield of the reaction by leading to favored formation of the malondiamide, anilines were preferentially used.¹⁵¹ In particular, *para*-substituted anilines with different electronic properties of the *para*-substituent were chosen to assess the impact of the substituent on the chemical reactivity and on the inhibitory potency.



Scheme 3.8 - Synthesis of azetidine-2,4-diones **77**, using the method described by Golik.¹⁵¹

Reagents and conditions: (i) RNH₂ (1 eq), TEA (2.6 eq), dioxane, reflux.

3,3-Gem-dimethyl ($R^1 = R^2 = \text{Me}$, **77**) derivatives were synthesized from commercially available dimethyl malonyl dichloride. Compound **77h** was synthesized as an isoster analogue of the 3-oxo- β -sultam **35** (previously presented in Figure 1.12, Chapter 1).

This method suffered a drawback by giving low yields (Table 3.1). But it allowed the synthesis of 4-oxo- β -lactam derivatives in a simply and unique step.

Table 3.1 - Synthesized 4-oxo- β -lactams **77a-i**.

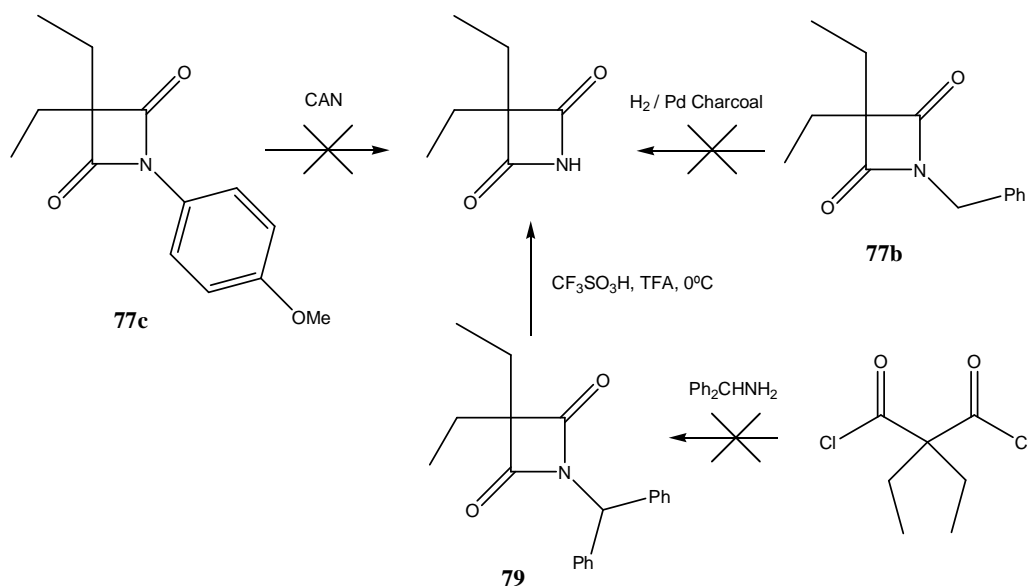
Compound	R^1	R	Yield (%)
77a	Et	CH ₂ CO ₂ Et	16
77b	Et	CH ₂ Ph	9
77c	Et	C ₆ H ₄ -4-OMe	11
77d	Et	C ₆ H ₄ -4-Me	10
77e	Et	C ₆ H ₅	15
77f	Et	C ₆ H ₄ -4-Cl	14
77g	Et	C ₆ H ₄ -4-CN	19
77h	Me	CH ₂ Ph	4
77i	Me	C ₆ H ₄ -4-Cl	6

In most cases, decreasing the basicity of the primary amine increased the yield for the cyclisation process. In this way, *N*-aryl derivatives **77c-g** provided better yields than the *N*-benzyl derivative **77b** (the best was obtained for the *p*-cyano derivative). On the other hand, highly reactive dimethylmalonyl dichloride provided lower yields than the diethyl counterpart.

3.2.3 Attempted Synthesis of *N*-Unsubstituted 4-Oxo- β -lactam from *N*-Protected Azetidine-2,4-diones

Once synthesized these 4-oxo- β -lactams, more attempts were made for the synthesis of the *N*-1 unsubstituted key intermediate **71**. Since the main difficulty on the

published routes for **71** arose from the difficulty on cyclisation of the ring (Section 3.2.1), attempted *N*-deprotection strategies of potential *N*-protected azetidine-2,4-diones were used (Scheme 3.9).

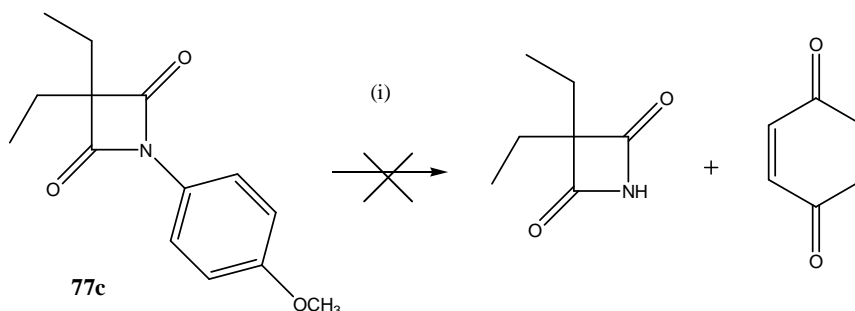


Scheme 3.9 - Attempted synthesis of *N*-unsubstituted 4-oxo- β -lactams based on *N*-protected azetidine-2,4-diones.

3.2.3.1 Attempted Oxidative *N*-Dearylation of *N*-(*p*-Methoxy)-phenylazetidine-2,4-dione, **77c**

Keeping in mind the well-known oxidative *N*-dearylation of *N*-(*p*-methoxy)-phenylazetidine-2-ones (simple β -lactams, 1 eq.) using ceric ammonium nitrate (CAN, 3 eq.)¹⁵², this method was used for the preparation of the *N*-unsubstituted 4-oxo- β -lactam from **77c** (Scheme 3.10). TLC analysis of the reaction mixture after 4h of reaction (eluant hexane/EtOAc 8:2), revealed starting **77c** ($R_f = 0.72$) and the formation of a new compound with a lower R_f value ($R_f = 0.38$). However, after work-up (extraction with EtOAc and purification by column chromatography) only starting material **77c** was recovered (47%). An alternative approach was investigated by using silica-gel supported cerium ammonium nitrate,¹⁵³ but this procedure also

failed. Both $^1\text{H-NMR}$ and ESI-MS analysis of the product after work-up were inconsistent with the expected product and could not be assigned to another structure.

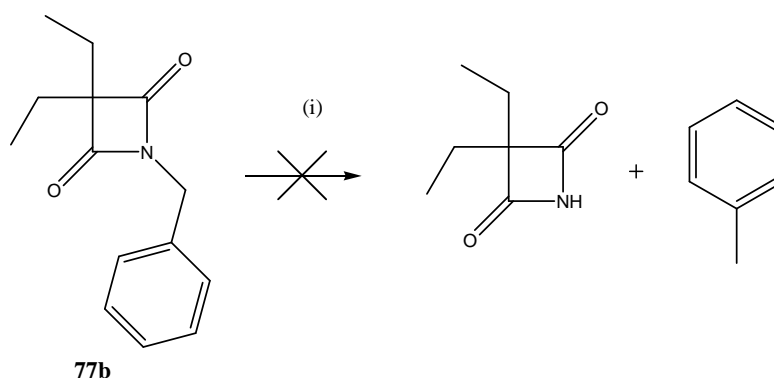


Scheme 3.10 - Attempted synthesis of *N*-unsubstituted 4-oxo- β -lactam from **77c**. Reagents and conditions: (i) CAN (ceric ammonium nitrate), $\text{CH}_3\text{CN}/\text{H}_2\text{O}$.

3.2.3.2 Attempted *N*-Debenzylation of **77b** by Catalytic Hydrogenation

The removal of the *N*-benzyl group from a wide variety of compounds is well-known. Thus, the following approach was considered (Scheme 3.11).

High pressure catalytic hydrogenation by using a Parr hydrogenator was carried out,¹⁵⁴ but no reaction took place after 28 h of stirring in methanol at room temperature (**77b**, 86% recovered). The reaction was repeated using formic acid or acetic acid, but only **77b** was recovered after work-up. Surprisingly, **77b** was likely to be “inert” under such severe conditions.



Scheme 3.11 - Attempted synthesis of *N*-unsubstituted 4-oxo- β -lactam from **77b**. Reagents and conditions: (i) H_2 / Pd Charcoal, Parr hydrogenator, MeOH or formic acid.

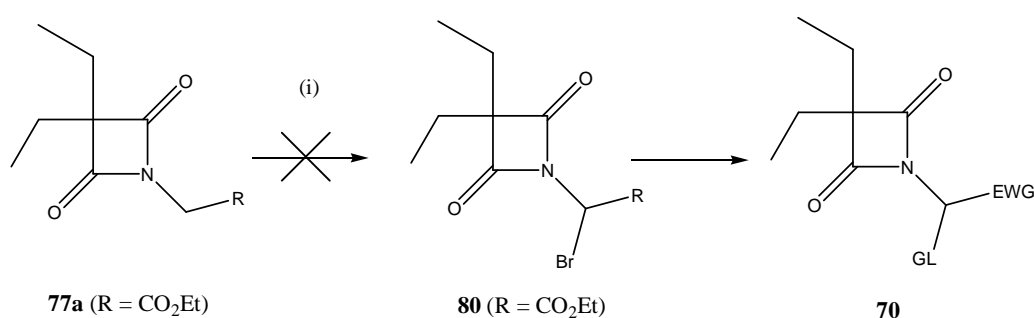
3.2.3.3 Attempted Deprotection of *N*-benzhydryl azetidine-2,4-dione, **79**

The route involving deprotection of the *N*-benzhydryl protecting group¹⁵⁵ by using triflic acid in TFA at 0 °C,¹⁵⁶ began with the attempted preparation of **79** (Scheme 3.9). Following the described procedure for obtention of azetidine-2,4-diones, the diethyl malonyl dichloride reacted with benzhydrylamine Ph₂CHNH₂, but **79** was not detected after work-up. NMR analysis of the product was consistent with the disubstitution product (malondiamide) **78**, R = Ph₂CH, R¹ = Et (12% yield). This route was no further investigated.

3.2.4 Attempted Bromination at C-1' of Azetidine-2,4-diones

Since it was not feasible to synthesize *N*-unsubstituted azetidine-2,4-diones for further reaction to prepare *N*-substituted derivatives, a different strategy was considered, which consisted in the bromination at C-1' of **77a** by using NBS with a radical initiator (Scheme 3.12).

The brominated compound **80** may function as a building molecule for **70** (Scheme 3.12). However, no bromination reaction took place after 24 h of reflux, being recovered the starting azetidine-2,4-dione **77a** (79%). Attempted benzylic bromination of **77b** also failed. This route was no further investigated.



Scheme 3.12 - Attempted bromination of 77a. Reagents and conditions: (i) NBS, CCl₄, benzoyl peroxide, reflux. EWG of compound **70** is CO₂Et.

In fact, none of the 4-oxo- β -lactams studied by molecular modelling techniques was able to be synthesized. Thus, in this phase of the project, it was of interest to perform preliminary studies on both serine protease inhibition and intrinsic chemical reactivity with the prepared 4-oxo- β -lactams **77**.

3.2.5 NMR Spectral Characterisation

The ^1H -NMR spectrum of compound **73** (Scheme 3.5) presents prochiral methylene protons on the diethyl substituent. These protons are attached to a prochiral carbon atom and are therefore non-equivalent. Each of these protons presents a doublet of quadruplets, due to geminal coupling with each other and with the neighbours CH_2CH_3 , as presented in Figure 3.1. The proposed splitting pattern for each proton is illustrated in Figure 3.2. Similar situation was found for compounds **74**, **75** and **76**.

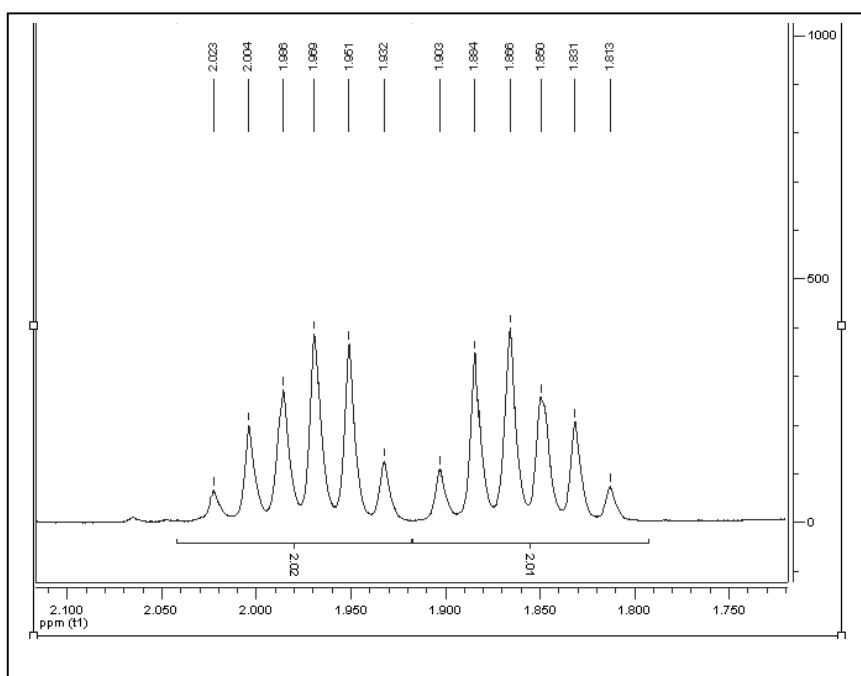


Figure 3.1 - Expansion of the observed signals of the spectrum of ^1H NMR for the methylene protons $-\text{CH}_2\text{CH}_3$ of the diethyl substituent of compound **73**.

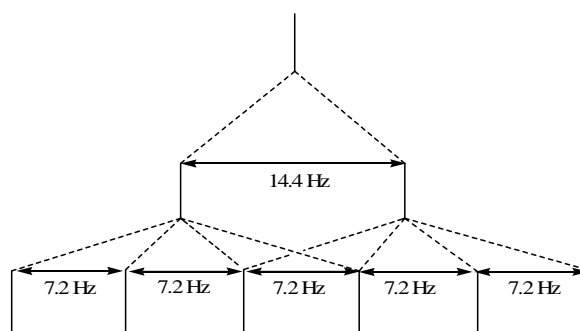


Figure 3.2 - Splitting pattern diagram for each methylene proton of the diethyl group of compound **73**.

With regard to 4-oxo- β -lactams **77**, all of them presented a plane of symmetry. Thus, the methylene protons of the gem-diethyl substituent at C-3 of **77a-g** are equivalent, and appear as a quartet in the $^1\text{H-NMR}$ spectra, integrating for 4 protons; while the protons of the methyl groups appear as a triplet, integrating for 6 protons. The methylene protons of *N*-benzyl derivatives give a singlet (eg. Figure 3.3a).

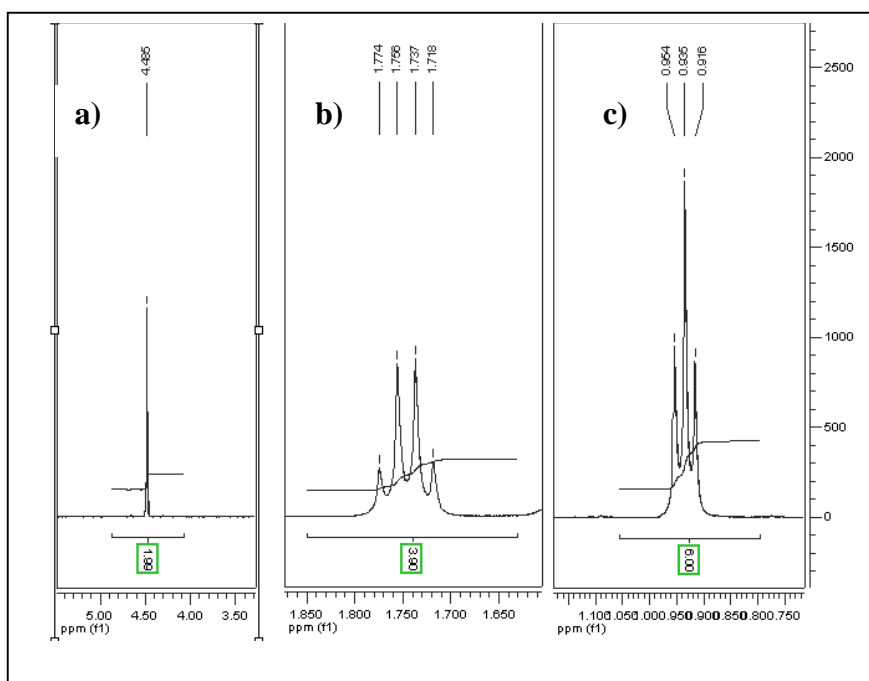


Figure 3.3 - Expansion of the observed signals of the spectrum of $^1\text{H NMR}$ for *a*) the singlet corresponding to two methylene protons $-\text{CH}_2\text{Ph}$, *b*) the quartet corresponding to four CH_2CH_3 protons and *c*) the triplet corresponding to six CH_2CH_3 protons of compound **77b**.

For the C-3 gem-dimethyl derivatives, **77h-i**, the six methyl protons are equivalent and appear as a singlet in the $^1\text{H-NMR}$ spectra. For the synthesized 4-oxo- β -lactams presenting a substituent on the *para* position of the aromatic ring at N-1, the aromatic protons belong to the AA'BB' system (Figure 3.4), being chemically equivalent by symmetry but magnetically non-equivalent.

It would be expected H_A proton coupling with H_B and then to the H_A' , in such a way that: $J(\text{H}_\text{A}\text{H}_\text{B}) = J(\text{H}_\text{A}\text{H}_\text{B}')$ and $J(\text{H}_\text{A}\text{H}_\text{A}') = J(\text{H}_\text{B}\text{H}_\text{B}')$, being $J(\text{H}_\text{A}\text{H}_\text{B}) > J(\text{H}_\text{A}\text{H}_\text{A}')$. However, the signals of these protons appear as broad doublets in the $^1\text{H-NMR}$ spectrum (400 MHz).

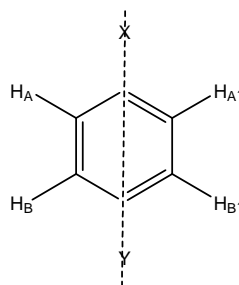


Figure 3.4 - AA'BB' protons in a 1,4-disubstituted aromatic ring.

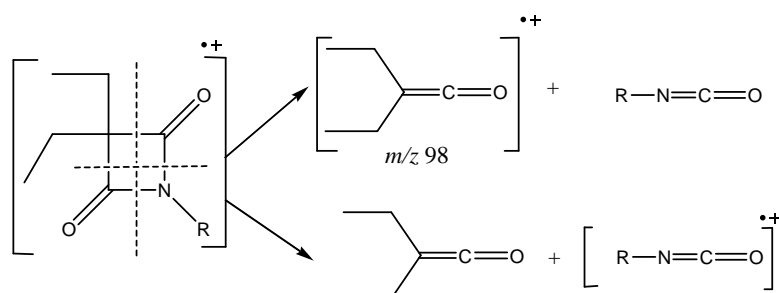
As a result of the plane of symmetry, both carbonyl carbon atoms C-2 and C-4 of all 4-oxo- β -lactams **77** are equivalent and give only one signal on the $^{13}\text{C-NMR}$ spectra.

3.2.6 IR Spectroscopy

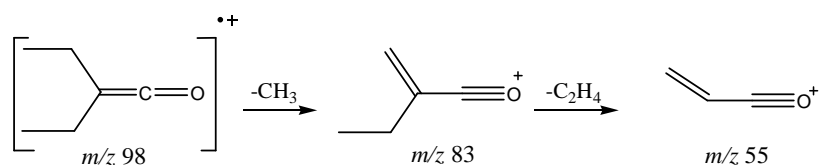
All synthesized 4-oxo- β -lactams **77** presented two bands due to carbonyl stretching: one high intensity C=O IR stretching band, which frequency is nearly 1730 cm^{-1} (asymmetric stretching) and a low intensity band, corresponding to symmetric stretching, nearly 1860 cm^{-1} .

3.2.7 Mass Spectroscopy

The synthesized 4-oxo- β -lactams were analyzed by mass spectrometry, using the electron-impact method of ionisation. A common route of fragmentation observed for all azetidin-2,4-diones **77** is the opening of the ring with formation of a ketene ion fragment and isocyanates. For the 3,3-diethyl derivatives **77a-g** some characteristic fragments were detected, identified in Schemes 3.13 and 3.14 (m/z).



Scheme 3.13 - Fragmentation of 3,3-diethylazetidin-2,4-diones with formation of diethylketene and the respective isocyanate.



Scheme 3.14 - Further fragmentation of the diethylketene ion.

Similarly, by fragmentation of the 3,3-dimethylazetidin-2,4-dione, **77h-i**, the dimethylketene is formed ($m/z = 70$).

3.3. ALKALINE HYDROLYSIS STUDIES OF 4-OXO- β -LACTAMS

3.3.1 Results and Discussion

The chemical reactivity studies began with the selection of the wavelength to be used in the UV-kinetic measurements (as described earlier for the alkaline hydrolysis of *N*-carbamoylazetidin-2-ones in Chapter 2, Section 2.2), and an example of a repeated spectral scanning for the reaction of hydroxide ion with a 4-oxo- β -lactam is given in *Appendix 3, Figure A3.1*.

Table 3.2 - Azetidine-2,4-diones (4-oxo- β -lactams) studied in the present work on the intrinsic chemical reactivity and indication of the selected wavelength for kinetic measurements by UV spectroscopy.

Compound	λ (nm)
77b	221
77c	247
77d	260
77e	247
77f	260
77g	280
77h	255
77i	260

The obtained k_{obs} values for each hydroxide-ion concentration used are given in *Appendix 3, Section A3.1*. The second-order rate constants for the ring-opening by alkaline hydrolysis were determined graphically and the respective plots of k_{obs} versus $[\text{OH}^-]$ will follow.

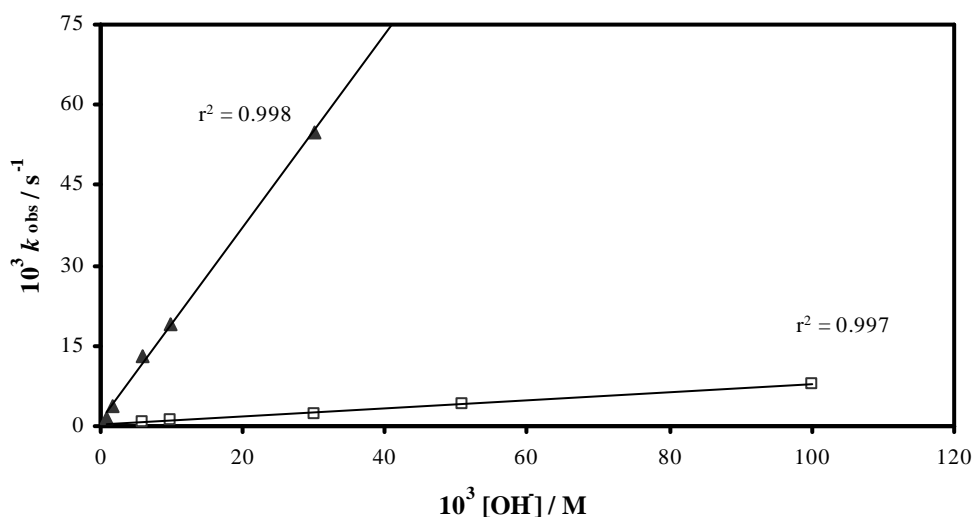


Figure 3.5 - Plot of the pseudo-first-order rate constants, k_{obs} for the alkaline hydrolysis of the *N*-benzyl derivatives **77b** (●) and **77h** (□), against hydroxide concentration, at 25 °C, ionic strength 0.5 M. Points are experimental and the lines are from linear regression analysis of the data, giving $k_{\text{OH}^-} = 0.0742 \pm 0.002 \text{ M}^{-1}\text{s}^{-1}$ for **77b** and $k_{\text{OH}^-} = 1.80 \pm 0.05 \text{ M}^{-1}\text{s}^{-1}$ for **77h**.

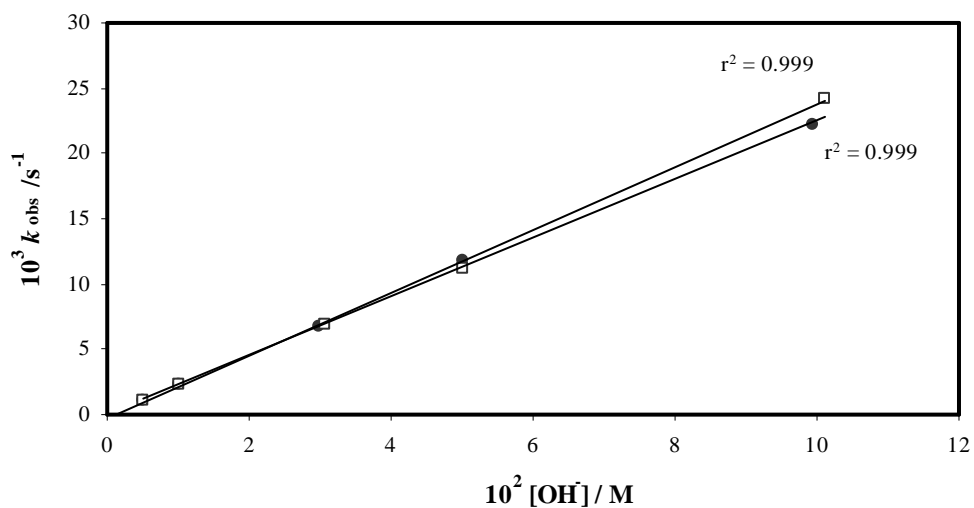


Figure 3.6 - Plot of the pseudo-first-order rate constants, k_{obs} for the alkaline hydrolysis of the 3,3-diethyl-*N*-(*p*-methoxyphenyl)-azetidine-2,4-dione **77c** (●), and *N*-(*p*-methylphenyl) counterpart **77d** (□), against hydroxide concentration, at 25 °C, ionic strength 0.5 M. Points are experimental and the lines are from linear regression analysis of the data, giving $k_{\text{OH}^-} = 0.225 \pm 0.004 \text{ M}^{-1}\text{s}^{-1}$ for **77c** and $0.240 \pm 0.004 \text{ M}^{-1}\text{s}^{-1}$ for **77d**.

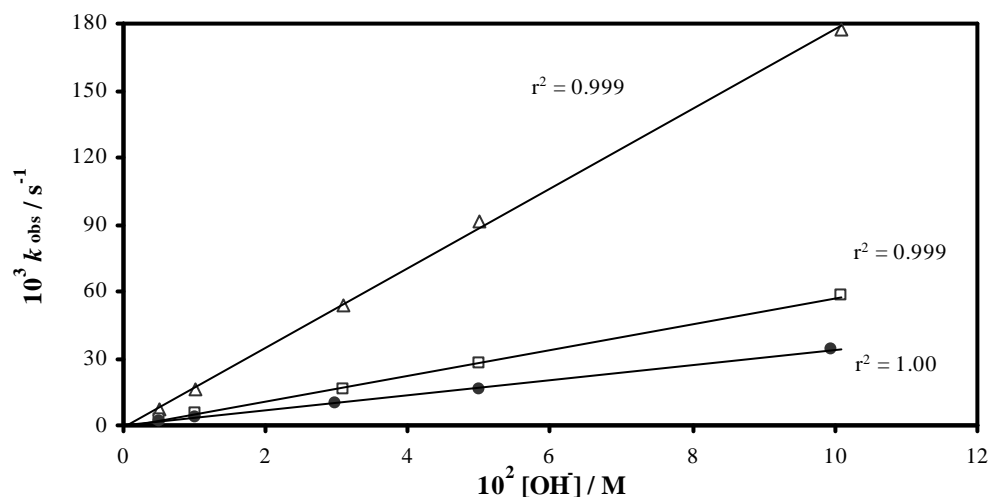


Figure 3.7 - Plot of the pseudo-first-order rate constants, k_{obs} for the alkaline hydrolysis of the *p*-unsubstituted, **77e** (\bullet), the *p*-chloro **77f** (\square) and the *p*-cyanophenyl **77g** (Δ) 4-oxo- β -lactams, against hydroxide concentration, at 25 °C, ionic strength 0.5 M. Points are experimental and the lines are from linear regression analysis of the data, giving $k_{\text{OH}^-} = 0.340 \pm 0.003 \text{ M}^{-1}\text{s}^{-1}$ for **77e**, $0.581 \pm 0.008 \text{ M}^{-1}\text{s}^{-1}$ for **77f** and $1.78 \pm 0.02 \text{ M}^{-1}\text{s}^{-1}$ for **77g**.

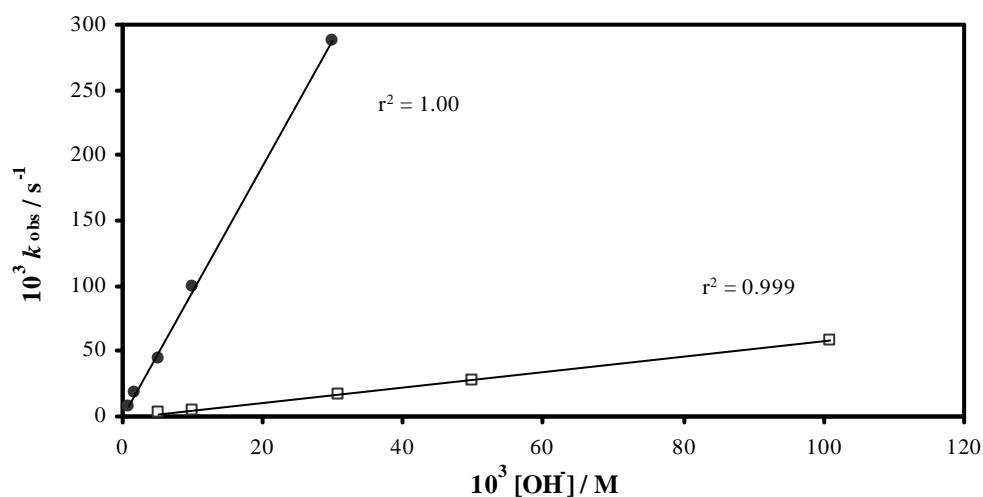


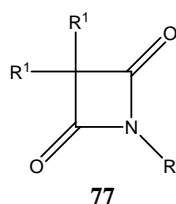
Figure 3.8 - Plot of the pseudo-first-order rate constants, k_{obs} for the alkaline hydrolysis of **77i** (\bullet) against hydroxide concentration, at 25 °C, ionic strength 0.5 M. For comparison, the results for the 3,3-diethyl counterpart **77f** (\square) were included. Points are experimental and the lines are from linear regression analysis of the data, giving $k_{\text{OH}^-} = 9.67 \pm 0.12 \text{ M}^{-1}\text{s}^{-1}$ for **77i**.

A summary of the second-order rate constants for the alkaline hydrolysis of the studied 4-oxo- β -lactams **77b-i** is presented in Table 3.3.

3.3.1.1 Structure Activity Relationships for the Alkaline Hydrolysis

By alkaline hydrolysis reaction, nucleophilic attack of hydroxide-ion at a carbonyl carbon with β -lactam ring opening occurs. It is of interest to evaluate the effect of substitution on N-1 and C-3 on the rate of the reaction (Table 3.3).

Table 3.3 - The second-order rate constants, k_{OH^-} , for the alkaline hydrolysis of 4-oxo- β -lactams **77**, at 25 °C and ionic strength adjusted to 0.5 M with NaClO₄. The σ_p values are given as an indicator of the polar effect of the substituent in the *para* position of the aromatic ring.



Compound	R ¹	R	σ_p ^{a, b}	$k_{\text{OH}^-} / \text{M}^{-1}\text{s}^{-1}$
77b	Et	CH ₂ Ph	-	0.0742 ± 0.002
77c	Et	C ₆ H ₄ -4-OMe	-0.28	0.225 ± 0.004
77d	Et	C ₆ H ₄ -4-Me	-0.14	0.240 ± 0.004
77e	Et	C ₆ H ₅	0	0.340 ± 0.003
77f	Et	C ₆ H ₄ -4-Cl	0.24	0.581 ± 0.008
77g	Et	C ₆ H ₄ -4-CN	0.70	1.78 ± 0.02
77h	Me	CH ₂ Ph	-	1.80 ± 0.05
77i	Me	C ₆ H ₄ -4-Cl	0.24	9.67 ± 0.12

^a Referred to the *para*-substituent on the aromatic ring; ^b From reference ¹²⁵.

The substitution of the *N*-benzyl by *N*-phenyl in 4-oxo- β -lactams changes the leaving group from an amide to an anilide and causes an increase in the rate of ring opening by hydroxide ion, as **77e** is 5-fold more reactive than **77b**. *N*-Substitution would be expected to have a large effect on rate-limiting C-N fission but a much smaller one if nucleophilic attack on the carbonyl carbon and formation of the tetrahedral intermediate is the rate-limiting step. Electron withdrawing substituents (such as 4-cyanophenyl, **77g** and 4-chlorophenyl, **77f**) produce a modest increase the rate of the alkaline hydrolysis, whereas electron donating groups with lone pairs on the atoms adjacent to the π system (4-OMe, **77c**), decrease k_{OH} , by increasing the electron density through a resonance donating effect (Figure 3.9). Overall, **77g** is nearly 8-fold more reactive than **77c**. These relative rates suggest that the rate-limiting step is hydroxide-ion attack and formation of the tetrahedral intermediate.

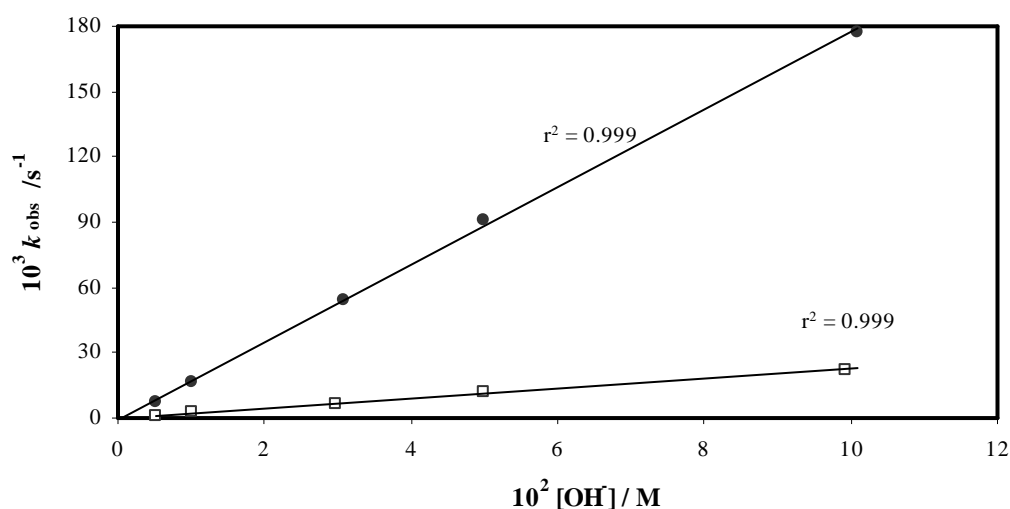


Figure 3.9 - Comparison of the chemical reactivity towards hydroxide between the less reactive 3,3-diethyl-*N*-aryl derivative **77c** (□), and the most reactive one, **77g** (●), at 25 °C.

For the 3,3-diethyl-*N*-aryl derivatives **77c-g**, a good correlation between the kinetic data and the electronic parameter σ_p of the *para*-substituent on the aromatic ring was found, giving a Hammett ρ_p value of 0.96 (Figure 3.10). This ρ_p value is positive, being indicative of the development of significant negative charge on the transition

state. This is consistent with rate limiting formation of the tetrahedral intermediate in the hydroxide-ion catalyzed reaction.

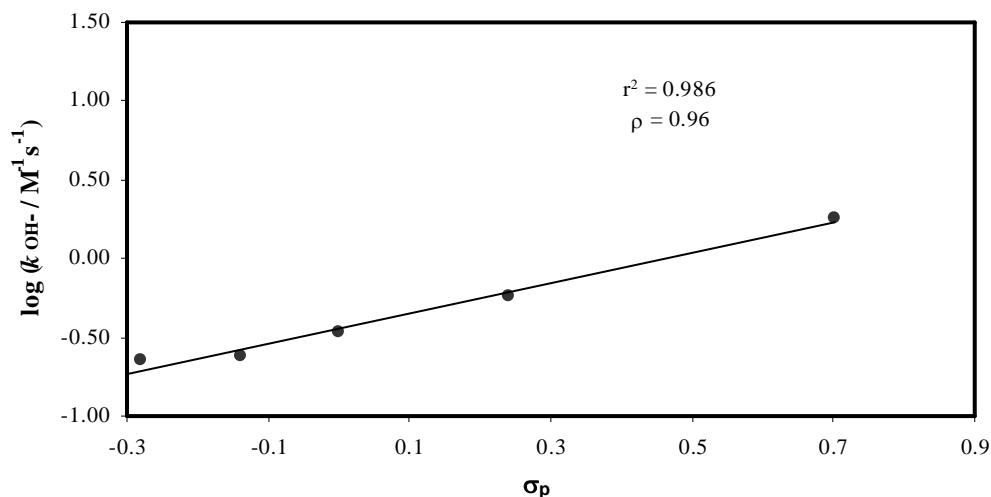
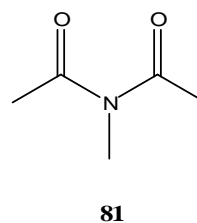


Figure 3.10 - Hammett plot for the second-order rate constants for the alkaline hydrolysis, k_{OH^-} , of **77c-g** at 25°C, yielding a ρ_p value of 0.96. Line is from linear regression analysis of the data.

There is a large steric effect of substituents α to the carbonyl carbon on the rate of alkaline hydrolysis. The α -gem-diethyl compounds **77b** and **77f** are about 20-fold less reactive than the corresponding α -gem-dimethyl compounds **77h** and **77i** (Figures 3.5 and 3.8), which is also compatible with rate limiting formation of the tetrahedral intermediate.

It is also important to note that the strained cyclic imide **77h** presented similar reactivity to that reported for the acyclic imide **81** (k_{OH^-} 1.54 $M^{-1}s^{-1}$),⁷² showing that there is no significant rate enhancement due to ring strain, once again compatible with the rate limiting step being the formation of the tetrahedral intermediate.



The mechanism for the alkaline hydrolysis of 4-oxo- β -lactams **77** is illustrated in Figure 3.11. The hydrolysis product is the corresponding α -amido acids, **82**.

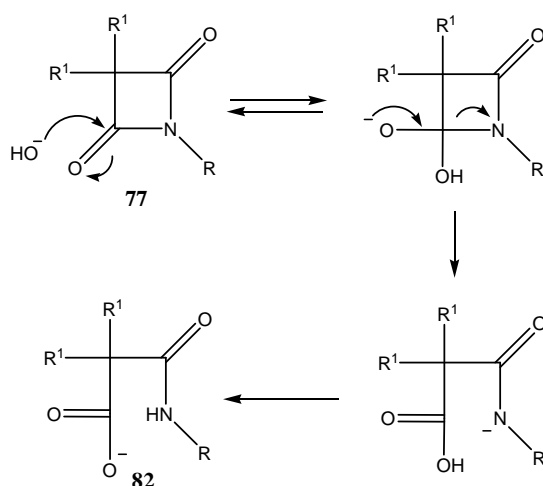
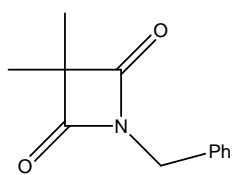


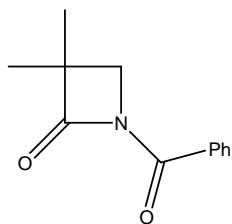
Figure 3.11 - The mechanism of alkaline hydrolysis of 4-oxo-β-lactams **77**.

Interestingly, at this stage of the project, another laboratory has also been investigating 4-oxo-β-lactams, in particular, **77h**, as a peptidomimetic template for elastase inhibition, and been performing alkaline hydrolysis studies to evaluate the intrinsic chemical reactivity as well. Thus, it was reported that the second-order rate constant for alkaline hydrolysis of **77h** at 30 °C, 1% DMSO (v/v), and 1.0 M ionic strength is $k_{\text{OH}^-} = 8.38 \text{ M}^{-1}\text{s}^{-1}$.¹⁵⁷ Furthermore, this result was compared with the alkaline hydrolysis of *N*-benzoyl-β-lactam **83**, in the same condition, in order to evaluate the effect of an exo- and endo-cyclic *N*-acyl substituent on the intrinsic chemical reactivity. In fact, compound **77h** has an increased ring strain compared to **83**, due to the incorporation of the *N*-acyl group into the four-membered ring. However, it was reported that k_{OH^-} for **77h** was, remarkably, only 7-fold greater than that for the corresponding *N*-benzoyl-β-lactam **83**, demonstrating the surprisingly small effect of introducing another 3-coordinate carbon, formally a sp^2 centre, in the already strained four-membered ring. Indeed, for both derivatives, the rate-limiting step is the formation of the tetrahedral intermediate and the release of strain does not occur in the transition state.¹⁵⁷

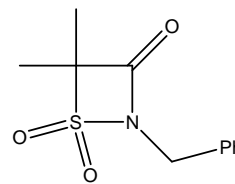
Since 4-oxo-β-lactams were designed as a result of an isosteric substitution at 3-oxo-β-lactams, in order to improve hydrolytic stability, as stated in Section 1.9, the most remarkable result from alkaline hydrolysis studies of 4-oxo-β-lactams is the notably lower intrinsic chemical reactivity compared to 3-oxo-β-lactams like **35**.



77h



83



35

3.4. PPE INHIBITION STUDIES

3.4.1 Results and Discussion

In a preliminary study of 4-oxo- β -lactams as elastase inhibitors, the synthesized compounds were tested against serine protease PPE and the obtained results are presented next. Firstly, PPE inhibition assays were performed using the incubation method.¹³⁶ However, incubation resulted in most cases (**77c-g**), in a very rapid time-dependent loss of activity, which did not allow the determination of the inhibition constants.

Therefore, inhibition was studied at 25 °C using the progress curve method,¹⁴² by monitoring continuously the hydrolysis of the reporter substrate, *N*-succinyl-(L-Ala)₃-*p*-nitroanilide at 390 nm.

Different concentrations [I] for each **77c-g** derivative were assayed and typical slow-binding inhibition progress curves were obtained, as illustrated in Figure 3.12. Progress curves data were analysed by slow binding kinetics.¹⁴² Thus, the initial and steady state velocities v_i and v_s , and the pseudo-first-order rate constants, k_{obs} , were calculated similarly with the previously described for HLE inhibition studies, in Chapter 2, using Equation 2.6.

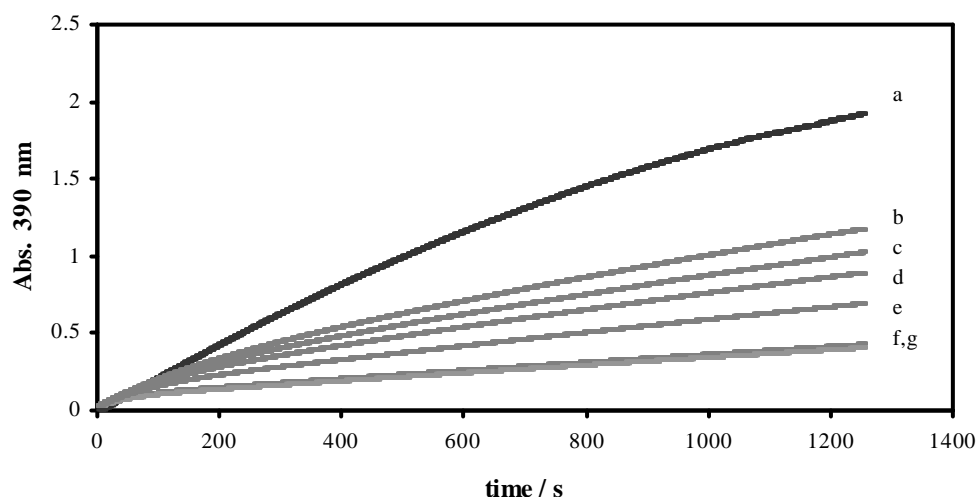


Figure 3.12 - Progress curves for slow-binding inhibition of PPE by 77f. Reaction conditions: [PPE] = 0.2 μ M, [*N*-Suc-(L-Ala)₃-*p*-NA] = 0.3 mM, 0.1 M HEPES buffer, pH 7.2, 5% DMSO, 25 °C. Inhibitor concentrations: (a), in absence of inhibitor; (b), 10; (c), 15; (d), 20; (e), 30; (f), 60; (g) and 75 μ M.

The obtained k_{obs} values for each inhibitor are presented in *Appendix 3, Table A3.2*. The final plots of k_{obs} versus [I] for **77c-g** are illustrated in Figures 3.13-15.

The plots of k_{obs} versus the concentration of 4-oxo- β -lactams **77c-g** were linear and thus consistent with the inhibition mechanism depicted earlier in Scheme 2.6, Section 2.3.2.2 (Mechanism A).

In this way, **77c-g** react with the enzyme as alternate substrate inhibitors, leading to the acylation of the active site serine residue, EI, followed by slow hydrolysis to regenerate the free enzyme.

The linear dependence of k_{obs} versus concentration of inhibitor [I], as well as the observation that the initial velocities, v_i , are all identical and equal the initial velocity in the absence of inhibitor (Figure 3.13), suggest that isomerization of the acyl-enzyme did not occur under the inhibitor concentration range used. Thus, the inhibitory potencies of 4-oxo- β -lactams **77c-g**, given by k_{on} values, were calculated using Equations 2.7 and 2.8.

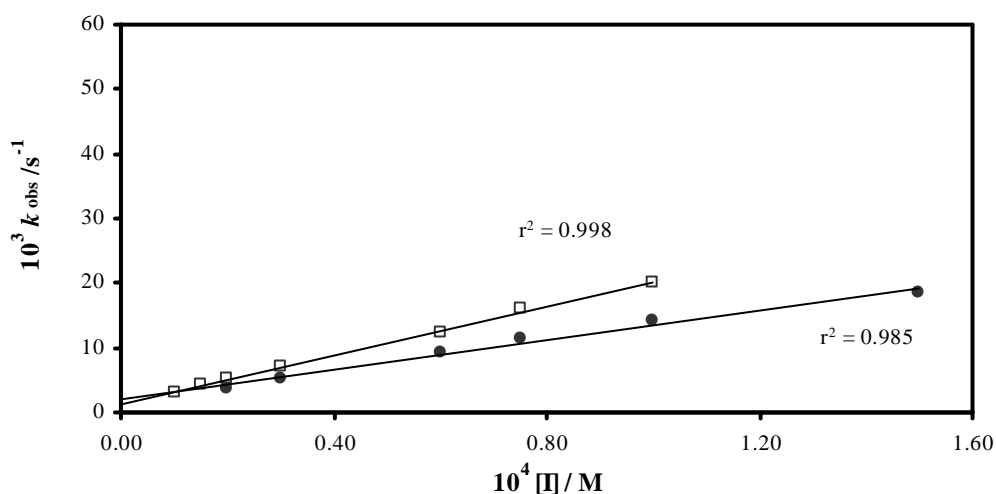


Figure 3.13 - Effect of inhibitor concentration on the onset of inhibition of PPE by 77c (●) and 77d (□), at 25 °C. Points are experimental and lines are from linear regression analysis of data, giving: $k_{off} = 2.02 \times 10^{-3} s^{-1}$ (ordinate intercept) and $k_{on}' = 115 \pm 7.1 M^{-1}s^{-1}$ (slope) for 77c; and $k_{off} = 1.35 \times 10^{-3} s^{-1}$ and $k_{on}' = 189 \pm 3.7 M^{-1}s^{-1}$ for 77d. By correction using Equation 2.8, $k_{on} = 124 \pm 7.6 M^{-1}s^{-1}$ for 77c and $k_{on} = 204 \pm 4.0 M^{-1}s^{-1}$ for 77d. K_i was obtained by the ratio k_{off}/k_{on}

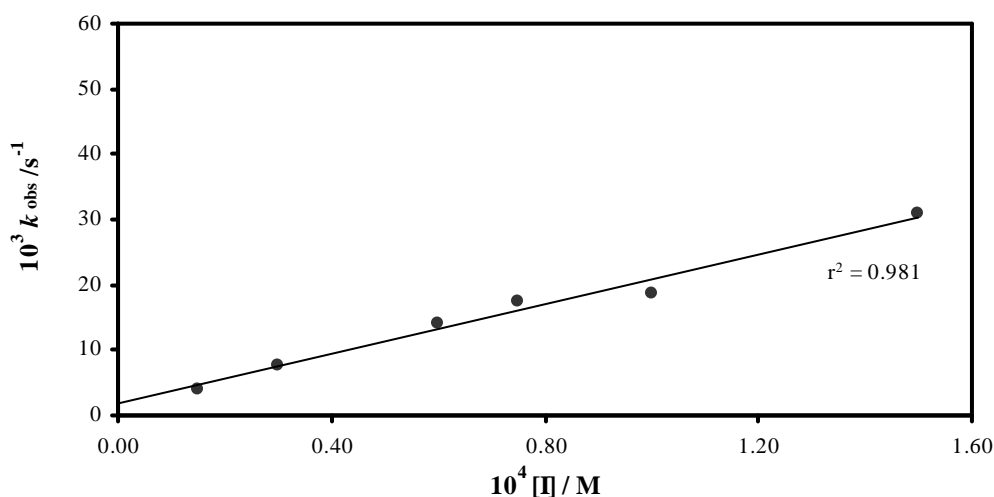


Figure 3.14 - Effect of inhibitor concentration on the onset of inhibition of PPE by 77e at 25 °C. Points are experimental and the line is from linear regression analysis of the data, giving $k_{off} = 1.81 \times 10^{-3} s^{-1}$ (intercept) and $k_{on}' = 191 \pm 13.5 M^{-1}s^{-1}$ (slope). By correction using Equation 2.8, $k_{on} = 206 \pm 14 M^{-1}s^{-1}$. K_i was obtained by the ratio k_{off}/k_{on}

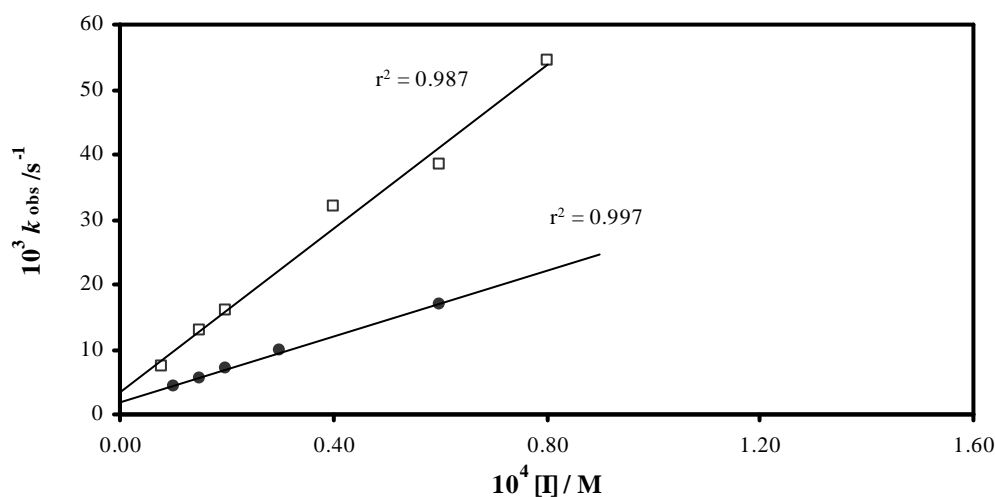


Figure 3.15- Effect of inhibitor concentration on the onset of inhibition of PPE by **77f** (●) and **77g** (□). Points are experimental and the lines are from linear regression analysis of the data, giving $k_{off} = 1.97 \times 10^{-3} s^{-1}$ and $k_{on}' = 251 \pm 8.2$ for **77f**; and $k_{off} = 2.91 \times 10^{-3} s^{-1}$ and $k_{on}' = 629 \pm 36 M^{-1}s^{-1}$ for **77g**. By correction using Equation 2.8, $k_{on} = 271 \pm 8.2 M^{-1}s^{-1}$ for **77f** and $679 \pm 39 M^{-1}s^{-1}$ for **77g**. K_i was obtained by the ratio k_{off}/k_{on}

In these preliminary studies, a simplistic way was used to obtain k_{off} , by the intercept of the plots of k_{obs} versus the inhibitor concentration (Figures 3.13-3.15), and thus K_i was obtained by the ratio k_{off}/k_{on} .

However, a different way to determine K_i uses Equations 2.10 and 2.11. In *Appendix 3, Section A3.2.1* the analysis of the inhibition kinetics and the determination of K_i based on these equations for a representative compound, **77e**, are presented. In this way, k_{off} is given by Equation 2.9. The obtained K_i and k_{off} values from this method were consistent with those obtained from Figure 3.15. The kinetic parameters for PPE inhibition by 4-oxo- β -lactams **77c-g** are listed below (Table 3.4) and discussion of these results will be made later in this chapter (Section 3.4.1.1).

In contrast to the slow-binding inhibition kinetics displayed by 3,3-diethyl-*N*-aryl-4-oxo- β -lactams **77c-g**, progress curves for the 3,3-dimethyl analogue **77i** presented strictly linear time courses for the hydrolysis of substrate, i.e. no initial exponential phase towards a steady-state was observed. Thus, the Kitz and Wilson's method of

incubation was used to investigate the time-dependent inhibition.¹³⁶ However, incubation of 15 mM of **77i** with PPE, in a molar ratio inhibitor to enzyme of 15, led to a labile PPE inhibition, followed by a rapid increase in enzymatic activity to nearly 90% within a few *minutes* of reaction (Figure 3.16).

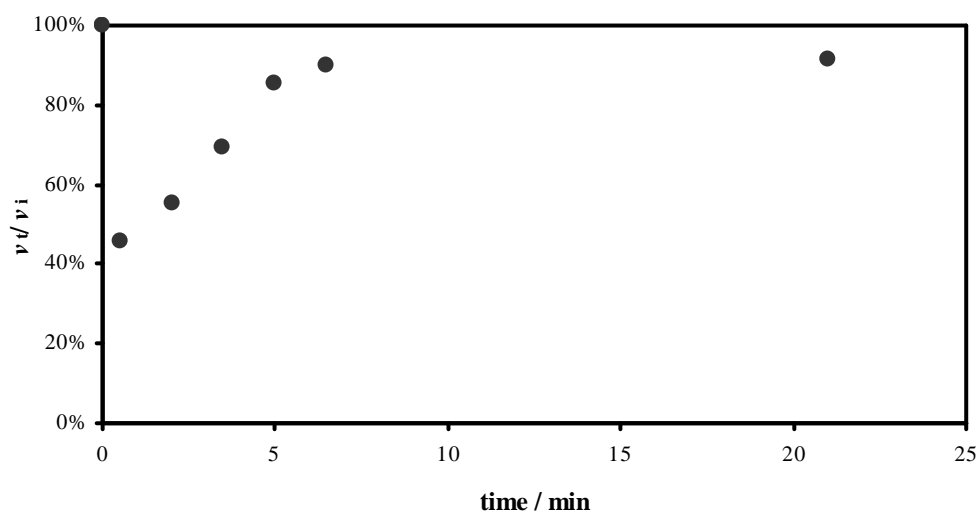


Figure 3.16 - Plot of the remaining PPE activity after incubation with **77i** ([I] = 15 mM) at 25 °C, pH 7.2, [I]/[E] = 15, leading to a rapid increase of enzymatic activity. Points are experimental and reflect the withdrawn aliquots at different time intervals from the incubation mixture for measuring the enzymatic activity.

For comparison, the 3,3-diethyl counterpart **77f**, which was found to be an effective irreversible inhibitor of PPE, was also studied using the incubation method. Thus, it was possible to investigate the stability of the corresponding acyl-enzyme complex. In contrast to Figure 3.16, Figure 3.17 suggests that the interaction of **77f** with PPE leads to a stable acyl-enzyme, EI, which slowly breaks down and regenerates the free, active enzyme, E, within a few *hours* of reaction and the inhibitor function as alternate substrate inhibitor of PPE, accordingly to Scheme 2.6, with an almost complete recovery of enzymatic activity. In fact, the less sterically hindered dimethyl derivative **77i** allowed the acyl-enzyme to undergo a more rapid hydrolysis (see discussion later in this chapter), and the Lineweaver-Burke plot (Figure 3.18) was used to determine the inhibition kinetic. The respective concentrations of substrate and initial rates are given in *Appendix 3, Section A3.2.2*.

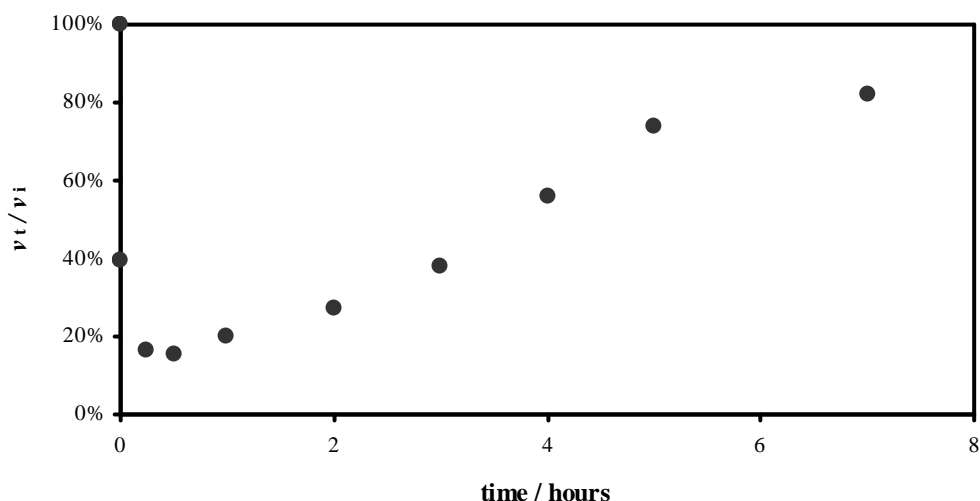


Figure 3.17 - Time-dependent loss of enzymatic activity. Excess of inhibitor 77f ($[I] = 150 \mu\text{M}$) was incubated with PPE ($[E] = 10 \mu\text{M}$) in 0.1 M HEPES buffer, pH 7.2, 25 °C. Points are experimental and reflect withdrawn aliquots at different time intervals for measuring the enzymatic activity.

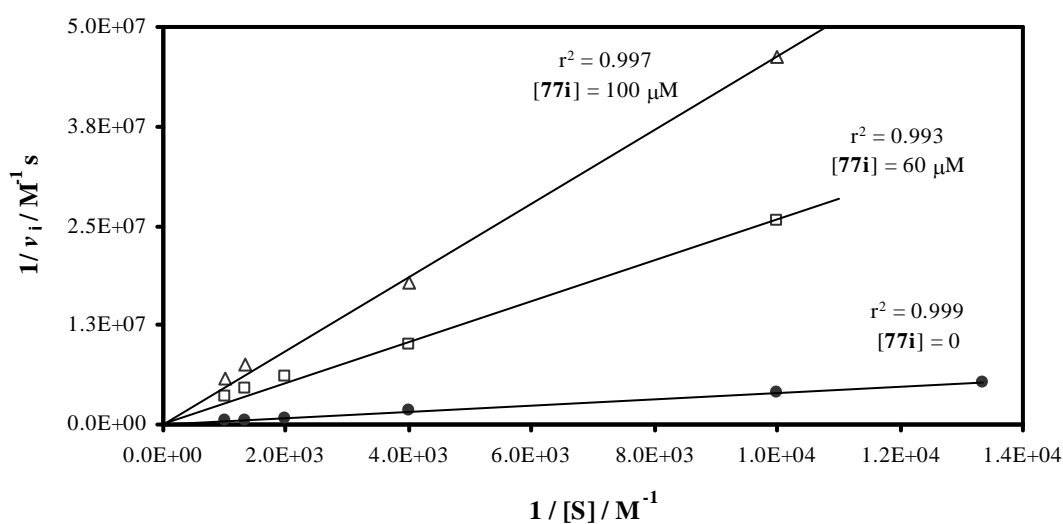
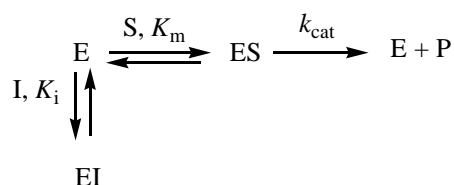


Figure 3.18 - Lineweaver-Burke plot for the PPE catalyzed hydrolysis of the substrate: in the absence of inhibitor (\bullet); and in the presence of 77i at 100 μM , $[I]/[E] = 100$ (Δ) and at 60 μM , $[I]/[E] = 60$ (\square). Points are experimental and lines are from linear regression analysis of data. At 100 μM , the obtained K_i was 9.29 μM , being in good agreement with that obtained at 60 μM (10.8 μM). Thus, the K_i value for 77i, given by the average, is 10 μM .

The trend lines in Figure 3.18 have the same ordinate intercept, indicating that V_{\max} is unaltered, but an increase in apparent K_m' agrees with Equation 3.1. Thus, **77i** behaves as a competitive reversible inhibitor of PPE and K_i was determined graphically.

$$K_m' = K_m (1 + [I] / K_i) \quad (3.1)$$

Besides the equilibrium between the enzyme and the substrate ES, a rapid reversible equilibrium is established between the enzyme and the inhibitor EI (Scheme 3.15), giving $K_i = 10 \mu\text{M}$. For **77h** a similar behavior was found, and the respective plot is depicted in Figure 3.19, giving $K_i = 184 \mu\text{M}$ (see data in Appendix 3, Section A3.2.2).



Scheme 3.15 - Competitive reversible enzyme inhibition mechanism.

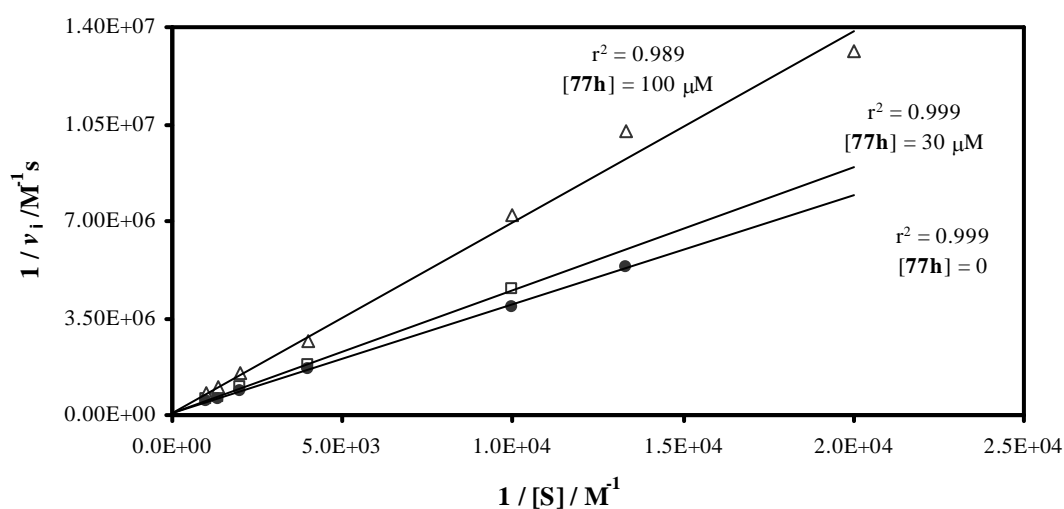


Figure 3.19 - Lineweaver-Burke plot for the PPE catalyzed hydrolysis of the substrate, in the absence of inhibitor (\bullet) and in the presence of inhibitor **77h** at $30 \mu\text{M}$, $[I]/[E] = 30$ (\square) and at $100 \mu\text{M}$, $[I]/[E] = 100$ (Δ). Points are experimental and lines are from linear regression analysis of data, giving $K_i = 184 \mu\text{M}$ for **77h**.

By contrast, the *N*-alkyl-3,3-diethyl derivatives **77a** and **77b** were found to be non-inhibitors of PPE, even when assayed at a final concentration of 60 μM . Next, the results of PPE inhibition studies for the whole set of 4-oxo- β -lactam **77** is presented (Table 3.4).

In order to explore the relationships between intrinsic chemical reactivity and enzyme inhibitory activity, the values for the second-order rate constant for alkaline hydrolysis, k_{OH^-} , for the same compounds are included in Table 3.4 and also the respective EREFs. Thus, the results of inhibitory activity are analyzed in conjunction with the data from reactivity studies.

Table 3.4 - Kinetic parameters for PPE inhibition at pH 7.2 and 25 °C by 4-oxo- β -lactams **77. For comparison, k_{OH^-} for the alkaline hydrolysis of the same compounds at 25 °C are included and also the respective EREFs.**

Compound	$K_i / \mu\text{M}$	$k_{\text{on}} / \text{M}^{-1}\text{s}^{-1}$	$10^3 k_{\text{off}} / \text{s}^{-1}$	$k_{\text{OH}^-} / \text{M}^{-1}\text{s}^{-1}$	EREF
77a	NI ^a	NI ^a	-	-	-
77b	NI ^a	NI ^a	-	0.0742	-
77c	16.3	124 \pm 7.6	2.02	0.225	551
77d	6.62	204 \pm 4.0	1.35	0.240	850
77e	8.78 ^b	206 \pm 14	1.81 ^b	0.340	606
77f	7.28	271 \pm 8.2	1.97	0.581	466
77g	4.29	679 \pm 39	2.91	1.78	381
77h	184	-	-	1.80	-
77i	10.0	-	-	9.67	-

^a No inhibition; ^b By using Equations 2.10-2.11, $K_i = 20.2 \pm 1.7 \mu\text{M}$ and $k_{\text{off}} = 4.15 \times 10^{-3} \text{ s}^{-1}$, as presented in Appendix 3, Section A3.2.2.

3.4.1.1 Structure Activity Relationships and Molecular Modeling

Inhibition of PPE by 4-oxo- β -lactams is a result of Ser-195 nucleophilic attack at one of the carbonyl carbons of the 4-oxo- β -lactam (cyclic imide), with ring opening, and expulsion of an amide leaving group by C-N bond fission. It is of interest to evaluate the effect of the substituents on C-3 and N-1 on the inhibitory potency against PPE. Inspection of Table 3.4 indicates that the most potent inhibitors contain an *N*-aryl group as well as two ethyl groups at C-3. In contrast, *N*-alkyl-4-oxo- β -lactams are either inactive (**77a-b**) or weak inhibitors that rapidly regenerate the active enzyme (**77h**).

Free Energy Relationships for PPE Catalyzed Hydrolysis of 77c-g. The rate of PPE inhibition by 3,3-diethyl-*N*-aryl 4-oxo- β -lactams **77c-g** was found to be linearly correlated with the Hammett σ_p values for the substituent at the *para* position on the aromatic ring, giving a ρ_p value of 0.68 (Figure 3.20). For comparison, the Hammett plot for alkaline hydrolysis of the same compounds at 25 °C is conveniently repeated in this figure.

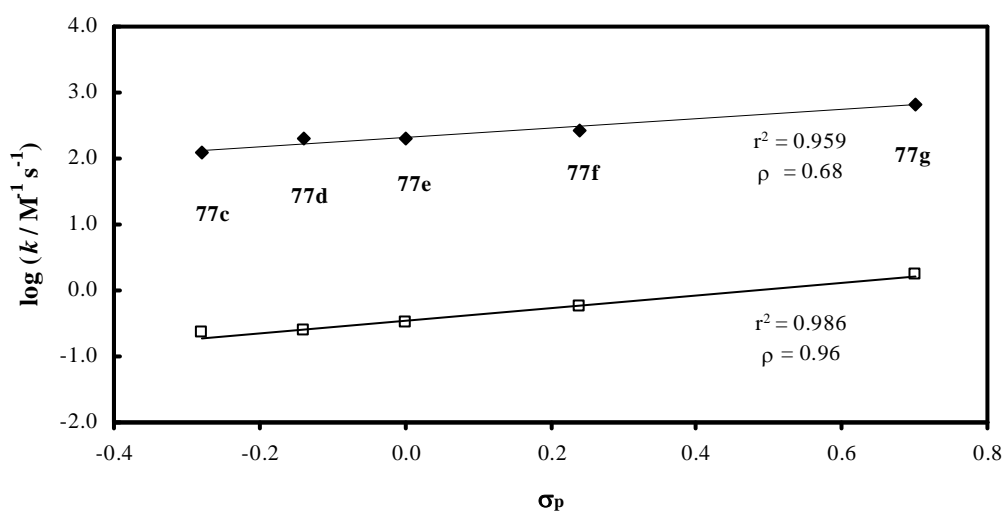


Figure 3.20 - Hammett plots for the second-order rate constants, k_{on} , for the inhibition of PPE by 4-oxo- β -lactams **77c-g** (\blacklozenge) and for the hydroxide-ion-catalyzed hydrolysis, k_{OH^-} , of the same compounds (\square) at 25°C.

The obtained positive ρ_p value for the PPE-catalyzed reaction is consistent with the development of significant negative charge on the transition state, indicative of rate limiting formation of the tetrahedral intermediate.

In comparison to PPE inhibition studies, the alkaline hydrolysis of 4-oxo- β -lactams **77c-g** gave a Hammett ρ_p value of 0.96, suggesting a much greater change in charge on going to the transition state. Both enzyme catalyzed acylation and alkaline hydrolysis of the 4-oxo- β -lactams involve rate limiting nucleophilic attack on the β -lactam carbonyl carbon, and the strain energy of the four-membered ring is not released in the transition state. The different Hammett ρ values indicate that the attack of serine residue occurs at an earlier position along the reaction coordinate compared with the hydroxide-ion-catalyzed hydrolysis.

This is consistent with the Hammond postulate in that these results suggest that the 4-oxo- β -lactam scaffold promotes the enzyme's ability to use its catalytic apparatus to stabilise the transition state and increase the rate of serine acylation, which might be achieved by favourable non-covalent binding of enzyme and inhibitor, stabilization of the tetrahedral intermediate in the oxyanion hole of the active site and compensation for the entropy loss required in the bimolecular reaction, being reflected in the EREF values (Table 3.4).

The hydrolysis of 4-oxo- β -lactams catalyzed by PPE is represented in Figure 3.21, being in accordance with Scheme 2.6 (Chapter 2). These inhibitors function as acylating agents of PPE to yield an acyl-enzyme complex **84**, which suffers deacylation (hydrolysis), regenerating the free enzyme.

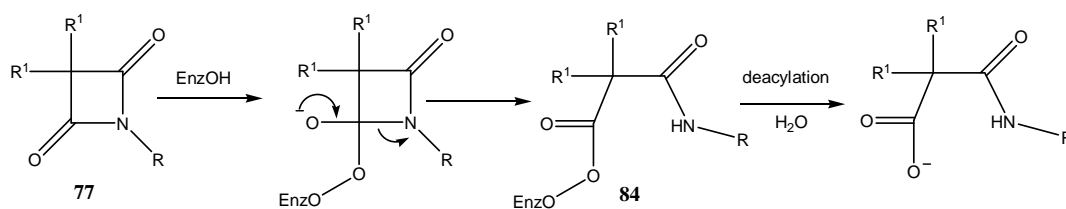


Figure 3.21 - The hydrolysis of 4-oxo- β -lactams mediated by PPE.

Table 3.4 indicates that the most active inhibitor contains a 4-CN electron-withdrawing substituent on the *N*-aromatic ring (**77g**) that increase the chemical reactivity of the carbonyl carbon towards nucleophilic attack of the Ser-195 hydroxyl group (inductive effect) and is nearly 5 fold more potent than **77c**, which is the less active inhibitor of this series and contains an electron donating substituent (4-OMe) (Figure 3.22).

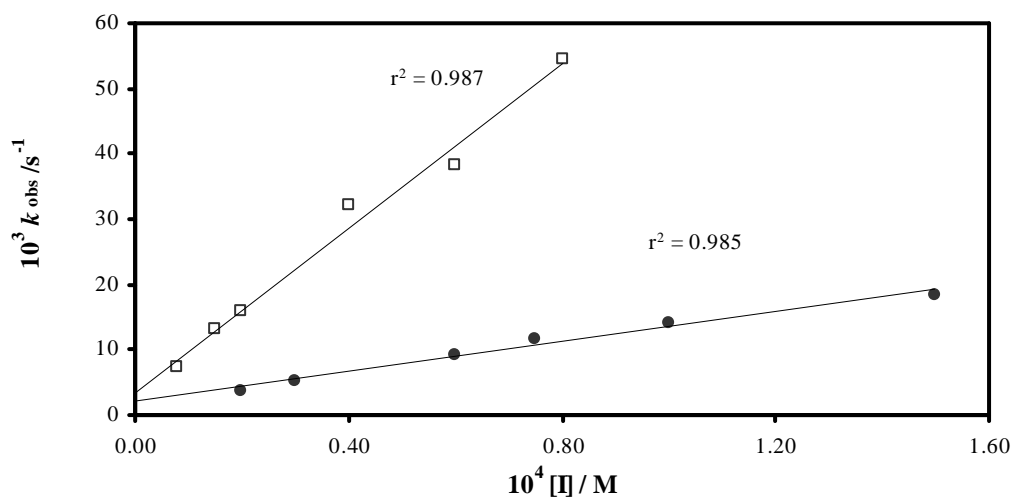


Figure 3.22 - Comparison between the effect of 4-oxo- β -lactam concentration on the onset of inhibition of PPE by **77c** (◆), the most potent inhibitor of the series and **77g** (□), the less potent one, at 25 °C. Points are experimental and lines are from linear regression analysis.

Therefore, increasing the intrinsic chemical reactivity of 4-oxo- β -lactams **77c-g** increases the rate of PPE acylation (Table 3.4), giving a good correlation (Figure 3.23, $r^2 = 0.922$). For these compounds, k_{OH} - functions as a guide to indicate the potential acylating power as serine enzyme PPE inhibitors.

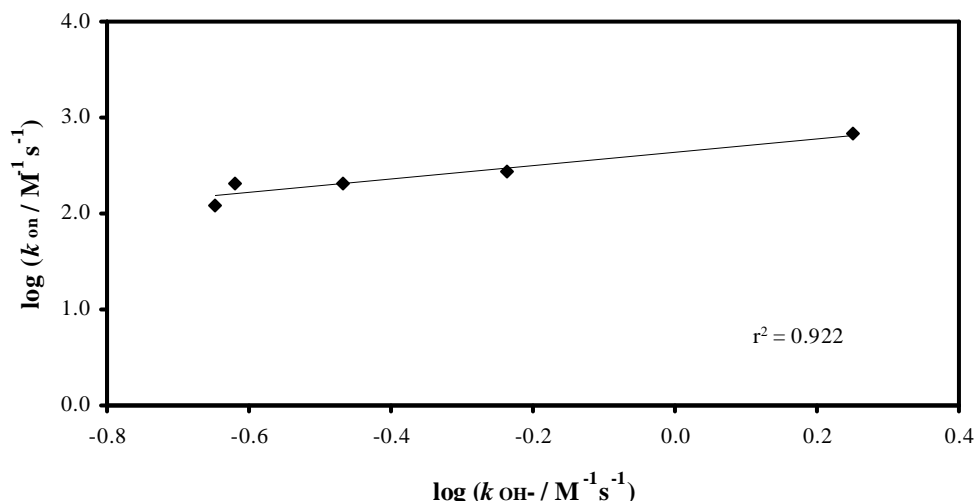


Figure 3.23 - Linear correlation between the second-order rate constant for PPE inhibition, k_{on} and the second-order rate constant for alkaline hydrolysis, k_{OH^-} . Line is from linear regression analysis of data.

Molecular Modeling Studies. To rationalize the trends observed in the enzyme assays, the molecular interactions between some 4-oxo- β -lactams **77** and PPE were investigated using the automated GOLD docking program (see Experimental Section for details). These studies were performed by Dr. Rita Guedes (iMed.UL, Lisbon). Docking of the most potent inhibitor **77g** into the active site of PPE revealed that only one ethyl substituent of the 3,3-diethyl group lies in the S_1 pocket (Figure 3.24A). This binding mode is not much different than that observed for the interaction of 3,3-diethyl- β -lactams with HLE, in which both ethyl substituents are accommodated in the larger S_1 pocket.¹⁰⁹ The distance between the closest carbonyl carbon of **77g** and the Ser-195 hydroxyl oxygen atom is about 3.18 Å (4.79 Å for the other carbonyl carbon atom), which indicates that nucleophilic attack by Ser-195 to the 4-oxo- β -lactam is possible. Interestingly, the “reactive” carbonyl of **77g** is not involved in the H-bond network with the so-called oxyanion hole defined by the backbone NHs of Gly-193 and Ser-195: the distance between the amidic hydrogen atoms of Gly-193 and Ser-195 to the carbonyl oxygen atom is 6.75 and 5.28 Å, respectively. This result may indicate that the oxyanion hole is not used to stabilize the TI derived from **77g**. However, some several key interactions seem to stabilize **77g** in the active site.

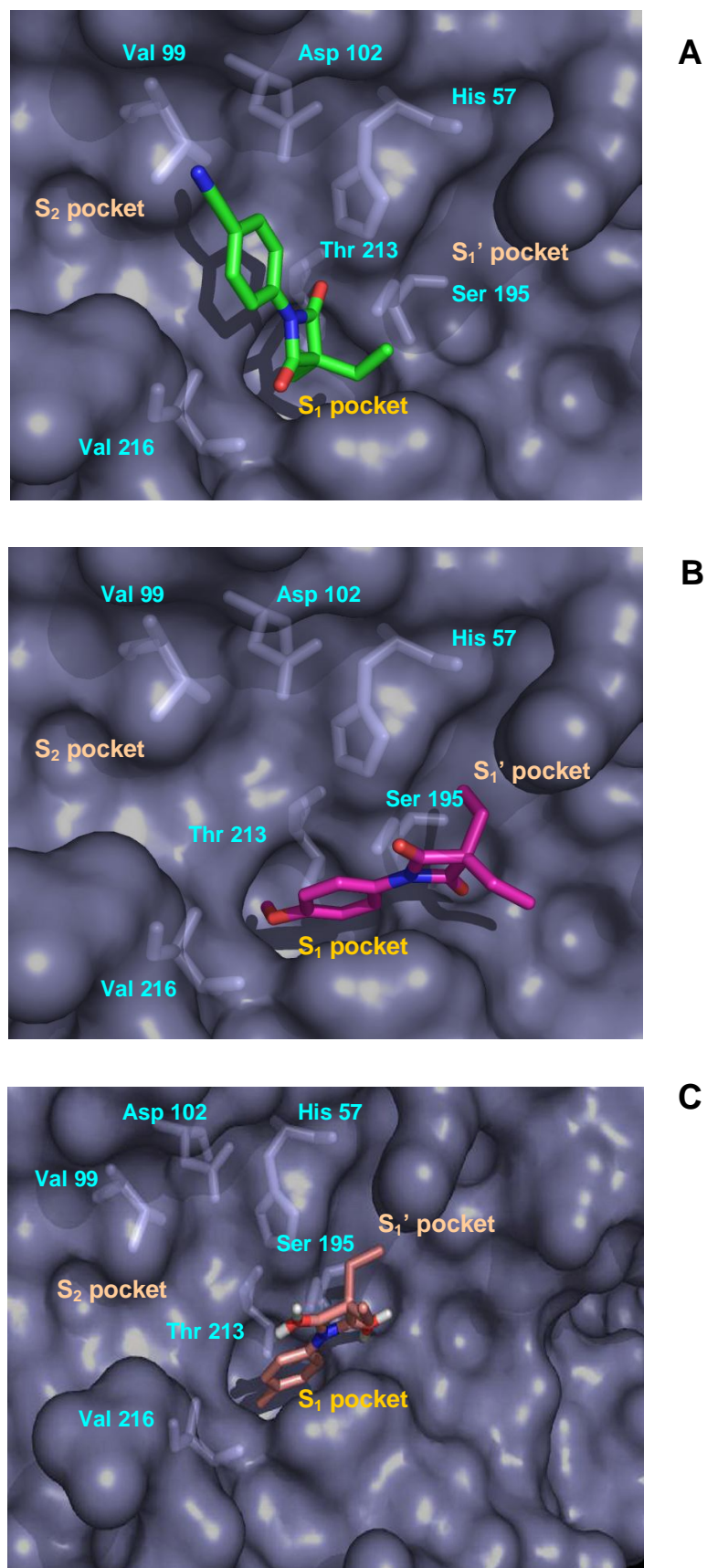


Figure 3.24 - Docking of 77g (A), 77c (B) and 77d (C) in the active site of PPE (see text for details).

First, strong hydrogen bonds involve the oxygen atom of the reactive carbonyl group and the NH of His-57 and the hydroxyl group of Ser-195. Second, an additional hydrogen bond involves the oxygen atom of the unreactive carbonyl and the amide group of Gln-192. Finally, enhanced Van der Waals contacts between the *N*-aryl moiety with Val-99, Phe-215 and His-57 were observed.

For compound **77c**, a less potent inhibitor, an inverted binding mode was observed, in which the 4-OMe substituent of the aromatic ring lies on the S_1 pocket, while one of the ethyl substituents is close to the S_1' pocket (Figure 3.24B). The distance between the closest carbonyl carbon and the Ser-195 hydroxyl oxygen atom is 3.62 Å (4.38 Å for the other carbonyl carbon atom). However, in contrast to **77g**, the “reactive” carbonyl of **77c** is involved in the H-bond network with the NHs of Gly-193 and Ser-195, which suggests that the oxyanion hole may be used to stabilize the resulting TI and to compensate the energy required for the enzyme to overcome the distance between Ser-195 and the carbonyl carbon. Compound **77d** also presents the *N*-aryl moiety sitting in the S_1 pocket of the enzyme (Figure 3.24C), but in this case the distance between the closest carbonyl carbon and the Ser-195 hydroxyl oxygen atom is 3.27 Å, i.e. close to that of **77g**. This binding mode suggests that nucleophilic attack by Ser-195 to the 4-oxo- β -lactam **77d** is feasible and is consistent with the EREF value of 850, the highest of the present series of compounds **77**.

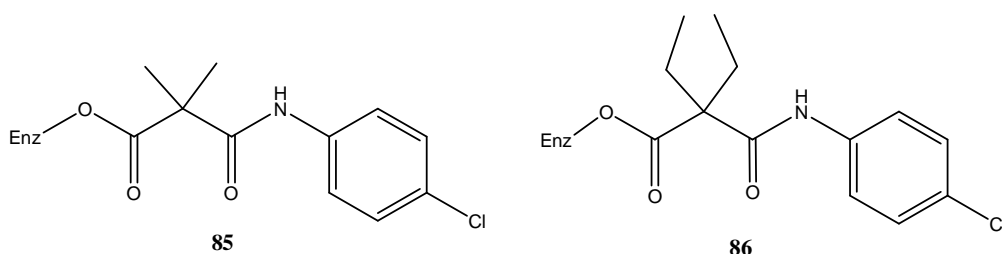
Indeed, as 4-oxo- β -lactam **77** have two acyl centers, there could be interaction of either the C-3 (as in **77g**) or the *N*-1 substituents (as in **77c-d**), with the S_1 binding pocket. In principle the latter could reduce the rate of acylation as a result of non-productive binding.

The Effects of the Substituent at C-3. It is known that the C-3 substituents allow interaction with the S_1 binding pocket of PPE, being preferred small hydrophobic substituents with two carbon atoms.¹⁰⁴ However, the C-3 dimethyl 4-oxo- β -lactam **77h**, interacts with PPE in a similar binding mode to that of the C-3 diethyl derivatives **77c-d**, i.e. aromatic ring lying on the S_1 pocket (Appendix 3, Figure A3.6)

and with the “reactive” carbonyl involved in the oxyanion hole H-bond network, as revealed by docking studies.

The bigger gem-diethyl group at C-3 only provided enzyme inhibition when combined with chemically more electron-withdrawing *N*-aryl substituents, being the *N*-alkyl analogues non inhibitors. For the 3,3-diethyl derivatives, expulsion of an anilide by C-N fission from the decomposition of TI, contributes significantly to the time-dependent inhibition of PPE rather than an aliphatic amide (being **77c-g** irreversible inhibitors while **77a-b**, non-inhibitors). By contrast, both *N*-alkyl and *N*-aryl 3,3-dimethyl derivatives **77h-i** inhibited PPE, but rapidly regenerated the free-active enzyme.

An important criterion for the successful inhibition of serine enzymes by an acylation process depends upon the lifetime of the acyl-enzyme intermediate. The less sterically hindered acyl-enzyme intermediate **85**, formed by reaction of the 3,3-dimethyl derivative **77i** with PPE, suffered rapid hydrolysis (Figure 3.16), while the correspondent acyl-enzyme **86**, obtained by reaction of its 3,3-diethyl counterpart **77f**, persisted during hours (Figure 3.17). The bigger gem-diethyl group is likely to significantly block attack by water of the active site at the acyl-enzyme ester of **86**, increasing its lifetime.



Thus, **77f** is an effective time-dependent irreversible inhibitor of PPE because of its relatively fast acylation and slow deacylation of the enzyme, while the dimethyl counterpart **77i**, although being a potential time-dependent inhibitor, allow the enzyme to turnover rapidly due to a relatively facile deacylation pathway, behaving macroscopically as a competitive inhibitor.

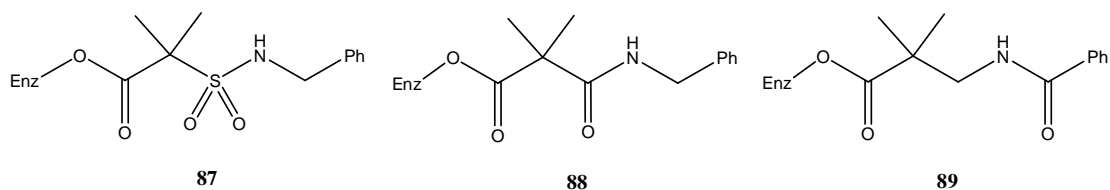
4-Oxo- β -lactams versus 3-Oxo- β -sultams in PPE Inhibition. Since 4-oxo- β -lactams were designed as isosteric analogues of previously discussed 3-oxo- β -sultams, it was of interest to compare the inhibitory properties for both scaffolds. As discussed in Section 1.6.2.2, PPE inhibition by 3-oxo- β -sultams results in a stable acyl-enzyme complex from enzyme-mediated ring opening by C-N bond fission, and expulsion of the sulfonamide leaving group.¹¹⁶

On the other hand, reaction of 4-oxo- β -lactams **77** with PPE involves serine nucleophilic attack at a reactive carbonyl carbon, with expulsion of a poorer amide leaving group, which may improve selectivity against the target enzyme. It is interesting to note that the *N*-benzyl-3,3-dimethyl-4-oxo- β -lactam **77h** has also been studied as inhibitor of PPE by W. Tsang et al, from a different laboratory, and the correspondent results are interesting to be discussed here. It was reported that the rate of formation, k_{on} , and breakdown, k_{off} , of the acyl-enzyme obtained by reaction of PPE with **77h** are, respectively, $63 \text{ M}^{-1}\text{s}^{-1}$ and 0.00997 s^{-1} , at pH 6.¹⁵⁷ Interestingly, moving the C-4 carbonyl group of **77h** to N-1 to give the corresponding *N*-acyl- β -lactam **83** (Section 3.3.1.1) decreased the rate of PPE acylation, as the respective k_{on} was reported to be $16.2 \text{ M}^{-1}\text{s}^{-1}$.¹⁵⁷ This result reflects the superior inhibitory property of the 4-oxo- β -lactam scaffold over simple β -lactams.

The same author found that the rate of PPE acylation by **77h** is 12-fold slower than that observed for the 3-oxo- β -sultam counterpart, **35** (**35**, Figure 1.12, $k_{\text{on}} = 7.68 \times 10^2 \text{ M}^{-1}\text{s}^{-1}$), with the same enzyme and at pH 6.0. By contrast, the rate of deacylation in the reaction of PPE with **77h** was reported to be 500-fold faster than that of the reactivation of the enzyme inhibited with **35** (**35**, $k_{\text{off}} = 2.08 \times 10^{-5} \text{ s}^{-1}$).¹⁵⁷

Nucleophilic attack at the carbonyl centre of **35** and that of **77h** generates a sulfonamide and an amide leaving group, respectively, being the correspondent acyl-enzyme complexes compounds **87** and **88**. Accordingly to W. Tsang, although sulfonamides and amides have different electronic properties (for example, sulfonamides are generally more acidic than amides by about 5 $\text{p}K_{\text{a}}$ units),¹⁵⁸ the stability of the acyl ester of the acyl enzymes was unlikely to be affected by this property as the groups were some distance from the acyl ester. However, the sulfonyl group of **87**, being bigger in size, was likely to severely impair attack by water for deacylation, increasing the half-life of **87**, and thus explaining the decrease by 500-

fold on the rate of deacylation compared with that observed with the amide leaving group, **88**.¹⁵⁷ The acyl-enzyme generated from the C-4 unsubstituted *N*-benzoyl β -lactam **83** has the structure shown in **89** and, despite the presence of the gem-dimethyl group, moving the carbonyl group further down in the ring-opened product reduced steric congestion around the acyl-enzyme ester, decreasing its half-life compared to **88**.



In the present study, good PPE irreversible inhibitory activity was found for 3,3-diethyl-*N*-aryl derivatives **77c-g**. Thus, the 4-oxo- β -lactams represent an attractive new class of serine proteases inhibitors.

These exciting results prompted this project to find out the effectiveness of 4-oxo- β -lactam as a suitable scaffold to design potent irreversible inhibitors of the therapeutic target HLE.

CHAPTER 4

AZETIDINE-2,4-DIONES (4-OXO- β -LACTAMS) AS
POTENT AND SELECTIVE INHIBITORS OF HLE

4. AZETIDINE-2,4-DIONES (4-OXO- β -LACTAMS) AS POTENT AND SELECTIVE INHIBITORS OF HLE

4.1. 4-OXO- β -LACTAM-BASED INHIBITOR DESIGN RATIONALE

Based on the promising results obtained for 4-oxo- β -lactams inhibitors of serine protease PPE, it was reasoned that this nucleus might inactivate the therapeutic target HLE via a similar acylation mechanism.

Thus, besides the synthesized azetidine-2,4-diones (Chapter 3), differently N-1 and C-3 substituted 4-oxo- β -lactams were prepared, in order to investigate the structure-activity relationships (SAR) towards HLE. These structural modifications attempt to improve both inhibitory potency and target selectivity, exploiting S_1 and S' subsites of the enzyme (Figure 4.1).

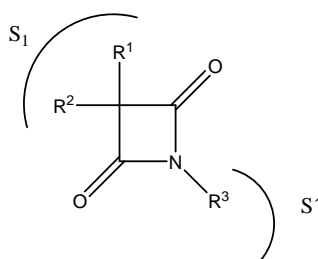


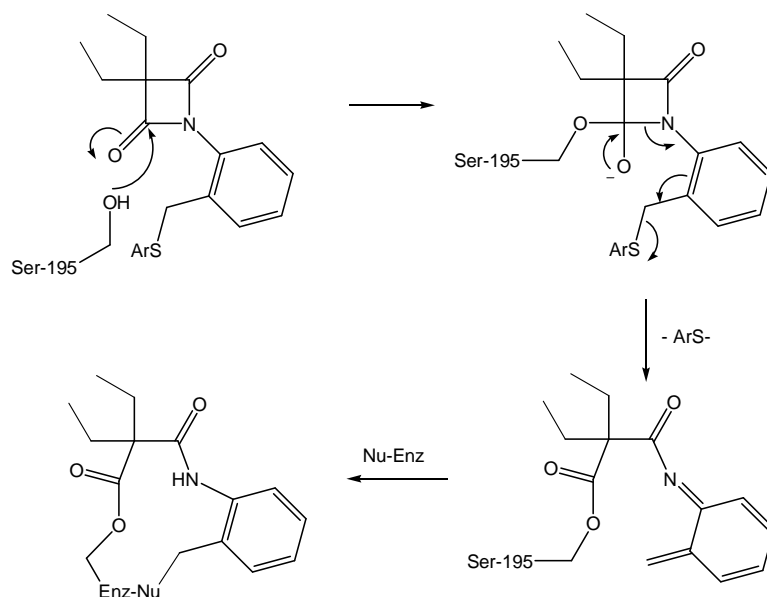
Figure 4.1 – Schematic drawing of the spatial arrangement of C-3 and N-1 substituents of azetidine-2,4-diones in the active site of HLE.

Therefore, different groups at C-3 (gem-diethyl, gem-dimethyl, ethylbenzyl, methylbenzyl, ethyl-*iso*-butyl, ethyl-*n*-butyl) were incorporated to evaluate the impact at the S_1 binding pocket of HLE for molecular recognition versus other neutrophil serine proteases (Cat G and PR3).

The effect of different amide leaving groups by C-N fission in the rate of serine acylation was explored, by varying N-1 from *N*-benzyl, -phenyl, -naphthyl and -3-pyridinyl substituents. Precedent literature stated that substitution at N-1 in β -lactams

allows interaction with the S_1' subsite of HLE.^{97, 109} On the other hand, aryl/heterocyclic sulfides and sulfonyl substituents have been successfully used in the design of HLE inhibitors based on different templates, such as the 1,2,5-thiadiazolidin-3-one 1,1-dioxide scaffold (**15**, Section 1.5.4, Chapter 1).^{86, 159, 160} Those substituents were used as recognition elements to probe the S_1' - S_3' subsites of serine proteases, in order to afford selective mechanism-based irreversible inhibitors. Subtle structural differences in the S' subsites of HLE with closely related proteases, such as PR3, have been explored in this manner. In fact, in contrast to PR3, the overall character of these subsites in HLE is hydrophobic, enabling hydrophobic binding interactions with the aryl/heterocyclic sulfides to improve selectivity.

With this background, and in an effort to obtain highly potent and selective irreversible inhibitors based on the azetidine-2,4-dione scaffold, it was rationalized that *N*-aryl derivatives with a *para*- or *ortho*- thioether function, could act as potential mechanism-based inhibitors of this enzyme. These derivatives were designed in analogy with the *N*-aryl azetidin-2-one **32** discussed in Chapter 1 (Figure 1.10). The expected suicide-type mechanism of enzyme inactivation (which is somehow similar to the one depicted in Figure 1.10), is given in Scheme 4.1 for an *ortho*-thioether functionalized azetidine-2,4-dione.



Scheme 4.1 Expected “double-hit” mechanism for HLE inactivation by 4-oxo- β -lactams containing a potential thiol leaving group.

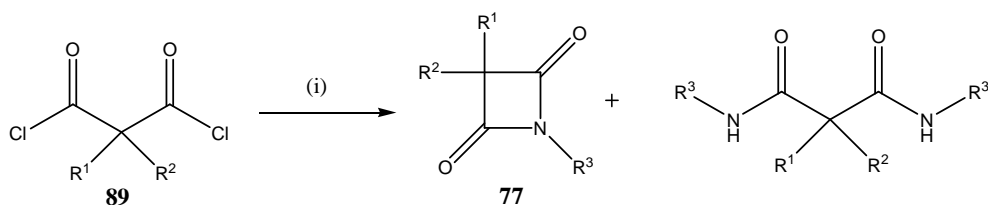
Accordingly, nucleophilic attack of the serine residue at a carbonyl carbon atom would lead to ring-opening with departure of the thiol leaving group, generating a reactive acyl-enzyme, which ultimately would suffer Michael addition (“double-hit” inhibition mechanism).

Taking into account that i) reported mechanism-based selective inhibitors of HLE used the phenylsulfonyl leaving group for binding into the S_n' subsites (eg. 1,2,5-thiadiazolidin-3-one 1,1-dioxide scaffold)⁸⁵ and ii) in this work the phenylsulfonyl substituent best activated the azetidin-2-one scaffold towards HLE, as discussed in Chapter 2, a 4-oxo- β -lactam presenting this group was also synthesized, by oxidation the sulfur atom of the corresponding sulfide moiety.

Besides these substituents, other functionalities at N-1 were interesting to be investigated for 4-oxo- β -lactam-based HLE inhibitors, such as *N*-sulfonyl derivatives, since the electron-withdrawing sulfonyl group would activate the β -lactam motif.

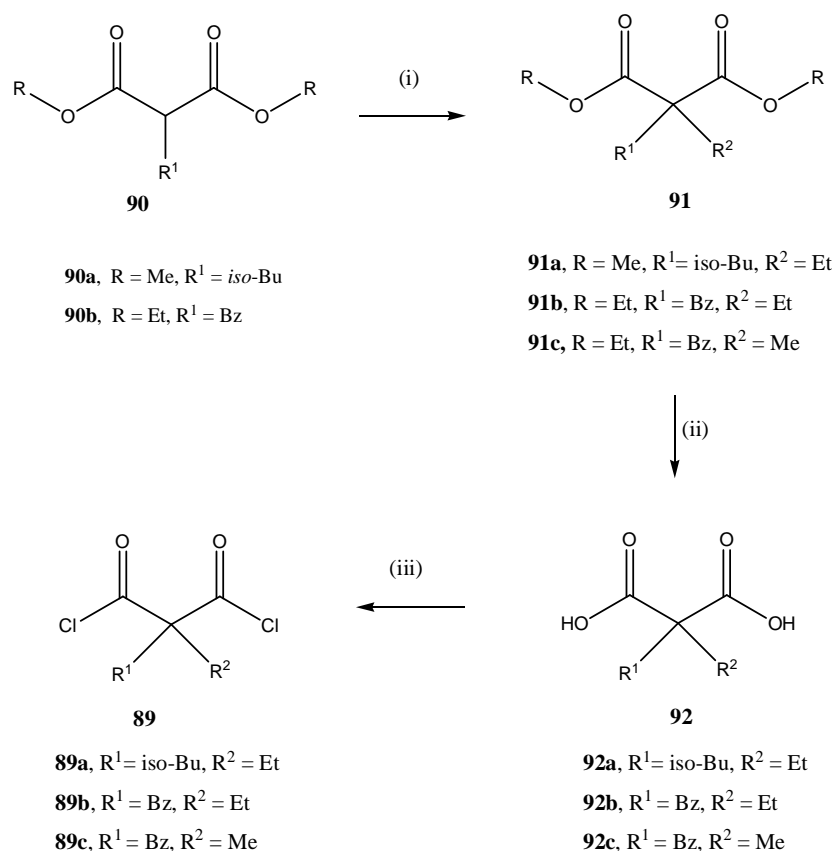
4.2. SYNTHESIS

4-Oxo- β -lactams **77** with different C-3 and N-1 substituents were synthesized, and the procedure used in most cases consisted in the condensation of the appropriate malonyl dichloride with a primary amine, in the presence of TEA (Scheme 4.2). As already stated in the previous chapter, diethyl and dimethyl malonyl dichlorides **89** (Scheme 4.2, respectively $R^1 = R^2 = \text{Et}$ and $R^1 = R^2 = \text{Me}$) are commercially available, while 2-ethyl-2-*iso*-butyl, 2-ethyl-2-benzyl and 2-methyl-2-benzyl malonyl dichlorides (**89a-c**) were obtained by synthesis (Scheme 4.3).



Scheme 4.2 - Synthesis of 4-oxo- β -lactams **77**. Reagents and conditions: (i) $R^3\text{NH}_2$, TEA, dioxane, reflux.

Thus, commercially available 2-monosubstituted malonates **90**, were alkylated to give the corresponding 2,2-disubstituted derivatives **91**, then hydrolyzed to the corresponding di-acids **92**, which subsequently reacted with thionyl chloride to afford the respective dichlorides **89a-c** (Scheme 4.3). Synthesized compounds **89a-c** were used immediately, without any purification.



Scheme 4.3 - Synthesis of disubstituted malonyl dichlorides **89 from the appropriate malonates **90**.** Reagents and conditions: (i) NaEtO⁻, R²I, reflux; (ii) exc. NaOH aq., reflux; (iii) exc. SOCl₂, reflux.

The azetidine-2,4-diones synthesized by this method are listed in Table 4.1, including those derivatives studied in Chapter 3, **77a-i**.

Table 4.1 - Azetidine-2,4-diones **77** synthesized using the method illustrated in Scheme 4.2.

Compound	R ¹	R ²	R ³	Yield (%)
77a	Et	Et	CH ₂ CO ₂ Et	16
77b	Et	Et	CH ₂ Ph	9
77c	Et	Et	C ₆ H ₄ -4-OMe	11
77d	Et	Et	C ₆ H ₄ -4-Me	10
77e	Et	Et	C ₆ H ₅	15
77f	Et	Et	C ₆ H ₄ -4-Cl	14
77g	Et	Et	C ₆ H ₄ -4-CN	19
77h	Me	Me	CH ₂ Ph	4
77i	Me	Me	C ₆ H ₄ -4-Cl	6
77j	Et	Et	C ₆ H ₄ -2-Me	6
77k	Et	Et	pyridin-3'-yl	47
77l	Et	Et	6'-methylpyridin-3'-yl	39
77m	Et	Et	1'-naphthyl	5
77n	Et	<i>iso</i> -Bu	C ₆ H ₅	12
77o	Et	CH ₂ Ph	C ₆ H ₅	22
77p	Me	CH ₂ Ph	C ₆ H ₅	5
77q	Me	Me	C ₆ H ₅	11

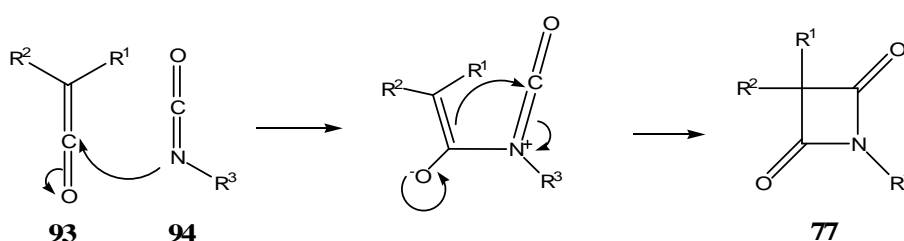
As already observed in the previous chapter, decreasing the basicity of the primary amine increased the yield for the cyclisation process (particularly remarkable for pyridinyl derivatives). However, in most cases this method gave the azetidine-2,4-diones **77** in poor yields. Thus, a different strategy was investigated for synthesis of azetidine-2,4-diones.

4.2.1 Cycloaddition of Ketenes Generated *in situ* with Isocyanates

The synthesis of azetidine-2,4-diones **77** was also reported previously as a result of cycloaddition of ketenes **93** and isocyanates **94** (Scheme 4.4) in good yields.^{150, 161, 162} Ketenes **96** are characterized by a carbon atom doubly bond to an oxygen atom as well as to another carbon atom. The HOMO is perpendicular to the plane of ketene, while LUMO is on ketene plane, thus allowing polarization of the oxygen and the β -

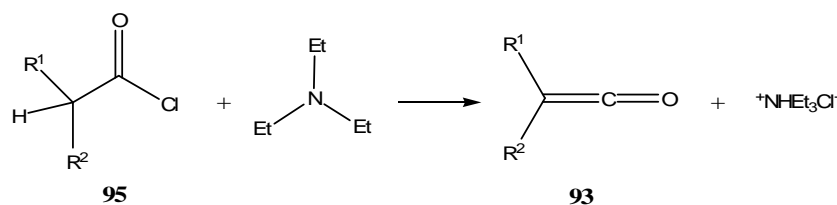
carbon, which is attached to the R^1 and R^2 substituents. By contrast, the α -carbon has a slight positive charge, being more susceptible for nucleophilic attack, explaining the high reactivity of these compounds. Disubstituted ketenes are more stable than monosubstituted counterparts, and larger the R^1 and R^2 substituents, higher is the stability, with an increased ketene lifetime (mainly due to steric reasons).

Staudinger first reported (1913) the reaction of ketenes **93** with isocyanates **94** to give azetidine-2,4-diones, **77** ($R^1 = R^2 = R^3 = \text{Ph}$).¹⁶¹ The proposed mechanism for the cycloaddition reaction is presented in Scheme 4.4.



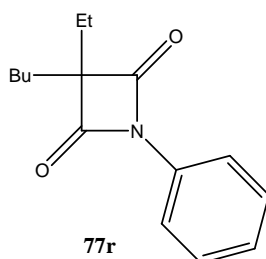
Scheme 4.4 - Proposed mechanism for the cycloaddition of ketenes and isocyanates.

Some published procedures for the cycloaddition synthesis of azetidine-2,4-diones used ketenes generated by pyrolysis.^{161, 162} This process for ketene generation was not studied in this work, since it requires cumbersome /specialized equipment and tricky conditions.¹⁶³ A different published procedure for obtaining ketenes consisted in the *in situ* dehydrohalogenation reaction of the respective acid chloride **95**, using a tertiary amine such as triethylamine (Scheme 4.5).^{164, 165}

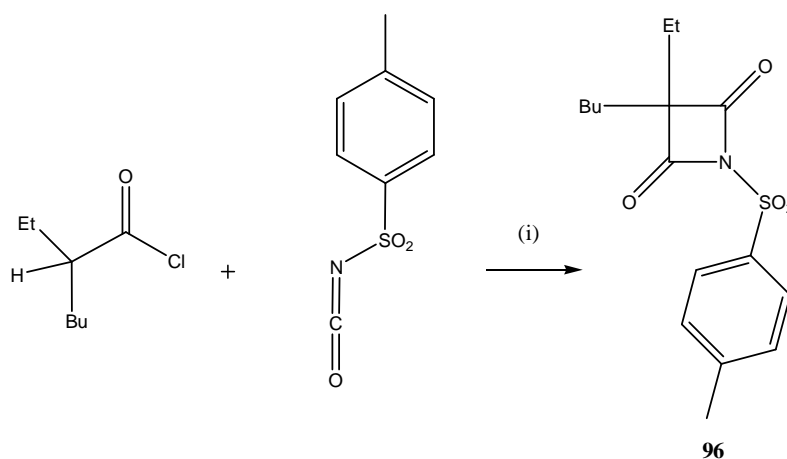


Scheme 4.5 - Ketene generated by reaction of the respective acid chloride with triethylamine.

In this way, 3-butyl-3-ethyl-*N*-phenylazetidine-2,4-dione, **77r** was synthesized using the technique described by Dai *et al.*¹⁶⁵ Thus, TEA (1.2 eq.) was added dropwise over a period of 4–6 h to a solution of 2-ethylhexanoyl chloride **95** ($R^1 = \text{Et}$, $R^2 = n\text{-Bu}$, 1 eq.) and phenyl isocyanate **94** ($R^3 = \text{Ph}$, 1.9 eq.) in xylene, so that the *in situ* ethylbutylketene concentration was maintained at a minimum throughout the reaction, in order to enhance the yield. Then, the reaction mixture was refluxed (xylene was used as solvent) and after work-up **77r** was obtained in reasonable yield (39%).

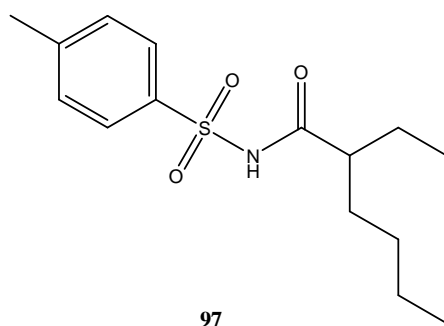


Because ethylbutylketene is much more stable and easier to handle at room temperature than dimethyl or diethylketene,¹⁶⁵ this ketene, generated from the respective acid chloride, was selected for the attempted synthesis of 3-butyl-3-ethyl-*N*-tosylazetidine-2,4-dione **96** is illustrated in Scheme 4.6.



Scheme 4.6 Attempted synthesis of 3-butyl-3-ethyl-*N*-tosylazetidine-2,4-dione **96**. Reagents and conditions: (i) TEA, THF, rt + reflux.

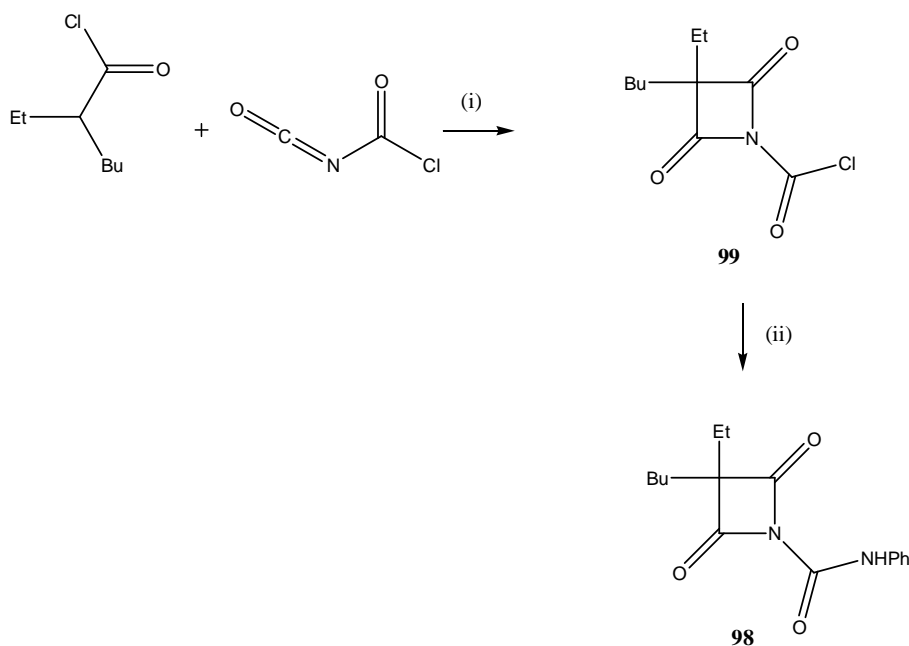
By reflux, the medium turned from colorless to brown, and thus only 20 min of reflux were allowed. However, after workup, the cycloaddition product **96** was not obtained and the isolated product was the 2-ethyl-*N*-tosylhexanamide **97** (40 % yield). This product is likely to be the result of hydrolysis and subsequent decarboxylation of highly reactive azetidine-2,4-dione **96**. Another explanation would be the hydrolysis of the tosyl isocyanate to give the corresponding sulfonamide, which would react with the ketene. Nevertheless, since the tosylamine has a reduced nucleophilic power due to the electron-withdrawing sulfone function, this route seems to be less important for **97**.



The strategy of cycloaddition of ketenes and isocyanates was also investigated to prepare *N*-acyl azetidine-2,4-diones **98** (Scheme 4.7). Thus, reaction of chlorocarbonyl isocyanate **94** ($R^3 = \text{COCl}$, 1.3 eq.) with ethylbutylketene (generated *in situ* from 2-ethylhexanoyl chloride **95**, $R^1 = \text{Et}$, $R^2 = n\text{-Bu}$, 1 eq. and TEA, 1.1 eq.) was carried out in inert atmosphere at room temperature, adopting described procedures.¹⁴⁸ After 2h30 of reaction, that is, more 30 min. than the time reported for **99** using ethylbutylketene generated by pyrolysis, aniline (1.1 eq.) was carefully added (Scheme 4.7) (evolution of hydrogen chloride).

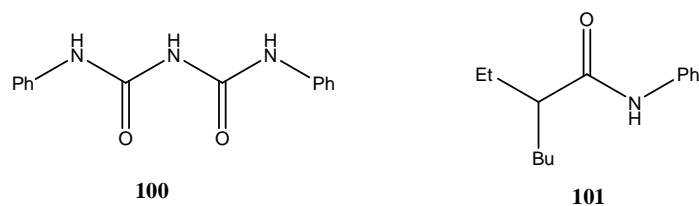
The reaction mixture was stirred at rt and TLC analysis revealed the formation of new products. A white solid precipitated in the reaction medium, which was filtered-off and purified by column chromatography. Compound **100** was isolated, which is a result of the reaction of two molecules of aniline with one of chlorocarbonyl isocyanate. Purification of the solid in the filter also afforded a white solid that gave a complex $^1\text{H-NMR}$ spectrum, inconsistent with the desired product and, even

combined with data from mass spectrometry, it could not be assigned to another structure. The solvent of the filtrate was removed under reduced pressure, and the residue purified by column chromatography on silica gel. However, **98** was not isolated and compounds **100** (purified from the solid and the filtrate in a total yield of 33%, the major product) and **101** (20% yield) were obtained.



Scheme 4.7 - Attempted synthesis of 3-butyl-3-ethyl-N-phenylcarbamoylazetidine-2,4-dione 98.

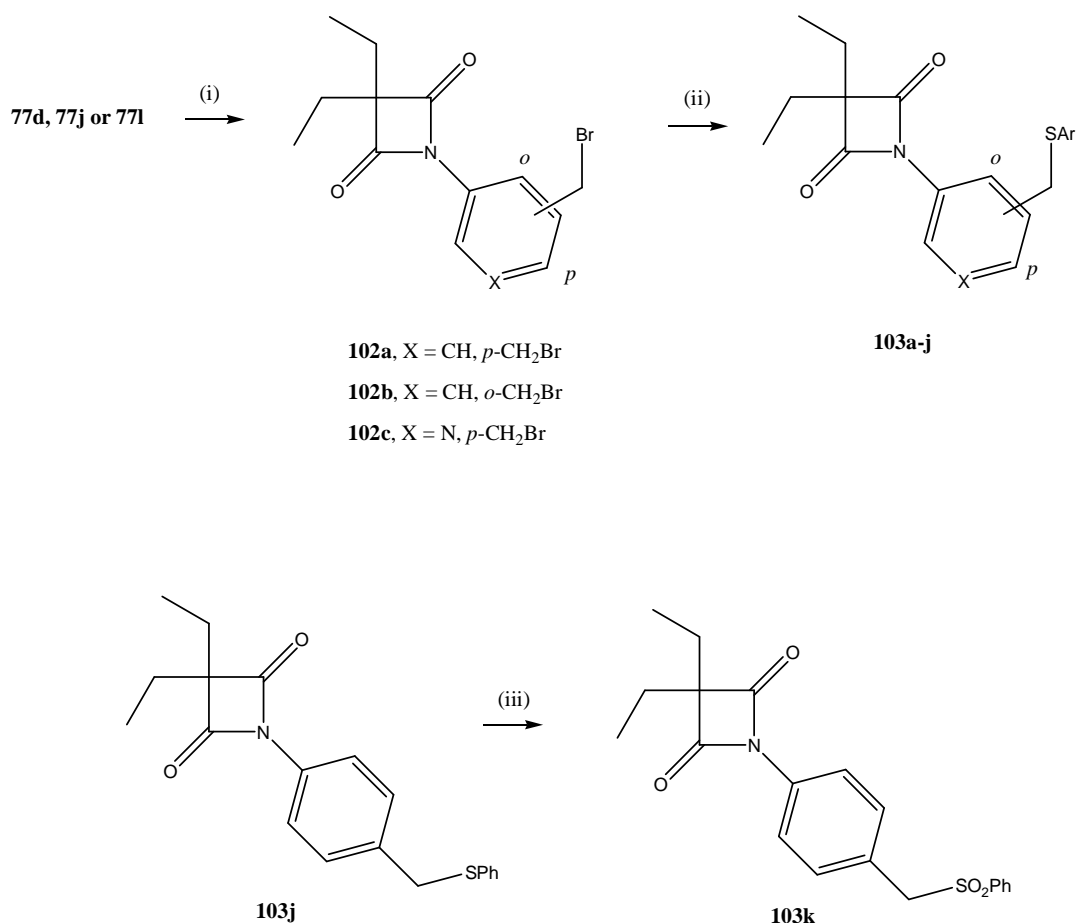
Reagents and conditions: (i) TEA, THF, rt; (ii) aniline, rt.



This strategy for *N*-acyl derivatives was no further investigated. Similarly, no further attempts were made for *N*-sulfonyl 4-oxo- β -lactams. In fact, the intrinsic chemical reactivity of these activated 4-oxo- β -lactams was likely to be exceedingly high, compromising their interest as potential therapeutic agents.

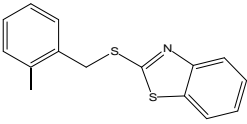
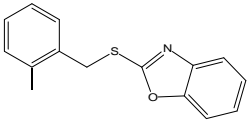
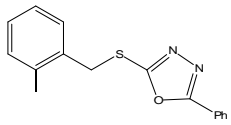
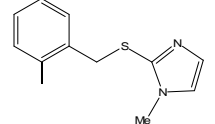
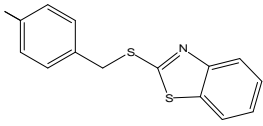
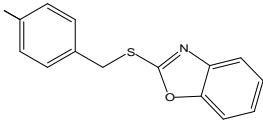
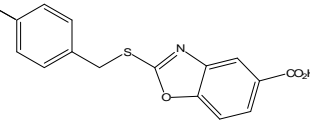
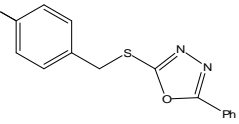
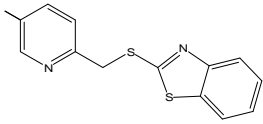
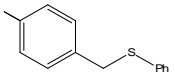
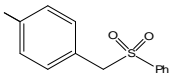
4.2.2 Thioether Functionalized *N*-aryl-azetidine-2,4-diones

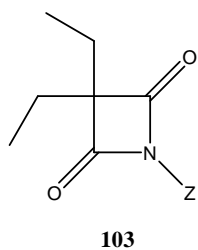
Derivatives **103a-j** were synthesized by first converting *N*-methylaryl 4-oxo- β -lactams **77d**, **77j** and **77l** into their *N*-bromomethylaryl derivatives **102a-c** (Scheme 4.8 and Table 4.3), using NBS, and then reacting these with the appropriate thiol in the presence of triethylamine. Compound **103k** was prepared by oxidation of the corresponding sulfide **103j** using *meta*-chloro-perbenzoic acid (MCPBA) (Scheme 4.8). The synthesized final azetidine-2,4-diones **103** are listed in Table 4.2.



Scheme 4.8 – Synthesis of *N*-heteroarylthiomethyl azetidine-2,4-diones **103a-k**. Reagents and conditions: (i) NBS, CCl₄, benzoyl peroxide; (ii) ArSH, Et₃N, THF; (iii) *meta*-chloro-perbenzoic acid (MCPBA), DCM.

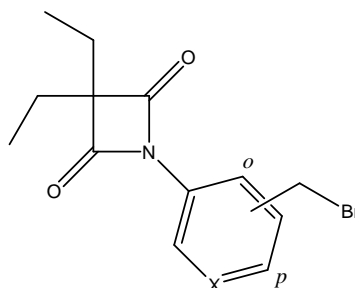
Table 4.2 - Synthesized *N*-heteroarylthiomethyl azetidine-2,4-diones 103a-k.

Compound	Z	Yield (%)
103a		68
103b		95
4.15c		87
103d		70
103e		73
103f		59
103g		24
103h		71
103i		61
103j		79
103k		83



Compound **103g** was prepared by reaction of **102a** with synthesized 2-mercaptobenzoxazole-5-carboxylic acid (**51**, Scheme 2.3, Chapter 2).

Table 4.3 - Key intermediates *N*-bromomethylaryl azetidine-2,4-diones **102a-c**.



102a-c

Compound	X	Bromomethyl position	Yield (%)
102a	CH	<i>para</i>	71
102b	CH	<i>ortho</i>	66
102c	N	<i>para</i>	36

4.2.3 NMR Spectral Characterisation

Similarly to that discussed in Chapter 3, all synthesized 4-oxo- β -lactam derivatives presenting a gem-diethyl substituent at C-3 presented a quartet (integrating for four protons) and a triplet (integrating for six protons) in the $^1\text{H-NMR}$ spectra, corresponding respectively to the methylene and methyl protons.

In the same way, the methylene protons of the benzyl substituent at C-3 of compounds **77o** and **77p** are equivalent and give a singlet in the $^1\text{H-NMR}$ spectra. Likewise, the methylene protons of the ethyl substituent at C-3 of compounds **77n-o** and **77r** give a quartet, integrating for two protons.

The two methylene protons of the $N\text{-C}_6\text{H}_5\text{CH}_2\text{X}$ substituent at N-1 ($\text{X} = \text{Br}$ or SAr) of compounds **102** and **103** appear as a singlet in the $^1\text{H-NMR}$ spectra, integrating for two protons (δ ranging 4.5-4.6 for **102** and 4.1- 4.7 ppm for **103**).

4.2.4 IR Spectroscopy

All 4-oxo- β -lactams synthesized displayed two carbonyl carbon stretching bands in the IR spectra: one high intensity band (corresponding to asymmetric stretching) at nearly 1730 cm^{-1} and a low intensity band (symmetric stretching) at nearly 1860 cm^{-1} .

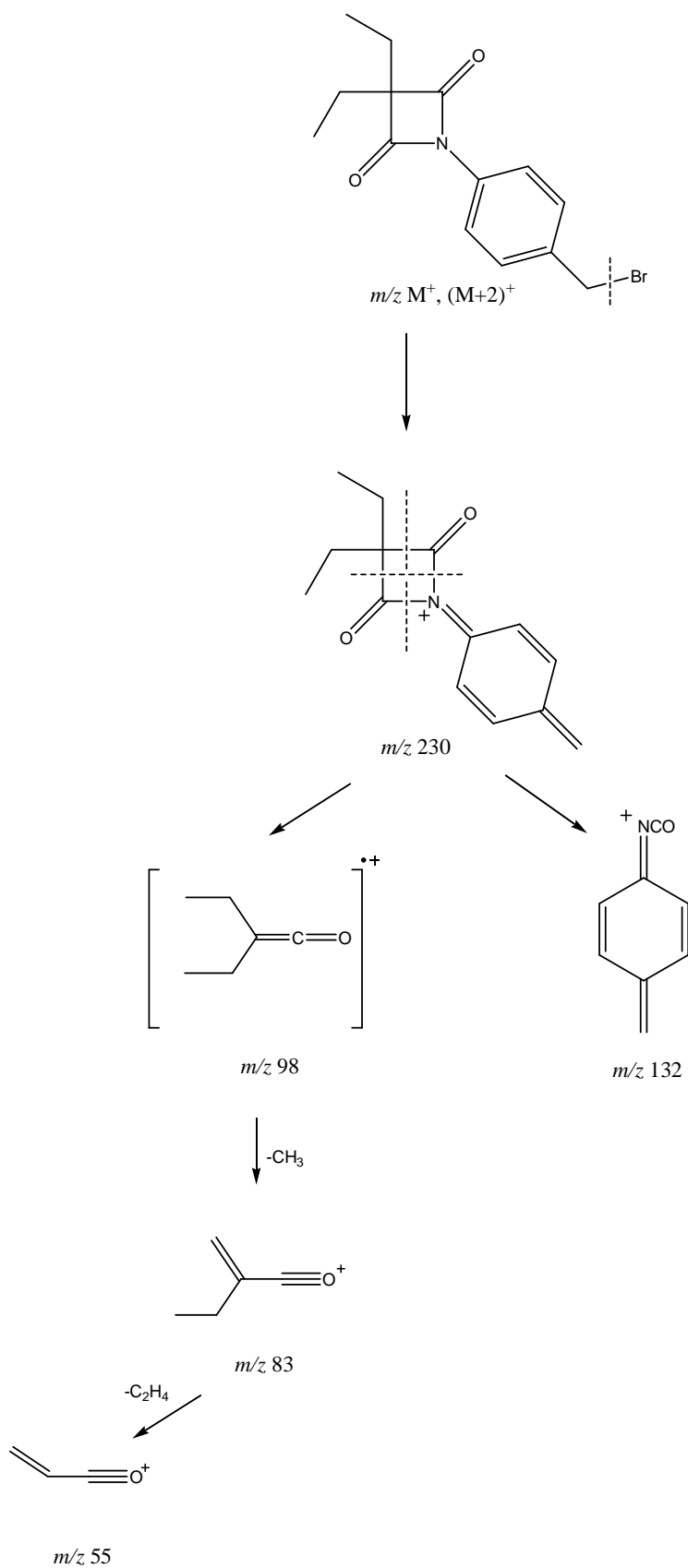
4.2.5 Mass Spectroscopy

All synthesized 4-oxo- β -lactams were analysed using the electron-impact method of ionization. Compounds **77** presented a common fragmentation route, involving formation of ketene ion and isocyanate fragment, in the same way as discussed in Chapter 3, Section 3.2.7.

4-Oxo- β -lactams **102** presented the expected double molecular ion at $m/z = M^+$ and $(M+2)^+$. A common fragmentation route was observed, involving loss of the terminal bromine atom, and formation of the respective quinone methide imine ion (m/z 230 for **102a-b** and 231 for **102c**, due to the replacement of one *CH* by a nitrogen atom *N* on the aromatic ring), which subsequently fragmented to the respective isocyanate and diethylketene. As an example, the fragmentation pathway for **102a** is given in Scheme 4.9.

All 4-oxo- β -lactams **103** also presented a similar fragmentation route, due to C-S fission to form the quinone methide imine ion, which further fragmented to the corresponding isocyanate and diethylketene.

For the *para*-substituted analogues **103e-h** and **103j-k**, the same quinone methide imine ion illustrated in Scheme 4.9, as well as identical further fragments were observed. For **103i** the isocyanate differed in one unit of mass ($m/z = 133$). In addition, an isocyanate still linked to the sulfur moiety was also found for this compound, as a result of an earlier 4-membered ring fission.



Scheme 4.9 - Fragmentation of 3,3-diethyl-N-(4-(bromomethyl)phenyl)-azetidine-2,4-dione, 102a.

4.3. ENZYME INHIBITION STUDIES

4.3.1 HLE Inhibition Studies: Results and Discussion

With exception for the bromomethylphenyl intermediates **102**, all synthesized azetidine-2,4-diones were assayed against HLE to evaluate the inhibitory activity. In fact, due to the presence of bromide as a potential leaving group, **102** would lead to potential toxic effects associated with bromide, with no interest as drug candidates.

The progress curve method was used for kinetic studies of HLE inhibition.¹⁴² All 4-oxo- β -lactams **77** and **103** displayed time-dependent inhibition of HLE and for each inhibitor several concentrations were tested. The exception was compound **77q**, as only one concentration of this inhibitor was assayed ($[I] = 0.5 \mu\text{M}$). The progress curves presented an initial exponential phase followed by a linear steady-state turnover of the substrate and were analyzed by the formalism of slow binding kinetics, using the Equation 2.6, presented at Section 2.3.2.2, Chapter 2.

For the more potent inhibitors, **103e-j**, an extremely rapid enzyme inactivation at very low inhibitor concentrations was found. In these experimental conditions, in which the inhibitor concentration was not much higher than that of HLE (i.e. $< 10[E]$), the progress curves had the same shape as those described by Equation 2.6, but were fitted by non-linear least-squares regression analysis to Equation 4.1, which accounts for the tight-binding nature of those inhibitors.²¹ Examples of typical progress curves for HLE inhibition by 4-oxo- β -lactams **77a**, **77l** and **103f**, at different concentrations are given in Figures 4.2-4.4, respectively. It is important to note that **77a** is one of the least potent inhibitors tested, while **103f** is the most potent one.

$$A = v_s t + [(v_i - v_s)(1 - \gamma) / k_{obs} \gamma] \ln \{ [1 - \gamma \exp(-k_{obs} t)] / (1 - \gamma) \} + A_0 \quad (4.1)$$

where

$$\gamma = ([E] / [I]) [1 - (v_s / v_i)]^2 \quad (4.2)$$

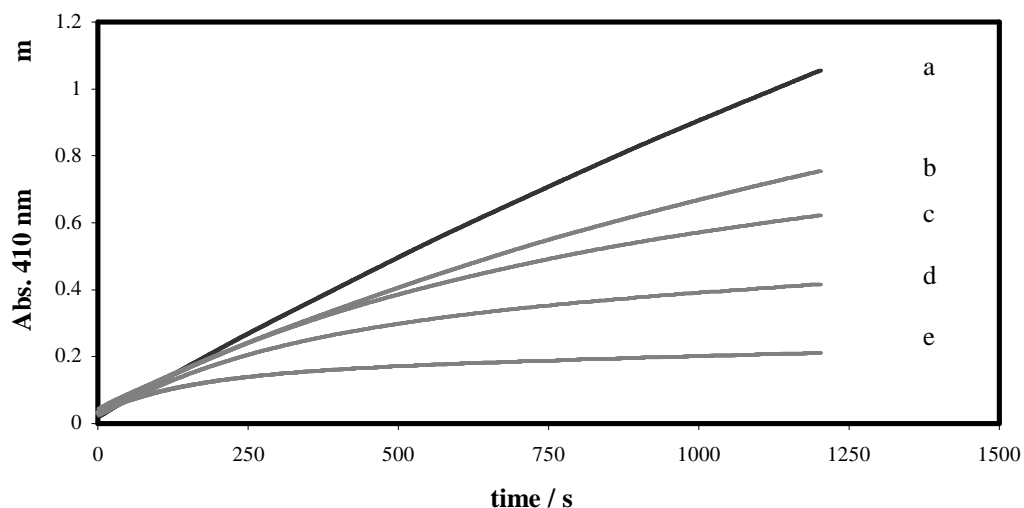


Figure 4.2- Typical progress curves for the inhibition of HLE by 77a. Reaction conditions: [HLE] = 20 nM, [MeOSuc-Ala-Ala-Pro-Val-*p*-NA] = 1 mM, 0.1 M HEPES buffer, pH 7.2, 3% DMSO, 25 °C. Inhibitor concentrations: (a) in absence of inhibitor, (b) 2500, (c) 10000, (d) 25000 and (e) 50000 nM.

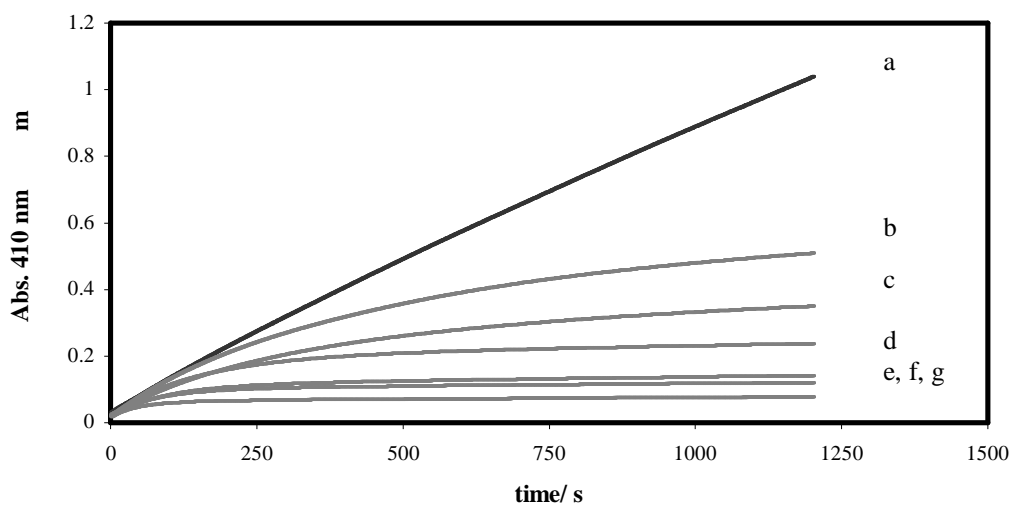


Figure 4.3 - Typical progress curves for the inhibition of HLE by 77l. Reaction conditions: [HLE] = 20 nM, [MeOSuc-Ala-Ala-Pro-Val-*p*-NA] = 1 mM, 0.1 M HEPES buffer, pH 7.2, 3% DMSO, 25 °C. Inhibitor concentrations: (a) in absence of inhibitor, (b) 75, (c) 100, (d) 250, (e) 375, (f) 500 and (g) 750 nM.

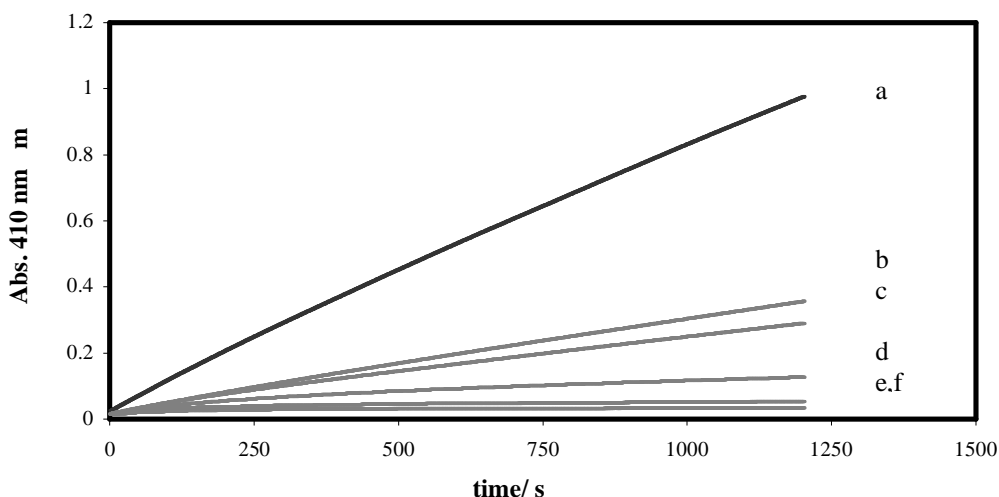


Figure 4.4 - Typical progress curves for HLE inhibition by compound 103f. Reaction conditions: [HLE] = 20 nM, [MeO-Suc-(L-Ala)₂-L-Pro-L-Val-*p*-NA] = 1mM, 0.1M HEPES buffer, pH 7.2, 3% DMSO, 25 °C. Inhibitor concentrations: (a) absence of inhibitor, (b) 6.25, (c) 12.5, (d) 25, (e) 50 and (f) 75 nM.

For each compound, the progress curves data for each concentration were fitted by non-linear regression analysis to the appropriate Equation (2.6 or 4.1), through a routine ENZFIT software. This programme was developed at iMed.UL by Prof. Luís Gouveia, enabling calculation of v_i , v_s and k_{obs} parameters with high accuracy (fitting residuals typically less than +/-0.001 Abs units).

The obtained k_{obs} values for compounds **77** and **103** (given in *Appendix 4, Section A4.1.1, Table A4.1*), displayed a linear or a hyperbolic dependence with the concentration of inhibitor, [I], in accordance with the previously discussed mechanisms A or B for slow-binding enzyme inhibition (Figure 2.28, Chapter 2).

In most cases (**77a-c**, **77e**, **77h-p**, **77r**, **103d-e**, **103h-j**) the plots of k_{obs} versus concentration of [I] were linear, in agreement with mechanism A, as can be seen at Figure 4.5 and at *Appendix 4, Section A4.1.2, Figures A4.1-12*. Good linear regressions using Equation 2.7 (Chapter 2) gave the apparent second-order rate constants for HLE acylation, k_{on}' , with high accuracy. Subsequent corrections by Equation 2.8 (Chapter 2) afforded k_{on} values as an index of the inhibitory potency.

In such situations, the initial velocities, v_i , are all identical and equal the initial velocity in the absence of inhibitor, v_0 (eg., Figures 4.2 and 4.3). The steady-state dissociation constants of the enzyme-inhibitor complex, K_i were calculated using the steady-state velocities, v_s , together with v_0 , fitting by non-linear regression to Equation 2.10 (using GraphPad Prism™ software), and then correcting through Equation 2.11. Therefore, K_i values were affected by the errors presented by those previous parameters, but, in most cases, the respective uncertainty presented quite acceptable values with no signs of bias. The data for determination of K_i , as well as the respective plots of v_s versus the concentration of inhibitor, are given in *Appendix 4, Section A4.1.3*. The first-order rate constant for deacylation, k_{off} , were given by Equation 2.9.

As an example, the determination of kinetic parameters for HLE inhibition by compound **771** (mechanism A) from data shown in Figure 4.3 is presented next (Table 4.4 and Figures 4.5 and 4.6).

Table 4.4 - k_{obs} and v_s obtained from non-linear regression analysis using Equation 2.6 for HLE inhibition by compound 771.

10^9 [771] / M	$10^3 k_{\text{obs}} / \text{s}^{-1}$	$10^5 v_s / \text{s}^{-1}$
0	-	104.3
75.0	3.18	12.96
100	3.44	8.24
250	7.03	3.30
375	10.0	2.36
500	12.4	1.58
750	18.7	1.09

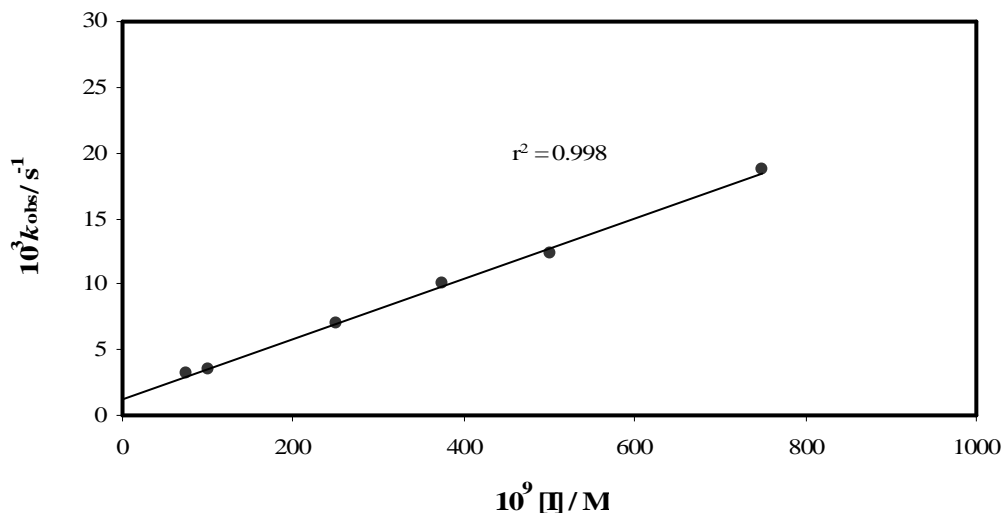


Figure 4.5 - Effect of inhibitor concentration on the onset of inhibition of HLE by 77I. The values for k_{obs} were obtained as average of as least duplicate assays from fits to Equation 2.6 of data shown in Figure 4.3. Points are experimental and the line is from linear regression analysis of the data presented in Appendix 4, Table A4.1, 77I, giving $k_{on}' = (2.30 \pm 0.05) \times 10^4 M^{-1}s^{-1}$ accordingly to mechanism A. By correction using Equation 2.8, $k_{on} = (1.67 \pm 0.04) \times 10^5 M^{-1}s^{-1}$ for 77I.

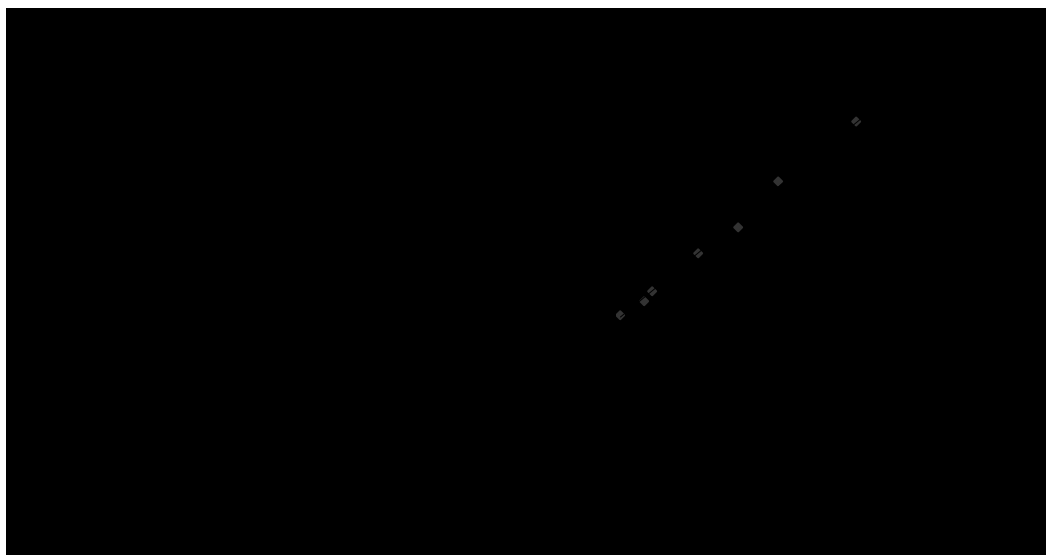


Figure 4.6 - Plot of the steady-state rates versus [I] for the inhibition of HLE by compound 77I. The values for the steady-state rates were obtained from fits to the data shown in Figure 4.3. Points are experimental and the line is from non linear regression analysis of the data shown in Appendix 4, Table A4.2, 77I, using Equation 2.10, for $K_i' = 9.69 \pm 0.50$ nM, which gave after correction using Equation 2.11, $K_i = 1.33 \pm 0.07$ nM. The insert is a Dixon plot to show the linearity.

For the remaining inhibitors (**77d**, **77f-g**, **103a-c**, **103f-g**), a hyperbolic plot of k_{obs} versus $[I]$ was observed (eg. Figure 4.7). In such cases, the initial velocities decrease with increasing the inhibitor concentration (eg. Figure 4.4). Thus, it suggested that a preassociation complex EI accumulated under the experimental conditions used, which then isomerized relatively slowly to the tight or stable complex, EI*, in agreement with mechanism B of Figure 2.28. By non-linear regression analysis using Equation 2.12 (Section 2.3.2.2), k_{inact} (the first-order rate constant for the chemical inactivation step), K_i' (the apparent dissociation constant for EI) and k_{off} were obtained. The corrected K_i was given by Equation 2.11 and the overall dissociation constant for EI*, K_i^* , was calculated from Equation 4.3.

As an example, the determination of the inhibition parameters for compound **103f** is presented in Figure 4.7.

$$K_i^* = K_i \left(\frac{k_{\text{off}}}{k_{\text{inact}} + k_{\text{off}}} \right) \quad (4.3)$$

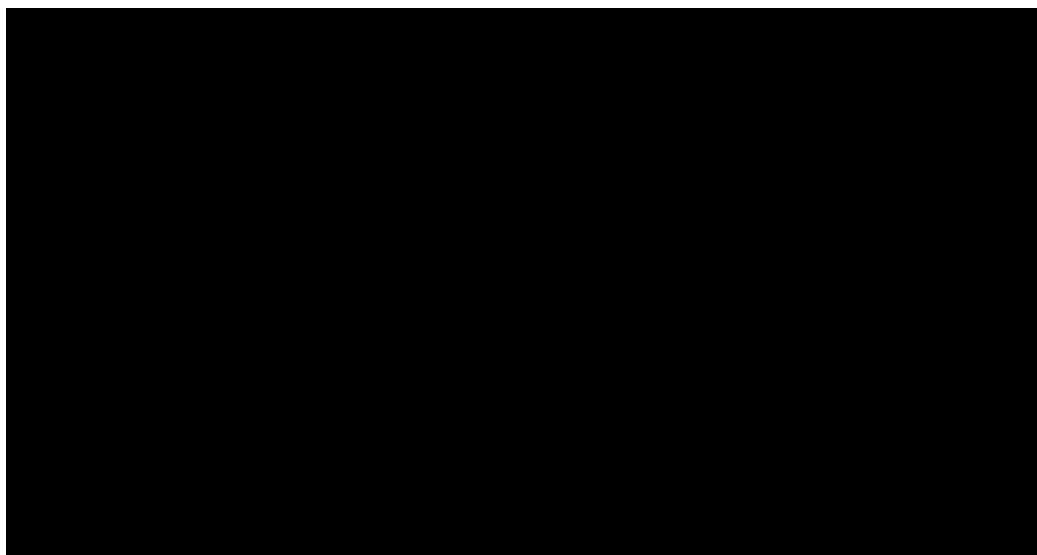


Figure 4.7 - Effect of inhibitor concentration on the onset of inhibition of HLE by 103f. The values for the pseudo-first order rate constants (Appendix 4, Table A4.2, **103f**) were obtained from fits to the data shown in Figure 4.4, using Equation 4.1. The solid line was obtained using non-linear regression analysis to Equation 2.12. From this plot, $k_{\text{inact}} = (9.57 \pm 0.08) \times 10^{-3} \text{ s}^{-1}$, $K_i' = 21.4 \pm 5.6 \text{ nM}$ and $k_{\text{off}} = (1.23 \pm 0.36) \times 10^{-3} \text{ s}^{-1}$. By correction (Equation 2.11), $K_i = 2.96 \pm 0.78 \text{ nM}$ and $K_i^* = 0.34 \text{ nM}$.

The overall dissociation constant for **103f**, K_i^* , defined by Equation 4.3, was found to be 0.34 nM, while K_i was found to be 2.96 nM. In fact, accordingly to the mechanism B of slow binding inhibition, K_i^* is lower than K_i , and conforms to the observed formation of EI* during the experimental assay. The second-order rate constant for the formation of EI*, k_{on} , given by Equation 2.13 (Section 2.3.2.2), was found to be $3.24 \times 10^6 \text{ M}^{-1}\text{s}^{-1}$ for **103f**. Remarkably, this association rate constant compare favorably with those of other very potent HLE inhibitors. For example, the k_{on} value for HLE inactivation by **103f** is one order of magnitude higher than that reported for β -lactam L-680,833 (compound **27**, Chapter 1).¹⁰³

The plots of k_{obs} versus the inhibitor concentration for the remaining compounds **77d**, **77f-g**, **103a-c** and **103g** are presented in *Appendix 4, Section A4.1.4*. The value of k_{off} for compounds **77d**, **77f** and **103c** could not be distinguished from zero, and thus the corresponding K_i^* were not determined.

The relevant kinetic data for the whole set of 4-oxo- β -lactams are outlined in Table 4.5. The k_{on} values, ranging from 2×10^2 to $3 \times 10^6 \text{ M}^{-1}\text{s}^{-1}$, were used as an index of inhibitory potency. Discussion of these results will be made in Section 4.3.1.1.

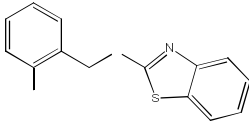
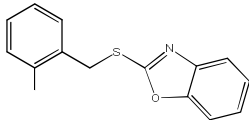
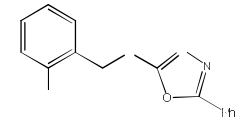
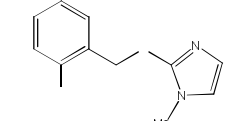
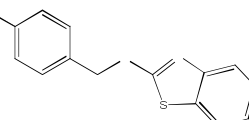
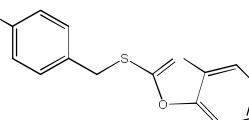
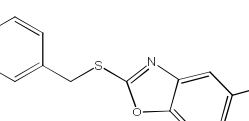
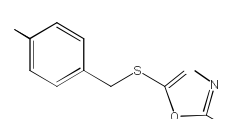
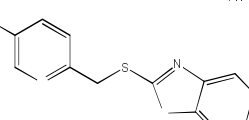
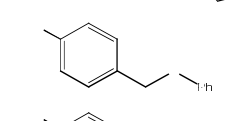
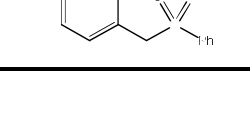
To study the efficiency of inactivation, titration of enzymatic activity studies were performed, in which HLE was incubated during 30 minutes with different concentrations of **77g** at pH 7.2 (see data in *Appendix 4, Section A4.1.5*). The fractional remaining activity was found to be proportional to the molar ratio of inhibitor to enzyme, as illustrated in Figure 4.8. The extrapolation of the linear part of the curve to the line to $v_i/v_i = 0$ (complete inactivation) gives the partition ratio; approximately 1.5 molecules of **77g** are required to completely inactivate one molecule of enzyme. This result suggests that **77g** is a very efficient irreversible inhibitor of HLE, and is consistent with the formation of a tight complex as revealed by the hyperbolic dependence of k_{obs} versus [I]. Similar low partition ratios were also reported for monocyclic β -lactams inhibitors of HLE, as 1.3 molecules of β -lactam L-680,833 (compound **27**, Chapter 1) are required to inactivate HLE to approximately 99%.¹³⁷

4. Azetidine-2,4-diones as Potent and Selective Inhibitors of HLE

Table 4.5 - Kinetic data for HLE inhibition by 4-oxo- β -lactams. See text for definition of each kinetic parameter.

Comp	R ¹	R ²	R ³	$k_{on}/M^{-1}s^{-1}$	k_{off}/s^{-1}	k_{inact}/s^{-1}	K_i (or K_i^*)/nM
77a	Et	Et	CH ₂ CO ₂ Et	7.33x10 ²	1.61x10 ⁻⁴	--	219
77b	Et	Et	CH ₂ Ph	1.76x10 ³	2.01x10 ⁻⁴	--	114
77c	Et	Et	C ₆ H ₄ -4-OMe	3.05x10 ⁵	2.16x10 ⁻⁴	--	0.708
77d	Et	Et	C ₆ H ₄ -4-Me	6.47x10 ⁵	~0	3.12x10 ⁻²	48.2 (ND)
77e	Et	Et	C ₆ H ₅	2.41x10 ⁵	2.92x10 ⁻⁴	--	1.21
77f	Et	Et	C ₆ H ₄ -4-Cl	6.61x10 ⁵	~0	3.83x10 ⁻²	57.9 (ND)
77g	Et	Et	C ₆ H ₄ -4-CN	5.08x10 ⁵	7.08x10 ⁻⁴	3.23x10 ⁻²	63.5 (1.36 ^a)
77h	Me	Me	CH ₂ Ph	6.21x10 ³	2.14x10 ⁻⁴	--	34.4
77i	Me	Me	C ₆ H ₄ -4-Cl	3.94x10 ⁵	9.38x10 ⁻³	--	23.8
77j	Et	Et	C ₆ H ₄ -2-Me	1.11x10 ³	2.58x10 ⁻⁴	--	233
77k	Et	Et	pyridin-3'-yl	1.01 x10 ⁵	2.26x10 ⁻⁴	--	2.24
77l	Et	Et	6'-methylpyridin-3'-yl	1.66 x10 ⁵	2.22x10 ⁻⁴	--	1.33
77m	Et	Et	1'-naphthyl	4.35x10 ³	1.48x10 ⁻⁴	--	33.9
77n	Et	<i>iso</i> -Bu	C ₆ H ₅	2.85x10 ⁴	1.10x10 ⁻⁴	-	3.87
77o	Et	CH ₂ Ph	C ₆ H ₅	2.00x10 ³	2.54x10 ⁻⁴	--	127
77p	Me	CH ₂ Ph	C ₆ H ₅	2.67x10 ²	1.19x10 ⁻³	--	4450

4. Azetidine-2,4-diones as Potent and Selective Inhibitors of HLE

77q	Me	Me	C ₆ H ₅	1.87×10^5 ^c	ND	--	ND
77r	Et	<i>n</i> -Bu	C ₆ H ₅	2.86×10^5	2.42×10^{-4}	--	0.85
103a	Et	Et		1.50×10^4	1.49×10^{-3}	4.24×10^{-3}	283 (73.7 ^a)
103b	Et	Et		3.49×10^4	2.74×10^{-4}	7.15×10^{-3}	205 (7.57 ^a)
103c	Et	Et		5.99×10^4 ^a	~0	2.12×10^{-2}	353 (ND)
103d	Et	Et		1.26×10^3	2.56×10^{-4}	--	203
103e	Et	Et		1.15×10^6	9.40×10^{-4}	--	0.82
103f	Et	Et		3.24×10^6	1.23×10^{-3}	9.57×10^{-3}	2.96 (0.34 ^a)
103g	Et	Et		1.77×10^6	1.99×10^{-3}	1.68×10^{-2}	9.50 (1.01 ^a)
103h	Et	Et		2.28×10^6	2.56×10^{-3}	--	1.12
103i	Et	Et		3.18×10^6	1.59×10^{-3}	--	0.50
103j	Et	Et		1.17×10^6	2.08×10^{-3}	--	1.78
103k	Et	Et		1.46×10^6	1.32×10^{-3}	--	0.90

^a Value for K_i^* (using Equation 4.3); ^b $k_{obs}/[I]$ determined at [77q] = 0.5 μM

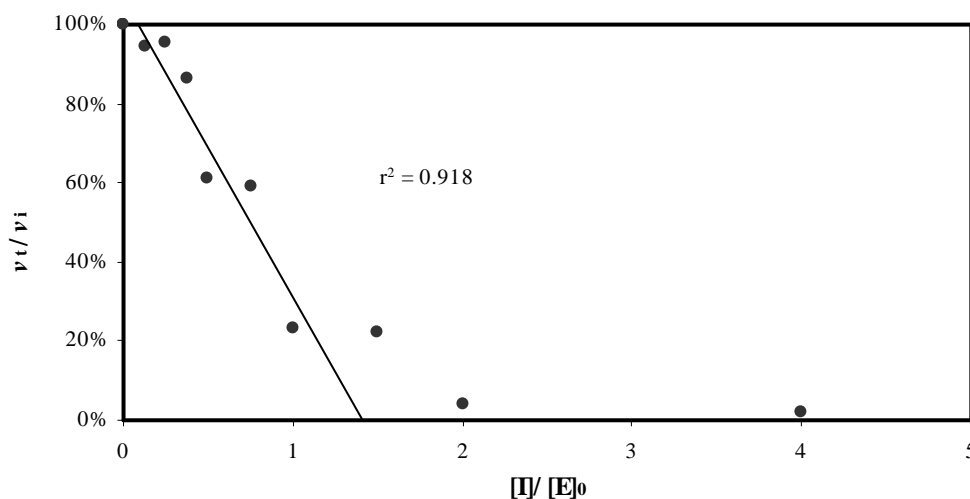


Figure 4.8- Inactivation of HLE as a function of the ratio $[77g]/[\text{enzyme}]$ at a fixed $[\text{HLE}]$ of $10 \mu\text{M}$. Various amounts of inhibitor **77g** (25-800 nM) in 0.1M pH 7.2 HEPES buffer were incubated at $25 \text{ }^\circ\text{C}$ for 30 min, then aliquots were withdrawn and measured for the remaining enzyme activity. Points are experimental and the line is from linear regression analysis of data shown in Appendix 4, Table A4.3, giving a partition ratio of nearly 1.5.

4.3.1.1 Structure Activity Relationships

Substitution at C-3. *N*-phenylazetidine-2,4-diones **77e** and **77n-q** and **77r** were assayed against HLE, and it was found that the rate of HLE inhibition depends on the size of the substituent at C-3. The gem-diethyl **77e**, as well as the ethyl-*n*-butyl **77r** were the most potent inhibitors of this series, as measured by the corresponding k_{on} values. By replacing one ethyl substituent in **77e** by a larger benzyl moiety, as in **77o**, the inhibitory potency (k_{on}) decreases by 120-fold and increased K_i ca. 100-fold. By changing the gem-diethyl group of **77e** to a methylbenzyl moiety, i.e. **77p**, drastically decreases the k_{on} value by 900-fold, and dramatically increases the K_i nearly 3700-fold. In addition, the *iso*-butyl derivative is nearly 8-fold less potent than **77e**. In contrast, the most potent inhibitor in the *N*-phenyl series was the 3-ethyl-3-*n*-butyl derivative, **77r**, with $k_{\text{on}} = 2.9 \times 10^5 \text{ M}^{-1}\text{s}^{-1}$ and $K_i = 0.85 \text{ nM}$. Overall, these results are consistent with the known preference of HLE for small hydrophobic aliphatic substituents at C-3 of monocyclic β -lactams for optimal interaction with the S_1

binding pocket of the enzyme.⁹⁷ As previous work had demonstrated that an ethyl-*n*-butyl substituent rather than a gem-diethyl group on C-3 of monobactams, have a reduced inhibitory activity in vivo (probably due to a greater protein binding)⁹⁷, the gem-diethyl series were preferentially synthesized.

Furthermore, the C-3 gem-diethyl derivative **77f** is nearly 2-fold more active than the gem-dimethyl counterpart **77i**, and allows accumulation of the acyl-enzyme (hyperbolic kinetics), as the k_{off} value is indistinguishable from zero. Thus, it reflects an increased affinity to HLE, while the gem-dimethyl counterpart shows a linear dependence of k_{obs} with [I]. By contrast, for the *N*-benzylazetidine-2,4-diones, the gem-dimethyl derivative **77h** is nearly 4-fold more active than its gem-diethyl counterpart **77b**.

Substitution at N-1. Derivatives with different *N*-aryl and *N*-alkyl substituents on N-1 were tested, in order to evaluate the effect of the ability of the amide leaving group by C-N bond fission on the inhibitory potency of 3,3-diethyl-4-oxo- β -lactams. Replacing the *N*-benzyl by an *N*-phenyl derivative significantly increases in the rate of enzyme inhibition, as the k_{on} value for **77e** is nearly 137-fold higher than that of **77b**. This effect can be ascribed to the different leaving group abilities of the amide formed from the decomposition of the tetrahedral intermediate generated from **77e** and **77b**.

However, the amide leaving group ability is not the only factor affecting inhibitory potency. For example, the *N*-1-naphthyl derivative, **77m**, is 55 times less reactive towards HLE than its *N*-phenyl counterpart, **77e**, suggesting that rigid substituents at this position may be responsible for some non-productive binding interactions.

Compound **77d** is 583-fold more potent than **77j**, the *ortho* positional isomer, and may reflect the less stereochemically hindered carbonyl carbon of **77d** towards nucleophilic attack.

The inhibitory potency of 4-oxo- β -lactams **77c-g** towards HLE does not correlate with the Hammett σ_p value of substituents at the aromatic moiety (σ_p values were presented in Table 3.3, Chapter 3). Thus, all *p*-substituted derivatives of this set (**77c-**

d and **77f-g**) were found to be more potent inhibitors than **77e**, *p*-unsubstituted, being the inhibitory potency independent on the electron-withdrawing strength of the appendage. Analysis of the data for the *N*-aryl, **77c-g**, and *N*-(3'-pyridyl), **77k-l**, series indicate that potency is not significantly affected by the electronic properties of substituents in the aromatic moiety. For example, the 4-methylphenyl and 4-chlorophenyl derivatives (**77d** and **77f**, respectively) have roughly the same k_{on} values (ca. $6.5 \times 10^5 \text{ M}^{-1}\text{s}^{-1}$), which were ca. 3- and 6-fold higher than those of the unsubstituted and 3'-pyridyl counterparts, **77e** and **77k**, respectively. This can be explained by a significant degree of molecular recognition of these derivatives by HLE.

For both *ortho* and *para* *N*-functionalized derivatives **103**, the incorporation of a thioether function *ortho* or *para* to the azetidine ring nitrogen, improved the inhibitory potency (k_{on}) towards HLE when compared to the unfunctionalized counterparts **77j**, **77d** and **77l**. For example, **103a**, **103e** and **103i** are respectively 14, 2 and 20-fold more potent than the methylphenyl analogues **77j**, **77d** and **77l**.

Remarkably, all *para*-substituted derivatives of the set of compounds containing a thioether function (i.e. **103e-k**) afforded extraordinarily high inhibitory potencies, with values of k_{on} ranging from 1.2×10^6 to $3.2 \times 10^6 \text{ M}^{-1}\text{s}^{-1}$, and very low K_{i} values, ranging from 0.50 to 9.5 nM. These inhibitors are even more potent than previously reported monocyclic β -lactams inhibitors of HLE, such as L-680,833 (**27**, Chapter 1, $k_{\text{on}} = 6.22 \times 10^5 \text{ M}^{-1}\text{s}^{-1}$).¹⁰³ The high inhibitory potency of **103e-k** against HLE is remarkably of the same order of magnitude of DMP-777 (compound **29**, Chapter 1, $k_{\text{on}} = 3.78 \times 10^6 \text{ M}^{-1}\text{s}^{-1}$),¹⁰⁶ which was reported to be in Phase II clinical trials for cystic fibrosis, juvenile rheumatoid arthritis and emphysema.⁶

In contrast, the *ortho*-substituted derivatives **103a-d** demonstrated lower k_{on} and much higher K_{i} values than the corresponding *para*-analogues, in line with results observed for their unfunctionalized analogues, **77d** and **77j**. For example, *para*-substituted inhibitors **103e**, **103f** and **103h** presented higher k_{on} values than the corresponding **103a-c**, respectively by nearly 90-, 80- and 40-fold. In addition, **103e** has a 345-fold lower K_{i} than **103a**.

Two inhibitors from the *para*-substituted set, **103f** and **103g**, exhibited a hyperbolic dependence of k_{obs} versus [I] (Figure 4.7 and Figure A4.38, Appendix 4, Section A4.1.4). Since both are derivatives of the thiol 2-mercaptobenzoxazole, one may suspect that this moiety allows specific interaction within the active site of the enzyme, thereby facilitating formation of a specific preassociation enzyme-inhibitor complex.

Replacing the oxygen atom of the benzoxazole moiety of **103f** by a sulfur atom, giving a benzothiazole moiety (as in **103e**), decreases the inhibitory potency by nearly 3-fold. This reinforces the idea that the benzoxazole substituent effects a gain in molecular recognition, with its oxygen atom involved in hydrogen bonding within the active site. Interestingly, the incorporation of a *meta* nitrogen atom into the aromatic ring, as in **103i**, improves inhibitory potency when compared to its carba counterpart, **103e**. This finding contrasts with the lower potency of **77k** and **77l** compared with the corresponding *N*-phenyl analogues. The electron-withdrawing phenylsulfone moiety of **103k** allows a better acylation rate and a lower K_i than the corresponding sulfide **103j**.

Stability of the acyl-enzyme complex. In order to study the stability of the acyl-enzyme complex, HLE was incubated with a 5-fold excess of **103a** or **103e**, respectively the *ortho*- or *para*-substituted methyl-(2-mercaptobenzothiazole) derivatives. Either **103a** or **103e** led to a very rapid time-dependent inactivation of HLE, enabling the formation of a tight acyl-enzyme adduct which persists during hours and slowly regenerates the free, active enzyme (the half-life for enzyme reactivation is nearly 5 hours for both, as shown in Figures 4.9 and 4.10). While incubation of HLE with **103a** allowed a complete regain of enzymatic activity within 24h, the *para* isomer **103e** allowed a partial regain.

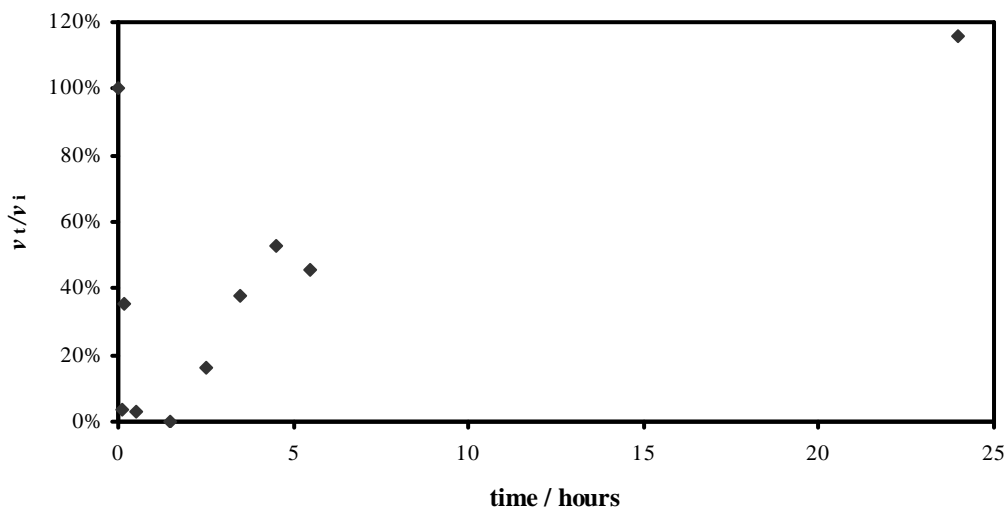


Figure 4.9 - 1 μ M of inhibitor 103a was incubated with 0.2 μ M of HLE in 0.1 M pH 7.2 HEPES buffer, at 25°C. Points are experimental and reflect aliquots withdrawn at different time intervals from the incubation mixture for determining remaining enzymatic activity.

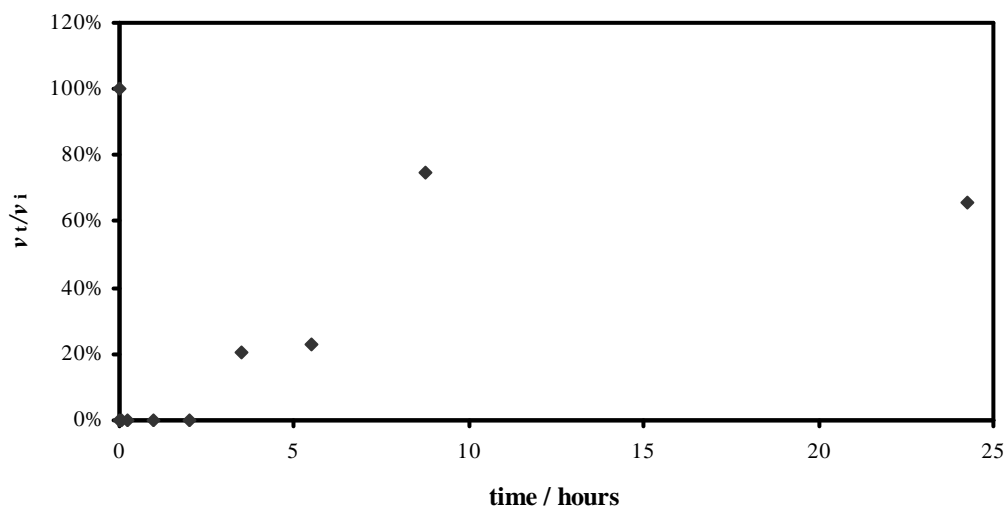


Figure 4.10 - 1 μ M of inhibitor 103e was incubated with 0.2 μ M of HLE in 0.1 M pH 7.2 HEPES buffer, at 25°C. Points are experimental and reflect aliquots withdrawn at different time intervals from the incubation mixture for determining remaining enzymatic activity.

4.3.1.2 Molecular Modeling Studies

In order to gain further insight and understanding into the observed inhibitory potencies shown by 4-oxo- β -lactams, molecular docking simulations were performed using inhibitors **77p**, **103e**, **103f** and **103i**. The molecular interactions between these compounds and the HLE were performed by Dr. Rita C. Guedes (iMed.UL, Lisbon), using the program GOLD¹⁶⁶ (PDB code 1HNE). The top 15 conformations (i.e. those with the highest GoldScore fitness score) were visually analyzed for hydrophobic interactions between the ligand and the residues defining the S₁ pocket and the distance between the O _{γ} oxygen atom of Ser-195 and both 4-oxo- β -lactam carbonyl carbon atoms (O _{γ} Ser195-CO).

Modeling **103e** into the active site of HLE revealed multiple attractive binding interactions. Both ethyl substituents at C-3 of the 4-oxo- β -lactam moiety are accommodated in the S₁ pocket where they interact with Val-190, Phe-192 and Val-216 (Figure 4.11A). This binding mode is in good agreement with that observed for 3,3-diethylazetidin-2-ones with HLE.¹⁰⁹ Enhanced van der Waals contacts between the benzothiazole moiety with Leu-99 and His-57 were also observed. The O _{γ} Ser195-CO distances for **103e** are 2.6 and 2.8 Å, suggesting that nucleophilic attack by Ser-195 at the 4-oxo- β -lactam is likely to be a facile process. Moreover, the carbonyl of **103e** closest to Ser-195 is involved in the H-bond network of the so-called oxyanion hole defined by the backbone NHs of Gly-193 and Ser-195, suggesting that the oxyanion hole is used to stabilize the tetrahedral intermediate derived from **103e**.

Docking of **103f** and **103i** into the active site of HLE revealed two binding poses: the normal pose (12 and 14 conformations out of the top 15 solutions, respectively), in which the ethyl groups at C-3 of the 4-oxo- β -lactam moiety sit in the S₁ pocket and the carbonyl carbon atoms lie close to the Ser-195 hydroxyl oxygen atom (O _{γ} Ser195-CO = 2.5/2.7 Å and 2.5/2.8 Å, respectively, Figure 4.11B and C); and the inverted pose, in which the benzothiazole (**103i**) and benzoxazole (**103f**) moieties are within the S₁ site, while the four-membered ring is sitting outside the active site. The inverted binding mode does not favour HLE acylation, as the average shortest O _{γ} Ser195-CO distance is 5.3 Å.

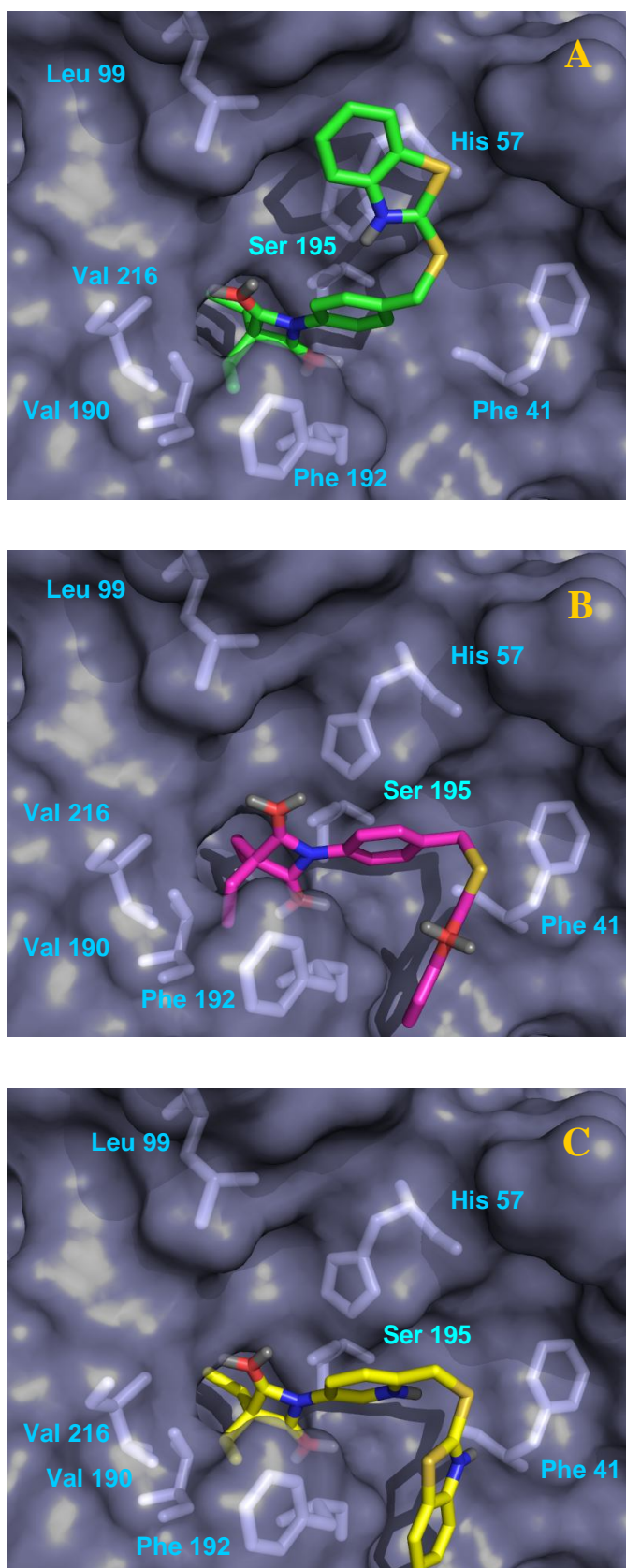


Figure 4.11 - Docking poses of 103e (A), 103f (B), and 103i (C) in the active site of HLE, obtained from PDB 1HNE. Pictures were prepared using Pymol.¹⁶⁷

However, its low frequency of occurrence is consistent with the observed inhibitory efficiency (three-fold higher k_{on} values for **103f** and **103i** as compared with **103e**). The presence of such inverted binding modes in top ranking conformations has been reported for other potent irreversible thrombin inhibitors.¹⁶⁸ In contrast, all top ranking docking solutions of **77p** correspond to the inverted pose, with the *N*-phenyl group inside the S_1 pocket and an average shortest $O_{\gamma_{\text{Ser195}}}$ -CO distance of 5.5 Å (Figure 4.12), a result entirely consistent with the weaker HLE inhibition profile of **77p**.

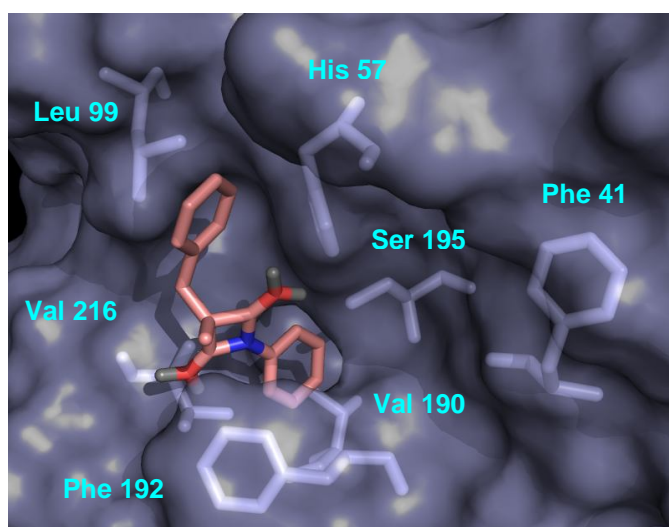


Figure 4.12 - Docking pose of **77p** in the active site of HLE, obtained from PDB 1HNE. (Picture prepared using Pymol).¹⁶⁷

4.3.2 Selectivity Studies

4.3.2.1 Proteinase 3 Inhibition Studies

PR 3 inhibition studies were performed using the progress curve method, by measuring the release of *p*-nitroaniline from the hydrolysis of the chromogenic substrate MeO-Suc-(L-Ala)₂-L-Pro-L-Val-*p*-NA (the same used for HLE inhibition assays). This substrate is known to be hydrolyzed less efficiently by PR3 than HLE, due to a 100-

fold lower proteolytic coefficient $k_{\text{cat}}/K_{\text{m}}$ for PR3.¹⁶⁹ Thus, it required longer experiences for monitoring PR3-catalyzed reactions.

Only one concentration of each representative 4-oxo- β -lactam was tested, at least in duplicate, and the progress curves were analysed by the formalism of slow binding kinetics as described for HLE inhibition. An example of progress curves for PR3 inhibition is depicted in *Appendix 4, Section A4.2, Figure A4.39*. The obtained pseudo-first-order rate constants for PR3 inhibition by 4-oxo- β -lactams are given in *Appendix 4, Table A4.4*. The inhibitory activities for the assayed compounds, expressed in terms of the bimolecular rate constant $k_{\text{obs}}/[I]$ in $\text{M}^{-1}\text{s}^{-1}$, are given in Table 4.6.

With the exception of **77g** and **77p**, all 4-oxo- β -lactams assayed were found to be time-dependent inhibitors of PR3, although with significantly lower activity compared with HLE. The most potent inhibitor towards PR3 was found to be the sulfone **103k**, with a second-order rate constant of nearly $5 \times 10^3 \text{ M}^{-1}\text{s}^{-1}$. In contrast, the sulfide counterpart **103j** was found to be a weak inhibitor of PR3. Compound **103f**, which was the most potent 4-oxo- β -lactam inhibitor against HLE, was ca. 10^5 times less potent inhibitor of PR3.

Dual inhibition of HLE and PR3 is not surprising as it reflects the close similarity of the primary specificity S_1 sites of both enzymes²⁹ and is consistent with similar observations previously described for other scaffolds.⁸⁶ As both of these neutrophil serine proteases are involved in inflammation and extracellular matrix destruction observed in pulmonary diseases, a potent inhibition of HLE combined with a weaker inhibition of PR3, may be an advantage for therapeutics.

4.3.2.2 Cathepsin G Inhibition Studies

Cathepsin G inhibition studies were also performed using the progress curve method.¹⁴² Assays were performed at 25 °C, 0.1 M pH 7.5 HEPES buffer, by monitoring the release of *p*-nitroaniline from the enzyme-catalyzed hydrolysis of the substrate *N*-Suc-L-(Ala)₂-L-Pro-L-Phe-*p*-NA. One or two concentrations (near to the limit of solubility) of representative 4-oxo- β -lactams were assayed at least in

duplicate and an example is illustrated in *Appendix 4, Section A4.3, Figure A4.4*. The obtained k_{obs} values are given in *Table A4.4*. The inhibitory activities, expressed in terms of the bimolecular rate constant $k_{\text{obs}}/[\text{I}]$, are given in *Table 4.6*. By contrast with PR3 assays, most of these derivatives were inactive (**77o**, **77p**, **103b**, **103f**, **103g**, **103i**, **103j**) or only weakly active against Cat G (*Table 4.6*).

Table 4.6 - Inhibitory activity of selected 4-oxo- β -lactams against neutrophil serine proteases HLE, PR3 and Cat G

Compound	$k_{\text{on}}/\text{M}^{-1}\text{s}^{-1}$	$k_{\text{obs}}/[\text{I}]/\text{M}^{-1}\text{s}^{-1}$	
	HLE	Proteinase 3	Cathepsin G
77g	5.08×10^5	16% ^a	36.5
77m	4.35×10^3	ND	35.6
77o	2.00×10^3	20.2	NI
77p	2.67×10^2	22% ^b	NI
77r	2.86×10^5	ND	47.3
103b	3.49×10^4	361	NI
103f	3.24×10^6	29.6	NI
103g	1.77×10^6	689	NI
103i	3.18×10^6	4080	NI
103j	1.17×10^6	122	ND
103k	1.46×10^6	4998	41.4

NI: no inhibition at 60 μM ; ND: not determined; ^a at 10 μM ; ^b at 60 μM

In particular, the most potent inhibitors towards HLE, compounds **103f** and **103k**, were found to be non inhibitors of Cat G, even when assayed at 20 and 5 μM , respectively. A similar selectivity pattern was also observed for **103g**, while the sulfone derivative **103k** inhibited all three serine proteases with a HLE/PR3/Cat G

ratio of $3.5 \times 10^4/120/1$. Indeed, while sulfide **103j** was found to be non inhibitor of cathepsin G, its sulfone counterpart **103k** inhibited this enzyme, giving $k_{on} = 41.4 \text{ M}^{-1} \text{ s}^{-1}$.

The fact that most 4-oxo- β -lactams assayed did not inhibit Cat G is consistent with the known substrate specificity, since this enzyme has a trypsin and a chymotrypsin-like preference for P_1 , accepting aromatic and positively charged side chains.²⁹ Surprisingly, neither the methyl benzyl (**77p**) nor the ethyl benzyl (**77o**) derivatives inhibited Cat G at 60 μM , despite the presence of an aromatic substituent at P_1 . This result may be ascribed to the restricted conformational mobility imparted by the geminal ethyl and methyl groups at C-3.

4.3.2.3 Papain Inhibition Studies

The group of derivatives assayed for activity against PR3 and Cat G (Table 4.6) was also evaluated against papain, a cystein protease. These compounds were found to be inactive even when incubated at 50-100 μM for 1h at 25 °C with papain, suggesting a high degree of selectivity of the azetidine-2,4-dione scaffold towards serine proteases.

4.3.2.4 PPE Inhibition versus HLE Inhibition

N-aryl-4-oxo- β -lactams **77c-g**, previously studied against porcine pancreatic elastase (PPE) (Chapter 3), were found to be much more potent inhibitors of HLE. In fact, the second-order rate constant for HLE inactivation for these compounds ranges from 2.4×10^5 to $6.6 \times 10^5 \text{ M}^{-1} \text{ s}^{-1}$, some three orders of magnitude larger than those previously discussed for PPE inhibition (Table 3.4, Chapter 3). The observed relative inhibitory potencies for **77c-g** accords with the S_1 binding pocket of HLE being larger than that of PPE,²⁷ thereby allowing optimal interaction with the diethyl group at the C-3 of the 4-oxo- β -lactam moiety. Furthermore, the tight preassociation inhibitor-HLE complex (mechanism B) observed for compounds **77d**, **77f** and **77g** contrasts with the simple association mechanism reported for PPE inhibition.

By contrast with HLE inhibition, compounds **77c-g** showed a good Hammett correlation towards PPE (as discussed in Figure 3.20, Chapter 3), indicating that PPE is much more susceptible to intrinsic chemical reactivity effects rather than favorable binding interactions by **77**. *N*-alkyl derivatives **77a-b**, which were non-inhibitors of PPE, were found to be time-dependent irreversible inhibitors of HLE.

4.4. HYDROLYTIC STABILITY STUDIES

The postulated mechanism of inactivation by compounds **103** was previously given in Scheme 4.1. In order to confirm the departure of the thiol leaving group to generate a highly reactive quinone methide imine function and provide valuable insights regarding the mechanism of action, a representative derivative **103f** was incubated in hydroxide buffer at 25 °C, being the reaction monitored by UV spectroscopy (Figure 4.13a).

Equimolar 2-mercaptobenzoxazole (used as standard) was separately incubated with hydroxide at 25 °C, for identification of a characteristic band in UV spectra, which was nearly at 295 nm (Figure 4.13b).

It was expected to observe that band, corresponding to 2-mercaptobenzoxazole, from the reaction of **103f** with hydroxide, as a result of nucleophilic attack of hydroxide at a carbonyl carbon atom and four-membered ring opening, with departure of the thiol. However, the incubation of **103f** with hydroxide did not generate any band at 295 nm (Figure 4.13a).

Thus, it suggests that there is no expulsion of the thiol from nucleophilic attack of **103** (it does not function as a leaving group). If this is the case, derivatives **103** are not mechanism-based inhibitors because they cannot form the reactive acyl-enzyme for a “double-hit mechanism”, but simple acylating agents of HLE.

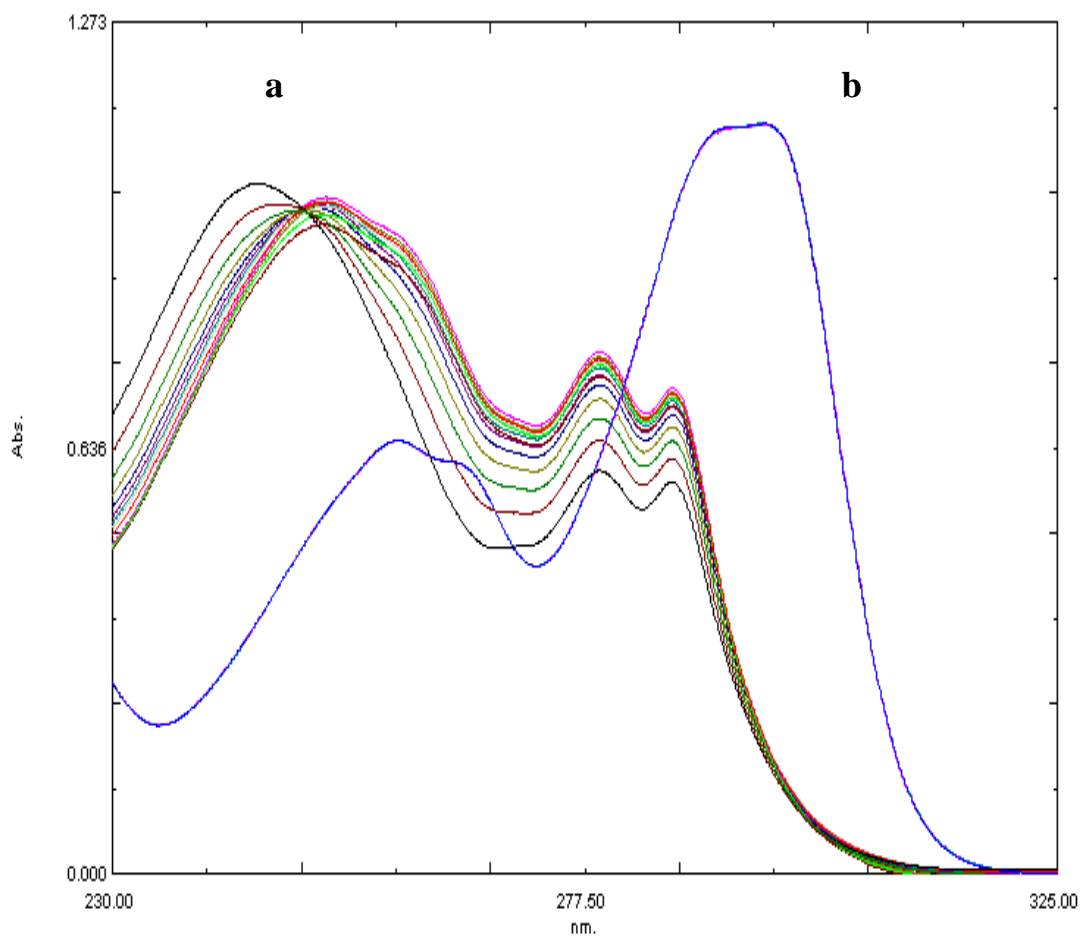
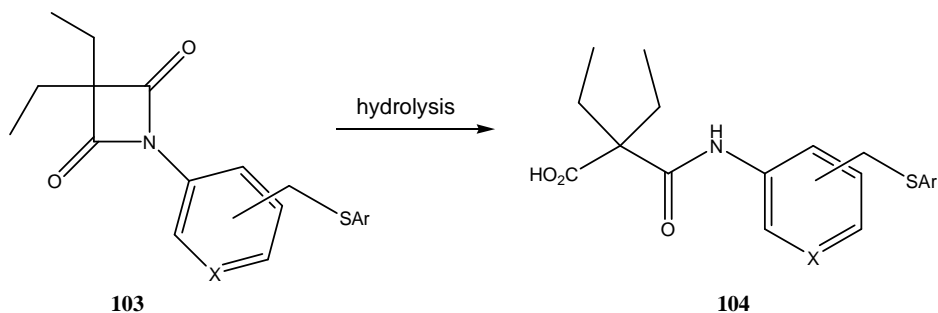


Figure 4.13 - UV spectra depicting the reactions, at 25 °C of (a) **103f** (150 μ M) and (b) 2-mercaptobenzoxazole (150 μ M) in 10 mM NaOH, containing NaClO₄ to maintain the ionic strength at 0.5 M (reaction monitored by 120 sec/scan, being depicted scans 1, 2, 3, 4, 5, 6, 7, 8, 10, 20, 30, 40, 50).

4.4.1 The Product of Hydrolysis of **103**

The product of alkaline hydrolysis of azetidine-2,4-diones is the corresponding *N*-aryl-2,2-diethylpropanedioic acid monoamide **104** (Scheme 4.10). As an example, a reaction of **103a** with excess of sodium hydroxide was performed, to give the corresponding ring-opened product **104**. From this result one may conclude that

departure of the thiol leaving group would not be an efficient process under physiological conditions.



Scheme 4.10 - The alkaline hydrolysis product of 4-oxo- β -lactam **103** is the corresponding α -amidoacid, **104**, without departure of the thiol leaving group.

Thus, nucleophilic attack at **103**, leading to β -lactam ring opening, does not involve expulsion of the thiol leaving group, being these results in consonance with those obtained by spectrophotometrically monitoring the reaction of **103f** with hydroxide ion (Figure 4.13). So, compounds **103** behave as simple alternate substrate inhibitors (acylating agents) of HLE and the formation of the electrophilic quinone methide imine by C-N fission is likely to do not occur.

As a result, the mechanism of HLE inactivation by 4-oxo- β -lactams **103** is similar to that discussed for **77** in Chapter 3 for PPE inactivation (Figure 3.21): serine nucleophilic attack at a carbonyl carbon to form a stable acyl-enzyme by four-membered ring-opening.

In order to support and establish unequivocally the reaction mechanism of **103** with HLE, attempted X-ray crystallography studies of this enzyme with selected derivatives were performed. However, the attempted obtention of the acyl-enzyme crystal structure remained unsuccessful.

4.4.2 Stability in pH 7.4 Buffer and in 80% Human Plasma

The promising results obtained for *in vitro* inhibitory potency and selectivity of 4-oxo- β -lactams, prompted to obtain further insight to the mechanism of hydrolysis and stability of **103**. The stability of selected compounds (**103a**, **103e**, **103i** and **103k**) was evaluated in pH 7.4 phosphate buffer saline and in 80% human plasma at 37 °C.

Indeed, stability towards hydrolysis is a prerequisite for maintaining the therapeutically useful concentrations in biological fluids, such as pulmonary epithelial lining fluid and plasma.

As an example, the profiles of mean concentration of **103a** versus time after incubation in phosphate buffer saline (PBS) and 80% human plasma, at 37 °C, are shown in Figures 4.14 and 4.15, respectively. These plots allowed the determination of the respective half-lives, by exponential regression analysis of data. Calibration curves, used for the quantification of assayed compounds, as well as the plots for determination of the half-lives for **103e**, **103i** and **103k** are given in *Appendix 4, Section A4.4, Figures A4.41-50*. The obtained results for stability in phosphate buffer saline and human plasma are listed in Table 4.7.

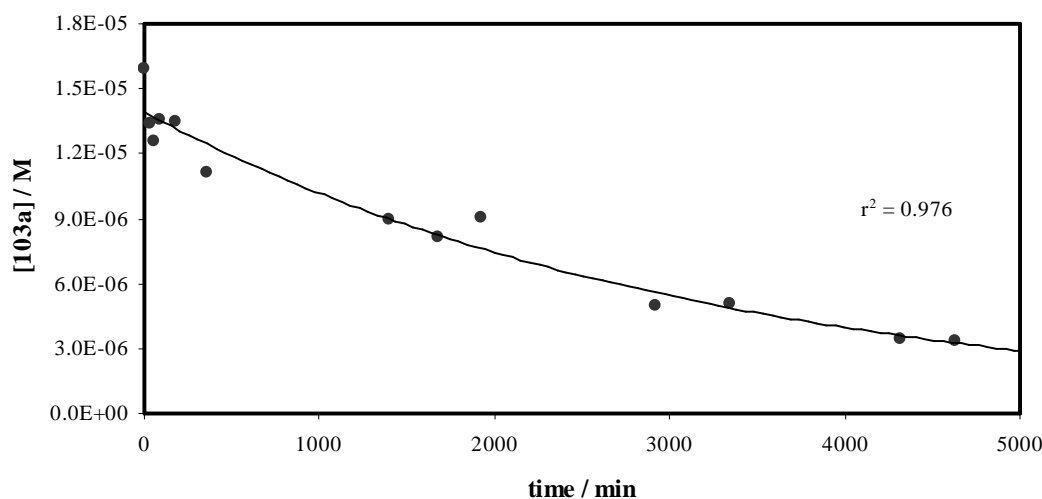


Figure 4.14 - Profile of concentration of 103a versus time after incubation in phosphate buffer saline, at 37 °C. Points are experimental and line is from exponential regression analysis of data, giving the kinetic rate constant of hydrolysis $k = 3.14 \times 10^{-4} \text{ min}^{-1}$. From this value, the half-life was determined, $t_{1/2} = 37\text{h}$.

In human plasma, these compounds were rapidly hydrolyzed, with half-lives ranging from 0.1 to ca. 2h. These half-lives were lower than that in phosphate buffer, indicating that these compounds are very susceptible to the hydrolysis catalyzed by plasma enzymes (as esterases). This situation is notable for compound **103i**, as the half-life for the hydrolysis in human plasma was found to be ca. 65 times lower than that in PBS (Table 4.7).

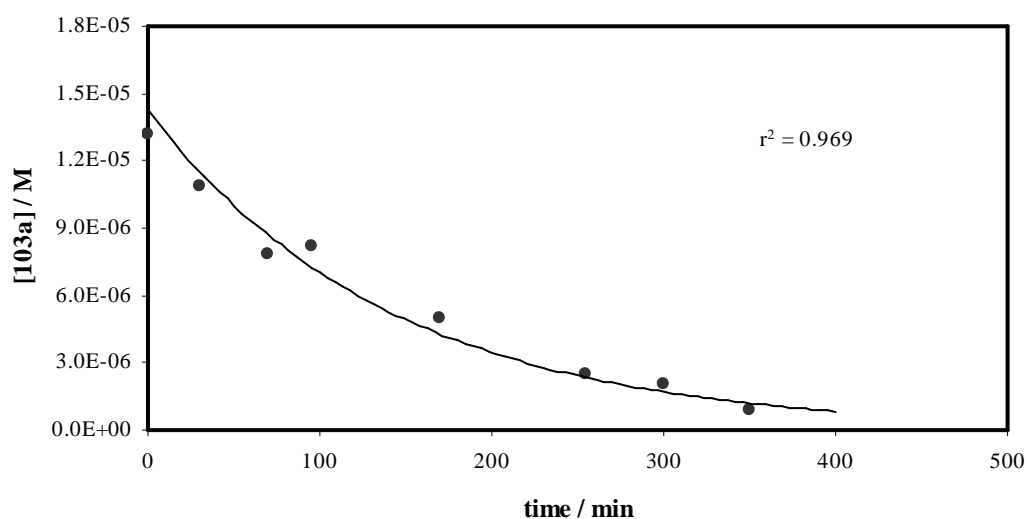


Figure 4.15 - Profile of concentration of **103a** versus time after incubation in 80% human plasma, at 37 °C. Points are experimental and line is from exponential regression analysis of data, giving the kinetic rate constant of hydrolysis $k = 7.08 \times 10^{-3} \text{ min}^{-1}$. From this value, the half-life was determined, $t_{1/2} = 1.63\text{h}$.

Table 4.7 - Aqueous and plasma stability at 37 °C for compounds **103a**, **103e**, **103i** and **103k**.

Compound	$t_{1/2} / \text{h}$	
	Buffer pH 7.4	80% Human plasma
103a	37	1.6
103e	10	0.4
103i	13	0.2
103k	1.0	0.1

Compound **103k** was found to be the most reactive compound in both PBS and plasma and may be a consequence of the powerful electron-withdrawing sulfone function, activating the 4-oxo- β -lactam carbonyl carbon towards nucleophilic attack.

The obtained results for these derivatives are in line with the pronounced susceptibility of neutral β -lactam derivatives (e.g. penicillin esters) to undergo plasma-catalyzed hydrolysis of the β -lactam ring.¹⁷⁰ Similarly, the previously reported half-life of cephalosporin sulfones in PBS pH 7.4 is 1.1 h.³⁴ By contrast, *N*-carbamoyl-azetidine-2-ones, as **27**, were reported to be much more stable, for more than 23 days, in PBS pH 7.5, at 37 °C.^[35]

These results indicate that the oral availability of 4-oxo- β -lactams might be limited by compound stability.

4.5. BIODISTRIBUTION STUDIES OF A SELECTED 4-OXO- β -LACTAM

In anticipation of using 4-oxo- β -lactams in rodent efficacy models, a biodistribution study in mice was carried out with a representative derivative, **103k**. These studies were kindly performed by Dr. Sandra Simões, from INETI/iMed.UL. All experimental procedures were carried out with the permission of the local laboratory committee, and in accordance with international accepted principles.

Thus, **103k** was determined after administration of a single dose of 30 mg/kg, given intraperitoneally in mice, in mice blood and tissues (lung, spleen and liver), at different times after the challenge, in an *ex vivo* study.

Three mice per time point were used. At appropriate time intervals, blood was collected into heparinised tubes and stored at -30 °C and mice were euthanized. The lung, spleen and liver of mice were removed and stored at -70 °C. A control group of mice was used, which did not receive the administration of **103k**. Standard solutions of **103k** were prepared for calibration curves and the quantification of the 4-oxo- β -lactam in mice blood and tissues was performed by HPLC (see Experimental Section for extraction and quantification details). Data used for calibration curves are given in *Appendix 4*, Tables A4.7-A4.10.

Figures 4.16, 4.17 and 4.18 show, respectively, the mean-total mice blood, spleen and lung concentration-time profile after administration of **103k**. Compound **103k** was not detected in mice liver.

Blood levels of **103k** decreased rapidly after ip administration in mice, in particular within the first 10 min, due to the hydrolytic instability. A similar pattern was observed in mice spleen and lung. The obtained C_{max} values of **103k** are 1207 ± 440 $\mu\text{g}/\text{total blood}$, 179 ± 30 $\mu\text{g}/\text{g spleen}$ and 106 ± 440 $\mu\text{g}/\text{g lung}$, suggesting that **103k** distributes well into tissues.

Although in a lower concentration than the observed for spleen, the 4-oxo- β -lactam **103k** reached the lungs (major target). By contrast, this compound was completely eliminated within 5 min in this tissue (Figure 4.18), suggesting a potential reaction of **103k** with mice elastase. Interestingly, after an initial clearance from blood, levels of **103k** increased after 30 min of administration and a similar situation was found in tissues, with relevance in lung, where **103k** appeared again after 30 min after the challenge.

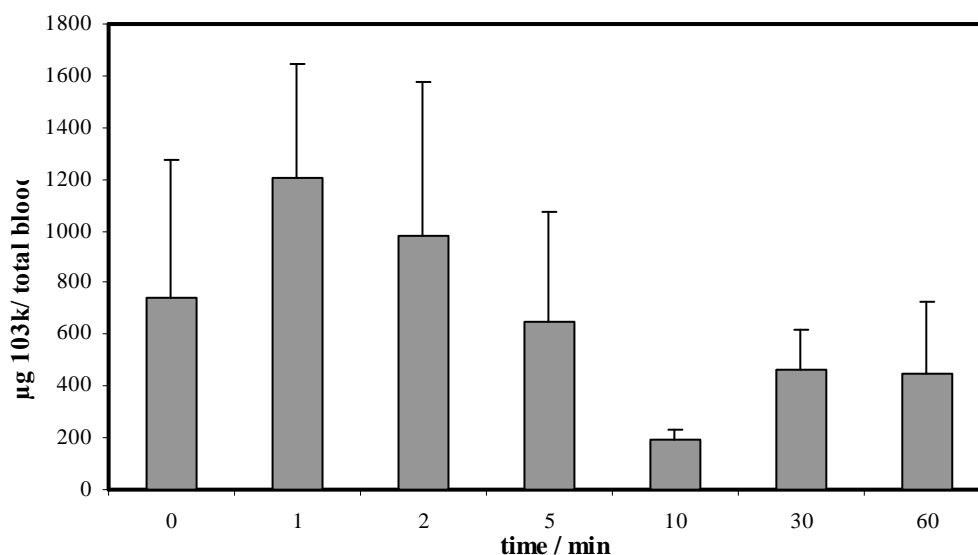


Figure 4.16 - Mean pharmacokinetic profile in total mice blood after administration of a ip 30 mg/kg dosage of **103k**. Data are mean \pm sd.

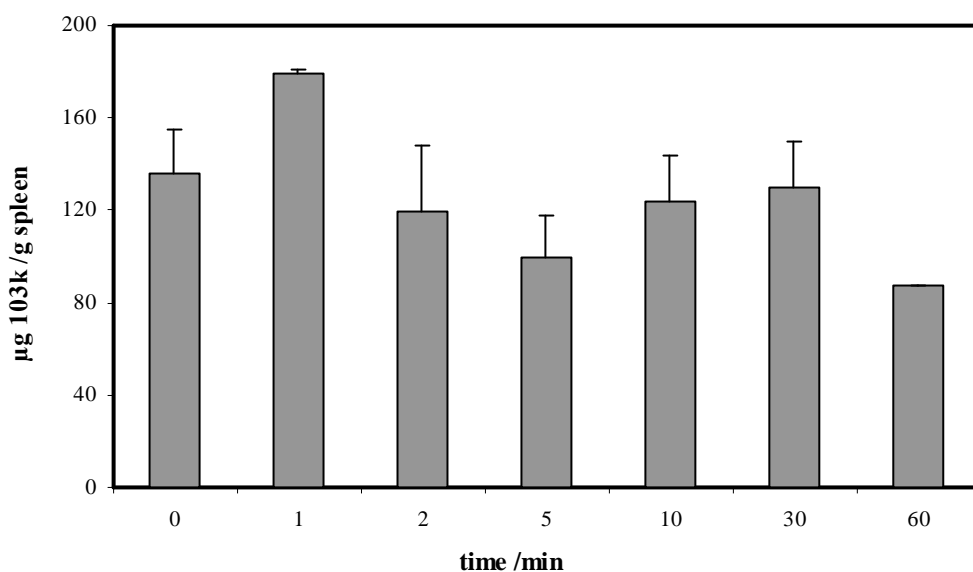


Figure 4.17 - Mean pharmacokinetic profile in mice spleen after administration of ip 30 mg/kg dosage of 103k. Data are mean \pm sd.

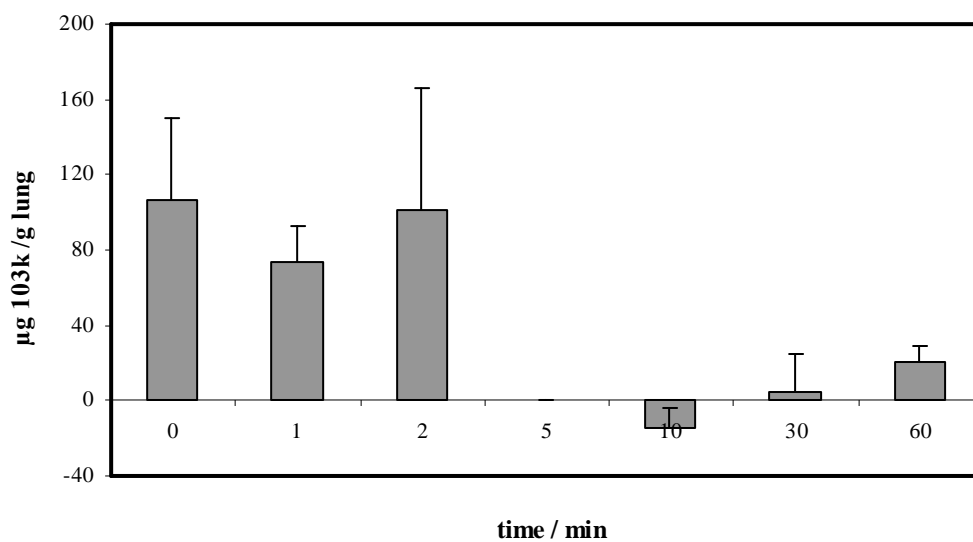


Figure 4.18 - Mean pharmacokinetic profile in mice lung after administration of a ip 30 mg/kg dosage of 103k. Data are mean \pm sd.

A biliar clearance is a very likely elimination pathway, with **103k** entering in an enterohepatic cycle, which might explain the increase of concentrations in blood and lungs after 30 min of administration. It is important to note that **103k** was undetectable in liver, which suggests a high metabolism by liver enzymes. This result agrees with the high reactivity of this compound, demonstrated in Section 4.4. For comparison, reference β -lactam DMP-777 (**29**, Section 1.6.2, Chapter 1) was reported to have a half-life of 1.8 h in rat blood after a 5 mg/kg dose given iv, and to be degraded in a pathway believed to be catalyzed by esterases, with β -lactam ring opening. Similarly, elimination of this compound involved metabolism in liver, followed by excretion of the metabolites in feces, *via* bile.¹⁷¹

CHAPTER 5

CONCLUSIONS

5. CONCLUSIONS

From the results presented in the previous chapters, one may conclude that potent time-dependent β -lactam-based irreversible inhibitors of elastases, including simple azetidin-2-ones or azetidine-2,4-diones, were achieved.

- For the *N*-carbamoylazetidin-2-one derivatives, nucleophilic attack at the β -lactam carbonyl carbon results in ring opening with expulsion of the leaving group at C-4. 3,3-Unsubstituted **47b-d** inhibited PPE (k_{on} values ranged from 11.3 to 290 $M^{-1}s^{-1}$), while 3,3-gem-diethyl analogues **47e-k** inhibited HLE (k_{on} values ranged from 310 to 14600 $M^{-1}s^{-1}$). A proof of the covalent bond established between the enzyme and the inhibitor was obtained by X-ray crystallography studies of the acyl-enzyme complex resulting from reaction of PPE with **47d**.

- In both alkaline hydrolysis and elastase inactivation, the rate limiting step is the formation of the tetrahedral intermediate, and the β -lactam ring opening is not concerted with the departure of the substituent from C-4. However, HLE-catalyzed reaction is likely to involve a more favorable pathway than the hydroxide-ion catalyzed one, resulting in an earlier transition-state (lower ρ_1 value). Thus, hydrophobic interactions of the gem-diethyl group of **47e-k** with the S_1 binding pocket of HLE seem to improve the inhibitory potency and EREF by molecular recognition.

- A moderate correlation was found between intrinsic chemical reactivity and HLE inactivation by C-4 substituted azetidin-2-ones. Electron-withdrawing sulfone derivatives **47h-j** provided not only the more active inhibitors (even more potent than the reference **47k** from Merck Research Laboratories), but also the more reactive compounds towards hydroxide, being efficient in activating the β -lactam scaffold towards nucleophilic attack (inductive effect).

- Preliminary studies with azetidine-2,4-diones, designed as isoster analogues of 3-oxo- β -sultams, revealed that these compounds are effective irreversible inhibitors of PPE. Enzyme inhibition is a result of nucleophilic attack of the catalytic serine residue at one of the carbonyl carbons, with ring opening to form a stable acyl-enzyme complex. On the other hand, while 3-oxo- β -sultams are unsuitable for therapeutic

application due to a very high intrinsic chemical reactivity (Section 1.6.2.2),¹¹⁶ their 4-oxo- β -lactam analogues were found to be dramatically less reactive towards hydroxide, as **77h** is 100 000-fold less reactive than its 3-oxo- β -sultam counterpart **35**. Not only the magnitude of k_{OH^-} for most of **77** derivatives is within the range acceptable for a pharmacologically useful acylating agent (that is, k_{OH^-} values ranging 10^{-1} - $1.0 \text{ M}^{-1}\text{s}^{-1}$, as shown in Table 3.3),⁷² but also **77g** is almost as potent as **35**, indicating the effectiveness of the 4-oxo- β -lactam (azetidine-2,4-dione) scaffold as a therapeutically important lead structure to design serine protease inhibitors.

- 4-Oxo- β -lactams were found to be very potent inhibitors of HLE and both linear and hyperbolic dependences of pseudo-first order rate constants, k_{obs} , with the inhibitor concentration were observed. The inhibitory potency, expressed by k_{on} values, ranges from 2×10^2 to $3 \times 10^6 \text{ M}^{-1}\text{s}^{-1}$. Small alkyl substituents at C-3 such as a gem-diethyl group improved the inhibitory potency when compared to gem-methyl benzyl or ethyl benzyl groups.

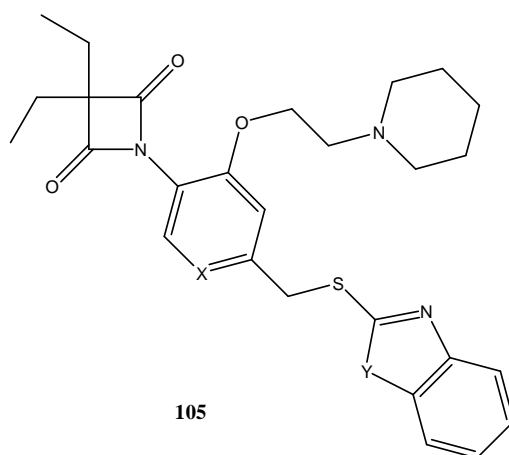
- The same derivatives assayed against PPE presented nearly three orders of magnitude larger k_{on} values towards HLE (**77c-g**) and, by contrast, inhibitory activity against HLE does not parallel chemical reactivity towards hydroxide, indicating good molecular recognition by the human enzyme. In addition, representative 4-oxo- β -lactams **77** and **103** were found to be relatively selective towards HLE, when compared to proteinase 3 and cathepsin G, but displayed absolute specificity when compared to cystein protease papain.

- The best inhibitor of this thesis was compound **103f**, with a remarkable k_{on} value of $3.24 \times 10^6 \text{ M}^{-1}\text{s}^{-1}$, which is one order of magnitude superior to that reported for Merck's derivative **27** (Chapter 1)¹⁰³ and of the same order that reported for **29** (Chapter 1).⁶ Docking studies, performed for selected 4-oxo- β -lactam inhibitors, supported the trends observed in the HLE inhibition assays.

- Although designed as potential mechanism-based inhibitors, derivatives **103** function as simple acylating agents (alternate substrate inhibitors), as the departure of the thiol leaving group does not occur under physiological conditions. Mass spectrometry techniques (ESI-MS) would be useful in identifying the inhibitor-complexed HLE structure. Although being very potent HLE inhibitors, compounds

103 suffer a drawback for systemic use. Indeed, the results obtained from hydrolytic stability as well as biodistribution studies suggest that these compounds are exceedingly reactive, being susceptible to off-target reactions, particularly by plasma and liver enzymes (esterases). However, these inhibitors might find pharmacological applicability as potential drug candidates suitable for aerosolization, a route of administration employed for other agents used for lung diseases.⁹³

- New azetidine-2,4-diones, retaining the optimized potency and with an improved hydrolytic stability, would be useful drug candidates for COPD and other inflammatory disorders. Derivatives **77**, such as **77d**, provided high levels of inhibitory potency against HLE combined with good hydrolytic stability, being important candidates for further optimization using computer-assisted techniques. An interesting approach for optimization of **103** is suggested in **105** (X = CH, N; Y = O, S). The *ortho* substituent may increase hydrolytic stability and the half-life of the acyl-enzyme complex. In addition, it is known that the basic piperidinoethoxy group increases water solubility and allows the penetration of the inhibitor into the bronchoalveolar fluid.¹⁷²



- Taken together, the results from this thesis demonstrate the superior activity of azetidine-2,4-dione over both 3-oxo- β -sultams and simple azetidin-2-one in the design of serine protease inhibitors. The use of the 4-oxo- β -lactam (azetidine-2,4-dione) scaffold as a lead template for potential drug candidates for COPD is the ultimate and most important goal of the research line initiated in this thesis. A fine

5. Conclusions

balance between intrinsic chemical reactivity, target selectivity, hydrolytic instability, stability of the acyl-enzyme complex, biodistribution and toxicity is important to achieve suitable inhibitors for therapeutic application.

CHAPTER 6

EXPERIMENTAL SECTION

6. EXPERIMENTAL SECTION

6.1. SYNTHESIS

6.1.1 Reagents, solvents and chromatography

Reagent grade chemicals were bought from Sigma-Aldrich and Merck. TEA was dried over potassium hydroxide and distilled under atmospheric pressure. Dichloromethane (DCM) was dried by distillation from calcium hydride. THF, benzene, toluene and dioxane were dried by distillation from sodium-benzophenone. The remaining compounds were used without further purification. Column chromatography was performed with silica gel (Merck, 230-400 mesh ATM). Preparative TLC was performed on silica gel GF₂₅₄ (Merck 1.07730). TLC was performed on pre-coated silica gel 60 F₂₅₄ (Merck) and visualized under UV light and / or by exposure to iodine vapour. All the reactions were monitored by TLC unless otherwise stated.

6.1.2 Equipment

Melting points were determined using a Kofler camera Bock Monoscope M and are uncorrected. The infrared spectra were collected on a Nicolet Impact 400 FTIR infrared spectrophotometer using thin films on NaCl plates (wavenumbers in cm⁻¹) and the NMR spectra on a Bruker 400 Ultra-Shield (¹H 400 MHz; ¹³C 100.61 MHz), in CDCl₃ (unless otherwise stated); chemical shifts, δ , are expressed in ppm (parts *per* million), coupling constants, J , are expressed in hertz (Hz). The spectra for **76** was collected on a Jeol JNM-300 (¹H 300 MHz; ¹³C 75 MHz). Carbon signal assignments were made also using DEPT technique. Low-resolution mass spectra were recorded using VG Mass Lab 20-250 EIMS or VG Quattro mass spectrometers. Elemental analyses were performed using an EA 1110 CE Instruments automatic analyser, at Medac Ltd., Brunel Science Centre, Englefield Green, Egham, TW20 0JZ, UK or a EA1108 automatic analyser, at University of Santiago de Compostela.

6.1.3 Experimental Procedures and Product Characterization

Synthesis of 4-Acetoxy-3,3-diethyl-azetidin-2-one, **42b** from 2-ethylbutyraldehyde (**48**)

1-Acetoxy-2-ethyl-1-butene (**49**)⁹⁸

A solution of commercial 2-ethylbutyraldehyde, **48** (1.09 mol, 136 ml), acetic anhydride (1.48 mol, 140 ml) and sodium acetate (0.14 mol, 11.18 g) was heated to reflux during 2 days. Then, the reaction mixture was slowly poured into a mixture of DCM, water and ice (respectively, 182 ml: 182 ml: 90.8 ml). The solution was neutralized (pH 7) by very slowly addition of solid sodium carbonate (100 g) (CO₂ evolution). The layers were separated, and the aqueous layer was extracted with DCM (200 ml). The organic layer was washed with saturated NaCl and dried over Na₂SO₄. The filtrate was concentrated and the residue was purified by distillation to yield 131.1 g (85%) of the enol acetate as a colorless liquid, b.p. 85-115° C at 75 mm Hg (lit. 65 - 90 °C at 90 mm Hg), ν_{\max} (film) 3088 (C=C), 1751 (C=O), 1227 (C-O), 1120 (C-O); δ ¹H-NMR 0.93 (3H, t, $J = 7.2$, CH₂CH₃), 0.97 (3H, t, $J = 7.6$, CH₂CH₃), 1.96 (2H, q, $J = 7.2$, CH₂CH₃), 2.06 (3H, s, COCH₃), 2.09 (2H, q, $J = 7.6$, CH₂CH₃), 6.80 (1 H, s, C=CH).

4-Acetoxy-3,3-diethyl-azetidin-2-one (**42b**)⁹⁸

A solution of 1-acetoxy-2-ethyl-1-butene, **49** (0.598 mol, 84.92 g) in dcm (150 ml) was cooled in an ice-ethanol bath. Chlorosulfonyl isocyanate (CSI, 0.709 mol, 100g) was added careful and slowly. The solution was allowed to warm to room temperature and stirred overnight. Then, the reaction mixture was diluted with ether and added very slowly to ice-cold NaHCO₃ solution containing Na₂SO₃, maintaining the temperature below 5 °C. The solution was stirred with a mechanical stirrer for 1.5 h. The aqueous layer was extracted with ether and the combined organic layers were washed with water, saturated NaCl and dried. The solvent was removed under reduced pressure and recrystallized with hexane (-10 °C), to afford a light yellow solid (36.92 g, 34%), m.p. 24 - 29 °C, ν_{\max} (film) 3267 (NH), 1786 (C=O), 1746 (C=O), 1233 (C-O), 1033 (C-O); δ ¹H- NMR 1.00 (3H, t, $J = 7.2$, CH₂CH₃), 1.03 (3H, t, $J =$

7.2, CH_2CH_3), 1.65-1.90 (4H, m, CH_3CH_2), 2.14 (3H, s, OCH_3), 5.60 (1H, s, C-4-H), 6.51 (1H, brs, N-H), δ ^{13}C -NMR 8.45 (CH_2CH_3), 8.72 (CH_2CH_3), 20.96 (OCH_3), 21.59 (CH_2CH_3), 23.56 (CH_2CH_3), 67.68 (C-3), 79.77 (C-4), 171.11 (C=O), 171.84 (C=O); ESI-MS m/z 208 (MNa^+).

4-Phenoxyazetid-2-one (43a)

To a solution of phenol (2.14 mmol, 201 mg) in acetone (2.2 ml), was added NaOH 1 M (2.6 mmol; 2.6 ml) with stirring for 20 minutes at room temperature. Then **42a** (1.94 mmol, 250.3 mg) in acetone (1.7 ml) was added. The solution was concentrated under reduced pressure and extracted with diethyl ether (2 x 70 ml). The organic layers were washed with NaHCO_3 5% (2 x 60 ml), followed by drying (MgSO_4) and concentration gave the crude, which was purified by column chromatography on silica gel (elution with DCM-EtOAc 9.5:0.5), to yield a pale yellow solid (66 mg, 21%); m.p. 72-73 °C; ν_{max} (film) 3234 (NH); 1744 (C=O), 1259 (C-O), 1058 (C-O); δ ^1H -NMR 3.12 (1H, d, $J = 15.2, 1.2$, C-3-H), 3.35 (1H, ddd, $J = 15.2, 3.6, 2.4$, C-3-H), 5.68 (1H, dd, $J = 3.6, 1.2$, C-4-H), 6.55 (1H, brs, N-H), 6.86-6.88 (2H, dd, $J = 7.2, 1.2$, C-H_{ortho}), 7.06 (1H, t, $J = 7.2$, C-H_{para}), 7.33 (2H, dt, $J = 7.2, 1.2$, C-H_{meta}); δ ^{13}C -NMR 46.20 (C-3), 76.31 (C-4), 115.74 (C-H), 122.64 (C-H), 129.94 (C-H), 155.90 (C), 166.26 (C=O); ESI-MS m/z 164 (MH^+).

3,3-Diethyl-4-phenoxyazetid-2-one (43b)¹⁰⁹

Prepared as described for **43a**, using phenol (3.89 mmol, 366 mg) and **42b** (3.53 mmol, 650 mg) as starting materials. Purified by column chromatography (elution with diethyl ether - light petroleum (1:1) to yield white crystals (320 mg, 42%); m.p. 56-58 °C (lit.¹⁰⁹ 53-56 °C); ν_{max} (film) 3256 (NH), 1764 (C=O), 1231 (C-O), 1083; δ ^1H -NMR 1.03 (3H, t, $J = 7.6$, CH_2CH_3), 1.04 (3H, t, $J = 7.6$, CH_2CH_3), 1.73-1.87 (3H, m, CH_2CH_3), 1.96 (1H, dq, $J = 14.4, 7.6$, CH_2CH_3), 5.37 (1H, s, C-4-H), 6.46 (1H, brs, N-H), 6.88 (2H, d, $J = 7.6$, C-H_{ortho}), 7.05 (1H, t, $J = 7.6$, C-H_{para}), 7.33 (2H, d, $J = 7.6$ Hz, C-H_{meta}); δ ^{13}C -NMR 8.64 (CH_2CH_3), 8.90 (CH_2CH_3), 21.72

(CH₂CH₃), 23.80 (CH₂CH₃), 64.68 (C-3), 83.41 (C-4), 115.87 (C-H), 122.41 (C-H), 129.84 (C-H), 156.40 (C), 172.57 (C=O); ESI-MS, *m/z* 219 (MH⁺).

6-(3,3-diethyl-4-oxoazetidin-2-yloxy)naphthalene-2-carboxylic acid (43c)

Prepared from 6-hydroxynaphthalene-2-carboxylic acid (1.65 mmol, 311 mg), **42b** (1.5 mmol, 272 mg) and NaOH 1 M (3.7 mmol; 3.7 ml), using the method described for **43a**. The reaction mixture was acidified with HCl (pH 2) with stirring and cooled and the crude product was filtered-off. The organic layer was washed with water, HCl 10 % and saturated NaCl. The combined residue was purified by flash chromatography using a gradient of EtOAc /ether, to yield white crystals (103 mg, 22%), m.p. 197-200 °C, ν_{\max} (film), 3216 (NH), 3200- 2600 (large O-H), 1748 (C=O), 1684 (C=O), 1204 (C-O), 936 (C-O); δ ¹H-NMR (DMSO) 0.98 (3H, t, *J* = 7.6, CH₂CH₃), 1.0 (3H, t, *J* = 7.6, CH₂CH₃), 1.64-1.93 (4H, m, CH₃CH₂), 5.65 (1H, s, C-4-H), 7.27 (1H, dd, *J* = 8.8, 2.4, C-H), 7.40 (1H, d, *J* = 2.4, C-H), 7.87 (1H, d, *J* = 8.8), 7.96 (1H, dd, *J* = 8.8, 2.4, C-H), 8.08 (1H, d, *J* = 8.8, C-H), 8.55 (1H, s, C-H), 9.07 (1H, s, N-H); δ ¹³C-NMR (DMSO) 8.40 (CH₂CH₃), 8.82 (CH₂CH₃), 21.25 (CH₂CH₃), 23.18 (CH₂CH₃), 63.42 (C-3), 82.05 (C-4), 108.70 (C-H), 119.61 (C-H), 125.80 (C-H), 126.58 (C), 127.25 (C-H), 127.87 (C), 130.52 (C-H), 131.36 (C-H), 136.30 (C), 155.87 (C), 167.48 (C=O), 172.42 (C=O); ESI-MS, *m/z* 312 (M-H).

4-Phenylthioazetidin-2-one (44a)

To a solution of 4-acetoxyazetidin-2-one **42a** (2 mmol, 258 mg) in benzene (20 ml) was added thiophenol (4 mmol, 440 μ l) and the reaction mixture was heated to reflux, adapting previously described techniques.¹²² The solution was washed with aqueous Na₂CO₃ (3 x 20 ml), dried (MgSO₄) and concentrated under reduced pressure. The residue was purified by chromatography on silica gel (elution with DCM-EtOAc 9.5:0.5), furnishing the desired product as white crystals (0.186 mg, 52%); m.p. 73 °C; ν_{\max} (film) 3205 (NH), 1740 (C=O); δ ¹H-NMR 2.91 (1H, ddd, *J* = 15.6, 2.4, 1.2, C-3-H), 3.40 (1H, ddd, *J* = 15.6, 4.8, 2.4, C-3-H), 5.04 (1H, dd, *J* = 4.8, 2.4, C-4-H), 6.21 (1H, brs, N-H), 7.38-7.39 (3H, m, C-H), 7.47-7.51 (2H, m, C-H); δ ¹³C-NMR 45.42

(C-3), 54.22 (C-4), 128.75 (C-H_{para}), 129.44 (C-H), 131.27 (C), 133.58 (C-H), 165.67 (C=O); ESI-MS, *m/z* 180 (MH⁺).

3,3-Diethyl-4-(phenylthio)azetidin-2-one (44b)^{107, 109, 120}

Prepared as described for **44a**, using **42b** (2 mmol, 370 mg) and thiophenol (4 mmol, 440 μ l) and purified by chromatography on silica gel (elution with diethyl ether - light petroleum 6:4), to yield the product (230.64 mg, 49 %) as a yellow oil, ν_{\max} (film) 3240 (NH), 1755 (C=O); δ ¹H-NMR 0.95 (3H, t, *J* = 7.2, CH₂CH₃), 1.10 (3H, t, *J* = 7.2, CH₂CH₃); 1.68-2.05 (4H, m, CH₃CH₂), 4.79 (1H, s, C-4-H), 6.73 (1H, brs, N-H), 7.26-7.44 (5H, m, C-H); δ ¹³C-NMR 8.56 (CH₂CH₃), 8.88 (CH₂CH₃), 22.84 (CH₂CH₃), 24.49 (CH₂CH₃), 66.95 (C-3), 77.20 (C-4), 127.89 (C-H_{para}), 129.44 (C-H), 132.16 (C), 134.82 (C-H), 171.10 (C=O); EI-MS *m/z* 235 (M⁺)

3,3-Diethyl-4-(benzoxazol-2-ylthio)-azetidin-2-one (44c)^{107, 109}

Prepared from **42b** (1.01 mmol, 186 mg) and 2-mercaptobenzoxazole (1.30 mmol, 196.44 mg), using the same method described earlier for **43a**. Recrystallized from DCM-hexane; to yield white crystals (120 mg, 43 %), m.p. 177-179 °C (lit.¹⁰⁹ 178-179 °C); ν_{\max} (film) 3237 (NH), 1776 (C=O); 1595, 1466, 1364, 1265 (C-O), 1141 (C-O), 921; δ ¹H-NMR 0.88 (3H, t, *J* = 7.2, CH₂CH₃), 1.18 (3H, t, *J* = 7.2, CH₂CH₃), 1.52 (1H, dq, *J* = 14.4, 7.2, CH₂CH₃), 1.69 (1H, dq, *J* = 14.4, 7.2, CH₂CH₃), 1.90 (1H, dq, *J* = 14.4, 7.2, CH₂CH₃), 2.04 (1H, dq, *J* = 14.4, 7.2, CH₂CH₃), 6.29 (1H, s, C-4-H), 6.34 (1H, brs, N-H), 7.29-7.31 (2H, m, C-H), 7.39-7.41 (1H, m, C-H), 7.60-7.62 (1H, m, C-H); δ ¹³C-NMR 8.07 (CH₂CH₃), 8.80 (CH₂CH₃), 21.52 (CH₂CH₃), 24.09 (CH₂CH₃), 67.53 (C-3), 70.39 (C-4), 110.77 (C-H), 112.00 (C-H), 124.55 (C-H), 125.18 (C-H), 131.19 (C), 146.98 (C), 172.47 (C=O), 179.64 (C); ESI-MS *m/z* 277 (MH⁺).

2-(3,3-Diethyl-4-oxoazetidin-2-ylthio)benzoxazole-5-carboxylic acid (44d)

Prepared as described for **43c**, from **42b** (1.35 mmol, 250 mg), **51** (1.49 mmol, 291 mg) and NaOH 1 M (3.34 mmol, 3.34 ml). The product was recrystallized from THF:

hexane, to yield the product as a solid (0.179 mg, 42%), m.p. 205-206 °C; ν_{\max} (film) 3300-2500 (large, O-H), 1761 (C=O of lactam), 1688 (of acid), 1356, 1268 (C-O), 1141; δ $^1\text{H-NMR}$ (DMSO) 0.76 (3H, t, $J = 7.2$, CH_2CH_3), 1.06 (3H, t, $J = 7.2$, CH_2CH_3), 1.35 (1H, dq, $J = 14.4, 7.2$, CH_2CH_3), 1.51 (1H, dq, $J = 14.4, 7.2$, CH_2CH_3), 1.76-1.91 (2H, m, CH_2CH_3), 6.00 (1H, s, C-4- H), 7.74 (1H, d, $J = 8.4$, C-7'- H), 7.98 (1H, dd, $J = 8.4, 1.6$, C-6'- H), 8.14 (1H, d, $J = 1.6$, C-4'- H), 9.15 (1H, brs, N- H), 13.42 (1H, brs, COOH); δ $^{13}\text{C-NMR}$ 8.42 (CH_2CH_3), 9.12 (CH_2CH_3), 21.78 (CH_2CH_3), 23.82 (CH_2CH_3), 66.49 (C-3), 70.46 (C-4), 111.16 (C-H), 113.33 (C-H), 126.71 (C-H), 128.41 (C), 131.86 (C), 149.77 (C), 166.81 (C=O), 171.62 (C=O of lactam), 179.59 (C); ESI-MS m/z 319 (M-H).

2-Mercaptobenzoxazole-5-carboxylic acid (51)

A mixture of 3-amino-4-hydroxybenzoic acid (5 mmol, 766 mg) and potassium ethyl xanthate (5.5 mmol, 882 mg) in ethanol 95%-water (6:1) was refluxed for 3h. The reaction mixture was concentrated, and acidified to pH 2 with stirring and cooled. The product separated as grey crystals (517 mg, 53%) being filtered-off, dried and used without any further purification; ν_{\max} (film) 3216 (NH), 3200-2500 (large, O-H); 1699 (C=O), 1459, 1274 (C-O), 1146, 1107; δ $^1\text{H-NMR}$ (DMSO) 7.53 (1H, d, $J = 8.8$, C-7'- H), 7.74 (1H, d, $J = 1.2$, C-4'- H), 7.85 (1H, dd, $J = 8.4, 1.2$, C-6'- H); δ $^{13}\text{C-NMR}$ 109.93 (C-H), 111.24 (C-H), 125.84 (C-H), 127.42 (C), 131.22 (C), 150.93 (C), 166.61 (C=O), 180.58 (NCS), ESI-MS m/z 194.08 (M-H).

3,3-Diethyl-4-(benzothiazol-2-ylthio)-azetidin-2-one (44e)

Prepared from **42b** (1.35 mmol, 249mg) and 2-mercaptobenzothiazole (1.49 mmol, 249 mg), as described for **43a**. Purified by column chromatography on silica gel (elution with DCM-EtOAc 9.5 : 0.5), to furnish white crystals (67 mg, 17%), m.p. 186-189 °C; ν_{\max} (film) 3266 (NH), 1756 (C=O), 1453; δ $^1\text{H-NMR}$ 0.88 (3H, t, $J = 7.2$, CH_2CH_3), 1.20 (3H, t, $J = 7.2$, CH_2CH_3), 1.53-1.62 (1H, m, CH_2CH_3), 1.77 (1H, dq, $J = 14.4, 7.2$, CH_2CH_3), 1.97-2.13 (2H, m, CH_2CH_3), 6.21 (1H, brs, N- H), 6.90 (1H, s, C-4- H), 7.32-7.40 (2H, m, C- H), 7.50 (1H, dd, $J = 8.4, 1.6$, C- H), 8.00 (1H, d, $J = 8.4$, C- H); δ $^{13}\text{C-NMR}$ 7.95 (CH_2CH_3), 8.73 (CH_2CH_3), 21.72 (CH_2CH_3), 24.50

(CH₂CH₃), 67.68 (C-3), 71.29 (C-4), 114.43 (C-H), 121.48 (C-H), 124.70 (C-H), 126.86 (C-H), 127.24 (C), 141.75 (C), 172.11 (C=O), 190.57 (NCS); ESI-MS *m/z* 293 (MH⁺).

3,3-Diethyl-4-(1-methyl-1H-imidazol-2-ylthio)-azetidin-2-one (44f)

Prepared from **42b** (1.62 mmol, 300 mg) and 2-mercapto-*N*-methylimidazole (1.79 mmol, 204 mg), as described for **43a**, and purified by column chromatography on silica gel (elution with DCM-EtOAc 9.5: 0.5), to yield the product as white crystals (92 mg, 25%). This compound was also synthesized using the method described for **44a**, from **42b** (0.54 mmol, 100 mg) and 2-mercapto-*N*-methylimidazole (1.08 mmol, 123.30 mg) with addition of triethylamine (1.08 mmol, 150 μ l), to yield white crystals (78.9 mg, 53%), m.p. 174-176 °C, ν_{\max} (film) 3288 (NH), 1765 (C=O); δ ¹H-RMN 0.82 (3H, t, *J* = 7.6, CH₂CH₃), 1.14 (3H, t, *J* = 7.6, CH₂CH₃), 1.33 (1H, dq, *J* = 15.2, 7.6, CH₂CH₃), 1.48 (1H, dq, *J* = 15.2, 7.6, CH₂CH₃), 1.86 (1H, dq, *J* = 15.2, 7.6, CH₂CH₃), 1.97 (1H, dq, *J* = 15.2, 7.6, CH₂CH₃), 3.67 (3H, s, N-CH₃), 6.05 (1H, s, C-4-*H*), 6.74 (1H, d, *J* = 2.4, C-*H*), 6.80 (1H, brs, N-*H*), 6.97 (1H, d, *J* = 2.4, C-*H*); δ ¹³C-RMN 8.00 (CH₂CH₃), 8.82 (CH₂CH₃), 21.46 (CH₂CH₃), 23.88 (CH₂CH₃), 34.61 (N-CH₃), 66.41 (C-3), 67.66 (C-4), 114.43 (C-H), 118.12 (C-H), 162.29 (NCS), 173.47 (C=O); ESI-MS *m/z* 240 (MH⁺).

3,3-Diethyl-4-(5-phenyl-1,3,4-oxadiazol-2-ylthio)-azetidin-2-one (44g)

Prepared as described for **44a**, using **42b** (0.81 mmol, 150 mg) and 2-mercapto-5-phenyl-1,3,4-oxadiazole (1.62 mmol, 289 mg), with addition of triethylamine (1.62 mmol, 226 μ l). The product was recrystallized from DCM/hexane, to afford pale yellow crystals (116 mg, 35%), m.p. 169.170 °C, ν_{\max} (film) 3262 (NH), 1783 (C=O), 1416; δ ¹H-RMN 0.93 (3H, t, *J* = 7.2, CH₂CH₃), 1.15 (3H, t, *J* = 7.2, CH₂CH₃), 1.60 (1H, dq, *J* = 14.4, 7.2, CH₂CH₃), 1.83-1.93 (2H, m, CH₂CH₃), 2.01 (1H, dq, *J* = 14.4, 7.2, CH₂CH₃), 5.97 (1H, s, C-4-*H*), 6.44 (1H, brs, N-*H*), 7.54-7.61 (3H, m, C-*H*), 7.98 (2H, d, *J* = 7.2, C-*H*); ¹³C-RMN 8.04 (CH₂CH₃), 8.79 (CH₂CH₃), 20.25 (CH₂CH₃), 23.25 (CH₂CH₃), 67.42 (C-3), 68.75 (C-4), 122.09 (C), 126.63 (C-H), 129.28 (C-H), 132.75 (C-H) 159.52 (C), 171.66 (C), 176.19 (C=O); ESI-MS *m/z* 304 (MH⁺).

4-Phenylsulphonylazetid-2-one (45a)¹⁰⁷

To a stirred solution of 4-phenylthioazetid-2-one, **44a** (1.79 mmol, 320 mg) in DCM (6 ml), previously cooled in an ice bath during 10 minutes, 70% MCPBA (4.469 mmol, 1200 mg) was added. After 30 minutes in an ice bath, the mixture was allowed to reach room temperature and stirred. After completion of the reaction, DCM (5 ml) was added to the mixture. This organic layer was successively washed with 5% NaHCO₃ solution (3 x 10 ml), brine (3 x 10 ml) then dried (MgSO₄) and the solvent removed under reduced pressure. Purified by column chromatography on silica gel (elution with DCM till elution of vestigial **44a**, then only EtOAc was used), to furnish the product as white solid (298.3 mg, 79%), m.p. 133-135 °C, ν_{\max} (film) 3249 (NH), 1763 (C=O), 1337 (S=O), 1123 (S=O), δ ¹H-RMN 3.25 (1H, ddd, $J = 15.6, 2.4, 1.2$, C-3-*H*), 3.34 (1H, ddd, $J = 15.6, 4.8, 2.4$, C-3-*H*), 4.76 (1H, dd, $J = 4.8, 2.4$, C-4-*H*), 6.43 (1H, brs, N-*H*), 7.66 (2H, t, $J = 8.8$, C-*H*_{meta}), 7.78 (1H, dt, $J = 8.8, 1.2$, C-*H*_{para}), 7.97 (2H, dd, $J = 8.8, 1.2$, C-*H*_{ortho}), δ ¹³C-RMN 41.67 (C-3), 64.88 (C-4), 128.29 (C-*H*_{para}), 129.39 (C-*H*), 129.78 (C-*H*), 134.64 (C), 164.46 (C=O); ESI-MS m/z 234 (MNa⁺).

3,3-Diethyl-4-phenylsulphonylazetid-2-one (45b)^{107, 109}

Prepared from **44b** (1.95 mmol, 350 mg) and 70% MCPBA (3.90 mmol, 963 mg 70%), as described for **45a**. Purified by column chromatography (elution with ether - hexane (8:2), to yield a white solid (255.8 mg, 62%), m.p. 155-157 °C (lit.¹⁰⁹ 156-158 °C), ν_{\max} (film) 3215 (NH), 1764 (C=O), 1458, 1335 (S=O), 1150 (S=O); δ ¹H-RMN 0.96 (3H, t, $J = 7.6$, CH₂CH₃), 1.09 (3H, t, $J = 7.6$, CH₂CH₃), 1.72 (1H, dq, $J = 15.0, 7.6$, CH₂CH₃), 1.94 (1H, dq, $J = 15.0, 7.6$, CH₂CH₃), 2.06 (1H, dq, $J = 15.0, 7.6$, CH₂CH₃), 2.39 (1H, dq, $J = 15.0, 7.6$, CH₂CH₃), 4.33 (1H, s, C-4-*H*), 6.26 (1H, brs, N-*H*), 7.62 (2H, t, $J = 7.2$, C-*H*_{meta}), 7.72 (1H, t, $J = 7.2$, C-*H*_{para}), 7.93 (2H, d, $J = 7.2$, C-*H*_{ortho}), δ ¹³C-RMN 8.57 (CH₂CH₃), 8.59 (CH₂CH₃), 20.32 (CH₂CH₃), 24.85 (CH₂CH₃), 67.85 (C-3), 74.29 (C-4), 128.55 (C-*H*), 129.75 (C-*H*), 134.84 (C-*H*_{para}), 138.15 (C), 171.10 (C=O); ESI-MS m/z 268 (MH⁺)

3,3-Diethylazetidin-2-one (46)¹⁰⁹

To a solution of a 4-acetoxy-3,3-diethylazetidin-2-one **42b** (800 mg, 4.32 mmol) in absolute EtOH (4 ml) at 0 °C, was added slowly NaBH₄ (178 mg, 4.72 mmol). The mixture was stirred for further 40 minutes. Then, the reaction mixture was filtered and the solvent evaporated. The resulting residue was washed with EtOAc (180 ml) and filtered. The solid in the filter was washed with DCM (20 ml). The organic solutions were combined, concentrated under reduced pressure and the residue purified by chromatography on silica gel (elution with DCM-EtOAc 7:3). The product was recovered as a colourless oil (163 mg, 30%); ν_{\max} (film) 3265; 1743; δ ¹H-RMN 0.95 (6H, t, $J = 7.5$, (CH₂CH₃)₂), 1.69 (4H, q, $J = 7.5$, (CH₂CH₃)₂), 3.09 (2H, s, C-4-H₂), 5.78 (1H, brs, N-H); δ ¹³C-RMN 8.78 (CH₂CH₃), 25.30 (CH₂CH₃), 45.12 (C-4), 61.59 (C-3), 174.18 (C=O); ESI-MS m/z 128 (MH⁺).

Synthesis of *N*-carbamoylazetidin-2-ones 47

N-Benzylcarbamoylazetidin-2-one (47a)^{120, 173}

Benzyl isocyanate (4.22 mmol, 521 μ l) and subsequently triethylamine (4.22 mmol, 588 μ l) were slowly added to a solution of the commercially available azetidin-2-one (3.52 mmol, 250 mg) in dichloromethane (3 ml). The reaction was stirred at room temperature. After completion of the reaction, the solution was evaporated under reduced pressure to give the crude product. Purified by column chromatography on silica gel (DCM-EtOAc 9.5:0.5) to yield white crystals (477 mg, 66%); m.p. 62-64 °C (lit¹⁷³ oil); ν_{\max} (film) 3335 (NH), 1764 (C=O of lactam), 1685 (C=O of urea); δ ¹H-RMN 3.08 (2H, t, $J = 4.8$, C-3-H), 3.68 (2H, t, $J = 4.8$, C-4-H), 4.50 (2H, d, $J = 6.0$, CH₂Ph), 6.89 (1H, brs, N-H), 7.28 - 7.38 (5H, m, C-H); δ ¹³C-RMN 36.06 (CH₂ of lactam), 37.21 (CH₂ of lactam), 43.70 (CH₂Ph), 127.59 (C-H_{para}), 127.64 (C-H), 128.72 (C-H), 137.93(C), 150.09 (C=O of urea), 167.11 (C=O of lactam); ESI-MS m/z 205 (MH⁺); Anal. calcd. for C₁₁H₁₂N₂O₂: C, 64.69, H, 5.92, N, 13.72; found: C, 64.55, H, 6.10, N, 13.66.

***N*-Benzylcarbamoyl-4-phenoxyazetididin-2-one (47b)**

Prepared as described for **47a**, using **43a** (0.30 mmol, 48.3 mg), benzyl isocyanate (0.36 mmol, 44 μ l) and triethylamine (0.36 mmol, 50 μ l). Purified by column chromatography on silica gel (elution with DCM-EtOAc 9.5 : 0.5) to afford white crystals (75 mg, 85%); m.p. 129-130 °C; ν_{\max} (film) 3368 (NH), 1780 (C=O of lactam), 1708 (C=O of urea), 1492, 1225 (C-O), 1073 (C-O); δ ¹H-RMN 3.17 (1H, dd, J = 16.0, 1.2, C-3-*H*), 3.46 (1H, dd, J = 16.0, 4.4, C-3-*H*), 4.50 (1H, dd, J = 14.4, 5.6, CH₂Ph), 4.55 (1H, dd, J = 14.4, 5.6, CH₂Ph), 6.07 (1H, dd, J = 4.4, 1.2, C-4-*H*), 6.88 (1H, brs, N-*H*), 7.10 (1H, t, J = 7.2, C-*H*), 7.15 (2H, d, J = 8.0, C-*H*), 7.31–7.39 (7H, m, C-*H*); δ ¹³C-RMN 43.76 (C-3), 45.51 (CH₂Ph), 78.76 (C-4), 117.14 (C-H_{para}), 123.21 (C-H_{para}), 127.00 (C-H), 128.78 (C-H), 129.43 (C-H), 129.72 (C-H), 137.56 (C), 146.13 (C), 156.14 (C=O of urea), 164.42 (C=O of lactam); ESI-MS m/z 297.5 (MH⁺); Anal. calcd. for C₁₇H₁₆N₂O₃: C, 68.91, H, 5.44, N, 9.45; found, C, 69.12, H, 5.61, N, 9.19.

***N*-Benzylcarbamoyl-4-phenylthioazetididin-2-one (47c)¹²⁰**

Prepared as described for **47a**, using **44a** (0.67 mmol, 120 mg), benzyl isocyanate (0.80 mmol, 100 μ l) and triethylamine (0.80 mmol, 112 μ l). Purified by column chromatography on silica gel (elution with DCM-EtOAc 9.5 : 0.5) to afford white crystals (169 mg, 80%), m.p. 78-79 °C (lit.¹²⁰ oil), ν_{\max} (film) 3366 (NH), 1773 (C=O of lactam), 1699 (C=O of urea), 1529; δ ¹H-RMN 2.88 (1H, dd, J = 16.4, 2.8, C-3-*H*), 3.40 (1H, dd, J = 16.4, 5.6, C-3-*H*), 4.47 (1H, dd, J = 15.0, 6.0, CH₂Ph), 4.54 (1H, dd, J = 15.0, 6.0, CH₂Ph), 5.29 (1H, dd, J = 5.6, 2.8, C-4-*H*), 6.81 (1H, brs, N-*H*), 7.30–7.39 (9H, m, C-*H*), 7.55 (1H, dd, J = 8.4, 1.6, C-*H*); δ ¹³C-RMN 43.68 (CH₂), 43.99 (CH₂), 56.69 (C-4), 127.69 (C-H_{para}), 127.72 (C-H_{para}), 128.77 (C-H), 129.29 (C-H), 129.31 (C-H), 129.36 (C-H), 135.25 (C), 137.83 (C), 149.63 (C=O of urea), 165.43 (C=O of lactam); ESI-MS m/z 334.8 (MNa⁺); Anal. calcd. for C₁₇H₁₆N₂O₂S: C, 65.36, H, 5.16, N, 8.97; found C 65.12, H 5.11, N 8.98.

***N*-Benzylcarbamoyl-4-phenylsulfonylazetid-2-one (47d)**

Prepared as described for **47a**, using **45** (0.31 mmol, 65 mg), benzyl isocyanate (0.37 mmol, 46 μ l) and triethylamine (0.37 mmol, 52 μ l). Purified by column chromatography on silica gel (elution with DCM-EtOAc 9.5:0.5), to yield white crystals (85.9 mg, 81%), m.p. 159-161 $^{\circ}$ C, ν_{\max} (film) 3374 (NH), 1789 (C=O of lactam), 1711 (C=O of urea), 1316 (S=O), 1150 (S=O); δ 1 H-RMN 3.48 (1H, dd, J = 16.8, 6.0, C-3-*H*), 3.67 (1H, dd, J = 16.8, 2.8, C-3-*H*), 4.33 (1H, dd, J = 14.8, 6.0, CH₂Ph), 4.39 (1H, dd, J = 14.8, 6.0, CH₂Ph), 5.20 (1H, dd, J = 6.0, 2.8, C-4-*H*), 6.65 (1H, brs, N-*H*), 7.23 (2H, dd, J = 8.0, 1.2, C-*H*_{ortho}), 7.31 -7.38 (3H, m, C-*H*), 7.58 (2H, t, J = 8.0, C-*H*), 7.74 (1H, dt, J = 8.0, 1.2, C-*H*), 7.96 (2H, dd, J = 8.0, 0.8, C-*H*_{ortho}); δ 13 C-RMN 39.43 (C-3), 43.86 (CH₂Ph), 65.84 (C-4), 127.58 (C-*H*), 127.79 (C-*H*_{para}), 128.77 (C-*H*), 129.28 (C-*H*), 129.39 (C-*H*), 134.88 (C-*H*_{para}), 136.75 (C), 137.28 (C), 148.39 (C=O of urea), 164.27 (C=O of lactam); EI-MS m/z : 344.00 (M⁺)(13.74); Anal. calcd. for C₁₇H₁₆N₂O₄S: C, 59.29, H, 4.68, N, 8.13; found C, 59.41, H, 4.55; N, 8.01.

***N*-Benzylcarbamoyl-3,3-diethylazetid-2-one (47e)¹²⁰**

Prepared as described for **47a**, using **46** (1.20 mmol, 152 mg), benzyl isocyanate (1.44 mmol, 177 μ l) and triethylamine (1.44 mmol, 200 μ l). Purified by column chromatography on silica gel (elution with DCM-EtOAc 9.5:0.5) to afford the product (257 mg, 83%) as colourless oil; ν_{\max} (film) 3364 (NH), 1757 (C=O of lactam), 1702 (C=O of urea), 1535; δ 1 H-RMN 1.00 (6H, t, J = 7.6, (CH₂CH₃)₂), (4H, q, J = 7.6, (CH₂CH₃)₂), 3.42 (2H, s, C-4-*H*), 4.50 (2H, d, J = 6.0, CH₂Ph), 6.93 (1H, brs, N-*H*), 7.28-7.38 (5H, m, C-*H*); δ 13 C-RMN 8.70 (CH₂CH₃), 25.71 (CH₂CH₃), 43.75 (CH₂), 47.04 (CH₂), 59.31 (C-3), 127.55 (C-*H*_{para}), 127.65 (C-*H*), 128.71 (C-*H*), 137.98 (C), 150.95 (C=O of urea), 172.83 (C=O of lactam); ESI-MS m/z 261 (MH⁺); Anal. calcd. for C₁₅H₂₀N₂O₂: C, 69.20, H, 7.74, N, 10.76; found C, 68.80, H, 7.80, N, 10.59.

***N*-Benzylcarbamoyl-3,3-diethyl-4-phenoxyazetidin-2-one (47f)**⁹⁹

Prepared as described for **47a**, using **43b** (1.40 mmol, 305.50 mg), benzyl isocyanate (1.68 mmol, 207 μ l) and triethylamine (1.68 mmol, 234 μ l). Purified by column chromatography on silica gel (elution with DCM-EtOAc 9.5:0.5), to furnish the product as white crystals (398 mg, 81%), m.p. 58-59 °C; ν_{\max} (film) 3366 (NH), 1770 (C=O of lactam), 1710 (C=O of urea), 1534, 1492, 1221 (C-O), 1086 (C-O); δ ¹H-RMN 1.00 (3H, t, J = 7.6, CH₂CH₃), 1.06 (3H, t, J = 7.6, CH₂CH₃), 1.77–1.84 (3H, m, CH₂CH₃), 1.99 (1 H, dq, J = 14.4, 7.2, CH₂CH₃), 4.47 (1H, dd, J = 15.6, 6.0, CH₂Ph), 4.51 (1H, dd, J = 15.6, 6.0, CH₂Ph), 5.68 (1H, s, C-4-H), 6.93 (1H, brs, N-H), 7.07 (1H, t, J = 7.2, C-H); δ ¹³C-RMN 8.58 (CH₂CH₃), 8.84 (CH₂CH₃), 21.23 (CH₂CH₃), 23.86 (CH₂CH₃), 43.75 (CH₂Ph), 64.35 (C-3), 86.76 (C-4), 117.76 (C-H), 123.17 (C-H_{para}), 127.63 (C-H_{para}), 127.67 (C-H), 128.76 (C-H), 129.67 (C-H), 137.66 (C), 150.14 (C), 157.47 (C=O of urea), 172.23 (C=O of lactam); ESI-MS m/z 353 (MH⁺); Anal. calcd. for C₂₁H₂₄N₂O₃: C, 71.57, H, 6.86, N, 7.95; found C, 71.84, H, 6.78, N, 8.18.

***N*-Benzylcarbamoyl-3,3-diethyl-4-phenylthioazetidin-2-one (47g)**

Prepared as described for **47a**, using **44b** (1.10 mmol, 262 mg), benzyl isocyanate (1.43 mmol, 180 μ l) and triethylamine (1.43 mmol, 200 μ l). Purified by column chromatography on silica gel (elution with DCM-EtOAc 9.5:0.5), and recrystallized from DCM/hexane to furnish the product as white crystals (278.9 mg, 69%), m.p. 79-80 °C, ν_{\max} (film) 3360 (NH), 1758 (C=O of lactam), 1700 (C=O of urea), 1523, 845; δ ¹H-RMN 0.94 (3H, t, J = 8.0, CH₂CH₃), 1.12 (3H, t, J = 8.0, CH₂CH₃), 1.75-1.98 (3H, m, CH₂CH₃), 1.99 (1 H, dq, J = 14.4, 7.2, CH₂CH₃), 4.51 (1H, dd, J = 15.6, 6.0, CH₂Ph), 4.55 (1H, dd, J = 15.6, 6.0, CH₂Ph), 5.06 (1H, s, C-4-H), 6.95 (1H, brs, N-H); 7.28-7.39 (8H, m, C-H); 7.77 (2H, d, J = 8.0, C-H); δ ¹³C-RMN 8.43 (CH₂CH₃), 9.01 (CH₂CH₃), 23.11 (CH₂CH₃), 24.74 (CH₂CH₃), 43.74 (CH₂Ph), 63.95 (C-3), 71.42 (C-4), 127.60 (C-H_{para}), 127.65 (C-H), 128.17 (C-H_{para}), 128.74 (C-H), 129.19 (C-H), 133.24 (C-H), 137.71 (C), 150.13 (C=O of urea), 172.04 (C=O of lactam); EI-MS m/z 368.15 (M⁺)(4.08%); Anal. calcd. for C₂₁H₂₄N₂O₂S: C, 68.45, H, 6.56, N, 7.60; found, C, 68.22, H, 6.93, N, 8.03.

3-Benzylpyrimidine-2,4(1H,3H)-dione (60), from large scale reaction of 47d with exc. sodium methoxide

N-Benzylcarbamoyl-4-phenylsulfonylazetidino-2-one, **47d** (0.29 mmol, 100 mg), was added to a solution of sodium methoxide (1.5 mmol) in methanol (15 ml). The reaction mixture was stirred at room temperature and monitored by TLC. The solvent was removed under reduced pressure and the residue was taken up in water (20 ml), acidified with HCl 10% until pH 2 and extracted with EtOAc (3x 30 ml). After drying and evaporating off the solvent, the residue was purified by column chromatography on silica gel (elution with DCM-EtOAc 8:2), to yield the product 3-benzylpyrimidine-2,4(1H,3H)-dione, **60**, as a white solid (46.4 mg, 79%); m.p. 177-179 °C (lit.,¹⁵⁶ 181-182 °C) ; ν_{\max} (film) 3084 (NH), 1625 (C=O), 1601 (NC=ON); δ ¹H-RMN 5.12 (2H, s, CH₂Ph), 5.81 (1H, dd, *J* = 7.2, 1.2, HC=CHN), 7.14 (1H, dd, *J* = 7.2, 6.0, HC=CHN), 7.26-7.34 (3H, m, C-H); 7.46 (2H, d, *J* = 7.2, C-H_{ortho}); 9.35 (1H, brs, N-H); δ ¹³C-RMN 43.71 (CH₂Ph), 102.26 (HC=CHN), 127.70 (C-H_{para}), 128.46 (C-H), 128.80 (C-H), 136.49 (C), 138.17 (HC=CHN), 151.09 (NHC=ON), 163.12 (C=OCH); EI-MS *m/z* 202.05 (M⁺)(100%); Anal. calcd. for C₁₁H₁₀N₂O₂, C, 65.34, H, 4.98, N, 13.85; found, C, 65.65, H, 5.25, N, 13.41.

Attempted ring-closure of 2,2-diethylmalonamic acid and derivatives.**Ethyl 2-cyano-2-ethylbutanoate (73)¹⁴⁶**

Sodium metal (10 mmol, 230 mg) in small pieces was added slowly to dry EtOH (5 ml). When the reaction had subsided, ethyl 2-cyanoacetate **72** (10 mmol, 1.07 ml) was added and the mixture stirred at 50 °C for 15 min. Iodoethane (10 mmol, 808 μ l) was added dropwise and the resulting mixture refluxed for 90 min, and then cooled to 20 °C. Subsequently, more sodium (10 mmol, 230 mg) in dry EtOH (5 ml) was added, and after 5 min., an additional iodoethane (10 mmol, 808 μ l), and the solution refluxed for 4h. The solvent was removed under reduced pressure, the residue washed with water and extracted with diethyl ether, to yield the product as a red wine colored liquid (1284 mg, 76%), ν_{\max} (film) 2241 (CN), 1741 (C=O), 1460, 1237 (C-O), 1020 (C-O); δ ¹H-RMN 1.64 (6H, t, *J* = 7.2, (CH₂CH₃)₂), 1.35 (3H, t, *J* = 7.2, OCH₂CH₃), 1.87 (2H, dq, *J* = 14.4, 7.2, CCH₂CH₃), 1.98 (2H, dq, *J* = 14.4, 7.2, CCH₂CH₃), 4.30

(2H, q, $J = 7.2$, OCH₂CH₃); δ ¹³C-RMN 10.01 (CCH₂CH₃), 14.38 (OCH₂CH₃), 30.75 (CCH₂CH₃), 51.82 (C), 62.72 (OCH₂CH₃), 119.41 (CN), 169.31 (C=O); EI-MS m/z 169.22 (M⁺)(1.90%).

2,2-Diethylmalonamic acid (74)¹⁴⁶

Compound **73** (6.11 mmol, 1034 mg) was added with cooling and stirring to conc. sulphuric acid at 90 °C, held at 100-110 °C for 30 min. and poured onto ice. Extracted with EtOAc and recrystallized from EtOH to give the product as white crystals (243 mg, 31%), m.p. 149-150 °C (lit.¹⁴⁶ 142-144 °C); ν_{\max} (film) 3401 (NH), 3227 (NH), 1705 (C=O of acid), 1640 (C=O of amide), 1479, 1305, 1214, 1085; δ ¹H-RMN (DMSO) 0.95 (6H, t, $J = 7.2$, (CH₂CH₃)₂), 1.77 (2H, dq, $J = 14.4$, 7.2, (CH₂CH₃)₂), 2.19 (2H, dq, $J = 14.4$, 7.2, CCH₂CH₃), 5.95 (1H, brs, N-H), 6.57 (1H, brs, N-H); δ ¹³C-RMN 9.27 (CCH₂CH₃), 26.85 (CCH₂CH₃), 58.09 (C), 172.60 (C=O), 175.11 (C=O); EI-MS m/z 159.18 (M⁺)(47.75%), 144 (M-CH₃)⁺ (100.00%), 129 (M-CO₂H)⁺ (91.46).

2-Cyano-2-ethylbutanoyl chloride (75)¹⁴⁷

To compound **74** (12.58 mmol, 2000 mg) suspended in dry toluene (15 ml) in inert atmosphere, was added simultaneously for 15 min. dry pyridine (15 mmol, 1.22 ml) and thionyl chloride (34 mmol, 2.48 ml) at 15-20 °C, refluxed for 30 min, the salt filtered-off and the yellow filtrate distilled in reduced pressure, to yield the product (740 mg, 37%), b.p. 28 °C (0.4 mm Hg); ν_{\max} (film) 2254 (CN), 1784 (C=O), 1459; δ ¹H-RMN (300 MHz) 1.07 (6H, t, $J = 7.2$, (CH₂CH₃)₂), 1.89 (2H, dq, $J = 14.4$, 7.2, CCH₂CH₃), 2.06 (2H, dq, $J = 14.4$, 7.2, CCH₂CH₃); δ ¹³C-RMN (300 MHz) 9.60 (CCH₂CH₃), 30.56 (CCH₂CH₃), 61.36 (C), 117.27 (CN), 171.82 (C=O); ESI-MS m/z 160 (MH⁺).

2,2-Diethylmalonamic acid ethyl ester (76)¹⁴⁶

Compound **73** (5.92 mmol, 1000 mg) was added with cooling to 30 ml of conc. sulphuric acid at 90 °C, the temperature maintained at 95-100 °C for 5 min., and

poured onto ice. The oil was extracted with diethyl ether and ethyl acetate, the organic layer washed with sodium carbonate, water and dried. The solvent was removed under reduced pressure to give the product as a pale yellow solid (232 mg, 21%), m.p. 77-78 °C (lit.¹⁴⁶ 73-75 °C), ν_{\max} (film) 3399 (NH), 3194(NH), 1716 (C=O of ester), 1669 (C=O of amide), 1228, 1133, 1010; δ ¹H-RMN 0.77 (6H, t, $J = 7.2$, (CH₂CH₃)₂), 1.26 (3H, t, $J = 7.2$, OCH₂CH₃), 1.76 (2H, dq, $J = 14.4, 7.2$, CCH₂CH₃), 1.98 (2H, dq, $J = 14.4, 7.2$, CCH₂CH₃), 4.15 (2H; q, $J = 7.2$, OCH₂CH₃), 5.69 (1H, brs, N-H), 7.86 (1H, brs, N-H); δ ¹³C-RMN 9.61 (CCH₂CH₃), 14.00 (OCH₂CH₃), 30.04 (CCH₂CH₃), 59.36 (C), 61.22 (OCH₂CH₃), 173.53 (C=O), 174.97 (C=O); EI-MS m/z 187.15 (M⁺)(0.02%), 144.15 (M-CONH₂)⁺ (7.29%).

Synthesis of azetidine-2,4-diones by condensation of malonyl dichlorides with primary amines

Ethyl 2-(3,3-diethyl-2,4-dioxoazetidin-1-yl)acetate (77a)¹⁵¹

To a solution of diethylmalonyl dichloride (25 mmol, 4925 mg) in dry dioxane (15 ml) was added under nitrogen ethyl glycinate hydrochloride (25 mmol, 3475 mg) in the same solvent (15 ml). Then, a solution of triethylamine (90 mmol, 9107 mg) in dry dioxane was added dropwise during 1.5 h and the reaction mixture refluxed for nearly 6h. The residue was purified by column chromatography on silica gel using mixtures of toluene and EtOAc as eluant to yield the diethylmalonyldiglycinate **78** (R = CH₂CO₂Et, R¹ = R² = Et) as the by-product, and the product as a colourless oil (920 mg, 16%); ν_{\max} (film) 1887 (C=O symm), 1737 (C=O assym.); δ ¹H-NMR 1.07 (6H, t, $J = 7.6$, (CH₂CH₃)₂), 1.30 (3H, t, $J = 7.2$, OCH₂CH₃), 1.82, (4H, q, $J = 7.6$, (CH₂CH₃)₂), 4.10 (2H, s, NCH₂CO), 4.25 (2H, q, $J = 7.2$, OCH₂CH₃); δ ¹³C-NMR 9.27 (CCH₂CH₃), 14.08 (OCH₂CH₃), 23.62 (CCH₂CH₃), 39.28 (NCH₂CO), 62.23 (OCH₂CH₃), 71.30 (C-3), 165.93 (C=O of ester), 173.59 (C=O of 4-oxo- β -lactam); EI-MS m/z 228.20 (M)⁺ (0.51%); 98.05 ((CH₃CH₂)₂C=C=O)⁺ (100.00%), 83.05 [((CH₃CH₂)₂C=C=O)-CH₃]⁺ (56.68%); 55 (C₃H₃O)⁺ (12.92 %); Anal. calcd. for C₁₁H₁₇NO₄: C, 58.14, H, 7.54, N, 6.16; found C, 58.40, H, 7.24, N, 5.77.

3,3-Diethyl-1-benzylazetidine-2,4-dione (77b)

Prepared as described for **77a**, using diethylmalonyl dichloride (15 mmol, 2956 mg), benzylamine (15 mmol, 1622 mg) and triethylamine (36 mmol, 3649 mg) as catalyst. Purified by chromatography on silica gel using toluene: EtOAc as eluant (from 9.8:0.2 to 9.2:0.8) and then recrystallized from hexane to yield the product as white crystals (243 mg, 9%); m.p. 46-47 °C; ν_{\max} (film) 1873 (C=O symm), 1717 (C=O assym.), 1458; δ ¹H-NMR 0.94 (6H, t, $J = 7.6$, (CH₂CH₃)₂), 1.75 (4H, q, $J = 7.6$, (CH₂CH₃)₂), 4.48 (2H, s, CH₂Ph), 7.32-7.37 (5H, m, C-H); δ ¹³C-NMR 9.18 (CH₂CH₃), 23.67 (CH₂CH₃), 42.17 (CH₂Ph), 70.98 (C-3), 128.14 (C-H_{para}), 128.28 (C-H), 128.88 (C-H), 135.06 (C), 174.24 (C=O); EI-MS m/z 231.15 (M)⁺ (4.07%), 133.05 (PhCH₂NCO)⁺ (1.32%), 98.05 ((CH₃CH₂)₂C=C=O)⁺ (100.00%), 90.95 (C₇H₇)⁺ (29.31%), 82.95 [((CH₃CH₂)₂C=C=O)-CH₃]⁺ (65.79%), 54.95 (C₃H₃O)⁺ (38.23%); Anal. calcd. for C₁₄H₁₇NO₂, C, 72.70, H, 7.41, N, 6.06; found, C 72.55 %, H 7.43 %, N 5.81 %.

3,3-Diethyl-1-(*p*-methoxyphenyl)azetidine-2,4-dione (77c)

Prepared as described for **77a**, using diethylmalonyl dichloride (15 mmol, 2956 mg) and 4-anisidine (15 mmol, 1605 mg) as primary amine. Purified by chromatography on silica gel using toluene: EtOAc (9.2: 0.8), yielding yellow oil (412 mg, 11%), ν_{\max} (film) 1849 (C=O symm.), 1736 (C=O assym.), 1513, 1250 (C-O), 1029 (C-O); δ ¹H-NMR 1.08 (6H, t, $J = 7.6$, (CH₂CH₃)₂), 1.86 (4H, q, $J = 7.6$, (CH₂CH₃)₂), 3.84 (3H, s, OCH₃), 6.94 (2H, d, $J = 8.8$, C-H), 7.76 (2H, d, $J = 8.8$, C-H); δ ¹³C-NMR 9.25 (CH₂CH₃), 23.95 (CH₂CH₃), 55.51 (OCH₃), 71.94 (C-3), 114.34 (C-H), 120.89 (C-H), 127.82 (C), 157.84 (C), 172.25 (C=O); EI-MS m/z 247.30 (M)⁺ (71.03%); 149.15 (4-(OCH₃)PhNCO)⁺ (100.00%), 134.15 (NCOC₆H₄O)⁺ (25.29%), 98.05 ((CH₃CH₂)₂C=C=O)⁺ (5.85%), 82.95 [((CH₃CH₂)₂C=C=O)-CH₃]⁺ (7.49%); Anal. calcd. for C₁₄H₁₇NO₃, C, 68.00, H, 6.93, N, 5.66; found, C, 67.60, H, 6.53, N, 5.79.

3,3-Diethyl-1-(*p*-tolyl)azetidine-2,4-dione (77d)

Prepared as described for **77a**, using diethylmalonyl dichloride (15 mmol, 2956 mg) and 4-toluidine (15 mmol, 1605 mg). Purified by chromatography on silica gel using

toluene: EtOAc (9:1) as eluant, to afford white crystals (343 mg, 10%), m.p. 41-44 °C; ν_{\max} (film) 1844 (C=O symm.), 1739 (C=O assym.), 1517; δ $^1\text{H-NMR}$ 1.08 (6H, t, $J = 7.6$, $(\text{CH}_2\text{CH}_3)_2$), 1.87 (4H, q, $J = 7.6$, $(\text{CH}_2\text{CH}_3)_2$), 2.37 (3H, s, $p\text{-CH}_3$), 7.23 (2H, d, $J = 8.4$, C-H), 7.73 (2H, d, $J = 8.4$, C-H); δ $^{13}\text{C-NMR}$ 9.24 (CH_2CH_3), 21.18 ($p\text{-CH}_3$), 23.95 (CH_2CH_3), 72.01 (C-3), 119.19 (C-H), 129.75 (C-H), 131.33 (C), 136.69 (C), 172.27 (C=O); EI-MS m/z 231.15 (M) $^+$ (5.76%), 97.95 $(\text{C}_3\text{H}_5\text{O})^+$ (94.15%), 82.95 $(\text{C}_3\text{H}_5\text{O}-\text{CH}_3)^+$ (100.00%), 54.95 ($\text{C}_3\text{H}_3\text{O}^+$) (47.58%); Anal. calcd. for $\text{C}_{14}\text{H}_{17}\text{NO}_2$, C, 72.70, H, 7.41, N, 6.06; found, C, 72.73, H, 6.59, N, 6.56.

3,3-Diethyl-1-phenylazetidine-2,4-dione (77e)¹⁶⁵

Prepared as described for **77a**, using diethylmalonyl dichloride (15 mmol, 2956 mg) and aniline (15 mmol, 1397 mg). Purified by column chromatography on silica gel using toluene: EtOAc (9.0, 1.0), to give a colourless oil (474 mg, 15%) (lit¹⁶⁵: mp. 86–87°C); ν_{\max} (film) 1863 (C=O symm.), 1740 (C=O asymm.), 1595, 1458; δ $^1\text{H-NMR}$ 1.09 (6H, t, $J = 7.6$, $(\text{CH}_2\text{CH}_3)_2$), 1.88 (4H, q, $J = 7.6$, $(\text{CH}_2\text{CH}_3)_2$), 7.29 (1H, dt, $J = 7.6$, 1.2, C- H_{para}), 7.73 (2H, dt, $J = 7.6$, 1.2, C- H_{meta}), 7.86 (2H, dd, $J = 7.6$, 1.2, C- H_{ortho}); δ $^{13}\text{C-NMR}$ 9.25 (CH_2CH_3), 23.96 (CH_2CH_3), 72.14 (C-3), 119.23 (C-H), 126.76 (C- H_{para}), 129.26 (C-H), 133.85 (C), 172.26 (C=O); EI-MS m/z 217.15 (M) $^+$ (18.05%); 118.95 (PhNCO) $^+$ (14.21%), 98.05 $(\text{C}_3\text{H}_5\text{O})^+$ (100.00%), 82.95 $(\text{C}_3\text{H}_5\text{O}-\text{CH}_3)^+$ (90.98%), 54.95 ($\text{C}_3\text{H}_3\text{O}^+$) (47.22%); Anal. calcd. for $\text{C}_{13}\text{H}_{15}\text{NO}_2$, C, 71.87, H, 6.96, N, 6.45; found, C, 72.09, H, 6.83, N, 6.46.

1-(*p*-Chlorophenyl)-3,3-diethylazetidine-2,4-dione (77f)

Prepared as described for **77a**, using diethylmalonyl dichloride (15 mmol, 2956 mg) and 4-chloroaniline (15 mmol, 1695 mg). Purified by column chromatography on silica gel using toluene: EtOAc (8.0, 2.0), yielding the product as white crystals (544 mg, 14%), m.p. 43-46 °C; ν_{\max} (film) 1868 (C=O symm.), 1741 (C=O asymm.), 1496, 1463, 1037; δ $^1\text{H-NMR}$ 1.08 (6H, t, $J = 7.6$, $(\text{CH}_2\text{CH}_3)_2$), 1.88 (4H, q, $J = 7.6$, $(\text{CH}_2\text{CH}_3)_2$), 7.40 (2H, d, $J = 8.8$, C-H), 7.83 (2H, d, $J = 8.8$, C-H); δ $^{13}\text{C-NMR}$ 9.23 (CH_2CH_3), 23.93 (CH_2CH_3), 72.38 (C-3), 120.41 (C-H), 129.42 (C-H), 132.12 (C),

132.32 (C), 171.96 (C=O); EI-MS m/z 251.05 (M)⁺ (48.25%), 253.05 (M+2)⁺ (15.90%), 153.00 (4-ClPhNCO)⁺ 28.31%, 155.00 (4-ClPhNCO+2) (9.49%), 98.05 ((CH₃CH₂)₂C=C=O)⁺ (100.00%), 82.95 [((CH₃CH₂)₂C=C=O)-CH₃]⁺ (77.26%), 55.00 (C₃H₃O)⁺ (44.43%); Anal. calcd. for C₁₃H₁₄NO₂Cl, C, 62.03, H, 5.61, N, 5.56, found, C, 62.31, H, 5.41, N, 5.81.

3,3-Diethyl-*p*-(2,4-dioxoazetid-1-yl)benzotrile (77g)

Prepared as described for **77a**, using diethylmalonyl dichloride (15 mmol, 2956 mg) and 4-cyanoaniline (15 mmol, 1772 mg). Purified by column chromatography on silica gel using hexane: EtOAc (8.0, 2.0), to yield the product as white crystals (687 mg, 19%), m.p. 106-109 °C; ν_{\max} (film) 2229 (CN), 1873 (C=O symm.), 1746 (C=O asymm.), 1385; δ ¹H-NMR 1.09 (6H, t, J = 7.6, (CH₂CH₃)₂), 1.90 (4H, q, J = 7.6, (CH₂CH₃)₂), 7.74 (2H, d, J = 8.8, C-H), 8.03 (2H, d, J = 8.8, C-H); δ ¹³C-NMR 9.21 (CH₂CH₃), 23.96 (CH₂CH₃), 72.87 (C-3), 110.10 (C), 118.14 (CN), 119.29 (C-H), 133.49 (C-H), 137.19 (C), 171.70 (C=O); EI-MS m/z 242.15 (M)⁺ (24.63%), 144.00 (4-(CN)PhNCO)⁺ (5.22%), 98.00 ((CH₃CH₂)₂C=C=O)⁺ (100.00%), 83.00 [((CH₃CH₂)₂C=C=O)-CH₃]⁺ (89.18%), 55.00 (C₃H₃O)⁺ (28.77%); Anal. calcd. for C₁₄H₁₄N₂O₂, C, 69.41, H, 5.82, N, 11.56; found, C, 69.58, H, 5.87, N, 11.57.

3,3-Dimethyl-1-benzylazetid-2,4-dione (77h)

Prepared as described for **77a**, using dimethylmalonyl dichloride (15 mmol, 2535 mg), benzylamine as primary amine (15 mmol, 1622 g) and triethylamine (36 mmol 3649 mg) as catalyst. The resulting reaction mixture was refluxed for 14h. Purified by chromatography on silica gel, using toluene: EtOAc as eluant (from 9.8:0.2 to 9.0:1.0), yielding white crystals (122 mg, 4%), m.p. 69-71 °C, ν_{\max} (film) 1874 (C=O symm.), 1719 (C=O asymm.), 1400; δ ¹H-NMR 1.38 (6H, s, (CH₃)₂), 4.46 (2H, s, CH₂Ph), 7.33-7.39 (5H, m, C-H); δ ¹³C-NMR 17.44 (CH₃), 42.78 (CH₂Ph), 60.66 (C-3), 127.99 (C-H), 128.17 (C-H), 129.00 (C-H), 134.77 (C), 175.05 (C=O); EI-MS m/z 203.30 (M)⁺ (100.00%), 133.05 (PhCH₂NCO)⁺ (36.41%), 90.95 (C₇H₇)⁺ (52.26%), 70.05 ((CH₃)₂C=C=O)⁺ (66.30 %); Anal. calcd. for C₁₂H₁₃NO₂, C, 70.92, H, 6.45, N, 6.89; found, C, 71.16, H, 5.92, N, 6.81.

3,3-Dimethyl-1-(*p*-Chlorophenyl)-azetidine-2,4-dione (77i)

Synthesized as described for **77a**, using dimethylmalonyl dichloride (25 mmol, 4225 mg) and 4-chloroaniline (25 mmol, 2820 mg), the reaction mixture being refluxed for 8h. Purified by column chromatography using hexane: EtOAc as eluant (8.4: 1.6) to afford white crystals (351 mg, 6%), m.p. 81-84 °C; ν_{\max} (film) 1858 (C=O symm.), 1735 (C=O asym.), 1493; δ ¹H-NMR 1.51 (6H, s, (CH₃)₂), 7.40 (2H, d, *J* = 8.8, C-H), 7.82 (2H, d, *J* = 8.8, C-H); δ ¹³C-NMR 17.76 (CH₃), 62.03 (C-3), 120.33 (C-H), 129.42 (C-H), 132.12 (C), 132.81 (C), 172.62 (C=O); EI-MS *m/z* 223.00 (M)⁺ (96.36 %), 225.00 (M+2)⁺ (32.71%), 153.00 (4-ClPhNCO)⁺ (33.19%), 155.00 (4-ClPhNCO+2)⁺ (11.09%), 70.00 ((CH₃)₂C=C=O)⁺ (100.00%); Anal. calcd. for C₁₁H₁₀NO₂Cl, C, 59.07; H, 4.51; N, 6.26; Cl, 15.85; found, C, 59.03; H, 4.12; N, 6.38.

3,3-Diethyl-1-*o*-tolylazetidine-2,4-dione (77j)

Prepared as described for **77a** using diethylmalonyl dichloride (15 mmol, 2956 mg) and *ortho*-toluidine (15 mmol, 1605 mg). The product was purified by chromatography on silica gel using hexane/EtOAc (8:2), and subsequently by preparative TLC, yielding the product as a colorless oil (346 mg, 6%); ν_{\max} (film) 1868 (C=O symm.), 1740 (C=O a symm.); δ ¹H-NMR 1.15 (6H, t, *J* = 7.6, (CH₂CH₃)₂), 1.90 (4H, q, *J* = 7.6, (CH₂CH₃)₂), 2.38 (3H, s, *o*-CH₃), 7.26-7.27 (2H, m, C-H), 7.30-7.32 (2H, m, C-H); δ ¹³C-NMR 9.52 (CH₂CH₃), 18.83 (*o*-CH₃), 24.11 (CH₂CH₃), 70.80 (C-3), 125.59 (C-H), 126.68 (C-H), 129.03 (C-H), 129.83 (C), 131.43 (C-H), 133.83 (C), 172.84 (C=O); EI-MS *m/z* 231 (M)⁺ 11.97 %, 133.00 (*o*-MePhNCO)⁺ (4.74%), 98.00 ((CH₃CH₂)₂C=C=O)⁺ (100.00%), 83.00 [((CH₃CH₂)₂C=C=O)-CH₃]⁺ (67.41%), 55.00 (C₃H₃O)⁺ (28.77%); Anal. calcd. for C₁₄H₁₇NO₂, C, 72.70, H, 7.41, N, 6.06; found, C, 70.69, H, 7.88, N, 5.85.

3,3-Diethyl-1-(pyridin-3-yl)azetidine-2,4-dione (77k)

Prepared as described for **77a** using diethylmalonyl dichloride (15 mmol) and 3-aminopyridine (15 mmol). Purified by column chromatography on silica gel using DCM/EtOAc (9.5:0.5), to give a light yellow solid, m.p. 38 °C (1520 mg, 47%), ν_{\max}

(film) 1869 (C=O symm.), 1743 (C=O asymm.); δ $^1\text{H-NMR}$ 1.10 (6H, t, $J = 7.6$, $(\text{CH}_2\text{CH}_3)_2$), 1.90 (4H, q, $J = 7.6$, $(\text{CH}_2\text{CH}_3)_2$), 7.38 (1H, ddd, $J = 8.4, 4.8, 0.4$, C'5- H), 8.35 (1H, ddd, $J = 8.4, 2.8, 1.6$, C- H), 8.55 (1H, dd, $J = 4.8, 1.6$, C- H), 9.16 (1H, d, $J = 2.8$, C'2- H); δ $^{13}\text{C-NMR}$ 9.22 (CH_2CH_3), 23.93 (CH_2CH_3), 72.40 (C-3), 123.84 (C- H), 126.21 (C- H), 130.83 (C), 140.77 (C- H), 147.71 (C- H), 171.73 (C=O); EI-MS m/z 218.15 (M) $^+$ (16.44%), 120.00 (PyrNCO) (11.45%), 98.00 ($(\text{CH}_3\text{CH}_2)_2\text{C}=\text{C}=\text{O}$) $^+$ 75.53%, 83.00 [$(\text{CH}_3\text{CH}_2)_2\text{C}=\text{C}=\text{O}$]- CH_3] $^+$ (67.41%), 58.00 (CH_2NCO) $^+$ (100.00%), 55.00 ($\text{C}_3\text{H}_3\text{O}$) $^+$ (42.74%); Anal. calcd. for $\text{C}_{12}\text{H}_{14}\text{N}_2\text{O}_2$, C, 66.04; H, 6.47; N, 12.84; found, C, 66.29; H, 6.53; N, 13.07.

3,3-Diethyl-1-(6-methylpyridin-3-yl)azetidine-2,4-dione (77l)

Prepared as described for **77a**, using diethylmalonyl dichloride (0.0075 mol) and 5-amino-2-methylpyridine (0.0075 mol). Purified by column chromatography on silica gel using DCM/EtOAc (9.5:0.5) and recrystallized from DCM-hexane, to give white crystals (678 mg, 39%), m.p. 44-45 °C ; ν_{max} (film) 1862 (C=O symm.), 1741 (C=O asymm.); δ $^1\text{H-NMR}$ 1.09 (6H, t, $J = 7.6$, $(\text{CH}_2\text{CH}_3)_2$), 1.89 (4H, q, $J = 7.6$, $(\text{CH}_2\text{CH}_3)_2$), 2.59 (3H, s, p - CH_3), 7.22 (1H, d, $J = 8.4$, C'5- H), 8.04 (1H, dd, $J = 8.4, 2.4$, C'6- H), 9.01 (1H, d, $J = 2.4$, C'2- H); δ $^{13}\text{C-NMR}$ 9.22 (CH_2CH_3), 23.91 (CH_2CH_3), 24.25 (p - CH_3), 72.25 (C-3), 123.34 (C), 126.74 (C- H), 129.24 (C- H), 140.13 (C- H), 156.83 (C), 171.80 (C=O); EI-MS m/z 232.09 (M) $^+$ 33.14%; 134.03 (6-MePyrNCO) $^+$ (41.21%), 98.00 ($(\text{CH}_3\text{CH}_2)_2\text{C}=\text{C}=\text{O}$) $^+$ (100.00%), 83.00 [$(\text{CH}_3\text{CH}_2)_2\text{C}=\text{C}=\text{O}$]- CH_3] $^+$ (80.34%), 55.00 ($\text{C}_3\text{H}_3\text{O}$) $^+$ (29.94%); Anal. calcd. for $\text{C}_{13}\text{H}_{16}\text{N}_2\text{O}_2$, C, 67.22; H, 6.94; N, 12.06; found, C, 66.81; H, 6.85; N, 11.71.

3,3-Diethyl-1-(naphthalen-1-yl)azetidine-2,4-dione (77m). Prepared as described for **77a**, using diethylmalonyl dichloride (15 mmol) and naphthalen-1-amine (15 mmol). Purified by column chromatography on silica gel using hexane/EtOAc (8:2), recrystallized from hexane, to yield a white solid (196 mg, 5%), m.p. 49-50 °C, ν_{max} (film) 1868 (C=O symm.), 1739 (C=O asymm.); δ $^1\text{H-NMR}$ 1.26 (6H, t, $J = 7.6$, $(\text{CH}_2\text{CH}_3)_2$), 2.00 (4H, q, $J = 7.6$, $(\text{CH}_2\text{CH}_3)_2$), 7.50-7.64 (4H, m, C- H), 7.89-7.93 (3H, m, C- H); δ $^{13}\text{C-NMR}$ 9.63 (CH_2CH_3), 24.25 (CH_2CH_3), 71.32 (C-3), 123.06 (C-

H), 123.32 (C-H), 125.21 (C-H), 126.77 (C-H), 127.17 (C), 127.20 (C-H), 127.90 (C), 128.47 (C-H), 129.43 (C-H), 134.36 (C), 173.26 (C=O); EI-MS m/z 267.15 (M)⁺ (10.41%), 169.05 (1-NaphNCO)⁺ (100.00%), 98.00 ((CH₃CH₂)₂C=C=O)⁺ (17.97%), 83.00 [((CH₃CH₂)₂C=C=O)-CH₃]⁺ (24.44%), 55.00 (C₃H₃O)⁺ (21.72%); Anal. calcd. for C₁₇H₁₇NO₂, C, 76.38; H, 6.41; N, 5.24; found, C, 76.31; H, 6.34; N, 5.23.

3-Ethyl-3-isobutyl-1-phenylazetidine-2,4-dione (77n). Prepared as described for **77a** using 2-ethyl-2-isobutylmalonyl dichloride **89a** (14 mmol) and aniline (14 mmol). The product was purified by chromatography on silica gel using hexane/EtOAc (9:1), yielding the desired product as a colorless oil (420 mg, 12%), ν_{\max} (film) 1860 (C=O symm.), 1737 (C=O asymm.); δ ¹H-NMR 1.00 (6H, d, J = 6.4, CH(CH₃)₂), 1.08 (3H, t, J = 7.6, CH₂CH₃), 1.75 (2H, d, J = 6.4, CH₂CH), 1.81-1.91 (3H, m, CH + CH₂CH₃), 7.29 (1H, dt, J = 7.6, 1.2, C-*H*_{para}), 7.44 (2H, dt, J = 7.6, 1.2, C-*H*_{meta}), 7.86 (2H, dd, J = 7.6, 1.2, C-*H*_{ortho}); δ ¹³C-NMR 9.09 (CH₂CH₃), 23.66 (CH(CH₃)₂), 25.04 (CH₂CH₃), 25.26 (CH(CH₃)₂), 39.80 (CH₂CH), 70.89 (C-3), 119.20 (C-H), 126.77 (C-H), 129.29 (C-H), 133.93 (C), 172.46 (C=O); EI-MS m/z 245.13 (M)⁺ (6.87%), 126.09 [(CH₃CH₂)((CH₃)₂CHCH₂)C=C=O]⁺ (100.00%), 119.03 (PhNCO)⁺ (6.68%), 98.00 ((CH₃CH₂)₂C=C=O)⁺ (26.52%), 83.00 [((CH₃CH₂)₂C=C=O)-CH₃]⁺ (64.45%), 55.00 (C₃H₃O)⁺ (87.73%); Anal. calcd. for C₁₅H₁₉NO₂, C, 73.44; H, 7.81; N, 5.71; found, C, 71.83; H, 7.93; N, 5.61.

3-Benzyl-3-ethyl-1-phenylazetidine-2,4-dione (77o)

Prepared as described for **77a** using 2-benzyl-2-ethylmalonyl dichloride **89b** (8.1 mmol) and aniline (8.1 mmol). The product was purified by chromatography on silica gel using hexane/EtOAc (8:2), and recrystallized from hexane, yielding white crystals (488 mg, 22%), m.p. 76-77 °C, ν_{\max} (film) 1855 (C=O symm.), 1733 (C=O asymm.); δ ¹H-NMR 1.11 (3H, t, J = 7.6, CH₂CH₃), 1.95 (2H, q, J = 7.6, CH₂CH₃), 3.10 (2H, s, CH₂Ph), 7.20-7.24 (2H, m, C-H), 7.27-7.28 (4H, m, C-H), 7.33 (2H, dt, J = 7.6, 1.2, C-H), 7.52 (2H, dd, J = 7.6, 1.2, C-H); δ ¹³C-NMR 9.33 (CH₂CH₃), 24.42 (CH₂CH₃), 37.38 (CH₂Ph), 73.37 (C-3), 119.61 (C-H), 126.90 (C-H), 127.38 (C-H), 128.57 (C-H), 129.11 (C-H), 129.63 (C-H), 132.99 (C), 134.86 (C), 171.36 (C=O); EI-MS m/z

279.04 (M)⁺ (75.54%), 160.03 [(CH₃CH₂)(CH₂Ph)C=C=O]⁺ (100.00%), 145.01 {[(CH₃CH₂)(CH₂Ph)C=C=O]-CH₃}⁺ (58.10%), 119.00 (PhNCO)⁺ (18.09%), 117.02 {[(CH₃CH₂)(CH₂Ph)C=C=O]-CO}⁺ (78.89%), 91.00 (PhCH₂)⁺ (75.73%), 77.01 (Ph)⁺ (21.86%); Anal. calcd. for C₁₈H₁₇NO₂, C, 77.40; H, 6.13; N, 5.01; found, C, 77.22; H, 6.08; N, 5.08.

3-Benzyl-3-methyl-1-phenylazetidine-2,4-dione (77p)

Prepared as described for **77a** using 2-benzyl-2-methylmalonyl dichloride **89c** (16 mmol) and aniline (16 mmol). Purified by column chromatography on silica gel using hexane/ethyl acetate (8:2), subsequently by preparative TLC and recrystallized from DCM-hexane to yield white crystals (182 mg, 5%), m.p. 54-55 °C, ν_{\max} (film) 1852 (C=O symm.), 1740 (asymm.); δ ¹H-NMR 1.57 (3H, s, CH₃), 3.10 (2H, s CH₂Ph), 7.20-7.24 (2H, m, C-H), 7.27-7.29 (4H, m, C-H), 7.33 (2H, dt, *J* = 7.6, 1.2, C-H), 7.56 (2H, dd, *J* = 7.6, 1.2, C-H); δ ¹³C-NMR 16.27 (CH₃), 38.65 (CH₂Ph), 73.03 (C-3), 119.48 (C-H), 126.92 (C-H), 127.56 (C-H), 128.60 (C-H), 129.12 (C-H), 129.56 (C-H), 134.86 (C), 136.16 (C), 171.51 (C=O); EI-MS *m/z* 265.07 (M)⁺ (81.34%), 146.19 [(CH₃)(CH₂Ph)C=C=O]⁺ (97.98%), 119.06 (PhNCO)⁺ (29.01%), 91.05 (PhCH₂)⁺ (78.17%), 77.04 (Ph)⁺ (25.17%); Anal. calcd. for C₁₇H₁₅NO₂, C, 76.96; H, 5.70; N, 5.28; found, C, 76.88; H, 5.59; N, 5.24.

3,3-Dimethyl-1-phenylazetidine-2,4-dione (77q)

Prepared as described for **77a** using dimethylmalonyl dichloride (6 mmol) and aniline (6 mmol). The addition of TEA was performed for the period of 6 h. Purified by column chromatography on silica gel using hexane/EtOAc (8:2), and subsequently by preparative TLC, recrystallized from hexane to yield white crystals (123 mg, 11%), m.p. 35 °C (lit.¹⁶⁵ m.p. 36 °C); ν_{\max} (film) 1858 (C=O symm.), 1737 (C=O asymm.); δ ¹H-NMR 1.51 (6H, s, (CH₃)₂), 7.29 (1H, dt, *J* = 7.6, 1.2, C-H_{para}), 7.34 (2H, dt, *J* = 7.6, 1.2, C-H_{meta}), 7.86 (2H, dd, *J* = 7.6, 1.2, C-H_{ortho}); δ ¹³C-NMR 17.77 (CH₃), 61.78 (C-3), 119.10 (C-H), 126.77 (C-H_{para}), 129.26 (C-H), 134.33 (C), 172.96 (C=O); EI-MS *m/z* 189.00 (M)⁺ (22.37%); 119.00 (PhNCO)⁺ (8.50%), 70.00 ((CH₃)₂C=C=O)⁺

(100.00%); Anal. calcd. for $C_{11}H_{11}NO_2$, C, 69.83; H, 5.86; N, 7.40; found, C, 70.15, H, 6.37, N, 7.75.

3-Butyl-3-ethyl-1-phenylazetidine-2,4-dione (**77r**)¹⁶⁵

A solution of triethylamine (12 mmol) in dry xylene (10 ml) was added dropwise over a period of 7 h to a solution of phenyl isocyanate (19 mmol) and 2-ethylhexanoyl chloride (10 mmol) in dry xylene (30 ml). The reaction mixture was refluxed for 11h, cooled to room temperature, filtered from triethylamine hydrochloride. The solvent was removed under reduced pressure, and the residue was purified by chromatography on silica gel, yielding the desired product as colorless oil (955 mg, 39%) (lit. m.p. 103-104 °C¹⁶⁵); ν_{\max} (film) 1861 (C=O symm.), 1741 (C=O asymm.); δ ¹H-NMR 0.92 (3H, t, $J = 8.0$, CH_2CH_3), 1.09 (3H, t, $J = 8.0$, CH_2CH_3), 1.35-1.47 (4H, m, $CH_2CH_2CH_2CH_3$), 1.79-1.83 (2H, m, $CH_2CH_2CH_2CH_3$), 1.88 (2H, q, $J = 8.0$, CH_2CH_3), 7.29 (1H, t, $J = 8.0$, C- H_{para}), 7.44 (2H, t, $J = 8.0$, C- H_{meta}), 7.87 (2H, d, $J = 8.0$, C- H_{ortho}); δ ¹³C-NMR 9.23 (CH_2CH_3), 13.79 (CH_2CH_3), 22.84 ($CH_2CH_2CH_2CH_3$), 24.34 ($CH_2CH_2CH_2CH_3$), 26.97 (CH_2), 30.60 (CH_2), 71.49 (C-3), 119.35 (C-H), 126.75 (C- H_{para}), 129.26 (C-H), 133.91 (C), 172.38 (C=O); EI-MS m/z 245.20 (M)⁺ (4.38%), 126.10 [$(CH_3CH_2)(CH_3(CH_2)_3)C=C=O$]⁺ (24.33%), 119.05 (PhNCO)⁺ (8.31%), 98.05 ($((CH_3CH_2)_2C=C=O)$)⁺ (100.00%), 83.05 [$((CH_3CH_2)_2C=C=O)-CH_3$]⁺ (24.44%), 55.00 (C₃H₅O)⁺ (21.72%); Anal. calcd. for $C_{15}H_{19}NO_2$, C, 73.44; H, 7.81; N, 5.71; found, C, 71.95 %; H, 8.33 %; N, 4.59 %.

2,2-Diethylmalonyldiglycinate (**78**, R = CH_2COOEt , R¹ = Et)¹⁵¹

Prepared from reaction of diethylmalonyl dichloride and ethyl glycinate hydrochloride, being a by-product from the synthesis of **77a**. Purified as described for **77a**, being the second fraction to be eluted (1620 mg, 20%), m.p. 108-109 (lit.¹⁵¹ 109-110 °C), ν_{\max} (film) 3464 (NH), 3329 (NH), 1743 (C=O of ester), 1664 (C=O of amide), 1645 (C=O of amide), 1388, 1245 (C-O), 1020 (C-O); δ ¹H-NMR 0.90 (6H, t, $J = 7.6$, $(CH_2CH_3)_2$), 1.30 (6H, t, $J = 7.2$, 2-O CH_2CH_3), 1.95 (4H, q, $J = 7.6$, $(CH_2CH_3)_2$), 4.06 (4H, d, $J = 5.6$, 2-NH CH_2), 4.22 (4H, q, $J = 7.2$, 2-O CH_2CH_3), 8.04 (2H, brs, 2 NH).

***N*-1,*N*-3-Dibenzhydryl-2,2-diethylmalonamide (78, R = CHPh₂, R¹ = R² = Et)**

Prepared as described for **77a**, using diethylmalonyl dichloride (15 mmol, 2956 mg), benzhydrylamine (15 mmol, 2.66 ml) and triethylamine (36 mmol, 5 ml). Purified by flash column chromatography, to afford a yellow solid (882 mg, 12%), v_{\max} (film) 3303 (NH), 3254 (NH), 1697 (C=O of amide), 1437, 1171, 1084; δ ¹H-NMR 0.83 (6H, t, $J = 7.6$, (CH₂CH₃)₂), 1.96 (4H, q, (CH₂CH₃)₂), 6.29 (2H, d, $J = 6.0$, 2 NHCHPh₂), 7.22-7.38 (20H, m, C-H), 7.90 (2H, brs, 2 NH).

Synthesis of 2,2-disubstituted malonyl dichlorides 89 from malonates 91

Dimethyl 2-ethyl-2-isobutylmalonate (91a)

Sodium hydride (60%, 17.7 mmol, 708 mg) was added very slowly under nitrogen to a solution of dimethyl 2-isobutylmalonate (16 mmol, 3.0 ml) in dry THF (50 ml) at 0 °C. The resulting mixture was then stirred at rt for 2h (hydrogen gas evolution). Then, iodoethane (17.7 mol, 1.42 ml) was added dropwise and the reaction mixture was stirred at rt for 12 h and refluxed for 1h30. The solvent was removed under reduced pressure and the residue was dissolved in diethyl ether (30 ml), washed with water (3 x 30 ml) and dried over anhydrous sodium sulfate. The solvent was removed to give the product as a yellow oil (2520 mg, 72%), used without any purification; v_{\max} (film) 1735 (br, C=O), 1457, 1438, 1232 (C-O), 1225 (C-O), 1150 (C-O), 1131 (C-O); δ ¹H-NMR 0.82 (3H, t, $J = 7.6$, CH₂CH₃), 0.88 (6H, d, $J = 6.8$, CH(CH₃)₂), 1.62 (1H, m, CH(CH₃)₂), 1.89 (2H, $J = 6.8$, CH₂CH), 1.99 (2H, $J = 7.6$, CH₂CH₃), 3.72 (6H, s, OCH₃); δ ¹³C-NMR 8.61 (CH₂CH₃), 23.65 (CH(CH₃)₂), 25.17 (CH(CH₃)₂), 25.28 (CH₂CH₃), 41.02 (CH₂CH), 53.53 (OCH₃), 56.29 (C-2), 172.46 (C=O).

Diethyl 2-benzyl-2-ethylmalonate (91b)

Sodium metal (44 mmol, 1012 mg) was added in small pieces to dry EtOH (120 ml) under a nitrogen atmosphere. When the reaction had subsided, diethyl 2-benzylmalonate (40 mmol, 9.30 ml) was added dropwise over a period of 20 min. and the mixture reacted for 30 min. at 50 °C. To the resulting solution was added dropwise iodoethane (44 mmol, 3.53 ml) and the mixture refluxed for 2h30. The mixture was

cooled to rt and the solvent was removed under reduced pressure. The residue was diluted in diethyl ether (80 ml), washed with water (3 x 80 ml) and dried over anhydrous sodium sulfate. The solvent was removed under reduced pressure to give a colorless oil (11.11 g, 58%), used without any purification; ν_{\max} (film) 1731 (br, C=O), 1451, 1425, 1275 (C-O), 1238 (C-O), 1187, 1106 (C-O), 1024 (C-O); δ $^1\text{H-NMR}$ 0.95 (3H, t, $J = 7.2$, CH_2CH_3), 1.26 (6H, t, $J = 7.2$, $2\text{-OCH}_2\text{CH}_3$), 1.85 (2H, q, $J = 7.2$, CH_2CH_3), 3.26 (2H, s, CH_2Ph), 4.20 (4H, q, $J = 7.2$, $2\text{-OCH}_2\text{CH}_3$), 7.10 (2H, d, $J = 7.2$, C-H_{ortho}), 7.23-7.28 (3H, m, C-H); δ $^{13}\text{C-NMR}$ 8.65 (CH_2CH_3), 14.10 (OCH_2CH_3), 24.73 (CH_2CH_3), 37.45 (CH_2Ph), 59.30 (C-2), 61.15 (OCH_2CH_3), 126.87 (C-H_{para}), 128.24 (C-H), 129.89 (C-H), 136.31 (C), 171.34 (C=O).

Diethyl 2-benzyl-2-methylmalonate (**91c**)¹⁷⁴

Prepared as described for **91a**, using diethyl 2-benzylmalonate (12.7 mmol, 3.0 ml), sodium hydride (60%, 14 mmol, 561 mg) and iodomethane (14 mmol, 0.87 ml), to afford the product as a yellow oil (1804 mg, 53.5%), used without any purification; ν_{\max} (film) 1732 (br, C=O), 1454, 1275 (C-O), 1241 (C-O), 1187 (C-O), 1106 (C-O); δ $^1\text{H-NMR}$ 1.28 (6H, t, $J = 7.2$, OCH_2CH_3), 1.36 (3H, s, CCH_3), 3.25 (2H, s, CH_2Ph), 4.21 (4H, q, $J = 7.2$, OCH_2CH_3), 7.13 (2H, d, $J = 7.2$, C-H_{ortho}), 7.25-7.30 (3H, m, C-H); δ $^{13}\text{C-NMR}$ 14.21 (OCH_2CH_3), 20.12 (CCH_3), 41.50 (CH_2Ph), 55.23 (C-2), 61.70 (OCH_2CH_3), 127.27 (C-H_{para}), 128.57 (C-H), 130.60 (C-H), 136.63 (C), 172.33 (C=O).

2-Ethyl-2-isobutylmalonic acid (**92a**)

91a (11.48 mmol, 2480 mg) was treated with a solution of sodium hydroxide (2 M) at rt for 6h and then the reaction mixture refluxed for 12h. The solvent was removed under reduced pressure and the residue was dissolved in water (60 ml), acidified to pH 1 (HCl conc.) and extracted with EtOAc. The organic layer was dried over anhydrous sodium sulfate. The solvent was removed under reduced pressure to yield the product as white crystals (682 mg, 32%); m.p. 117-118 °C, ν_{\max} (film) 3505-2500 (br, O-H of acid), 1705 (br, C=O), 1460, 1239 (C-O), 1025 (C-O); δ $^1\text{H-NMR}$ 0.91 (3H, t, $J = 7.2$, CH_2CH_3), 0.92 (6H, d, $J = 6.8$, $\text{CH}(\text{CH}_3)_2$), 1.69 (1H, m, $\text{CH}(\text{CH}_3)_2$),

1.98 (2H, $J = 6.8$, CH_2CH), 2.05 (2H, $J = 7.2$, CH_2CH_3), 10.41 (2H, brs); δ ^{13}C -NMR 8.62 (CH_2CH_3), 23.85 ($\text{CH}(\text{CH}_3)_2$), 25.16 ($\text{CH}(\text{CH}_3)_2$), 25.08 (CH_2CH_3), 40.92 (CH_2CH), 58.51 (C-2), 178.02 (C=O).

2-Benzyl-2-ethylmalonic acid (92b)

Prepared as described for **92a**, using **91b** (18 mmol, 5000 mg) as starting material to afford the product as white crystals (3608 g, 75%), m.p. 129-131 °C, ν_{max} (film) 3476-2500 (br, O-H of acid), 1703 (C=O), 1459, 1255 (C-O), 1207 (C-O); δ ^1H -NMR 1.03 (3H, t, $J = 7.2$, CH_2CH_3), 2.05 (2H, q, $J = 7.2$, CH_2CH_3), 3.32 (2H, s, CH_2Ph), 4.20 (4H, q, $J = 7.2$, 2- OCH_2CH_3), 7.21-7.32 (5H, m, C-H); δ ^{13}C -NMR 9.05 (CH_2CH_3), 26.99 (CH_2CH_3), 39.64 (CH_2Ph), 60.06 (C-2), 127.39 (C- H_{para}), 128.53 (C-H), 129.67 (C-H), 135.24 (C), 177.26 (C=O).

2-Benzyl-2-methylmalonic acid (92c)

Prepared as described for **92a**, using **91c** (6.17 mmol, 1632 mg) to afford the product as white crystals (558 mg, 43%), m.p. 115-118 °C, ν_{max} (film) 3480-2500 (br, O-H of acid), 1704 (C=O), 1460 (C-O-H), 1256 (C-O); δ ^1H -NMR 1.47 (3H, s, CCH_3), 3.31 (2H, s, CH_2Ph), 7.22 (2H, d, $J = 7.6$, C- H_{ortho}), 7.28-7.33 (3H, m, C-H); δ ^{13}C -NMR 19.78 (CCH_3), 41.20 (CH_2Ph), 54.94 (C-2), 127.30 (C- H_{para}), 128.43 (C-H), 130.20 (C-H), 135.32 (C), 177.22 (C=O).

2-Ethyl-2-isobutylmalonyl dichloride (89a)

2-Ethyl-2-isobutylmalonic acid (**92a**, 14.24 mmol, 3204 mg) refluxed with thionyl chloride (10 ml) under inert atmosphere. After 24h, the remaining thionyl chloride was removed under reduced pressure to afford a brown oil (3494 mg, 92%), used immediately without any purification.

2-Benzyl-2-ethylmalonyl dichloride (89b)

Prepared as described for **89a**, using **92b** (13.5 mmol, 3000mg) to afford the product as an oil (3486 mg, 83%), used immediately without any purification.

2-Benzyl-2-methylmalonyl dichloride (89c)

Prepared as described for **89a**, using **92c** (2.30 mmol, 480 mg), to afford the product as a brown oil (496 mg, 88%), used immediately without any purification.

Reaction of *p*-toluenesulfonyl isocyanate with ethylbutylketene generated *in situ* to give 2-ethyl-*N*-tosylhexanamide (97)

To a solution of *p*-toluenesulfonyl isocyanate (93 mmol, 1.42 ml), in dry THF (20 ml) at 0°C and under an atmosphere of nitrogen, 2-ethylhexanoyl chloride (4.9 mmol, 0.85 ml) was added. Then, triethylamine (0.82 ml) in THF (15 ml) was added dropwise during 5h and the mixture refluxed for 20 min.. Purified by column chromatography, using DCM/EtOAc (9.5: 0.5), to afford the product as white crystals (586 mg, 40%), m.p. 93-94 °C, ν_{\max} (film) 3232, 1702, 1344 (S=O), 1172 (S=O); δ ¹H-NMR 0.78 (3H, t, $J = 7.2$, CH₃), 0.79 (3H, t, $J = 7.2$, CH₃), 0.99-1.22 (4H, m, CH₂CH₂CH₃), 1.35 (4H, m, CHCH₂CH₃ + CHCH₂CH₂), 2.11 (1H, tt, $J = 8.8, 5.2$, CH₂CHCH₂), 2.46 (3H, s, *p*-CH₃), 7.36 (2H, d, $J = 8.4$, C-H), 7.97 (2H, d, $J = 8.4$, C-H), 9.08 (1H, brs, N-H); δ ¹³C-NMR 11.55 (CH₂CH₃), 13.82 (CH₂CH₃), 21.68 (*p*-CH₃), 22.57 (CH₂CH₂CH₃), 25.46 (CH₂), 29.28 (CH₂), 31.79 (CH₂), 49.24 (CH₂CHCH₂), 128.34 (C-H), 129.57 (C-H), 135.57 (C), 145.11 (C), 74.41 (C=O), EI-MS m/z 241.15 (M-C₄H₁₀)⁺ (2.70%), 198.23 (M-C₇H₁₆)⁺ (2.02%), 91.05 (C₇H₇)⁺ (51.44%); Anal. calcd. for C₁₅H₂₃NO₃S, C, 60.58, H, 7.79, N, 4.71; found, C, 61.02, H, 7.64, N, 4.58.

Reaction of chlorocarbonyl isocyanate with ethylbutylketene generated *in situ* - compounds 100 and 101.

***N*¹-(phenylurea)-*N*³-carbonylaniline (100)**

To a solution of chlorocarbonyl isocyanate (11.99 mmol, 0.96 ml) in dry THF (10 ml) at 0 °C under nitrogen was added 2-ethylhexanoyl chloride (9.22 mmol, 1.6 ml). Next

triethylamine (10.14 mmol, 1.41 ml) in THF (5 ml) was added dropwise during 4h. The reaction mixture was stirred for 2h30h at rt. Then, aniline (10.14 mmol, 0.93 ml) was added, followed by an additional stirring for 3h. The mixture was concentrated and cooled. An insoluble white solid was filtered-off. The solid in the filter was purified by column chromatography (gradient elution with DCM-EtOAc 9.5: 0.5 to 9.0: 1.0). On the other hand, the THF from the filtrate was removed under reduced pressure and the residue purified by column chromatography. In both purifications, the most polar fraction corresponded to **100**, obtained as white crystals (388 mg, 33%), m.p. 218-219 °C, ν_{\max} (film) 3729 (NH), 3382 (NH), 1684 (C=O), 1600, 1542; δ $^1\text{H-NMR}$ (DMSO) 7.08 (2H, t, $J = 7.2$, C- H_{para}), 7.34 (4H, t, $J = 7.2$, C- H_{meta}), 7.49 (4H, d, $J = 7.2$, C- H_{ortho}), 9.10 (1H, s, $\text{N}^2\text{-H}$), 9.72 (2H, brs, $\text{N}^1\text{-H} + \text{N}^2\text{-H}$); δ $^{13}\text{C-NMR}$ 119.23 (C-H), 123.83 (C-H), 129.43 (C-H), 138.33 (C), 152.46 (C=O); EI-MS m/z 255.10 (M) $^+$ (41.33%), 135.00 (C₇H₇N₂O) $^+$ (45.98%), 93.00 (C₆H₇N) $^+$ (100.00%); Anal. calcd. for C₁₄H₁₃N₃O₂, C, 65.87, H, 5.13, N, 16.46; found, C, 65.17, H, 5.94, N, 16.11.

2-Ethyl-N-phenylhexanamide (101)

Formed as a by-product from the reaction described above for **100**, and purified by column chromatography from the filtrate, to afford the product as white crystals (404 mg, 20%), m.p. 66-67 °C, ν_{\max} (film) 3289 (NH), 1651 (C=O), 1600, 1530, 1239; δ $^1\text{H-NMR}$ 0.90 (3H, t, $J = 7.2$, CH₂CH₃), 0.98 (3H, t, $J = 7.2$, CH₂CH₃), 1.30-1.35 (4H, m, CH₂CH₂), 1.53-1.77 (4H, m, CHCH₂CH₃ + CHCH₂), 2.11 (1H, m, CH₂CHCH₂), 7.13 (1H, t, $J = 7.6$, C- H_{para}), 7.18 (1H, brs, N-H), 7.34 (2H, t, $J = 7.6$, C- H_{meta}), 7.57 (4H, d, $J = 7.6$, C- H_{ortho}); δ $^{13}\text{C-NMR}$ 12.11 (CH₂CH₃), 13.96 (CH₂CH₃), 22.80 (CH₂CH₂CH₃), 26.23 (CH₂), 29.88 (CH₂), 32.61 (CH₂), 50.85 (CH₂CHCH₂), 119.93 (C-H), 124.21 (C-H), 128.98 (C-H), 137.93 (C), 174.44 (C=O); EI-MS m/z 219.26 (M) $^+$ (4.82%), 177.02 (M-C₄H₁₀) (8.40%), 120.05 (C₇H₆NO) $^+$ (2.50%), 93.05 (C₆H₇N) $^+$ (54.19%), 57 (C₄H₉) $^+$ (100.00%), Anal. calcd. for C₁₄H₂₁NO, C, 76.67, H, 9.65, N, 6.39; found, C, 76.10, H, 9.60, N, 5.98.

Synthesis of bromomethylarylazetidine-2,4-diones 102**1-(4-(Bromomethyl)phenyl)-3,3-diethylazetidine-2,4-dione (102a)**

A mixture of **77d** (0.346 mmol, 80.00 mg), *N*-bromosuccinimide (NBS) (0.364 mmol, 64.79 mg) and benzoyl peroxide (70%, 0.0346 mmol, 11.96 mg) in tetrachloromethane (8 ml) was heated under reflux for nearly 12h. Benzoic acid by-product was removed by filtration and the solvent removed under reduced pressure. Purified by column chromatography using hexane/EtOAc 9.5:0.5, to yield white crystals (76.2 mg, 71%), m.p. 71-72 °C, ν_{\max} (film) 1865 (C=O symm.), 1740 (C=O asymm.); δ ¹H-NMR 1.08 (6H, t, $J = 7.6$, CH₂CH₃), 1.88 (4H, q, $J = 7.6$, CH₂CH₃), 4.50 (2H, s, CH₂Ph), 7.47 (2H, dd, $J = 7.2$, 2.0, C-H), 7.86 (2H, dd, $J = 7.2$, 2.0, C-H); δ ¹³C-NMR 9.25 (CH₂CH₃), 23.98 (CH₂CH₃), 32.62 (CH₂Br), 72.35 (C-3), 119.45 (C-H), 130.01 (C-H), 133.73 (C), 136.27 (C-H), 172.06 (C=O); EI-MS m/z 310.00 (M)⁺ (3.42%); 312.00 (M+2)⁺ (3.40%); 230.15 (66.76%), 132.00 (C₇H₆NCO)⁺ (100.00%), 98.00 ((CH₃CH₂)₂C=C=O)⁺ (51.86%), 83.00 [((CH₃CH₂)₂C=C=O)-CH₃]⁺ (47.92%), 55.00 (C₃H₃O)⁺ (12.21%).

1-(2-(Bromomethyl)phenyl)-3,3-diethylazetidine-2,4-dione (102b)

Prepared as described for **102a**, using **77j** (0.282 mmol, 65.14 mg). Purification of the residue by column chromatography gave the product and recovery of remaining **77j** with the same R_f in TLC using hexane/EtOAc (8:2). Thus, the yield was determined on the basis of 400-MHz ¹H NMR of the mixture. The product **102b** (57.7 mg, 66%) was obtained as an oil, used without any further purification; ν_{\max} (film) 1869 (C=O symm.), 1740 (C=O asymm.); δ ¹H-NMR 1.19 (6H, t, $J = 7.6$, CH₂CH₃), 1.97 (4H, q, $J = 7.6$, CH₂CH₃), 4.64 (2H, s, CH₂Br), 7.35-7.44 (3H, m, C-H), 7.49 (1H, dd, $J = 7.6$, 2.0, C-H); EI-MS m/z 310.00 (M)⁺ (1.41%); 312.00 (M+2)⁺ (1.39%), 230.15 (M-Br)⁺ (4.30%), 132.00 (C₇H₆NCO)⁺ (12.45%), 98.00 ((CH₃CH₂)₂C=C=O)⁺ (100.00%), 83.00 [((CH₃CH₂)₂C=C=O)-CH₃]⁺ (60.83%), 55.00 (C₃H₃O)⁺ (13.87%).

1-(6-(Bromomethyl)pyridin-3-yl)-3,3-diethylazetidine-2,4-dione (102c)

Prepared as described for **102a**, using **771** (0.522 mmol, 121.8 mg) and purified using DCM as eluant, to yield a pink oil (58.7 mg, 36%), ν_{\max} (film) 1868 (C=O symm.), 1741 (C=O asymm.); δ $^1\text{H-NMR}$ 1.10 (6H, t, $J = 7.6$, CH_2CH_3), 1.91 (4H, q, $J = 7.6$, CH_2CH_3); 4.61 (2H, s, CH_2Br), 7.56 (1H, d, $J = 8.4$, C-H), 8.23 (1H, dd, $J = 8.4$, 2.8, C-H), 9.13 (1H, d, $J = 2.8$, C-H); δ $^{13}\text{C-NMR}$ 9.25 (CH_2CH_3), 23.96 (CH_2CH_3), 32.45 (CH_2Br), 72.66 (C-3), 128.46 (C-H), 130.10 (C), 130.95 (C-H), 141.42 (C-H), 148.94 (C), 171.43 (C=O); EI-MS m/z 311.00 (M) $^+$ (8.30%), 313.00 (M+2) $^+$ (8.27%), 231.04 (M-Br) $^+$ (51.9%), 98.00 ($(\text{CH}_3\text{CH}_2)_2\text{C}=\text{C}=\text{O}$) $^+$ (100.00%), 83.00 [$(\text{CH}_3\text{CH}_2)_2\text{C}=\text{C}=\text{O}$]- CH_3] $^+$ (63.44%), 55.00 ($\text{C}_3\text{H}_3\text{O}$) $^+$ (17.92%).

Synthesis of thiofunctionalized azetidine-2,4-diones (103a-j) from 102**1-(2-((Benzo[d]thiazol-2-ylthio)methyl)phenyl)-3,3-diethylazetidine-2,4-dione (103a)**

To a solution of **102b** (0.193 mmol, 60 mg) and 2-mercaptobenzothiazole (0.212 mmol, 35.5 mg) in dry THF (5 ml), triethylamine (0.212 mmol, 29 μl) was added. The reaction was stirred at room temperature for nearly 6h, being monitored by TLC. Upon completion, triethylamine hydrochloride was removed by filtration, the solvent removed under reduced pressure, and the residue purified first by chromatography on silica gel and subsequently by preparative TLC. Elution with DCM-hexane 7:3, yielded a white solid, m.p. 73-75 $^\circ\text{C}$ (52 mg, 68%); ν_{\max} (film) 1868 (C=O symm.), 1738 (C=O asymm.), 1456, 1371; δ $^1\text{H-NMR}$ 1.15 (6H, t, $J = 7.6$, CH_2CH_3), 1.93 (4H, q, $J = 7.6$, CH_2CH_3), 4.72 (2H, s, PhCH_2S), 7.28-7.36 (4H, m, C-H), 7.44 (1H, t, $J = 8.0$, C-H), 7.67 (1H, ddd, $J = 8.0$, 1.2, 0.4, C-H), 7.75 (1H, d, $J = 8.0$, C-H), 7.91 (1H, d, $J = 8.0$, C-H); δ $^{13}\text{C-NMR}$ 9.45 (CH_2CH_3), 23.98 (CH_2CH_3), 34.02 (PhCH_2S), 70.80 (C-3), 121.02 (C-H), 121.69 (C-H), 124.36 (C-H), 125.98 (C-H), 126.09 (C-H), 128.84 (C-H), 129.25 (C-H), 129.89 (C), 131.42 (C-H), 132.06 (C), 135.39 (C), 153.05 (C), 165.42 (SCNS), 172.87 (C=O). EI-MS m/z 396.15 (M) $^+$ (32.99%), 298.00 [M- $(\text{CH}_3\text{CH}_2)_2\text{C}=\text{C}=\text{O}$] $^+$ (30.36%), 132.00 ($\text{C}_7\text{H}_6\text{NCO}$) $^+$ (100.00%), 98.00 ($(\text{CH}_3\text{CH}_2)_2\text{C}=\text{C}=\text{O}$) $^+$ (8.82%), 83.00 [$(\text{CH}_3\text{CH}_2)_2\text{C}=\text{C}=\text{O}$]- CH_3] $^+$ (23.27%), 55.00

(C₃H₃O)⁺ (25.55%); Anal. calcd. for C₂₁H₂₀N₂O₂S₂, C, 63.61, H, 5.08, N, 7.06; found, C, 61.43, H, 5.87, N, 6.90.

1-(2-((Benzo[d]oxazol-2-ylthio)methyl)phenyl)-3,3-diethylazetidine-2,4-dione (103b)

Prepared from **102b** (0.284 mmol, 88 mg) and 2-mercaptobenzoxazole (0.314 mmol, 47.18 mg), as described for **103a**, and purified similarly and using the same eluent, to give a white solid (103 mg, 95%), m.p. 63-66 °C, ν_{\max} (film) 1868 (C=O symm.), 1740 (C=O asymm.), 1498; δ ¹H-NMR 1.17 (6H, t, $J = 7.6$, CH₂CH₃), 1.95 (4H, q, $J = 7.6$, CH₂CH₃), 4.66 (2H, s, PhCH₂S), 7.28 (1H, dt, $J = 7.6$, 1.2, C-H), 7.30 (1H, dt, $J = 7.6$, 1.2, C-H), 7.33-7.38 (3H, m, C-H), 7.43 (1H, ddd, $J = 7.6$, 1.2, 0.4, C-H), 7.62 (1H, ddd, $J = 7.6$, 1.2, 0.4, C-H); 7.68-7.71 (1H, m, C-H); δ ¹³C-NMR 9.42 (CH₂CH₃), 23.94 (CH₂CH₃), 32.92 (PhCH₂S), 70.79 (C-3), 109.92 (C-H), 118.62 (C-H), 123.98 (C-H), 124.34 (C-H), 125.88 (C-H), 128.98 (C-H), 129.24 (C-H), 129.88 (C), 131.46 (C-H), 131.83 (C), 141.83 (C), 151.98 (C), 163.74 (OCNS), 172.85 (C=O); EI-MS m/z 380.15 (M)⁺ (29.76%); 230.15 (M-SAr)⁺ (7.15%), 132.00 (C₇H₆NCO)⁺ (100.00%), 98.00 ((CH₃CH₂)₂C=C=O)⁺ (8.53%), 83.00 [((CH₃CH₂)₂C=C=O)-CH₃]⁺ (19.72%), 55.00 (C₃H₃O)⁺ (22.36%); Anal. calcd. for C₂₁H₂₀N₂O₃S, C, 66.29, H, 5.30, N, 7.36, S, 8.43; found, C, 66.54, H, 5.35, N, 7.26, S, 8.45.

1-(2-((5-Phenyl-1,3,4-oxadiazol-2-ylthio)methyl)phenyl)-3,3-diethylazetidine-2,4-dione (103c)

Prepared as described for **103a**, using **102b** (0.177 mmol, 54.8 mg) and 5-phenyl-1,3,4-oxadiazole-2-thiol (0.194 mmol, 34.6 mg), and purified similarly using DCM-hexane 8:2 as eluant, to yield white crystals (63 mg, 87%), m.p. 110-112 °C, ν_{\max} (film) 1857 (C=O symm.), 1740 (C=O asymm.), 1467, 1371; δ ¹H-NMR 1.18 (6H, t, $J = 7.6$, CH₂CH₃), 1.95 (4H, q, $J = 7.6$, CH₂CH₃), 4.67 (2H, s, PhCH₂S), 7.35-7.40 (3H, m, C-H), 7.48-7.56 (3H, m, C-H), 7.71 (1H, dd, $J = 6.0$, 2.0, C-H), 7.99 (2H, dd, $J = 8.0$, 1.6, C-H); δ ¹³C-NMR 9.47 (CH₂CH₃), 23.99 (CH₂CH₃), 33.57 (PhCH₂S), 70.83 (C-3), 123.50 (C), 125.96 (C-H), 126.69 (C-H), 129.05 (C-H), 129.24 (C-H),

129.27 (C-H), 129.96 (C), 131.18 (C), 131.73 (C-H), 131.83 (C-H), 163.35 (NCO), 166.03 (NCO), 172.74 (C=O); EI-MS m/z 407.20 (M)⁺ (11.73%), 230.05 (M-SAr)⁺ (15.70%), 132.00 (C₇H₆NCO)⁺ (100.00%), 98.00 ((CH₃CH₂)₂C=C=O)⁺ (16.95%), 83.00 [((CH₃CH₂)₂C=C=O)-CH₃]⁺ (34.22%), 77.00 (Ph)⁺ (51.84%), 55.00 (C₃H₃O)⁺ (30.05%); Anal. calcd. for C₂₂H₂₁N₃O₃S, C, 64.85, H, 5.19, N, 10.31, S, 7.87; found, C, 63.62, H, 5.29, N, 9.71, S, 7.48.

1-(2-((1-Methyl-1H-imidazol-2-ylthio)methyl)phenyl)-3,3-diethylazetidine-2,4-dione (103d)

Prepared from **102b** (0.169 mmol, 52.4 mg) and 1-methyl-1H-imidazole-2-thiol (0.186 mmol, 21.2 mg) as described for **103a**, and purified similarly using EtOAc-acetone 9:1 as eluant, to yield a pale yellow solid (40.9 mg, 70%), m.p. 61-63 °C, ν_{\max} (film) 1874 (C=O symm.), 1738 (C=O asymm.), 1456, 1373; δ ¹H-NMR 1.17 (6H, t, $J = 7.6$, CH₂CH₃), 1.94 (4H, q, $J = 7.6$, CH₂CH₃), 3.11 (3H, s, N-CH₃), 4.22 (2H, s, PhCH₂S), 6.80 (1H, s, C-H), 6.93 (1H, d, $J = 7.6$, C-H), 7.10 (1H, s, C-H), 7.15 (1H, dt, $J = 7.6$, 1.6, C-H), 7.25-7.32 (2H, m, C-H); δ ¹³C-NMR 9.50 (CH₂CH₃), 23.95 (CH₂CH₃), 33.19 (N-CH₃), 37.31 (PhCH₂S), 70.68 (C-3), 122.77 (C-H), 126.32 (C-H), 128.60 (C-H), 128.96 (C-H), 129.32 (C-H), 129.42 (C), 130.90 (C-H), 133.82 (C), 139.92 (NCNS), 172.89 (C=O); EI-MS m/z 343.00 (M)⁺ (14.24%), 230.05 (M-SAr)⁺ (9.11%), 132.00 (C₇H₆N=C=O)⁺ (100.00%), 98.00 ((CH₃CH₂)₂C=C=O)⁺ (11.05%), 83.00 [((CH₃CH₂)₂C=C=O)-CH₃]⁺ (18.10%), 55.00 (C₃H₃O)⁺ (24.05%); Anal. calcd. for C₁₈H₂₁N₃O₂S, C, 62.95, H, 6.16, N, 12.23, S, 9.34; found, C, 62.82, H, 6.98, N, 11.76, S, 8.87.

1-(4-((Benzo[d]thiazol-2-ylthio)methyl)phenyl)-3,3-diethylazetidine-2,4-dione (103e)

Prepared from **102a** (0.097 mmol, 30 mg) and 2-mercaptobenzothiazole (0.106 mmol, 17.8 mg), as described for **103a** and purified similarly using DCM-hexane 7:3 as eluant, to yield a white solid (28 mg, 73%), m.p. 102-104 °C, ν_{\max} (film) 1861 (C=O symm.), 1737 (C=O asymm.), 1514, 1457; δ ¹H-NMR 1.07 (6H, t, $J = 7.6$, CH₂CH₃), 1.86 (4H, q, $J = 7.6$, CH₂CH₃), 4.60 (2H, s, PhCH₂S), 7.32 (1H, dt, $J = 7.6$, 1.2, C-H),

7.45 (1H, dt, $J = 7.6, 1.2$, C-H), 7.53 (2H, d, $J = 8.4$, C-H), 7.76 (1H, dd, $J = 7.6, 0.4$, C-H), 7.83 (2H, d, $J = 8.4$, C-H), 7.92 (1H, dd, $J = 7.6, 0.4$, C-H); δ ^{13}C -NMR 9.25 (CH₂CH₃), 23.96 (CH₂CH₃), 37.07 (PhCH₂S), 72.25 (C-3), 119.37 (C-H), 121.06 (C-H), 121.60 (C-H), 124.41 (C-H), 126.13 (C-H), 130.06 (C-H), 133.22 (C), 135.08 (C), 135.36 (C), 153.06 (C), 165.77 (SCNS), 172.10 (C=O); EI-MS m/z 396.10 (M)⁺ (16.55%); 298.00 ([M-((CH₃CH₂)₂C=C=O)]⁺ (7.91%), 132.00 (C₇H₆NCO)⁺ (100.00%), 83.00 [((CH₃CH₂)₂C=C=O)-CH₃]⁺ (6.57%), 55.00 (C₃H₃O)⁺ (6.48%); Anal. calcd. for C₂₁H₂₀N₂O₂S₂, C, 63.61, H, 5.08, N, 7.06, S, 16.17; found C, 62.11, H, 5.28, N, 6.91, S, 16.03.

1-(4-((Benzo[d]oxazol-2-ylthio)methyl)phenyl)-3,3-diethylazetidine-2,4-dione (103f)

Prepared from **102a** (0.145 mmol, 45.0 mg) and 2-mercaptobenzoxazole (0.160 mmol, 24.2 mg) as described for **103a**, and purified similarly using DCM-hexane 7:3 as eluant, to yield white crystals (32.4 mg, 59%), m.p. 96-98 °C, ν_{max} (film) 1857 (C=O symm.), 1738 (C=O asymm.), 1506, 1453; δ ^1H -NMR 1.07 (6H, t, $J = 7.6$, CH₂CH₃), 1.86 (4H, q, $J = 7.6$, CH₂CH₃), 4.57 (2H, s, PhCH₂S), 7.28 (1H, dt, $J = 7.6, 1.2$, C-H), 7.32 (1H, dt, $J = 7.6, 1.2$, C-H), 7.47 (1H, d, $J = 7.6$, C-H), 7.55 (2H, d, $J = 8.4$, C-H), 7.65 (1H, d, $J = 7.6$, C-H), 7.84 (2H, d, $J = 8.4$, C-H); δ ^{13}C -NMR 9.25 (CH₂CH₃), 23.97 (CH₂CH₃), 36.02 (PhCH₂S), 72.30 (C-3), 109.98 (C-H), 118.50 (C-H), 119.42 (C-H), 124.12 (C-H), 124.44 (C-H), 130.03 (C-H), 133.40 (C), 134.63 (C), 141.83 (C), 151.93 (C), 164.05 (OCNS), 172.09; EI-MS m/z 380.01 (M)⁺ (57.89%), 230.05 (M-SAr)⁺ (57.97%), 131.99 (C₇H₆NCO)⁺ (100.00%), 98.03 ((CH₃CH₂)₂C=C=O)⁺ (11.05%), 83.02 [((CH₃CH₂)₂C=C=O)-CH₃]⁺ (10.24%), 55.00 (C₃H₃O)⁺ (10.96%); Anal. calcd. for C₂₁H₂₀N₂O₃S, C, 66.29, H, 5.30, N, 7.36, S, 8.43; found, C, 65.98, H, 4.88, N, 7.23, S, 8.13.

2-(((4-(3,3-Diethyl-2,4-dioxoazetidin-1-yl)benzyl)sulfanyl)benzo[d]oxazole-5-carboxylic acid (103g)

Prepared from **102a** (0.225 mmol, 69.7 mg), 2-mercaptobenzoxazole-5-carboxylic acid, **51**, (0.247 mmol, 48.5 mg) and triethylamine (0.472 mmol, 66 μl), as described

for **103a**. The reaction mixture was acidified with HCl until pH 2 and extracted with EtOAc. After drying and evaporating off the solvent, the residue was purified by column chromatography on silica gel, and subsequently by preparative TLC (elution with EtOAc), to yield a yellow solid (22.4 mg, 24%), m.p. 166-171 °C, ν_{\max} (film) 4000-2500 (br, O-H of acid), 1855 (C=O symm.), 1733 (C=O asymm.), 1683 (C=O of acid); δ $^1\text{H-NMR}$ (DMSO) 1.07 (6H, t, $J = 7.6$, CH_2CH_3), 1.87 (4H, q, $J = 7.6$, CH_2CH_3), 4.65 (2H, s, PhCH_2S), 7.52 (1H, d, $J = 8.8$, C-H), 7.56 (2H, d, $J = 8.4$, C-H), 7.86 (2H, d, $J = 8.4$, C-H), 8.11 (1H, d, $J = 8.8$, C-H), 8.41 (1H, s, NCC-H); δ $^{13}\text{C-NMR}$ (DMSO) 9.25 (CH_2CH_3), 23.97 (CH_2CH_3), 36.12 (PhCH_2S), 72.32 (C-3), 109.88 (C-H), 119.47 (C-H), 121.05 (C-H), 126.78 (C-H), 130.09 (C-H), 133.48 (C), 134.35 (C), 135.76 (C), 142.02 (C), 151.52 (C), 166.02 (C), 169.87 (C=O of acid), 172.09 (C=O of imide); EI-MS m/z 424.20 (M^+) (1.37%), 230.15 (M-SAr^+) (12.29%), 132.05 ($\text{C}_7\text{H}_6\text{NCO}^+$) (100.00%), 98.05 ($(\text{CH}_3\text{CH}_2)_2\text{C}=\text{C}=\text{O}^+$) (6.86%), 83.05 [$(\text{CH}_3\text{CH}_2)_2\text{C}=\text{C}=\text{O}-\text{CH}_3^+$] (14.26%), 55.05 ($\text{C}_3\text{H}_3\text{O}^+$) (12.63%); Anal. calcd. for $\text{C}_{22}\text{H}_{20}\text{N}_2\text{O}_5\text{S}$, C, 62.25, H, 4.75, N, 6.60, S, 7.55; found, C, 61.87, H, 4.66, N, 6.30, S, 7.21.

1-(4-((5-Phenyl-1,3,4-oxadiazol-2-ylthio)methyl)phenyl)-3,3-diethylazetidine-2,4-dione (**103h**)

Prepared from **102a** (0.290 mmol, 90.0 mg) and 5-phenyl-1,3,4-oxadiazole-2-thiol (0.319 mmol, 56.9 mg), as described for **103a**, and purified similarly using DCM-hexane 9:1, to yield white crystals (83.5 mg, 71%), m.p. 120-122 °, ν_{\max} (film) 1855 (C=O symm.), 1735 (C=O asymm.), 1512; δ $^1\text{H-NMR}$ 1.07 (6H, t, $J = 7.6$, CH_2CH_3), 1.87 (4H, q, $J = 7.6$, CH_2CH_3), 4.53 (2H, s, PhCH_2S), 7.49-7.54 (3H, m, C-H), 7.55 (2H, d, $J = 8.4$, C-H), 7.85 (2H, d, $J = 8.4$, C-H), 8.01 (2H, dd, $J = 8.4$, 1.6, C-H); δ $^{13}\text{C-NMR}$ 9.22 (CH_2CH_3), 23.97 (CH_2CH_3), 36.27 (PhCH_2S), 72.29 (C-3), 119.49 (C-H), 123.53 (C-H), 126.68 (C-H), 129.06 (C-H), 130.10 (C-H), 131.74 (C-H), 133.34 (C), 134.30 (C), 147.38 (C), 163.50 (NCOS), 172.07 (C=O), EI-MS m/z 407.08 (M^+) (39.01%), 230.08 (M-SAr^+) (61.96%), 132.02 ($\text{C}_7\text{H}_6\text{NCO}^+$) (100.00%), 98.05 ($(\text{CH}_3\text{CH}_2)_2\text{C}=\text{C}=\text{O}^+$) (15.20%), 83.03 [$(\text{CH}_3\text{CH}_2)_2\text{C}=\text{C}=\text{O}-\text{CH}_3^+$] (20.42%), 55.07 ($\text{C}_3\text{H}_3\text{O}^+$) (18.60%); Anal. calcd. for $\text{C}_{22}\text{H}_{21}\text{N}_3\text{O}_3\text{S}$, C, 64.85; H, 5.19; N, 10.31; S, 7.87; found, C, 64.66; H, 5.17; N, 10.41; S, 7.91.

1-(6-((Benzo[d]thiazol-2-ylthio)methyl)pyridin-3-yl)-3,3-diethylazetidione-2,4-dione (103i)

Prepared from **102c** (0.151 mmol, 47.1 mg) and 2-mercaptobenzothiazole (0.166 mmol, 27.8 mg), as described for **103a**, and purified similarly using DCM as eluant, to yield a white solid (36.6 mg, 61%); m.p. 129-131 °C; ν_{\max} (film) 1868 (C=O symm.), 1741 (C=O asymm.), 1489; δ $^1\text{H-NMR}$ 1.08 (6H, t, $J = 7.6$, CH_2CH_3), 1.88 (4H, q, $J = 7.6$, CH_2CH_3), 4.76 (2H, s, ArCH_2S), 7.33 (1H, dt, $J = 8.4$, 1.6, C-H), 7.44 (1H, dt, $J = 8.4$, 1.6, C-H), 7.66 (1H, d, $J = 8.4$, C-H), 7.77 (1H, dd, $J = 8.4$, 0.4, C-H), 7.91 (1H, d, $J = 8.4$, C-H), 8.12 (1H, dd, $J = 8.4$, 2.4, C-H), 9.11 (1H, d, $J = 2.4$ NCCHN); δ $^{13}\text{C-NMR}$ 9.23 (CH_2CH_3), 23.94 (CH_2CH_3), 38.60 (ArCH_2S), 72.46 (C-3), 121.09 (C-H), 121.56 (C), 123.85 (C-H), 124.42 (C-H), 126.12 (C-H), 126.87 (C-H), 129.72 (C-H), 135.4 (C-H), 140.36 (C), 152.99 (C), 154.85 (C), 165.69 (NCSS), 171.61 (C=O); EI-MS m/z 396.97 (M) $^+$ (62.79%), 298.92 [$\text{M}-((\text{CH}_3\text{CH}_2)_2\text{C}=\text{C}=\text{O})$] $^+$ (100.00%), 166.93 (2-mercapto-benzothiazol) $^+$, 132.99 (93.27%), 98.05 ($((\text{CH}_3\text{CH}_2)_2\text{C}=\text{C}=\text{O})$) $^+$ (11.79%), 83.02 [$((\text{CH}_3\text{CH}_2)_2\text{C}=\text{C}=\text{O})-\text{CH}_3$] $^+$ (23.22%), 55.06 ($\text{C}_3\text{H}_3\text{O}$) $^+$ (29.59%); Anal. calcd. for $\text{C}_{20}\text{H}_{19}\text{N}_3\text{O}_2\text{S}_2$, C, 60.43, H, 4.82, N, 10.57, S, 16.13; found C, 60.01, H, 5.03, N, 10.22.

3,3-Diethyl-1-(4-((phenylthio)methyl)phenyl)azetidione-2,4-dione (103j)

Prepared as described above for **103a**, by reaction of **102a** (0.229 mmol, 71.1 mg) with thiophenol (0.252 mmol, 26 μl), and purified using DCM-hexane 7:3 as eluant, to yield a colorless oil (61.4 mg, 79%), ν_{\max} (film) 1849 (C=O symm.), 1736 (C=O asymm.); δ $^1\text{H-NMR}$ 1.08 (6H, t, $J = 7.6$, CH_2CH_3), 1.86 (4H, q, $J = 7.6$, CH_2CH_3); 4.12 (2H, s, PhCH_2S), 7.20-7.31 (5H, m, C-H); 7.34 (2H, d, $J = 8.4$, C-H), 7.77 (2H, d, $J = 8.4$, C-H); δ $^{13}\text{C-NMR}$ 9.26 (CH_2CH_3), 23.95 (CH_2CH_3), 38.71 (ArCH_2S), 72.15 (C-3), 119.24 (C-H), 126.65 (C-H), 128.95 (C-H), 129.61 (C-H), 130.13 (C-H), 132.76 (C), 135.72 (C), 136.28 (C), 172.17 (C=O); EI-MS m/z 339.20 (M) $^+$ (2.37%), 230.15 (M-SPh) $^+$ (20.70%), 132.05 ($\text{C}_7\text{H}_6\text{NCO}$) $^+$ (100.00%), 98.05 ($((\text{CH}_3\text{CH}_2)_2\text{C}=\text{C}=\text{O})$) $^+$ (1.92%), 83.05 [$((\text{CH}_3\text{CH}_2)_2\text{C}=\text{C}=\text{O})-\text{CH}_3$] $^+$ (4.45%), 77.05 (Ph) $^+$ (5.65%), 55.00 ($\text{C}_3\text{H}_3\text{O}$) $^+$ (3.45%); Anal. calcd. for $\text{C}_{20}\text{H}_{21}\text{NO}_2\text{S}$, C, 70.77; H, 6.24; N, 4.13; S, 9.45; found, C, 69.66, H, 5.83; N, 3.86; S, 8.82.

Oxidation of 103j with 3-chloroperbenzoic acid to give 3,3-Diethyl-1-(4-((phenylsulfonyl)methyl)phenyl)azetidine-2,4-dione (103k)

3-Chloroperbenzoic acid (MCPBA, 0.382 mmol) was gently added to a cold solution of the thioether **103j** (0.153 mmol, 51.9 mg) in DCM (10 ml). The reaction mixture was warmed to room temperature and monitored by TLC. After completion of the reaction (after nearly 40 min.), the solvent was removed under reduced pressure and the product purified by column chromatography, and recrystallized from DCM-hexane, to yield a white solid (47.4 mg, 83%), m.p. 143-145, ν_{\max} (film) 1856 (C=O symm.), 1737 (C=O asymm.), 1315 (S=O), 1153 (S=O); δ $^1\text{H-NMR}$ 1.08 (6H, t, $J = 7.6$, CH_2CH_3), 1.88 (4H, q, $J = 7.6$, CH_2CH_3), 4.32 (2H, s, PhCH_2S), 7.16 (2H, d, $J = 8.0$, C-H), 7.52 (2H, t, $J = 8.0$, C-H), 7.66 (1H, t, $J = 8.0$, C-H), 7.71 (2H, dd, $J = 8.0$, 1.6, C-H), 7.79 (2H, d, $J = 8.0$, C-H); δ $^{13}\text{C-NMR}$ 9.24 (CH_2CH_3), 23.91 (CH_2CH_3), 62.33 (ArCH_2S), 72.31 (C-3), 119.13 (C-H), 126.43 (C), 128.60 (C-H), 129.11 (C-H), 131.76 (C-H), 133.97 (C-H), 134.23 (C), 137.79 (C), 172.04 (C=O); EI-MS 230.15 ($\text{M-SO}_2\text{Ar}$) $^+$ (22.19%), 132.05 ($\text{C}_7\text{H}_6\text{NCO}$) $^+$ (100.00%), 98.05 ($(\text{CH}_3\text{CH}_2)_2\text{C}=\text{C}=\text{O}$) $^+$ (4.96%), 83.05 [$(\text{CH}_3\text{CH}_2)_2\text{C}=\text{C}=\text{O}-\text{CH}_3$] $^+$ (12.02%), 77.05 (Ph) $^+$ (30.42%), 55.00 ($\text{C}_3\text{H}_3\text{O}$) $^+$ (12.21%); Anal. calcd. for $\text{C}_{20}\text{H}_{21}\text{NO}_4\text{S}$, C, 64.67; H, 5.70; N, 3.77; S, 8.63; found C, 64.43; H, 5.94; N, 3.56; S, 8.31.

Product of the hydrolysis of 4-oxo- β -lactam 104

To a solution of **103a** (0.2 mmol, 79.3 mg) in a mixture of water / THF (1:1, 4 ml) was added 1 ml of a 1M NaOH solution. When all substrate was consumed, the solvent was evaporated under reduced pressure, the residue suspended in a solution of 5% HCl and extracted with ethyl acetate (25 ml). After drying with anhydrous Na_2SO_4 , the solvent was evaporated and the residue was purified by column chromatography (elution with EtOAc) to yield 45 mg (54%) of the hydrolysis product **104** as an oil. δ $^1\text{H-NMR}$ ($\text{D}_2\text{O}/\text{DMSO}$) 0.94 (6H, t, $J = 7.4$, CH_2CH_3), 1.82 (4H, q, $J = 7.4$, CH_2CH_3), 4.58 (2H, s, PhCH_2S), 7.09-7.57 (5H, m, C-H), 7.85 (1H, d, $J = 8.2$, C-H), 7.94 (1H, d, $J = 8.1$, C-H), 7.98 (1H, d, $J = 8.2$, C-H).

6.2. ALKALINE HDROLYSIS STUDIES (CHEMICAL KINETICS)

All kinetic measurements were carried out at 25.0 ± 0.1 °C and with an ionic strength adjusted to 0.5 M by addition of NaClO₄. Due to substrate solubility problems all buffers contained 20% (v/v) acetonitrile. Rate constants were determined using UV spectrophotometry by recording the decrease of substrate absorbance at fixed wavelength (**47b**, 250; **47e**, 224; **47f**, 238; **77b and 77h**, 221; **77c**, 247, **77d**, **77f** and **77i** 260; **77e**, 255; **77g**, 280 nm), using a spectrophotometer equipped with a temperature controller. In a typical run, reaction was initiated by adding a 15 µl aliquot of a 10⁻² M stock solution of **47** in acetonitrile to a cuvette containing 3 ml of the buffer solution. The pseudo-first-order rate constants, k_{obs} , were obtained by least-squares treatment of $\log(A_t - A_\infty)$ data, where A_t and A_∞ represent the absorbance at time t and at time infinity, respectively. Rate constants derived using this method were reproducible to $\pm 5\%$.

6.3. ENZYME INHIBITION STUDIES

6.3.1 PPE Inhibition Studies

6.3.1.1 PPE Inactivation by the Incubation Method

Inhibition of PPE was assayed by Kitz and Wilson's incubation method.¹³⁶ In a typical experiment, 50 µl of inhibitor solution in DMSO was incubated at 25 °C with 750 µl of 0.1 M HEPES buffer, pH 7.2, and 200 µl of PPE solution (50 µM in 0.1 M HEPES buffer, pH 7.2). Aliquots (100 µl) were withdrawn at different time intervals and transferred to a cuvette thermostatted at 25 °C, containing 895 µl of 0.1 M HEPES buffer, pH 7.2, and 5 µl of *N*-Suc-Ala-Ala-Ala-*p*NA (12.5 mM in DMSO). The absorbance was monitored at 390 nm for 50 seconds and the gradients of the slopes obtained of initial rate used as a measure of enzyme activity. The values of k_{obs} for all compounds tested were determined in duplicates or triplicates from exponential regression-type analysis from plots of v_t/v_i versus incubation time, where v_t is the

initial rate at time t and v_i is the initial rate of the control incubation without inhibitor. Accordingly, Equation 2.3 (Section 2.3.1.3) was used. The plots of k_{obs} versus $[I]$ were linear and the inhibitory potency was determined in terms of the bimolecular rate constant $k_{\text{obs}}/[I] = k_{\text{inact}}/K_i$ (Equation 2.5, Section 2.3.1.3).

6.3.1.2 PPE Inactivation by the Progress Curve Method

PPE inhibition was analyzed by the progress curve method.¹⁴² The enzymatic reactions were initiated by addition of 10 μl of PPE (20 μM in HEPES buffer, 0.1 M, pH 7.2) to a cuvette thermostated at 25 $^{\circ}\text{C}$, containing 940 μl of HEPES buffer (0.1 M, pH 7.2), 20 μl of DMSO, 20 μl of substrate (15 mM in DMSO) and 10 μl of inhibitor (in DMSO). The absorbance was continuously monitored at 390 nm for 20 minutes. The final concentrations were: $[\text{PPE}] = 200 \text{ nM}$, $[\text{substrate}] = 0.3 \text{ mM}$ and $[\text{DMSO}] = 5\% \text{ (v/v)}$. Several inhibitor concentrations from 8 to 150 μM were used. Control assays, in which the inhibitor was omitted, ran linearly. The pseudo-first order rate constants, k_{obs} , for the inhibition of PPE were determined according to the slow binding inhibition model¹⁴² (mechanism A of Figure 2.28, Section 2.3.2.2) and involved the fitting of product concentration as a function of time to Equation 2.6 by non-linear regression analysis using the routine ENZFIT (a Microsoft ExcelTM workbook with in-house developed Visual Basic for Applications (VBA) procedures developed at the Faculty of Pharmacy, Lisbon). The inhibitory potency, given by k_{on} , was determined using Equations 2.7 and 2.8 and K_i was determined using Equation 2.9.

6.3.1.3 Titration of PPE (Partition Ratio)

PPE solutions (200 μl of 50 μM in 0.1 M HEPES buffer, pH 7.2) were incubated at 25 $^{\circ}\text{C}$ with different concentrations of inhibitor solutions in 0.1 M HEPES buffer, pH 7.2, in a final volume of 1 ml. After 30 min incubation, a 100 μl aliquot of the reaction mixture was withdrawn and assayed for remaining enzyme activity as described previously in Section 6.3.1.1. The partition ratio was determined from the intercept to

the x axis of the linear plot of the remaining activity ($[E]_t/[E]_0$), expressed as v_t/v_i , versus the initial ratio of inhibitor to enzyme ($[I]/[E]_0$).

6.3.2 HLE Inhibition Studies

6.3.3 HLE Inactivation by the Progress Curve Method

Inactivation of HLE was studied at 25 °C by mixing 10 μ l of HLE stock solution (2 μ M in 0.05 M acetate buffer, pH 5.5) to a solution containing 10 μ l of inhibitor in DMSO, 20 μ l of substrate MeOSuc-Ala-Ala-Pro-Val-*p*-nitroanilide (50 mM in DMSO) and 960 μ l of 0.1 M HEPES buffer pH 7.2, and the absorbance was continuously monitored at 410 nm for 20 minutes. Control assays in which the inhibitor was omitted, ran linearly. Depending on the ratio inhibitor to enzyme, progress curves were fitted to Equation 2.6 or 4.1. The k_{obs} values, calculated from the progress curves, were fitted against the inhibitor concentration, accordingly to the slow association (linear) or the isomerization (hyperbolic) mechanisms (respectively, mechanisms A or B of Figure 2.28). k_{on} , K_i and k_{off} values were determined using the appropriate equations given in Section 2.3.2.2.

6.3.4 HLE Inactivation by the Incubation Method

HLE inactivation was performed using the incubation method to evaluate the stability of the acyl-enzyme complex of compounds **103a** and **103e**. Thus, 10 μ l of inhibitor (0.1 mM in DMSO) were incubated with 980 μ l of HEPES buffer (0.1 M; pH 7.2) and 10 μ l of HLE stock solution (20 μ M in 0.05 M acetate buffer, pH 5.5) at 25 °C. Aliquots (100 μ l) were withdrawn at different time intervals and transferred to a cuvette thermostated at 25 °C, containing 880 μ l of 0.1 M HEPES buffer pH 7.2 and 20 μ l of substrate MeOSuc-Ala-Ala-Pro-Val-*p*-NA (50 mM in DMSO). The absorbance was monitored at 410 nm for 50 seconds. The amount of enzyme activity v_t/v_i was determined by the ratio of the activity of an enzyme solution containing

inhibitor by the activity of a control assay (containing no inhibitor) at the same time point.

6.3.4.1 Titration of HLE (Partition Ratio)

10 μl of HLE stock solutions (20 μM in 0.05 M acetate buffer, pH 5.5) were incubated at 25 $^{\circ}\text{C}$ with different concentrations of inhibitor **77g** in DMSO (10 μl) and 980 μl of 0.1 M HEPES buffer, pH 7.2. After incubating the reaction mixture for 30 minutes, a 100 μl aliquot was withdrawn and assayed for remaining enzyme activity, as described previously (Section 6.3.4). The partition ratio was determined from the intercept to the x axis of the linear plot of the remaining activity ($[\text{E}]_t/[\text{E}]_0$), *versus* the initial ratio of inhibitor to enzyme ($[\text{I}]/[\text{E}]_0$).

6.3.5 Inhibition Assay for Cathepsin G

Inactivation of cathepsin G was studied at 25 $^{\circ}\text{C}$ using the progress curve method,¹⁴² by mixing 100 μl of enzyme stock solution (680 nM in 0.05 M acetate buffer, pH 5.5) to a solution containing 10 μl of inhibitor in DMSO, 20 μl of substrate Suc-Ala-Ala-Pro-Phe-*p*-nitroanilide (42.5 mM in DMSO) and 870 μl of 0.1 M HEPES buffer pH 7.5, and the absorbance was continuously monitored at 410 nm for 20 minutes. Control assays, in which the inhibitor was omitted, ran linearly. Data were treated as described above, involving the fitting of product concentration as a function of time to Equation 2.6 (Section 2.3.2.2) by non-linear regression analysis, to afford k_{obs} . The inhibitory potency was given as the ratio $k_{\text{obs}}/[\text{I}]$.

6.3.6 Inhibition Assay for Proteinase 3

Inactivation of proteinase 3 was studied at 25 $^{\circ}\text{C}$ by mixing 70 μl of enzyme stock solution (325 nM in 0.05 M pH 6 acetate buffer, 150 mM NaCl) to a solution containing 10 μl of inhibitor in DMSO, 75 μl of substrate MeOSuc-Ala-Ala-Pro-Val-*p*-nitroanilide (50 mM in DMSO) and 835 μl of 0.1 M pH 7.2 HEPES buffer, and the absorbance was continuously monitored at 410 nm for 10000 seconds. Control assays,

in which the inhibitor was omitted, ran linearly. Progress curves data were treated as described above (Section 6.3.5).

6.3.7 Inhibition Assay for Papain

Papain (1mg/ml) was activated as described¹⁷⁵ and the activated enzyme (300 μ l) was studied using the incubation method, at 25 °C, by incubation with 50 μ l of the inhibitor in 650 μ l of 50 mM pH 7.0 K₂HPO₄/KH₂PO₄ buffer, containing 2.5 mM EDTA. At different times, aliquots (100 μ l) were withdrawn and transferred to a cuvette thermostated at 25 °C, containing 100 μ l of benzoyl-*S*-arginine-*p*-nitroanilide substrate (10 mM in DMSO) and 800 μ l of 50 mM pH 7.0 K₂HPO₄/KH₂PO₄ buffer, containing 2.5 mM EDTA. The absorbance was monitored during 4 min at 410 nm. The activity of control assays, without the inhibitor, was assumed to present 100% of activity. Data were treated as described.¹⁷⁵

6.4. X-RAY CRYSTALLOGRAPHY STUDIES

Porcine pancreatic elastase (PPE) was incubated with inhibitor **47d** for 30 min. Good quality crystals were grown in 200 mM sodium sulfate and 100 mM sodium acetate at pH 5.1 (293 K) using the sitting drop vapour-diffusion method. X-Ray diffraction data were measured at EMBLX11 beamline at theDORISstorage ring, DESY, Hamburg (Germany), to 1.66 Å resolution. The data were integrated with MOSFLM¹⁷⁶ and scaled using SCALA.¹⁷⁷ Relevant statistics on data collection and processing are given in *Appendix 1, Table A1.4*. The crystals soaked with the inhibitor solution belong to the same space group and show similar cell parameters as the native ones, so the structure was solved by Fourier synthesis. The initial rigid body refinement step yielded an *R*-work and *R*-free of 27.7 and 30.5%, respectively. Further crystallographic refinement was performed with Refmac¹⁷⁸ and the electron density maps were inspected with COOT.¹⁷⁹ The refined model of PPE in complex with inhibitor **47d** shows an *R*-factor of 15.6% and *R*-free of 18.6%.

The structure is generally well defined within the electron density maps, showing an average *B* factor of 10.5 Å² for all protein atoms. The final model comprises 240 amino acid residues, 316 water molecules, the inhibitor **47d** without the C-4 phenylsulfinate leaving group, two glycerol molecules, one sulfate ion and one sodium ion, which is hexa-coordinated to side-chain atoms of Glu-80, Asp-77, Gln-75, Asn-72, Glu-70 and a water molecule. Alternate conformations were modelled for the side chains of Gln-23, Gln-75, Val-83 and Ser-189, with 50% occupancy each. All protein residues lie within allowed regions of the Ramachandran plot. The overall protein structure of the **47d**-PPE complex is very similar to that of the native enzyme (PDB code 1QNJ) and superposition of the C-α atoms shows a r.m.s. deviation of 0.089 Å. The numbering of **47d**-PPE complex follows the common practice of using the bovine chymotrypsinogen A numbering.¹⁸⁰

The coordinates of **47d**-PPE complex have been deposited in the Protein Data Bank (PDB)⁶⁶ with identification code 2V35 and the corresponding structure factors with id code 2V35SF.

6.5. HYDROLYSIS OF SELECTED 4-OXO-β-LACTAMS IN PHOSPHATE BUFFER SOLUTION (PBS) AND HUMAN PLASMA

6.5.1 Hydrolysis of Selected β-Lactams in pH 7.4 Phosphate Buffer Solution

The kinetics of hydrolysis was studied using HPLC. Usually, a 15 μl aliquot of a 10⁻² M stock solution of the compound in acetonitrile was added to 2.5 ml of thermostated PBS (37°C). At regular intervals, samples of the reaction mixture were analyzed by HPLC as described below (Section 6.5.3).

6.5.2 Hydrolysis in Human Plasma

Human plasma was obtained from the pooled, heparinised blood of healthy donors, and was frozen and stored at -20°C prior to use. For the hydrolysis experiments, the compounds were incubated at 37°C in human plasma that had been diluted to 80% (v/v) with pH 7.4 isotonic phosphate buffer. At appropriate intervals, aliquots of 100

μl were added to 200 μl of acetonitrile to both quench the reaction and precipitate plasma proteins. These samples were centrifuged and the supernatant analyzed by HPLC for the presence of initial compound, as described below (Section 6.5.3).

6.5.3 HPLC Analysis

The analytical high-performance liquid chromatography (HPLC) system comprised a Merck Hitachi L-7100 pump with an Shimadzu SPD-6AV UV detector, a manual sample injection module equipped with a 20 mL loop, a Merck LichroCART 250-4 RP8 (5 μm) column equipped with a Merck Lichrocart pre-column (Merck, Germany). As mobile phase it was used isocratic solvent systems of acetonitrile/water (65:35) for compounds 6a, 6e and 6i, The column effluent was monitored at 225 nm for **103a** and 220 nm for compounds **103e** and **103i**.

6.6. BIODISTRIBUTION STUDY IN MICE

Male NMRI (20-22 g) were obtained from Charles River (Barcelona, Spain). The animals were kept under standard conditions and fed *ad libitum*. All of the experimental procedures were carried out with the permission of the local laboratory committee, and in accordance with international accepted principles.

Each mice group received a single 30 mg/kg dose of **103k** given by intraperitoneal (ip) injection and three mice per time point were used. At appropriate time intervals, blood was collected into heparinised tubes and stored at -30 °C and mice were euthanized. The lung, spleen and liver of mice were removed and stored at -70 °C. A control group of mice was used, which did not receive the administration of **103k**.

6.6.1 Determination of 103k by HPLC in Mice Blood and Tissues

6.6.1.1 Chromatographic system

Plasma and tissue levels of **103k** were determined by HPLC. The HPLC system consisted of a 32 Katarat Software (Beckman Instruments, Inc.), a Midas Spark 1.1

autoinjector and a Diode-Array 168 detector (Beckman Instruments, Inc.). The wavelength of this detector was set to 280 nm. The analytical column was a LiChroCART® (250-4.6), Purospher® Star RP-8 (5µm) (Merck, Darmstadt, Germany). The mobile phase consisted of 0.05M potassium dihydrogen phosphate and 0.05M sodium acetate (pH adjusted to 4.0 with acetic acid) - acetonitrile (53:47, v/v) with a flow rate of 1 mL/min at 25 °C, according to Gaspar *et al*¹⁸¹ with adaptations. The retention time was approximately 5.2 min. in blood samples and 5.0 min. in organs samples.

6.6.1.2 Preparation of Standard Solutions

Standard solutions of **103k** (5-120 µg/mL) were prepared by weighing the appropriate amount of bulk **103k** and dissolving it in acetonitrile and further dilution with mobile phase. Three eight-point calibration curves, with a loop of 100 µL, were used for the quantification of **103k** in plasma and tissues. A stock solution of 50 µg/mL was stored at -30 °C and a sample of this stock solution was always injected together with the analysed samples to verify the precision of the obtained concentrations of **103k** in samples and controls from their peak area concentration response.

6.6.1.3 Extraction of 103k from Blood and Tissues

Levels of **103k** in blood and tissues were determined by HPLC after an extraction procedure according to Battaglia *et al*¹⁸² and Benedetti *et al*,¹⁸³ adapted by Gaspar *et al*.¹⁸¹ Briefly, 500 µL of blood were mixed with 250 µL of buffer 0.05M potassium dihydrogen phosphate and 0.05M sodium acetate (pH adjusted to 4.0 with acetic acid) and extracted twice with 1 mL of a DCM: isooctane mixture (2:3, v/v) under stirring (15 min), followed by a centrifugation step at 1200×g for 10 min in a GPR centrifuge (Beckman Instruments, Inc.). Liver, lung and spleen tissues were thawed and aliquots of ca. 100 mg were weighed out for each sample mixed with 500 µL of buffer and extracted twice with 2300 µL of dichloromethane: isooctane mixture by mechanical shaking for 30 min at room temperature, followed by a centrifugation step at 1200×g for 10 min in a GPR centrifuge. The organic extracts were pooled and evaporated to dryness under nitrogen. The residue was dissolved in 1500 µL of mobile phase,

filtered and then injected into the HPLC system. To determine the efficiency of the extraction procedures, a known amount of **103k** was added to blood and solid tissues removed from mice that had not received **103k** administration and then submitted to the same above-mentioned extraction protocol.

All data are presented as mean \pm sd. Differences between groups were evaluated for statistical significance using one-way analysis of variance. A *p* value less than 0.05 was considered statistically significant.

6.7. MOLECULAR MODELING

Molecular modeling studies of inhibitors into the active site of HLE were performed with the flexible GOLD 3.0 (Genetic Optimization for Ligand Docking)¹⁶⁶ docking program.

GOLD program uses a genetic algorithm in order to explore the full range of ligand conformational and rotational flexibility, being the results ranked using the goldscore scoring function.¹⁸⁴ This function is defined as the sum of four components (protein-ligand hydrogen bond energy, protein-ligand van der Waals energy, ligand internal van der Waals energy and ligand torsional strain energy).

The HLE structure used (PDB code 1HNE¹⁸⁵) was obtained by deletion from the active site of the ligand (MeOSuc-Ala-Ala-Pro-Ala chloromethyl ketone) present in the crystal structure. Hydrogen atoms were added and correct protonation state of histidine residues were assigned according to their surrounding environment. The HLE structure was energy minimized and charges were added (using Chimera software)^{186,187} Then, in order to validate the optimized structure of the HLE, the respective deleted inhibitor was docked at the active site of the enzyme and the obtained final complex gave a SD < 2Å.

Geometries of inhibitors studied were energy-minimized using density functional theory.¹⁸⁸ (These calculations were performed with the B3LYP^{189, 190} hybrid functional Gaussian03 software package.¹⁹¹ After geometry optimizations, partial charges were included (Chimera software).^{187, 192}

6.7.1 Virtual Screening

For each inhibitor (*Appendix 2*), 20 runs for virtual screening were performed, using GOLD docking program. A constrain was introduced for calculations: the distance between the oxygen atom of Ser-195 and the carbonyl carbon C-2 should be more than 1.5 and less than 3.5 Å. Each run produced a score for the best fitted conformation of the inhibitor at the enzyme active site.

6.7.2 Molecular Docking

Each ligand was subjected to 10,000 docking runs (with a population size of 100; 100,000 genetic algorithm operations; 5 islands). The top 15 solutions (i.e. those with the highest fitness score) were visually analyzed for: (i) the hydrophobic and hydrophilic interactions between the ligand and enzyme surfaces and (ii) the distance between the Ser-195 hydroxyl oxygen atom and the carbonyl carbon atoms of each β -lactam.

APPENDICES

APPENDIX 1

A1.1 Alkaline hydrolysis of compounds 47b, 47e and 47f

Table A1.1 - Effect of concentration of OH⁻ on the pseudo-first-order rate constant for the alkaline hydrolysis of compounds 47b, 47e and 47f, at 25 °C and ionic strength adjusted to 0.5 M with NaClO₄.

47b

$10^2 [\text{OH}^-] / \text{M}$	$10^2 k_{\text{obs}} / \text{s}^{-1}$
3.06	2.48
3.07	3.29
4.74	3.45
4.95	5.06
9.85	10.90
1.60	19.10
19.80	19.20

47e

$10^2 [\text{OH}^-] / \text{M}$	$10^4 k_{\text{obs}} / \text{s}^{-1}$
2.95	0.54
4.95	0.70
10.10	1.65
19.80	3.24

47f

$10^2 [\text{OH}^-] / \text{M}$	$10^4 k_{\text{obs}} / \text{s}^{-1}$
3.07	1.66
4.95	2.72
9.85	5.64
19.80	13.65

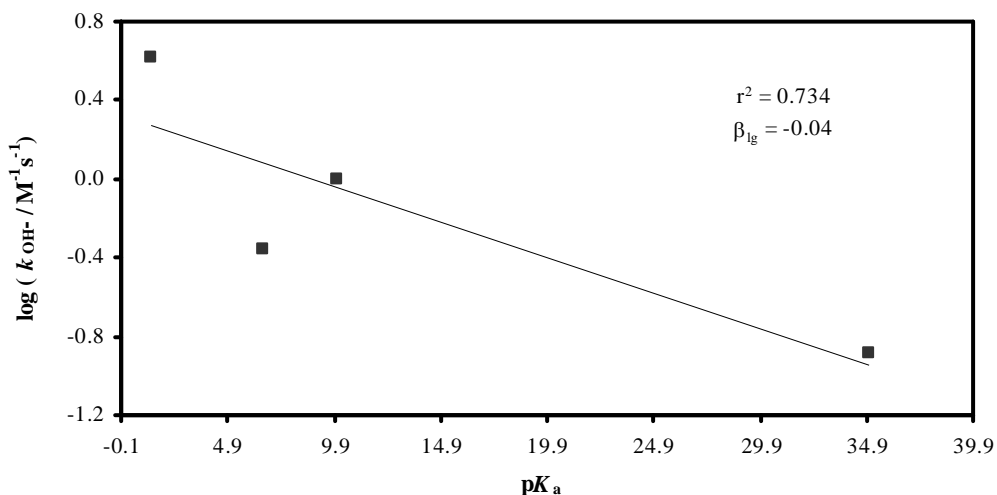


Figure A1.1 - Brønsted plot for the second-order rate constant for alkaline hydrolysis of 47a-d against the pK_a of the corresponding leaving groups at C-4, at 25°C, in 20% acetonitrile (v/v), giving a β_{lg} value of -0.04.

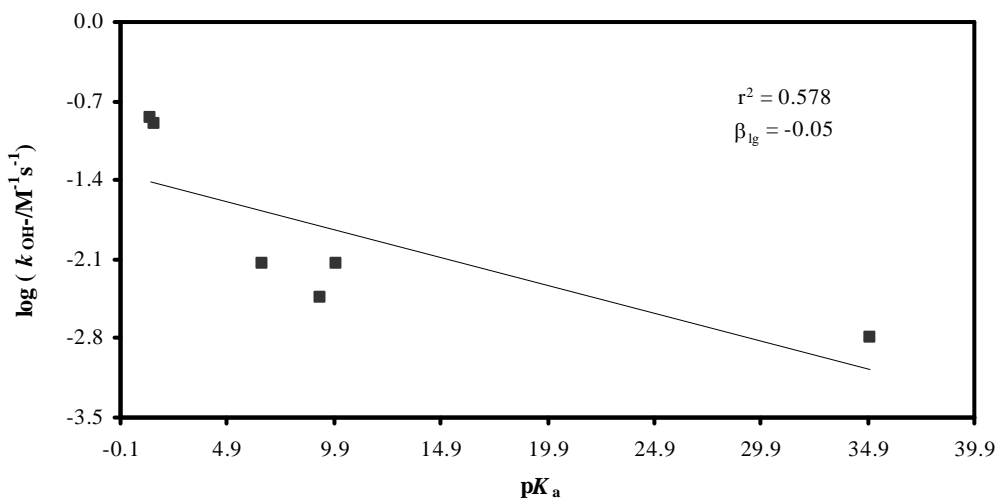


Figure A1.2 - Brønsted plot for the second-order rate constant for alkaline hydrolysis of 47e-j against the pK_a of the corresponding leaving groups at C-4, at 25°C, in 20% acetonitrile (v/v), giving a β_{lg} value of -0.05.

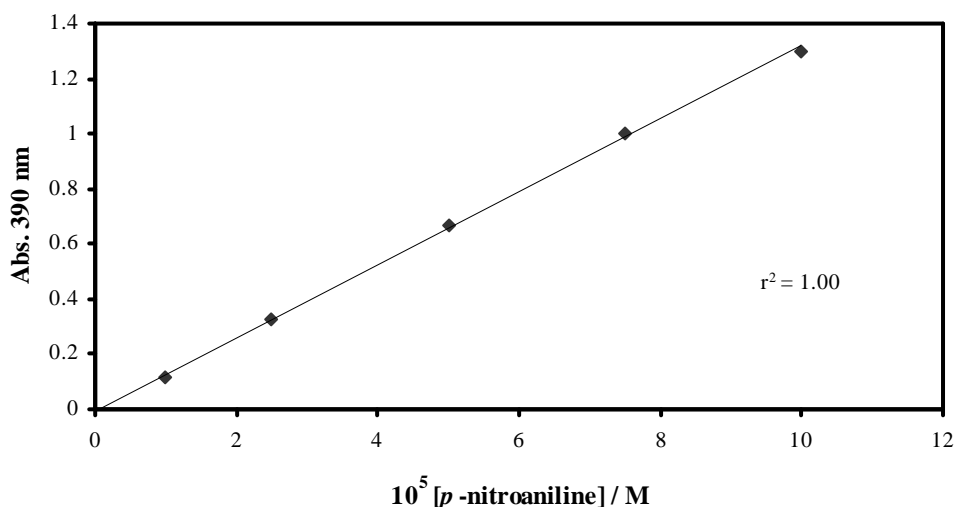
A1.2 Determination of the molar extinction coefficient for *p*-nitroaniline, ϵ_{390} 

Figure A1.3 - Beer-Lambert plot for determination of the molar extinction coefficient for *p*-nitroaniline, at 390 nm, ϵ_{390} , 25 °C, in 0.1 M HEPES buffer, pH 7.2, 6% DMSO (v/v), using a cuvette in which $l = 1$ cm.

From this plot, the molar extinction coefficient for *p*-nitroaniline at 390 nm, ϵ_{390} , is $1.32 \times 10^4 \text{ M}^{-1}\text{cm}^{-1}$. This value is in good agreement with the one reported in the literature, $\epsilon_{390} = 1.24 \times 10^4 \text{ M}^{-1}\text{cm}^{-1}$.¹⁹³

A1.3 Determination of the K_m

PPE activity was monitored over a period of 1 min, at 390 nm, 25 °C, in 0.1M HEPES buffer, pH 7.2, 6% DMSO (v/v), using different concentrations of substrate ([S] in the cuvette ranging from 75 μM to 1 mM), and being [PPE] = 1 μM . Each concentration was assayed at least two times. The initial rates, v_i , were determined in $\Delta A \text{ s}^{-1}$. Rates

in Ms^{-1} were obtained by dividing the initial rate v_i , in $\Delta A \text{ s}^{-1}$ by the obtained molar extinction coefficient for *p*-nitroaniline, ϵ_{390} .

Table A1.2 - Concentrations of the chromogenic substrate used for determination of the K_m and the respective initial rates of the PPE-mediated hydrolysis, in $\Delta A \text{ s}^{-1}$ and $\text{M}^{-1}\text{s}^{-1}$, at 390 nm, 25 °C, in 0.1 M pH 7.2 HEPES buffer, 6% DMSO (v/v).

$10^5 [\text{S}] / \text{M}$	$v_i / \Delta A \text{ s}^{-1}$	v_i / Ms^{-1}
7.5	2.46×10^{-3}	1.86×10^{-7}
10	3.36×10^{-3}	2.55×10^{-7}
25	7.80×10^{-3}	5.91×10^{-7}
50	1.53×10^{-2}	1.16×10^{-6}
75	2.15×10^{-2}	1.64×10^{-6}
100	2.50×10^{-2}	1.89×10^{-6}

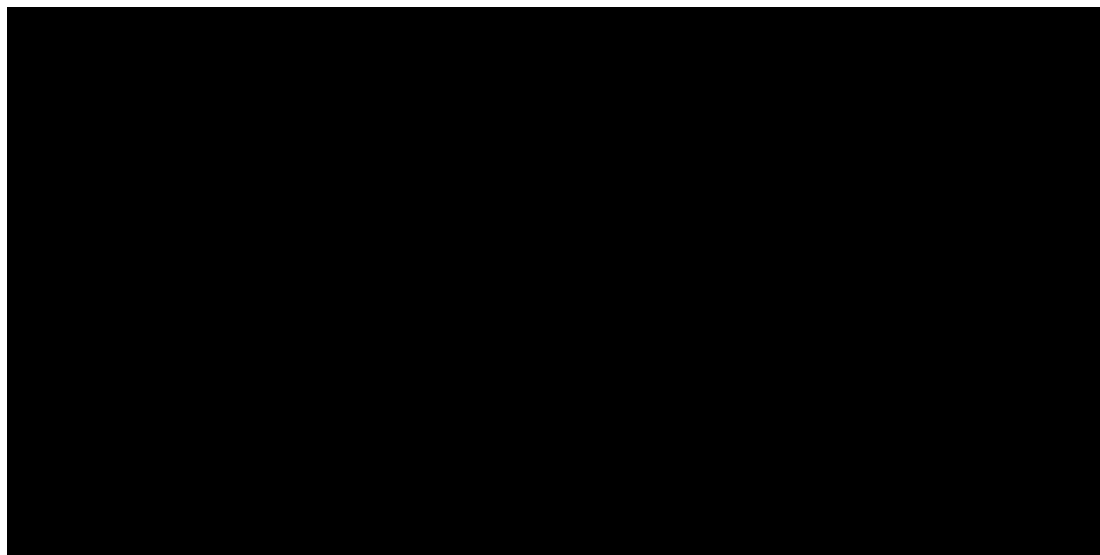


Figure A1.4 - Michaelis-Menten plot for the hydrolysis of the chromogenic substrate of PPE, at 390 nm, 25 °C, in 0.1 M pH 7.2 HEPES buffer, 6% DMSO (v/v). Concentrations of substrate [S] and v_i in Ms^{-1} are from Table A1.2. Points are experimental and line is from non-linear regression analysis.

A1.4 PPE Inhibition Studies**Table A1.3 -Pseudo-first-order rate constant, k_{obs} , for the inactivation of PPE by β -lactams 47b-d, at 25 °C, in 0.1 M HEPES buffer, pH 7.2.****47b**

10^4 [47b] / M	$10^3 k_{obs} / s^{-1}$
0.20	0.26
1.25	1.84
2.50	2.62
5.00	5.86

47c

10^4 [47c] / M	$10^3 k_{obs} / s^{-1}$
1.00	2.40
2.00	4.99
3.30	7.98
5.00	11.1

47d

10^4 [47d] / M	$10^3 k_{obs} / s^{-1}$
0.10	2.45
0.20	5.06
0.40	10.3
0.50	14.4

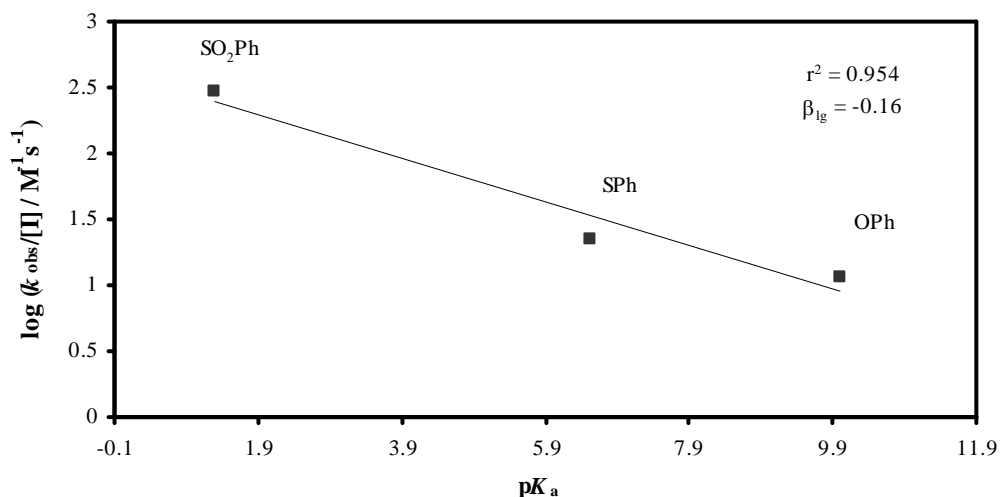


Figure A1.5 - Brønsted plot of the second-order rate constant for PPE inactivation $k_{\text{obs}}/[I]$ by 47b-d against the $\text{p}K_{\text{a}}$ of the leaving group at C-4, giving a β_{lg} value of -0.16.

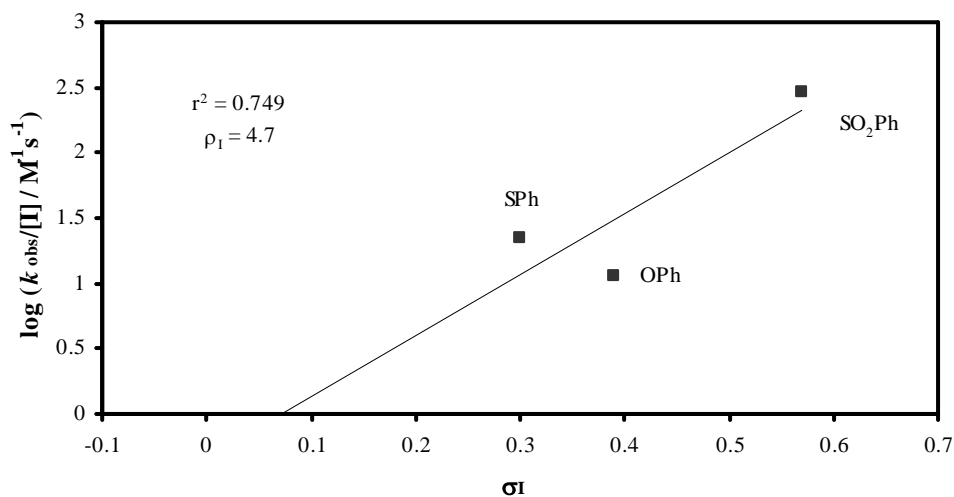


Figure A1.6 - Plot of the second-order rate constants for PPE inactivation, $k_{\text{obs}}/[I]$, by 47b-d against the σ_{I} value of the substituent at C-4, giving $\rho_{\text{I}} = 4.7$.

Table A1.4 - Data collection and crystallographic refinement statistics for the porcine pancreatic elastase structure bound to 47d.

X-ray data-collection wavelength (Å)	0.82
Space group	P2 ₁ 2 ₁ 2 ₁
Unit cell parameters (Å)	a = 50.25, b = 57.94, c = 74.69
Resolution range (Å)	37.95-1.66
Refined model	
R-factor (%)	15.6
R-free (%)	18.6
N° of non H protein atoms	1833
N° of solvent molecules	320
Average B-factor (Å²)	
Protein only	10.5
Inhibitor only	24.4
Solvent molecules	25.9
Ramachandran plot	
Residues in most most favoured regions of (%)	87.4
Residues in additional allowed regions (%)	12.6
r.m.s. deviations	
bond angles (°)	0.01
angle lengths (Å)	1.22

A1.5 HLE Inhibition Studies

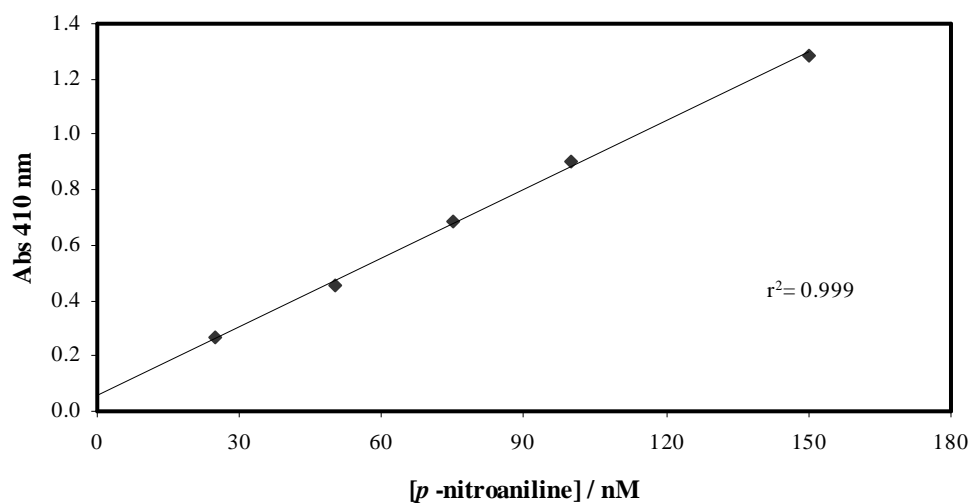


Figure A1.7 - Beer-Lambert plot for determination of the molar extinction coefficient for *p*-nitroaniline, at 410 nm, ϵ_{410} , 25 °C, in 0.1 M HEPES buffer, pH 7.2, using a cuvette in which $l = 1$ cm.

From this plot, the molar extinction coefficient for *p*-nitroaniline at 410 nm is $\epsilon_{410} = 8.25 \times 10^3 \text{ M}^{-1}\text{cm}^{-1}$. This value is in agreement with the one reported in the literature, $\epsilon_{410} = 8.80 \times 10^3 \text{ M}^{-1}\text{cm}^{-1}$.¹⁹⁴

Table A1.5 - Pseudo-first-order rate constant, k_{obs} , for the inactivation of HLE by β -lactams 47f-h and 47k at 25 °C, in 0.1 M HEPES buffer, pH 7.2.

47f		47g	
10^6 [47f] / M	$10^3 k_{\text{obs}} / \text{s}^{-1}$	10^6 [47g] / M	$10^3 k_{\text{obs}} / \text{s}^{-1}$
15	5.59	100	3.52
10	4.08	50	3.28
5.0	2.77	10	2.48
2.0	1.72	2.0	1.08

47h		47k	
$10^6 [47h] / M$	$10^3 k_{obs} / s^{-1}$	$10^6 [47g] / M$	$10^3 k_{obs} / s^{-1}$
25	3.63	20	3.21
10	3.56	15	3.14
2.0	1.96	7.5	2.53
		2.0	1.43

Table A1.6 - The dependence of the steady-state rate, v_s , with the inhibitor concentration for compound 47f, allowing the determination of K_i .

47f	
$10^6 [47f] / M$	$10^5 v_s / \Delta A s^{-1}$
15	2.05
10	1.78
5.0	5.88
2.0	9.41
0	27.0

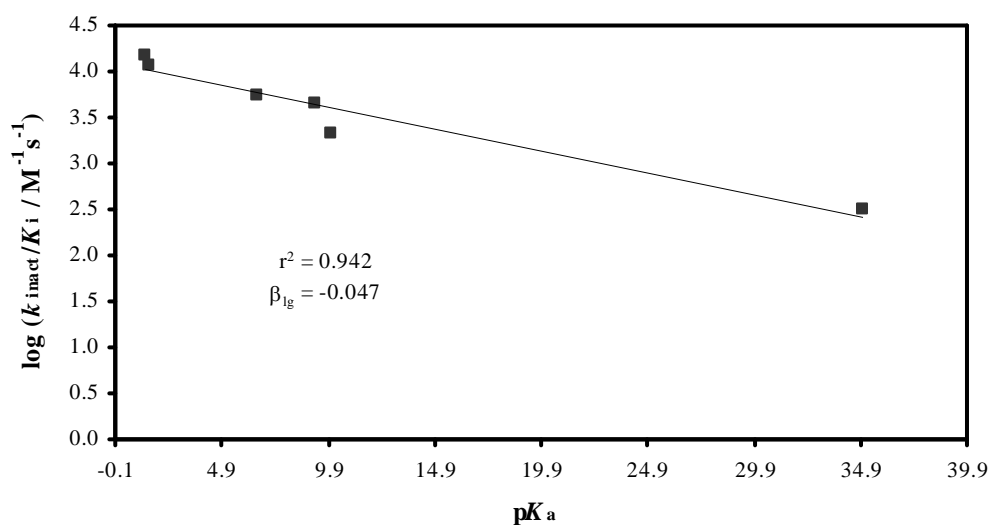
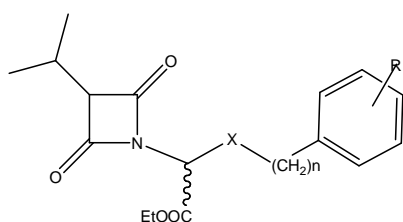
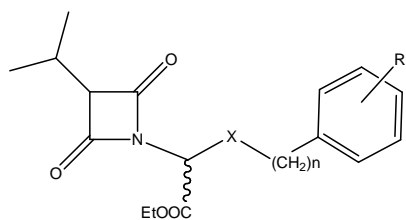


Figure A1.8 - Brønsted plot of the second-order rate constant for HLE inactivation k_{inact}/K_i against the pK_a of the leaving group at C-4, giving a β_{ig} value of -0.047.

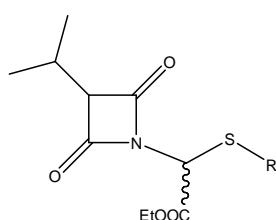
APPENDIX 2

Table A2.1- Database of 4-oxo- β -lactams created for virtual screening studies with HLE.

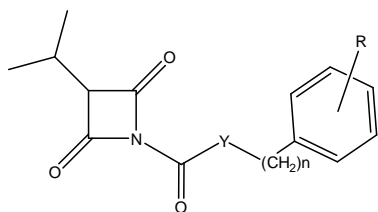
Compound	R	Config.
A1R	Benzyl	R
A1S	Benzyl	S
A2R	Phenyl	R
A2S	Phenyl	S
A3R	C ₆ H ₄ -4-OCH ₃	R
A3S	C ₆ H ₄ -4-OCH ₃	S
A4R	C ₆ H ₄ -4-CH ₃	R
A4S	C ₆ H ₄ -4-CH ₃	S
A5R	Methyl	R
A5S	Methyl	S
A6R	C ₆ H ₄ -2-CO ₂ H	R
A6S	C ₆ H ₄ -2-CO ₂ H	S
A7R	C ₆ H ₄ -4-CO ₂ H	R
A7S	C ₆ H ₄ -4-CO ₂ H	S



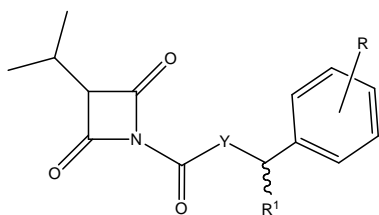
Compound	X	n	R	Config.
A8R	O	0	H	R
A8S	O	0	H	S
A9R	O	0	4-Methyl	R
A9S	O	0	4-Methyl	S
A10R	O	0	4-COOH	R
A10S	O	0	4-COOH	S
A11R	SO	0	H	R
A11S	SO	0	H	S
A12R	SO ₂	0	H	R
A12S	SO ₂	0	H	S
A13R	SO ₂	1	H	R
A13S	SO ₂	1	H	S



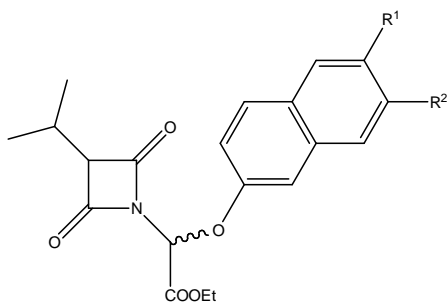
Compound	R	Config.
A14R	2-(5-phenyl-1,3,4-oxadiazole)	R
A14S	2-(5-phenyl-1,3,4-oxadiazole)	S
A15R	2-benzoxazole	R
A15S	2-benzoxazole	S
A16R	2-(benzoxazole-5-COOH)	R
A16S	2-(benzoxazole-5-COOH)	S
A17R	2-(benzoxazole-6-COOH)	R
A17S	2-(benzoxazole-6-COOH)	S
A18R	2-benzothiazole	R
A18S	2-benzothiazole	S
A19R	2-(1-methylimidazole)	R
A19S	2-(1-methylimidazole)	S
A20R	Phenyl	R
A20S	Phenyl	S
A21R	2-(1-methylbenzimidazole)	R
A21S	2-(1-methylbenzimidazole)	S
A22R	2-(benzimidazole)	R
A22S	2-(benzimidazole)	S
A23R	CH ₂ COPh	R
A23S	CH ₂ COPh	S
A24R	CH ₂ -2-pyridinyl	R
A24S	CH ₂ -2-pyridinyl	S



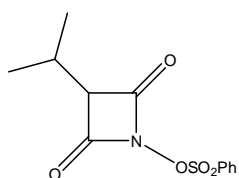
Compound	Y	n	R
A25	NH	1	H
A26	NH	0	H
A27	CH ₂	0	H
A28	O	0	H
A29	NH	1	4-Me
A30	NH	1	3-OMe, 4-Me
A31	NH	1	3-Me, 4-OMe
A32	NH	1	3,4-Me ₂



Compound	Y	R ¹	R	Config.
A33R	NH	Et	H	R
A33S	NH	Et	H	S
A34R	NH	Pr	H	R
A34S	NH	Pr	H	S

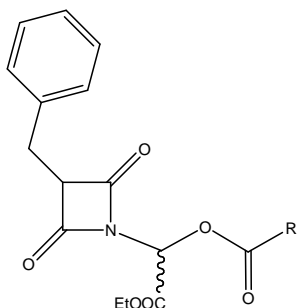


Compound	R ¹	R ²	Config.
A35	COOH	H	R
A36	COOH	H	S
A37	H	COOH	R
A38	H	COOH	S

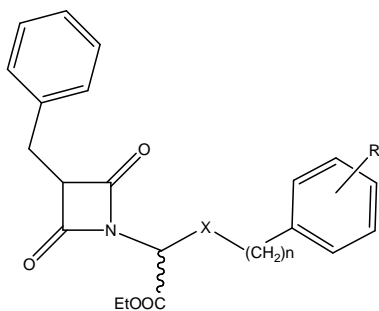


Compound

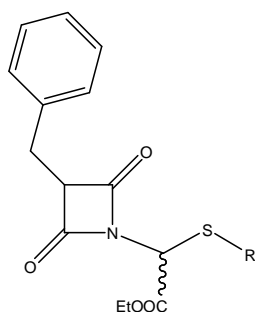
A39



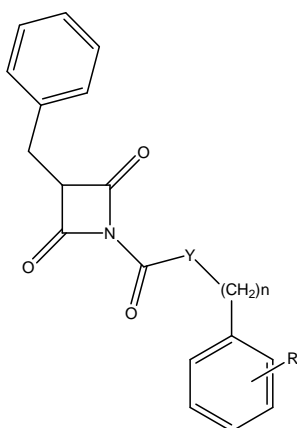
Compound	R	Config.
A40R	Benzyl	R
A40S	Benzyl	S
A41R	Ph	R
A41S	Ph	S
A42R	C ₆ H ₄ -4-OCH ₃	R
A42S	C ₆ H ₄ -4-OCH ₃	S
A43R	C ₆ H ₄ -4-CH ₃	R
A43S	C ₆ H ₄ -4-CH ₃	S
A44R	Methyl	R
A44S	Methyl	S
A45R	C ₆ H ₄ -2-CO ₂ H	R
A45S	C ₆ H ₄ -2-CO ₂ H	S
A46R	C ₆ H ₄ -4-CO ₂ H	R
A46S	C ₆ H ₄ -4-CO ₂ H	S



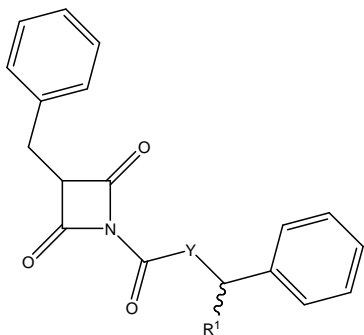
Compound	X	n	R	Config.
A47R	O	0	H	R
A47S	O	0	H	S
A48R	O	0	4-Methyl	R
A48S	O	0	4-Methyl	S
A49R	O	0	4-COOH	R
A49S	O	0	4-COOH	S
A50R	SO	0	H	R
A50S	SO	0	H	S
A51R	SO ₂	0	H	R
A51S	SO ₂	0	H	S
A52R	SO ₂	1	H	R
A52S	SO ₂	1	H	S



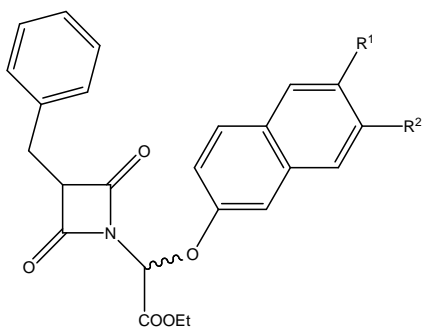
Compound	R	Config.
A53R	2-(5-phenyl-1,3,4-oxadiazole)	R
A53S	2-(5-phenyl-1,3,4-oxadiazole)	S
A54R	2-benzoxazole	R
A54S	2-benzoxazole	S
A55R	2-(benzoxazole-5-COOH)	R
A55S	2-(benzoxazole-5-COOH)	S
A56R	2-(benzoxazole-6-COOH)	R
A56S	2-(benzoxazole-6-COOH)	S
A57R	2-benzothiazole	R
A57S	2-benzothiazole	S
A58R	2-(1-methylimidazole)	R
A58S	2-(1-methylimidazole)	S
A59R	Phenyl	R
A59S	Phenyl	S
A60R	2-(1-methylbenzimidazole)	R
A60S	2-(1-methylbenzimidazole)	S
A61R	2-(benzimidazole)	R
A61S	2-(benzimidazole)	S
A62R	CH ₂ COPh	R
A62S	CH ₂ COPh	S
A63R	CH ₂ -2-pyridinyl	R
A63S	CH ₂ -2-pyridinyl	S



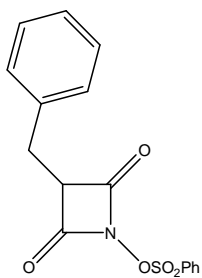
Compound	Y	n	R
A64	NH	1	H
A65	NH	0	H
A66	CH ₂	0	H
A67	O	0	H
A68	NH	1	4-Me
A69	NH	1	3-OMe, 4-Me
A70	NH	1	3-Me, 4-OMe
A71	NH	1	3,4-Me ₂



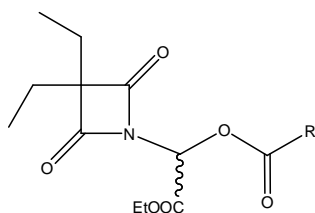
Compound	Y	R ¹	Config.
A72R	NH	Et	R
A72S	NH	Et	S
A73	NH	Pr	R
A74	NH	Pr	S



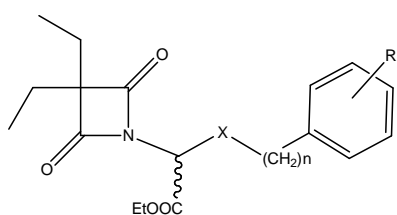
Compound	R ¹	R ²	Config.
A75	COOH	H	R
A76	COOH	H	S
A77	H	COOH	R
A78	H	COOH	S



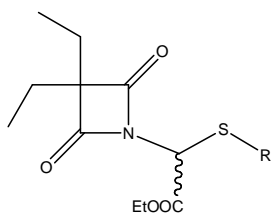
Compound
A79



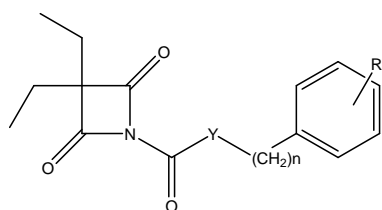
Compound	R	Config.
A80R	Benzyl	R
A80S	Benzyl	S
A81R	Phenyl	R
A81S	Phenyl	S
A82R	C ₆ H ₄ -4-OCH ₃	R
A82S	C ₆ H ₄ -4-OCH ₃	S
A83R	C ₆ H ₄ -4-CH ₃	R
A83S	C ₆ H ₄ -4-CH ₃	S
A84R	Methyl	R
A84S	Methyl	S
A85R	C ₆ H ₄ -2-CO ₂ H	R
A85S	C ₆ H ₄ -2-CO ₂ H	S
A86R	C ₆ H ₄ -4-CO ₂ H	R
A86S	C ₆ H ₄ -4-CO ₂ H	S



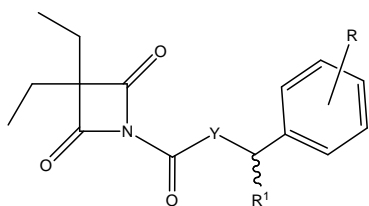
Compound	X	n	R	Config.
A87R	O	0	H	R
A87S	O	0	H	S
A88R	O	0	4-Methyl	R
A88S	O	0	4-Methyl	S
A89R	O	0	4-COOH	R
A89S	O	0	4-COOH	S
A90R	SO	0	H	R
A90S	SO	0	H	S
A91R	SO ₂	0	H	R
A91S	SO ₂	0	H	S
A92R	SO ₂	1	H	R
A92S	SO ₂	1	H	S



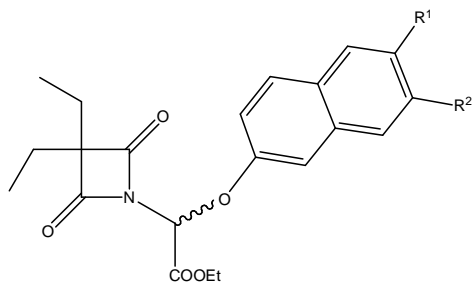
Compound	R	Config.
A93R	2-(5-phenyl-1,3,4-oxadiazole)	R
A93S	2-(5-phenyl-1,3,4-oxadiazole)	S
A94R	2-benzoxazole	R
A94S	2-benzoxazole	S
A95R	2-(benzoxazole-5-COOH)	R
A95S	2-(benzoxazole-5-COOH)	S
A96R	2-(benzoxazole-6-COOH)	R
A96S	2-(benzoxazole-6-COOH)	S
A97R	2-benzothiazole	R
A97S	2-benzothiazole	S
A98R	2-(1-methyl imidazole)	R
A98S	2-(1-methyl imidazole)	S
A99R	Phenyl	R
A99S	Phenyl	S
A100R	2-(1-methyl benzimidazole)	R
A100S	2-(1-methyl benzimidazole)	S
A101R	2-(benzimidazole)	R
A101S	2-(benzimidazole)	S
A102R	CH ₂ COPh	R
A102S	CH ₂ COPh	S
A103R	CH ₂ -2-pyridinyl	R
A103S	CH ₂ -2-pyridinyl	S



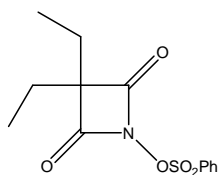
Compound	Y	n	R
A104	NH	1	H
A105	NH	0	H
A106	CH ₂	0	H
A107	O	0	H
A108	NH	1	4-Me
A109	NH	1	3-OMe, 4-Me
A110	NH	1	3-Me, 4-OMe
A111	NH	1	3,4-Me ₂



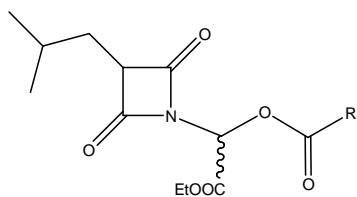
Compound	Y	R ¹	R	Config.
A112R	NH	Et	H	R
A112S	NH	Et	H	S
A113	NH	Pr	H	R
A114	NH	Pr	H	S



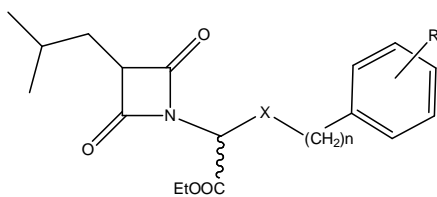
Compound	Config.	R ¹	R ²
A115	R	COOH	H
A116	S	COOH	H
A117	R	H	COOH
A118	S	H	COOH



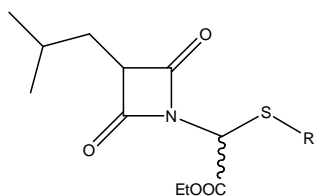
Compound
A119



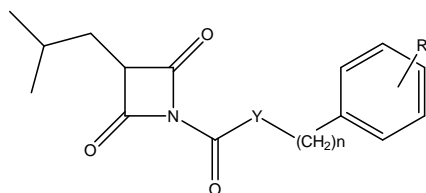
Compound	R	Config.
A120R	Benzyl	R
A120S	Benzyl	S
A121R	Phenyl	R
A121S	Phenyl	S
A122R	C ₆ H ₄ -4-OCH ₃	R
A122S	C ₆ H ₄ -4-OCH ₃	S
A123R	C ₆ H ₄ -4-CH ₃	R
A123S	C ₆ H ₄ -4-CH ₃	S
A124R	Methyl	R
A124S	Methyl	S
A125R	C ₆ H ₄ -2-CO ₂ H	R
A125S	C ₆ H ₄ -2-CO ₂ H	S
A126R	C ₆ H ₄ -4-CO ₂ H	R
A126S	C ₆ H ₄ -4-CO ₂ H	S



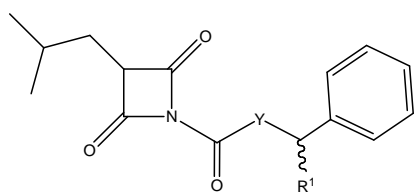
Compound	X	n	R	Config.
A127R	O	0	H	R
A127S	O	0	H	S
A128R	O	0	4-Methyl	R
A128S	O	0	4-Methyl	S
A129R	O	0	4-COOH	R
A129S	O	0	4-COOH	S
A130R	SO	0	H	R
A130S	SO	0	H	S
A131R	SO ₂	0	H	R
A131S	SO ₂	0	H	S
A132R	SO ₂	1	H	R
A132S	SO ₂	1	H	S



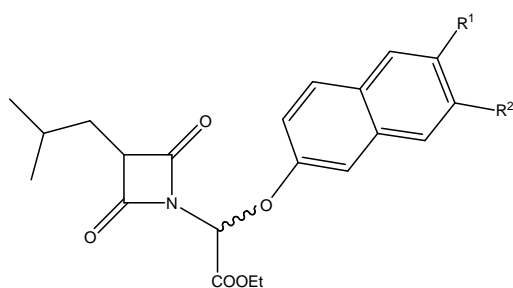
Compound	R	Config.
A133R	2-(5-phenyl-1,3,4-oxadiazole)	R
A133S	2-(5-phenyl-1,3,4-oxadiazole)	S
A134R	2-benzoxazole	R
A134S	2-benzoxazole	S
A135R	2-(benzoxazole-5-COOH)	R
A135S	2-(benzoxazole-5-COOH)	S
A136R	2-(benzoxazole-6-COOH)	R
A136S	2-(benzoxazole-6-COOH)	S
A137R	2-benzothiazole	R
A137S	2-benzothiazole	S
A138R	2-(1-methyl imidazole)	R
A138S	2-(1-methyl imidazole)	S
A139R	Phenyl	R
A139S	Phenyl	S
A140R	2-(1-methyl benzimidazole)	R
A140S	2-(1-methyl benzimidazole)	S
A141R	2-(benzimidazole)	R
A141S	2-(benzimidazole)	S
A142R	CH ₂ COPh	R
A142S	CH ₂ COPh	S
A143R	CH ₂ -2-pyridinyl	R
A143S	CH ₂ -2-pyridinyl	S



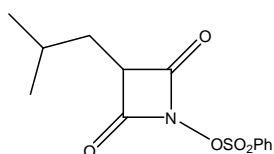
Compound	Y	n	R
A144	NH	1	H
A145	NH	0	H
A146	CH ₂	0	H
A147	O	0	H
A148	NH	1	4-Me
A149	NH	1	3-OMe, 4-Me
A150	NH	1	3-Me, 4-OMe
A151	NH	1	3,4-Me ₂



Compound	Y	R ¹	R	Config.
A152R	NH	Et	H	R
A152S	NH	Et	H	S
A153R	NH	Pr	H	R
A153S	NH	Pr	H	S



Compound	R ¹	R ²	Config.
A154R	COOH	H	R
A154S	COOH	H	S
A155R	H	COOH	R
A155S	H	COOH	S



Compound
A156

From this database, the compounds that afforded the best fitness score were **A1**, **A40** and **A80** (both *R* and *S* enantiomers)

APPENDIX 3

A3.1 Alkaline Hydrolysis Studies of 4-Oxo- β -lactams **77**

Spectral scanning for the reaction of hydroxide-ion with **77d**

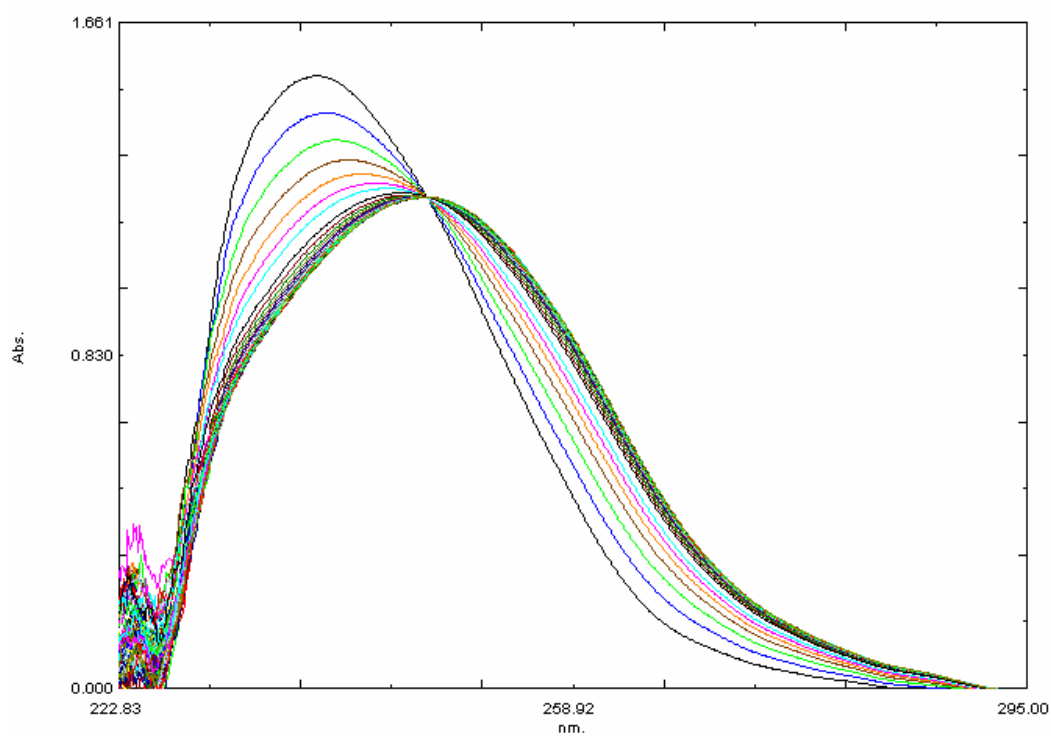


Figure A3.1 - UV spectra depicting the reaction, at 25 °C, of 77d (10^{-4} M) with OH^- 0.1 M (ionic strength 0.5 M), scan intervals: 100 sec. An isosbestic point was found. The wavelength selected to monitor the kinetic reaction was 260 nm.

Table A3.1 - Effect of concentration of OH⁻ on the pseudo-first-order rate constant for the alkaline hydrolysis of compounds 77b-i, at 25 °C and ionic strength adjusted to 0.5 M with NaClO₄.

N-Benzyl derivatives 77b and 77h

77b

$10^3 [\text{OH}^-] / \text{M}$	$10^3 k_{obs} / \text{s}^{-1}$
5.80	0.713
9.90	1.04
30.0	2.19
51.0	4.16
100	7.65

77h

$10^3 [\text{OH}^-] / \text{M}$	$10^3 k_{obs} / \text{s}^{-1}$
0.77	1.62
1.7	3.81
5.8	13.2
9.9	19.0
30	54.8

N-Aryl derivatives 77c-g and 77i

77c

$10^2 [\text{OH}^-] / \text{M}$	$10^3 k_{obs} / \text{s}^{-1}$
0.50	1.03
1.01	2.32
2.98	6.73
5.00	11.8
9.94	22.2

77d

$10^2 [\text{OH}^-] / \text{M}$	$10^3 k_{obs} / \text{s}^{-1}$
0.50	1.08
1.01	2.28
3.08	6.94
5.00	11.3
10.1	24.2

77e

$10^2 [\text{OH}^-] / \text{M}$	$10^3 k_{obs} / \text{s}^{-1}$
0.50	1.56
1.01	3.30
2.98	10.2
5.00	16.6
9.94	33.8

77f

$10^2 [\text{OH}^-] / \text{M}$	$10^3 k_{obs} / \text{s}^{-1}$
0.50	2.43
1.01	5.12
3.08	16.4
5.00	27.4
10.1	58.2

77g		77i	
$10^2[\text{OH}^-] / \text{M}$	$10^3 k_{\text{obs}} / \text{s}^{-1}$	$10^3[\text{OH}^-] / \text{M}$	$10^3 k_{\text{obs}} / \text{s}^{-1}$
0.50	7.53	0.77	7.56
1.01	16.6	1.70	18.0
3.08	53.8	5.05	44.7
5.00	91.4	10.1	99.6
10.10	178	29.8	288

A3.2 - PPE Inhibition by 4-Oxo- β -lactams 77

Table A3.2 - Pseudo-first-order rate constant, k_{obs} , for the inactivation of PPE by 4-oxo- β -lactams 77c-g, at 25 °C, in 0.1 M HEPES buffer, pH 7.2.

77c		77d	
$10^4 [77\text{c}] / \text{M}$	$10^3 k_{\text{obs}} / \text{s}^{-1}$	$10^4 [77\text{d}] / \text{M}$	$10^3 k_{\text{obs}} / \text{s}^{-1}$
0.20	3.65	0.10	3.10
0.30	5.19	0.15	4.20
0.60	9.26	0.20	5.14
0.75	11.5	0.30	7.18
1.00	14.1	0.60	12.3
1.50	18.5	0.75	16.0
		1.00	20.0

77e		77f	
$10^4 [77\text{e}] / \text{M}$	$10^3 k_{\text{obs}} / \text{s}^{-1}$	$10^4 [77\text{f}] / \text{M}$	$10^3 k_{\text{obs}} / \text{s}^{-1}$
0.15	3.99	0.10	4.34
0.30	7.79	0.15	5.55
0.60	14.0	0.20	7.03
0.75	17.5	0.30	9.91
1.00	18.6	0.60	16.8
1.50	30.9		

77g

$10^4[\mathbf{77g}] / \text{M}$	$10^3 k_{obs} / \text{s}^{-1}$
0.08	7.44
0.15	13.07
0.20	16.05
0.40	32.01
0.60	38.40
0.80	54.47

A3.2.1 - Analysis of the Inhibition Kinetics and Determination of K_i for **77e**

The analysis of the inhibition kinetics of PPE for determination of K_i by 3,3-diethyl-*N*-phenylazetidine-2,4-dione **77e** is illustrated in Figures A3.2 and A3.3.

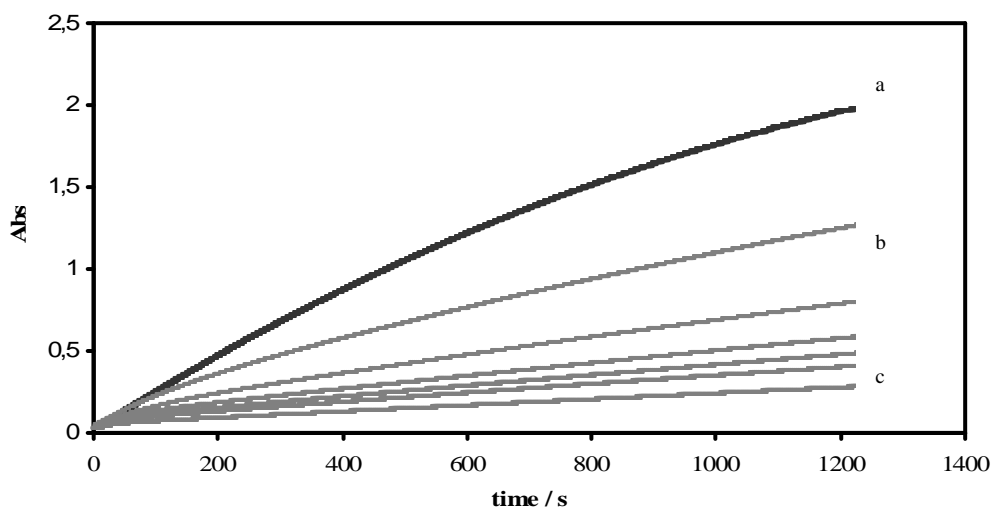


Figure A3.2 - Progress curves for the slow-binding inhibition of PPE by compound **77e.** Reaction conditions: [PPE] = 0.2 μM , [N-Suc-(L-Ala)₃-p-NA] = 0.3 mM, 0.1 M HEPES buffer, pH 7.2, 5% DMSO, 25 $^\circ\text{C}$. Inhibitor concentrations: (a), in absence of inhibitor; (b), 15; (c), 30; (d), 60; (e), 75; (f), 100; (g), 150 μM .

The data shown in Figure A3.2 were fitted by non-linear regression analysis accordingly to slow binding kinetics, as previously discussed, to obtain the best-fit parameters for v_i , v_s and k_{obs} for **77e**, Table A3.3.

Table A3.3 - The dependence of the kinetic parameters of PPE inhibition, k_{obs} , v_i and v_s with the inhibitor concentration for the 4-oxo- β -lactam **77e.**

$10^4[\mathbf{77e}] / \text{M}$	$10^3 k_{obs} / \text{s}^{-1}$	$10^4 v_i / \Delta\text{A s}^{-1}$	$10^4 v_s / \Delta\text{A s}^{-1}$
0	-		13.4
0.15	3.99	18.2	7.53
0.30	7.79	14.9	5.35
0.60	14.0	14.2	3.75
0.75	17.5	12.9	3.10
1.00	18.6	10.9	2.58
1.50	30.9	10.1	1.94

The apparent second-order rate constant k_{on}' was obtained from k_{obs} plotted versus $[I]$, illustrated in Figure 3.14, Chapter 3, and was then corrected using Equation 2.8 (Section 2.3.2.2) to give k_{on} .

The apparent steady-state dissociation constant of the enzyme-inhibitor complex, K_i' was calculated using the steady-state velocities, v_s (Table A3.3) fitting by non-linear regression to Equation 2.10, as shown in Figure A3.3. Then, K_i value was calculated by correction using Equation 2.11.

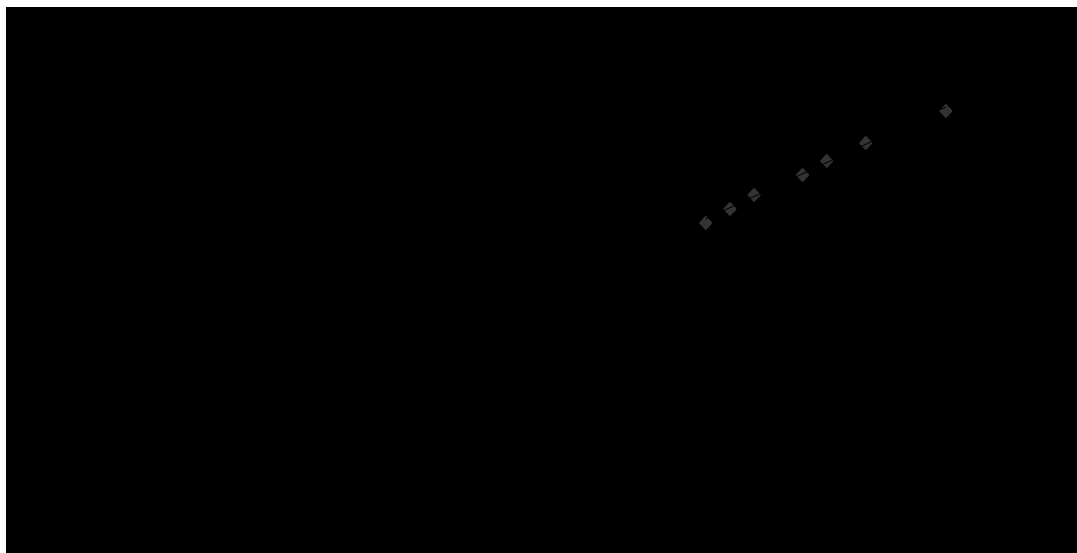


Figure A3.3 - Plot of the steady-state rates versus [I] for the inhibition of PPE by compound 77e. Points are experimental and were obtained from fits of the curves shown in Figure A3.2 and the line is from non-linear regression analysis of the steady state rates v_s versus inhibitor concentration (Table A3.3), using Equation 2.10, for $K_i' = 21.8 \pm 1.1 \mu\text{M}$. (The insert is a Dixon plot to show the linearity).

Thus, as presented in Figure A3.3, $K_i' = 21.8 \pm 1.1 \mu\text{M}$ for **77e**. By correction using Equation 2.11, $K_i = 20.2 \pm 1.7 \mu\text{M}$ for **77e**.

Then, the k_{off} value was calculated from K_i and k_{on} values using Equation 2.9, giving $k_{\text{off}} = 4.15 \times 10^{-3} \text{ s}^{-1}$.

A3.2.2 Inhibition of PPE by compounds 77h-i

Table A3.4 – Kinetic data for the hydrolysis of the chromogenic substrate of PPE in the presence of 77i. (Initial rates for the reaction in the absence of inhibitor were given in Table A1.2).

$10^5 [S] / M$	$[77i] = 60 \mu M$	$[77i] = 100 \mu M$
	v_i / Ms^{-1}	v_i / Ms^{-1}
10.0	3.89×10^{-8}	2.16×10^{-8}
25.0	9.96×10^{-8}	5.61×10^{-8}
50.0	1.69×10^{-7}	-
75.0	2.19×10^{-7}	1.33×10^{-7}
100	2.85×10^{-7}	170×10^{-7}

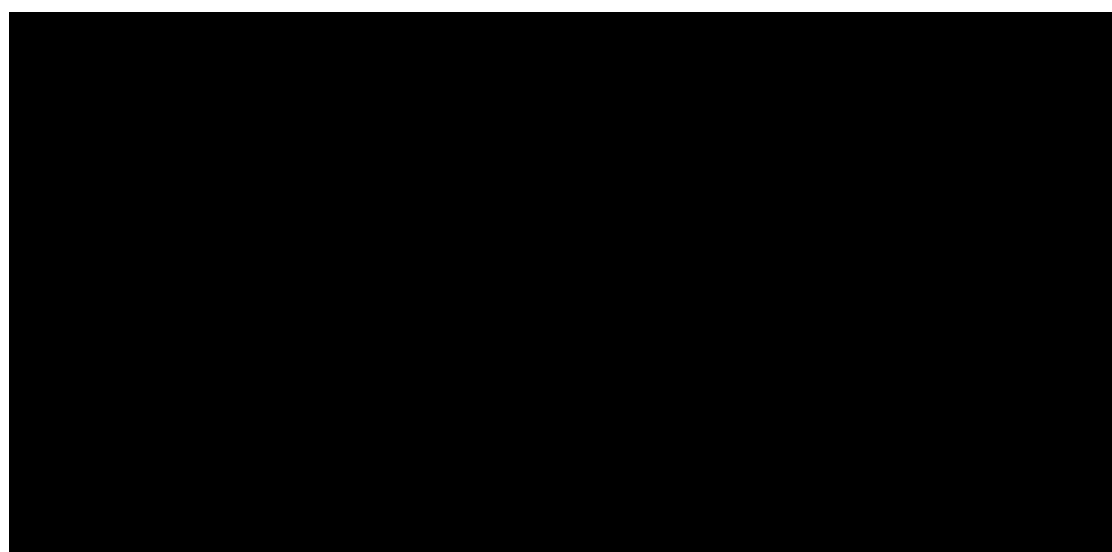


Figure A3.4 - Michaelis-Menten plot for the hydrolysis of the chromogenic substrate of PPE, in the absence of inhibitor (●), and in the presence of 60 μM (□) and 100 μM of 77i (▲), at 390 nm, 25 °C, in 0.1 M HEPES buffer, pH 7.2, 6% DMSO (v/v). Points are experimental and lines are from non-linear regression analysis of the data. The respective Lineweaver-Burke plot was obtained from linear analysis of data $1/v_i/M^{-1}s$ versus $1/[S]/M^{-1}$, as illustrated in Chapter 3, Section 3.4.1, Figure 3.18.

Table A3.5 – Kinetic data for the hydrolysis of the chromogenic substrate of PPE in the presence of 77h. (Initial rates for the reaction in the absence of inhibitor were given in Table A1.2).

$10^5 [S] / M$	[77h] = 60 μM	[77h] = 100 μM
	$v_i / M^{-1}s^{-1}$	v_i / Ms^{-1}
5.0	-	7.63×10^{-8}
7.5	-	9.77×10^{-8}
10	2.19×10^{-7}	1.38×10^{-7}
25	5.56×10^{-7}	3.72×10^{-7}
50	1.02×10^{-6}	6.55×10^{-7}
75	1.46×10^{-6}	9.85×10^{-7}
100	1.81×10^{-6}	1.28×10^{-6}

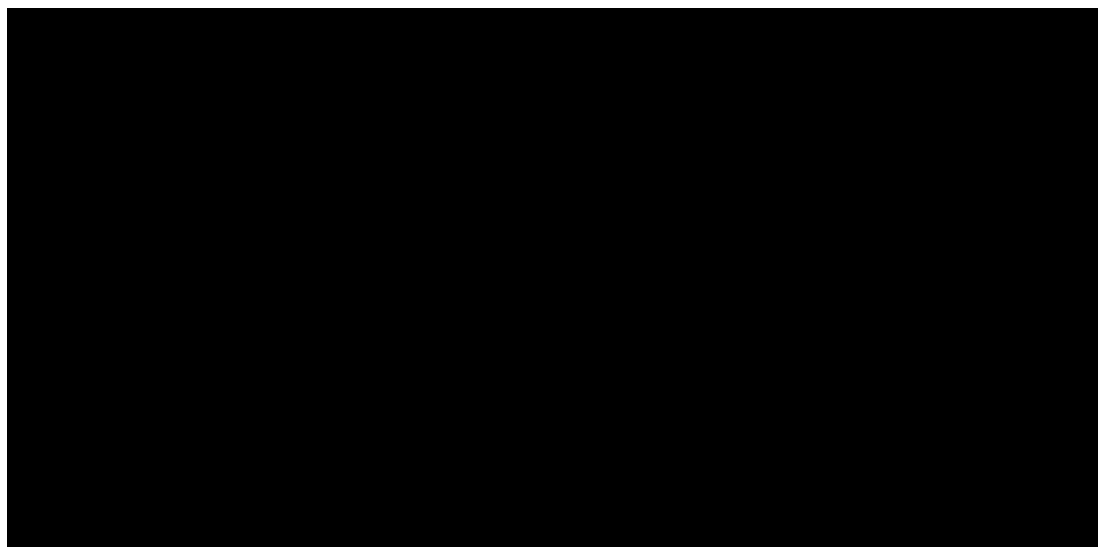


Figure A3.5 - Michaelis-Menten plot for the hydrolysis of the chromogenic substrate of PPE, in the absence of inhibitor 77h (●), and in the presence of 30 μM (□) and 100 μM of 77h (▲), at 390 nm, 25 °C, in 0.1 M HEPES buffer, pH 7.2, 6% DMSO (v/v). Points are experimental and lines are from non-linear regression analysis of the data. From this data, the respective Lineweaver-Burke plot was obtained from linear analysis of data $1/v_i/M^{-1}s$ versus $1/[S]/M^{-1}$, as illustrated in Chapter 3, Section 3.4.1, Figure 3.19.

A.3.2.3 Molecular Modeling of 77h at the Active Site of PPE.

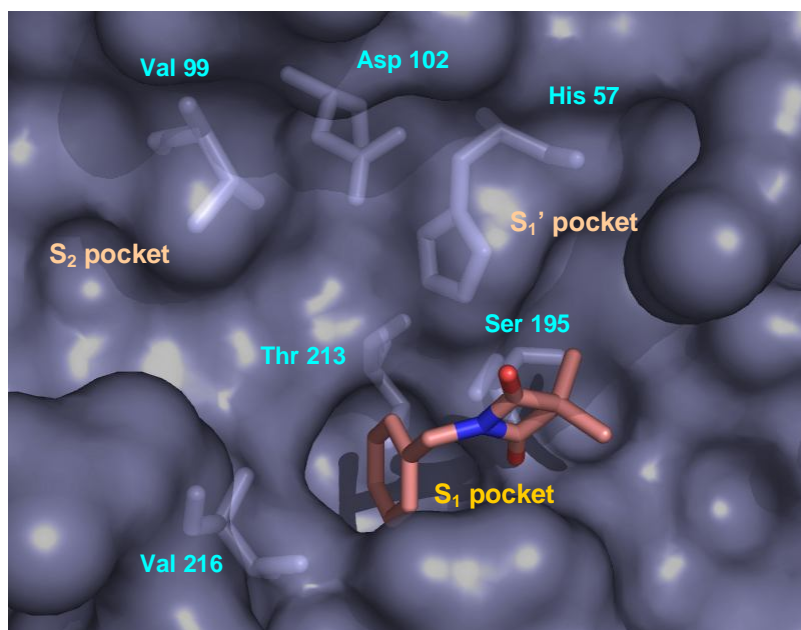


Figure A3.6 - Docking of 77h at the active site of PPE. The aromatic ring of the *N*-benzyl moiety lies in the S₁ pocket of PPE.

APPENDIX 4

A4.1 HLE Inactivation Studies by 4-Oxo- β -lactams (77 and 103)

A4.1.1 Obtained Pseudo-First Order Rate Constants of HLE Inhibition

Table A4.1 - Pseudo-first-order rate constant, k_{obs} , for the inactivation of HLE by 4-oxo- β -lactams 77 and 103, at 25 °C, in 0.1 M HEPES buffer, pH 7.2.

77a		77b	
10^6 [77a] / M	$10^3 k_{obs} / s^{-1}$	10^6 [77b] / M	$10^3 k_{obs} / s^{-1}$
2.5	1.54	3.0	1.95
10	1.83	10	3.50
25	3.54	30	8.23
50	6.17	75	19.40

77c		77d	
10^9 [77c] / M	$10^3 k_{obs} / s^{-1}$	10^9 [77d] / M	$10^3 k_{obs} / s^{-1}$
50	3.61	75	4.19
150	9.02	150	7.79
300	15.2	300	13.2
500	22.8	500	16.9

77e		77f	
10^9 [77e] / M	$10^3 k_{obs} / s^{-1}$	10^9 [77f] / M	$10^3 k_{obs} / s^{-1}$
50	2.95	50	3.52
100	5.12	100	6.29
150	6.24	300	15.2
300	11.8	500	20.3
600	21.3	750	23.6

77g

$10^9 [77g] / M$	$10^3 k_{obs} / s^{-1}$
50	3.98
80	5.24
100	6.58
250	12.2
500	17.5

77h

$10^6 [77h] / M$	$10^3 k_{obs} / s^{-1}$
1.50	2.58
3.00	4.45
7.50	8.57
30.0	27.3

77i

$10^9 [77i] / M$	$10^3 k_{obs} / s^{-1}$
50.0	6.94
100	13.52
250	19.07
500	33.02

77j

$10^6 [77j] / M$	$10^3 k_{obs} / s^{-1}$
2.5	1.96
5.0	2.15
10.0	2.68
20.0	4.58

77k

$10^9 [77k] / M$	$10^3 k_{obs} / s^{-1}$
100	2.85
200	4.39
500	9.51
1000	15.3

77l

$10^9 [77l] / M$	$10^3 k_{obs} / s^{-1}$
75	3.18
100	3.44
250	7.03
375	10.04
500	12.4

77m

$10^6 [77m] / M$	$10^3 k_{obs} / s^{-1}$
0.5	1.88
2.0	2.44
5.0	4.60
10	7.68
20	13.4

77n

$10^9 [77n] / M$	$10^3 k_{obs} / s^{-1}$
500	2.55
750	3.22
1000	4.26
1500	5.82
2000	8.53

77o

$10^6 [77o] / \text{M}$	$10^3 k_{obs} / \text{s}^{-1}$
2.0	1.76
4.0	2.04
5.0	2.72
7.5	2.89
10	3.96
15	5.06
20	6.74

77p

$10^6 [77p] / \text{M}$	$10^3 k_{obs} / \text{s}^{-1}$
20	2.25
38	2.72
50	3.38

77q

$10^6 [77q] / \text{M}$	$10^3 k_{obs} / \text{s}^{-1}$
0.50	12.9

77r

$10^9 [77r] / \text{M}$	$10^3 k_{obs} / \text{s}^{-1}$
50.0	2.68
100	4.07
200	7.17
300	12.6
400	16.0

103a

$10^6 [103a] / \text{M}$	$10^3 k_{obs} / \text{s}^{-1}$
0.5	2.35
1.0	2.83
2.5	3.87
5.0	4.48

103b

$10^6 [103b] / \text{M}$	$10^3 k_{obs} / \text{s}^{-1}$
0.50	2.22
1.25	3.09
2.50	5.08
5.00	5.95
10.0	6.31

103c

$10^6 [103c] / \text{M}$	$10^3 k_{obs} / \text{s}^{-1}$
0.50	2.83
1.25	5.24
2.50	9.15
5.00	14.23
10.0	15.15

103d

$10^6 [103d] / \text{M}$	$10^3 k_{obs} / \text{s}^{-1}$
2.0	1.94
5.0	2.17
20	5.06
40	8.63
50	10.0

103e

10^9 [103e] / M	$10^3 k_{obs} / s^{-1}$
6.25	4.07
12.5	4.41
25.0	5.57
37.5	8.74
50.0	10.7

103f

10^9 [103f] / M	$10^3 k_{obs} / s^{-1}$
6.25	3.18
12.5	5.24
25.0	6.03
50.0	7.84
75.0	8.80

103g

10^9 [103g] / M	$10^3 k_{obs} / s^{-1}$
6.25	3.43
12.5	4.55
25.0	6.21
37.5	8.31
50.0	8.87

103h

10^9 [103h] / M	$10^3 k_{obs} / s^{-1}$
6.25	2.21
12.5	3.79
25.0	7.58
37.5	11.98

103i

10^9 [103i] / M	$10^3 k_{obs} / s^{-1}$
6.25	3.74
12.5	6.13
25.0	12.6
37.5	17.1

103j

10^6 [103j] / M	$10^3 k_{obs} / s^{-1}$
10.0	3.80
25.0	6.55
50.0	8.77
75.0	14.4
100	18.3

103k

10^9 [103k] / M	$10^3 k_{obs} / s^{-1}$
6.25	4.07
12.5	4.41
25.0	5.57
37.5	8.74
50.0	10.7

A4.1.2 Plots of the pseudo-first-order rate constants, k_{obs} , versus the inhibitor concentration for HLE inhibition by 77 and 103, in accordance to the mechanism A of Figure 2.28.

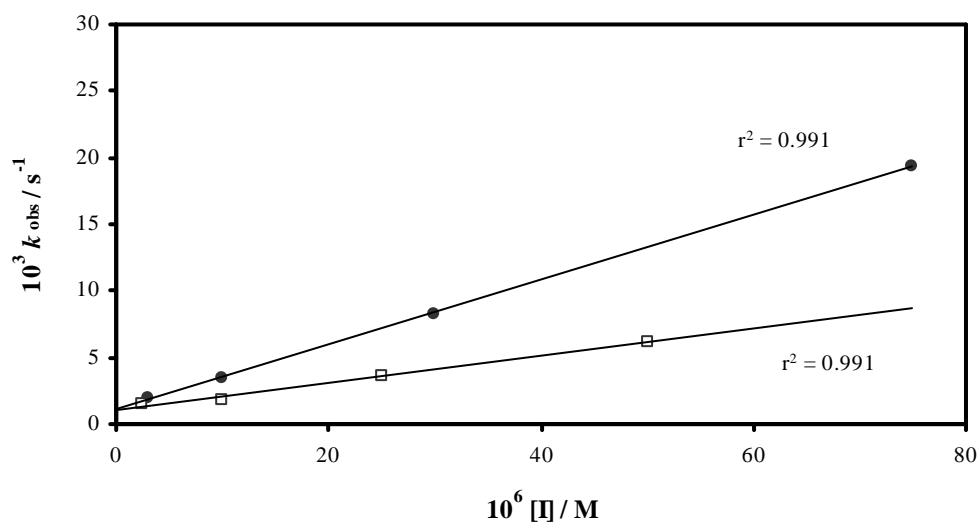


Figure A4.1 - Effect of inhibitor concentration on the onset of inhibition of HLE by 77a (\square) and 77b (\bullet). Points are experimental and the lines are from linear regression analysis of the data, giving $k_{\text{on}}' = (1.01 \pm 0.05) \times 10^2 \text{ M}^{-1}\text{s}^{-1}$ for 77a and $k_{\text{on}}' = (2.43 \pm 0.03) \times 10^2 \text{ M}^{-1}\text{s}^{-1}$ for 77b. By correction using Equation 2.8, $k_{\text{on}} = (7.33 \pm 0.34) \times 10^2 \text{ M}^{-1}\text{s}^{-1}$ for 77a and $k_{\text{on}} = (1.76 \pm 0.02) \times 10^3 \text{ M}^{-1}\text{s}^{-1}$ for 77b.

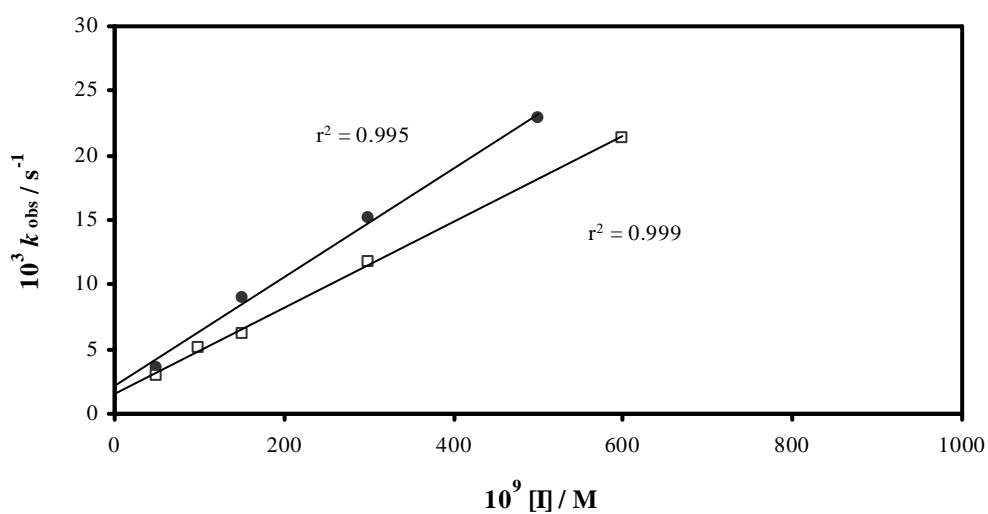


Figure A4.2 - Effect of inhibitor concentration on the onset of inhibition of HLE by 77c (\bullet) and 77e (\square). Points are experimental and the lines are from linear regression analysis of the data, giving k_{on}'

$= (4.21 \pm 0.21) \times 10^4 \text{ M}^{-1}\text{s}^{-1}$ for **77c**; and $k_{\text{on}}' = (3.32 \pm 0.07) \times 10^4 \text{ M}^{-1}\text{s}^{-1}$ for **77e**. By correction using Equation 2.8, $k_{\text{on}} = (3.05 \pm 0.16) \times 10^5 \text{ M}^{-1}\text{s}^{-1}$ for **77c** and $(2.41 \pm 0.05) \times 10^5 \text{ M}^{-1}\text{s}^{-1}$ for **77e**.

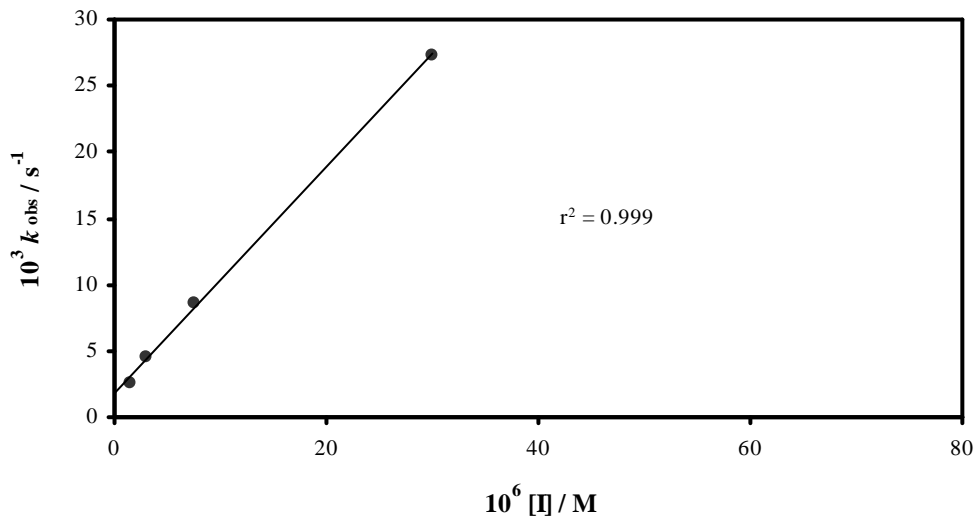


Figure A4.3 - Effect of inhibitor concentration on the onset of inhibition of HLE by 77h. Points are experimental and the line is from linear regression analysis of the data, giving $k_{\text{on}}' = (8.57 \pm 0.19) \times 10^2 \text{ M}^{-1}\text{s}^{-1}$. By correction using Equation 2.8, $k_{\text{on}} = (6.21 \pm 0.14) \times 10^3 \text{ M}^{-1}\text{s}^{-1}$.

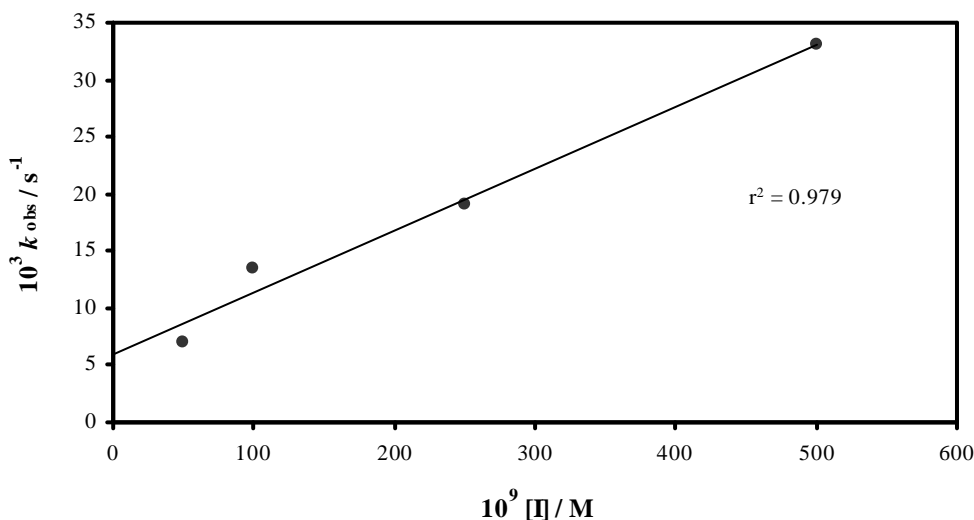


Figure A4.4 - Effect of inhibitor concentration on the onset of inhibition of HLE by 77i. Points are experimental and the line is from linear regression analysis of the data, giving $k_{\text{on}}' = (5.43 \pm 0.56) \times 10^4 \text{ M}^{-1}\text{s}^{-1}$. By correction using Equation 2.8, $k_{\text{on}} = (3.94 \pm 0.40) \times 10^5 \text{ M}^{-1}\text{s}^{-1}$.

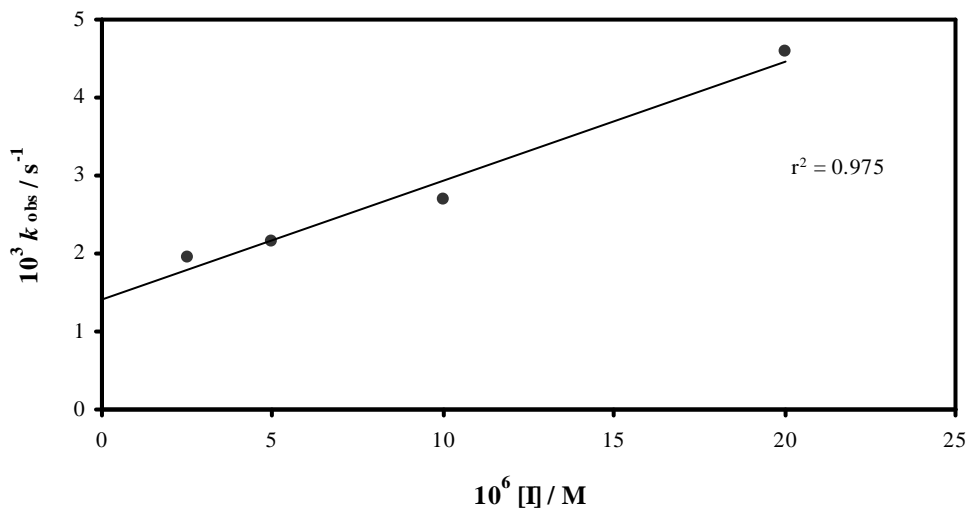


Figure A4.5 - Effect of inhibitor concentration on the onset of inhibition of HLE by 77j. Points are experimental and the line is from linear regression analysis of the data, giving $k_{on}' = (1.53 \pm 0.11) \times 10^2 \text{ M}^{-1}\text{s}^{-1}$. By correction using Equation 2.8, $k_{on} = (1.11 \pm 0.08) \times 10^3 \text{ M}^{-1}\text{s}^{-1}$.

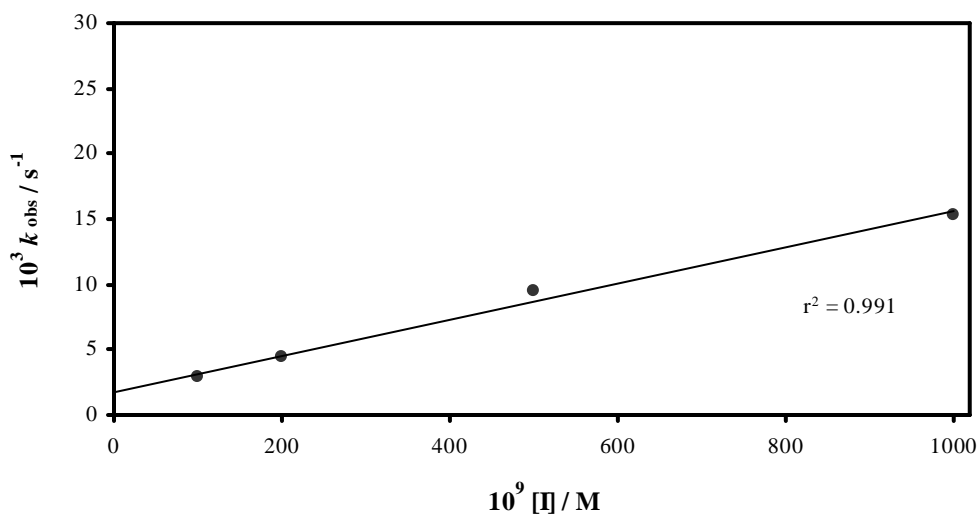


Figure A4.6 - Effect of inhibitor concentration on the onset of inhibition of HLE by 77k. Points are experimental and the line is from linear regression analysis of the data, giving $k_{on}' = (1.30 \pm 0.15) \times 10^4 \text{ M}^{-1}\text{s}^{-1}$. By correction using Equation 2.8, $k_{on} = (1.01 \pm 0.11) \times 10^5 \text{ M}^{-1}\text{s}^{-1}$.

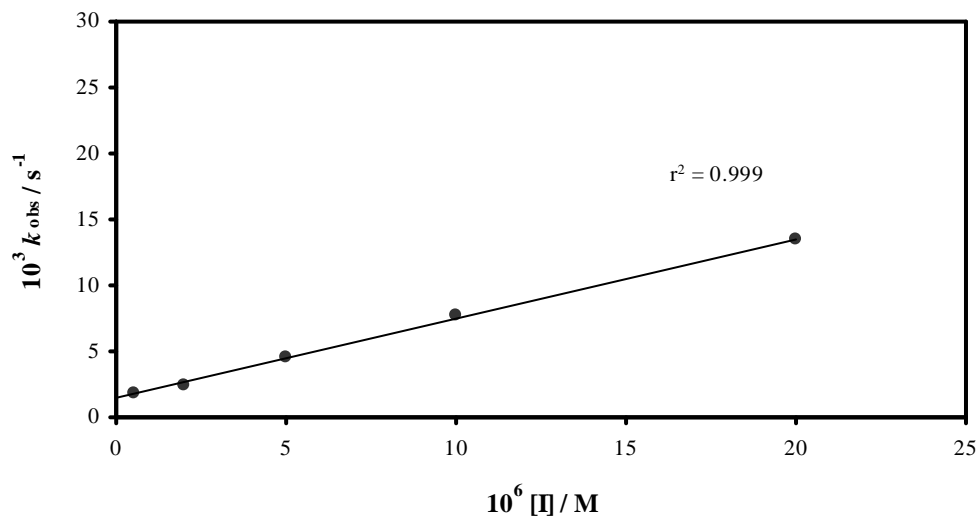


Figure A4.7 - Effect of inhibitor concentration on the onset of inhibition of HLE by 77m. Points are experimental and the line is from linear regression analysis of the data, giving $k_{on}' = (6.00 \pm 0.14) \times 10^2 M^{-1}s^{-1}$. By correction using Equation 2.8, $k_{on} = (4.35 \pm 0.10) \times 10^3 M^{-1}s^{-1}$.

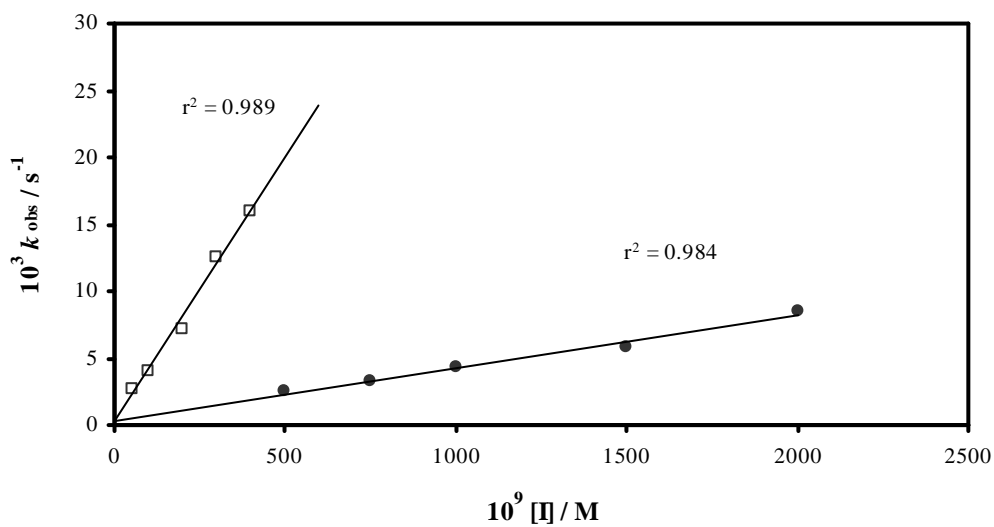


Figure A4.8 - Effect of inhibitor concentration on the onset of inhibition of HLE by 77n (●) and 77r (□). Points are experimental and the lines are from linear regression analysis of the data, giving $k_{on}' = (3.93 \pm 0.20) \times 10^3 M^{-1}s^{-1}$ for 77n and $k_{on}' = (3.94 \pm 0.17) \times 10^4 M^{-1}s^{-1}$ for 77r. By correction using Equation 2.8, $k_{on} = (2.85 \pm 0.14) \times 10^4 M^{-1}s^{-1}$ for 77n and $k_{on} = (2.86 \pm 0.12) \times 10^5 M^{-1}s^{-1}$ for 77r.

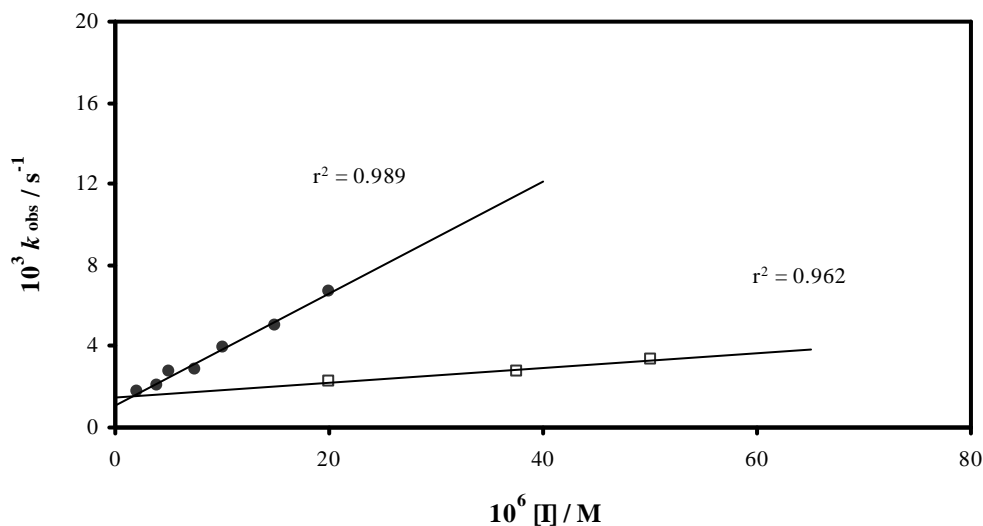


Figure A4.9 - Effect of inhibitor concentration on the onset of inhibition of HLE by **77o** (●) and **77p** (□). Points are experimental and the lines are from linear regression analysis of the data, giving $k_{on}' = (2.76 \pm 0.14) \times 10^2 \text{ M}^{-1}\text{s}^{-1}$ for **77o** and $k_{on}' = (3.68 \pm 0.41) \times 10^1 \text{ M}^{-1}\text{s}^{-1}$ for **77p**. By correction using Equation 2.8, $k_{on} = (2.00 \pm 0.10) \times 10^3 \text{ M}^{-1}\text{s}^{-1}$ for **77o** and $k_{on} = (2.67 \pm 0.30) \times 10^2 \text{ M}^{-1}\text{s}^{-1}$ for **77p**.

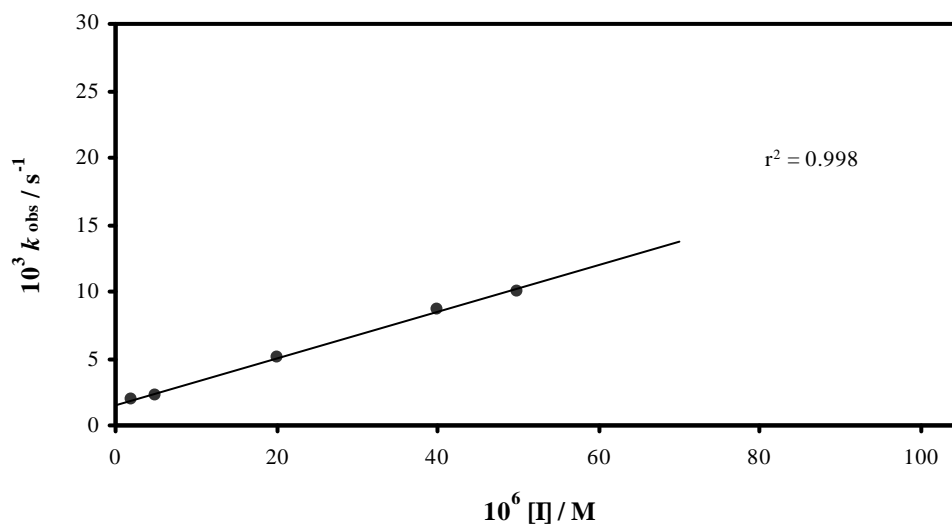


Figure A4.10 - Effect of inhibitor concentration on the onset of inhibition of HLE by **103d**. Points are experimental and the line is from linear regression analysis of the data, giving $k_{on}' = (1.74 \pm 0.04) \times 10^2 \text{ M}^{-1}\text{s}^{-1}$. By correction using Equation 2.8, $k_{on} = (1.26 \pm 0.03) \times 10^3 \text{ M}^{-1}\text{s}^{-1}$.

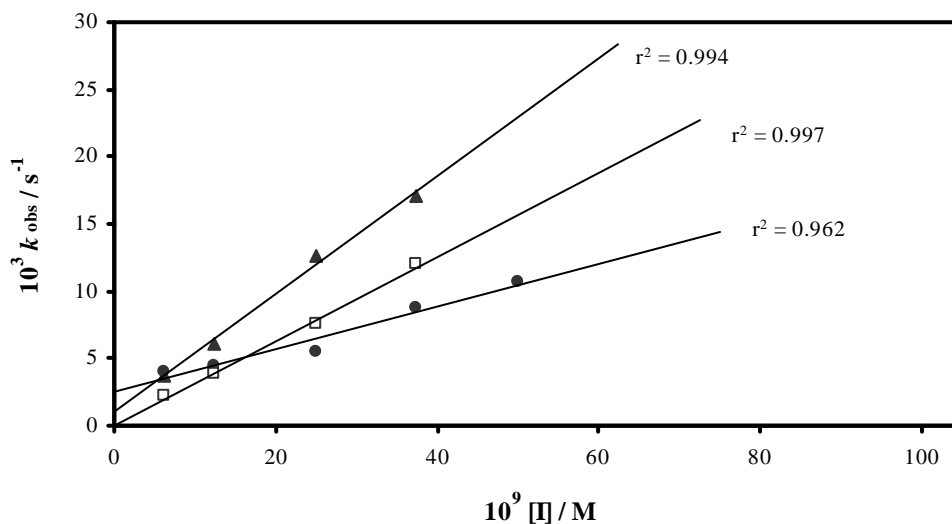


Figure A4.11 - Effect of inhibitor concentration on the onset of inhibition of HLE by **103e** (●), **103h** (□) and **103i** (▲). Points are experimental and the lines are from linear regression analysis of the data, giving $k_{on}' = (1.59 \pm 0.13) \times 10^5 \text{ M}^{-1}\text{s}^{-1}$ for **103e**, $(3.14 \pm 0.13) \times 10^5 \text{ M}^{-1}\text{s}^{-1}$ for **103h** and $(4.38 \pm 0.24) \times 10^5 \text{ M}^{-1}\text{s}^{-1}$ for **103i**. By correction using Equation 2.8, $k_{on} = (1.15 \pm 0.09) \times 10^6 \text{ M}^{-1}\text{s}^{-1}$ for **103e**, $(2.28 \pm 0.09) \times 10^6 \text{ M}^{-1}\text{s}^{-1}$ for **103h** and $(3.18 \pm 0.15) \times 10^6 \text{ M}^{-1}\text{s}^{-1}$ for **103i**.

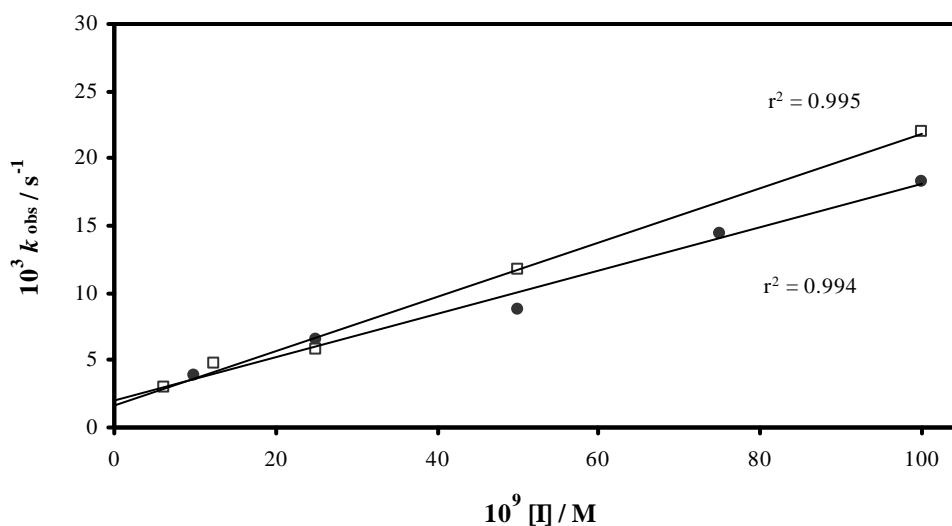


Figure A4.12 - Effect of inhibitor concentration on the onset of inhibition of HLE by **103j** (●) and **103k** (□). Points are experimental and the lines are from linear regression analysis of the data, giving $k_{on}' = (1.61 \pm 0.07) \times 10^5 \text{ M}^{-1}\text{s}^{-1}$ for **103j** and $(2.02 \pm 0.10) \times 10^5 \text{ M}^{-1}\text{s}^{-1}$ for **103k**. By correction using Equation 2.8 (Section 2.3.2.1), $k_{on} = (1.17 \pm 0.05) \times 10^6 \text{ M}^{-1}\text{s}^{-1}$ for **103j** and $k_{on} = (1.47 \pm 0.07) \times 10^6 \text{ M}^{-1}\text{s}^{-1}$ for **103k**.

A4.1.3 Determination of K_i for 4-oxo- β -lactams that inhibited HLE accordingly to the mechanism A of Figure 2.28.

Table A4.2 - The dependence of the steady-state rates, v_s , with the inhibitor concentration for HLE inhibition

77a		77b	
10^6 [77a] / M	$10^5 v_s / \text{Abs.s}^{-1}$	10^6 [77b] / M	$10^5 v_s / \text{Abs.s}^{-1}$
0	95.6	0	68.5
2.5	35.2	3.0	15.8
10	14.2	10	3.15
25	9.98	30	0.99
50	5.05	75	0.41

77c		77e	
10^9 [77c] / M	$10^5 v_s / \text{Abs.s}^{-1}$	10^9 [77e] / M	$10^5 v_s / \text{Abs.s}^{-1}$
0	55.2	0	59.3
50	5.45	50	10.3
150	1.26	100	3.49
300	0.63	150	2.20
500	0.26	300	0.97
		600	0.22

77h		77i	
10^6 [77h] / M	$10^5 v_s / \text{Abs.s}^{-1}$	10^9 [77i] / M	$10^5 v_s / \text{Abs.s}^{-1}$
0	54.69	0	67.01
1.50	7.56	50.0	47.93
3.00	4.56	100	44.08
7.50	1.89	250	26.66
30.0	0.54	500	17.42

77j

$10^6 [77j] / \text{M}$	$10^5 \nu_s / \text{Abs.s}^{-1}$
0	77.3
2.5	34.0
5.0	18.4
10.0	8.20
20.0	5.10

77k

$10^9 [77k] / \text{M}$	$10^5 \nu_s / \text{Abs.s}^{-1}$
0	68.8
100	9.78
200	4.91
500	2.21
1000	0.89

77m

$10^6 [77m] / \text{M}$	$10^5 \nu_s / \text{Abs.s}^{-1}$
0	71.1
0.5	25.3
2.0	4.15
5.0	2.47
10	1.50
20	0.90

77n

$10^9 [77n] / \text{M}$	$10^5 \nu_s / \text{Abs.s}^{-1}$
0	128.0
500	7.63
750	3.68
1000	0.00
1500	2.12
2000	1.41

77o

$10^6 [77o] / \text{M}$	$10^5 \nu_s / \text{Abs.s}^{-1}$
0	149.5
2.0	48.47
4.0	29.17
5.0	23.22
7.5	13.29
10	11.06
15	6.85
20	5.78

77p

$10^6 [77p] / \text{M}$	$10^5 \nu_s / \text{Abs.s}^{-1}$
0	151.6
20	81.57
37.5	71.89
50	66.50

77r

$10^9 [77r] / M$	$10^5 v_s / \text{Abs.s}^{-1}$
0	109.2
50.0	16.7
100	0.21
200	0.43
300	0.65
400	0.44

103d

$10^6 [103d] / M$	$10^5 v_s / \text{Abs.s}^{-1}$
0	71.21
2	31.85
5	13.95
20	4.93
40	2.41
50	1.61

103h

$10^9 [103h] / M$	$10^5 v_s / \text{Abs.s}^{-1}$
0	73.76
6.25	48.26
12.5	40.53
25.0	7.24
37.5	2.26

103j

$10^6 [103j] / M$	$10^5 v_s / \text{Abs.s}^{-1}$
10.0	3.80
25.0	6.55
50.0	8.77
75.0	14.4
100	18.3

103e

$10^9 [103e] / M$	$10^5 v_s / \text{Abs.s}^{-1}$
0	65.07
6.25	39.42
12.5	19.51
25.0	7.33
37.5	9.00
50.0	1.05

103i

$10^9 [103i] / M$	$10^5 v_s / \text{Abs.s}^{-1}$
0	73.20
6.25	37.77
12.5	10.17
25.0	1.60
37.5	0.99

103k

$10^9 [103k] / M$	$10^5 v_s / \text{Abs.s}^{-1}$
0	72.01
6.25	34.76
12.5	37.16
25.0	6.94
37.5	1.47
50.0	0.72

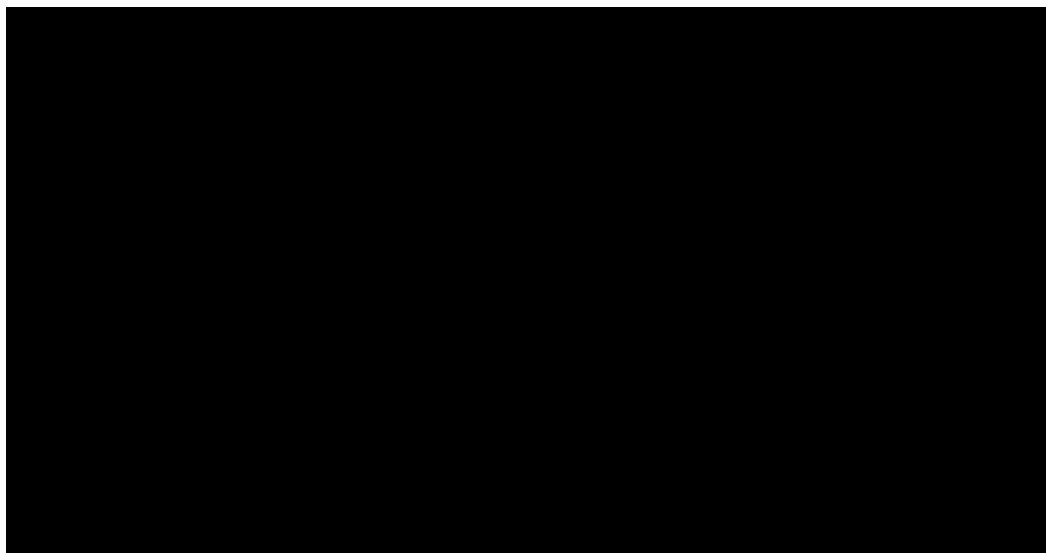


Figure A4.13 - Plot of the steady-state rate versus [I] for the inhibition of HLE by 77a. Points are experimental and the line is from non-linear regression analysis of data presented in Table A4.2, **77a**, using Equation 2.10, for $K_i' = 1590 \pm 200$ nM. After correction, the K_i value for **77a** is 219 ± 27.6 nM.

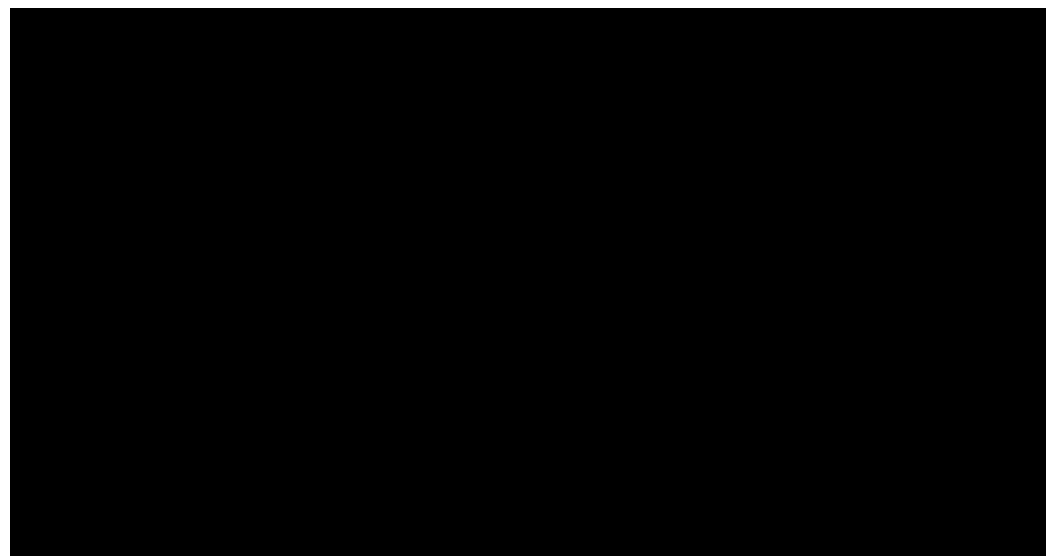


Figure A4.14 - Plot of the steady-state rate versus [I] for the inhibition of HLE by 77b. Points are experimental and the line is from non-linear regression analysis of data presented in Table A4.2, **77b**, using Equation 2.10, for $K_i' = 825 \pm 95.5$ nM. After correction, the K_i value for **77b** is 114 ± 13.2 nM.

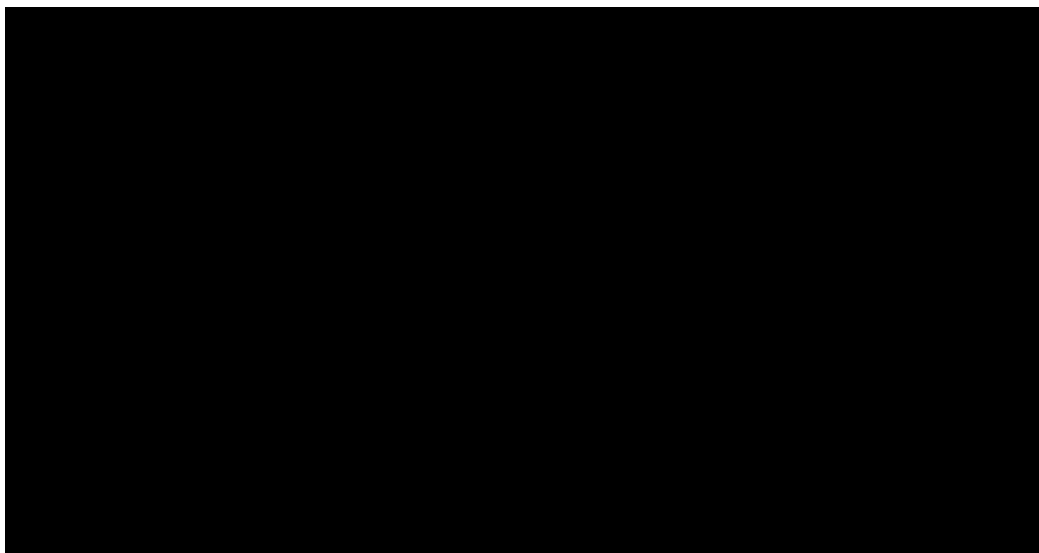


Figure A4.15 - Plot of the steady-state rate versus [I] for the inhibition of HLE by 77c. Points are experimental and the line is from non-linear regression analysis of data presented in Table A4.2, **77c**, using Equation 2.10, for $K_i' = 5.14 \pm 0.45$ nM. After correction, the K_i value for **77c** is 0.71 ± 0.06 nM.

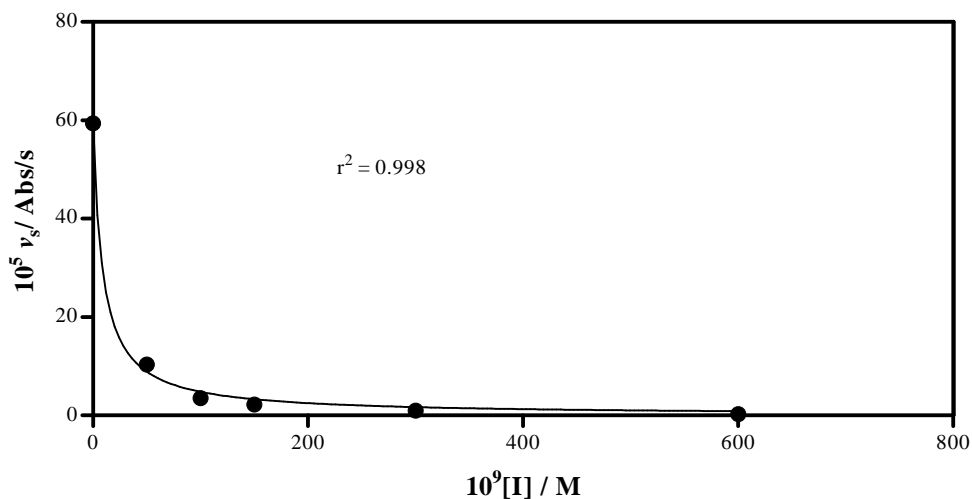


Figure A4.16 - Plot of the steady-state rate versus [I] for the inhibition of HLE by 77e. Points are experimental and the line is from non-linear regression analysis of data presented in Table A4.2, **77e**, using Equation 2.10, for $K_i' = 8.79 \pm 1.14$ nM. After correction, the K_i value for **77e** is 1.21 ± 0.16 nM.

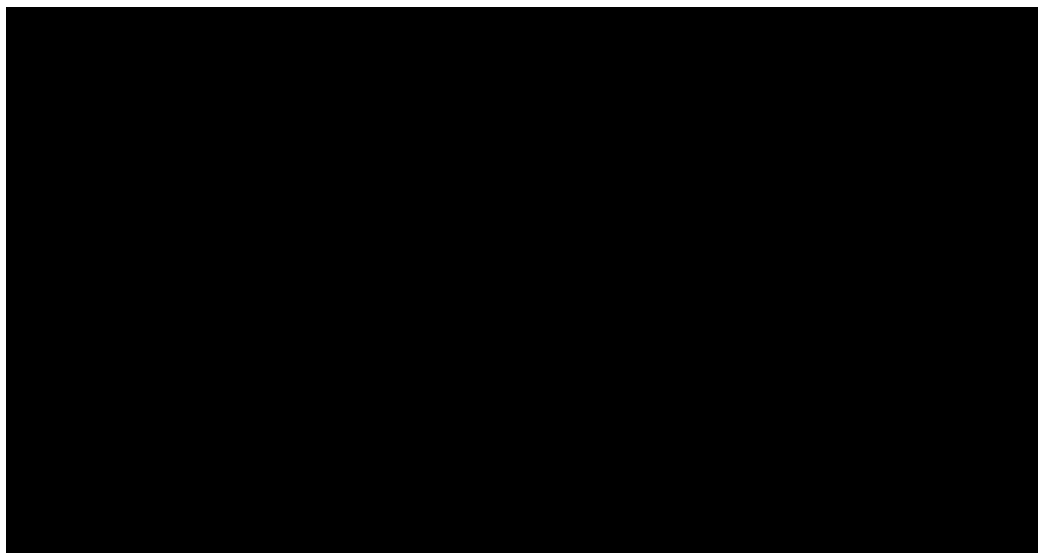


Figure A4.17 - Plot of the steady-state rate versus [I] for the inhibition of HLE by 77h. Points are experimental and the line is from non-linear regression analysis of data presented in Table A4.2, **77h**, using Equation 2.10, for $K_i' = 250 \pm 4.48$ nM. After correction, the K_i value for **77h** is 34.4 ± 1.17 nM.

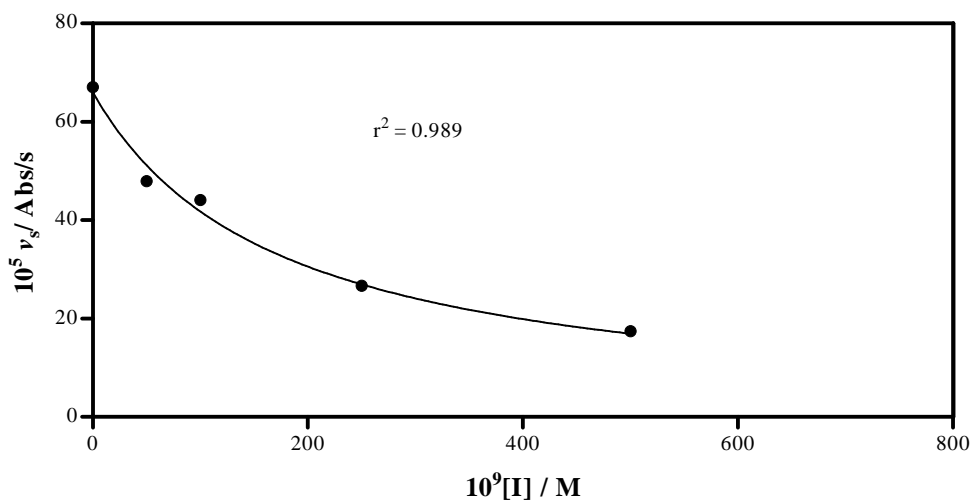


Figure A4.18- Plot of the steady-state rate versus [I] for the inhibition of HLE by 77i. Points are experimental and the line is from non-linear regression analysis of data presented in Table A4.2, **77i**, using Equation 2.10, for $K_i' = 173 \pm 20.3$ nM. After correction, the K_i value for **77i** is 23.8 ± 2.80 nM.

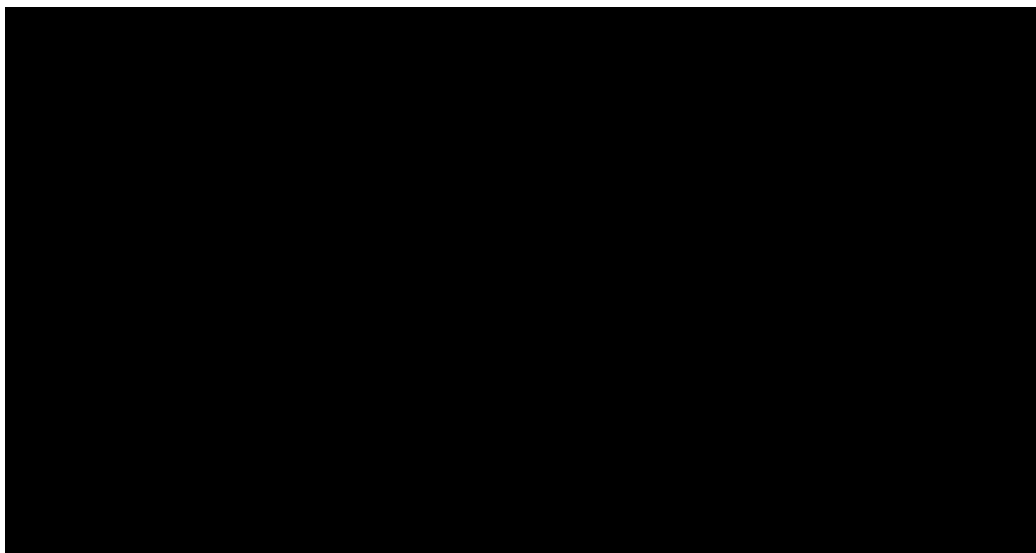


Figure A4.19 - Plot of the steady-state rate versus [I] for the inhibition of HLE by 77j. Points are experimental and the line is from non-linear regression analysis of data presented in Table A4.2, **77j**, using Equation 2.10, for $K_i' = 1687 \pm 180$ nM. After correction, the K_i value for **77j** is 233 ± 24.8 nM.

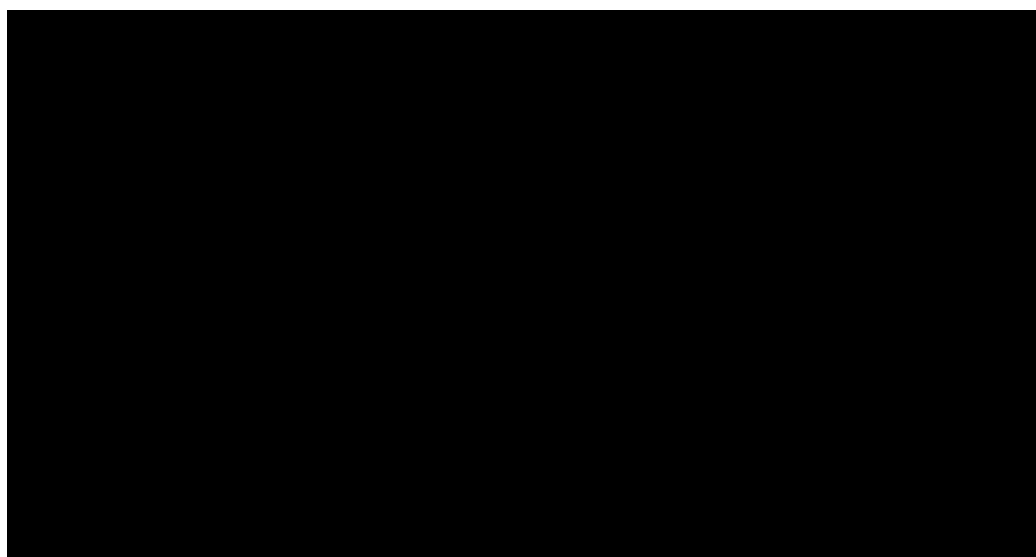


Figure A4.20 - Plot of the steady-state rate versus [I] for the inhibition of HLE by 77k. Points are experimental and the line is from non-linear regression analysis of data presented in Table A4.2, **77k**, using Equation 2.10, for $K_i' = 16.2 \pm 0.36$ nM. After correction, the K_i value for **77k** is 2.24 ± 0.05 nM.

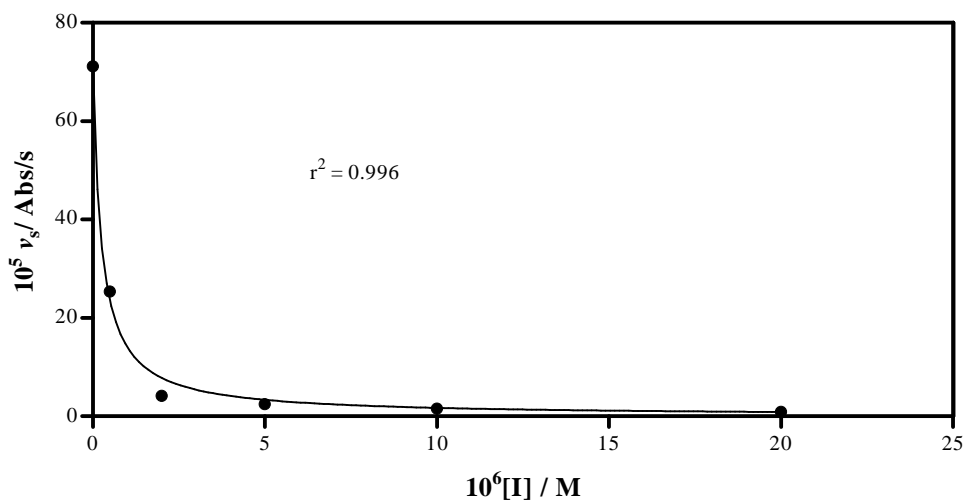


Figure A4.21 - Plot of the steady-state rate versus [I] for the inhibition of HLE by 77m. Points are experimental and the line is from non-linear regression analysis of data presented in Table A4.2, **77m**, using Equation 2.10, for $K_i' = 246 \pm 30.9$ nM. After correction, the K_i value for **77m** is 33.9 ± 4.26 nM.

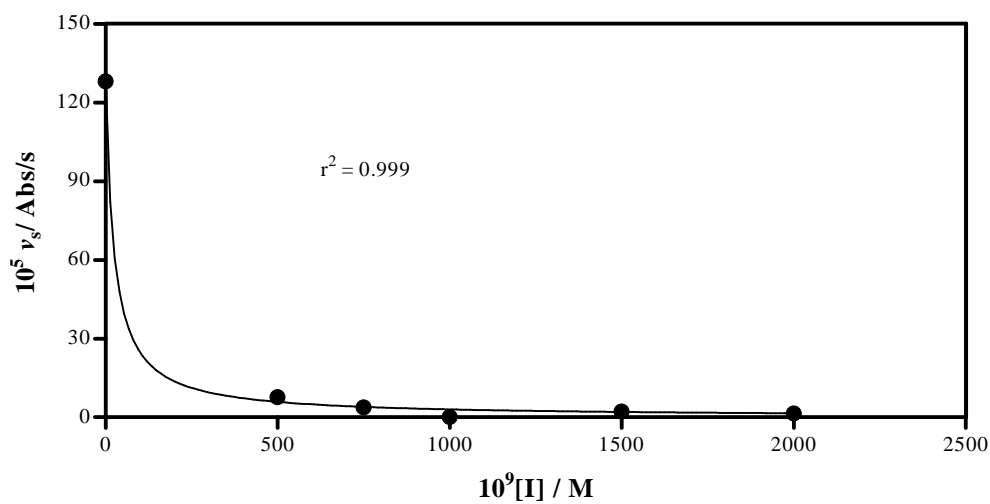


Figure A4.22 - Plot of the steady-state rate versus [I] for the inhibition of HLE by 77n. Points are experimental and the line is from non-linear regression analysis of data presented in Table A4.2, **77n**, using Equation 2.10, for $K_i' = 28.1 \pm 2.57$ nM. After correction, the K_i value for **77n** is 3.87 ± 0.35 nM.

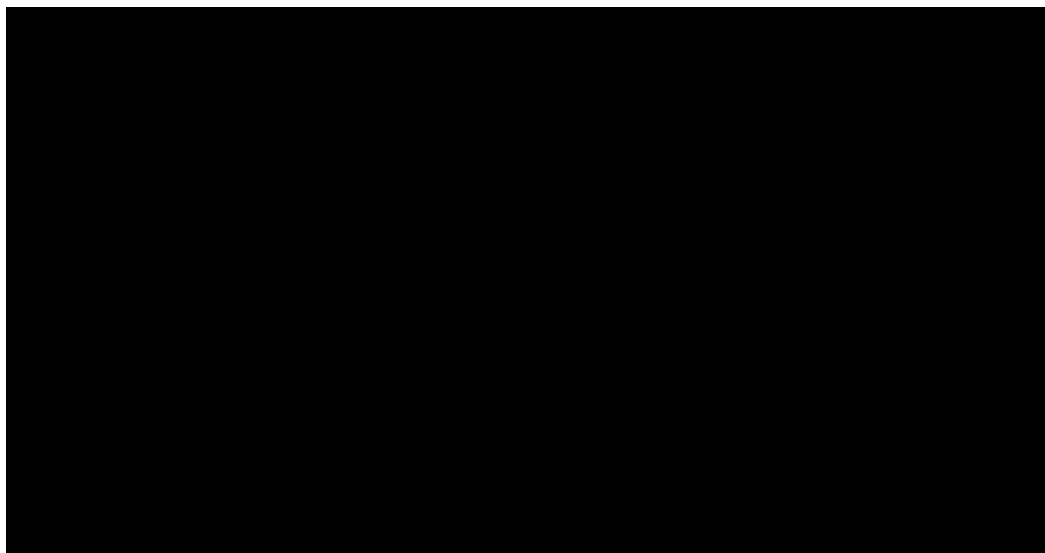


Figure A4.23 - Plot of the steady-state rate versus [I] for the inhibition of HLE by 77o. Points are experimental and the line is from non-linear regression analysis of data presented in Table A4.2, **77o**, using Equation 2.10, for $K_i' = 920 \pm 36.3$ nM. After correction, the K_i value for **77o** is 126 ± 5.01 nM.

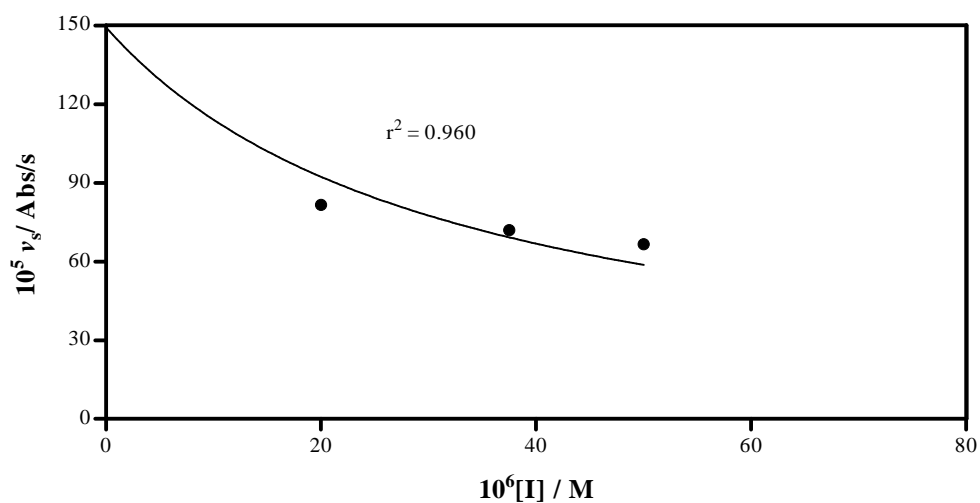


Figure A4.24 - Plot of the steady-state rate versus [I] for the inhibition of HLE by 77p. Points are experimental and the line is from non-linear regression analysis of data presented in Table A4.2, **77p**, using Equation 2.10, for $K_i' = 32200 \pm 6550$ nM. After correction, the K_i value for **77p** is 4450 ± 903 nM.

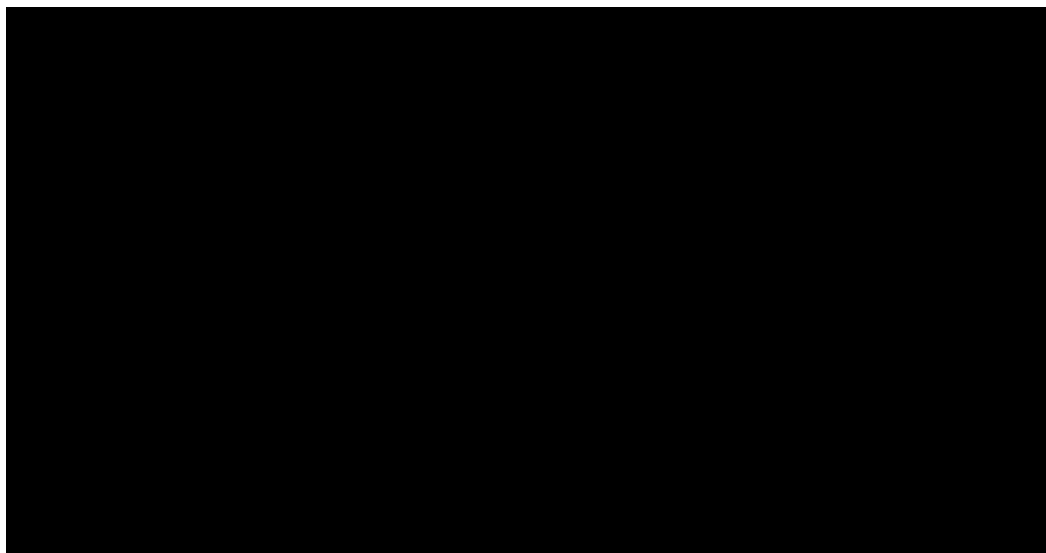


Figure A4.25 - Plot of the steady-state rate versus [I] for the inhibition of HLE by 77r. Points are experimental and the line is from non-linear regression analysis of data presented in Table A4.2, **77r**, using Equation 2.10, for $K_i' = 6.15 \pm 2.04$ nM. After correction, the K_i value for **77r** is 0.85 ± 0.28 nM.

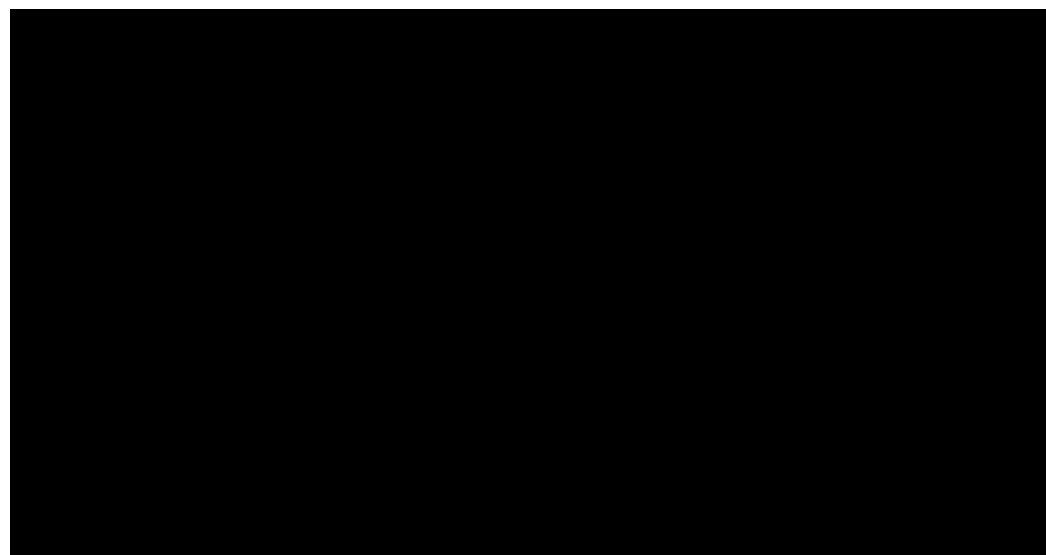


Figure A4.26 - Plot of the steady-state rate versus [I] for the inhibition of HLE by 103d. Points are experimental and the line is from non-linear regression analysis of data presented in Table A4.2, **103d**, using Equation 2.10, for $K_i' = 1470 \pm 104$ nM. After correction, the K_i value for **103d** is 203 ± 14 nM.

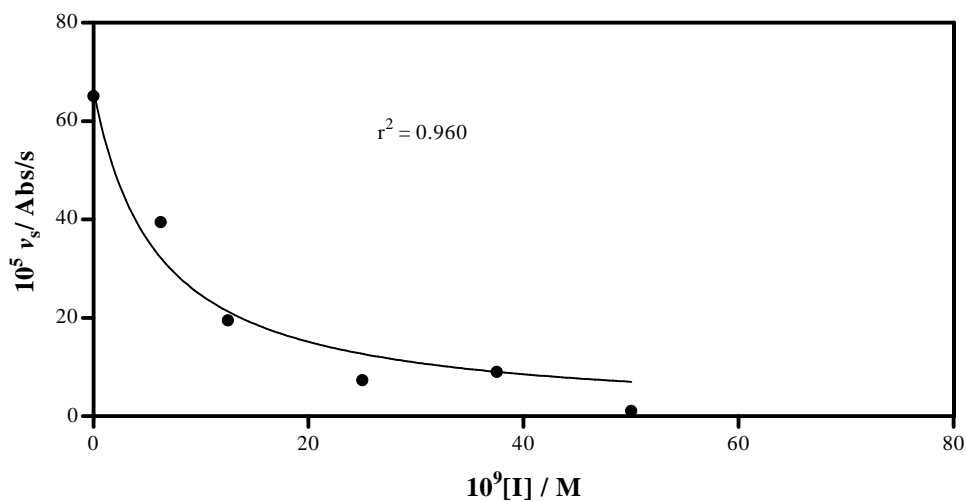


Figure A4.27 - Plot of the steady-state rate versus [I] for the inhibition of HLE by 103e. Points are experimental and the line is from non-linear regression analysis of data presented in Table A4.2, **103e**, using Equation 2.10, for $K_i' = 5.91 \pm 1.45$ nM. After correction, the K_i value for **103e** is 0.82 ± 0.20 nM.

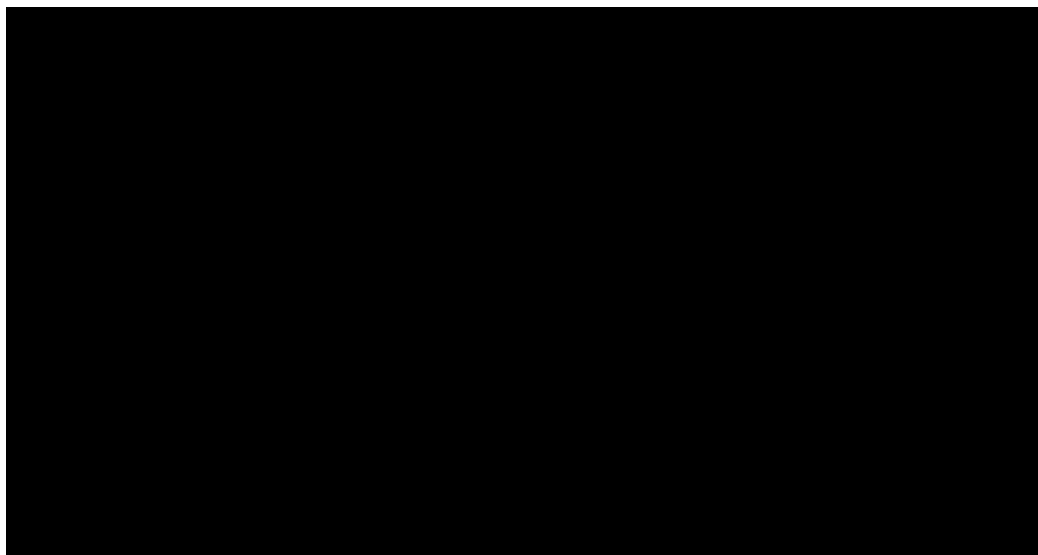


Figure A4.28 - Plot of the steady-state rate versus [I] for the inhibition of HLE by 103h. Points are experimental and the line is from non-linear regression analysis of data presented in Table A4.2, **103h**, using Equation 2.10, for $K_i' = 8.17 \pm 3.68$ nM. After correction, the K_i value for **103h** is 1.12 ± 0.51 nM.

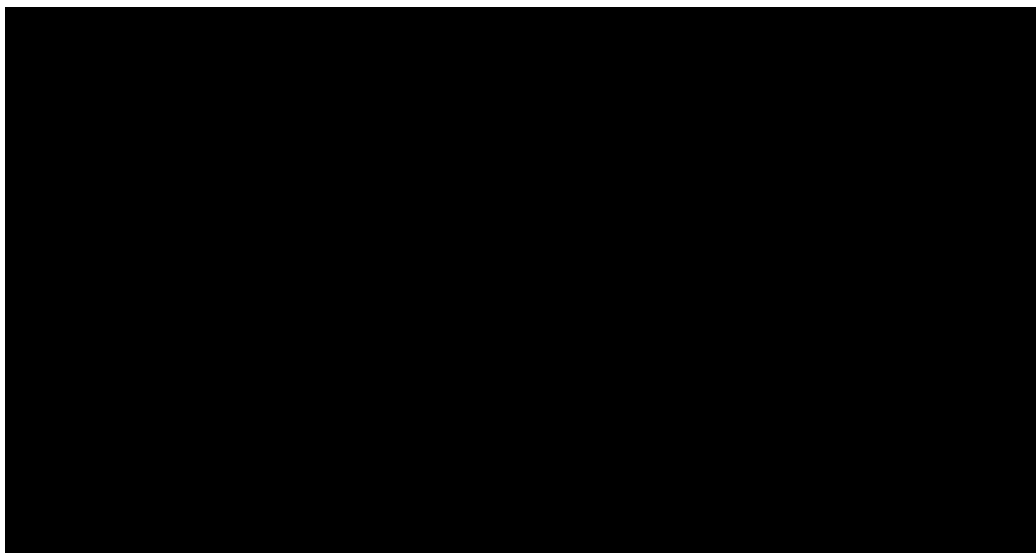


Figure A4.29 - Plot of the steady-state rate versus [I] for the inhibition of HLE by **103i**. Points are experimental and the line is from non-linear regression analysis of data presented in Table A4.2, **103i**, using Equation 2.10, for $K_i' = 3.64 \pm 1.52$ nM. After correction, the K_i value for **103i** is 0.50 ± 0.21 nM.

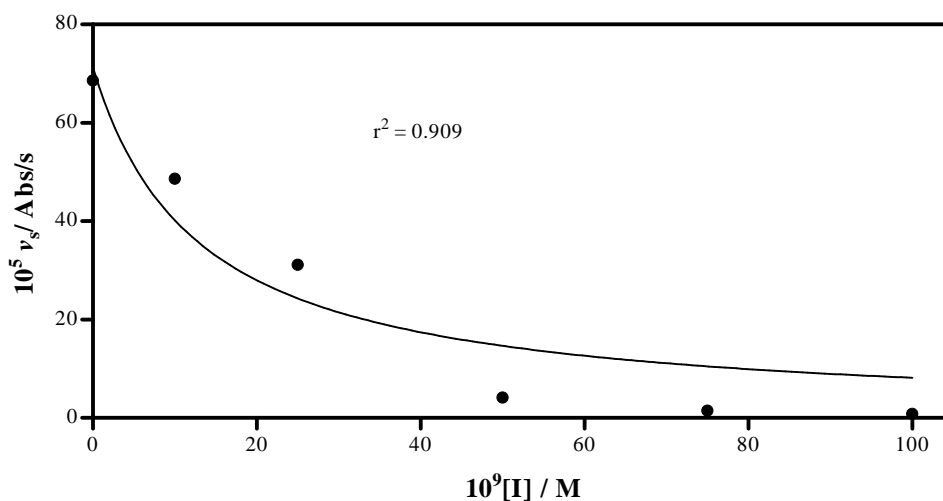


Figure A4.30 - Plot of the steady-state rate versus [I] for the inhibition of HLE by **103j**. Points are experimental and the line is from non-linear regression analysis of data presented in Table A4.2, **103j**, using Equation 2.10, for $K_i' = 12.9 \pm 5.20$ nM. After correction, the K_i value for **103j** is 1.78 ± 0.72 nM.

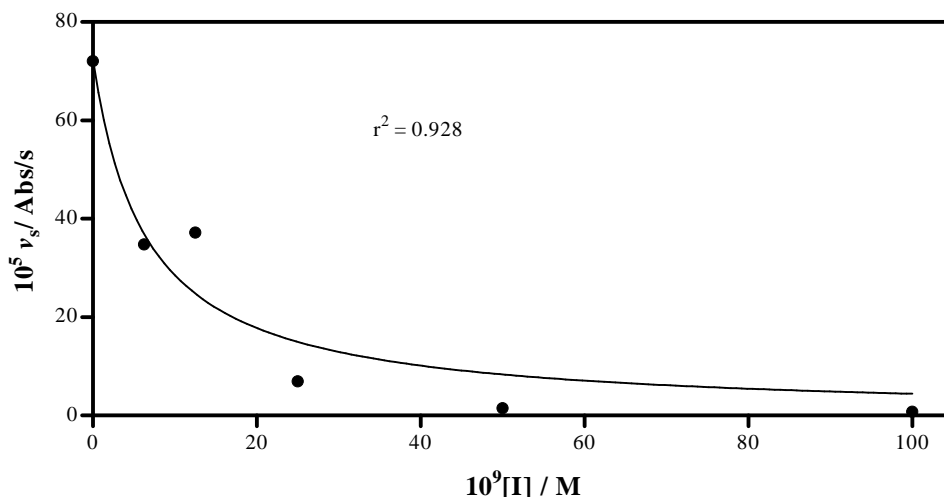


Figure A4.31 - Plot of the steady-state rate versus [I] for the inhibition of HLE by 103k. Points are experimental and the line is from non-linear regression analysis of data presented in Table A4.2, **103k**, using Equation 2.10, for $K_i' = 6.52 \pm 2.30$ nM. After correction, the K_i value for **103k** is 0.90 ± 0.32 nM.

A4.1.4 - Determination of Kinetic Parameters for HLE Inhibition that Conforms to the Mechanism B of Figure 2.28

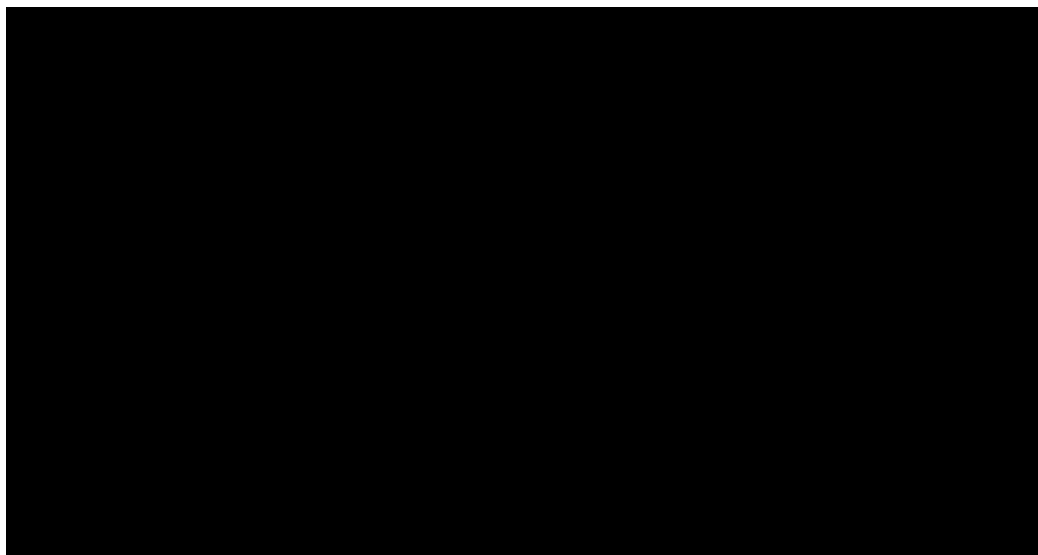


Figure A4.32 - Plot of the pseudo-first order rate constants for HLE inhibition by compound 77d. Points are experimental and the line is from non-linear regression analysis of data presented in Table A4.1, **77d**, using Equation 2.13, for $k_{inact} = (3.12 \pm 0.20) \times 10^{-2} s^{-1}$, $K_i' = 349 \pm 87$ nM. After correction, the K_i value for **77d** is 48.2 ± 12.0 nM. The k_{off} is impossible to tell apart from zero.

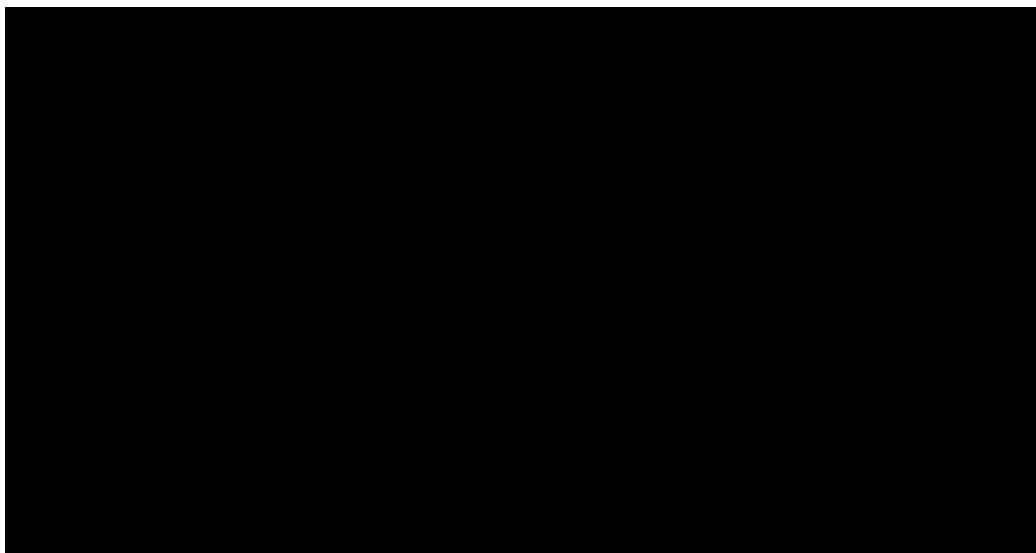


Figure A4.33 - Plot of the pseudo-first order rate constants for HLE inhibition by compound 77f. Points are experimental and the line is from non-linear regression analysis of data presented in Table A4.1, **77f**, using Equation 2.13, for $k_{\text{inact}} = (3.83 \pm 0.17) \times 10^{-2} \text{ s}^{-1}$, $K_i' = 420 \pm 63.2 \text{ nM}$. After correction, the K_i value for **77f** is $57.9 \pm 8.71 \text{ nM}$. The k_{off} is impossible to tell apart from zero.

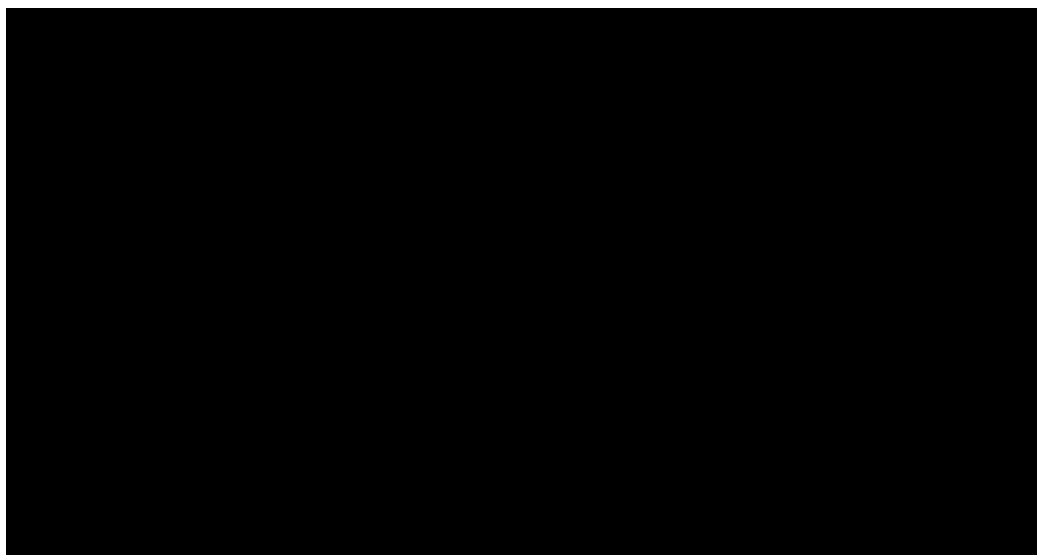


Figure A4.34 - Plot of the pseudo-first order rate constants for HLE inhibition by compound 77g. Points are experimental and the line is from non-linear regression analysis of data presented in Table A4.1, **77g**, using Equation 2.13, for $k_{\text{inact}} = (3.23 \pm 0.22) \times 10^{-2} \text{ s}^{-1}$, $K_i' = 461 \pm 80.7 \text{ nM}$ and $k_{\text{off}} = (7.08 \pm 4.32) \times 10^{-2} \text{ s}^{-1}$. After correction, the K_i value for **77g** is $63.5 \pm 11.1 \text{ nM}$ and K_i^* , given by Equation 4.4, is 1.36 nM .

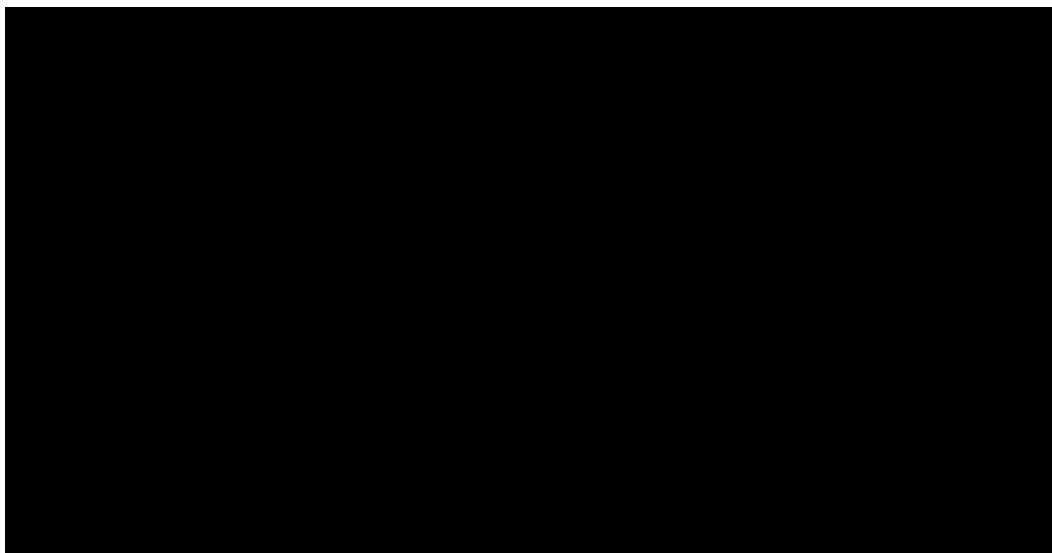


Figure A4.35 - Plot of the pseudo-first order rate constants for HLE inhibition by compound 103a. Points are experimental and the line is from non-linear regression analysis of data presented in Table A4.1, **103a**, using Equation 2.13, for $k_{\text{inact}} = (4.23 \pm 0.24) \times 10^{-2} \text{ s}^{-1}$, $K_i = 205 \pm 71 \text{ nM}$ and $k_{\text{off}} = (1.49 \pm 0.26) \times 10^{-2} \text{ s}^{-1}$. After correction, the K_i value for **103a** is $283 \pm 11.1 \text{ nM}$ and K_i^* , given by Equation 4.4, is 73.7 nM .

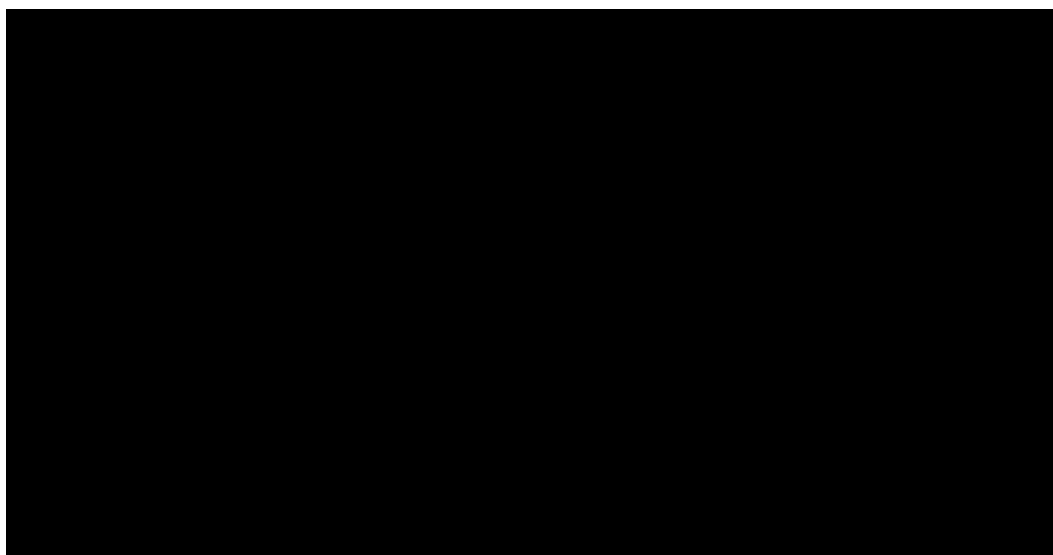


Figure A4.36 - Plot of the pseudo-first order rate constants for HLE inhibition by compound 103b. Points are experimental and the line is from non-linear regression analysis of data presented in Table A4.1, **103b**, using Equation 2.13, for $k_{\text{inact}} = (7.15 \pm 1.08) \times 10^{-2} \text{ s}^{-1}$, $K_i = 1490 \pm 980 \text{ nM}$ and $k_{\text{off}} = (2.74 \pm 1.14) \times 10^{-4} \text{ s}^{-1}$. After correction, the K_i value for **103b** is $205 \pm 135 \text{ nM}$ and K_i^* , given by Equation 4.4, is 7.57 nM .

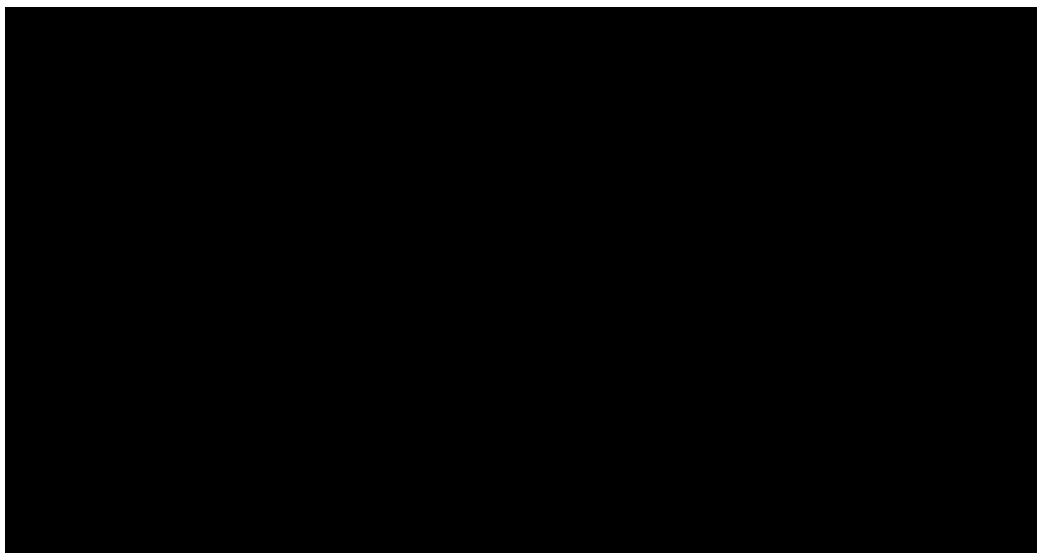


Figure A4.37 - Plot of the pseudo-first order rate constants for HLE inhibition by compound 103c. Points are experimental and the line is from non-linear regression analysis of data presented in Table A4.1, **103c**, using Equation 2.13, Section 2.3.2.2, for $k_{\text{inact}} = (2.12 \pm 0.23) \times 10^{-2} \text{ s}^{-1}$, $K_i' = 2560 \pm 1490 \text{ nM}$ and k_{off} is impossible to tell apart from zero. After correction, the K_i value for **103c** is $353 \pm 206 \text{ nM}$.

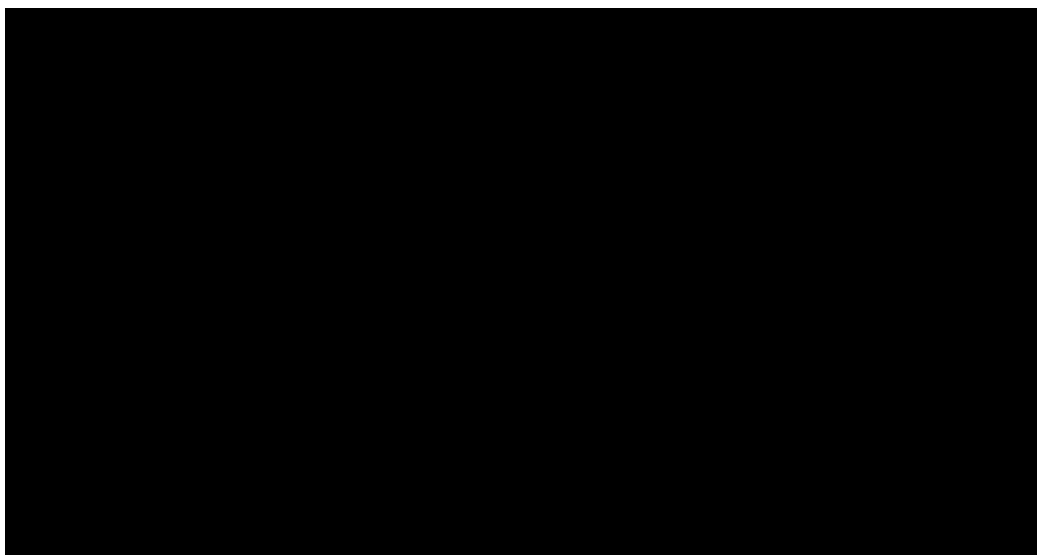


Figure A4.38 - Plot of the pseudo-first order rate constants for HLE inhibition by compound 103g. Points are experimental and the line is from non-linear regression analysis of data presented in Table A4.1, **103g**, using Equation 2.13, Section 2.3.2.2, for $k_{\text{inact}} = (1.68 \pm 0.42) \times 10^{-2} \text{ s}^{-1}$, $K_i' = 68.9 \pm 29 \text{ nM}$ and $k_{\text{off}} = (1.99 \pm 0.27) \times 10^{-3} \text{ s}^{-1}$. After correction, the K_i value for **103g** is $9.50 \pm 3.99 \text{ nM}$ and K_i^* , given by Equation 4.4, is 1.01 nM .

A4.1.5 - Titration of HLE Activity by 77g

Table A4.3 – Percentage of remaining HLE activity, v_t/v_i versus the initial ratio of inhibitor to enzyme, $[I]/[E]_0$, after a 30 min. incubation period with 77g at 25 °C.

$[I]/[E]_0$	v_t/v_i (%)
0	100
0.125	94.3
0.250	95.4
0.375	86.2
0.500	61.1
0.750	59.3
1.00	23.4
1.50	22.3
2.00	3.9
4.00	2.10

A4.2 Proteinase 3 Inhibition Studies

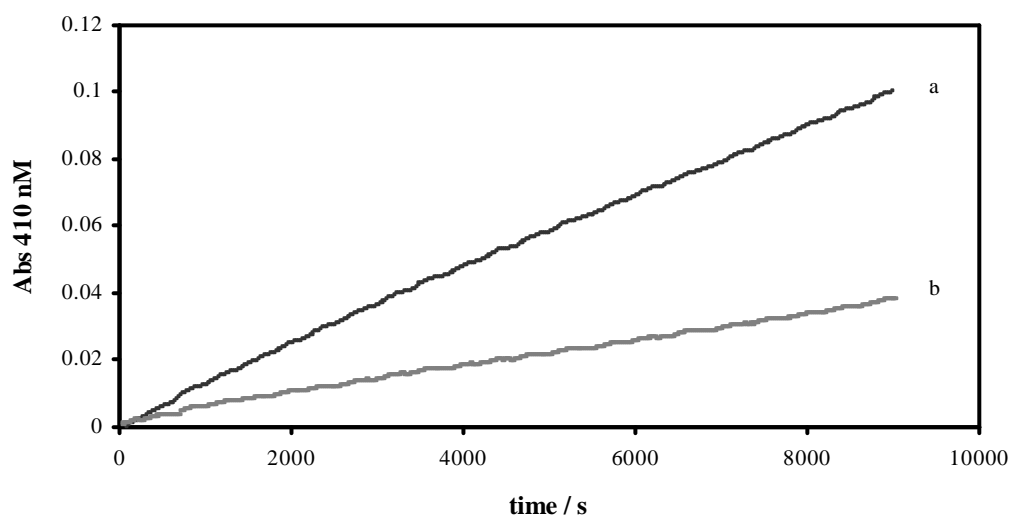


Figure A4.39 - Progress curve for PR3 inhibition by 103i. Reaction conditions: $[PR3] = 22.75$ nM, $[MeO-Suc-(L-Ala)_2-L-Pro-L-Val-p-NA] = 3.75$ mM, 0.1M, pH 7.2 HEPES buffer, 25 °C, (a) absence of inhibitor, (b) $[103i] = 50$ nM.

Table A4.4 - Pseudo-first-order rate constant, k_{obs} , for the time-dependent inactivation of PR3 by 4-oxo- β -lactams, at 25 °C, in 0.1 M, pH 7.2 HEPES buffer.

77o		103b	
10^6 [77o] / M	$10^4 k_{obs} / s^{-1}$	10^6 [103b] / M	$10^4 k_{obs} / s^{-1}$
30	6.06	1.0	3.61

103f		103g	
10^6 [77f] / M	$10^4 k_{obs} / s^{-1}$	10^9 [103g] / M	$10^4 k_{obs} / s^{-1}$
10	2.96	50	0.35

103i		103j	
10^9 [103g] / M	$10^4 k_{obs} / s^{-1}$	10^6 [103j] / M	$10^4 k_{obs} / s^{-1}$
50	20.4	10	12.2

103k	
10^9 [77k] / M	$10^4 k_{obs} / s^{-1}$
50	25.0

Table A4.5 – PR3 inhibition by 77g and 77p

77g	
$10^5 v_i / \text{Abs.s}^{-1}$ (in absence of 77g)	1.08
$10^5 v_i / \text{Abs.s}^{-1}$ (at [77g] = 10 μM)	0.91
Inhibitory activity 16%	

77p	
$10^5 v_i / \text{Abs.s}^{-1}$ (in absence of 77p)	0.91
$10^5 v_i / \text{Abs.s}^{-1}$ (at [77p] = 60 μM)	0.70
Inhibitory activity 22%	

A4.3 Cathepsin G Inhibition Studies

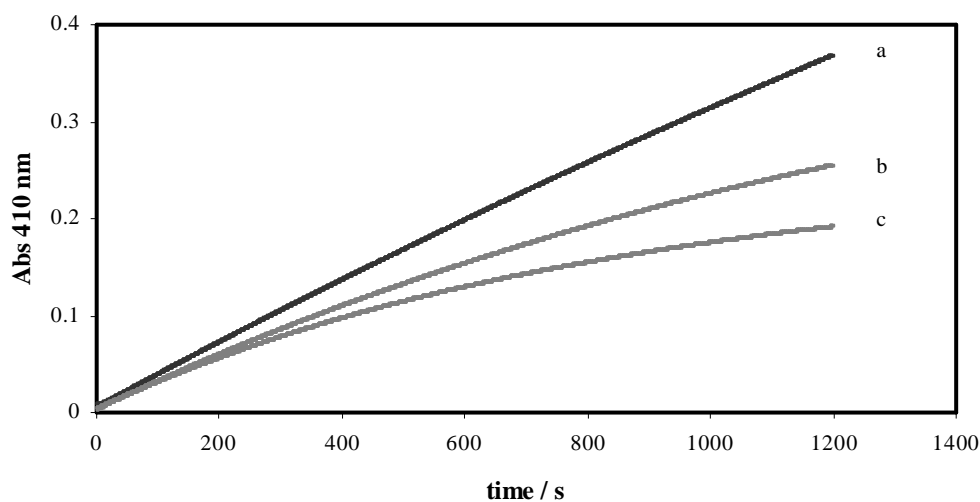


Figure A4.40 - Progress curve for Cat G inhibition by 77m. Reaction conditions: [Cat G] = 68 nM, [N-Suc-(L-Ala)₂-L-Pro-L-Phe-p-NA] = 0.85 mM, 0.1M, pH 7.5 HEPES buffer, 25 °C, (a) absence of inhibitor, (b) [77m] = 20 μM, (c) [77m] = 40 μM.

Table A4.6 - Pseudo-first-order rate constant, k_{obs} , for the time-dependent inactivation of Cat G by 4-oxo- β -lactams, at 25 °C, in 0.1 M, pH 7.5 HEPES buffer.

77g		77m	
10^6 [77g] / M	$10^4 k_{obs} / s^{-1}$	10^6 [77m] / M	$10^4 k_{obs} / s^{-1}$
60	21.9	20	7.99
		40	12.5

77r		103k	
10^6 [77r] / M	$10^4 k_{obs} / s^{-1}$	10^6 [103k] / M	$10^4 k_{obs} / s^{-1}$
20	9.46	40	16.6

A4.4 – Hydrolytic Stability Studies

A4.4.1 – Calibration curves

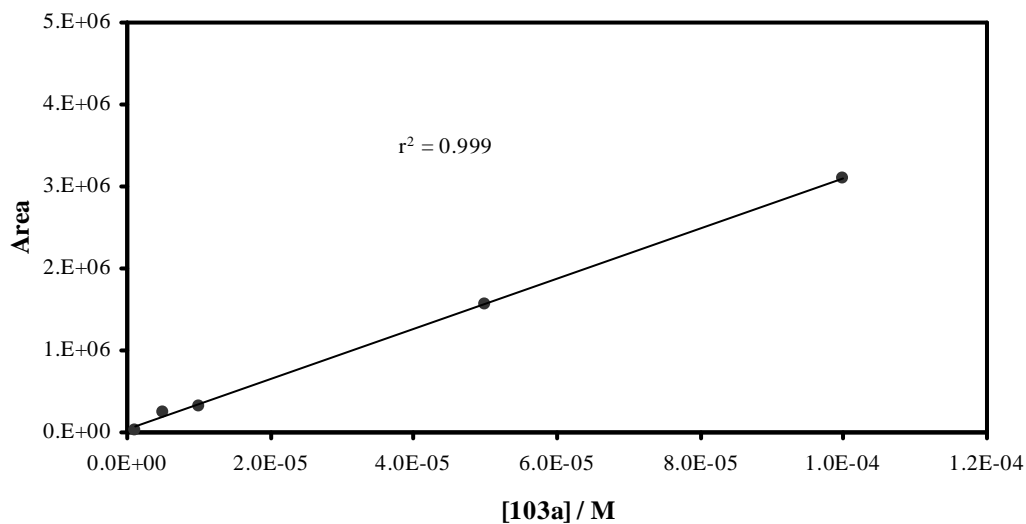


Figure A4.41 - Calibration curve for 103a. Points are experimental and the line is from linear regression analysis of data.

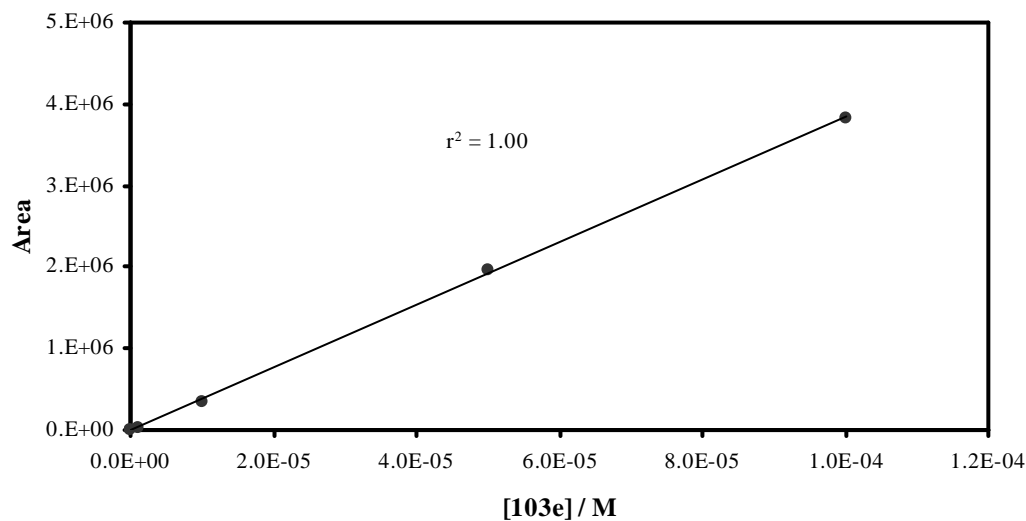


Figure A4.42 - Calibration curve for 103e. Points are experimental and the line is from linear regression analysis of data.

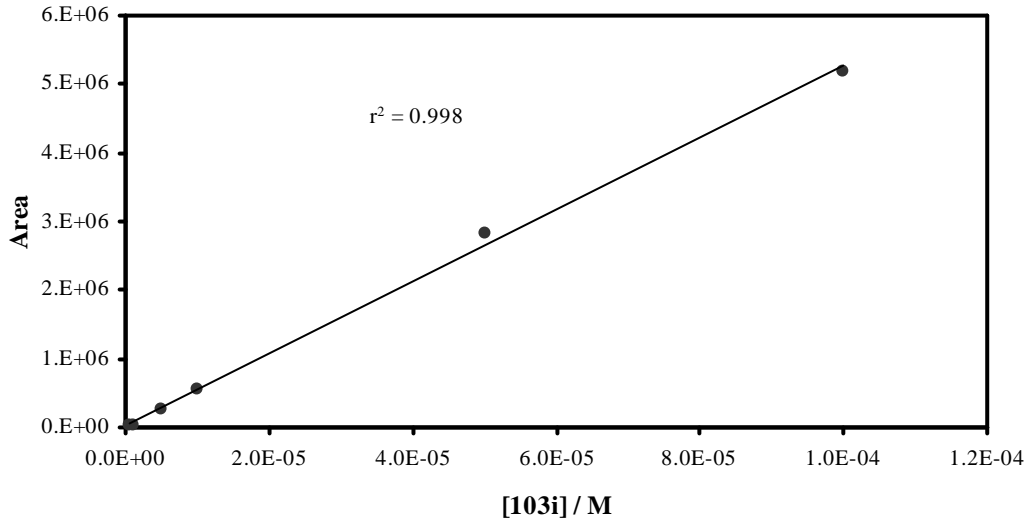


Figure A4.43 - Calibration curve for 103i. Points are experimental and the line is from linear regression analysis of data.

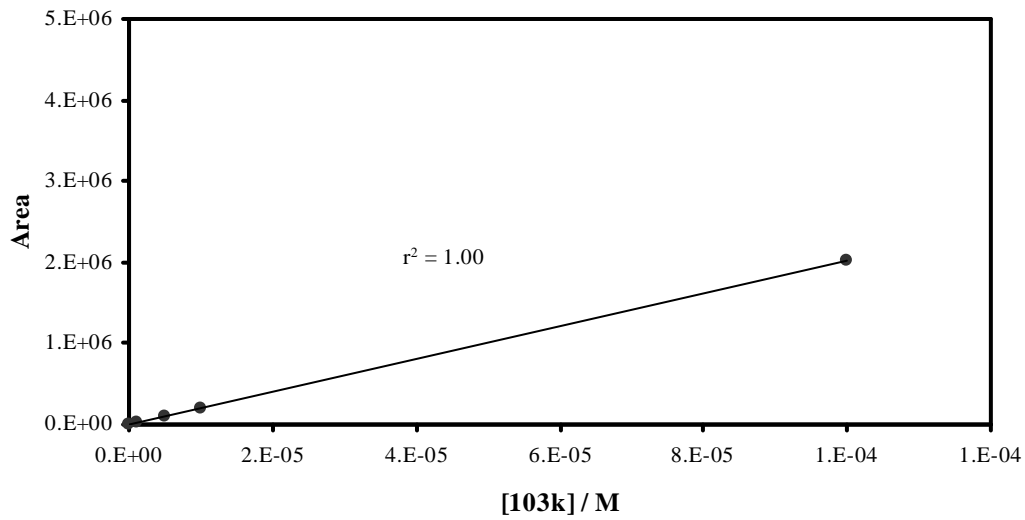


Figure A4.44 - Calibration curve for 103k. Points are experimental and line is from linear regression analysis of data.

A4.4.2 - Stability in pH 7.4 Phosphate Buffer Saline (PBS)

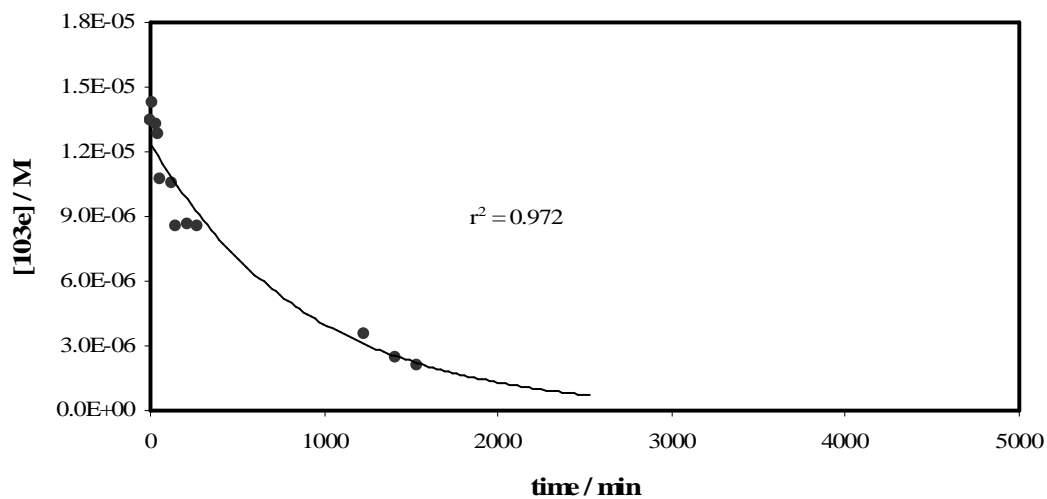


Figure A4.45 - Profile of concentration of 103e versus time after incubation in pH 7.4 PBS, at 37 °C. Points are experimental and line is from exponential regression analysis of data, giving the kinetic rate constant of hydrolysis $k = 1.13 \times 10^{-3} \text{ min}^{-1}$. From this value, the half-life was determined, $t_{1/2} = 10\text{h}$.

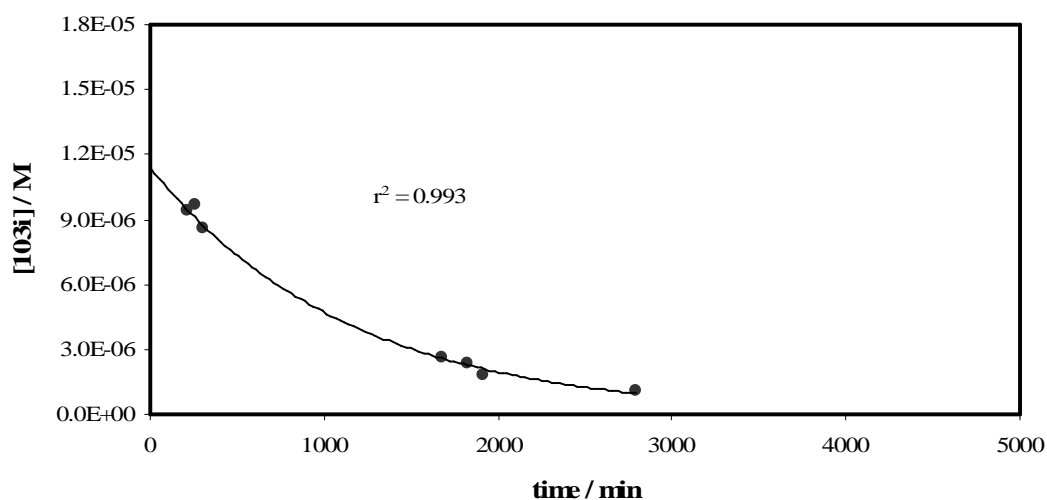


Figure A4.46 - Profile of concentration of 103i versus time after incubation in PBS, at 37 °C. Points are experimental and line is from exponential regression analysis of data, giving the kinetic rate constant of hydrolysis $k = 8.83 \times 10^{-4} \text{ min}^{-1}$. From this value, the half-life was determined, $t_{1/2} = 13\text{h}$.

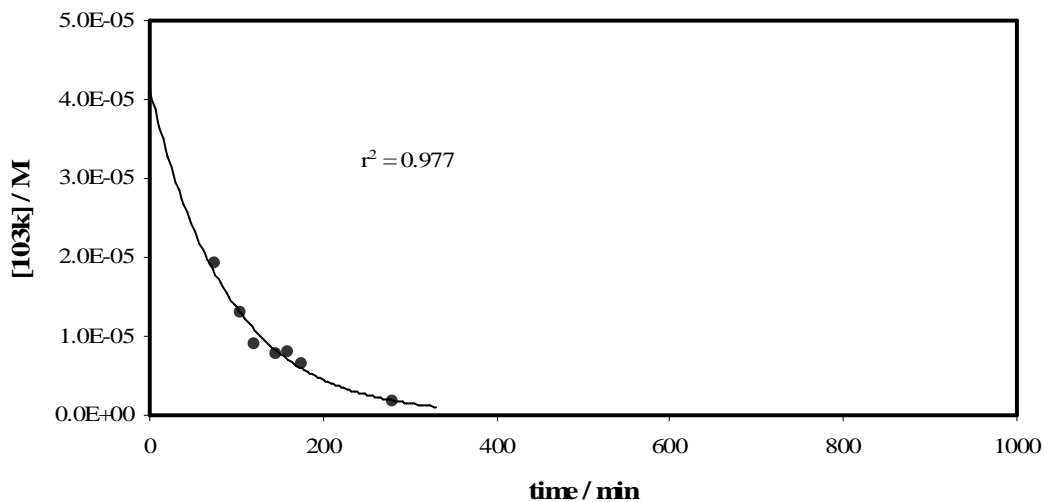


Figure A4.47 - Profile of concentration of 103k versus time after incubation in PBS, at 37 °C. Points are experimental and line is from exponential regression analysis of data, giving the kinetic rate constant of hydrolysis $k = 1.11 \times 10^{-2} \text{ min}^{-1}$. From this value, the half-life was determined, $t_{1/2} = 1.04\text{h}$.

A4.4.3 – Stability in 80% Human Plasma

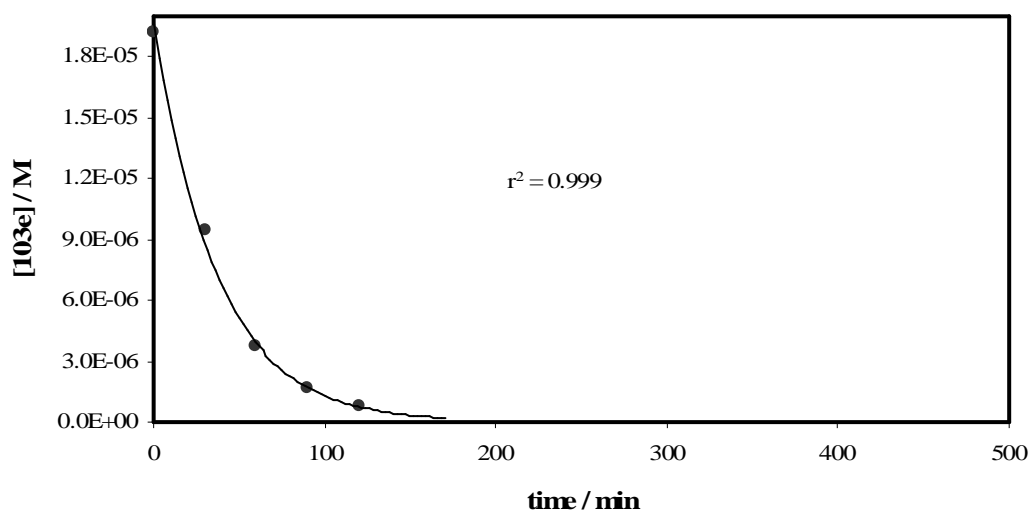


Figure A4.48 - Profile of concentration of 103e versus time after incubation in 80% human plasma, at 37 °C. Points are experimental and line is from exponential regression analysis of data,

giving the kinetic rate constant of hydrolysis $k = 2.72 \times 10^{-2} \text{ min}^{-1}$. From this value, the half-life was determined, $t_{1/2} = 0.42\text{h}$.

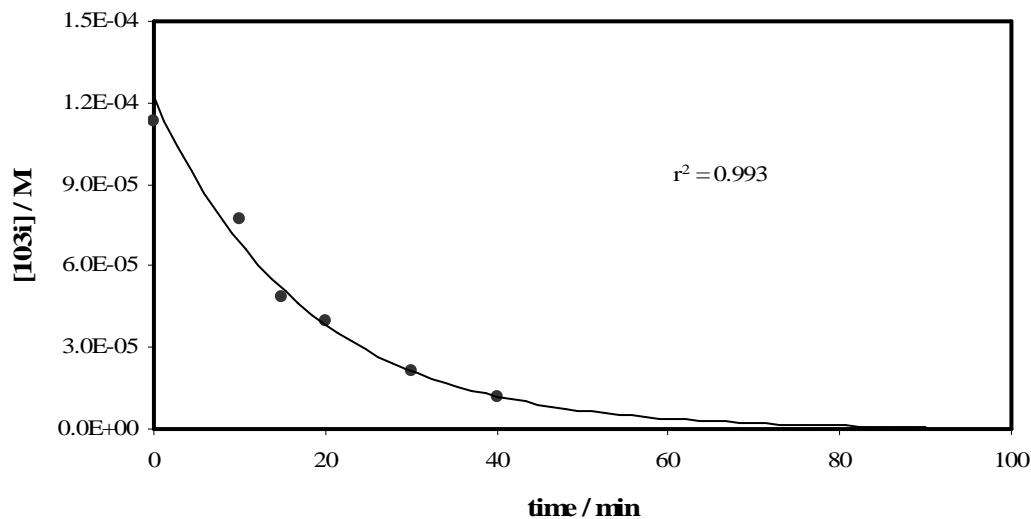


Figure A4.49 - Profile of concentration of 103i versus time after incubation in 80% human plasma, at 37 °C. Points are experimental and line is from exponential regression analysis of data, giving the kinetic rate constant of hydrolysis $k = 5.79 \times 10^{-2} \text{ min}^{-1}$. From this value, the half-life was determined, $t_{1/2} = 0.20\text{h}$.

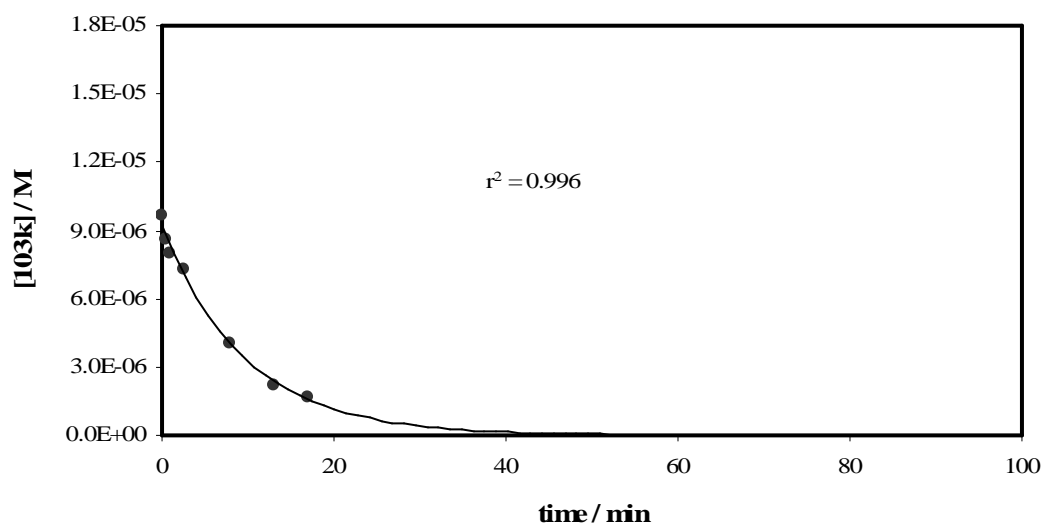


Figure A4.50 - Profile of concentration of 103k versus time after incubation in 80% human plasma, at 37 °C. Points are experimental and line is from exponential regression analysis of data, 300

giving the kinetic rate constant of hydrolysis $k = 1.04 \times 10^{-1} \text{ min}^{-1}$. From this value, the half-life was determined, $t_{1/2} = 0.11\text{h}$.

A4.5 – Biodistribution Studies

Table A4.7 - Data for calibration curve of 103k in mice blood, spleen, lung and liver

Blood	
[103k] / $\mu\text{g/ml}$	Area
9.0	602
13.5	1159
22.5	1729
45.0	5074
67.5	7920

Spleen	
[103k] / $\mu\text{g/ml}$	Area
9.0	1314
13.5	7177
22.5	10402

Lung	
[103k] / $\mu\text{g/ml}$	Area
9.0	3906
13.5	5500
22.5	8315

Liver	
[103k] / $\mu\text{g/ml}$	Area
9.0	4770
13.5	6368
22.5	8446

REFERENCES

REFERENCES

1. Nomenclature Committee of the International Union of Biochemistry and Molecular Biology (NC-IUBMB). <http://www.chem.qmul.ac.uk/iubmb/enzyme/> (February 2009).
2. Rawlings, N. D., Morton, F.R., Kok, C.Y., Kong, J. & Barrett, A.J. . MEROPS: the peptidase database. *Nucleic Acids Res* **2008**, 36, D320-D325.
3. National Library of Medicine - Medical Subject Headings. http://www.nlm.nih.gov/cgi/mesh/2009/MB_cgi?mode=&term=Serine+proteases (February 2009).
4. Hedstrom, L. Serine Protease Mechanism and Specificity. *Chem. Rev.* **2002**, 102, 4501-4523.
5. Page, M. J.; Di Cera, E. Serine Peptidases: Classification, Structure and Function. *Cell. Mol. Life Sci.* **2008**, 65, 1220-1236.
6. Ilies, M. A.; Scozzafava, A.; Supuran, C. T. Therapeutic Applications of Serine Protease Inhibitors. *Expert Opin. Ther. Pat.* **2002**, 12, 1181-1214.
7. Vandenameele, P.; Orrenius, S.; Zhivotovsky, B. Serine Proteases and Calpains Fulfill Important Supporting Roles in The Apoptotic Tragedy of The Cellular Opera. *Cell Death Differ.* **2005**, 12, 1219-1224.
8. Turk, B. Targeting Proteases: Successes, Failures and Future Prospects. *Nat. Rev. Drug Discov.* **2006**, 5, 785-799.
9. Abbenante, G.; Fairlie, D. P. Protease Inhibitors in the Clinic. *Med. Chem.* **2005**, 1, 71-104.
10. Turk, B. Recent Advances and Future Prospect in Protease Targeting - Part-II. *Curr. Pharm. Design* **2007**, 13, 347-348.
11. Walker, B.; Lynas, J. F. Strategies for the inhibition of serine proteases. *Cell. Mol. Life Sci.* **2001**, 58, 596-624.
12. Kwong, A. D.; McNair, L.; Jacobson, I.; George, S. Recent Progress in the Development of Selected Hepatitis C Virus NS3.4A Protease and NS5B Polymerase Inhibitors. *Curr. Opin. Pharmacol.* **2008**, 8, 522-531.

13. Dunbar, S. D.; Ornstein, D. L.; Zacharski, L. R. Cancer Treatment with Inhibitors of Urokinase-Type Plasminogen Activator and Plasmin. *Expert Opin. Invest. Drugs* **2000**, 9, 2085-2092.
14. Webber, M. M.; Waghray, A.; Bello, D. Prostate-Specific Antigen, a Serine Protease, Facilitates Human Prostate Cancer Cell Invasion. *Clin. Cancer Res.* **1995**, 1, 1089-1094.
15. Sommerhoff, C. P.; Schaschke, N. Mast Cell Tryptase β as a Target in Allergic Inflammation: An Evolving Story. *Curr. Pharm. Design* **2007**, 13, 313-332.
16. Reid, P.; Sallenave, J.-M. Neutrophil-Derived Elastases and Their Inhibitors: Potential Role in the Pathogenesis of Lung Disease. *Curr. Opin. Invest. Drugs* **2001**, 2, 59-67.
17. Jenne, D. E.; Tschopp, J.; Ludemann, J.; Utecht, B.; Gross, W. L. Wegener's Autoantigen Decoded. *Nature* **1990**, 346, 520-520.
18. Prezelj, A.; Anderuh, P. S.; Peternel, L.; Urleb, U. Recent Advances in Serine Protease Inhibitors as Anticoagulant Agents. *Curr. Pharm. Design* **2007**, 13, 287-312.
19. EMEA. *Public Assessment Report for Pradaxa*; 2008.
20. Konaklieva, M. I. β -Lactams as Inhibitors of Serine Enzymes. *Curr. Med. Chem. - Anti-Infective Agents* **2002**, 1, 215-238.
21. Copeland, R. A. *Evaluation of Enzyme Inhibitors in Drug Discovery: A Guide for Medicinal Chemists and Pharmacologists* John Wiley and Son New Jersey, 2005; p 296.
22. Schechter, I.; Berger, A. On the size of the active site in proteases. I. Papain. *Biochem. Biophys. Res. Comm.* **1967**, 27, 157-162.
23. Babine, R. E.; Bender, S. L. Molecular Recognition of Protein-Ligand Complexes: Applications to Drug Design. *Chem. Rev.* **1997**, 97, 1359-1472.
24. Leung, D.; Abbenante, G.; Fairlie, D. P. Protease Inhibitors: Current Status and Future Prospects. *J. Med. Chem.* **2000**, 43, 305-341.
25. Powers, J. C.; Asgian, J. L.; Ekici, O. D.; James, K. E. Irreversible Inhibitors of Serine, Cysteine, and Threonine Proteases. *Chemical Reviews* **2002**, 102, 4639-4750.
26. Borregaard, N.; Cowland, J. B. Granules of the Human Neutrophilic Polymorphonuclear Leukocyte. *Blood* **1997**, 89, 3503-3521.

27. Bode, W.; Meyer, E.; Powers, J. C. Human-Leukocyte and Porcine Pancreatic Elastase - X-Ray Crystal-Structures, Mechanism, Substrate-Specificity, and Mechanism-Based Inhibitors. *Biochemistry* **1989**, 28, 1951-1963.
28. Lee, W. L.; P.Downey, G. Leukocyte Elastase Physiological Functions and Role in Acute Lung Injury. *Am. J. Respir. Crit. Care Med.* **2001**, 164, 896-904.
29. Korkmaz, B.; Moreau, T.; Gauthier, F. Neutrophil Elastase, Proteinase 3 and Cathepsin G: Physicochemical Properties, Activity and Physiopathological Functions. *Biochimie* **2008**, 90, 227-242.
30. Kelly, E.; Greene, C. M.; McElvaney, N. G. Targeting neutrophil elastase in cystic fibrosis. *Expert Opin. Ther. Targets* **2008**, 12, 145-157.
31. Owen, C. A. Leukocyte Cell Surface Proteinases: Regulation of expression, Functions, and Mechanisms of Surface Localization. *Int. J. Biochem. Cell Biol.* **2008**, 40, 1246-1272.
32. Sinha, S.; Watorek, W.; Karr, S.; Gils, J.; Bode, W.; Travis, J. Primary Structure of Human Neutrophil Elastase. *Proc. Natl. Acad. Sci.* **1987**, 84, 2228-2232.
33. Pham, C. T. N. Neutrophil Serine Proteases Fine-tune the Inflammatory Response. *Int. J. Biochem. Cell Biol.* **2008**, 40, 1317-1333.
34. Brinkmann, V.; Reichard, U.; Goosmann, C.; Fauler, B.; Uhlemann, Y.; Weiss, D. S.; Weinrauch, Y.; Zychlinsky, A. Neutrophil Extracellular Traps Kill Bacteria. *Science* **2004**, 303, 1532-1535.
35. Dallegri, F.; Ottonello, L. Tissue Injury in Neutrophilic Inflammation. *Inflamm. Res.* **1997**, 46, 382-391.
36. Roughley, P. J.; Barrett, A. J. The Degradation of Cartilage Proteoglycans by Tissue Proteinases Proteoglycan Structure and Its Susceptibility to Proteolysis. *Biochem. J.* **1977**, 167, 629-637.
37. Dollery, C. M.; Owen, C. A.; Sukhova, G. K.; Krettek, A.; Shapiro, S. D.; Libby, P. Neutrophil Elastase in Human Atherosclerotic Plaques - Production by Macrophages. *Circulation* **2003**, 107, 2829-2836.
38. Pham, C. T. N. Neutrophil Serine Proteases: Specific Regulators of Inflammation. *Nature Rev. Immunol.* **2006**, 6, 541-550.
39. Lungarella, G.; Cavarra, E.; Lucattelli, M.; Martorana, P. A. The Dual Role of Neutrophil Elastase in Lung Destruction and Repair. *Int. J. Biochem. Cell Biol.* **2008**, 40, 1287-1296.

40. Carrell, R. α_1 -Antitrypsin: Molecular Pathology, Leukocytes, and Tissue damage. *J. Clin. Invest.* **1986**, 78, 1427-1431.
41. Kuzniar, J.; Kuzniar, T. J.; Marchewka, Z.; Lembas-Bogaczyk, J.; Rabczynski, J.; Kopec, W.; Klinger, M. Elastase Deposits in the Kidney and Urinary Elastase Excretion in Patients with Glomerulonephritis - Evidence for Neutrophil Involvement in Renal Injury. *Scand. J. Urol. Nephrol.* **2007**, 41, 527-534.
42. Schrijver, G.; Schalkwijk, J.; Robben, J. C. M.; Assmann, K. J. M.; Koene, R. A. P. Antiglomerular Basement-Membrane Nephritis in Beige Mice - Deficiency of Leukocytic Neutral Proteinases Prevents the Induction of Albuminuria in the Heterologous Phase. *J. Exp. Med.* **1989**, 169, 1435-1448.
43. Henriksen, P. A.; Sallenave, J. Human Neutrophil Elastase: Mediator and Therapeutic Target in Atherosclerosis. *Int. J. Biochem. Cell Biol.* **2008**, 40, 1095-1100.
44. Adkison, A. M.; Raptis, S. Z.; Kelley, D. G.; Pham, C. T. N. Dipeptidyl Peptidase I Activates Neutrophil-Derived Serine Proteases and Regulates the Development of Acute Experimental Arthritis. *J. Clin. Invest.* **2002**, 109, 363-371.
45. Abboud, R. T.; Vimalanathan, S. Pathogenesis of COPD. Part I. The Role of Protease-antiprotease Imbalance in Emphysema. *Int. J. Tuberc. Lung Dis.* **2008**, 12, 361-367.
46. Barnes, P. J.; Shapiro, S. D.; Pauwells, R. A. Chronic Obstructive Pulmonary Disease: Molecular and Cellular Mechanisms. *Eur. Respir. J.* **2003**, 22, 672-688.
47. Moraes, T. J.; Chow, C. W.; Downey, G. P. Proteases and Lung Injury. *Crit. Care Med.* **2002**, 13, S189-S194.
48. Voynow, J. A.; Fischer, B. M.; Zheng, S. Proteases and cystic fibrosis. *Int. J. Biochem. Cell Biol.* **2008**, 40, 1238-1245.
49. World Health Report 2000 statistical annex. World Health Organization. <http://www.who.int/whr/2000/en/statistics.htm>. (January 2009).
50. Pauwels, R. A.; Buist, A. S.; Calverley, P. M. A.; Jenkins, C. R.; Hurd, S. S. Global strategy for the diagnosis, management, and prevention of COPD, NHLBI/WHO Global Initiative for Chronic Lung Disease (GOLD). *Am. J. Respir. Crit. Care Med.* **2001**, 163, 1256-1276.
51. Lopez, A. D.; Murray, C. C. J. L. The global burden of disease, 1990-2020. *Nature Med.* **1998**, 4, 1241-1243.

52. Barnes, P. J. Peter J. Barnes. *N. Engl. J. Med.* **2000**, 343, 269-280.
53. Suki, B.; Lutchen, K. R.; Ingenito, E. P. On the Progressive Nature of Emphysema: Roles of Proteases, Inflammation, and Mechanical Forces. *Am. J. Respir. Crit. Care Med.* **2003**, 168, 516-521.
54. Barnes, P. J. New Treatments for COPD. *Nat. Rev. Drug Discov.* **2002**, 1, 437-446.
55. Lieberman, J. Elastase, Collagenase, Emphysema, and Alpha1-Antitrypsin Deficiency. *Chest* **1976**, 70, 62-67.
56. Laurell, C. B.; Eriksson, S. Electrophoretic Alpha1-Globulin Pattern of Serum in Alpha1-Antitrypsin Deficiency. *Scand. J. Clin. Lab. Invest.* **1963**, 15, 132-&.
57. Gadek, J. E.; Fells, G. A.; Crystal, R. G. Cigarette-Smoking Induces Functional Antiprotease Deficiency in the Lower Respiratory-Tract of Humans. *Science* **1979**, 206, 1315-1316.
58. Powers, J. C. Elastase Inhibitors for Treatment of Emphysema Approaches to Synthesis and Biological Evaluation *J. Enz. Inhib.* **1987**, 1, 311-319.
59. Barnes, P. J.; Hansel, T. T. Prospects for New Drugs for Chronic Obstructive Pulmonary Disease. *The Lancet* **2004**, 364, 985-996.
60. Janoff, A.; Sloan, B.; Weinbaum, G.; Damiano, V.; Sandhaus, R. A.; Elias, J.; Kimbel, P. Experimental Emphysema Induced with Purified Human Neutrophil Elastase - Tissue Localization of Instilled Protease. *Am. Rev. Respir. Dis.* **1977**, 115, 461-478.
61. Chua, F.; Laurent, G. J. Neutrophil Elastase: Mediator of Extracellular Matrix Destruction and Accumulation. *Proc. Am. Thorac. Soc.* **2006**, 3, 424-427.
62. Hirche, T. O.; Crouch, E. C.; Espinola, M.; Brokelman, T. J.; Mecham, R. P.; DeSilva, N.; Cooley, J.; Remold-O'Donnell, E.; Belaaouaj, A. Neutrophil Serine Proteinases Inactivate Surfactant Protein D by Cleaving within a Conserved Subregion of the Carbohydrate Recognition Domain. *J. Biolog. Chem.* **2004**, 279, 27688-27698.
63. Chughtai, B.; O'Riordan, T. G. Potential Role of Inhibitors of Neutrophil Elastase in Treating Diseases of the Airway. *Journal of Aerosol Med. - Depos. Clear. Eff. Lung* **2004**, 17, 289-298.

64. Zhong, J.; Groutas, W. C. Recent Developments in the Design of Mechanism-based and Alternate Substrate Inhibitors of Serine Proteases. *Curr. Top. Med. Chem.* **2004**, *4*, 1203-1216.
65. Stoller, J. K.; Aboussouan, L. S. α 1-Antitrypsin Deficiency. *The Lancet* **2005**, *365*, 2225-2236.
66. PDB. www.rcsb.org/pdb
67. Skiles, J. W.; Jeng, A. Y. Therapeutic Promises of Leukocyte Elastase and Macrophage Metalloelastase Inhibitors for the Treatment of Pulmonary Emphysema. *Exp. Opin. Ther. Pat.* **1999**, *9*, 869-895.
68. Bernstein, P. R.; Andisik, D.; Bradley, P. K.; Bryant, C. B.; Ceccarelli, C.; Damewood, J. R.; Earley, R.; Edwards, P. D.; Feeney, S.; Gomes, B. C.; Kosmider, B. J.; Steelman, G. B.; Thomas, R. M.; Vacek, E. P.; Veale, C. A.; Williams, J. C.; Wolanin, D. J.; Woolson, S. A. Nonpeptidic Inhibitors of Human-Leukocyte Elastase. 3. Design, Synthesis, X-Ray Crystallographic Analysis, and Structure-Activity-Relationships for a Series of Orally-Active 3-Amino-6-Phenylpyridin-2-One Trifluoromethyl Ketones. *J. Med. Chem.* **1994**, *37*, 3313-3326.
69. Ohbayashi, H. Current Synthetic Inhibitors of Human Neutrophil Elastase. *Exp. Opin. Ther. Pat.* **2002**, *12*, 65-84.
70. Ohbayashi, H. Current Synthetic Inhibitors of Human Neutrophil Elastase in 2005. *Exp. Opin. Ther. Pat.* **2005**, *15*, 759-771.
71. Marangoni, A. G. *Enzyme Kinetics: A Modern Approach*. John Wiley & Sons: New Jersey, 2002; p 248
72. Sykes, N. O.; Macdonald, S. J. F.; Page, M. I. Acylating Agents as Enzyme Inhibitors and Understanding Their Reactivity for Drug Design. *J. Med. Chem.* **2002**, *45*, 2850-2856.
73. Imaki, K.; Okada, T.; Nakayama, Y.; Nagao, Y.; Kobayashi, K.; Sakai, Y.; Mohri, T.; Amino, T.; Nakai, H.; Kawamura, M. Non-Peptidic Inhibitors of Human Neutrophil Elastase: The Design and Synthesis of Sulfonamide-Containing Inhibitors. *Bioorg. Med. Chem.* **1996**, *4*, 2115-2134.
74. Nakayama, Y.; Odagaki, Y.; Fujita, S.; Matsuoka, S.; Hamanaka, N.; Nakai, H.; Toda, M. Clarification of Mechanism of Human Sputum Elastase Inhibition by a New Inhibitor, ONO-5046, Using Electrospray Ionization Mass Spectrometry. *Bioorg. Med. Chem. Lett.* **2002**, *12*, 2349-2353.

75. Kawabata, K.; Suzuki, M.; Sugitani, M.; Imaki, K.; Toda, M.; Miyamoto, T. Ono-5046, a Novel Inhibitor of Human Neutrophil Elastase. *Biochem. Biophys. Res. Comm.* **1991**, 177, 814-820.
76. Krantz, A.; Spencer, R. W.; Tam, T. F.; Liak, T. J.; Copp, L. J.; Thomas, E. M.; Rafferty, S. P. Design and Synthesis of 4H-3,1-Benzoxazin-4-ones as Potent Alternate Substrate Inhibitors of Human Leukocyte Elastase. *J. Med. Chem.* **1990**, 33, 464-479.
77. Krantz, A.; Spencer, R. W.; Tam, T. F.; Thomas, E.; Copp, L. J. Design of Alternate Substrate Inhibitors of Serine Proteases. Synergistic Use of Alkyl Substitution to Impede Enzyme-Catalysed Deacylation. *J. Med. Chem.* **1987**, 30, 589-591.
78. Silverman, R. B. *The Organic Chemistry of Drug Design and Drug Action*. Academic Press: NY, 1992.
79. Powers, J. C.; Oleksyszyn, J.; Narasimhan, S. L.; Kam, C. M.; Radhakrishnan, R.; Meyer, E. F. Reaction of Porcine Pancreatic Elastase with 7-Substituted 3-Alkoxy-4-chloroisocoumarins: Design of Potent Inhibitors Using the Crystal Structure of the Complex Formed with 4-Chloro-3-ethoxy-7-guanidinoisocoumarin. *Biochemistry* **1990**, 29, 3108-3118.
80. Harper, J. W.; Hemmi, K.; Powers, J. C. Reaction of Serine Proteases with Substituted Isocoumarins: Discovery of 3,4-Dichloroisocoumarin, a New General Mechanism Based Serine Protease Inhibitor. *Biochemistry* **1985**, 24, 1831-1841.
81. Groutas, W. C.; Brubaker, M. J.; Chong, L. S.; Venkataraman, R.; Huang, H.; Epp, J. B.; Kuang, R.; Hoidal, J. R. Design, Synthesis and Biological Evaluation of Succinimide Derivatives as Potential Mechanism-Based Inhibitors of Human-Leukocyte Elastase, Cathepsin-G and Proteinase-3. *Bioorg. Med. Chem.* **1995**, 3, 375-381.
82. Groutas, W. C.; Stanga, M. A.; Castrisos, J. C.; Schatz, E. J. Hydantoin Derivatives. A New Class of Inhibitors of Human Leukocyte Elastase. *J. Enz. Inhib. Med. Chem.* **1990**, 3, 237-243.
83. Neumann, U.; Gutschow, M. N-(Sulfonyloxy)Phthalimides and Analogs Are Potent Inactivators of Serine Proteases. *J. Biol. Chem.* **1994**, 269, 21561-21567.

84. Groutas, W. C.; Houserarchield, N.; Chong, L. S.; Venkataraman, R.; Epp, J. B.; Huang, H.; McClenahan, J. J. Efficient Inhibition of Human-Leukocyte Elastase and Cathepsin-G by Saccharin Derivatives. *J. Med. Chem.* **1993**, *36*, 3178-3181.
85. Groutas, W. C.; Kuang, R.; Venkataraman, R.; Epp, J. B.; Ruan, S.; Prakash, O. Structure-Based Design of a General Class of Mechanism-Based Inhibitors of the Serine Proteinases Employing a Novel Amino Acid-Derived Heterocyclic Scaffold. *Biochemistry* **1997**, *36*, 4739-4750.
86. He, S.; Kuang, R. Z.; Venkataraman, R.; Tu, J.; Truong, T. M.; Chan, H. K.; Groutas, W. C. Potent Inhibition of Serine Proteases by Heterocyclic Sulfide Derivatives of 1,2,5-Thiadiazolidin-3-one 1,1 dioxide. *Bioorg. Med. Chem.* **2000**, *8*, 1713-1717.
87. Lai, Z.; Gan, X. D.; Wei, L. Q.; Alliston, K. R.; Yu, H. Y.; Li, Y. H.; Groutas, W. C. Potent Inhibition of Human Leukocyte Elastase by 1,2,5-Thiadiazolidin-3-one 1,1 dioxide-based Sulfonamide Derivatives. *Arch. Biochem. Biophys.* **2004**, *429*, 191-197.
88. Doherty, J. B.; Ashe, B. M.; Argenbright, L. W.; Barker, P. L.; Bonney, R. J.; Chandler, G. O.; Dahlgren, M. E.; Dorn, C. P.; Finke, P. E.; Firestone, R. A.; Fletcher, D.; Hagmann, W. K.; Mumford, R.; Ogrady, L.; Maycock, A. L.; Pisano, J. M.; Shah, S. K.; Thompson, K. R.; Zimmerman, M. Cephalosporin Antibiotics Can Be Modified to Inhibit Human-Leukocyte Elastase. *Nature* **1986**, *322*, 192-194.
89. Shah, S. K.; Finke, P. E.; Brause, K. A.; Chandler, G. O.; Ashe, B. M.; Weston, H.; Maycock, A. L.; Mumford, R. A.; Doherty, J. B. Monocyclic β -Lactam Inhibitors of Human Leukocyte Elastase. Stereospecific Synthesis and Activity of 3,4-Disubstituted-2-azetidinones. *Bioorg. Med. Chem. Lett.* **1993**, *3*, 2295-2298.
90. Navia, M. A.; Springer, J. P.; Lin, T. Y.; Williams, H. R.; Firestone, R. A.; Pisano, J. M.; Doherty, J. B.; Finke, P. E.; Hoogsteen, K. Crystallographic Study of a β -Lactam Inhibitor Complex with Elastase at 1.84-Å Resolution. *Nature* **1987**, *327*, 79-82.
91. Knight, W. B.; Maycock, A. L.; Green, B. G.; Ashe, B. M.; Gale, P.; Weston, H.; Finke, P. E.; Hagmann, W. K.; Shah, S. K.; Doherty, J. B. Mechanism of Inhibition of Human Leukocyte Elastase by Two Cephalosporin Derivatives. *Biochemistry* **1992**, *31*, 4980-4986.

92. Page, M. I. The Mechanisms of Reactions of β -Lactam Antibiotics. *Adv. Phys. Org. Chem.* **1987**, *23*, 165-270.
93. Finke, P. E.; Shah, S. K.; Ashe, B. M.; Ball, R. G.; Blacklock, T. J.; Bonney, R. J.; Brause, K. A.; Chandler, G. O.; Cotton, M.; Davies, P.; Dellea, P. S.; Dorn, C. P.; Fletcher, D. S.; Ogrady, L. A.; Hagmann, W. K.; Hand, K. M.; Knight, W. B.; Maycock, A. L.; Mumford, R. A.; Osinga, D. G.; Sohar, P.; Thompson, K. R.; Weston, H.; Doherty, J. B. Inhibition of Human-Leukocyte Elastase .4. Selection of a Substituted Cephalosporin (L-658,758) as a Topical Aerosol. *J. Med. Chem.* **1992**, *35*, 3731-3744.
94. Firestone, R. A.; Barker, P. L.; Pisano, J. M.; Ashe, B. M.; Dahlgren, M. E. Monocyclic Beta-Lactam Inhibitors of Human-Leukocyte Elastase. *Tetrahedron* **1990**, *46*, 2255-2262.
95. Underwood, D. J.; Green, B. G.; Chabin, R.; Mills, S.; Doherty, J. B.; Finke, P. E.; Maccoss, M.; Shah, S. K.; Burgey, C. S.; Dickinson, T. A.; Griffin, P. R.; Lee, T. E.; Swiderek, K. M.; Covey, T.; Westler, W. M.; Knight, W. B. Mechanism of Inhibition of Human-Leukocyte Elastase by β -Lactams .3. Use of Electrospray-Ionization Mass-Spectrometry and 2-Dimensional NMR Techniques to Identify β -Lactam-Derived E-I Complexes. *Biochemistry* **1995**, *34*, 14344-14355.
96. Green, B. G.; Chabin, R.; Mills, S.; Underwood, D. J.; Shah, S. K.; Kuo, D.; Gale, P.; Maycock, A. L.; Liesch, J.; Burgey, C. S.; Doherty, J. B.; Dorn, C. P.; Finke, P. E.; Hagmann, W. K.; Hale, J. J.; MacCoss, M.; Westler, W. M.; Knight, W. B. Mechanism of Inhibition of Human Leucocyte Elastase by β -Lactams. 2. Stability, Reactivation Kinetics, and Products of β -Lactam-Derived E-I Complexes. *Biochemistry* **1995**, *34*, 14331-14343.
97. Finke, P. E.; Shah, S. K.; Fletcher, D. S.; Ashe, B. M.; Brause, K. A.; Chandler, G. O.; Dellea, P. S.; Hand, K. M.; Maycock, A. L.; Osinga, D. G.; Underwood, D. J.; Weston, H.; Davies, P.; Doherty, J. B. Orally-Active β -Lactam Inhibitors of Human Leukocyte Elastase. 3. Stereospecific Synthesis and Structure-Activity-Relationships for 3,3-Dialkylazetidino-2-ones. *J. Med. Chem.* **1995**, *38*, 2449-2462.
98. Shah, S. K.; Dorn, C. P.; Finke, P. E.; Hale, J. J.; Hagmann, W. K.; Brause, K. A.; Chandler, G. O.; Kissinger, A. L.; Ashe, B. M.; Weston, H.; Knight, W. B.; Maycock, A. L.; Dellea, P. S.; Fletcher, D. S.; Hand, K. M.; Mumford, R. A.;

Underwood, D. J.; Doherty, J. B. Orally Active β -Lactam Inhibitors of Human-Leukocyte Elastase. 1- Activity of 3,3-Diethyl-2-Azetidinones. *J. Med. Chem.* **1992**, 35, 3745-3754.

99. Hagmann, W. K.; Kissinger, A. L.; Shah, S. K.; Finke, P. E.; Dorn, C. P.; Brause, K. A.; Ashe, B. M.; Weston, H.; Maycock, A. L.; Knight, W. B.; Dellea, P. S.; Fletcher, D. S.; Hand, K. M.; Osinga, D.; Davies, P.; Doherty, J. B. Orally Active β -Lactam Inhibitors of Human Leukocyte Elastase. 2. Effect of C-4 Substitution. *J. Med. Chem.* **1993**, 36, 771-777.

100. Hagmann, W. K.; Thompson, K. R.; Shah, S. K.; Finke, P. E.; Ashe, B. M.; Weston, H.; Maycock, A. L.; Doherty, J. B. The Effect of *N*-Acyl Substituents on the Stability of Monocyclic β -Lactam Inhibitors of Human Leukocyte Elastase. *Bioorg. Med. Chem. Lett.* **1992**, 2, 681-684.

101. Hagmann, W. K.; Shah, S. K.; Dorn, C. P.; O'Grady, L. A.; Hale, J. J.; Finke, P. E.; Thompson, K. R.; Brause, K. A.; Ashe, B. M.; Weston, H.; Dahlgren, M.; Maycock, A. L.; Dellea, P. S.; Hand, K. M.; Osinga, D. G.; Bonney, R. J.; Davies, P.; Fletcher, D. S.; Doherty, J. B. Prevention of Human Leukocyte Elastase-mediated Lung Damage by 3-Alkyl-4-Azetidinones. *Bioorg. Med. Chem. Lett.* **1991**, 1, 545-550.

102. Fletcher, D.; Osinga, D.; Hand, K.; Dellea, P.; Ashe, B.; Mumford, R.; Davies, P.; Hagmann, W.; Finke, P.; Doherty, J.; Bonney, R. A Comparison of α_1 -Proteinase Inhibitor Methoxysuccinyl-Ala-Ala-Pro-Val-Chloromethylketone and Specific β -Lactam Inhibitors in an Acute Model of Human Polymorphonuclear Leukocyte Elastase-induced Lung Hemorrhage in the Hamster. *Am. Rev. Respir. Dis.* **1990**, 141, 672-677.

103. Doherty, J. B.; Shah, S. K.; Finke, P. E.; Jr., C. P. D.; Hagmann, W. K.; Hale, J. J.; Kissinger, A. L.; Thompson, K. R.; Brause, K.; Chandler, G. O.; Knight, W. B.; Maycock, A. L.; Ashe, B. M.; Weston, H.; Gale, P.; Mumford, R. A.; Andersen, O. F.; Williams, H. R.; Nolan, T. E.; Frankenfield, D. L.; Underwood, D.; Vyas, K. P.; Kari, P. H.; Dahlgren, M. E.; Mao, J.; Fletcher, D. S.; Dellea, P. S.; Hand, K. M.; Osinga, D. G.; Peterson, L. B.; Williams, D. T.; Metzger, J. M.; Bonney, R. J.; Humes, J. L.; Pacholok, S. P.; Hanlon, W. A.; Opas, E.; Stolk, J.; Davies, P. Chemical, Biochemical, Pharmacokinetic, and Biological Properties of L-680,833: A

Potent, Orally Active Monocyclic β -Lactam Inhibitor of Human Polymorphonuclear Leukocyte elastase. *Proc. Nat. Acad. Sci.* **1993**, 90, 8727-8731.

104. Knight, W. B.; Green, B. G.; Chabin, R. M.; Gale, P.; Maycock, A. L.; Weston, H.; Kuo, D. W.; Westler, W. M.; Dorn, C. P.; Finke, P. E.; Hagmann, W. K.; Hale, J. J.; Liesch, J.; MacCoss, M.; Navia, M. A.; Shah, S. K.; Underwood, D.; Doherty, J. B. Specificity, Stability, and Potency of Monocyclic β -Lactam Inhibitors of Human Leucocyte Elastase. *Biochemistry* **1992**, 31, 8160-8170.

105. Merck. Pulmonary-Allergy, Dermatological, Gastrointestinal & Arthritis: β -Lactams as Inhibitors of Human Leukocyte Elastase. *Exp. Opin. Ther. Pat.* **1994**, 4, 1519-1522.

106. Finke, P. E.; Dorn, C. P.; Kissinger, A. L.; Shah, S. K.; Ball, R. G.; Chabin, R.; Davie, P.; Della, P. S.; Doherty, J. B.; Durette, P. L.; Fletcher, D. S.; Griffin, P. R.; Green, B. G.; Hale, J. J.; Hanlon, W. A.; Hand, K. M.; Humes, J. L.; Kieczkowski, G. R.; Klatt, T. D.; Lanza, T. J.; Knight, W. B.; Maccoss, M.; Miller, D. S.; Mumford, R. A.; Pacholok, S. G.; Peterson, L. P.; Poe, M.; Underwood, D. J.; Williams, D. T.; Williams, H. R. In *Orally-Active, Intracellular Inhibitors of Human-Leukocyte Elastase (Hle)*, 22nd National Meeting of the American Chemical Society., Chicago, Aug, 1995; Chicago, 1995; pp 83-MEDI.

107. Clemente, A.; Domingos, A.; Grancho, A. P.; Iley, J.; Moreira, R.; Neres, J.; Palma, N.; Santana, A. B.; Valente, E. Design, Synthesis and Stability of N-Acyloxymethyl- and N-Aminocarbonyloxymethyl-2-azetidinones as Human Leukocyte Elastase Inhibitors. *Bioorg. Med. Chem. Lett.* **2001**, 11, 1065-1068.

108. Beauve, C.; Bouchet, M.; Touillaux, R.; Fastrez, J.; Marchand-Brynaert, J. Synthesis, Reactivity and Biochemical Evaluation of 1,3-Substituted Azetidin-2-ones as Enzyme Inhibitors. *Tetrahedron* **1999**, 55, 13301-13320.

109. Moreira, R.; Santana, A. B.; Iley, J.; Neres, J.; Douglas, K. T.; Horton, P. N.; Hursthouse, M. B. Design, Synthesis, and Enzymatic Evaluation of N^1 -Acyloxyalkyl- and N^1 -Oxazolidin-2,4-dion-5-yl-substituted β -Lactams as Novel Inhibitors of Human Leukocyte Elastase. *J. Med. Chem.* **2005**, 48, 4861-4870.

110. Doucet, C.; Vergely, I.; ReboudRavaux, M.; Guilhem, J.; Kobaiter, R.; Joyeau, R.; Wakselman, M. Inhibition of Human Leukocyte Elastase by Functionalized N-Aryl-3,3-dihalogenoazetidin-2-ones. Stereospecific Synthesis and

Chiral Recognition of Dissymmetrically C-3-Substituted β -Lactams. *Tetrahedron: Asymm.* **1997**, 8, 739-751.

111. Wakselman, M.; Joyeau, R.; Kobaiter, R.; Boggetto, N.; Vergely, I.; Maillard, J.; Okochi, V.; Montagne, J. J.; Reboudraux, M. Functionalized N-Aryl Azetidines as Novel Mechanism-Based Inhibitors of Neutrophil Elastase. *FEBS Lett.* **1991**, 282, 377-381.

112. Vergely, I.; Boggetto, N.; Okochi, V.; Golpayegani, S.; Reboudraux, M.; Kobaiter, R.; Joyeau, R.; Wakselman, M. Inhibition of Human-Leukocyte Elastase by Functionalized N-Aryl Azetidines - Substituent Effects at C-3 and Benzylic Positions. *Eur. J. Med. Chem.* **1995**, 30, 199-208.

113. Aoyama, Y.; Uenaka, M.; Konoike, T.; Hayasaki-Kajiwara, Y.; Naya, N.; Nakajima, M. Inhibition of Serine Proteases: Activity of 1,3-Diazetidines-2,4-diones. *Bioorg. Med. Chem. Lett.* **2001**, 11, 1691-1694.

114. Cainelli, G.; Galletti, P.; Garbisa, S.; Giacomini, D.; Sartor, L.; Quintavalla, A. 4-Alkylidene-azetidines-2-ones: Novel Inhibitors of Leukocyte Elastase and Gelatinase. *Bioorg. Med. Chem.* **2003**, 11, 5391-5399.

115. Dell'Aica, I.; Sartor, L.; Galletti, P.; Giacomini, D.; Quintavalla, A.; Calabrese, F.; Giacometti, C.; Brunetta, E.; Piazza, F.; Agostini, C.; Garbisa, S. Inhibition of Leukocyte Elastase, Polymorphonuclear Chemoinvasion, and Inflammation-Triggered Pulmonary Fibrosis by a 4-Alkylidene- β -lactam with a Galloyl Moiety. *J. Pharm. Exp. Ther.* **2006**, 316, 539-546.

116. Tsang, W. Y.; Ahmed, N.; Harding, L. P.; Hemming, K.; Laws, A. P.; Page, M. I. Acylation versus Sulfonylation in the Inhibition of Elastase by 3-Oxo- β -Sultams. *J. Am. Chem. Soc.* **2005**, 127, 8946-8947.

117. Ahmed, N.; Tsang, W. Y.; Page, M. I. Acyl vs Sulfonyl Transfer in N-Acyl β -Sultams and 3-Oxo- β -sultams. *Org. Lett.* **2003**, 6, 201-203.

118. Laws, A. P.; Page, M. I. The Effect of the Carboxy Group on the Chemical and Beta-Lactamase Reactivity of Beta-Lactam Antibiotics. *J. Chem. Soc. - Perkin Trans. 2* **1989**, 1577-1581.

119. Page, M. I.; Laws, A. P.; Slater, M. J.; Stone, J. R. Reactivity of β -Lactams and Phosphoramidates and Reactions with β -Lactamase. *Pure Appl. Chem.* **1995**, 67, 711-717.

120. Martins, L. Derivados β -Lactâmicos como Potenciais Inibidores da Elastase Humana. Master Thesis, University of Lisbon, Lisbon, 2002.
121. Gu, H. Z.; Fedor, L. R. Base-Catalyzed Elimination of *para*-Substituted Thiophenoxides from 4-(Arylthio)Azetidin-2-Ones. *J. Org. Chem.* **1990**, *55*, 5655-5657.
122. Shah, S.; Finke, P. E.; Doherty, J. B.; Barker, P.; Hagmann, W.; Dorn, C. P.; Firestone, R. A. New substituted azetidinones as anti-inflammatory and antidegenerative agents. EP0337549A1, 1989.
123. Vanallan, J. A.; Deacon, B. D. 2-Mercaptobenzimidazole - 2-Benzimidazolethiol. *Org. Syntheses* **1950**, *30*, 56-57.
124. Buncel, E.; Menon, B. Carbanion Mechanisms .6. Metalation of Arylmethanes by Potassium Hydride-18 Crown-6 Ether in Tetrahydrofuran and Acidity of Hydrogen. *J. Am. Chem. Soc.* **1977**, *99*, 4457-4461.
125. Perrin, D. D.; Dempsey, B.; Serjeant, E. P. *pK_a Predictions for Organic Acids and Bases*. Chapman and Hall: London, 1981.
126. Charton, M. Definition of Inductive Substituent Constants. *J. Org. Chem.* **1964**, *29*, 1222-&.
127. Hammond, G. S. A Correlation of Reaction Rates. *J. Am. Chem. Soc.* **1955**, *77*, 334-338.
128. Boyd, D. B.; Hermann, R. B.; Presti, D. E.; Marsh, M. M. Electronic-Structures of Cephalosporins and Penicillins .4. Modeling Acylation by β -Lactam Ring. *J. Med. Chem.* **1975**, *18*, 408-417.
129. Page, M. I.; Proctor, P. Mechanism of β -Lactam Ring-Opening in Cephalosporins. *J. Am. Chem. Soc.* **1984**, *106*, 3820-3825.
130. Proctor, P.; Gensmantel, N. P.; Page, M. I. The Chemical-Reactivity of Penicillins and Other β -Lactam Antibiotics. *J. Chem. Soc., Perkin Trans. 2* **1982**, 1185-1192.
131. Valente, E.; Gomes, J. R. B.; Moreira, R.; Iley, J. Kinetics and Mechanism of Hydrolysis of N-Acyloxymethyl Derivatives of Azetidin-2-one. *J. Org. Chem.* **2004**, *69*, 3359-3367.
132. Page, M. I. The Mechanisms of Reactions of β -Lactam Antibiotics. *Acc. Chem. Res.* **1984**, *17*, 144-151.

133. Page, M. I. The Reactivity of β -Lactams, the Mechanism of Catalysis and the Inhibition of β -Lactamases. *Curr. Pharm. Design* **1999**, 5, 895-913.
134. Page, M. I.; Laws, A. P. The Chemical Reactivity of β -Lactams, β -Sultams and β -Phospholactams. *Tetrahedron* **2000**, 56, 5631-5638.
135. Hinchliffe, P. S.; Wood, J. M.; Davis, A. M.; Austin, R. P.; Beckett, R. P.; Page, M. I. Structure-reactivity Relationships in the Inactivation of Elastase by β -Sultams. *Org. Biomol. Chem.* **2003**, 1, 67-80.
136. Kitz, R.; Wilson, I. B. Esters of Methanesulfonic Acid as Irreversible Inhibitors of Acetylcholinesterase. *J. Biol. Chem.* **1962**, 237.
137. Chabin, R.; Green, B. G.; Gale, P.; Maycock, A. L.; Weston, H.; Dorn, C. P.; Finke, P. E.; Hagmann, W. K.; Hale, J. J.; Maccoss, M.; Shah, S. K.; Underwood, D.; Doherty, J. B.; Knight, W. B. Mechanism of Inhibition of Human-Leukocyte Elastase by Monocyclic β -Lactams. *Biochemistry* **1993**, 32, 8970-8980.
138. Taylor, P.; Anderson, V.; Dowden, J.; Flitsch, S. L.; Turner, N. J.; Loughran, K.; Walkinshaw, M. D. Novel Mechanism of Inhibition of Elastase by β -Lactams Is Defined by Two Inhibitor Crystal Complexes. *J. Biolog. Chem.* **1999**, 274, 24901-24905.
139. Kuzin, A. P.; Nukaga, M.; Nukaga, Y.; Hujer, A.; Bonomo, R. A.; Knox, J. R. Inhibition of the SHV-1 β -Lactamase by Sulfones: Crystallographic Observation of Two Reaction Intermediates with Tazobactam. *Biochemistry* **2001**, 40, 1861-1866.
140. Padayatti, P. S.; Helfand, M. S.; Totir, M. A.; Carey, M. P.; Hujer, A. M.; Carey, P. R.; Bonomo, R. A.; Akker, F. v. d. Tazobactam Forms a Stoichiometric *trans*-Enamine Intermediate in the E166A Variant of SHV-1 β -Lactamase: 1.63 Å Crystal Structure. *Biochemistry* **2004**, 43, 843-848.
141. Massova, I.; Mobashery, S. Molecular Bases for Interactions between β -Lactam Antibiotics and β -Lactamases. *Acc. Chem. Res.* **1997**, 30, 162-168.
142. Morrison, J. F.; Walsh, C. T. The behavior and significance of slow-binding enzyme inhibitors. *Adv. Enzymol.* **1988**, 61, 201-301.
143. Gutschow, M.; Neumann, U. Novel Thieno[2,3-d][1,3]oxazin-4-ones as Inhibitors of Human Leukocyte Elastase. *J. Med. Chem.* **1998**, 41, 1729-1740.
144. Shah, S. K.; Brause, K. A.; Chandler, G. O.; Finke, P. E.; Ashe, B. M.; Weston, H.; Knight, W. B.; Maycock, A. L.; Doherty, J. B. Inhibition of Human

- Leukocyte Elastase. 3. Synthesis and Activity of 3'-Substituted Cephalosporins. *J. Med. Chem.* **1990**, 33, 2529-2535.
145. Buynak, J. D.; Rao, A. S.; Ford, G. P.; Carver, C.; Adam, G.; Geng, B.; Bachmann, B.; Shobassy, S.; Lackey, S. 7-Alkylidenecephalosporin Esters as Inhibitors of Human Leukocyte Elastase. *J. Med. Chem.* **1997**, 40, 3423-3433.
146. Testa, E.; Fontanella, L.; Cristiani, G. F.; Mariani, L. Auf das Zentralnervensystem wirkende Substanzen XV. Über Azetidin-2,4-Dione (Malonimide). *Helv. Chim. Acta* **1959**, 42, 2370-2379.
147. Testa, E.; Fontanella, L. Auf Das Zentralnervensystem Wirkende Substanzen, XXIV. Über Azetidindione-(2.4), II. *Ann. Chem.-Justus Liebig* **1962**, 660, 118-134.
148. Oku, J.; Padias, A. B.; Hall, H. K.; East, A. J. Poly(3-Butyl-3-Ethylmalonimide) by Ring-Opening Polymerization. *Macromolecules* **1987**, 20, 2314-2315.
149. Graf, R.; Mundlos, E. Addition Compounds from Ketenes and Isocyanates. DE 1098515, 1961.
150. Ebnother, A.; Jucker, E.; Rissi, E.; Rutschmann, J.; Schreier, E.; Steiner, R.; Suess, R.; Vogel, A. Über Azetidin-2,4-Dione (Malonimide). *Helv. Chim. Acta* **1959**, 42, 918-955.
151. Golik, U. Synthesis of Malonimide Derivatives as Potential Penicillin Analogs. *J. Heter. Chem.* **1972**, 9, 21-24.
152. Kronenthal, D. R.; Han, C. Y.; Taylor, M. K. Oxidative N-dearylation of 2-azetidionones. p-Anisidine as a source of azetidinone nitrogen. *J. Org. Chem.* **1982**, 47, 2765-2768.
153. Ali, M. H.; Niedbalski, M.; Bohnert, G.; Bryant, D. Silica-Gel-Supported Cerium Ammonium Nitrate (CAN): A Simple and Efficient Solid-Supported Reagent for Oxidation of Oxygenated Aromatic Compounds to Quinones. *Syn. Commun.* **2006**, 36, 1715-1759.
154. Hartung, W. H.; Simonoff, R. Hydrogenolysis of Benzyl Groups Attached to Oxygen, Nitrogen, or Sulfur. *Organic Reactions* **1953**, 7, 263-326.
155. Laurent, M.; Belmans, M.; Kemps, L.; Cérésiat, M.; Marchand-Brynaert, J. A New Method of N-Benzhydryl Deprotection in 2-Azetidinone Series. *Synthesis* **2003**, 4, 570-576.

156. Wu, F.; Buhendwa, M. G.; Weaver, D. F. Benzhydryl as an Efficient Selective Nitrogen Protecting Group for Uracils. *J. Org. Chem.* **2004**, *69*, 9307-9309.
157. Tsang, W. The Chemical and Biological Activities of β -Sultams. PhD Thesis, The University of Huddersfield, Huddersfield, 2005.
158. King, J. F. *The Chemistry of Sulphonic Acids, Esters and Their Derivatives*. John Wiley: Chichester, 1991.
159. Li, Y.; Yang, Q.; Dou, D.; Alliston, K. R.; Groutas, W. C. Inactivation of Human Neutrophil Elastase by 1,2,5-Thiadiazolidin-3-one 1,1 Dioxide-based Sulfonamides. *Bioorg. Med. Chem.* **2008**, *16*, 692-698.
160. Li, Y.; Dou, D. F.; He, G. J.; Lushington, G. H.; Groutas, W. C. Mechanism-based inhibitors of serine proteases with high selectivity through optimization of S' subsite binding. *Bioorg. Med. Chem.* **2009**, *17*, 3536-3542.
161. Staudinger, H.; Endle, R. Ketene - The formation of δ -lactones from diphenyl ketene. *Justus Liebigs Ann. Chem.* **1913**, *401*, 263-292.
162. Martin, J. C.; Burpitt, R. D.; Gott, P. G.; Harris, M.; Meen, R. H. Ketenes .13. Reactions of Ketenes with Heterocumulenes. *J. Org. Chem.* **1971**, *36*, 2205-&.
163. Hafez, A. M. Generation of Highly Reactive Ketenes and Their Synthetic Utility as Intermediates in the Asymmetric Synthesis of Biologically Active Molecules. PhD Thesis, The Johns Hopkins University, Baltimore, 2003.
164. Poshkus, A. C.; Herweh, J. E. A New Reaction between Cyclohexanecarbonyl Chloride and Phenyl Isocyanate. *J. Org. Chem.* **1965**, *30*, 2466-2469.
165. Dai, S. A.; Juang, T.; Chen, C.; Chang, H.; Kuo, W.; Suo, W.; Jeng, R. Synthesis of N-Aryl Azetidine-2,4-diones and Polymalonamides Prepared from Selective Ring-Opening Reactions. *J. Appl. Polym. Sci.* **2007**, *103*, 3591-3599.
166. CCDC Software Ltd; Cambridge, UK.
167. DeLano, W. L. *The PyMOL Molecular Graphics System*, DeLano Scientific: San Carlos, CA, 2002.
168. Frederick, R.; Robert, S.; Charlier, C.; Wouters, J.; Masereel, B.; Pochet, L. Mechanism-based thrombin inhibitors: Design, synthesis, and molecular docking of a new selective 2-oxo-2H-1-benzopyran derivative. *J. Med. Chem.* **2007**, *50*, 3645-3650.
169. Koehl, C.; Knight, C. G.; Bieth, J. G. Compared Action of Neutrophil Proteinase 3 and Elastase on Model Substrates - Favorable Effect of S' -P'

Interactions on Proteinase 3 Catalysis. *Journal of Biological Chemistry* **2003**, 278, 12609-12612.

170. Nielsen, N. M.; Bundgaard, H. Facile Plasma-Catalysed Degradation of Penicillin Alkyl Esters but with No Liberation of the Parent Penicillin. *J. Pharm. Pharmacol.* **1988**, 40, 506-509.

171. Vincent, S. H.; Painter, S. K.; LufferAtlas, D.; Karanam, B. V.; McGowan, E.; Cioffe, C.; Doss, G.; Chiu, S. H. L. Orally active inhibitors of human leukocyte elastase .2. Disposition of L-694,458 in rats and rhesus monkeys. *Drug Metab. Dispos.* **1997**, 25, 932-939.

172. Varga, M.; Kapui, Z.; Bátori, S.; Nagy, L. T.; Vasvári-Debreczy, L.; Mikus, E.; Urbán-Szabó, K.; Arányi, P. A Novel Orally Active Inhibitor of HLE. *European Journal of Medicinal Chemistry* **2003**, 38, 421-425.

173. Gérard, S.; Galleni, M.; Dive, G.; Brynaert, J. M. Synthesis and Evaluation of N1/C4-Substituted β -Lactams as PPE and HLE Inhibitors. *Bioorganic & Medicinal Chemistry* **2004**, 12, 129-138.

174. Lee, H. S.; Kim, D. H. Synthesis and Evaluation of α,α -Disubstituted-3-mercaptopropanoic Acids as Inhibitors for Carboxypeptidase A and Implications with Respect to Enzyme Inhibitor Design. *Bioorg. Med. Chem.* **2003**, 11, 4685-4691.

175. Valente, C.; Moreira, R.; Guedes, R. C.; Iley, J.; Jaffar, M.; Douglas, K. T. The 1,4-naphthoquinone scaffold in the design of cysteine protease inhibitors. *Bioorg. Med. Chem.* **2007**, 15, 5340-5350.

176. Leslie, A. G. W. Joint CCP4 + ESF-EAMCB Newsletter on Protein Crystallography, 26. http://www.mrc-lmb.cam.ac.uk/harry/mosflm/mosflm_user_guide.html. (2009).

177. Bailey, S. The Ccp4 Suite - Programs for Protein Crystallography. *Acta Crystallogr. D - Biol. Crystallog.* **1994**, 50, 760-763.

178. Murshudov, G. N.; Vagin, A. A.; Dodson, E. J. Refinement of macromolecular structures by the maximum-likelihood method. *Acta Crystallogr. D - Biol. Crystallog.* **1997**, 53, 240-255.

179. Krissinel, E. B.; Winn, M. D.; Ballard, C. C.; Ashton, A. W.; Patel, P.; Potterton, E. A.; McNicholas, S. J.; Cowtan, K. D.; Emsley, P. The New CCP4 Coordinate Library as a Toolkit for the Design of Coordinate-Related Applications in Protein Crystallography. *Acta Crystallogr. D - Biol. Crystallog.* **2004**, 60, 2250-2255.

180. Hartley, B. S. Amino-Acid Sequence of Bovine Chymotrypsinogen-A. *Nature* **1964**, 201, 1284-1287.
181. Gaspar, M. M.; Cruz, A.; Penha, A. E.; Reymao, J.; Sousa, A. C.; Eleuterio, C. V.; Domingues, S. A.; Fraga, A. G.; Filho, A. L.; Cruz, M. E. M.; Pedrosa, J. Rifabutin encapsulated in liposomes exhibits increased therapeutic activity in a model of disseminated tuberculosis. *Int. J. Antimicrob. Agents* **2008**, 31, 37-45.
182. Battaglia, R.; Pianezzola, E.; Salgarollo, G.; Zini, G.; Benedetti, M. S. Absorption, Disposition and Preliminary Metabolic Pathway of C-14 Rifabutin in Animals and Man. *J. Antimicrob. Chemother.* **1990**, 26, 813-822.
183. Benedetti, M. S.; Pianezzola, E.; Brianceschi, G.; Jabes, D.; Dellabruna, C.; Rocchetti, M.; Poggesi, I. An Investigation of the Pharmacokinetics and Autoinduction of Rifabutin Metabolism in Mice Treated with 10 Mg/Kg/Day 6 Times a Week for 8 Weeks. *J. Antimicrob. Chemother.* **1995**, 36, 247-251.
184. Jones, G.; Willett, P.; Glen, R. C.; Leach, A. R.; Taylor, R. Development and validation of a genetic algorithm for flexible docking. *J. Mol. Biol.* **1997**, 267, 727-748.
185. Navia, M. A.; McKeever, B. M.; Springer, J. P.; Lin, T.; Williams, H. R.; Fluder, E. M.; Dorn, C. P.; Hoogsteen, K. Structure of Human Neutrophil Elastase in Complex with a Peptide Chloromethyl Ketone Inhibitor at 1.84-Å Resolution. *Proc. Nat. Acad. Sci.* **1989**, 86, 7-11.
186. Cornell, W. D.; Cieplak, P.; Bayly, C. I.; Gould, I. R.; Merz, K. M.; Ferguson, D. M.; Spellmeyer, D. C.; Fox, T.; Caldwell, J. W.; Kollman, P. A. A 2nd Generation Force-Field for the Simulation of Proteins, Nucleic-Acids, and Organic-Molecules. *J. Amer. Chem. Soc.* **1995**, 117, 5179-5197.
187. Pettersen, E. F.; Goddard, T. D.; Huang, C. C.; Couch, G. S.; Greenblatt, D. M.; Meng, E. C.; Ferrin, T. E. UCSF chimera - A visualization system for exploratory research and analysis. *J. Comput. Chem.* **2004**, 25, 1605-1612.
188. Parr, R. G.; Yang, W. *Density Functional Theory of the Electronic Structure of Molecules*. Oxford University Press: Oxford, UK, 1989.
189. Becke, A. D. Density Functional Thermochemistry 3. The Role of Exact Exchange. *J. Chem. Phys.* **1993**, 98, 5648-5652.

190. Lee, C. T.; Yang, W. T.; Parr, R. G. Development of the Colle-Salvetti Correlation-Energy Formula into a Functional of the Electron-Density. *Phys. Rev. B* **1988**, *37*, 785-789.
191. Frisch, M.; et, a. *Gaussian 03*, Revision C.02, Gaussian Inc.; Wallingford CT, 2004.
192. Wang, J. M.; Wang, W.; Kollman, P. A.; Case, D. A. Automatic atom type and bond type perception in molecular mechanical calculations. *J. Mol. Graph. Model.* **2006**, *25*, 247-260.
193. Wood, J. The reactivity of β -sultams and their application as enzyme inhibitors. PhD Thesis, The University of Huddersfield, Huddersfield, 2001.
194. Colson, E.; Wallach, J.; Hauteville, M. Synthesis and Anti-Elastase Properties of 6-Amino-2-phenyl-4H-3,1-benzoxazin-4-one Aminoacyl and Dipeptidyl Derivatives. *Biochimie* **2005**, *87*, 223-230.

Publications resulting from this thesis

- I. Oliveira, T. F.; **Mulchande, J.**; Moreira, R.; Iley, J.; Archer, M. Crystallization and Preliminary Diffraction Studies of Porcine Pancreatic Elastase in Complex with a Novel Inhibitor. *Protein Pept. Lett.* **2007**, 14, 93-95.
- II. **Mulchande, J.**; Martins, L.; Moreira, R.; Archer, M.; Oliveira, T. F.; Iley, J. The Efficiency of C-4 Substituents in Activating the β -Lactam Scaffold towards Serine Proteases and Hydroxide Ion. *Org. Biomol. Chem.* **2007**, 5, 2617-2626.
- III. **Mulchande, J.**; Guedes, R. C.; Tsang, W. Y.; Page, M. I.; Moreira, R.; Iley, J. Azetidine-2,4-diones (4-Oxo- β -lactams) as Scaffolds for Designing Elastase Inhibitors. *J. Med. Chem.* **2008**, 51, 1783-1790.
- IV. **Mulchande, J.**; Oliveira, R.; Carrasco, M.; Gouveia, L.; Guedes, R. C.; Iley, J.; Moreira, R. Azetidine-2,4-diones (4-Oxo- β -lactams) Are Potent and Selective Inhibitors of Human Leukocyte Elastase. *J. Med. Chem.* (*in press*).
- V. **Mulchande, J.**; Simões, S. I.; Gaspar, M. M.; Eleutério, C. V.; Oliveira, R.; Cruz, M. E. M.; Moreira, R.; Iley, J. Synthesis, Stability, Biochemical and Pharmacokinetic Properties of a New Potent and Selective 4-Oxo- β -lactam Inhibitor of Human Leukocyte Elastase. *J Pharm. Pharmacol.* (*in preparation*).
- VI. **Mulchande, J.**; Lopes, F.; Moreira, R., Azetidin-2-ones and Related Systems as Enzyme Inhibitors: Synthesis and Reactivity. *Heterocycles Review Book* (book chapter), Research Signpost Ed. (*in preparation*).

Crystallization and Preliminary Diffraction Studies of Porcine Pancreatic Elastase in Complex with a Novel Inhibitor

Tânia F. Oliveira^a, Jalmira Mulchande^b, Rui Moreira^b, Jim Iley^c and Margarida Archer^{a,*}

^aInstituto de Tecnologia Química e Biológica, Universidade Nova de Lisboa, ITQB-UNL, Av. República, Apt. 127, 2781-901 Oeiras, Portugal; ^bCEFC, Faculdade de Farmácia, Universidade de Lisboa, Av. Forças Armadas, 1600-083 Lisboa, Portugal; ^cChemistry Department, The Open University, Milton Keynes, MK7 6AA, UK

Abstract: Porcine pancreatic elastase (PPE) was crystallized in complex with a novel inhibitor at pH 5 and X-ray diffraction data were collected at a synchrotron source to 1.66 Å. Crystals belong to the orthorhombic space group P2₁2₁2₁, with unit cell parameters a = 50.25 Å, b = 57.94 Å and c = 74.69 Å. PPE is often used as model for drug target, due to its structural homology with the important therapeutic target human leukocyte elastase (HLE). Elastase is a serine protease that belongs to the chymotrypsin family, which has the ability to degrade elastin, an important component in connective tissues. Excessive elastin proteolysis leads to a number of pathological diseases.

Keywords: Human leukocyte elastase, Porcine pancreatic elastase, β-Lactams inhibitors, Crystallization.

INTRODUCTION

Human leukocyte elastase (HLE, EC 3.4.21.37) is a serine protease released from polymorphonuclear leukocytes (neutrophils) in response to inflammatory stimuli and mediators [1]. HLE degrades very efficiently various tissue matrix proteins such as elastin and in healthy individuals its proteolytic activity is regulated by potent endogenous anti-proteases such as α₁-antitrypsin and secretory leukocyte proteinase inhibitor [2]. Imbalance between HLE and its endogenous inhibitors leads to excessive elastin proteolysis and destruction of connective tissues in a number of inflammatory diseases such as pulmonary emphysema, adult respiratory distress syndrome (ARDS), chronic bronchitis, chronic obstructive pulmonary disease (COPD), pulmonary hypertension and rheumatoid arthritis [3-6], as well as in other pulmonary pathophysiological states, e.g. cystic fibrosis [7].

The design of low molecular-weight inhibitors of elastases has received considerable attention due to their potential therapeutic usefulness [8, 9]. Understanding the nature of inhibition and structure of the ligand-enzyme complex is a fundamental step in any structure-based lead optimization project. This is particularly true for mechanism-based inhibitors that can lead to a double-hit inactivation process [10]. β-Lactams (azetidins-2-ones) are potent inhibitors of a wide range of enzymes that contain serine as the catalytic residue [11-13]. Many structural and inhibition studies with β-lactams have been conducted with the readily available porcine pancreatic elastase (PPE) [14, 15]. Indeed, the sequence identity between PPE and HLE is ca. 40% [16], and despite small differences in the primary specificity pockets [1], PPE is considered to be a good model for HLE to be used in preliminary inhibition studies.

Herein we report the crystallization and preliminary X-ray diffraction analysis of PPE inactivated with the β-lactam (Fig. 1), which contains a potential leaving group at C-4 position of the four-membered ring. Compound JM54 (Fig. 1) is a novel potent irreversible inhibitor of PPE ($k_{\text{obs}}/[\text{I}]$ of 290 M⁻¹s⁻¹) that requires only ca. 1 mol. equivalent to inactivate the enzyme [17]. We aim towards a detailed structural characterization of the molecular interactions of PPE with this potential mechanism-based inhibitor.

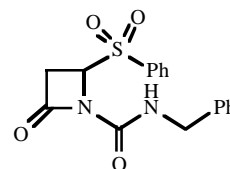


Figure 1. Molecular structure of the synthesized inhibitor JM54.

MATERIALS AND METHODS

Crystallization

Elastase from porcine pancreas (E.C. 3.4.21.36) was purchased from Serva (Cat No 20929) and was used without any further purification. The protein (MW of 25.9 kDa) was dissolved in bidistilled water to a concentration of 40 mg/ml. A concentrated solution (~150 mM) of the synthesized inhibitor JM54, was freshly prepared in DMSO. JM54 was incubated with PPE for 30 minutes at room temperature (inhibitor in a 10 molar excess, final concentration of 10% DMSO). The crystallization trials were set up at 293 K using the sitting drop vapour-diffusion method, and were based on previously known crystallization conditions [18, 19]. PPE co-crystallized with the inhibitor JM54 in 200 mM sodium sulfate and 100 mM sodium acetate at pH 5.1 yielded good quality crystals. Native crystals were also grown under the same experimental conditions to test soaking procedures with the inhibitor.

*Address correspondence to this author at the Instituto de Tecnologia Química e Biológica, Universidade Nova de Lisboa, ITQB-UNL, Av. República, Apt. 127, 2781-901 Oeiras, Portugal; E-mail: archer@itqb.unl.pt

X-Ray Data Collection and Phasing

Crystals were cryoprotected with the reservoir solution supplemented with 30% glycerol and were flash cooled in liquid nitrogen (100 K). X-ray diffraction data were collected to 1.66 Å at EMBL X11 beamline at the DORIS storage ring, DESY, Hamburg (Germany), using a wavelength of 0.82 Å. A total of 136 images were collected on a MARCCD-165 mm detector with an oscillation angle of 1.5° and an exposure time of 20 s per frame. The X-ray data were integrated and scaled using MOSFLM [20] and SCALA programs [21]. Since the crystals obtained for the enzyme:inhibitor complex were isomorphous to the native ones and belonged to the same space group, the structure was solved by Fourier synthesis [18, 19]. A rigid-body refinement step was performed with Refmac [22] yielding an R-work and R-free of 27.7 and 30.5%, respectively.

RESULTS AND DISCUSSION

The crystal quality was optimized by varying the PPE concentration (10 to 40 mg/ml), and by trying different protein:reservoir volumes and ratios. The best crystals were obtained by mixing equal volumes (1-2 µl) of PPE/JM54 mixture (~40 mg/ml) and reservoir solution. The reservoir solution contained 200 mM sodium sulfate and 100 mM sodium acetate at pH 5.1. Crystals grew within 1 to 3 days to maximum dimensions of approximately 0.8 x 0.5 x 0.1 mm (Fig. 2). X-ray diffraction data were collected at EMBL/DESY synchrotron, Hamburg to 1.66 Å (Fig. 3). Data collection and processing statistics are given in Table 1. Crystals belong to the orthorhombic space group $P2_12_12_1$ with unit cell parameters $a = 50.25$ Å, $b = 57.94$ Å and $c = 74.69$ Å. The calculated V_M [23] is 2.1 Å³/Da, which corresponds to a solvent content of ~ 41% and one molecule per asymmetric unit. Crystals of native PPE [18, 19] and PPE/inhibitor complexes [24-26] grown under the same experimental conditions show similar cell parameters. The initial calculated maps showed electron density near the catalytic triad, which corresponds to the inhibitor. Model fitting and further refinement is now in progress.

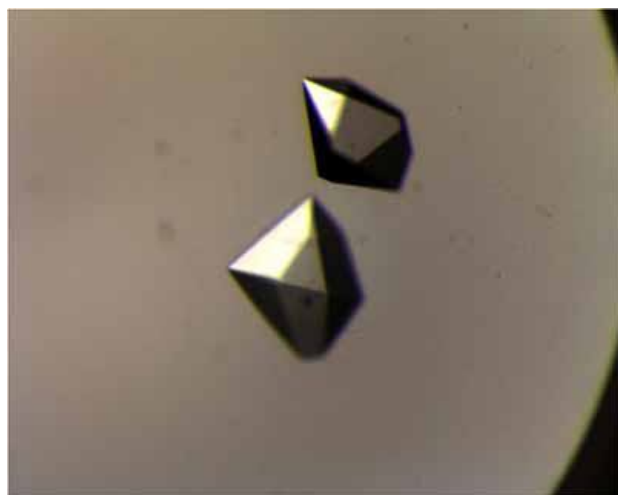


Figure 2. Crystals of PPE/JM54 complex with dimensions - 0.6 x 0.4 x 0.4 mm

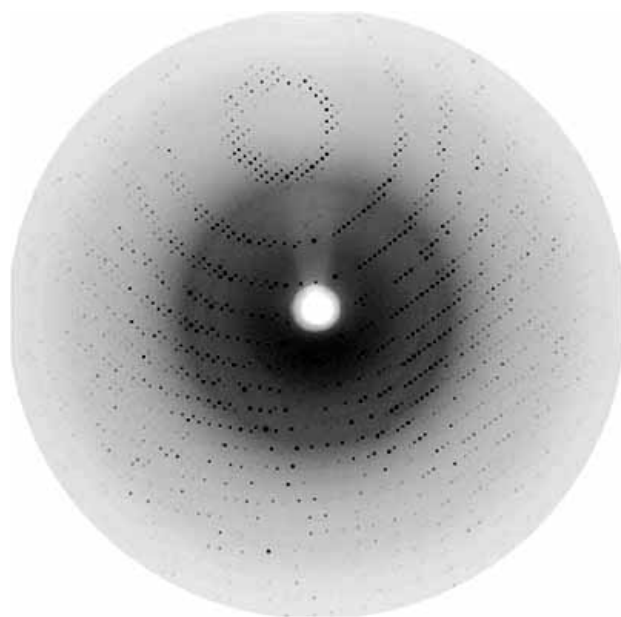


Figure 3. Diffraction pattern of the PPE/JM54 crystal collected at the X11 beamline at DESY-Hamburg.

Table 1. X-Ray Data Collection Statistics

Wavelength (Å)	0.82
Resolution range (Å)	37.95 - 1.66
Space group	$P2_12_12_1$
Unit cell parameters (Å)	$a = 50.25, b = 57.94, c = 74.69$
Total reflections	177649
Unique reflections	26474
Completeness (%)	96.9 (79.8)
Redundancy	4.3 (4.1)
R_{merge}^* (%)	3.0 (9.3)
$I/\sigma(I)$	27.4 (14.7)

Values in parenthesis show the statistics of the highest resolution shell (1.75 - 1.66 Å).
 $* R_{\text{merge}} = \frac{\sum_{hkl} \sum_i |I_i(hkl) - \bar{I}(hkl)|}{\sum_{hkl} \sum_i I_i(hkl)}$ where I_i is the i^{th} measurement.

ACKNOWLEDGMENTS

The authors thank Fundação para a Ciência e Tecnologia for an FCT fellowship to T.F.O (project POCI/BIA-PRO/55621/2004) and the pluriannual funding to the CECF research unit and ITQB. J.M. thanks FCT and the European Social Fund (ESF) for the award of Ph.D. research grant (SFRH/BD/17534/2004). Support from the European Community - Research Infrastructure Action under the FP6 was provided to collect X-ray diffraction data at EMBL/DESY, Hamburg.

ABBREVIATIONS

PPE = Porcine Pancreatic Elastase

HLE = Human Leukocyte Elastase

DMSO = Dimethyl Sulfoxide

REFERENCES

- [1] Bode, W., Meyer, E., Jr. and Powers, J.C., (1989) *Biochem.*, 28, 1951-1963.
- [2] Barnes, P.J., (2000) *N. Engl. J. Med.*, 343, 269-280.
- [3] Cowan, K.N., Heilbut, A., Humpl, T., Lam, C., Ito, S. and Rabinovitch, M., (2000) *Nat. Med.*, 6, 698-702.
- [4] Ohbayashi, H., (2005) *Expert. Opinion on Therapeutic Patents*, 15, 759-771.
- [5] Donnelly, L.E. and Rogers, D.F., (2003) *Drugs*, 63, 1973-1998.
- [6] Fujita, J., Nelson, N.L., Daughton, D.M., Dobry, C.A., Spurzem, J.R., Irino, S. and Rennard, S.I., (1990) *Am Rev. Respir. Dis.*, 142, 57-62.
- [7] Griese, M., von Bredow, C., Birrer, P. and Schams, A., (2001) *Pulm. Pharmacol. Ther.*, 14, 461-467.
- [8] Malhotra, S., Man, S.F. and Sin, D.D., (2006) *Expert Opin. Emerg. Drugs*, 11, 275-291.
- [9] Bernstein, P.R., Edwards, P.D. and Williams, J.C., (1994) *Prog. Med. Chem.*, 31, 59-120.
- [10] Powers, J.C., Asgian, J.L., Ekici, O.D. and James, K.E., (2002) *Chem. Rev.*, 102, 4639-4750.
- [11] Konaklieva, M.I., (2002) *Curr. Med. Chem. Anti-Infective Agents*, 1, 215-238.
- [12] Konaklieva, M.I. and Plotkin, B.J., (2004) *Mini Rev. Med. Chem.*, 4, 721-739.
- [13] Leung, D., Abbenante, G. and Fairlie, D.P., (2000) *J. Med. Chem.*, 43, 305-341.
- [14] Wilmouth, R.C., Kassamally, S., Westwood, N.J., Sheppard, R.J., Claridge, T.D., Aplin, R.T., Wright, P.A., Pritchard, G.J. and Schofield, C.J., (1999) *Biochemistry*, 38, 7989-7998.
- [15] Wilmouth, R.C., Clifton, I.J. and Neutze, R., (2000) *Nat Prod Rep*, 17, 527-533.
- [16] Sinha, S., Watorek, W., Karr, S., Giles, J., Bode, W., Travis, J., (1987) *Proc. Natl. Acad. Sci., USA*, 84, 2229-2232.
- [17] Mulchande, J., Martins, L. and Moreira, R., (2006) *Drugs Fut.*, 31, 194.
- [18] Weiss, M.S., Panjikar, S., Nowak, E. and Tucker, P.A., (2002) *Acta Cryst. D*, 58, 1407-1412.
- [19] Wurtele, M., Hahn, M., Hilpert, K. and Hohne, W., (2000) *Acta Cryst. D*, 56, 520-523.
- [20] Leslie, A.G.W., (1992) Joint CCP4 + ESF-EAMCB Newsl. Protein Crystallogr., 26.
- [21] Collaborative Computational Project, N. 4, (1994) *Acta Cryst. D*, 50, 760-763.
- [22] Murshudov, G.N., Vagin, A.A. and Dodson, E.J., (1997) *Acta Cryst. D*, 53, 240-255.
- [23] Matthews, B.W., (1968) *J. Mol. Biol.*, 33, 491-497.
- [24] Ay, J., Hilpert, K., Krauss, N., Schneider-Mergener, J. and Hohne, W., (2003) *Acta Cryst. D*, 59, 247-254.
- [25] Kinoshita, T., Kitatani, T., Warizaya, M. and Tada, T., (2005) *Acta Cryst. F*, 61, 808-811.
- [26] Wilmouth, R.C., Clifton, I.J., Robinson, C.V., Roach, P.L., Aplin, R.T., Westwood, N.J., Hajdu, J. and Schofield, C.J., (1997) *Nat. Struct. Biol.*, 4, 456-462.

The efficiency of C-4 substituents in activating the β -lactam scaffold towards serine proteases and hydroxide ion†

Jalmira Mulchande,^a Luísa Martins,^a Rui Moreira,^{*a} Margarida Archer,^b Tania F. Oliveira^b and Jim Iley^c

Received 2nd May 2007, Accepted 26th June 2007

First published as an Advance Article on the web 16th July 2007

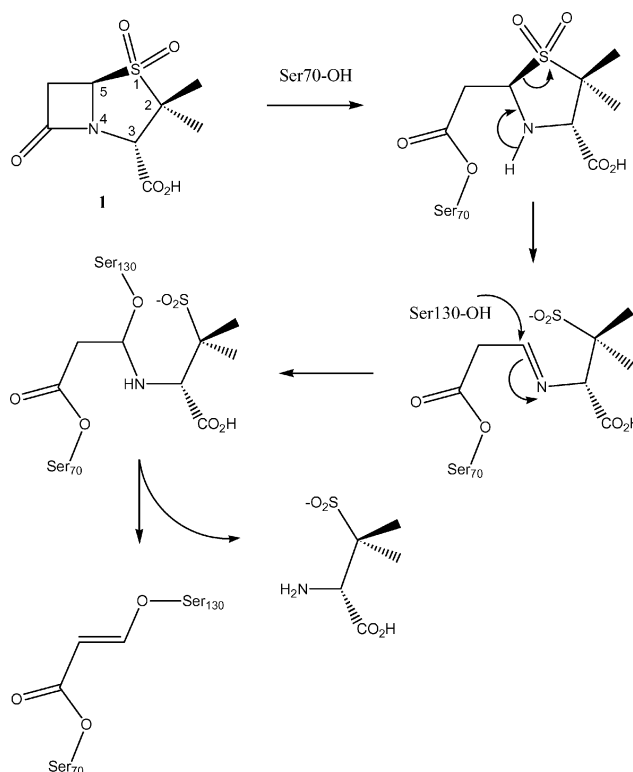
DOI: 10.1039/b706622h

The presence of a leaving group at C-4 of monobactams is usually considered to be a requirement for mechanism-based inhibition of human leukocyte elastase by these acylating agents. We report that second-order rate constants for the alkaline hydrolysis and elastase inactivation by *N*-carbamoyl monobactams are independent of the pK_a of the leaving group at C-4. Indeed, the effect exerted by these substituents is purely inductive: electron-withdrawing substituents at C-4 of *N*-carbamoyl-3,3-diethylmonobactams increase the rate of alkaline hydrolysis and elastase inactivation, with Hammett ρ_1 values of 3.4 and 2.5, respectively, which indicate the development of a negative charge in the transition-states. The difference in magnitude between these ρ_1 values is consistent with an earlier transition-state for the enzymatic reaction when compared with that for the chemical process. These results suggest that the rate-limiting step in elastase inactivation is the formation of the tetrahedral intermediate, and that β -lactam ring-opening is not concerted with the departure of a leaving group from C-4. Monobactam sulfones emerged as potent elastase inhibitors even when the ethyl groups at C-3, required for interaction with the primary recognition site, are absent. For one such compound, a 1 : 1 enzyme–inhibitor complex involving porcine pancreatic elastase has been examined by X-ray crystallography and shown to result from serine acylation and sulfinic acid departure from the β -lactam C-4.

Introduction

β -Lactams are potent inhibitors of a wide range of enzymes that contain a catalytic serine residue, including the hepatitis C virus serine protease, penicillin-binding proteins (PBPs), β -lactamases and human leukocyte elastase (HLE).^{1–7} The efficiency of β -lactams as enzyme inhibitors depends on the molecular recognition by the protein as well as on the intrinsic chemical reactivity of the β -lactam, both of which affect the rate at which these inhibitors acylate the serine residue.⁸

Among the most extensively studied enzymatic reactions of β -lactams is the inhibition of class A β -lactamases by penam sulfone inhibitors such as sulbactam, **1** (Scheme 1), tazobactam and their analogues.^{9–15} Reaction of penam sulfones with the catalytic Ser70 involves β -lactam ring-opening and leads to the departure of a sulfinic acid leaving group from C-5 and formation of an imine (Scheme 1).^{1,14} The imine then undergoes a cascade of reactions including nucleophilic attack by the Ser130 hydroxyl group to form a stable acrylate ester capable of preventing hydrolysis of the acyl-enzyme, and thus leading to irreversible inhibition.¹¹ The oxidation state of the sulfur atom in the penam plays a role in potency: while sulbactam is a potent β -lactamase inhibitor, its penicillanate counterpart is only a substrate of β -lactamase,



Scheme 1

while the corresponding sulfoxides are both substrate and weak inactivators.¹⁰ It is worth noting that β -lactamase inhibition by clavulanic acid, **2**, requires intramolecular hydrogen bonding from

^ai-Med-UL, Faculdade de Farmácia, Universidade de Lisboa, Av. Forças Armadas, 1600-083, Lisboa, Portugal

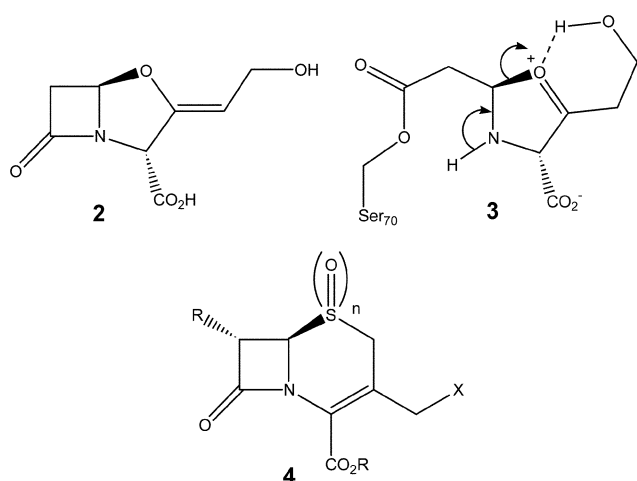
^bInstituto de Tecnologia Química e Biológica, Universidade Nova de Lisboa, ITQB-UNL, Av., República, Apt. 127, 2781-901, Oeiras, Portugal

^cDepartment of Chemistry, The Open University, Milton Keynes, MK7 6AA, UK

† Electronic supplementary information (ESI) available: X-Ray data collection statistics. See DOI: 10.1039/b706622h

the C-9 hydroxyl group to assist the departure of an oxonium oxygen from C-5, *i.e.* **3** (species **3** results from proton transfer from a water molecule, Wat673, to the carbon–carbon double bond of the acyl-enzyme).¹⁶ These results suggest that departure of a good leaving group from the C-5 carbon atom of penams and clavams is required to achieve irreversible inhibition of enzymes containing a catalytic serine residue.^{10,17}

Cephalosporins are time-dependent inhibitors of HLE inhibitors, and, similarly to penams, the oxidation state of the sulfur atom also plays a role in potency, with sulfones (**4**, $n = 2$) showing considerably greater activity than the corresponding sulfides (**4**, $n = 0$) or β -sulfoxides (**4**, $n = 1$), while α -sulfoxides are inactive.^{18–21} However, the identity of the species giving rise to inhibition remains to be defined. X-Ray crystallography indicates that inactivation of HLE by cephalosporin sulfones containing a good leaving group at C-3' (*e.g.* **4**, X = AcO) preferably involves reaction with His57 at this position rather than sulfinic acid departure from C-6 and thiazine ring-opening.²²



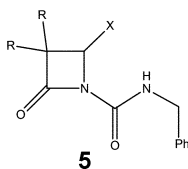
Monobactams containing potential leaving groups at C-4 have also been developed as mechanism-based inhibitors of HLE,^{23–25} although the requirement of leaving-group departure to achieve irreversible inactivation is still controversial. Crystallography²⁶ and mass spectrometry²⁷ studies indicate that the reaction of monobactams containing a C-4 aryloxy substituent with HLE involves the departure of a phenol, possibly concerted with C–N bond fission and β -lactam ring-opening.²⁸ However, the observation that the second-order rate-constants for HLE inactivation by monobactams with no leaving group at C-4 do not differ significantly from those of monobactams containing a phenol²⁸ suggests that leaving group ability is not essential to inactivate the enzyme. Understanding how β -lactam substituents affect molecular recognition by the enzyme and “chemical reactivity” is most useful in designing more potent enzyme inhibitors. We report here a study on the chemistry of elastase inactivation by model monobactams, **5** (Scheme 2, Table 1) with the objective of elucidating how C-4 substituents contribute to the chemical reactivity towards the catalytic serine. The results herein presented show that the effect exerted by these substituents is largely inductive and that sulfones at C-4 are particularly efficient in activating the β -lactam scaffold towards elastase.

Results and discussion

1. Chemistry

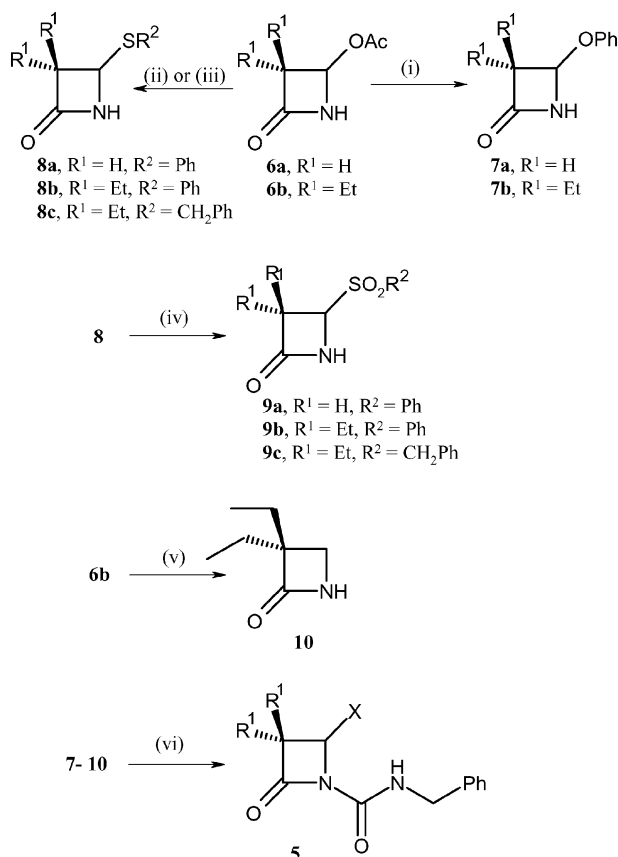
The synthesis of compounds **5** used the appropriate 4-acetoxiazetid-2-one **6**²⁴ as the starting material to give direct access to the differently C-4-substituted azetid-2-one key intermediates **7–10** (Scheme 2). Reaction of 4-acetoxiazetid-2-ones **6** with phenol²⁴ (or thiols²⁹) and sodium hydroxide in acetone at room temperature gave the corresponding C-4-substituted β -lactams **7** and **8**, respectively. Alternatively, **8a** was synthesised by refluxing **6a** with thiophenol in benzene.³⁰ Treatment of thioethers **8** with 3-chloroperbenzoic acid (MCPBA) yielded the

Table 1 Second-order rate constants, k_{OH^-} , for the hydroxide-catalyzed hydrolysis of 4-substituted azetid-2-ones, **5**, at 25 °C and the kinetic parameters for the time-dependent inactivation of porcine pancreatic elastase (**5a–d**) and human leukocyte elastase (**5e–k**) in pH 7.2 buffer at 25 °C



Compound	R	X	$\text{p}K_{\text{a}}(\text{XH})$	$(k_{\text{inact}}/K_{\text{i}})/\text{M}^{-1} \text{s}^{-1}$	$10^2 k_{\text{OH}^-}/\text{M}^{-1} \text{s}^{-1}$	EREF ^f
5a	H	H	3.5 ⁵³	NI ^f	13.0	—
5b	H	OPh	9.92 ⁵⁴	11.5 ^a	99.0	11.6
5c	H	SPh	6.52 ⁵⁴	22.0 ^a	44.1	50.0
5d	H	SO ₂ Ph	1.29 ⁵⁵	290 ^a	416	70.0
5e	Et	H	3.5 ⁵³	310 ^b	0.164	1.89 × 10 ⁵
5f	Et	OPh	9.92 ⁵⁴	2280 ^b	0.722	3.15 × 10 ⁵
5g	Et	SPh	6.52 ⁵⁴	5760 ^{b,c}	0.713	8.08 × 10 ⁵
5h	Et	SO ₂ Ph	1.29 ⁵⁵	15 200 ^{b,d}	14.2	1.07 × 10 ⁵
5i	Et	SCH ₂ Ph	9.27 ⁵⁴	4464 ^b	0.362	1.23 × 10 ⁶
5j	Et	SO ₂ CH ₂ Ph	1.45 ⁵⁵	11 741 ^b	12.7	9.24 × 10 ⁴
5k	Et	OC ₆ H ₄ -4-CO ₂ H	8.90 ⁵⁴	8320 ^{b,e}	ND ^f	ND ^f

^a Against PPE. ^b Against HLE. ^c **5g**: $K_{\text{i}} = 0.633 \mu\text{M}$, $k_{\text{inact}} = 3.64 \times 10^{-3} \text{s}^{-1}$. ^d **5h**: $K_{\text{i}} = 0.267 \mu\text{M}$, $k_{\text{inact}} = 4.06 \times 10^{-3} \text{s}^{-1}$. ^e **5k**: $K_{\text{i}} = 0.454 \mu\text{M}$, $k_{\text{inact}} = 3.78 \times 10^{-3} \text{s}^{-1}$. ^f NI: no inhibition, ND: not determined, EREF: enzyme rate enhancement factor.



Scheme 2 Reagents and conditions: (i) PhOH, NaOH, acetone; (ii) R²SH, NaOH, acetone; (iii) PhSH (2 mol equiv.), C₆H₆, reflux; (iv) MCPBA, DCM; (v) NaBH₄, EtOH; (vi) PhCH₂NCO, TEA, DCM.

corresponding sulfones **9** (Scheme 2). The C-4 unsubstituted intermediate **10** was synthesised by reduction of **6b** with NaBH₄ in ethanol at 0 °C.³¹ Finally, reaction of intermediates **7–10** with benzyl isocyanate gave the desired compounds **5** in good yield.

2. Enzyme inhibition studies

The series of β-lactams, **5a–d**, lacking substituents at the C-3 position was prepared to assess the impact of a leaving group at C-4 on porcine pancreatic elastase (PPE) inhibition when interaction with the S₁ primary recognition site³² of elastase is reduced. PPE is a readily available elastase that shares a conserved catalytic triad consisting of Ser195, His57 and Asp102 with HLE.³³ The primary specificity pocket of PPE is slightly less hydrophobic and smaller than that of HLE, showing preference for small aliphatic side chains such as alanine.³³ The kinetic studies carried out at pH 7.2 and 25 °C, using the incubation method,³⁴ showed that β-lactams **5b–d** containing leaving groups are time-dependent inhibitors of PPE, while the C-4-unsubstituted counterpart **5a** is inactive up to a concentration of 1 mM. The second-order rate constants for PPE inactivation, k_{inact}/K_1 (Table 1) were determined from the plots of pseudo-first-order inhibition rate constant, k_{obs} , versus [I] (Fig. 1). The sulfone derivative **5d** proved to be a potent inhibitor of PPE, with a k_{inact}/K_1 value of 290 M⁻¹ s⁻¹, thus suggesting that the sulfone group is a very powerful activator of the β-lactam carbonyl carbon atom towards the Ser195 hydroxyl group, even in

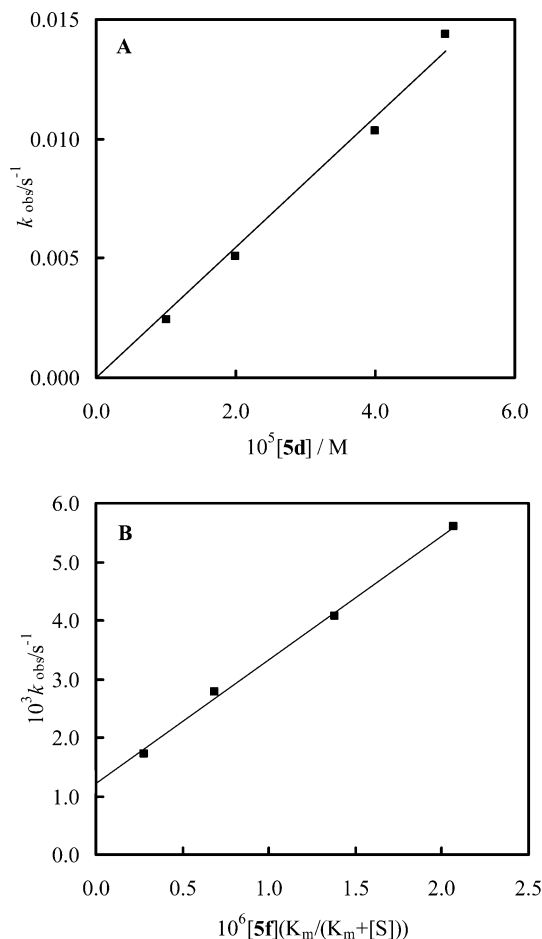


Fig. 1 Dependence of k_{obs} for enzyme inhibition on inhibitor concentration: (A), **5d**, porcine pancreatic elastase; (B), **5f**, human leucocyte elastase.

the absence of an adequate molecular recognition moiety at C-3 in the β-lactam scaffold.

Further evidence of the efficiency of **5d** as an irreversible inhibitor of PPE comes from the titration of enzyme activity. The number of equivalents required to inactivate PPE was calculated by plotting the fraction of remaining enzyme activity, v/v_0 , after a 30 min incubation period versus the initial ratio of inhibitor to enzyme, *i.e.* [I]/[E]₀. For levels of inhibition of up to 90% of the original enzyme activity, the extent of inactivation was found to depend linearly on the inhibitor-to-enzyme molar ratio (Fig. 2), and extrapolation of the line to $v/v_0 = 0$ shows that it required approximately 1.2 equiv. of **5d** to completely inactivate PPE. Interestingly, such high inhibitory efficiency is similar to that reported for HLE inactivation by 3,3-diethylmonobactams and cephalosporins.^{33,35}

In contrast to the C-3-unsubstituted series, their 3,3-diethyl counterparts **5e–j** were completely inactive against PPE in concentrations up to 0.5 mM. However, β-lactams **5e–j** inhibited HLE very efficiently in a time-dependent fashion. The pseudo-first-order rate-constants, k_{obs} , for HLE inactivation were determined using the progress-curve method.³⁶ For compound **5f**, a linear dependence of k_{obs} on inhibitor concentration was observed (Fig. 1B); and correction for the concentration and Michaelis constant of the substrate yielded the second-order rate constant for

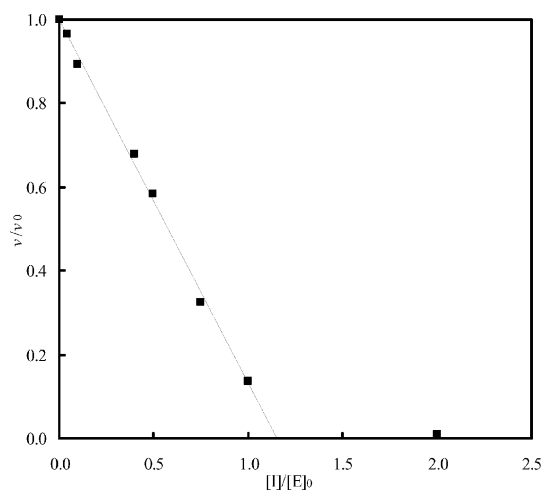


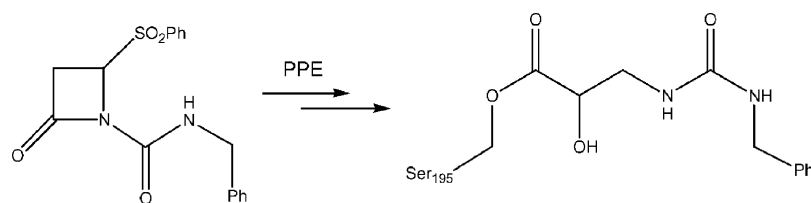
Fig. 2 Inactivation of porcine pancreatic elastase as a function of the molar ratio of inhibitor **5d** to enzyme. PPE (10 μ M) and various amounts of inhibitor **5d** (20–0.4 μ M) in 0.1 M HEPES buffer, pH 7.25, were incubated at 25 $^{\circ}$ C for 30 min, and aliquots were withdrawn for assay.

inhibition, k_{inact}/K_i , as the slope (Table 1). For compounds **5g** and **5h**, the individual kinetic parameters K_i and k_{inact} were obtained by determining k_{obs} as a function of the inhibitor concentration,²⁸ while for the remaining β -lactams (**5e**, **5i** and **5j**) the k_{inact}/K_i values

were determined by calculating $k_{\text{obs}}/[I]$ (Table 1). The second-order rate-constants for HLE inactivation, k_{inact}/K_i , are within the range of 10^3 to 10^4 $\text{M}^{-1} \text{s}^{-1}$, which reflects the stringent S_1 subsite specificity of this enzyme toward hydrophobic substituents with three or four carbon atoms.^{25,31,33,37}

3. X-Ray crystallography studies

PPE was incubated with **5d** for 30 min. Good quality crystals were grown and subjected to X-ray analysis.³⁸ The electron density maps at the catalytic site indicate that PPE inactivation by **5d** involves β -lactam ring-opening, as revealed by the ester formed with Ser195 O γ (Fig. 3). Moreover, inspection of the maps calculated at 1.66 \AA resolution shows that acylation of PPE by **5d** also involves the departure of sulfinate from C-4. Interestingly, the crystal structure reveals the presence of a hydroxyl group at C-3 (β -lactam numbering) (Scheme 3). This hydroxyl group establishes H-bonds to water molecules while the ester carbonyl group is H-bonded to the NH backbone of Gln192. Furthermore, the adjacent urea NH groups are within H-bonding distance to water molecules, as shown in Fig. 3. This was a somewhat unexpected result when compared with those from previous X-ray crystallographic studies with other β -lactams containing leaving groups at C-4. For example, inactivation of PPE by 4-aryloxy-3,3-diethyl- β -lactams leads to a carbinolamine acyl-enzyme, resulting



Scheme 3 Covalent enzyme–inhibitor complex (see Fig. 3).

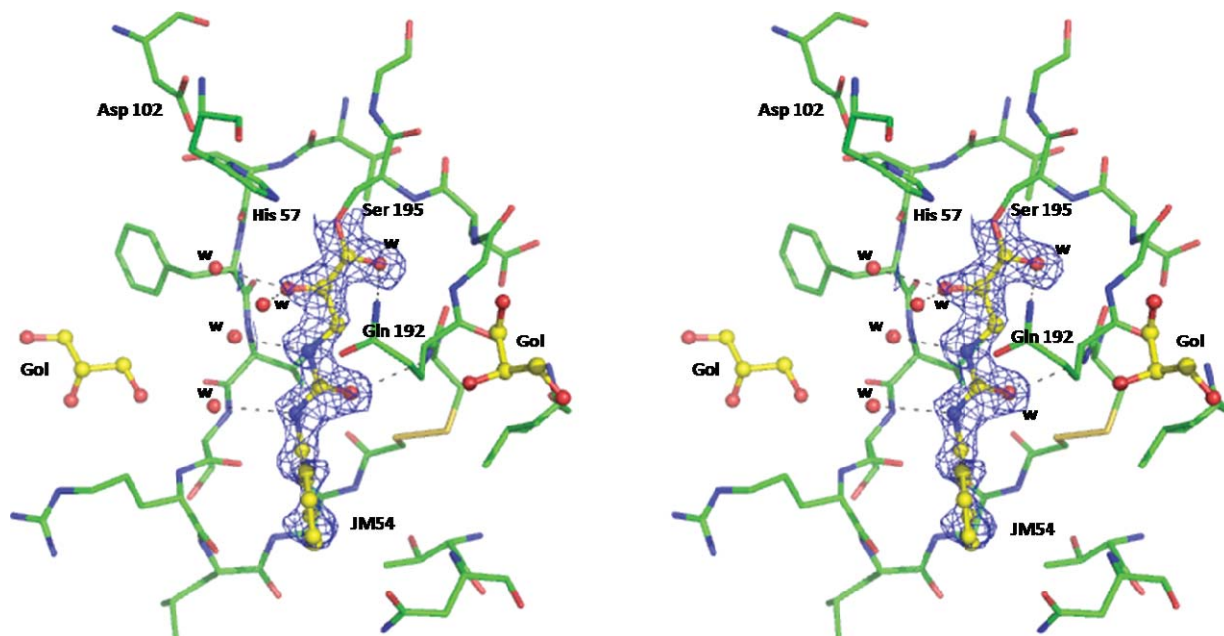
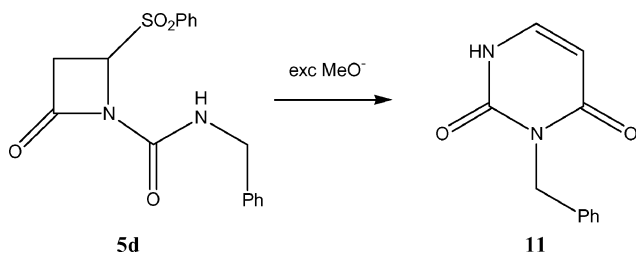


Fig. 3 A stereoview of the $|F_0| - |F_c|$ electron density map calculated, with Ser195 and inhibitor **5d** (code JM54) omitted from the model. The omit map is contoured at 3σ and shows the acyl-enzyme covalently linked to Ser195 with the corresponding interactions with PPE active site.

from reaction of water at C-4 of the imine intermediate.²⁶ When a single 1-hydroxyethyl substituent is present at C-3, an enamine acyl-enzyme is formed, presumably from a retro-aldol reaction on the imine precursor.²⁶

We wondered if this pattern of reactivity was inherent to **5d** or a function of the enzyme active site. Therefore we undertook reaction of inhibitor **5d** with sodium methoxide in methanol, which has been reported as a good model reaction for the acylation of serine enzymes.^{39,40} The product of this reaction was 3-benzylpyrimidine-2,4-(1*H*,3*H*)-dione, **11**, in 80% yield (Scheme 4). This result is consistent with MeO⁻-catalyzed β -lactam ring opening followed by pyrimidine ring formation and phenylsulfinate elimination (or first the elimination then the ring closure). Clearly, the enzyme active site must preclude the ring closure process; moreover, the imine resulting from Ser195 acylation and phenylsulfinate elimination would be expected to add water to C-4 (β -lactam numbering) rather than to the C-3 atom that is evident in Fig. 3, thus suggesting that a different pathway may be available in the active site of PPE subsequent to β -lactam ring-opening. Although the nature of such a pathway is currently unclear, it is unlikely to be the rate-limiting step in the enzyme inactivation process (see below). In this regard, it is of interest to note that the distance between C-4 (β -lactam numbering) of the PPE-**5d** complex and the C- α of Gln192 is only 3.4 Å; this close approach might suggest a reason as to why the presence of a hydroxyl group in the C-4 position is precluded.



Scheme 4

4. Alkaline hydrolysis

It has been suggested that the magnitude of the second-order rate-constant, k_{OH^-} , for the alkaline hydrolysis of potential inhibitors of enzymes containing a catalytic serine is a crude indicator for their ability to be effective and therapeutically useful acylating agents.^{39,41,42} Comparison of the k_{OH^-} values presented in Table 1 reveals that the reactivity of β -lactams **5** correlates poorly to the $\text{p}K_{\text{a}}$ of the leaving group at C-4 of the β -lactam moiety. A poor correlation between $\log k_{\text{OH}^-}$ values for the 3,3-diethyl series **5e-j** and the $\text{p}K_{\text{a}}$ of the leaving group at C-4 was observed, corresponding to a β_{lg} value of -0.05 , indicating that there is essentially no change in the effective charge on the leaving group on going from the ground state to the transition state. These results are comparable to those reported for the alkaline hydrolysis of the vinylogous cephalosporins containing a potential leaving group at C-3' (**4**, $n = 0$), for which a β_{lg} value close to zero was also determined.⁴³

In contrast, $\log k_{\text{OH}^-}$ values correlate with σ_1 values for the substituents at C-4, including those that are not expelled, yielding Hammett ρ_1 values of 2.8 and 3.4 for the series **5a-d** and **5e-j**,

respectively (Fig. 4). The Hammett ρ_1 values are large and positive, which indicates a substantial build-up of negative charge in the transition-state and that the effect exerted by C-4 substituents on the alkaline hydrolysis of **5** is purely inductive. The solvolysis of penicillins and cephalosporins involves decomposition of the tetrahedral intermediate *via* general-acid-catalysed N-protonation, *e.g.* **12**, or complexation with a metal ion, to effect C–N bond cleavage.⁴⁴ For compounds **5**, N-protonation is thermodynamically unfavourable. However, ureido anion expulsion from the tetrahedral intermediate may occur at a rate that is comparable or even faster than that for hydroxide ion, and thus the reaction may involve the rate-limiting attack of hydroxide on the β -lactam carbonyl atom.

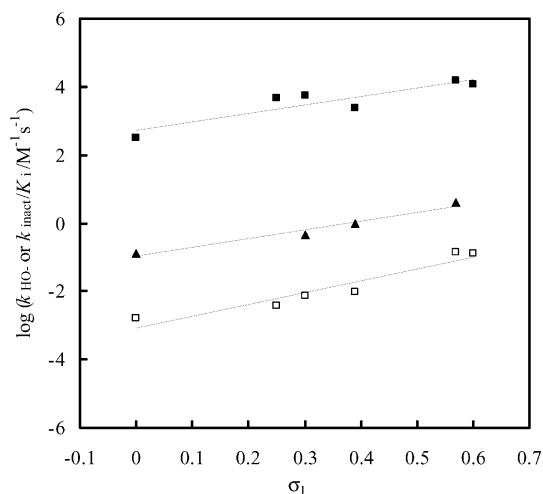
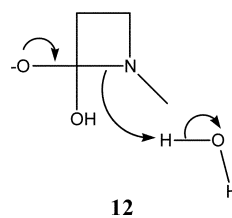


Fig. 4 Plots of second-order rate-constants for the alkaline hydrolysis of C-3-unsubstituted β -lactams **5a-d** (\blacktriangle) and 3,3-diethyl- β -lactams **5e-j** (\square), and of second-order rate-constants for HLE inactivation by 3,3-diethyl- β -lactams **5e-j** (\blacksquare), against σ_1 values for the X substituents in C-4.

The higher ρ_1 value determined for the 3,3-diethyl series when compared to that of the C-3 unsubstituted series is consistent with the formation of a high energy tetrahedral intermediate in which the two C–O bonds are eclipsed with the ethyl groups at C-3. According to the Hammond postulate, this implies that formation of such an intermediate involves a later transition state in which there is significant negative charge build-up, thereby being more susceptible to the electronic effects of the C-4 substituents. The ρ_1 value determined here for the monobactams **5** is higher than the corresponding ρ_1 value of 1.35 reported for the alkaline hydrolysis of cephalosporins,⁴⁴ a difference that almost certainly reflects the shorter distance between the electron-withdrawing substituents and the nitrogen atom in the β -lactam scaffold of **5**.

5. Structure–activity relationships

Insight into how a particular substituent promotes the ability of the enzyme to use its catalytic apparatus to increase the rate of acylation through β -lactam ring-opening can be obtained by the enzyme rate enhancement factor (EREF); this is the ratio of second-order rate-constant for enzyme inactivation to the second-order rate-constant for the alkaline hydrolysis, *i.e.* $(k_{\text{inact}}/K_i)/k_{\text{OH}^-}$.^{39,45} Remarkably, the 3,3-diethyl β -lactams **5e–j** exhibit EREF values *ca.* 10^4 times higher than those of their C-3 unsubstituted analogues **5b–d** (Table 1). The differences in EREF between the two series of β -lactams largely reflect the importance of the alkyl substituents at C-3 in promoting efficient molecular recognition by the S₁ site of the enzyme. This interaction probably positions the β -lactam carbonyl within the oxyanion hole, facilitating successful nucleophilic attack by Ser195, and thus enhancing the rate of β -lactam ring-opening.³¹ Clearly, the favourable binding energy between the enzyme and the C-3 substituents overcomes the strain energy in the tetrahedral intermediate *en route* to the acyl-enzyme.

As with alkaline hydrolysis, enzyme inactivation efficiency is largely independent on the $\text{p}K_{\text{a}}$ of the leaving group at C-4. For example, the second-order rate constant for PPE inactivation by the 4-phenylsulfonyl derivative **5d** is only 25 times higher than that of its 4-phenoxy analogue **5b**, despite the 9-fold difference between the leaving group abilities of phenylsulfinate and phenolate. Similarly, the 3,3-diethyl-4-phenylsulfonyl counterpart **5h** is only 6 times more potent as HLE inhibitor than its 4-phenoxy analogue **5f**. However, a good correlation was found between the logarithm of the second-order rate-constants of HLE inactivation and the σ_1 values for the substituents at C-4, including X = H (**5e**), which corresponds to a ρ_1 value of 2.5 for compounds **5e–j** (Fig. 4). This ρ_1 value is higher than that reported for HLE inactivation by cephalosporin sulfones (**4**, R = MeO, $n = 2$; $\rho_1 = 1.83^{20}$), again reflecting the shorter distance between the substituents and the nitrogen atom in the β -lactam scaffold **5**. Compared with the alkaline hydrolysis of **5** (ρ_1 of 3.4), the HLE reaction seems to involve an earlier transition-state with less negative charge buildup. This effect can be ascribed, at least in part, to the favourable non-covalent interactions with the primary specificity pocket, which allows the enzyme to stabilize the transition-state and to make full use of its catalytic machinery to increase the rate of acylation through β -lactam ring-opening. This is consistent with the EREF values for **5e–j** ranging from 10^5 to 10^6 , which indicate that HLE is facilitating the expulsion of the urea anion from the tetrahedral intermediate when compared to the hydroxide-induced hydrolysis.

In conclusion, the effectiveness of monobactams as elastase inhibitors is strongly dependent on the effect of C-3 substituents on the molecular recognition by the enzyme as well as on the effect of C-4 substituents on chemical reactivity that leads to serine acylation. The rate-limiting step in elastase inactivation is the formation of the tetrahedral intermediate, and β -lactam ring-opening is not concerted with the departure of a leaving group from C-4. Monobactam sulfones emerged as very potent inhibitors of elastase due to the strong electron-withdrawing properties of the sulfone, although the departure of sulfinate from C-4 might be relevant to the chemistry of enzyme inactivation.

Experimental

General

Melting points were determined using a Kofler camera Bock Monoscope M and are uncorrected. The infrared spectra were collected on a Nicolet Impact 400 FTIR infrared spectrophotometer and the NMR spectra on a Bruker 400 Ultra-Shield (400 MHz) in CDCl_3 ; chemical shifts, δ , are expressed in ppm, coupling constants, J , are expressed in Hz. Low-resolution mass spectra were recorded using VG Mass Lab 20–250, VG Quattro or HP5988A mass spectrometers. Elemental analyses were performed by Medac Ltd, Brunel Science Centre, Englefield Green, Egham, TW20 0JZ, UK, or by ITN, Chemistry Unit, Sacavém, Portugal. UV-vis assays were recorded either on Shimadzu UV-1603 or UV-2100 PC spectrophotometers. TLC was performed on Merck aluminium plates, silica gel 60 F₂₅₄, and visualized by UV light and/or iodine. Preparative column chromatography was performed on silica gel 60 from Merck (70–230 mesh ASTM). DCM, TEA and benzene were purified and dried before use. Solvents and buffer materials for enzyme assays were of analytical reagent grade and were purchased from Merck or Sigma. PPE, MeO-Suc-Ala-Ala-Pro-Val-*p*NA and *N*-Suc-Ala-Ala-Ala-*p*NA were purchased from Sigma, and HLE was purchased from Calbiochem.

General procedure for the synthesis of *N*-carbamoylazetidin-2-one derivatives

Benzyl isocyanate (4.2 mmol) and subsequently triethylamine (4.2 mmol) were slowly added to a solution of the appropriate azetidin-2-one **7–10** (3.5 mmol) in dichloromethane (3 mL). The reaction was stirred at room temperature and monitored by TLC. After completion of the reaction, the solution was evaporated under reduced pressure. The product was purified by column chromatography.

***N*-Benzylcarbamoylazetidin-2-one, 5a.** Purified by column chromatography on silica gel (dichloromethane–ethyl acetate 9.5 : 0.5); 66%; m.p. 62–64 °C (lit.,⁴⁶ oil); ν_{max} (film) 3335, 1764, 1685 cm^{-1} ; δ_{H} 3.08 (2H, t, $J = 4.8$); 3.68 (2H, t, $J = 4.8$); 4.50 (2H, d, $J = 6.0$); 6.89 (1H, brs); 7.28–7.38 (5H, m); δ_{C} 36.06, 37.21, 43.70, 127.59, 127.64, 128.72, 137.93, 150.59, 167.00; ESI-MS m/z 205.37 (MH^+); Anal. calcd. for $\text{C}_{11}\text{H}_{12}\text{N}_2\text{O}_2$: C, 64.69; H, 5.92; N, 13.72; found: C, 64.55; H, 6.10; N, 13.66.

***N*-Benzylcarbamoyl-4-phenoxyazetidin-2-one, 5b.** Purified by column chromatography on silica gel (elution with dichloromethane–ethyl acetate 9.5 : 0.5); 85%; m.p. 129–130 °C; ν_{max} (film) 3368, 1780, 1708 cm^{-1} ; δ_{H} 3.17 (1H, dd, $J = 16.0, 1.2$); 3.46 (1H, dd, $J = 16.0, 4.4$); 4.50 (1H, dd, $J = 14.4, 5.6$); 4.55 (1H, dd, $J = 14.4, 5.6$); 6.07 (1H, dd, $J = 4.4, 1.2$); 6.88 (1H, brs); 7.10 (1H, t, $J = 7.2$); 7.15 (2H, d, $J = 8.0$); 7.31–7.39 (7H, m); δ_{C} 43.76, 45.51, 78.76, 117.14, 123.21, 127.00, 128.78, 129.72, 137.56, 156.14, 164.42; ESI-MS m/z 297.52 (MH^+); Anal. calcd. for $\text{C}_{17}\text{H}_{16}\text{N}_2\text{O}_3$: C, 68.91, H, 5.44, N, 9.45; found: C, 69.12, H, 5.61, N, 9.19.

***N*-Benzylcarbamoyl-4-phenylthioazetidin-2-one, 5c.** Purified by column chromatography on silica gel (elution with dichloromethane–ethyl acetate 9.5 : 0.5); 80%; m.p. 78–79 °C, ν_{max}

(film) 3366, 3036, 2908, 1773, 1698 cm^{-1} ; δ_{H} 2.88 (1H, dd, $J = 16.4, 2.8$); 3.40 (1H, dd, $J = 16.4, 5.6$); 4.47 (1H, dd, $J = 15.0, 6.0$); 4.54 (1H, dd, $J = 15.0, 6.0$); 5.29 (1H, dd, $J = 5.6, 2.8$), 6.81 (1H, brs); 7.30–7.39 (9H, m); 7.55 (1H, dd, $J = 8.4, 1.6$); δ_{C} 43.68, 43.99; 56.69; 127.69, 127.72, 128.77, 129.29, 129.31, 129.36, 135.25, 137.83, 149.63, 165.43; ESI-MS m/z 334.84 (MNa^+); Anal. calcd. for $\text{C}_{17}\text{H}_{16}\text{N}_2\text{O}_2\text{S}$: C, 65.36; H, 5.16; N, 8.97; found C 65.12; H 5.11; N 8.98.

***N*-Benzylcarbamoyl-4-phenylsulfonylazetid-2-one, 5d.** Purified by column chromatography on silica gel (elution with dichloromethane–ethyl acetate 9.5 : 0.5); 81%; m.p. 159–161 °C; ν_{max} (film) 3374, 3064, 3031, 2978, 1789, 1711, 1316, 1150 cm^{-1} ; δ_{H} 3.48 (1H, dd, $J = 16.8, 6.0$); 3.67 (1H, dd, $J = 16.8, 2.8$); 4.33 (1H, dd, $J = 14.8, 6.0$); 4.39 (1H, dd, $J = 14.8, 6.0$); 5.20 (1H, dd, $J = 6.0, 2.8$), 6.65 (1H, brs); 7.23 (2H, dd, $J = 8.0, 1.2$); 7.31–7.38 (3H, m); 7.58 (2H, t, $J = 8.0$); 7.74 (1H, dt, $J = 8.0, 1.2$); 7.96 (2H, dd, $J = 8.0, 0.8$); δ_{C} 39.43, 43.86, 65.84, 127.58, 127.79, 128.77, 129.28, 129.39, 134.88, 136.75, 137.28, 148.39, 164.27; EI-MS m/z : 344.00 (M^+); Anal. calcd. for $\text{C}_{17}\text{H}_{16}\text{N}_2\text{O}_4\text{S}$: C, 59.29; H, 4.68; N, 8.13; found C, 59.41; H, 4.55; N, 8.01.

***N*-Benzylcarbamoyl-3,3-diethylazetid-2-one, 5e.** Purified by column chromatography on silica gel (elution with dichloromethane–ethyl acetate 9.5 : 0.5); 83% as a colourless oil, ν_{max} (film) 3364, 3071, 3031, 2969, 2924, 2875, 1757, 1702 cm^{-1} ; δ_{H} 1.00 (6H, t, $J = 7.6$); (4H, q, $J = 7.6$); 3.42 (2H, s); 4.50 (2H, d, $J = 6.0$); 6.93 (1H, brs); 7.28–7.38 (5H, m); δ_{C} 8.70, 25.71, 43.75, 47.04, 59.31, 127.44, 127.54, 127.65, 128.65, 128.71, 137.98, 150.95, 172.83; ESI-MS m/z 261.10 (MH^+); Anal. calcd. for $\text{C}_{15}\text{H}_{20}\text{N}_2\text{O}_2$: C, 69.20, H, 7.74, N, 10.76; found C, 68.95; H, 7.80; N, 10.59.

***N*-Benzylcarbamoyl-3,3-diethyl-4-phenoxyazetid-2-one, 5f²⁵.** Purified by column chromatography on silica gel (elution with dichloromethane–ethyl acetate 9.5 : 0.5); 81%; m.p. 58–59 °C; ν_{max} (film) 3366, 3064, 3031, 2970, 2939, 2880, 1770, 1710 cm^{-1} ; δ_{H} 1.00 (3H, t, $J = 7.6$ Hz); 1.06 (3H, t, $J = 7.6$); 1.77–1.84 (3H, m); 1.99 (1 H, dq, $J = 14.4, 7.2$); 4.47 (1H, dd, $J = 15.6, 6.0$); 4.51 (1H, dd, $J = 15.6, 6.0$); 5.68 (1H, s); 6.93 (1H, brs); 7.07 (1H, t, $J = 7.2$); 7.22–7.35 (9H, m); δ_{C} 8.58, 8.84, 21.23, 23.86, 43.75, 64.35, 86.76, 117.76, 123.17, 127.63, 127.67, 128.76, 129.67, 137.66, 150.14, 157.47, 172.23; ESI-MS m/z 353.29 (MH^+); Anal. calcd. for $\text{C}_{21}\text{H}_{24}\text{N}_2\text{O}_3$: C, 71.57, H, 6.86, N, 7.95; found 71.84, 6.78, 8.18.

***N*-Benzylcarbamoyl-3,3-diethyl-4-phenylthioazetid-2-one, 5g.** Purified by column chromatography on silica gel (elution with dichloromethane–ethyl acetate 9.5 : 0.5); 70%; m.p. 80–81 °C; ν_{max} (film) 3361, 3061, 2968, 1758, 1701 cm^{-1} ; δ_{H} 0.94 (3H, t, $J = 8.0$ Hz); 1.06 (3H, t, $J = 8.0$); 1.75–1.98 (3H, m); 1.99 (1 H, dq, $J = 14.4, 7.2$); 4.51 (1H, dd, $J = 15.6, 6.0$); 4.55 (1H, dd, $J = 15.6, 6.0$); 5.06 (1H, s); 6.95 (1H, brs); 7.28–7.39 (8H, m); 7.77 (2H, d, $J = 8.0$); δ_{C} 8.43, 9.01, 23.11, 24.74, 43.74, 63.95, 71.42, 127.60, 127.65, 128.17, 128.74, 129.19, 133.24, 137.71, 150.13, 172.04; EI-MS m/z 368.15 (M^+); Anal. calcd. for $\text{C}_{21}\text{H}_{24}\text{N}_2\text{O}_2\text{S}$: C, 68.45, H, 6.56, N, 7.60; found, C, 68.22, H, 6.65, N, 7.88.

***N*-Benzylcarbamoyl-3,3-diethyl-4-phenylsulfonylazetid-2-one, 5h.** Purified by column chromatography on silica gel (elution

with dichloromethane–ethyl acetate 9.5 : 0.5); 63%; m.p. 142–144 °C; ν_{max} (film) 3366, 3060, 3041, 2971, 1778, 1711, 1312, 1151 cm^{-1} ; δ_{H} 1.01 (3H, t, $J = 7.2$ Hz); 1.06 (3H, t, $J = 7.2$); 1.68 (1 H, dq, $J = 14.4, 7.2$); 1.95 (1 H, dq, $J = 14.4, 7.2$); 2.20 (1 H, dq, $J = 14.4, 7.2$); 2.47 (1 H, dq, $J = 14.4, 7.2$); 4.21 (1H, dd, $J = 14.8, 6.0$); 4.33 (1H, dd, $J = 14.8, 6.0$); 4.75 (1H, s); 6.66 (1H, brs); 7.14 (2H, d, $J = 7.6$); 7.19–7.28 (3H, m); 7.47 (2H, t, $J = 7.6$); 7.61 (1H, t, $J = 7.6$); 7.85 (2H, t, $J = 7.6$); δ_{C} 8.56, 8.90, 20.86, 25.12, 43.85, 67.05, 74.72, 127.43, 127.69, 128.74, 128.88, 129.18, 134.39, 137.36, 139.84, 148.99, 171.49; EI-MS m/z 400.05 (M^+); Anal. calcd. for $\text{C}_{21}\text{H}_{24}\text{N}_2\text{O}_4\text{S}$: C, 62.98, H, 6.04, N, 6.99; found, C, 63.11, H, 6.25, N, 7.12.

***N*-Benzylcarbamoyl-3,3-diethyl-4-benzylthioazetid-2-one, 5i.** Purified by column chromatography on silica gel (elution with dichloromethane–ethyl acetate 9.5 : 0.5); 53% as a yellow oil, ν_{max} (film) 3365, 1759, 1701 cm^{-1} ; δ_{H} 0.56 (3H, t, $J = 7.4$); 0.85 (3H, t, $J = 7.4$); 1.44–1.69 (4H, m); 3.99 (1H, d, $J = 12.8$); 4.06 (1H, d, $J = 12.8$); 4.31 (1H, dd, $J = 15.3, 6.1$); 4.36 (1H, dd, $J = 15.3, 6.3$); 4.70 (1H, s); 6.91 (1H, s); 7.10–7.27 (10H, m); δ_{C} 7.67; 8.90; 22.41; 24.44; 37.37; 43.61; 62.99; 65.84; 127.63; 127.72; 127.81; 129.01; 129.07; 129.80; 138.79; 139.62; 150.96; 172.35; HPLC-ESIMS m/z (MH^+) 383.52; Anal. calcd. for $\text{C}_{22}\text{H}_{26}\text{N}_2\text{O}_2\text{S}$: C, 69.08; H, 6.85; N, 7.32; found C, 69.10, H, 6.90; N, 7.30.

***N*-Benzylcarbamoyl-3,3-diethyl-4-benzylsulfonylazetid-2-one, 5j.** Purified by column chromatography on silica gel (elution with diethyl ether–light petroleum 1 : 1); 52%; m.p. 93–94 °C; ν_{max} (film) 3365, 1778, 1313, 1165 cm^{-1} ; δ_{H} 0.79 (3H, t, $J = 7.4$); 1.01 (3H, t, $J = 7.5$); 1.62 (1 H, dq, $J = 14.5, 7.3$); 1.84 (1H, dd, $J = 14.5, 7.3$); 2.08 (1H, dq, $J = 14.5, 7.4$); 2.52 (1H, dq, $J = 14.6, 7.4$); 4.48 (1H, d, $J = 13.9$); 4.53 (2H, d, $J = 5.9$); 4.62 (1H, s); 5.01 (1H, d, $J = 13.9$); 6.95 (1H, t, $J = 5.9$); 7.19–7.59 (10H, m); δ_{C} 8.27, 8.87, 20.90, 24.48, 44.12, 62.27, 66.46, 69.06, 127.59, 127.89, 128.91, 129.07, 131.37, 137.08, 150.20, 171.22; EI-MS m/z 413.8 (MH^+); Anal. calcd. for $\text{C}_{22}\text{H}_{26}\text{N}_2\text{O}_4\text{S}$: C, 63.75; H, 6.32; N, 6.76; found C, 63.70, H, 6.40; N, 6.60.

Large scale reaction of *N*-benzylcarbamoyl-4-phenylsulfonylazetid-2-one with excess sodium methoxide

N-Benzylcarbamoyl-4-phenylsulfonylazetid-2-one (0.29 mmol), **5d**, was added to a solution of sodium methoxide (1.5 mmol) in methanol (15 mL). The reaction mixture was stirred at room temperature and monitored by TLC. The solvent was removed under reduced pressure and the residue was taken up in water (20 mL), acidified with 10% HCl until pH 2 and extracted with ethyl acetate (3 × 30 mL). After drying and evaporating off the solvent, the residue was purified by column chromatography on silica gel (elution with dichloromethane–ethyl acetate 8 : 2), to yield the product, 3-benzylpyrimidine-2,4-(1*H*,3*H*)-dione, **11**, as a white solid (79%); m.p. 177–179 °C (lit.,⁴⁷ 181–182 °C); ν_{max} (film) 3084, 2965, 1625, 1601 cm^{-1} ; δ_{H} 5.12 (2H, s); 5.81 (1H, dd, $J = 7.2, 1.2$); 7.14 (1H, dd, $J = 7.2, 6.0$); 7.26–7.34 (3H, m); 7.46 (2H, d, $J = 7.2$); 9.35 (1H, brs); δ_{C} 43.71, 102.26, 127.70, 128.46, 128.80, 136.49, 138.17, 163.12; EI-MS m/z 202.05 (M^+); Anal. calcd. for $\text{C}_{11}\text{H}_{10}\text{N}_2\text{O}_2$, C, 65.34; H, 4.98; N, 13.85; found, C, 65.55, H, 5.25, N, 13.81.

Chemical kinetics

All kinetic measurements were carried out at 25.0 ± 0.1 °C and with an ionic strength adjusted to 0.5 M by addition of NaClO₄. Due to substrate solubility problems all buffers contained 20% (v/v) acetonitrile. Rate constants were determined using UV spectrophotometry by recording the decrease of substrate absorbance at fixed wavelength (**5a**, 220; **5b**, 250; **5c**, 260; **5d**, 255; **5e**, 224; **5f**, 238; **5g**, 260; **5h**, 225; **5i**, 240; **5j**, 240 nm), using a spectrophotometer equipped with a temperature controller. In a typical run, the reaction was initiated by adding a 15 µL aliquot of a 10^{-2} M stock solution of substrate in acetonitrile to a cuvette containing 3 mL of the buffer solution. The pseudo-first-order rate constants, k_{obs} , were obtained by least-squares treatment of $\log(A_t - A_\infty)$ data, where A_t and A_∞ represent the absorbance at time t and at time infinity, respectively. Rate constants derived using this method were reproducible to $\pm 5\%$.

Enzyme inactivation by the progress curve method

Inactivation of HLE was assayed at 25 °C by mixing 10 µL of HLE stock solution (2 µM in 0.05 M acetate buffer, pH 5.5) to a solution containing 10 µL of inhibitor in DMSO (200 µM), 20 µL of substrate MeO-Suc-Ala-Ala-Pro-Val-*p*NA (50 mM in DMSO) and 960 µL of 0.1 M HEPES buffer, pH 7.2, and the absorbance was continuously monitored at 410 nm for 20 minutes. Control assays, in which the inhibitor was omitted, ran linearly. The pseudo-first order rate constants, k_{obs} , for the inhibition of HLE were determined according to the slow-tight binding inhibition model³⁶ and involved the fitting of product concentration as a function of time to eqn (1) by non-linear regression analysis using the routine ENZFIT (developed at the Faculty of Pharmacy, Lisbon):

$$A = v_s t + \frac{(v_i - v_s)(1 - e^{-k_{\text{obs}} t})}{k_{\text{obs}}} + A_0 \quad (1)$$

where A is the absorbance at 410 nm, A_0 is the absorbance at $t = 0$, v_i is the initial rate of change of absorbance, v_s is the steady-state rate and k_{obs} is the first-order rate constant for the approach to the steady-state. The individual kinetic parameters K_i and k_{inact} were obtained by determining k_{obs} (in duplicate or triplicate) as a function of the inhibitor concentration and by fitting the experimental data to eqn (2).²⁵ When a linear dependence of k_{obs} on inhibitor concentration was observed (e.g. for **5f**), correction for substrate concentration and Michaelis constant yielded the second-order rate constant for inhibition (k_{inact}/K_i) as the slope, and the first-order rate for the dissociation of the E·I complex (k_{off}) as the intercept (eqn (3)) (see Fig. 1B). For the remaining β -lactams the k_{inact}/K_i values were determined in duplicate or triplicate by calculating $k_{\text{obs}}/[I]$ and then correcting for the substrate concentration and Michaelis constant using eqn (4).

$$k_{\text{obs}} = \frac{k_{\text{inact}}[I]}{K_i(1 + [S]/K_m) + [I]} \quad (2)$$

$$k_{\text{obs}} = k_{\text{off}} + \frac{(k_{\text{inact}}/K_i)[I]}{1 + [S]/K_m} \quad (3)$$

$$\frac{k_{\text{obs}}}{[I]} = \frac{k_{\text{inact}}/K_i}{1 + [S]/K_m} \quad (4)$$

Enzyme inactivation by the incubation method

Inhibition of PPE was assayed by Kitz and Wilson's incubation method.³⁴ In a typical experiment, 50 µL of inhibitor solution in DMSO was incubated at 25 °C with 750 µL of 0.1 M HEPES buffer, pH 7.2, and 200 µL of PPE solution (50 µM in 0.1 M HEPES buffer, pH 7.2). Aliquots (100 µL) were withdrawn at different time intervals and transferred to a cuvette thermostatted at 25 °C, containing 895 µL of 0.1 M HEPES buffer, pH 7.2, and 5 µL of *N*-Suc-Ala-Ala-Ala-*p*NA (12.5 mM in DMSO). The absorbance was monitored at 390 nm for 60 seconds and the gradients of the slopes obtained of initial rate used as a measure of enzyme activity. The values of k_{obs} for compounds **5b–d** were determined in duplicates or triplicates from plots of $\ln(v/v_0)$ versus incubation time, where v is the initial rate at time t and v_0 is the initial rate of the control incubation without inhibitor. The plots of k_{obs} versus $[I]$ were linear and the potency of the inhibitors was determined in terms of the bimolecular rate constant $k_{\text{inact}}/K_i = k_{\text{obs}}/[I]$.

Partition ratio

PPE solutions were incubated at 25 °C with different concentrations of **5d** solutions in 0.1 M HEPES buffer, pH 7.2, in a final volume of 1 mL. After 30 minutes incubation, a 100 µL aliquot of the reaction mixture was withdrawn and assayed for remaining enzyme activity as described previously.

X-Ray crystallographic studies

Porcine pancreatic elastase (PPE) was incubated with inhibitor **5d** for 30 min. Good quality crystals were grown in 200 mM sodium sulfate and 100 mM sodium acetate at pH 5.1 (293 K) using the sitting drop vapour-diffusion method.³⁸ X-Ray diffraction data were measured at EMBL X11 beamline at the DORIS storage ring, DESY, Hamburg (Germany), to 1.66 Å resolution. The data were integrated with MOSFLM⁴⁸ and scaled using SCALA.⁴⁹ Relevant statistics on data collection and processing are given in Table S1 (Supplementary material†). The crystals soaked with the inhibitor solution belong to the same space group and show similar cell parameters as the native ones, so the structure was solved by Fourier synthesis. The initial rigid body refinement step yielded an R -work and R -free of 27.7 and 30.5%, respectively. Further crystallographic refinement was performed with Refmac⁵⁰ and the electron density maps were inspected with COOT.⁵¹ The refined model of PPE in complex with inhibitor **5d** shows an R -factor of 15.6% and R -free of 18.6%.

The structure is generally well defined within the electron density maps, showing an average B factor of 10.5 Å² for all protein atoms. The final model comprises 240 amino acid residues, 316 water molecules, the inhibitor **5d** without the C-4 PhSO₂⁻ leaving group, two glycerol molecules, one sulfate ion and one sodium ion, which is hexa-coordinated to side-chain atoms of Glu80, Asp77, Gln75, Asn72, Glu70 and a water molecule. Alternate conformations were modelled for the side chains of Gln23, Gln75, Val83 and Ser189, with 50% occupancy each. All protein residues lie within allowed regions of the Ramachandran plot, and the relevant refinement statistics are presented in Table 2. The overall protein structure of the **5d**-PPE complex is very similar to that of the native enzyme (PDB code 1QNJ) and superposition of the

Table 2 Data collection and crystallographic refinement statistics for the porcine pancreatic structure bound to **5d**

Resolution range/Å	37.95–1.66
Refined model	
<i>R</i> -factor (%)	15.6
<i>R</i> -free (%)	18.6
No. of non-H protein atoms	1833
No. of solvent molecules	320
Average <i>B</i> -factor/Å ²	
Protein only	10.5
Inhibitor only	24.4
Solvent molecules	25.9
Ramachandran plot	
Residues in most favoured regions (%)	87.4
Residues in additional allowed regions (%)	12.6
Root-mean-square deviations	
Bond angles/°	0.01
Angle lengths/Å	1.22

C- α atoms shows a r.m.s. deviation of 0.089 Å. The numbering of **5d**–PPE complex follows the common practice of using the bovine chymotrypsinogen A numbering.⁵²

The coordinates of **5d**–PPE complex have been deposited in the Protein Data Bank (PDB) with identification code 2V35 and the corresponding structure factors with id code 2V35SF.

Acknowledgements

The authors thank the Fundação para a Ciência e Tecnologia (FCT, Portugal) for financial support to CECF/i-Med-UL and ESF for the financial support to collect X-ray diffraction data at EMBL/DESY, Hamburg (Research Infrastructure Action under the FP6). J.M. and T.F.O. acknowledge FCT for the PhD grants SFRH/BD/17534/2004 and SFRH/BD/29519/2006, respectively.

References

- 1 I. Massova and S. Mobashery, *Acc. Chem. Res.*, 1997, **30**, 162–168.
- 2 D. Leung, G. Abbenante and D. P. Fairlie, *J. Med. Chem.*, 2000, **43**, 305–341.
- 3 M. I. Konaklieva, *Curr. Med. Chem.: Anti-Infect. Agents*, 2002, **1**, 215–238.
- 4 J. Zhong and W. C. Groutas, *Curr. Top. Med. Chem.*, 2004, **4**, 1203–1216.
- 5 M. I. Konaklieva and B. J. Plotkin, *Mini-Rev. Med. Chem.*, 2004, **4**, 721–739.
- 6 J. C. Powers, J. L. Asgian, Ö. D. Ekicu and K. E. James, *Chem. Rev.*, 2002, **102**, 4639–4750.
- 7 P. R. Bernstein, P. D. Edwards and J. C. Williams, *Prog. Med. Chem.*, 1994, **31**, 59–120.
- 8 M. I. Page and A. P. Laws, *Tetrahedron*, 2000, **56**, 5631–5638.
- 9 U. Imtiaz, E. Billings, J. R. Knox, E. K. Manavathu, S. A. Lerner and S. Mobashery, *J. Am. Chem. Soc.*, 1993, **115**, 4435–4442.
- 10 U. Imtiaz, E. Billings, J. R. Knox and S. Mobashery, *Biochemistry*, 1994, **33**, 5728–5738.
- 11 A. P. Kuzin, M. Nukaga, Y. Nukaga, A. Hujer, R. A. Bonomo and J. R. Knox, *Biochemistry*, 2001, **40**, 1861–1866.
- 12 P. S. Padayatti, M. S. Helfand, M. A. Totir, M. P. Carey, A. M. Hujer, P. R. Carey, R. A. Bonomo and F. van den Akker, *Biochemistry*, 2004, **43**, 843–848.
- 13 T. Sun, C. R. Bethel, R. A. Bonomo and J. R. Knox, *Biochemistry*, 2004, **43**, 14111–14117.
- 14 P. S. Padayatti, M. S. Helfand, M. A. Totir, M. P. Carey, P. R. Carey, R. A. and F. van den Akker, *J. Biol. Chem.*, 2005, **280**, 34900–34907.
- 15 P. S. Padayatti, A. Sheri, M. A. Totir, M. S. Helfand, M. P. Carey, V. E. Anderson, P. R. Carey, C. R. Bethel, R. A. Bonomo, J. D. Buynak and F. van den Akker, *J. Am. Chem. Soc.*, 2006, **128**, 13235–13242.
- 16 K. Miyashita and S. Mobashery, *Bioorg. Med. Chem. Lett.*, 1995, **5**, 1043–1048.
- 17 R. C. Wilmouth, Y.-H. Li, P. A. Wright, T. D. W. Claridge, R. T. Aplin and C. J. Schofield, *Tetrahedron*, 2000, **56**, 5729–5733.
- 18 J. B. Doherty, B. M. Ashe, L. W. Argenbright, P. Barker, L. Bonney, G. O. Chandler, M. E. Dahlgren, C. P. Dorn, P. E. Finke, R. A. Firestone, D. Fletcher, W. K. Hagmann, R. Mumford, L. O'Grady, A. L. Maycock, J. M. Pisano, S. K. Shah, K. R. Thompson and M. Zimmerman, *Nature*, 1986, **322**, 192–194.
- 19 J. B. Doherty, B. M. Ashe, P. Barker, T. J. Blacklock, J. W. Butcher, G. O. Chandler, M. E. Dahlgren, P. Davies, C. P. Dorn, P. E. Finke, R. A. Firestone, W. K. Hagmann, T. Halgren, W. B. Knight, A. L. Maycock, M. A. Navia, L. O'Grady, J. M. Pisano, S. K. Shah, K. R. Thompson, H. Weston and M. Zimmerman, *J. Med. Chem.*, 1990, **33**, 2513–2521.
- 20 S. K. Shah, K. A. Brause, G. O. Chandler, P. E. Finke, B. M. Ashe, H. Weston, W. B. Knight, A. L. Maycock and J. B. Doherty, *J. Med. Chem.*, 1990, **33**, 2529–2535.
- 21 J. D. Buynak, *J. Med. Chem.*, 1997, **40**, 3423–3433.
- 22 M. A. Navia, J. P. Springer, T.-Y. Lin, H. R. Williams, R. A. Firestone, J. M. Pisano, J. B. Doherty, P. E. Finke and K. Hogsteen, *Nature*, 1987, **327**, 79–82.
- 23 R. A. Firestone, P. L. Barker, J. M. Pisano, B. M. Ashe and M. E. Dahlgren, *Tetrahedron*, 1990, **46**, 2255–2262.
- 24 S. K. Shah, C. P. Dorn, P. E. Finke, J. J. Hale, W. K. Hagmann, K. A. Brause, G. O. Chandler, A. L. Kissinger, B. M. Ashe, H. Weston, W. B. Knight, A. L. Maycock, P. S. Dellea, D. S. Fletcher, K. M. Hand, R. A. Mumford, D. J. Underwood and J. B. Doherty, *J. Med. Chem.*, 1992, **35**, 3745–3754.
- 25 W. K. Hagmann, A. L. Kissinger, S. K. Shah, P. E. Finke, C. P. Dorn, K. A. Brause, B. M. Ashe, H. Weston, A. L. Maycock, W. B. Knight, P. S. Dellea, D. S. Fletcher, K. M. Hand, D. Osinga, P. Davies and J. B. Doherty, *J. Med. Chem.*, 1993, **36**, 771–777.
- 26 P. Taylor, V. Anderson, J. Dowden, S. L. Flitsch, N. J. Turner, K. Loughran and M. D. Walkinshaw, *J. Biol. Chem.*, 1999, **274**, 24901–24905.
- 27 D. J. Underwood, B. G. Green, R. Chabin, S. Mills, J. B. Doherty, P. E. Finke, M. MacCoss, S. K. Shah, C. S. Burgey, T. A. Dickinson, P. R. Griffin, T. E. Lee, K. M. Swiderek, T. Covey, W. M. Westler and W. B. Knight, *Biochemistry*, 1995, **34**, 14344–14355.
- 28 R. Chabin, B. G. Green, P. Gale, A. L. Maycock, H. Weston, C. P. Dorn, P. E. Finke, W. K. Hagmann, J. J. Hale, M. MacCoss, S. K. Shah, D. Underwood, J. B. Doherty and W. B. Knight, *Biochemistry*, 1993, **32**, 8970–8980.
- 29 H. Gu and L. R. Fedor, *J. Org. Chem.*, 1990, **55**, 5655–5657.
- 30 *Eur. Pat.* 0 337 549 A1, 1989.
- 31 R. Moreira, A. B. Santana, J. Iley, J. Neres, K. T. Douglas, P. N. Horton and M. B. Hursthouse, *J. Med. Chem.*, 2005, **48**, 4861.
- 32 I. Schechter and A. Berger, *Biochem. Biophys. Res. Commun.*, 1967, **27**, 157–162.
- 33 W. Bode, E. Meyer, Jr. and J. C. Powers, *Biochemistry*, 1989, **28**, 1951–1963.
- 34 R. Kitz and I. B. Wilson, *J. Biol. Chem.*, 1962, **12**, 2940–2945.
- 35 B. G. Green, H. Weston, B. M. Ashe, J. Doherty, P. Finke, W. Hagmann, M. Lark, J. Mao, A. Maycock, V. Moore, R. Mumford, S. Shah, L. Walakovits and W. B. Knight, *Arch. Biochem. Biophys.*, 1991, **286**, 284–292.
- 36 J. F. Morrison and C. Walsh, *Adv. Enzymol. Relat. Areas Mol. Biol.*, 1988, **61**, 201–299.
- 37 A. Clemente, A. Domingos, A. P. Grancho, J. Iley, R. Moreira, J. Neres, N. Palma, A. B. Santana and E. Valente, *Bioorg. Med. Chem. Lett.*, 2001, **11**, 1065–1068.
- 38 T. F. Oliveira, J. Mulchande, R. Moreira, J. Iley and M. Archer, *Protein Pept. Lett.*, 2007, **14**, 93–95.
- 39 N. O. Sykes, S. J. F. Macdonald and M. I. Page, *J. Med. Chem.*, 2002, **45**, 2850–2856.
- 40 W. C. Groutas, N. Houser-Archfield, L. S. Chong, R. Venkataraman, J. B. Epp, H. Huang and J. J. McClenahan, *J. Med. Chem.*, 1993, **36**, 3178–3181.
- 41 J. M. Indelicato and C. E. Pasini, *J. Med. Chem.*, 1988, **31**, 1227–1230.
- 42 A. Krantz, R. W. Spencer, T. F. Tam, T. J. Liak, L. J. Copp, E. M. Thomas and S. P. Rafferty, *J. Med. Chem.*, 1990, **33**, 464–479.

-
- 43 P. Proctor, N. P. Gensmantel and M. I. Page, *J. Chem. Soc., Perkin Trans. 2*, 1982, 1185–1192.
- 44 M. I. Page, *Adv. Phys. Org. Chem.*, 1987, **23**, 165–210.
- 45 M. J. Slater, A. P. Laws and M. I. Page, *Bioorg. Chem.*, 2001, **29**, 77–95.
- 46 S. Gérard, M. Galleni, G. Dive and J. Marchand-Brynaert, *Bioorg. Med. Chem. Lett.*, 2004, **12**, 129–138.
- 47 F. Wu, M. G. Buhendwa and D. F. Weaver, *J. Org. Chem.*, 2004, **69**, 9307–9309.
- 48 A. G. W. Leslie, *Joint CCP4 + ESF-EAMCB Newsletter on Protein Crystallography*, MRC Laboratory of Molecular Biology, Cambridge, vol. 26, 1992, http://www.mrc-lmb.cam.ac.uk/harry/mosflm/mosflm_user_guide.html.
- 49 Collaborative Computational, Project no. 4, *Acta Crystallogr., Sect. D: Biol. Crystallogr.*, 1994, **50**, 760–763.
- 50 G. N. Murshudov, A. A. Vagin and E. J. Dodson, *Acta Crystallogr., Sect. D: Biol. Crystallogr.*, 1997, **53**, 240–255.
- 51 P. Emsley and K. Cowtan, *Acta Crystallogr., Sect. D: Biol. Crystallogr.*, 2004, **60**, 2126–2132.
- 52 B. S. Hartley, *Nature*, 1964, **201**, 1284–1287.
- 53 E. Buncl and B. Menon, *J. Am. Chem. Soc.*, 1977, **99**, 4457–4461.
- 54 D. D. Perrin, B. Dempsey and E. P. Serjeant, *pK_a Prediction for Organic Acids and Bases*, Chapman and Hall, London, 1981, p. 127.
- 55 H. Fujihara and N. Furukawa, in *The Chemistry of Sulfinic Acids, Esters and Their Derivatives*, ed. S. Patai, Wiley, New York, 1990, ch. 10, p. 275.

Azetidine-2,4-diones (4-Oxo- β -lactams) as Scaffolds for Designing Elastase InhibitorsJalmira Mulchande,[†] Rita C. Guedes,[†] Wing-Yin Tsang,[‡] Michael I. Page,^{‡,*} Rui Moreira,^{†,*} and Jim Iley[§]*iMed.UL, CECF, Faculdade de Farmácia, Universidade de Lisboa, Av. Forças Armadas, 1600-083 Lisboa, Portugal, Department of Chemical & Biological Sciences, University of Huddersfield, Huddersfield, HD1 3DH, U.K., and Department of Chemistry, The Open University, Milton Keynes, MK7 6AA, U.K.*

Received October 5, 2007

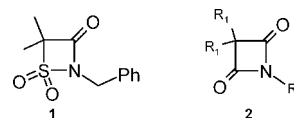
A new class of inhibitors 4-oxo- β -lactams (azetidine-2,4-diones), containing the required structural elements for molecular recognition, inhibit porcine pancreatic elastase (PPE) but show a dramatically lower reactivity toward hydroxide compared with the analogous inhibitors 3-oxo- β -sultams. Inhibition is the result of acylation of the active site serine and electron-withdrawing substituents at the *N*-(4-aryl) position in 3,3-diethyl-*N*-aryl derivatives increasing the rate of enzyme acylation and generating a Hammett ρ -value of 0.65. Compared with a ρ -value of 0.96 for the rates of alkaline hydrolysis of the same series, this is indicative of an earlier transition state for the enzyme-catalyzed reaction. Docking studies indicate favorable noncovalent interactions of the inhibitor with the enzyme. Compound **2i**, the most potent inhibitor against PPE, emerged as a very potent HLE inhibitor, with a second-order rate for enzyme inactivation of $\sim 5 \times 10^5 \text{ M}^{-1} \text{ s}^{-1}$.

Introduction

Human leukocyte elastase (HLE)^a is a member of the chymotrypsin superfamily of serine proteases that very efficiently degrades tissue matrix proteins such as elastin when released from the azurophilic granules of polymorphonuclear leukocytes because of inflammatory stimuli and mediators. The imbalance between HLE and its endogenous inhibitors leads to excessive elastin proteolysis and destruction of connective tissues in a number of inflammatory diseases such as pulmonary emphysema, adult respiratory distress syndrome, chronic bronchitis, chronic obstructive pulmonary disease, and rheumatoid arthritis.^{1–5}

β -Lactams are well-known as potent inhibitors of some enzymes that contain serine as the catalytic residue, including the bacterial penicillin binding proteins (PBPs) and Class A and Class C β -lactamases.⁶ β -Lactams have also been appropriately modified to develop active site-directed and mechanism-based inhibitors of HLE.^{7–9} Improvement of the rate of serine acylation by increasing the intrinsic chemical reactivity of the β -lactams has been used as a strategy to design more potent inhibitors.¹⁰ Recently, we have reported that 3-oxo- β -sultam, **1**, is a reasonably potent inhibitor of porcine pancreatic elastase (PPE), a model enzyme that shares $\sim 40\%$ homology and the catalytic triad consisting of Ser-195, His-57 and Asp-102 with HLE. Nucleophilic attack on 3-oxo- β -sultams **1** could involve either acylation or sulfonylation resulting from substitution at the carbonyl center and expulsion of the sulfonamide or from substitution at the sulfonyl center and expulsion of the amide, respectively. Inhibition of elastase by **1** occurs by acylation of the active site serine and so involves C–N fission and expulsion of sulfonamide.¹¹ By contrast, the alkaline hydrolysis of **1** occurs by hydroxide-ion attack on the sulfonyl center with S–N fission.

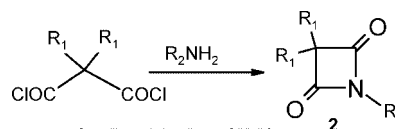
This is a very rapid process and occurs with a second-order rate constant, k_{OH} , value of $\sim 2 \times 10^5 \text{ M}^{-1} \text{ s}^{-1}$,¹² which is about 10^6 times higher than those of most clinically useful β -lactams.¹³ Highly reactive scaffolds may lead to a decrease the selectivity toward the target enzyme, increase susceptibility to metabolism, and reduce oral bioavailability.¹⁴ The mechanism of inhibition of elastase by **1** involves expulsion of the relatively good leaving sulfonamide group. Selectivity could be improved by replacing this group by a poorer leaving group such as an amide. We now report that isosteric analogues of **1**, azetidine-2,4-diones or 4-oxo- β -lactams, **2**, containing the required structural elements for molecular recognition by PPE and HLE, retain inhibitory activity while dramatically decreasing the reactivity toward hydrolysis by hydroxide ion.



Results and Discussion

Synthesis. 4-Oxo- β -lactams **2** were prepared in reasonable yields from the appropriate 2,2-disubstituted malonic acid chlorides and amines (Scheme 1). The corresponding malon-diamides were always obtained as side-products but were easily removed by column chromatography.

Scheme 1



- 2a** $R_1 = \text{Me}$, $R_2 = \text{CH}_2\text{Ph}$
2b $R_1 = \text{Me}$, $R_2 = \text{C}_6\text{H}_4\text{-4-Cl}$
2c $R_1 = \text{Et}$, $R_2 = \text{CH}_2\text{CO}_2\text{Et}$
2d $R_1 = \text{Et}$, $R_2 = \text{CH}_2\text{Ph}$
2e $R_1 = \text{Et}$, $R_2 = \text{C}_6\text{H}_4\text{-4-OMe}$
2f $R_1 = \text{Et}$, $R_2 = \text{C}_6\text{H}_4\text{-4-Me}$
2g $R_1 = \text{Et}$, $R_2 = \text{C}_6\text{H}_5$
2h $R_1 = \text{Et}$, $R_2 = \text{C}_6\text{H}_4\text{-4-Cl}$
2i $R_1 = \text{Et}$, $R_2 = \text{C}_6\text{H}_4\text{-4-CN}$

* To whom correspondence should be addressed. Phone: +44 1484 472531 (M.I.P.). Fax: +44 1484 473075 (M.I.P.). E-mail: m.i.page@hud.ac.uk (M.I.P.); rmoreira@ff.ul.pt (R.M.).

[†] Universidade de Lisboa.

[‡] University of Huddersfield.

[§] The Open University.

^a Abbreviations: EREF, enzyme rate enhancement factor; HEPES, *N*-[2-hydroxyethyl]piperazine-*N'*-[2-ethane sulfonic acid]; HLE, Human leukocyte elastase; PBP, penicillin binding proteins; PPE, porcine pancreatic elastase; TI, tetrahedral intermediate.

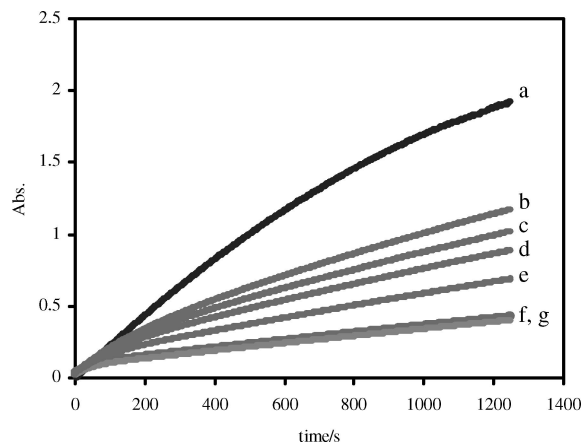


Figure 1. Progress curves for the inhibition of **2h**. Reaction conditions: [PPE] = 0.2 μ M, [Suc-(L-Ala)₃-p-NA] = 0.3 mM, 0.1 M HEPES buffer, pH 7.2, 5% DMSO, 25 °C. Inhibitor concentrations (μ M): (a) absence of inhibitor, (b) 10, (c) 15, (d) 20, (e) 30, (f) 60, (g) 75.

Scheme 2



PP Elastase Inhibition Studies. Enzyme activity was measured by the hydrolysis of reporter substrate *N*-succinyl-(L-Ala)₃-*p*-nitroanilide at 390 nm. Incubation of PPE with 4-oxo- β -lactams **2** resulted, in most cases, in very rapid time-dependent loss of activity (Figure 1), followed by a slower reactivation of enzyme activity. This is presumably attributable to acylation of the active site serine followed by slow hydrolysis and is described by Scheme 2, where EI corresponds to the acyl-enzyme. Therefore, inhibition was studied at 25 °C using the progress curve method,¹⁵ and the time courses for Figure 1 were fit by nonlinear regression analysis to eq 1

$$A = v_s t + (v_i - v_s)(1 - e^{-k_{\text{obs}} t})/k_{\text{obs}} + A_0 \quad (1)$$

where *A* is the absorbance at 390 nm, *A*₀ is the absorbance at *t* = 0, *v*_i is the initial rate of change of absorbance, *v*_s is the steady-state rate, and *k*_{obs} is the first-order rate constant for the approach to the steady-state. The plots of *k*_{obs} versus the concentration of **2** were linear and thus were consistent with the inhibition mechanism depicted in Scheme 2, which corresponds to eq 2.¹⁶ The linear dependence of *k*_{obs} on [I], as well as the observation that initial velocities, *v*_i, equalled the velocity in the absence of inhibitor, *v*₀, suggest that the acyl-enzyme EI did not accumulate in the inhibitor concentration range used. The graphical interpretation (Figure 2) of eq. 2 yields the second-order rate constant for inhibition, *k*_{on}, as the slope (Table 1) and the first-order rate for deacylation, *k*_{decayl}, as the intercept. The *K_i* values were calculated as *k*_{decayl}/*k*_{on}.

$$k_{\text{obs}} = (k_{\text{on}}[I]/\{1 + ([S]/K_m)\}) + k_{\text{decayl}} \quad (2)$$

An important criterion for the successful inhibition of serine enzymes by an acylation process depends upon the lifetime of the acyl-enzyme intermediate. A reactive intermediate will undergo rapid hydrolysis as in the normal pathway for the hydrolysis of substrates. In contrast to the slow-binding inhibition model displayed by 3,3-diethyl-substituted 4-oxo- β -lactams, **2e–i**, their 3,3-dimethyl counterparts, **2a** and **b** presented strictly linear time courses for the hydrolysis of substrate, that is, no initial exponential phase toward a steady-state was observed. Incubation of 7.5×10^{-4} M of *N*-benzyl-4,4-dimethyl-4-oxo-

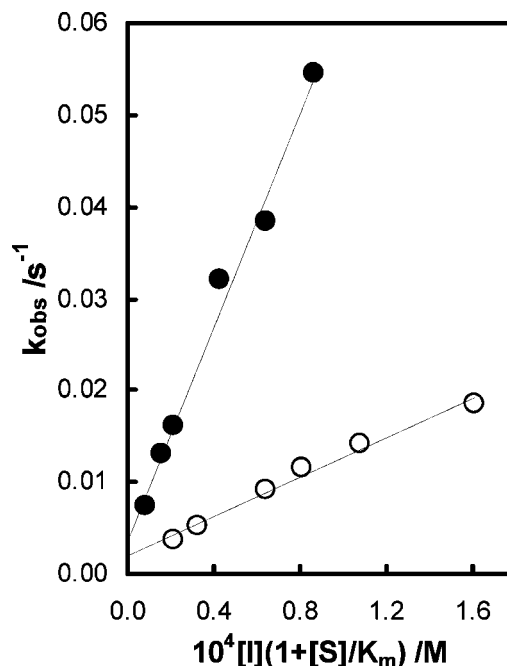


Figure 2. Effect of inhibitor concentration on the onset of inhibition of PPE by **2e** (○) and **2i** (●). Inhibitor concentration is corrected according to eq 2.

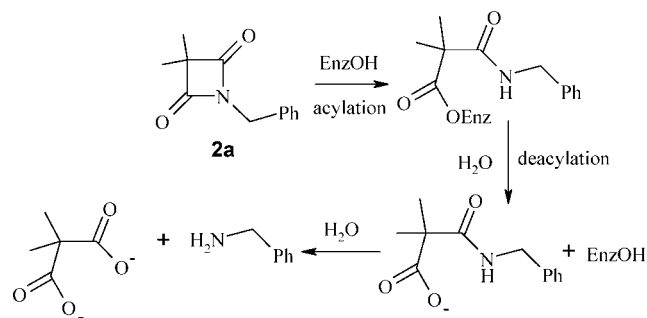
β -lactam **2a**, which was in 750-fold excess to PPE concentration, showed no decrease of enzyme activity when the incubated enzyme was diluted into assay cells containing the substrate. The less sterically hindered dimethyl derivative may act as a simple substrate for elastase. However, the reaction of **2a** with elastase was followed by UV-spectroscopy at 242 nm. The plot of absorbance versus time displayed biphasic kinetics, in which the concentration of 4-oxo- β -lactam **2a** decreases with time in a zero-order manner in the first phase of the reaction but changed to first-order kinetics in the second phase of the reaction. This apparent “saturation” behavior is compatible with slow deacylation of the acyl-enzyme intermediate, assuming the exponential decay of absorbance against time for the second phase of the reaction is caused by the hydrolysis of the ring-opened hydrolysis product (Scheme 3). The rate of formation and breakdown of the acyl-enzyme was obtained by fitting the absorbance versus time curve for the reaction of **2a** at high concentration of PPE to Scheme 2 using Dynafit,¹⁷ and the derived rate constants are given in Table 1. Increasing the enzyme concentration did not affect the rate of breakdown of the acyl enzyme intermediate but increased the rate of formation of the acyl-enzyme intermediate. Zero-order kinetics were observed if the rate of acylation is at least 30-fold greater than that of deacylation.

Interestingly, the rate of acylation in the reaction of *N*-benzyl-3,3-dimethyl-4-oxo- β -lactam **2a** with PPE elastase is 12-fold slower than that of inhibition by its 3-oxo- β -sultam counterpart **1** (**1**, *k*_{on} = 7.68×10^2 M⁻¹ s⁻¹),¹¹ with the same enzyme and at pH 6.0, whereas the rate of deacylation in the reaction of **2a** is 500-fold faster than that of the reactivation of the enzyme inhibited with **1** (**1**, *k*_{decayl} = 2.08×10^{-5} s⁻¹). Nucleophilic attack at the carbonyl center of **1** and that of **2** generates a sulfonamide and an amide leaving group, respectively. Although sulfonamides and amides have different electronic properties, for example, sulfonamides are generally more acidic than amides by about 5 p*K_a* units,¹⁸ the stability of the acyl ester of the acyl enzymes is unlikely to be affected by this property because the groups are some distance from the acyl ester.¹⁹ However, the

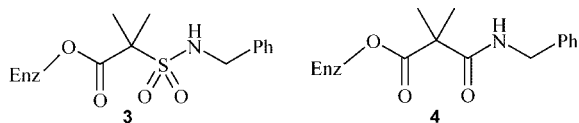
Table 1. Kinetic Parameters for the Inhibition of PPE at pH 7.2 by, and for the Alkaline Hydrolysis of, Azetidion-24-diones, **2, at 25 °C**

compound	R ¹	R ²	K _i (μM)	k _{on} (×10 ⁻² M ⁻¹ s ⁻¹)	k _{off} (×10 ³ s ⁻¹)	k _{OH⁻} (M ⁻¹ s ⁻¹)	EREF
2a	Me	CH ₂ Ph	184	0.63 ^a	0.997 ^a	1.80 ^b ; 8.38 ^c	
2b	Me	C ₆ H ₄ -4-Cl	10.0			9.67	
2c	Et	CH ₂ CO ₂ Et	NI	NI		ND	
2d	Et	CH ₂ Ph	NI	NI		0.0742	
2e	Et	C ₆ H ₄ -4-OMe	9.81	1.22	1.20	0.225	542
2f	Et	C ₆ H ₄ -4-Me	7.46	1.74	1.30	0.240	725
2g	Et	C ₆ H ₅	10.2	1.77	1.81	0.336	527
2h	Et	C ₆ H ₄ -4-Cl	8.47	2.32	1.97	0.581	400
2i	Et	C ₆ H ₄ -4-CN	6.02	5.83	3.53	1.78	328

^a pH 6.0. ^b T = 30 °C, 1% DMSO (v/v). ^c T = 25 °C, 20% CH₃CN (v/v).

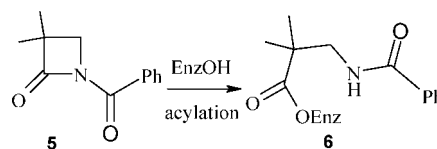
Scheme 3

α -tertiary center containing a *gem*-dimethyl group together with a sulfonyl group of a sulfonamide, **3**, is likely to significantly block attack by water at the active site, and the deacylation would be severely impaired. If this is the case, the sulfonamide leaving group being bigger in size, as in **3**, decreases the rate of deacylation by 500-fold compared with that observed with an amide leaving group, **4**.

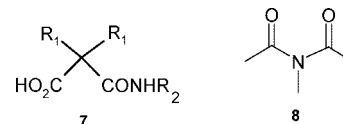


The effect of bulky substituents on the rate of deacylation is also demonstrated by the PPE catalyzed hydrolysis of *N*-benzoyl-3,3-dimethyl- β -lactam **5** (Scheme 4), which shows normal hydrolytic behavior and no accumulation of the acyl enzyme intermediate despite the presence of an α -*gem*-dimethyl group. The acyl enzyme generated from **5** has the structure **6** and presumably moving the exocyclic carbonyl further down the carbon chain in the ring-opened product **6** must reduce the steric congestion around the acyl enzyme ester, allowing rapid deacylation.

Alkaline Hydrolysis. The second-order rate constants, k_{OH^-} , for the alkaline hydrolysis of the 4-oxo- β -lactams **2** were also determined for comparison with those for PPE inhibition (Table 1). It has been suggested that the magnitude of the second-order rate constant, k_{OH^-} , for the alkaline hydrolysis of potential inhibitors of enzymes containing a catalytic serine is a crude indicator for their ability to be effective and therapeutically useful acylating agents.^{14,20,21} As a result of the symmetry of 4-oxo- β -lactams **2**, the two acyl centers are equivalent, and the hydrolysis products of 4-oxo- β -lactams **2** are the corresponding α -amido acids **7**. The second-order rate constant, k_{OH^-} , for the alkaline hydrolysis of **2a** is 8.38 M⁻¹ s⁻¹ (Table 1), which is, remarkably, only 7-fold greater than that for the corresponding *N*-benzoyl- β -lactam **5** and demonstrates the surprisingly small effect of introducing a second sp² center into the already strained four-membered ring. Furthermore, the strained cyclic imide **2a** shows reactivity similar to that of the acyclic imide **8** (k_{OH^-} =

Scheme 4

1.54 M⁻¹ s⁻¹),¹⁴ showing that there is no significant rate enhancement caused by ring strain, compatible with the limiting step of alkaline hydrolysis being the formation of the tetrahedral intermediate (TI).



It is of interest to compare the rate constants for alkaline hydrolysis for a series of four-membered rings β -lactams, **2** and **5**, and β -sultams, for example, **1**, with those for their reactions with elastase. The substitution of the *N*-benzyl by *N*-phenyl in 4-oxo- β -lactam changes the leaving group from an amide to an anilide and causes an increase in the rate of ring opening by hydroxide ion (e.g., **2g** is 5-fold more reactive than **2d**). *N*-Substitution would be expected to have a large effect on rate-limiting C–N fission but a much smaller one if nucleophilic attack on the carbonyl carbon and formation of the tetrahedral intermediate is the rate-limiting step. Electron-withdrawing substituents (such as 4-cyanophenyl **2i** and 4-chlorophenyl **2h**) produce a modest increase in the rate of the alkaline hydrolysis, whereas electron-donating groups (4-methoxyphenyl, **2e**), decrease k_{OH^-} . Overall, **2i** is nearly 8-fold more active than **2e**. These relative rates indicate that the rate-limiting step is hydroxide-ion attack and formation of the tetrahedral intermediate.

There is a large steric effect of substituents α to the carbonyl carbon on the rate of alkaline hydrolysis. The α -*gem*-diethyl compounds **2d** and **2h** are about 20-fold less reactive than the corresponding α -*gem*-dimethyl compounds **2a** and **2b**, which is also compatible with rate limiting formation of the tetrahedral intermediate.

Structure–Activity Relationships and Molecular Modeling. Inspection of Table 1 indicates that the most potent inhibitors contain an *N*-aryl group in addition to two ethyl groups at C-3. In contrast, *N*-alkyl-4-oxo- β -lactams are either inactive (**2c**, **d**) or weak inhibitors (**2a**) that regenerate the active enzyme. This suggests that the leaving group ability of the amide formed from the decomposition of the tetrahedral intermediate (TI) **9** contributes significantly to the time-dependent inhibition of PPE. The most-active inhibitor contains a 4-CN electron-withdrawing substituent on the *N*-aromatic ring (**2i**) and is nearly 5-fold more potent than **2e**, which contains an electron-donating substituent. Interestingly, log k_{on} values correlate with Hammett σ_p values,

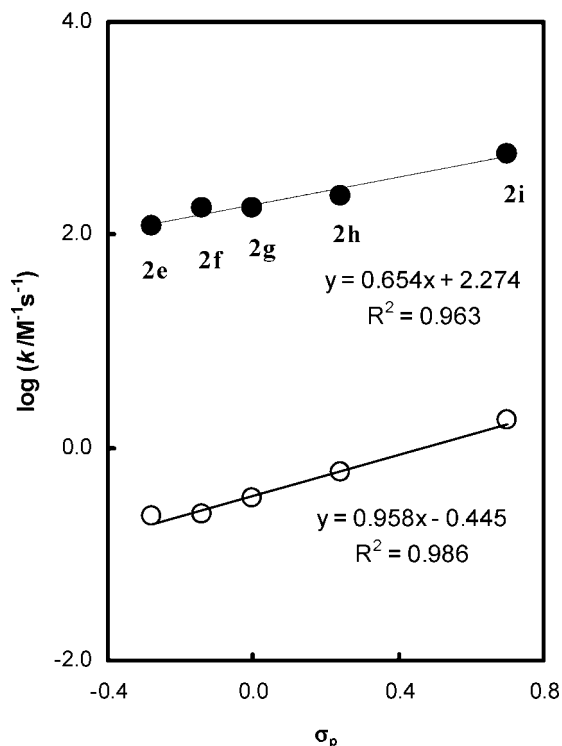
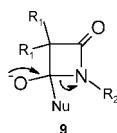


Figure 3. Hammett plots for the second-order rate constants, k_{on} , for the inhibition of PPE by 4-oxo- β -lactams **2e–i** (●) and for the hydroxide-ion-catalyzed hydrolysis, k_{OH^-} , of the same compounds (○) at 25 °C.

giving a ρ value of 0.65 (Figure 3), consistent with the reduction of the positive charge on the nitrogen amide caused by resonance rather than the development of significant negative charge on this atom in the transition-state. This is consistent with rate limiting formation of the tetrahedral intermediate in the enzyme catalyzed reaction. In comparison, the alkaline hydrolysis of 4-oxo- β -lactams gives a Hammett ρ value of 0.96 (Figure 3) suggesting a much greater change in charge on going to the transition state. Both enzyme-catalyzed acylation and alkaline hydrolysis of the 4-oxo- β -lactams involve nucleophilic attack on the β -lactam carbonyl. The different Hammett ρ values indicate the enzyme-catalyzed attack of serine occurs at an earlier position along the reaction coordinate leading to formation of the tetrahedral intermediate compared with the hydroxide-ion-catalyzed hydrolysis. This is consistent with the Hammond postulate in that these results suggest that the 4-oxo- β -lactam scaffold promotes the enzyme's ability to use its catalytic apparatus to stabilize the transition state and increase the rate of serine acylation, which might be achieved by favorable noncovalent binding of enzyme and inhibitor, stabilization of the TI in the oxyanion hole of the active site and compensation for the entropy loss required in the bimolecular reaction.



It has been suggested that the effectiveness of an enzyme in catalyzing a reaction can be indicated by the enzyme rate enhancement factor, EREF, which is evaluated by dividing the second-order rate constant for the enzyme catalyzed reaction, k_{on} , by that for hydrolysis of the same substrate catalyzed by

hydroxide ion, k_{OH^-} .¹⁴ The highest value of EREF was obtained for inhibitor **2f**: the enzyme increases the rate of reaction by 725-fold.

To rationalize the trends observed in the enzyme assays, the molecular interactions between the more active 4-oxo- β -lactams **2a**, **2e**, **2i** and HLE were investigated using the automated GOLD docking program (see Experimental Section for details). The primary recognition pocket, S_1 , for porcine elastase prefers small hydrophobic substituents with two carbon atoms.²² Docking of the most potent compound, **2i**, into the active site of PPE revealed that only one ethyl substituent of the 3,3-diethyl group lies in the S_1 pocket (Figure 4). This binding mode is not much different than that observed for the interaction of 3,3-diethyl- β -lactams with HLE, in which both ethyl substituents are accommodated in the larger S_1 pocket.¹⁰ The distance between the Ser-195 hydroxyl oxygen atom and the closest carbonyl carbon of **2i** is 3.18 Å (4.79 Å for the other carbonyl carbon atom), which indicates that nucleophilic attack by Ser-195 to the 4-oxo- β -lactam is possible. Interestingly, the “reactive” carbonyl of **2i** is not involved in the H-bond network with the so-called oxyanion hole defined by the backbone NHs of Gly-193 and Ser-195: the distances between the amidic hydrogen atoms of Gly-193 and Ser-195 to the carbonyl oxygen atom are 6.75 and 5.28 Å, respectively. This result may indicate that the oxyanion hole is not used to stabilize the TI derived from **2i**. However, several key interactions seem to stabilize **2i** in the active site. First, strong hydrogen bonds involve the oxygen atom of the reactive carbonyl and the NH of His-57 and the hydroxyl group of Ser-195. Second, an additional hydrogen bond involves the oxygen atom of the unreactive carbonyl and the amide group of Gln-192. Finally, enhanced van der Waals contacts between the N-aryl moiety with Val-99, Phe-215, and His-57 were observed.

For compound **2e**, a less potent inhibitor, an inverted binding mode was observed, in which the 4-OMe substituent of the aromatic ring lies on the S_1 pocket, while one of the ethyl substituents is close to the S_1' pocket (Figure 4). The distance between the closest carbonyl carbon and the Ser-195 hydroxyl oxygen atom is 3.62 Å (4.38 Å for the other carbonyl carbon atom). However, in contrast to **2i**, the reactive carbonyl of **2e** is involved in the H-bond network with the NHs of Gly-193 and Ser-195, which suggests that the oxyanion hole may be used to stabilize the resulting TI and to compensate the energy required for the enzyme to overcome the distance between Ser-195 and the carbonyl carbon. The 3,3-dimethyl-*N*-benzyl derivative **2a** also interacts with PPE with a similar binding mode to that of **2e**, that is, aromatic ring lying on the S_1 pocket (Figure 4) and with the reactive carbonyl involved in the oxyanion hole H-bond network. Compound **2f** also presents the *N*-aryl moiety sitting in the S_1 pocket of the enzyme (see Supporting Information), but in this case, the distance between the closest carbonyl carbon and the Ser-195 hydroxyl oxygen atom is 3.27 Å, that is, close to that of **2i**. This binding confirmation suggests that nucleophilic attack by Ser-195 to the 4-oxo- β -lactam is feasible and is consistent with the EREF value of 725, the highest of the present series of compounds **2**.

Because the 4-oxo- β -lactam inhibitors **2** have two acyl centers, there could be interaction of either the C-3 or the N-1 substituents with the S_1 binding pocket. In principle, the latter could reduce the rate of acylation as a result of nonproductive binding. However, the dominant effect of N-substituents is their influence the rate of C-N bond fission in breakdown of the TI **9**. Compound **2h**, containing a diethyl substituent at C-3 position is a time dependent and, effectively, irreversible inhibitor of

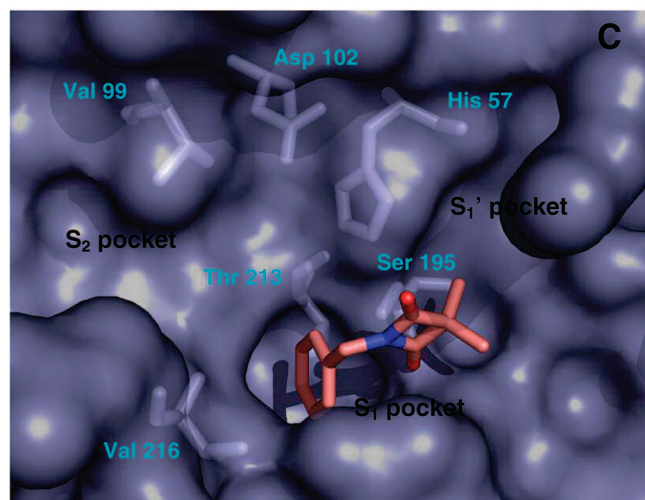
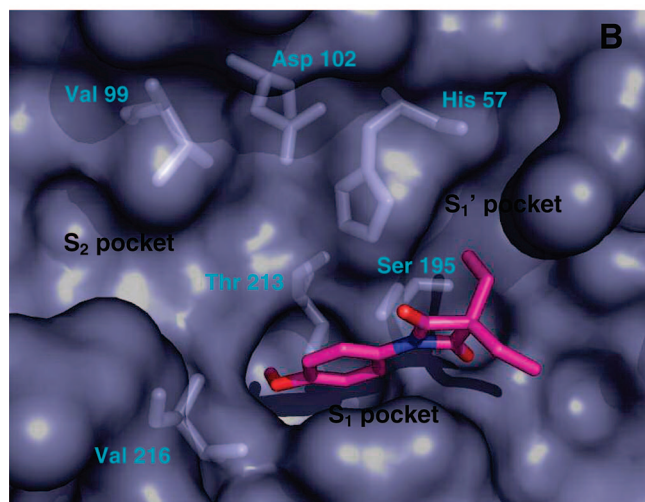
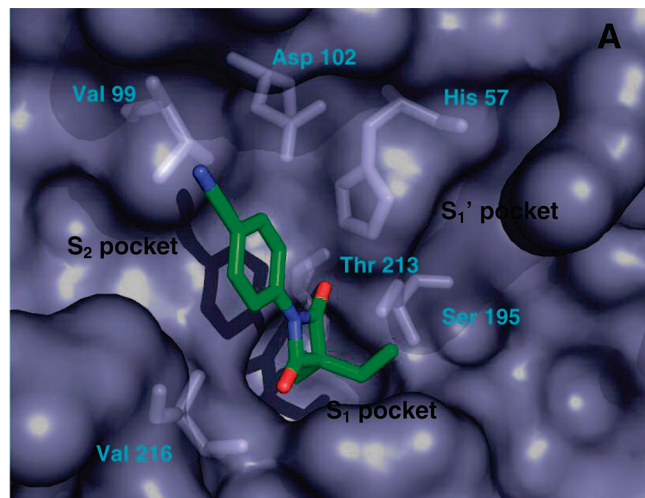


Figure 4. Docking of **2i** (A), **2e** (B), and **2a** (C) in the active site of PPE (see text for details of docking procedure).

PPE because of its relatively fast acylation of the enzyme, while the dimethyl counterpart **2b** is also a time dependent inhibitor, but because of a relatively facile deacylation pathway of the dimethyl acyl-enzyme does allow the enzyme to turnover. The almost complete recovery of enzymatic activity (Figure 5), monitored by checking the enzyme activity at different time intervals after incubation with **2h**, suggests that the interaction of **2** with PPE leads to a labile acyl-enzyme, EI, which breaks

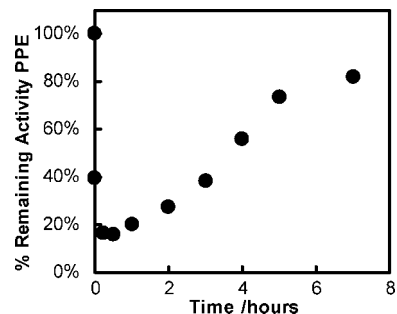


Figure 5. Time-dependent loss of enzymatic activity. Excess of inhibitor **2h** ($[I]_t = 150 \mu\text{M}$) was incubated with PPE ($[E]_t = 10 \mu\text{M}$) in 0.1 M HEPES buffer, pH 7.2, 25 °C, aliquots were withdrawn at different time intervals and assayed for enzymatic activity.

down and regenerates the free, active enzyme, E (Scheme 3), within a few hours and the inhibitor function as alternate substrate inhibitor of PPE.

HLE Inhibition. Taking into account the high k_{on} value obtained for compound **2i** against PPE, we assayed this compound against HLE. A nonlinear dependence of k_{obs} (determined by the progress curve method; eq. 1)¹⁵ on inhibitor concentration was observed (Supporting Information) and the individual kinetic parameters K_i (63.5 nM) and k_{inact} (0.0323 s⁻¹) were obtained according to eq 3.²² The corresponding second-order rate constant for inhibition, k_{inact}/K_i is $5.08 \times 10^5 \text{ M}^{-1}\text{s}^{-1}$, a value close to those reported for the most potent monocyclic β -lactams developed by Merck.²² This result (i) shows the usefulness of the 4-oxo- β -lactam scaffold for designing inhibitors for human elastase and (ii) indicates that **2i** is a promising lead for further optimization against HLE.

$$k_{\text{obs}} = k_{\text{inact}}[I]/\{K_i(1 + [S]/K_m) + [I]\} \quad (3)$$

Conclusion

This study has shown that 4-oxo- β -lactam derivatives can function as novel time dependent irreversible inhibitors of serine proteases when they contain 3,3-diethyl-*N*-aryl substituents. The title compounds were designed as a result of an isosteric replacement from 3-oxo- β -sultam, yielding more stable compounds to hydrolysis by nonspecific nucleophiles and reacting with the enzyme as active-site-directed inhibitors. The most-active inhibitors correspond to the most reactive compounds toward alkaline hydrolysis and contain electron-withdrawing substituents on the aromatic ring that increase the chemical reactivity of the carbonyl carbon toward nucleophilic attack of the Ser-195 hydroxyl group. The enzyme-mediated hydrolysis has an earlier transition state because of favorable hydrophobic and other noncovalent binding interactions between enzyme and inhibitor that can be used to compensate for unfavorable processes that contribute to the activation energy. In summary, 4-oxo- β -lactam derivatives represent an attractive new class of acyl-enzyme inhibitors of elastases and are suitable scaffolds that might find further applicability for the design of nonpeptidic inhibitors of other serine proteases.

Experimental Section

General. Melting points were determined using a Kofler camera Bock Monoscope M and are uncorrected. The infrared spectra were collected on a Nicolet Impact 400 FTIR infrared spectrophotometer, and the NMR spectra were collected on a Bruker 400 Ultra-Shield (400 MHz) in CDCl₃; chemical shifts, δ , are expressed in ppm, and coupling constants, J , are expressed in Hz. Low-resolution mass spectra were recorded using a HP5988A spectrometer, by RIAIDT, University of Santiago de Compostela, Spain. Elemental analyses

were performed by Medac Ltd., Brunel Science Centre, Englefield Green Egham TW20 0JZ, U.K., or by ITN, Chemistry Unit, Sacavém, Portugal. UV spectra and spectrophotometric assays were performed using Shimadzu UV-1603 or UV-2100 PC spectrometers. Thin layer chromatography was performed on a Merck grade aluminum plates, silica gel 60 F₂₅₄, and visualized by UV light or iodine. Preparative column chromatography was performed on silica gel 60 from Merck (70–230 mesh ASTM). Dioxane and TEA were purified and dried before use. Sodium hydroxide and hydrochloric acid solutions were prepared from dilution of standardized Tritisol stock solutions. Solvents and buffer materials for enzyme assays were of analytical reagent grade and were purchased from Merck or Sigma. PPE, MeO-Suc-Ala-Ala-Pro-Val-*p*-NA, and *N*-Suc-Ala-Ala-*p*-NA were purchased from Sigma, and HLE was purchased from Calbiochem.

General Procedure for the Synthesis of Azetidine-2,4-dione Derivatives. To a solution of the appropriate malonyl dichloride (0.015 mol) in dry dioxane (15 mL) was added under a nitrogen atmosphere a primary amine (0.015 mol) in the same solvent (15 mL). Subsequently, a solution of triethylamine (0.036 mol) in dry dioxane (15 mL) was added dropwise during 1.5 h, and the resulting mixture refluxed for 6 h, with the reaction progress being monitored by TLC. After the mixture was cooled, triethylamine hydrochloride was filtered off, and the solvent was removed under reduced pressure yielding a solid (malondiamide), recrystallized from dioxane/hexane. The mother liquor was concentrated under reduced pressure, and the residue was purified by chromatography on silica gel, affording the desired product (azetidine-2,4-dione).

1-Benzyl-3,3-dimethylazetidine-2,4-dione, 2a. Compound **2a** was prepared as described above, using dimethylmalonyl dichloride (2.535 g, 0.015 mol), benzylamine as primary amine (1.622 g, 0.015 mol), and triethylamine (3.649 g; 0.036 mol) as catalyst. The resulting reaction mixture was refluxed for 14 h. The product was purified by chromatography on silica gel, using toluene/ethyl acetate as eluant (from 9.8:0.2 to 9.0:1.0), yielding white crystals (0.122 g, 4%): mp 69–71 °C; Anal. (C₁₂H₁₃NO₂) C, N. H calcd 6.45; found 5.95; δ ¹H NMR 1.38 (6H, s), 4.46 (2H, s), 7.33–7.39 (5H, m); δ ¹³C NMR 17.44, 42.78, 60.66, 127.99, 128.17, 129.00, 134.77, 175.05.

1-(4-Chlorophenyl)-3,3-dimethylazetidine-2,4-dione, 2b. Compound **2b** was synthesized as described for **2a**, using dimethylmalonyl dichloride (4.225 g, 0.025 mol) and 4-chloroaniline (2.820 g, 0.025 mol), with the reaction mixture being refluxed for 8 h. The product was purified by column chromatography using hexane/ethyl acetate as eluant (8.4:1.6) to afford **2b** as white crystals (0.351 g, 6%): mp 81–84 °C; Anal. (C₁₁H₁₀NO₂Cl) C, H, N; δ ¹H NMR 1.51 (6H, s), 7.40 (2H, d, *J* = 8.8), 7.82 (2H, d, *J* = 8.8); δ ¹³C NMR 17.76, 62.03, 120.33, 129.42, 132.12, 132.81, 172.62.

Ethyl 2-(3,3-Diethyl-2,4-dioxazetidin-1-yl)acetate, 2c. Compound **2c** was prepared as described for **2a** using diethylmalonyl dichloride (4.925 g, 0.025 mol) and ethyl glycinate hydrochloride (3.475 g, 0.025 mol) but with more than 3 equiv of triethylamine (9.107 g, 0.09 mol). The residue was purified by column chromatography on silica gel using mixtures of toluene and ethyl acetate as eluant to yield a colorless oil (0.920 g, 16%): Anal. (C₁₁H₁₇NO₄) C, H, N; δ ¹H NMR 1.07 (6H, t, *J* = 7.6), 1.30 (3H, t, *J* = 7.2), 1.82, (4H, q, *J* = 7.6), 4.10 (2H, s), 4.25 (2H, q, *J* = 7.2); Lit.²⁴ 1.03 (3H, t, *J* = 7), 1.30 (3H, t, *J* = 7), 1.77 (4H, q, *J* = 7), 3.98 (2H, s), 4.21 ((2H, q, *J* = 7); δ ¹³C NMR 9.27, 14.08, 23.62, 39.28, 62.23, 71.30, 165.93, 173.59.

1-Benzyl-3,3-diethylazetidine-2,4-dione, 2d. Compound **2d** was prepared as described for **2a**, using diethylmalonyl dichloride (2.956 g, 0.015 mol), benzylamine (1.622 g, 0.015 mol) as primary amine, and triethylamine (3.649 g, 0.036 mol) as catalyst. The product was purified by chromatography on silica gel using toluene/ethyl acetate as eluant (from 9.8:0.2 to 9.2:0.8) and then recrystallized from hexane to yield the product as white crystals (0.243 g, 9%): mp 46–47 °C; Anal. (C₁₄H₁₇NO₂) C, H, N; δ ¹H NMR 0.94 (6H, t, *J* = 7.6), 1.75 (4H, q, *J* = 7.6), 4.48 (2H, s), 7.32–7.37 (5H, m); δ ¹³C NMR 9.18, 23.67, 42.17, 70.98, 128.14, 128.28, 128.88, 135.06, 174.24.

3,3-Diethyl-1-(4-methoxyphenyl)azetidine-2,4-dione, 2e. Compound **2e** was prepared as described for **2a**, using diethylmalonyl dichloride (2.956 g, 0.015 mol) and 4-anisidine (1.605 g, 0.015 mol) as primary amine. Purified by chromatography on silica gel using toluene/ethyl acetate (9.2:0.8), yielding yellow oil (0.412 g, 11%): Anal. (C₁₄H₁₇NO₃) C, H, N; δ ¹H NMR 1.08 (6H, t, *J* = 7.6), 1.86 (4H, q, *J* = 7.6), 3.84 (3H, s), 6.94 (2H, d, *J* = 8.8), 7.76 (2H, d, *J* = 8.8); δ ¹³C NMR 9.25, 23.95, 55.51, 71.94, 114.34, 120.89, 172.25.

3,3-Diethyl-1-(4-tolyl)azetidine-2,4-dione, 2f. Compound **2f** was prepared as described for **2a**, using diethylmalonyl dichloride (2.956 g; 0.015 mol) and 4-toluidine (1.605 g; 0.015 mol). The product was purified by chromatography on silica gel using toluene/ethyl acetate (9:1) as eluant, to afford white crystals (0.343 g, 10%): mp 41–44 °C; Anal. (C₁₄H₁₇NO₂) C, H calcd 7.41; found 6.59; N calcd 6.06; found 6.56; δ ¹H NMR 1.08 (6H, t, *J* = 7.6), 1.87 (4H, q, *J* = 7.6), 2.37 (3H, s), 7.23 (2H, d, *J* = 8.4), 7.73 (2H, d, *J* = 8.4); δ ¹³C NMR 9.24, 21.18, 23.95, 72.01, 119.19, 129.75, 131.33, 136.69, 172.27.

3,3-Diethyl-1-phenylazetidine-2,4-dione, 2g. Compound **2g** was prepared as described for **2a**, using diethylmalonyl dichloride (2.956 g, 0.015 mol) and aniline (1.397 g, 0.015 mol). It was purified by column chromatography on silica gel using toluene/ethyl acetate (9.0, 1.0) to give a colorless oil (0.474 g, 15%) (Lit.²⁴ mp. 86–87 °C): Anal. (C₁₃H₁₅NO₂) C, H, N; δ ¹H NMR 1.09 (6H, t, *J* = 7.6), 1.88 (4H, q, *J* = 7.6), 7.29 (1H, dt, *J* = 7.6, 1.2), 7.73 (2H, dt, *J* = 7.6, 1.2), 7.86 (2H, dd, *J* = 7.6, 1.2); δ ¹³C NMR 9.25, 23.96, 72.14, 119.23, 126.76, 129.26, 133.85, 172.26.

1-(4-Chlorophenyl)-3,3-diethylazetidine-2,4-dione, 2h. Compound **2h** was prepared as described for **2a**, using diethylmalonyl dichloride (2.956 g; 0.015 mol) and 4-chloroaniline (1.695 g, 0.015 mol). It was purified by column chromatography on silica gel using toluene/ethyl acetate (8.0, 2.0), yielding the product as white crystals (0.544 g, 14%): mp 43–46 °C; Anal. (C₁₃H₁₄NO₂Cl) C, H, N; δ ¹H NMR 1.08 (6H, t, *J* = 7.6), 1.88 (4H, q, *J* = 7.6), 7.40 (2H, d, *J* = 8.8), 7.83 (2H, d, *J* = 8.8); δ ¹³C NMR 9.23, 23.93, 72.38, 120.41, 129.42, 132.12, 132.32, 171.96.

4-(3,3-Diethyl-2,4-dioxazetidin-1-yl)benzonitrile, 2i. Compound **2i** was prepared as described for **2a**, using diethylmalonyl dichloride (2.956 g; 0.015 mol) and 4-cyanoaniline (1.772 g, 0.015 mol). It was purified by column chromatography on silica gel using hexane/ethyl acetate (8.0, 2.0), to yield the product as white crystals (0.687 g, 19%): mp 106–109 °C; Anal. (C₁₄H₁₄N₂O₂) C, H, N; δ ¹H NMR 1.09 (6H, t, *J* = 7.6), 1.90 (4H, q, *J* = 7.6), 7.74 (2H, d, *J* = 8.8), 8.03 (2H, d, *J* = 8.8); δ ¹³C NMR 9.21, 23.96, 72.87, 110.10, 118.14, 119.29, 133.49, 137.19, 171.70.

Chemical Kinetics. For all kinetic experiments, temperatures were maintained at 25.0 ± 0.1 °C, and the ionic strength was adjusted to 0.5 M by addition of NaClO₄. Sodium hydroxide solutions were prepared by dilution of standardized Tritisol stock solutions and contained 20% (v/v) CH₃CN. Stock solutions of compounds were prepared in CH₃CN. In a typical run, the reaction was initiated by the addition of a 30 μ L aliquot of a 10⁻² M stock solution of substrate to a cuvette containing 3 mL of the alkaline buffer solution. Curves were analyzed as first-order reactions. The pseudo-first-order rate constants, *k*_{obs}, were obtained by least-squares treatment of log(*A*_{*t*} - *A*_∞) data, where *A*_{*t*} and *A*_∞ represent the absorbance at time *t* and at time infinity, respectively. The wavelengths (nm) used were 221 for **2a** and **2d**, 260 for **2b**, **2f**, and **2h**, 247 for **2e**, 255 for **2g**, and 280 nm for **2i**.

Enzymatic Assays. PPE and HLE were assayed spectrophotometrically by monitoring the release of *p*-nitroaniline at 390 and 410 nm, respectively, from the enzyme mediated hydrolysis of the substrates, *N*-Suc-Ala-Ala-*p*-NA and MeO-Suc-Ala-Ala-*p*-NA at 25 °C to evaluate whether the inhibition is reversible or irreversible. Inactivation rates for time-dependent inhibition were determined continuously, according to the slow tight-binding inhibition model. Alternatively, in cases where no time-dependent inhibition was observed, the inhibitor constants *K*_{*i*} were calculated from Dixon plots.

Enzyme Inactivation by the Progress Curve Method. For the most-active compounds (**2e–2i**), PPE inhibition was analyzed by the progress curve method.^{15,25} The enzymatic reactions were initiated by addition of 10 μL of PPE (20 μM in HEPES buffer, 0.1 M, pH 7.2) to a cuvette thermostatted at 25 $^{\circ}\text{C}$, containing 940 μL of HEPES buffer (0.1 M, pH 7.2), 20 μL of DMSO, 20 μL of substrate (15 mM in DMSO), and 10 μL of inhibitor (**2e–2i** in DMSO). The absorbance was continuously monitored at 390 nm for 20 min. The final concentrations were $[\text{PPE}] = 200 \text{ nM}$, $[\text{substrate}] = 0.3 \text{ mM}$, and $[\text{DMSO}] = 5\% \text{ (v/v)}$. Several inhibitor concentrations from 8 to 150 μM were used. Control assays, in which the inhibitor was omitted, ran linearly. The pseudo-first-order rate constants, k_{obs} , for the inhibition of PPE were determined according to the slow tight-binding inhibition model¹⁵ and involved the fitting of product concentration as a function of time to eq 1 by nonlinear regression analysis using the routine ENZFIT (developed at the Faculty of Pharmacy, Lisbon).

Inactivation of HLE was assayed at 25 $^{\circ}\text{C}$ by mixing 10 μL of HLE stock solution (2 μM in 0.05 M acetate buffer, pH 5.5) to a solution containing 10 μL of inhibitor in DMSO (200 μM), 20 μL of substrate MeO-Suc-Ala-Ala-Pro-Val-p-NA (50 mM in DMSO), and 960 μL of 0.1 M HEPES buffer, pH 7.2, and the absorbance was continuously monitored at 410 nm for 20 min.

Enzyme Inactivation by the Incubation Method.²⁶ In a typical experiment, 50 μL of inhibitor **2h** (3 mM in DMSO) was incubated at 25 $^{\circ}\text{C}$ with 750 μL of HEPES buffer (0.1 M; pH 7.2) and 200 μL of PPE solution of 50 μM in HEPES buffer. Aliquots (100 μL) were withdrawn at different time intervals (30 s, 15 min, 30 min, 1 h, 2 h, 3 h, 4 h, 5 h, and 7 h) and transferred to a cuvette thermostatted at 25 $^{\circ}\text{C}$, containing 895 μL of HEPES buffer (0.1 M; pH 7.2) and 5 μL of substrate (12.5 mM). The absorbance was monitored at 390 nm for 50 s. The amount of enzyme activity was determined by comparison of the activity of a control assay (containing no inhibitor) with the activity of an enzyme solution containing inhibitor at the same time point. The experiment was repeated using inhibitor **2b** (aliquots withdrawn at 30 s, 2 min, 3.5 min, 5 min, 6.5 min, 21 min, and 60 min).

Molecular Modeling. The geometries of compounds **2** were energy minimized using density functional theory.²⁷ These calculations were performed with the B3LYP²⁸ hybrid functional and the 6-31+G(d,p) basis set implemented in Gaussian03 software package.²⁹ After geometry optimizations, partial charges were included using Amber's Antechamber module³⁰ (included with Chimera software).³¹ The PPE structure used was obtained by deletion from the active site of the ligand present in the crystal structure (the β -lactam ring-opened product of a *N*-sulfonylaryl β -lactam covalently linked to Ser-195; PDB accession code 1BTU).³² Hydrogen atoms were added, and the correct protonation states of histidine residues were assigned according to their surrounding environment. The PPE structure was energy minimized, and charges were added using the Amber united atom force field,³³ implemented in Chimera software.³¹ To assess the quality of our docking results, the ligand derived from the *N*-sulfonylaryl β -lactam was docked back into the 1BTU active site showing a very small root-mean-square deviation (rmsd) when compared with 1BTU crystal structure. Molecular docking studies of inhibitors **2** into the active site of PPE enzyme were performed with the flexible GOLD (Genetic Optimisation for Ligand Docking, version 3.0.1)³⁴ docking program using the goldscore scoring function.³⁵ Each ligand was initially energy minimized and then subjected to 10 000 docking runs (with a population size of 100; 100,000 genetic algorithm operations; 5 islands). The top 10 solutions (i.e., those with the highest fitness score) were visually analyzed for (i) the hydrophobic and hydrophilic interactions between the ligand and enzyme surfaces and (ii) the distance between the Ser-195 hydroxyl oxygen atom and the carbonyl carbon atoms of each 4-oxo- β -lactam **2**.

Acknowledgment. This work was supported in part by Fundação para a Ciência e Tecnologia (FCT, Portugal) through the project PTDC/QUI/64056/2006. J.M. acknowledges FCT for the PhD grant SFRH/BD/17534/2004.

Supporting Information Available: Analytical data, complete ref 29, plots of k_{obs} versus $[\text{I}]$ for **2f**, **2g**, and **2h** in PPE assays, plot of k_{obs} versus $[\text{I}]$ for **2i** in the HLE assay, and superimposition of docked structures of **2b**, **2e**, **2f**, and **2i** in PPE active site. This material is available free of charge via the Internet at <http://pubs.acs.org>.

References

- Barnes, P. J. Chronic obstructive pulmonary disease. *New Engl. J. Med.* **2000**, *343*, 269–280.
- Cowan, K. N.; Heilbut, A.; Humpl, T.; Lam, C.; Ito, S.; Rabinovitsch, M. Complete reversal of pulmonary hypertension in rats by a serine elastase inhibitor. *Nat. Med.* **2005**, *6*, 698–702.
- Ohbayashi, H. Current synthetic inhibitors of human neutrophil elastase in 2005. *Expert Opin. Ther. Pat.* **2005**, *15*, 759–771.
- Donnelly, L. E.; Rogers, D. F. Therapy for chronic obstructive pulmonary disease in the 21st century. *Drugs* **2003**, *63*, 1973–1998.
- Malhotra, S.; Man, S. F. P.; Sin, D. D. Emerging drugs for the treatment of chronic obstructive pulmonary disease. *Expert Opin. Emerging Drugs* **2006**, *11*, 275–291.
- Konaklieva, M. I. β -Lactams as inhibitors of serine enzymes. *Curr. Med. Chem.* **2002**, *1*, 215–238.
- Powers, J. C.; Asgjan, J. L.; Ekicu, Ö. D.; James, K. E. Irreversible inhibitors of serine, cysteine, and threonine proteases. *Chem. Rev.* **2002**, *102*, 4639–4750.
- Konaklieva, M. I.; Plotkin, B. J. The relationship between inhibitors of eukaryotic and prokaryotic serine proteases. *Mini-Rev. Med. Chem.* **2004**, *4*, 721–739.
- Leung, D.; Abbenante, G.; Fairlie, D. P. Protease inhibitors: Current status and future prospects. *J. Med. Chem.* **2000**, *43*, 305–341.
- Moreira, R.; Santana, A. B.; Iley, J.; Neres, J.; Douglas, K. T.; Horton, P. N.; Hursthouse, M. B. Design, synthesis and enzymatic evaluation of *N*-acyloxyalkyl- and *N*-oxazolidin-2,4-dion-5-yl-substituted β -lactams as novel inhibitors of human leukocyte elastase. *J. Med. Chem.* **2005**, *48*, 4861–4870.
- Tsang, W. Y.; Ahmed, N.; Hardling, L.; Hemming, K.; Laws, A. P.; Page, M. Acylation versus sulfonylation in the inhibition of elastase by 3-oxo- β -sultams. *J. Am. Chem. Soc.* **2005**, *127*, 8946–8947.
- Ahmed, N.; Tsang, W. Y.; Page, M. I. Acyl vs sulfonyl transfer in *N*-acyl β -sultams and 3-oxo- β -sultams. *Org. Lett.* **2004**, *6*, 201–203.
- Page, M. I. The mechanisms of reactions of β -lactams antibiotics. *Adv. Phys. Org. Chem.* **1987**, *23*, 165–270.
- Sykes, N. O.; Macdonald, S. J. F.; Page, M. I. Acylating agents as enzyme inhibitors and understanding their reactivity for drug design. *J. Med. Chem.* **2002**, *45*, 2850–2856.
- Morrison, J.; Walsh, C. The behaviour and significance of slow binding enzyme inhibitors. *Adv. Enzym.* **1988**, *61*, 201–299.
- Stein, R. L.; Strimpler, A. M.; Viscarello, B. R.; Wildonger, R. A.; Mauger, R. C.; Traino, D. A. Mechanism for slow-binding inhibition of human leukocyte elastase by valine-derived benzoxazinones. *Biochemistry* **1987**, *26*, 4126–4130.
- Kuzmic, P. Program DYNAPFIT for the analysis of enzyme kinetic data: Application to HIV proteinase. *Anal. Biochem.* **1996**, *237*, 260–273.
- King, J. F. In *The Chemistry of Sulphonic Acids, Esters and their Derivatives*; Patai, S., Rappoport, Z., Eds.; John Wiley: Chichester, U.K., 1991; pp. 249–259.
- Page, M. I. β -Sultams—Mechanism of reactions and use as inhibitors of serine proteases. *Acc. Chem. Res.* **2004**, *37*, 297–303.
- Indelicato, J. M.; Pasini, C. E. The acylating potential of γ -lactam antibacterials: Base hydrolysis of bicyclic pyrazolidinones. *J. Med. Chem.* **1988**, *31*, 1227–1230.
- Krantz, A.; Spencer, R. W.; Tam, T. F.; Liak, T. J.; Copp, L. J.; Thomas, E. M.; Rafferty, S. P. Design and synthesis of 4H-3,1-benzoxazin-4-ones as potent alternate substrate inhibitors of human leukocyte elastase. *J. Med. Chem.* **1990**, *33*, 464–479.
- Knight, W.; Green, B.; Chabin, R.; Gale, P.; Maycock, A.; Weston, H.; Kuo, D.; Westler, W.; Dorn, C.; Finke, P.; Haggmann, W.; Hale, J.; Liesch, J.; MacCoss, M.; Navia, M.; Shah, S.; Underwood, D.; Doherty, J. Specificity, stability, and potency of monocyclic β -lactam inhibitors of human leukocyte elastase. *Biochemistry* **1992**, *31*, 8160–8170.
- Golik, U. The synthesis of malonimide derivatives as potential penicillin analogs. *J. Heterocycl. Chem.* **1972**, *9*, 21–24.
- Dai, S. A.; Juang, T. Y.; Chen, C. P.; Chang, H. Y.; Kuo, W. J.; Su, W. C.; Jeng, R. J. Synthesis of *N*-aryl azetidino-2,4-diones and polymalonamides prepared from selective ring-opening reactions. *J. Appl. Polym. Sci.* **2007**, *103*, 3591–3599.
- Haggmann, W. K.; Kissinger, A. L.; Shah, S. K.; Finke, P. E.; Dorn, C. P.; Brause, K. A.; Ashe, B. M.; Weston, H.; Maycock, A. L.;

- Knight, W. B.; Della, P. S.; Fletcher, D. S.; Hand, K. M.; Osinga, D.; Davies, P.; Doherty, J. B. Orally active β -lactam inhibitors of human-leukocyte elastase. 2. Effect of C-4 substitution. *J. Med. Chem.* **1993**, *36*, 771–777.
- (26) Kitz, R.; Wilson, I. B. Esters of methanesulfonic acid as irreversible inhibitors of acetylcholinesterase. *J. Biol. Chem.* **1962**, *12*, 2940–2945.
- (27) Parr, R. G.; Yang, W. *Density Functional Theory of Atoms and Molecules*; Oxford University Press: Oxford, U. K., 1989.
- (28) (a) Becke, A. D. *J. Chem. Phys.* **1993**, *98*, 5648–5652. (b) Lee, C. T.; Yang, W.; Parr, R. G. *Phys. Rev. B* **1988**, *37*, 785–789.
- (29) Frisch, M. J. *Gaussian 03*, revision C.02; Gaussian, Inc.: Wallingford, CT, 2004.
- (30) Wang, J.; Wang, W.; Kollman, P. A.; Case, D. A. Automatic atom type and bond type perception in molecular mechanical calculations. *J. Mol. Graph. Model.* **2006**, *25*, 247.
- (31) For the UCSF Chimera package from the Resource for Biocomputing, Visualization, and Informatics at the University of CA, San Francisco (supported by NIH P41 RR-01081), see: Pettersen, E. F.; Goddard, T. D.; Huang, C. C.; Couch, G. S.; Greenblatt, D. M.; Meng, E. C.; Ferrin, T. E. UCSF Chimera—A visualization system for exploratory research and analysis. *J. Comput. Chem.* **2004**, *25*, 1605–1612.
- (32) Wilmouth, R. C.; Westwood, N. J.; Anderson, K.; Brownlee, W.; Claridge, T. D. W.; Clifton, I. J.; Pritchard, G. J.; Aplin, R. T.; Schofield, C. J. Inhibition of elastase by *N*-sulfonylaryl β -lactams: Anatomy of a stable acyl-enzyme complex. *Biochemistry* **1998**, *37*, 17506–17513.
- (33) Cornell, W. D.; Cieplak, P.; Bayly, C. I.; Gould, I. R.; Merz, K. M., Jr.; Ferguson, D. M.; Spellmeyer, D. C.; Fox, T.; Caldwell, J. W.; Kollman, P. A. A second generation force field for the simulation of proteins, nucleic acids and organic molecules. *J. Am. Chem. Soc.* **1995**, *117*, 5179–5197.
- (34) CCDC Software Ltd., Cambridge, U.K.
- (35) Jones, G.; Willett, P.; Glen, R. C.; Leach, A. R.; Taylor, R. Development and validation of a genetic algorithm for flexible docking. *J. Mol. Biol.* **1997**, *267*, 727–748.

JM701257H